

Det Kongelige Danske Videnskabernes Selskab

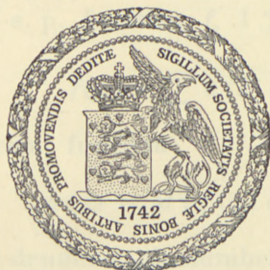
Matematisk-fysiske Meddelelser, bind 29, nr. 1

Dan. Mat. Fys. Medd. 29, no. 1 (1954)

ON THE DUAL SPACES
OF THE BESICOVITCH ALMOST
PERIODIC SPACES

BY

ERLING FØLNER



København 1954

i kommission hos Ejnar Munksgaard

Det Kongelige Danske Videnskabsnernes Selskab

Matematisk-fysiske Meddelelser, bind 23, nr. 1

1925

ON THE DUAL SPACES
OF THE BESICOVITCH ALMOST
PERIODIC SPACES

BY
HAROLD POINCARÉ



Printed in Denmark.

Bianco Lunos Bogtrykkeri A.S.

Introduction.

As is well known, see for instance [5], p. 36, for every p , $1 \leq p < \infty$, a B^p -a. p. function f is a function to which there exists a sequence of ordinary almost periodic functions φ_n such that

$$\|f - \varphi_n\|_{B^p} \rightarrow 0 \text{ for } n \rightarrow \infty.$$

Here the B^p -norm is defined by

$$\|f\|_{B^p} = \overline{\lim}_{T \rightarrow \infty} \left(\frac{1}{2T} \int_{-T}^T |f(x)|^p dx \right)^{\frac{1}{p}} = \left(\overline{M}\{ |f(x)|^p \} \right)^{\frac{1}{p}}.$$

If in particular $\|f\|_{B^p} = 0$, the function f is called a B^p -zero function. If we set $f \equiv g$ when $\|f - g\|_{B^p} = 0$, the equivalence classes for this relation are called B^p -a. p. points. Multiplication of a B^p -a. p. point by a complex constant, addition of two B^p -a. p. points, and the B^p -norm of a B^p -a. p. point are defined in the natural way. Thus the set of B^p -a. p. points becomes a linear metric space, [5], pp. 37—39. Since the B^p -a. p. space is complete, see for instance [5], pp. 54—57, it is a Banach space.

To every B^p -a. p. function f , $1 \leq p < \infty$, is associated a Fourier series

$$f(x) \sim \sum a(\lambda) e^{i\lambda x},$$

where the coefficient function

$$a(\lambda) = M\{ f(x) e^{-i\lambda x} \}$$

is $\neq 0$ only for a denumerable number of values λ , the so-called Fourier exponents of f , [2], p. 262. Since all functions in a B^p -a. p. point have the same Fourier series, this Fourier series is called the Fourier series of the B^p -a. p. point.

Let \mathbf{M} be an arbitrary module of real numbers, i. e., a set of real numbers which together with λ_1 and λ_2 also contains $\lambda_1 - \lambda_2$. A B^p -a. p. function (B^p -a. p. point) is called a B^p -a. p.— \mathbf{M} function (B^p -a. p.— \mathbf{M} point) if all its Fourier exponents belong to \mathbf{M} . The subspace of the B^p -a. p. space consisting of all B^p -a. p.— \mathbf{M} points is a linear closed subspace and hence a Banach space. If in particular \mathbf{M} is the module of all real numbers, the B^p -a. p.— \mathbf{M} space is the B^p -a. p. space itself.

We consider a complex bounded linear functional A on the space of B^p -a. p.— \mathbf{M} functions, i. e., a complex functional which satisfies

$$\begin{aligned} A(\lambda f) &= \lambda Af \quad (\lambda \text{ complex}) \\ A(f + g) &= Af + Ag \\ |Af| &\leq C \|f\|_{B^p}, \end{aligned}$$

where C is independent of f . Here we may assume C chosen as the smallest of its possible values. C is then called the norm of A and denoted by $\|A\|$. It is obvious that A takes the same value on all B^p -a. p.— \mathbf{M} functions in a B^p -a. p.— \mathbf{M} point. Thus A may also be considered as a bounded linear functional on the B^p -a. p.— \mathbf{M} space. With usual addition, usual multiplication by a complex constant, and the above norm, the set of bounded linear functionals on the B^p -a. p.— \mathbf{M} space is a Banach space, the so-called dual space of the B^p -a. p.— \mathbf{M} space.

We shall prove in the present paper that for $1 < p < \infty$ and any module \mathbf{M} of real numbers the dual space of the B^p -a. p.— \mathbf{M} space is the B^q -a. p.— \mathbf{M} space where q is determined by $1/p + 1/q = 1$. The isomorphism (i. e., the linear one-to-one isometric mapping) of the dual space of the B^p -a. p.— \mathbf{M} space on the B^q -a. p.— \mathbf{M} space is given by

$$A_g \rightarrow g \quad \text{where} \quad A_g f = M \{ f \bar{g} \}.$$

The dual space of the B^1 -a. p.— \mathbf{M} space will also be completely characterized.

We shall deduce this main result by two rather different methods. The first method is the most elementary one and uses only the ordinary theory of generalized almost periodic functions. It is based on previous results by R. Doss [7], [8], and is an

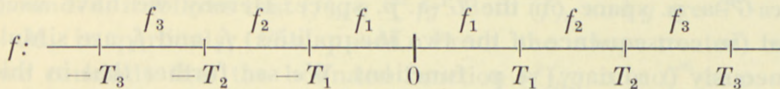
extension of the method used by Doss. This method is set forth in Part I of the paper.

The second method, which is set forth in Part II of the paper, consists in the establishment of a close correspondance between the B^p -a. p.—**M** points and the measurable p -integrable functions on the Bohr compactification of the real axis by all ordinary a. p.—**M** functions. When this correspondance is established, our main result concerning the dual space of the B^p -a. p.—**M** space, $1 \leq p < \infty$, is an immediate consequence of the generalization to the abstract case of F. Riesz's classical result concerning the dual space of the space L^p of measurable p -integrable functions, $1 \leq p < \infty$.

Part I.

1. Preparations.

1. We have mentioned in the Introduction that the B^p -a. p. space, $1 \leq p < \infty$, is a complete space; or, in other words, that if f_n is a B^p -fundamental sequence of B^p -a. p. functions: $\|f_m - f_n\|_{B^p} \rightarrow 0$ for $m, n \rightarrow \infty$, then there exists a B^p -a. p. function f such that $\|f - f_n\|_{B^p} \rightarrow 0$ for $n \rightarrow \infty$. We shall use moreover that f , as shown in [5], pp. 54—57, can be constructed "from pieces of the f_n " as indicated on the following figure



where $0 = T_0 < T_1 < T_2 < \dots \rightarrow \infty$ and the only extra demand to T_n is of the form

$$T_n > t(T_0, T_1, \dots, T_{n-1}), \quad n = 1, 2, \dots$$

When in the following the letter G is applied (instead of the usual B), this indicates that the theorems are true for all three types of generalized almost periodic functions, the Stepanoff a. p. functions, the Weyl a. p. functions, and the Besicovitch a. p. functions (for their definitions see for instance [5], pp. 33—39).

2. On account of Hölder's inequality we have $\|f\|_{G^{p_1}} \leq \|f\|_{G^{p_2}}$ for $1 \leq p_1 < p_2$. Hence a G^{p_2} -a. p. function (G^{p_2} -zero function) is also a G^{p_1} -a. p. function (G^{p_1} -zero function).

3. A bounded G^1 -a. p. function (bounded G^1 -zero function) is a G^p -a. p. function (G^p -zero function) for all p , $1 \leq p < \infty$; [5], p. 62. We shall call such a bounded G^1 -a. p. function (bounded G^1 -zero function) a G^∞ -a. p. function (G^∞ -zero function).

4. Deeper-lying theorem: A B^1 -a. p. point which contains a B^P -bounded function for a fixed P , $1 < P < \infty$, contains also a B^P -a. p. function. [5], pp. 99–106.

5. We consider the inequalities

$$\left| |f|^{\frac{1}{p}} \operatorname{sign} f - |\varphi|^{\frac{1}{p}} \operatorname{sign} \varphi \right| \leq 2^p |f - \varphi|$$

and

$$\left| |f|^p \operatorname{sign} f - |\varphi|^p \operatorname{sign} \varphi \right| \leq 2^p |f - \varphi| \left(|f| + |\varphi| \right)^{p-1},$$

where $1 \leq p < \infty$. See [6], pp. 220–221, exercise 10. These inequalities, the latter in connection with Hölder's inequality, show that the mapping

$$(1) \quad f_1 \rightarrow f_2,$$

where $f_2 = |f_1|^p \operatorname{sign} f_1$ and hence $f_1 = |f_2|^{\frac{1}{p}} \operatorname{sign} f_2$ is (or more correctly: may be considered as) a homeomorphic mapping of the G^p -a. p. space on the G^1 -a. p. space. Hereby we have used that (in consequence of the two inequalities) f_1 and f_2 are simultaneously (ordinary) a. p. functions. We see further that in this case they "majorize" each other; [4], p. 60. Hence (l. c.) f_1 and f_2 are simultaneously a. p.—**M** functions. Since a G^p -a. p.—**M** function is a function which can be G^p -approximated by a. p.—**M** functions (cf. 8. below), we conclude that if f_1 is a G^p -a. p.—**M** function, then f_2 is a G^1 -a. p.—**M** function, and conversely. Hence (1) is also a homeomorphic mapping of the G^p -a. p.—**M** space on the G^1 -a. p.—**M** space.

Combining this result and the corresponding result with p replaced by q , $1 \leq q < \infty$, we see finally that

$$f_1 \rightarrow f_2,$$

where $f_2 = |f_1|^{\frac{p}{q}} \text{sign } f_1$, and hence $f_1 = |f_2|^{\frac{q}{p}} \text{sign } f_2$ is a homeomorphic mapping of the G^p -a. p.— \mathbf{M} space on the G^q -a. p.— \mathbf{M} space for any module \mathbf{M} of real numbers. In particular, when f_1 is G^p -a. p.— \mathbf{M} , then f_2 is G^q -a. p.— \mathbf{M} , and conversely. Cf. [11], pp. 422—423.

6. If φ_n is a sequence of $G^{\alpha p}$ -a. p. functions which $G^{\alpha p}$ -converges to the $G^{\alpha p}$ -a. p. function f and ψ_n is a sequence of $G^{\alpha q}$ -a. p. functions which $G^{\alpha q}$ -converges to the $G^{\alpha q}$ -a. p. function g , for fixed $\alpha \geq 1$, $1 < p < \infty$, $1 < q < \infty$, $1/p + 1/q = 1$, then $\varphi_n \psi_n$ will G^α -converge to fg . This follows easily by application of Hölder's and Minkowski's inequalities. In particular, when f is a $G^{\alpha p}$ -a. p.— \mathbf{M} function and g is a $G^{\alpha q}$ -a. p.— \mathbf{M} function, then fg is a G^α -a. p.— \mathbf{M} function. Cf. [11], pp. 416—417.

If f is a G^α -a. p.— \mathbf{M} function and g is a G^∞ -a. p.— \mathbf{M} function for fixed $\alpha \geq 1$, then fg is a G^α -a. p.— \mathbf{M} function. In order to see this we introduce the cut-off function

$$(f(x))_n = \begin{cases} f(x) & \text{for } |f(x)| \leq n \\ n \text{ sign } f(x) & \text{for } |f(x)| \geq n. \end{cases}$$

Since

$$|(f)_n - (\varphi)_n| \leq |f - \varphi|$$

we see that if f is a p.— \mathbf{M} , then $(f)_n$ is a p.— \mathbf{M} as it is majorized by f ; [4], p. 60. It follows that in the general case $(f)_n$ is G^∞ -a. p.— \mathbf{M} . Further $(f)_n \xrightarrow{G^\alpha} f$ for $n \rightarrow \infty$; [5], pp. 44—45. Since g is bounded, it follows that $(f)_n g \xrightarrow{G^\alpha} fg$. Both $(f)_n$ and g are G^∞ -a. p.— \mathbf{M} , in particular G^2 -a. p.— \mathbf{M} . From the above-treated case we conclude that the bounded function $(f)_n g$ is a G^∞ -a. p.— \mathbf{M} function. Then the G^α -limit fg is a G^α -a. p.— \mathbf{M} function, as was to be proved.

7. Let \mathbf{M} be a denumerable module of real numbers $\alpha_1, \alpha_2, \dots$. By a sequence of Bochner—Fejér kernels belonging to \mathbf{M} we understand a sequence of non-negative trigonometric polynomials with exponents from \mathbf{M} , positive coefficients, mean values 1, and which converge formally to $\sum e^{i\alpha_n x}$. It follows that the coefficients are ≤ 1 .

Let

$$\sum a(\lambda_n) e^{i\lambda_n x} = \sum a(\lambda) e^{i\lambda x}$$

be a trigonometric series and \mathbf{M} an arbitrary denumerable module of real numbers $\alpha_1, \alpha_2, \dots$. Let

$$k_m(x) = \sum d_n^{(m)} e^{i\alpha_n x}$$

be a sequence of Bochner—Fejér kernels belonging to \mathbf{M} . Then

$$\sigma_m(x) = \sum d_n^{(m)} a(\alpha_n) e^{i\alpha_n x}$$

is called a Bochner—Fejér sequence belonging to \mathbf{M} of the trigonometric series. If every λ for which $a(\lambda) \neq 0$, belongs to \mathbf{M} , then the series is said to belong to \mathbf{M} , and σ_m is called a full Bochner—Fejér sequence of the series.

8. Let f be a G^p -a. p. function for a fixed p , $1 \leq p < \infty$, with the Fourier series

$$f(x) \sim \sum a(\lambda) e^{i\lambda x}.$$

Let \mathbf{M} be a denumerable module and σ_m a Bochner—Fejér sequence belonging to \mathbf{M} of the Fourier series. Then $\|\sigma_m\|_{G^p} \leq \|f\|_{G^p}$ (see [2], pp. 263—266). If $|f(x)| \leq C$ for all x , then $|\sigma_m(x)| \leq C$ for all x . If σ_m is a full Bochner—Fejér sequence of the series, then $\sigma_m \xrightarrow{G^p} f$ for $m \rightarrow \infty$; [2], pp. 262—266.

9. If $f \sim \sum a(\lambda) e^{i\lambda x}$ is a B^1 -a. p. function and $g(x) = \sum b(\lambda) e^{i\lambda x}$ is a trigonometric polynomial, then (obviously)

$$M\{f\bar{g}\} = \sum a(\lambda) \overline{b(\lambda)}.$$

If $f \sim \sum a(\lambda) e^{i\lambda x}$ is a B^p -a. p. function and $g \sim \sum b(\lambda) e^{i\lambda x}$ is a B^q -a. p. function for fixed p and q , $1 \leq p < \infty$, $1 < q \leq \infty$, $1/p + 1/q = 1$, and furthermore $a(\lambda) \overline{b(\lambda)} = 0$ for all λ , then

$$M\{f\bar{g}\} = 0.$$

In order to see this, let σ_m be a full Bochner—Fejér sequence of f . Then by 8. we have $\sigma_m \xrightarrow{B^p} f$ and, using also the above remark, $M\{\sigma_m \bar{g}\} = 0$. As a result of 6. the function $f\bar{g}$ is B^1 -a. p. and $M\{\sigma_m \bar{g}\} \rightarrow M\{f\bar{g}\}$. Thus $M\{f\bar{g}\} = 0$, as we had to show.

10. If a sequence A_m of bounded linear functionals on a

Banach space converges weakly, i. e., $A_m f$ converges for every f in the Banach space, then there exists a constant C such that $\|A_m\| \leq C$ for all m . See for instance [9], p. 21.

2. Necessary and sufficient conditions for a trigonometric series to be the Fourier series of a B^p -a. p. function for a given p , $1 \leq p \leq \infty$.

Doss, [7], p. 209, and [8], pp. 89—91, has proved the following two theorems.

Theorem A. *A necessary and sufficient condition for a trigonometric series $\sum a_n e^{i\lambda_n x}$ to be the Fourier series of a B^∞ -a. p. function is that for a full Bochner-Fejér sequence σ_m of the series there exists a constant C such that $|\sigma_m(x)| \leq C$ for all x and all m .*

Theorem B. *A necessary and sufficient condition for a trigonometric series $\sum a_n e^{i\lambda_n x}$ to be the Fourier series of a B^1 -a. p. function is that a full Bochner-Fejér sequence σ_m of the series has the following property: To every $\varepsilon > 0$ there exists a $\delta > 0$ such that $\overline{M}_E \{ |\sigma_m(x)| \} < \varepsilon$ for any measurable set E with upper mean-measure $\overline{m} E < \delta$.*

The remaining cases, $1 < p < \infty$, are dealt with in the following:

Theorem 1. *Let p be a fixed number, $1 < p < \infty$. A necessary and sufficient condition for a trigonometric series $\sum a_n e^{i\lambda_n x}$ to be the Fourier series of a B^p -a. p. function is that for a full Bochner-Fejér sequence σ_m of the series there exists a constant C such that $\|\sigma_m\|_{B^p} < C$ for all m .*

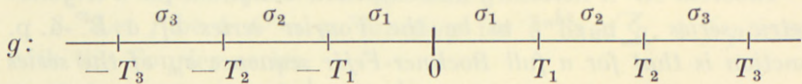
Proof. The necessity of the condition is clear, for if the series is the Fourier series of the B^p -a. p. function f , then as stated in I, 8. we have $\|\sigma_m\|_{B^p} \leq \|f\|_{B^p}$.

We shall now show that the condition is sufficient. Assuming the condition fulfilled, we show first that the series is the Fourier series of a B^1 -a. p. function; and we do this by showing that it fulfils the condition from Theorem B. Let E be an arbitrary measurable set of real numbers; let e denote the characteristic function of E ; and let σ_m be a full Bochner-Fejér sequence of the series. Determining q by $1/p + 1/q = 1$ we obtain by Hölder's inequality

$$\begin{aligned} \overline{M}_E \{ |\sigma_m(x)| \} &= \overline{M} \{ e(x) |\sigma_m(x)| \} \leq \\ (M \{ |\sigma_m|^p \})^{\frac{1}{p}} (\overline{M} \{ e^q \})^{\frac{1}{q}} &= \|\sigma_m\|_{B^p} (\overline{m}E)^{\frac{1}{q}} \leq C (\overline{m}E)^{\frac{1}{q}} \end{aligned}$$

and this tends to 0 for $\overline{m}E \rightarrow 0$. Hence the condition from Theorem B is fulfilled so that our series is the Fourier series of a B^1 -a. p. function h . Thus, by 1, 8. we have $\|h - \sigma_m\|_{B^1} \rightarrow 0$ for $m \rightarrow \infty$, in particular $\|\sigma_m - \sigma_n\|_{B^1} \rightarrow 0$ for $m, n \rightarrow \infty$.

We shall now determine a B^1 -limit function g from pieces of the σ_m as indicated on the following figure



and show that we can determine $0 = T_0 < T_1 < T_2 < \dots \rightarrow \infty$ so that $\|g\|_{B^p} < \infty$.

From

$$\|\sigma_m\|_{B^p}^p = \overline{\lim}_{T \rightarrow \infty} \frac{1}{2T} \int_{-T}^T |\sigma_m(x)|^p dx < C^p$$

follows

$$\overline{\lim}_{|T| \rightarrow \infty} \frac{1}{T} \int_0^T |\sigma_m(x)|^p dx < 2 C^p.$$

Hence there exists a t_m such that

$$\frac{1}{T} \int_0^T |\sigma_m(x)|^p dx < 2 C^p \quad \text{for } |T| > t_m,$$

and there exists an $s = s(T_{m-1})$ such that

$$\frac{1}{T - (\pm T_{m-1})} \int_{\pm T_{m-1}}^T |\sigma_m(x)|^p dx < 2 C^p \quad \text{for } \pm T > s(T_{m-1}),$$

respectively, $m = 1, 2, \dots$. Besides choosing $T_m > t(T_0, \dots, T_{m-1})$ which by 1, 1. secures the B^1 -convergence of σ_m towards g we choose $T > t_{m+1}$ and $T_m > s(T_{m-1})$ for $m = 1, 2, \dots$. Then for $T_m \leq T < T_{m+1}$ we get

$$\begin{aligned} \frac{1}{T} \int_0^T |g(x)|^p dx &= \frac{1}{T} \left[\int_0^{T_1} |\sigma_1(x)|^p dx + \cdots + \int_{T_{m-1}}^{T_m} |\sigma_m(x)|^p dx + \right. \\ &\quad \left. \int_{T_m}^T |\sigma_{m+1}(x)|^p dx \right] \leq \frac{1}{T} [2 C^p (T_1 - 0) + 2 C^p (T_2 - T_1) + \cdots \\ &\quad + 2 C^p (T_m - T_{m-1})] + \frac{1}{T} \int_0^T |\sigma_{m+1}(x)|^p dx < 2 C^p + 2 C^p = 4 C^p. \end{aligned}$$

For $-T_{m+1} < T \leq -T_m$ we get analogously that

$$\frac{1}{T} \int_0^T |g(x)|^p dx < 4 C^p.$$

Hence $\|g\|_{B^p} \leq 4^{1/p} C < \infty$, as desired.

We have seen that our series is the Fourier series of a B^1 -a. p. point which contains the B^p -bounded function g . It follows by the theorem in 1, 4. that the B^1 -a. p. point contains a B^p -a. p. function f . Thus our series is the Fourier series of a B^p -a. p. function f . This completes the proof of Theorem 1.

Corollary. Let $f \sim \sum a(\lambda) e^{i\lambda x}$ be a B^p -a. p. function for a fixed p , $1 < p < \infty$, and let \mathbf{M} be an arbitrary module of real numbers. Then the subseries

$$\sum_{\lambda \in \mathbf{M}} a(\lambda) e^{i\lambda x}$$

is the Fourier series of a B^p -a. p. function $f^{\mathbf{M}}$.

Proof. Without loss of generality we may assume \mathbf{M} to be denumerable. A Bochner-Fejér sequence σ_m belonging to \mathbf{M} of the original series $\sum a(\lambda) e^{i\lambda x}$ is plainly a Bochner-Fejér sequence belonging to \mathbf{M} of the subseries $\sum_{\lambda \in \mathbf{M}} a(\lambda) e^{i\lambda x}$, and for this latter series it is a full Bochner-Fejér sequence.

From 1, 8. it follows that $\|\sigma_m\|_{B^p} \leq \|f\|_{B^p}$. This implies, by Theorem 1, that $\sum_{\lambda \in \mathbf{M}} a(\lambda) e^{i\lambda x}$ is the Fourier series of a B^p -a. p. function, q. e. d.

Remark. The Corollary is also true when $p = 1$. (Cf. Doss [8], p. 91). The Corollary in the case $p = \infty$ is an immediate consequence of Theorem A.

It is natural to mention, in connection with the above theorems, the following theorem of PITT, [10], pp. 144—147, which generalizes the Hausdorff-Young Theorem for ordinary Fourier series.

Theorem C. *Let p and q be fixed numbers with $1/p + 1/q = 1$ and $1 < q \leq 2 \leq p < \infty$.*

(a) *If f is a B^q -a. p. function with the Fourier series $\sum a_n e^{i\lambda_n x}$ we have*

$$\left(\sum |a_n|^p\right)^{1/p} \leq \|f\|_{B^q}.$$

(b) *Every trigonometric series $\sum a_n e^{i\lambda_n x}$ with $\sum |a_n|^q < +\infty$ is the Fourier series of a B^p -a. p. function f , and*

$$\|f\|_{B^p} \leq \left(\sum |a_n|^q\right)^{1/q}.$$

Part (b) of this theorem will be applied in the following.

3. The dual space of the B^p -a. p.- \mathbf{M} space, $1 \leq p < \infty$.

Theorem 2. *Let \mathbf{M} be a module of real numbers and p, q fixed numbers, $1 < p < \infty$, $1 < q < \infty$, satisfying $1/p + 1/q = 1$. Let further g be a B^q -a. p.- \mathbf{M} function. Then there exists a B^p -a. p.- \mathbf{M} function f such that*

$$(2) \quad |M\{f\bar{g}\}| = \|f\|_{B^p} \|g\|_{B^q}.$$

Thus, when $A_g f = M\{f\bar{g}\}$ is considered as a bounded linear functional on the B^p -a. p.- \mathbf{M} space, the norm of A_g is equal to $\|g\|_{B^q}$.

Proof. As shown in 1. 5. the function $f = |g|^{q/p} \text{sign } g$ is a B^p -a. p.- \mathbf{M} function. An immediate calculation shows that it satisfies (2).

Theorem 3. *Let \mathbf{M} be a module of real numbers. Let further g be a B^∞ -a. p.- \mathbf{M} function. Then, when f runs over all B^1 -a. p.- \mathbf{M} functions and z runs over all B^∞ -zero functions we have*

$$(3) \quad \sup_f \frac{|M\{f\bar{g}\}|}{\|f\|_{B^1}} = \lim_{q \rightarrow \infty} \|g\|_{B^q} = \min_z \sup_x |g(x) + z(x)|.$$

In other words: When $A_g f = M\{f\bar{g}\}$ is considered as a bounded linear functional on the B^1 -a. p.- \mathbf{M} space, the norm of A_g is equal to

$$\lim_{q \rightarrow \infty} \|g\|_{B^q} = \min_z \sup_x |g(x) + z(x)|.$$

Proof. We shall begin by showing that the second sign of equality in (3) is valid and do this in two steps, one for \leq and one for \geq .

In order to show the inequality \leq , we shall prove that for any B^∞ -zero function z we have

$$\lim_{q \rightarrow \infty} \|g\|_{B^q} \leq \sup_x |g(x) + z(x)|.$$

Without changing the value of the left-hand side we can replace g by $g + z$ whereafter the inequality is clear.

In order to show the inequality \geq (and the existence of the minimum) we have to construct a B^∞ -zero function z such that

$$\lim_{q \rightarrow \infty} \|g\|_{B^q} \geq \sup_x |g(x) + z(x)|.$$

Let σ_m be a full Bochner-Fejér sequence of g . Then $\|\sigma_m\|_{B^q} \leq \|g\|_{B^q}$ for $1 \leq q < \infty$, so that

$$(4) \quad \lim_{q \rightarrow \infty} \|g\|_{B^q} \geq \lim_{q \rightarrow \infty} \|\sigma_m\|_{B^q} = \sup_x |\sigma_m(x)|$$

(for the last sign of equality, see [3], pp. 110—111). We construct now by **1**, 1. a B^1 -limit function f from pieces of the σ_m . Then it follows from (4) that

$$\lim_{q \rightarrow \infty} \|g\|_{B^q} \geq \sup_x |f(x)|$$

and obviously $f = g + z$ where z is a B^∞ -zero function.

Thus the second sign of equality in (3) is established.

We shall now prove that the sign \leq holds between the first and the third term in (3). When f is a B^1 -a. p. function, g a B^∞ -a. p. function, and z a B^∞ -zero function we have $M\{\overline{f\bar{g}}\} = M\{\overline{f(g+z)}\}$, which we obtain from $M\{(f)_n \bar{g}\} = M\{(f)_n \overline{(g+z)}\}$ when we let $n \rightarrow \infty$ (see end of **1**, 6). It follows that

$$\frac{M\{\overline{f\bar{g}}\}}{M\{|f|\}} = \frac{M\{\overline{f(g+z)}\}}{M\{|f|\}} \leq \sup_x |g(x) + z(x)|.$$

Finally we shall show that the sign \geq holds between the first and the second term in (3). On account of Theorem 2 there exists for every p , $1 < p < \infty$, a B^p -a. p.— \mathbf{M} (and hence B^1 -a. p.— \mathbf{M}) function f_p such that when $1/p + 1/q = 1$

$$|M\{f_p \bar{g}\}| = \|f_p\|_{B^p} \|g\|_{B^q} \geq \|f_p\|_{B^1} \|g\|_{B^q}.$$

Hence

$$\sup_p \frac{|M\{f_p \bar{g}\}|}{\|f_p\|_{B^1}} \geq \lim_{q \rightarrow \infty} \|g\|_{B^q}.$$

This completes the proof of Theorem 3.

It will now be natural to introduce in the set of B^∞ -a. p. functions the norm

$$\|f\|_{B^\infty} = \lim_{q \rightarrow \infty} \|f\|_{B^q} = \min_z \sup_x |f(x) + z(x)|$$

where z runs through all B^∞ -zero functions. Obviously a B^∞ -zero function z may be characterized as a B^∞ -a. p. function with $\|z\|_{B^\infty} = 0$. Now in the usual fashion we introduce B^∞ -a. p. points and organize them as a linear metric space. That the B^∞ -a. p. space is complete, and hence a Banach space, may for instance be deduced from Theorem 4, below. For an arbitrary module \mathbf{M} of real numbers we define in the usual way B^∞ -a. p.— \mathbf{M} functions and points. The subspace of B^∞ -a. p.— \mathbf{M} points is called the B^∞ -a. p.— \mathbf{M} space. It is linear and closed and hence a Banach space.

In the following theorem the term "isomorphic mapping" designates "linear one-to-one isometric mapping".

Theorem 4. Main Theorem. *Let \mathbf{M} be an arbitrary module of real numbers and p, q two numbers, $1 \leq p < \infty$, $1 < q \leq \infty$, satisfying $1/p + 1/q = 1$. Then the dual space of the B^p -a. p.— \mathbf{M} space is isomorphic to the B^q -a. p.— \mathbf{M} space. The isomorphic mapping is given by $A_g \rightarrow g$ where A_g is the bounded linear functional on the B^p -a. p.— \mathbf{M} space given by $A_g f = M\{f \bar{g}\}$.*

Proof. On account of Theorem 2 and Theorem 3 it suffices to show that every bounded linear functional on the B^p -a. p.— \mathbf{M} space has the form $A_g f = M\{f \bar{g}\}$ where g is a B^q -a. p.— \mathbf{M} function.

In the case $p = 1$ this statement was proved by Doss [8]

and was one of the main results of his interesting paper. With the previous preparations at our disposal we can easily treat the general case by his method.

We consider first the case where \mathbf{M} is a denumerable module of real numbers $\lambda_1, \lambda_2, \dots$. We put

$$A(e^{i\lambda_n x}) = \bar{a}_n$$

and form the trigonometric series

$$(5) \quad \sum a_n e^{i\lambda_n x}.$$

Let

$$k_m(x) = \sum d_n^{(m)} e^{i\lambda_n x}$$

be a sequence of Bochner-Fejér kernels belonging to \mathbf{M} (see 1, 7.). Then if

$$f \sim \sum b_n e^{i\lambda_n x}$$

is an arbitrary B^p -a. p.— \mathbf{M} function the sequence

$$\sigma_m(x) = \sum d_n^{(m)} b_n e^{i\lambda_n x}$$

is a Bochner-Fejér sequence belonging to \mathbf{M} of f . Further

$$A\sigma_m = \sum d_n^{(m)} b_n \bar{a}_n.$$

We shall show below that (5) is the Fourier series of a B^q -a. p.— \mathbf{M} function g . Then we get by 1, 9.

$$A\sigma_m = \sum d_n^{(m)} b_n \bar{a}_n = M\{\sigma_m \bar{g}\}.$$

Further, from $\|f - \sigma_m\|_{B^p} \rightarrow 0$ we get $M\{\sigma_m \bar{g}\} \rightarrow M\{f\bar{g}\}$ and $A\sigma_m \rightarrow Af$. Hence

$$Af = \lim_{m \rightarrow \infty} A\sigma_m = \lim_{m \rightarrow \infty} M\{\sigma_m \bar{g}\} = M\{f\bar{g}\},$$

as was to be proved.

That (5) really is the Fourier series of a B^q -a. p.— \mathbf{M} function is seen in the following way. The sequence

$$\tau_m(x) = \sum d_n^{(m)} a_n e^{i\lambda_n x}$$

is a Bochner-Fejér sequence belonging to \mathbf{M} of (5). We consider the sequence of bounded linear functionals A_m on the B^p -a. p.— \mathbf{M} space given by

$$A_m f = A \sigma_m = \sum d_n^{(m)} b_n \bar{a}_n = M \{ f \bar{\tau}_m \}.$$

Since $A \sigma_m \rightarrow Af$, the sequence A_m converges weakly to A in the Banach space in question. This implies, by the theorem in I. 10, the existence of a constant C such that

$$\|A_m\| \leq C \text{ for all } m.$$

From Theorem 2 and Theorem 3 it follows that $\|A_m\| = \|\tau_m\|_{B^q}$. In the special case $q = \infty$ we have

$$\|\tau_m\|_{B^\infty} = \lim_{p \rightarrow \infty} \|\tau_m\|_{B^p} = \sup_x |\tau_m(x)|.$$

Thus in the case $1 < q < \infty$ it follows from Theorem 1 and in the case $q = \infty$ from Theorem A that (9) is the Fourier series of a B^q -a. p. function. Of course this function is a B^q -a. p.— \mathbf{M} function. This completes the proof of the Main Theorem in the case of a denumerable module \mathbf{M} .

We now pass to the case of an arbitrary module \mathbf{M} . Let

$$A(e^{i\lambda x}) = \bar{a}_\lambda$$

for $\lambda \in \mathbf{M}$. We shall first show that there exists only a finite number of λ 's with $|\alpha_\lambda| > a$ when a is a positive constant. We do this indirectly by assuming that there exists an infinite sequence $\lambda_1, \lambda_2, \dots$ with $|\alpha_{\lambda_n}| > a$. Let k_n be a sequence of positive numbers with $\sum k_n = \infty$ and if $p \leq 2$ such that $\sum k_n^2 < \infty$ and if $p \geq 2$ such that $\sum k_n^{\frac{p}{p-1}} < \infty$. By Theorem C this implies, since $|\alpha_{\lambda_n}| \leq \|A\|$, that

$$\sum k_n \alpha_{\lambda_n} e^{i\lambda_n x}$$

is the Fourier series of a B^2 -a. p.— \mathbf{M} function for $p \leq 2$ and of a B^p -a. p.— \mathbf{M} function for $p \geq 2$ — and thus in any case of a B^p -a. p.— \mathbf{M} function.

Let σ_m be a Bochner-Fejér sequence of f corresponding to the module generated by $\lambda_1, \lambda_2, \dots$. Then

$$\sigma_m(x) = \sum c_n^{(m)} k_n a_{\lambda_n} e^{i\lambda_n x}$$

where $0 \leq c_n^{(m)} \leq 1$ and $c_n^{(m)} \rightarrow 1$ for fixed n and $m \rightarrow \infty$. Thus

$$A\sigma_m = \sum c_n^{(m)} k_n |a_{\lambda_n}|^2 \geq a^2 \sum c_n^{(m)} k_n \rightarrow \infty$$

for $m \rightarrow \infty$. Since $\sigma_m \xrightarrow{B^p} f$ implies $A\sigma_m \rightarrow Af$, we have obtained a contradiction.

In particular we have shown that there exists only a denumerable number of λ 's with $a_\lambda \neq 0$. The denumerable module generated by these λ 's is denoted by \mathbf{M}_1 and the elements of this module by $\lambda_1, \lambda_2, \dots$.

When we consider the contraction of A to the B^p -a. p.- \mathbf{M}_1 space, we conclude from the case of a denumerable module treated above that

$$\sum a_{\lambda_n} e^{i\lambda_n x}$$

is the Fourier series of a B^q -a. p.- \mathbf{M}_1 function g and that for any B^p -a. p.- \mathbf{M}_1 function we have $Af = M\{f\bar{g}\}$.

Now let f be a B^p -a. p.- \mathbf{M} function whose Fourier exponents do not belong to \mathbf{M}_1 . Then $Af = 0$ since f can be B^p -approximated by trigonometric polynomials without exponents in \mathbf{M}_1 . From 1, 9. we see that $M\{f\bar{g}\} = 0$. Hence also in this case we get $Af = M\{f\bar{g}\}$.

Finally, let f be an arbitrary B^p -a. p.- \mathbf{M} function. Then by the Corollary and the Remark, p. 11, we can write f in the form

$$f = f^{\mathbf{M}_1} + (f - f^{\mathbf{M}_1})$$

where $f^{\mathbf{M}_1}$ is a B^p -a. p.- \mathbf{M}_1 function and $f - f^{\mathbf{M}_1}$ is a B^p -a. p.- \mathbf{M} function whose Fourier exponents do not belong to \mathbf{M}_1 . From the two special cases just treated we get

$$\begin{aligned} Af &= A(f^{\mathbf{M}_1}) + A(f - f^{\mathbf{M}_1}) = \\ &M\{f^{\mathbf{M}_1}\bar{g}\} + M\{(f - f^{\mathbf{M}_1})\bar{g}\} = M\{f\bar{g}\}. \end{aligned}$$

This completes the proof of the Main Theorem.

Part II.

1. Bohr compactification of the real axis.

Let \mathbf{M} be an arbitrary module of real numbers. We consider the Bohr compactification $R'_{\mathbf{M}}$ of the group R of real numbers with usual topology by all (ordinary) a. p.— \mathbf{M} functions. See e. g. [1], pp. 477—478.

We denote by H the subgroup of R which consists of the x for which $e^{i\lambda x} = 1$ for all $\lambda \in \mathbf{M}$. In the uninteresting case when $\mathbf{M} = \{0\}$ we have $H = R$. If \mathbf{M} has the form $\{n\xi \mid n = 0, \pm 1, \dots\}$, we have $H = \{n \frac{2\pi}{\xi} \mid n = 0, \pm 1, \dots\}$. Otherwise $H = \{0\}$.

We shall make use of the following facts concerning $R'_{\mathbf{M}}$ (see the above quotation).

1) $R'_{\mathbf{M}}$ is a compact abelian group.
 2) When the groups $R'_{\mathbf{M}}$ and R/H are considered without their topologies, the group R/H is a subgroup of $R'_{\mathbf{M}}$. The set R/H lies everywhere dense in $R'_{\mathbf{M}}$. Incidentally, in the case $H = \{n \frac{2\pi}{\xi} \mid n = 0, \pm 1, \dots\}$, the group $R'_{\mathbf{M}}$ is identical with the topological group R/H .

3) When a continuous function on $R'_{\mathbf{M}}$ is contracted to R/H and the contracted function is extended by periodicity with H as periodicity module to R , the resulting function is an a. p.— \mathbf{M} function on R . Conversely, an a. p.— \mathbf{M} function φ on R has H as a periodicity module and may therefore be considered as a function on R/H , and this function extends itself in unique fashion by continuity in $R'_{\mathbf{M}}$ to a continuous function φ' on $R'_{\mathbf{M}}$. This correspondence $\varphi \leftrightarrow \varphi'$ between the a. p.— \mathbf{M} functions on R and the continuous functions on $R'_{\mathbf{M}}$ is of main importance in the following.

4) When $\varphi = e^{i\lambda x}$, $\lambda \in \mathbf{M}$, the function φ' is a continuous character on $R'_{\mathbf{M}}$. All continuous characters on $R'_{\mathbf{M}}$ can be obtained in this way. [Thus the module \mathbf{M} with discrete topology is the character group of $R'_{\mathbf{M}}$.]

5) Let M denote the Bohr mean and M_N the von Neumann mean, both in R , and let \int denote the Haar integral in R'_M with $\int 1 = 1$. Then for any a. p.— \mathbf{M} function φ on R we have

$$M\varphi = M_N\varphi = \int \varphi'.$$

2. Extension of the correspondence $\varphi \leftrightarrow \varphi'$ between the a. p.— \mathbf{M} functions on R and the continuous functions on R'_M to a correspondence between the B^p -a. p.— \mathbf{M} space over R and the space L^p over R'_M , $1 \leq p \leq \infty$.

As well-known for any fixed p , $1 \leq p < \infty$, the set of measurable p -integrable functions $g(x')$ on R'_M is organized as a Banach space L^p by the norm

$$\|g\|_p = \left(\int |g(x')|^p \right)^{\frac{1}{p}}$$

while for $p = \infty$ the set of essentially bounded measurable functions $g(x')$ on R'_M is organized as a Banach space L^∞ by the norm

$$\|g\|_\infty = \lim_{p \rightarrow \infty} \|g\|_p = \text{vrai max}_x |g(x')|.$$

Functions which are equal almost everywhere (a. e.) are considered to be the same function.

For this, and also for results used in the following, we refer the reader to Loomis' book [9], Chapter III, pp. 29—47.

We shall now prove the following

Correspondence Theorem. *Let \mathbf{M} be a module of real numbers. Then there exists a mapping $f \rightarrow f'$ of the set of B^1 -a. p.— \mathbf{M} functions on the set of integrable functions on R'_M which is an extension of the previous mapping $\varphi \rightarrow \varphi'$ of the set of a. p.— \mathbf{M} functions on the set of continuous functions on R'_M . This mapping has the following properties.*

1. For any fixed p , $1 \leq p \leq \infty$, the contraction of the mapping to the set of B^p -a. p.— \mathbf{M} functions is a linear isometric mapping of the set of B^p -a. p.— \mathbf{M} functions on the space L^p over R'_M . It may be considered as a one-to-one linear isometric mapping of the B^p -a. p.— \mathbf{M} space on the space L^p over R'_M .

2. For any B^1 -a. p.— \mathbf{M} function f we have

$$|f'| = |f'|, \quad (\Re f)' = \Re (f'), \quad (\Im f)' = \Im (f'), \\ (\bar{f})' = \overline{(f')}, \quad ((f)_n)' = (f')_n$$

and when f is real

$$(f^+)' = (f')^+ \quad \text{and} \quad (f^-)' = (f')^-.$$

3. If f is a B^p -a. p.— \mathbf{M} function and g is a B^q -a. p.— \mathbf{M} function, $1/p + 1/q = 1$, $1 \leq p \leq \infty$, $1 \leq q \leq \infty$, then

$$(fg)' = f'g'.$$

4. If the B^1 -a. p.— \mathbf{M} function f has the Fourier series $\sum a_n e^{i\lambda_n x}$, then f' has the Fourier series

$$\sum a_n (e^{i\lambda_n x})',$$

in particular $Mf = \int f'$.

5. If f is a B^p -a. p.— \mathbf{M} function for a fixed p , $1 \leq p < \infty$, and $1 \leq q < \infty$, then

$$(|f|^{\frac{p}{q}} \text{sign } f)' = |f'|^{\frac{p}{q}} \text{sign } f'.$$

6. The asymptotic distribution function of a real B^1 -a. p.— \mathbf{M} function f is identical with the distribution function of f' .

Proof. Let f be a B^p -a. p.— \mathbf{M} function for a fixed p , $1 \leq p < \infty$. Then there exists a sequence of a. p.— \mathbf{M} functions φ_n such that $\varphi_n \xrightarrow{B^p} f$. In particular $\|\varphi_m - \varphi_n\|_{B^p} \rightarrow 0$ for $m, n \rightarrow \infty$. Hence by 3) and 5) we get

$$\|\varphi'_m - \varphi'_n\|_p^p = \int |\varphi'_m - \varphi'_n|^p = \int (|\varphi_m - \varphi_n|^p)' = \|\varphi_m - \varphi_n\|_{B^p}^p \rightarrow 0$$

for $m, n \rightarrow \infty$. It follows that φ'_n will p -converge to a function g_p from L^p which is determined a. e. This function g_p depends only on f and not on the sequence φ_n . To see this, let ψ_n be another sequence of a. p.— \mathbf{M} functions which B^p -converges to f , and suppose that $\psi'_n \xrightarrow{p} h_p$. Then the combined sequence $\varphi'_1, \psi'_1, \varphi'_2, \psi'_2, \dots$ will B^p -converge to f , and it follows that $\varphi'_1, \psi'_1, \varphi'_2, \psi'_2, \dots$ will p -converge, in particular that $\varphi'_n - \psi'_n \xrightarrow{p} 0$. Hence $\|h_p - g_p\|_p = 0$.

We see also that if p_1 and p_2 are two values of p for which f is B^p -a. p.—**M**, then $g_{p_1} = g_{p_2}$ a. e., for if $1 \leq p_1 < p_2$ and $\varphi_n \xrightarrow{B^{p_2}} f$, then $\varphi_n \xrightarrow{B^{p_1}} f$, and we get $\varphi_n \xrightarrow{p_2} g_{p_2}$, $\varphi_n \xrightarrow{p_1} g_{p_1}$ the first of which implies that $\varphi_n \xrightarrow{p_1} g_{p_2}$ so that $\|g_{p_2} - g_{p_1}\|_{p_1} = 0$.

If in particular f is an a. p.—**M** function, then $f, f, \dots \xrightarrow{B^p} f$ and since $f', f', \dots \xrightarrow{p} f'$ we see that the function g corresponding to f is f' . Also in the general case when f is a B^1 -a. p.—**M** function the corresponding function g , defined by the above procedure, will be denoted by f' .

Now let f be a B^∞ -a. p.—**M** function. We shall show that f' belongs to L^∞ . Let $\sup_x |f(x)| = C$. There exists (I, 1, 8.) a sequence of a. p.—**M** functions φ_n which B^1 -converges to f and has $|\varphi_n(x)| \leq C$. Then $|\varphi_n'(x')| \leq C$ and $\varphi_n \xrightarrow{1} f'$ which implies $|f'(x')| \leq C$, a. e. Thus f' belongs to L^∞ , and furthermore $\text{vrai max}_x |f'(x')| \leq \sup_x |f(x)|$.

For a fixed p , $1 \leq p < \infty$, let f be a B^p -a. p.—**M** function. We choose a sequence of a. p.—**M** functions φ_n which B^p -converges to f . Then $\|\varphi_n\|_{B^p} \rightarrow \|f\|_{B^p}$, $\|\varphi_n'\|_p \rightarrow \|f'\|_p$, and $\|\varphi_n\|_{B^p} = \|\varphi_n'\|_p$ so that

$$\|f\|_{B^p} = \|f'\|_p.$$

If f is a B^1 -a. p.—**M** function and φ_n is chosen as usual we get $M\varphi_n \rightarrow Mf$, $\int \varphi_n' \rightarrow \int f'$, and $M\varphi_n = \int \varphi_n'$ so that

$$(1) \quad Mf = \int f'.$$

Let f and g be two B^1 -a. p.—**M** functions. Let φ_n and ψ_n be chosen correspondingly. Then we get successively, when a and b denote complex numbers, $a\varphi_n + b\psi_n \xrightarrow{B^1} af + bg$, $\varphi_n \xrightarrow{1} f'$, $\psi_n \xrightarrow{1} g'$, $(a\varphi_n + b\psi_n)' \xrightarrow{1} (af + bg)'$, $a\varphi_n' + b\psi_n' \xrightarrow{1} af' + bg'$. Since $(a\varphi_n + b\psi_n)' = a\varphi_n' + b\psi_n'$ we get

$$(af + bg)' = af' + bg'.$$

In an analogous way we obtain the relations in 2.

In order to prove 3. we consider first the case $1 < p < \infty$, and hence $1 < q < \infty$. That fg is B^1 -a. p.—**M** follows from I, 1, 6. Let φ_n and ψ_n be chosen in the usual way for f and g respectively. Then by I, 1, 6. we get $\varphi_n \psi_n \xrightarrow{B^1} fg$. Hence we get successively

$\varphi'_n \xrightarrow{p} f'$, $\psi'_n \xrightarrow{q} g'$, $(\varphi_n \psi_n)' \xrightarrow{1} (fg)'$, and $\varphi'_n \psi'_n \xrightarrow{1} f'g'$ (by the result corresponding to I, 1, 6. for the space L^p). Since $(\varphi_n \psi_n)' = \varphi'_n \psi'_n$ we get

$$(fg)' = f'g'.$$

Next, we consider the case $p = 1$, $q = \infty$. That fg is B^1 -a. p.—**M** follows from I, 1, 6. We showed there that $(f)_n g \xrightarrow{B^1} fg$. Hence $((f)_n g)' \xrightarrow{1} (fg)'$ since our mapping is linear and isometric. However, $(f)_n$ and g are B^∞ -a. p.—**M**, in particular B^2 -a. p.—**M**. Hence from the case just treated we get $((f)_n g)' = ((f)_n)'g' = (f')_n g'$ and this $\xrightarrow{1} f'g'$ since f' is in L^1 and g' in L^∞ . Thus also in this case $(fg)' = f'g'$. This completes the proof of 3.

From the special result (1) the general statement 4. is now an easy consequence.

The proof of 5. is analogous to the proof of 3. It uses I, 1, 5. instead of I, 1, 6. However, we shall not use 5. in the following.

Next, for any fixed p , $1 \leq p < \infty$, we consider an arbitrary function $g(x')$ from L^p . There exists a sequence of continuous functions φ'_n on R'_M which $\xrightarrow{p} g$. [As stated in 3) every continuous function on R'_M is of the form φ' where φ is an a. p.—**M** function.] Then $\|\varphi_m - \varphi_n\|_{B^p} = \|\varphi'_m - \varphi'_n\|_p \rightarrow 0$ for $m, n \rightarrow \infty$ and hence φ_n will B^p -converge to a B^p -a. p.—**M** function f for which $f' = g$. Since the mapping is linear and isometric, the B^p -a. p.—**M** functions f for which $f' = g$ are exactly the functions in a B^p -a. p.—**M** point. Thus the contraction of our mapping $f \rightarrow f'$ to the set of B^p -a. p.—**M** functions may be considered as a one-to-one mapping of the B^p -a. p.—**M** space on the space L^p . Obviously this mapping is linear and isometric. This proves 1. for $1 \leq p < \infty$.

Next we consider the case $p = \infty$. We have already seen that the set of B^∞ -a. p.—**M** functions is mapped into the space L^∞ and that $\|f'\|_\infty \leq \sup_x |f(x)|$.

Now let $g(x')$ be an arbitrary function from L^∞ and let $\|g\|_\infty = C$. Let φ_n be a sequence of a. p.—**M** functions such that $|\varphi'_n(x')| \leq C$ and $\varphi'_n \xrightarrow{1} g$. Then $\|\varphi_m - \varphi_n\|_{B^1} \rightarrow 0$ for $m, n \rightarrow \infty$ and hence by I, 1, 1. we can construct a B^1 -limit function f_0 of the sequence φ_n from pieces of the φ_n . It follows that $|f_0(x)| \leq C$ and that $f'_0 = g$. Since $\sup_x |f_0(x)| \leq \|g\|_\infty$ and since, as we have seen previously, all B^∞ -a. p.—**M** functions f which are mapped in g have

$$(2) \quad \sup_x |f(x)| \geq \|g\|_\infty,$$

we see that

$$(3) \quad \sup_x |f_0(x)| = \|g\|_\infty.$$

The B^∞ -a. p.— \mathbf{M} functions f which are mapped in the same g from L^∞ belong in particular to the same B^1 -a. p.— \mathbf{M} point, and hence they differ from each other by a bounded B^1 -zero function, i. e., a B^∞ -zero function. Thus they belong to the same B^∞ -a. p.— \mathbf{M} point. All functions in this point are mapped in the function g . Thus the contraction of the mapping $f \rightarrow f'$ to the set of B^∞ -a. p.— \mathbf{M} functions can be considered as a one-to-one linear mapping of the B^∞ -a. p.— \mathbf{M} space on the space L^∞ . From (2) and (3) we can now conclude that for any B^∞ -a. p.— \mathbf{M} function f we have

$$\|f'\|_\infty = \inf_z \sup_x |f(x) + z(x)| = \|f\|_{B^\infty}$$

where z runs through all B^∞ -zero functions. Thus the contracted mapping is isometric. Using that

$$\|f'\|_\infty = \lim_{p \rightarrow \infty} \|f'\|_p = \lim_{p \rightarrow \infty} \|f\|_{B^p}$$

we get the other expression

$$\|f\|_{B^\infty} = \lim_{p \rightarrow \infty} \|f\|_{B^p}$$

for the B^∞ -norm. This completes the proof of 1.

Finally we shall prove 6. Since this part of the Correspondence Theorem will not be used in the following we shall treat it shortly. It is known that every real B^1 -a. p. function possesses an asymptotic distribution function. We shall use a proof of this theorem which was communicated to the authors of [5] by JESSEN and published in [5], pp. 101—103; in order to save space we shall assume that the reader knows the proof and the notations used therein. It is easily seen that the function $\Phi(f(x))$ occurring l. c., p. 102 can be written

$$\Phi(f(x)) = 1 + \frac{(f(x) - \beta)^+ - (f(x) - \alpha)^+}{\beta - \alpha}.$$

Hence

$$(\Phi(f))' = \Phi(f')$$

so that

$$M_B \{ \Phi(f) \} = \{ \Phi(f') \}.$$

Then 6. is a simple consequence of the inequalities

$$\psi_1(\beta) \geq M_B \{ \Phi(f) \} \geq \psi(\alpha)$$

which were proved l. c., p. 102 and the corresponding inequalities for the function f' .

This completes the proof of the Correspondence Theorem.

3. Application of the Correspondence Theorem to a proof of the Main Theorem.

If in the Main Theorem we replace the B^p -a. p.— \mathbf{M} space by the space L^p and the B^q -a. p.— \mathbf{M} space by the space L^q and the mean value M by the Lebesgue integral \int , we obtain a classical result of F. RIESZ which is valid even for spaces L^p in the abstract case. A proof of this theorem is given in [9], Chapter III, p. 42 and p. 47.

By use of the Correspondence Theorem we shall now deduce our Main Theorem from F. RIESZ's result. Let p be a fixed number, $1 \leq p < \infty$. It follows easily from the Correspondence Theorem that the mapping

$$(4) \quad A \rightarrow A'$$

where A is a bounded linear functional on the B^p -a. p.— \mathbf{M} space and A' is the functional on the space L^p over R'_M defined by

$$A'f' = Af$$

is a one-to-one linear isometric mapping of the dual space of the B^p -a. p.— \mathbf{M} space on the dual space of the space L^p . However, on account of RIESZ's theorem the mapping

$$(5) \quad A'_g' \rightarrow g'$$

where

$$A'_{g'}(f') = \int f' \overline{(g')}$$

is a one-to-one linear isometric mapping of the dual space of L^p over R'_M on the space L^q over R'_M . Finally, by the Correspondence Theorem the mapping

$$(6) \quad g' \rightarrow g$$

is a one-to-one linear isometric mapping of the space L^q over R'_M on the B^q -a. p.— M space and

$$\int f' \overline{(g')} = M \{ f \bar{g} \}$$

for every B^p -a. p.— M function f and every B^q -a. p.— M function g . The mapping

$$A_g \rightarrow g$$

which results from the mappings (4), (5), (6) is then a one-to-one linear isometric mapping of the dual space of the B^p -a. p.— M space on the B^q -a. p.— M space, and

$$A_g f = A'_{g'}(f') = \int f' \overline{(g')} = M \{ f \bar{g} \}.$$

This completes the proof of the Main Theorem.

Appendix.

The following theorem shows that for a given module M of real numbers and a fixed p , $1 \leq p < \infty$, the B^p -a. p.— M space and the W^p -a. p.— M space have the same dual space.

Theorem. *Let M be a module of real numbers and p, q two numbers, $1 \leq p < \infty$, $1 < q \leq \infty$, satisfying $1/p + 1/q = 1$. Then the dual space of the W^p -a. p.— M space is isomorphic to the B^q -a. p.— M space. The isomorphic mapping is given by $A_g \rightarrow g$ where A_g is the bounded linear functional on the W^p -a. p.— M space given by $A_g f = M \{ f \bar{g} \}$.*

Proof. For any W^p -a. p. function f we have $\|f\|_{B^p} = \|f\|_{W^p}$, for by I, 1, 5. the function $|f(x)|^p$ is W^1 -a. p. so that

$$\lim_{T \rightarrow \infty} \frac{1}{T} \int_a^{a+T} |f(x)|^p dx$$

exists uniformly in a . Further every B^p -a. p.— \mathbf{M} function may be B^p -approximated by W^p -a. p.— \mathbf{M} functions, for it may even be B^p -approximated by a. p.— \mathbf{M} functions. It follows from this that every bounded linear functional on the W^p -a. p.— \mathbf{M} space extends itself in unique fashion by B^p -continuity to a bounded linear functional on the B^p -a. p.— \mathbf{M} space with the same norm as the original functional, and that conversely every bounded linear functional on the B^p -a. p.— \mathbf{M} space induces a bounded linear functional on the W^p -a. p.— \mathbf{M} space. Our theorem is then a consequence of the Main Theorem.

References.

- [1] H. ANZAI and S. KAKUTANI: Bohr compactifications of a locally compact abelian group I. Proc. Imp. Acad. Tokyo 19, 476—480 (1943).
- [2] A. S. BESICOVITCH and H. BOHR: Almost periodicity and general trigonometric series. Acta Math. 57, 203—292 (1931). H. BOHR: Collected mathematical works, II, C 27. København 1952.
- [3] H. BOHR: On the explicit determination of the upper limit of an almost-periodic function. J. London Math. Soc. 1, 109—112 (1926). H. BOHR: Collected mathematical works, II, C 13. København 1952.
- [4] H. BOHR: Ueber fastperiodische ebene Bewegungen. Comment. Math. Helv. 4, 51—64 (1932). H. BOHR: Collected mathematical works, II, C 29. København 1952.
- [5] H. BOHR and E. FÖLNER: On some types of functional spaces. A contribution to the theory of almost periodic functions. Acta Math. 76, 31—155 (1944). H. BOHR: Collected mathematical works, III, C 47. København 1952.
- [6] N. BOURBAKI: Éléments de mathématique. Première partie. Livre VI. Intégration. Actualités scientifiques et industrielles, 1175: Paris 1952.
- [7] R. DOSS: Contribution to the theory of almost periodic functions. Ann. Math. (2) 46, 196—219 (1945).
- [8] R. DOSS: Some theorems on almost periodic functions. Amer. J. Math. 72, 81—92 (1950).
- [9] L. H. LOOMIS: An introduction to abstract harmonic analysis. Toronto. New York. London. 1953.
- [10] H. R. PITT: On the Fourier coefficients of almost periodic functions. J. London Math. Soc. 14, 143—150 (1939).
- [11] H. D. URSELL: Parseval's theorem for almost periodic functions. Proc. London Math. Soc. (2) 32, 402—440 (1931).

Det Kongelige Danske Videnskabernes Selskab

Matematisk-fysiske Meddelelser, bind **29**, nr. 2

Dan. Mat. Fys. Medd. **29**, no. 2 (1954)

CAUSAL BEHAVIOUR OF FIELD
THEORIES WITH NON-LOCALIZABLE
INTERACTIONS

BY

MARVIN E. EBEL



København 1954

i kommission hos Ejnar Munksgaard

CONTENTS

	Pages
1. Introduction	3
2. Limitations on the Causality Condition	7
3. Measuring Processes	9
4. Asymptotic Expansion of the Integral	22
5. Discussion	28
References	31

The causal behaviour of field theories with non-localizable interactions of the Kristensen-Møller type is discussed in the perturbation approximation, with particular attention to interactions involving only particles with time-like momentum vectors. Causal behaviour is understood to imply that all observable particles of positive energy are propagated at a velocity less than the velocity of light. It is shown that the causal behaviour of the non-local interaction theories is determined both by the location of the singularities of the propagation function, and by the continuity of the various derivatives of the form function. It is further demonstrated that, by choosing these derivatives to be continuous in sufficiently high orders, the probability of observing signals propagating with a velocity greater than that of light may be made to decrease more rapidly than any arbitrary inverse power of the distance between the points at which the signal is observed. The relation of this work to other treatments of causality is discussed.

1. Introduction.

Considerable interest has recently been attached to discussions of field theories involving non-local interaction, that is, field theories in which the interaction term in the Lagrangian involves the field variables at different points in space and time. Following KRISTENSEN and MØLLER⁽¹⁾, this interaction term may be written as¹

$$L_{\text{int}} = - \int d^4x' d^4x'' d^4x''' \psi^+(x') \Phi(x'x''x''') \varphi(x'') \psi(x'''), \quad (1.1)$$

in which $\Phi(x'x''x''')$ is the form factor of the interaction and will in general be a product of a matrix operator and a function

¹ We shall use the notation $F(123)$ for $F(x_1^\mu, x_2^\mu, x_3^\mu)$. The adjoint field is denoted by ψ^+ , and may be taken as $\psi^+ = \psi^* \gamma_4$, with ψ^* the Hermitian conjugate to ψ . Further, the inner product of two four-vectors is indicated by $a \cdot b = a_\mu b^\mu = \mathbf{a} \cdot \mathbf{b} - a^0 b^0$.

of coordinates $F(x'x''x''')$. Utilizing the various invariance conditions which may be placed on F , we may expand it in momentum space as

$$F(x'x''x''') = (2\pi)^{-8} \int d^4l_1 d^4l_3 G(l_1 l_3) \left. \begin{aligned} & \times \exp i [l_1(x' - x'') + l_3(x''' - x'')] \end{aligned} \right\} \quad (1.2)$$

where G is a function only of l_1^2 , l_3^2 , and $(l_1 + l_3)^2$.

Of especial importance to any investigation of a theory of this type are the questions, first, whether such a generalization of the usual theory can bring about the desired convergence of integrals representing matrix elements, and second, if it can do this, what effects this generalization would have upon such properties of the theory as its causal behaviour. BLOCH⁽²⁾ and KRISTENSEN⁽³⁾ have shown that, in order to gain convergence to all orders of the coupling constant, it is sufficient (and probably necessary) to require that $G(l_1 l_3)$ vanish if any of the vectors l_1 , l_3 or $l_1 + l_3$ is space-like. This is a rather serious restriction; in fact, it eliminates the possibility of obtaining the usual local theory as a limiting case. It has been felt that such a restriction may perhaps lead to acausal behaviour for the particles described by the theory. It is the purpose of this paper to investigate in some detail the commensurability of such an assumption with the causality requirement, and to show in what sense we may say that causality is preserved. A theory will be said to exhibit causal behaviour if it predicts that all observable signals or particles of positive energy are propagated only in a forward direction in space-time, and at a velocity equal to or less than the velocity of light.

Discussions of the application of the requirement of causality to the non-local interaction are not new, of course. For example, BLOCH⁽²⁾, and later CHRÉTIEN and PEIERLS⁽⁴⁾, have determined what properties the form function must possess in order that the interaction be limited to a small region in space and time. In substance, their result is that, if the form function in momentum space, $G(l_1 l_3)$, is sufficiently smooth, then the interaction involves essentially only field variables at points close to each other. Smoothness here implies the continuity of the various higher derivatives of G with respect to l_1^2 , l_3^2 , and $(l_1 + l_3)^2$. This

question is, however, somewhat different from that discussed by FIERZ⁽⁵⁾ in his analysis of the causal behaviour of the local theory of quantum electrodynamics. It was pointed out there that, for the causality requirement to make sense, it is necessary to discuss only observable signals. This means that the predicted matrix element for some measuring process as a whole must be examined. It was shown that, if a particle (specifically, a photon) of positive energy is absorbed at an approximate distance r from its point of creation, such absorption must take place at a time at least r/c later than its time of emission. It is apparent that this discussion does not correspond to that given by Bloch or Chrétien and Peierls. A simple demonstration of this discrepancy is provided by a local theory in which the Feynman or causal Green's function $\Delta_F = \Delta^1 - 2i\bar{\Delta}$ is replaced by its complex conjugate Δ_F^* . This would certainly satisfy the conditions of Bloch, and Chrétien and Peierls, since the interaction would only involve the field variables at the same point. Nevertheless, such a theory would not satisfy the Fierz condition, which we might call "causality in the large", because the absorption of a particle of positive energy would actually occur before its emission. In the course of our examination of the properties of the restricted non-local interaction, we shall find the distinction between these conditions appearing in a rather natural way.

Perhaps it should be mentioned that this work is rather distinct from that of VAN KAMPEN⁽⁶⁾ and others, who have established rather general conditions on the S -matrix for scattering in classical and first-quantized theories. Their interest is mainly concentrated upon determining the properties for cross sections and bound states following from conditions which are, in a sense, weaker than those above, but which must be followed rigorously. This involves a somewhat different emphasis, resulting from a different point of view concerning the causality condition.

Essentially, it is possible to start from a given set of properties, including, say, some sort of causality condition, and from these to deduce certain characteristics which must be possessed by any theory containing these properties. This is the approach of van Kampen, mentioned above. On the other hand, it is also possible to begin with a definite theory or class of theories, and

to deduce to what extent this theory possesses certain desired properties. This is the approach which has been used by Fierz, and which will be adopted here. It contains one definite advantage; namely, if we begin with a causality condition, and use this to restrict the form of the theory, then we must, of course, use a condition which can be expressed in specific terms, and which must be adhered to rigorously. However, it has been pointed out previously that such a condition in a quantum theory will tend to be rather weak, primarily because of the inability to assign precise values of the momentum and position to a particle at two different times. Therefore, it seems better for our purposes to begin with that specific theory in which we are interested, and to examine its predictions for those processes which will exhibit most clearly its causal or acausal nature. These processes are just those which describe physical methods for measuring the velocity of propagation of a particle. The more general approach, while more difficult in application, might be expected to throw considerable light on the structure of S-matrix theory, particularly if the same sort of causality condition as that used here could be formulated in a more definite manner. One of the problems involved in such a treatment would be the construction of certain types of localized states. We shall attempt to avoid such difficult questions by the use of a more intuitive approach.

Several basic assumptions and limitations will be introduced here in order to simplify the discussion. The most important of these involves the application of perturbation theory to the calculation of matrix elements involved in determining the causal behaviour. In particular, we shall assume that, if the results of the lowest order perturbation calculation indicate a causal behaviour, such behaviour will carry over into the higher orders. Causality will be seen to be intimately connected with the form of a certain product of the Green's function Δ_F and form functions $F(x'x''x''')$. In the higher orders, the same product is merely repeated a number of times. If this product is of the proper form to ensure causality for the first non-vanishing term in the expansion, we may expect that the higher orders will not introduce difficulties. Wherever possible, we shall attempt to indicate what modifications are introduced in the higher orders. The entire structure of our analysis might not make any sense

if the perturbation method itself is not valid, of course. Such questions, while important, are not to be discussed here.

For convenience, only two types of particles will be considered, one possessing charge conjugate states and spin one-half, and one Majorana neutral particle. The fields describing the former will be denoted by ψ and ψ^+ , and φ will be used for the field of the neutral particle. Both the neutral particle and the coupling will be assumed to be scalar. At times we may find it convenient, for giving a physical picture of the processes considered, to refer to these particles as nucleons and mesons.

Finally, we shall only be concerned with the causal or acausal behaviour of the φ field; that is, we shall only require that the neutral particle have a velocity less than that of light. This makes it possible to treat the ψ and ψ^+ fields non-relativistically if desirable, which can simplify the discussion. It is obvious, of course, that a similar treatment of the causality properties of the ψ and ψ^+ fields could be given, with essentially no modification of the procedure.

2. Limitations on the Causality Condition.

As indicated previously, it is extremely difficult to give an exact criterion for causal behaviour of a theory, primarily due to the limitations imposed on the measuring process by the quantum nature of the theory. We shall now examine this limitation more closely. Essentially two types of measurements are involved in determining causal behaviour as defined previously. These are: the determination of the location of the particle at two different points in space-time, and the measurement of the sign of the energy of the particle. If the theory is second quantized, then of course the points of position measurement are just the points at which the creation and destruction of the particle in the given state occur.

It is rather clear that the operator measuring the position of a particle, the eigenfunctions of which are the so-called localized states of the particle, does not commute with the energy operator. This, however, is too much to expect; all we really would need for a precise formulation of the causality condition is that the position operator commute with the operator determining the

sign of the particle energy. Expressed in other words, we would require that the localized states of the system be composed only of positive (or only of negative) energy components. That this should be so seems extremely unlikely, and we therefore expect that the position of the particle, or its points of creation and destruction, may only be defined to within a certain distance. This distance may be taken to be of the order of the Compton wavelength of the particle, h/mc , which is the position uncertainty we would obtain using states which are described by the usual minimum wave packets familiar in ordinary quantum mechanics. Furthermore, we should also expect to be able to determine the sign of the energy of the particle with only a certain probability; this probability may be large, but not equal to one. With these limitations, our statement of causal behaviour becomes as follows: to the extent to which the energy of the particle is known to be positive, and to the extent to which its points of creation and destruction may be determined, these points must be separated by a time-like distance, and the point of destruction must occur later than that of creation. At first glance, we might be tempted to require also that the particle energy be greater than mc^2 , i.e., that the particle be real, not virtual. On the other hand, the existence of an appreciable probability for finding a virtual particle propagating at a velocity greater than c at a distance from its point of creation large compared to h/mc can also be considered to be a violation of causality. It seems reasonable, then, to include virtual particles in our discussion. This question does not arise in the usual local theory, for there we know that the range of the interaction produced by the exchange of a virtual particle of mass m is of the order of h/mc , no larger than the fundamental uncertainty in the position measurement. There appears to be no reason to expect this range to be any shorter in a non-local theory. Conversely, we also may regard this as a reason for not choosing our position measurement more accurate than h/mc , for the existence of virtual particles prevents any more accurate formulation of the causality condition.

With these considerations in mind, we now may give a general description of the type of process the investigation of which should prove most interesting and decisive with regard

to causality. We might expect such processes to be the simplest ones possible which create and subsequently destroy a meson; that is, the interaction of two nucleons by means of the meson field. The process should provide some method of determining where and when the meson is created and destroyed; this may be done by determining where the nucleons which emit and absorb the meson change state. Furthermore, the energy of the meson may be determined from a knowledge of the energy change of the nucleon involved in its emission. These requirements mean that the nucleon states must not be described by momentum eigenfunctions, but rather by some sort of wave packets, which also permit a certain localization in space and time. In principle, from a knowledge of the nucleon states in the infinite past and in the infinite future, we may deduce the properties of the particle field which transmits the interaction between the two nucleons. It does not matter whether we assume such interaction occurs by the exchange of one or many mesons; in either case the causality condition should be satisfied.

It also should be noted that, if the initial and final states of the nucleons are chosen to be free particle states, i.e., some superposition of plane waves, then an additional interaction with the meson or some other field must be introduced to provide long range (greater than h/mc) interaction between the nucleons. This is, of course, a consequence of the conservation of energy and momentum, which forbids the absorption or emission by free nucleons of any save virtual mesons. This additional interaction may either be with a prescribed external field, or else with the meson field or some other quantized field. In the latter case, the additional field also should be described by states which are represented by wave packets. In the next section, we shall present two types of processes which can throw light on the causal behaviour of the theory, and show that essentially the same answer would be obtained in an analysis of either of them.

3. Measuring Processes.

Whether or not a theory is causal can be determined from the predictions it makes for various special processes. In this section, we shall consider several representative examples of such pro-

cesses, which are of the general type discussed previously. We shall show that both of these "Gedanken" experiments lead to a condition essentially the same as that of Fierz.

In the interest of simplicity, we may begin with a case in which two nucleons in different potential wells interact by means of the intermediate meson field, the dropping of one nucleon from its initial state to a lower level causing the excitation of the system containing the other nucleon to a higher state. Since the treatment of bound states in a field-theoretical manner would introduce several complications into our discussion, we shall assume that the nucleons in the potential well are not described by a quantized field, but merely by simple Schrödinger wave functions. This means that we may not use a three-point form function, but rather consider only a non-local interaction between the meson field and a source density, represented by the nucleon wave functions. The corresponding problem in electrodynamics involves the exchange of excitation of two different atoms by means of the radiation field. The approximation of treating the nucleons by Schrödinger functions is somewhat better than the familiar semi-classical radiation theory, in that the possibility of virtual-pair formation by the meson field is contained in our discussion. Effects corresponding to the radiative corrections in emission and absorption are not included, however.

The use of a potential well serves to localize the emission and absorption of the meson in space, but not in time. In order also to establish a time for these events, we may consider that the population of the nucleon states varies as a result of other unspecified interactions with other particles. This changing population results in a time-dependent normalization for the particles in each potential well:

$$\int d^3\mathbf{x} \psi^*(\mathbf{x}, t) \psi(\mathbf{x}, t) = |f(t)|^2, \quad (3.1)$$

and might be described by introducing an additional imaginary potential $V' = i\hbar [\ln f(t)]'$ into the Schrödinger equation, which becomes

$$\left. \begin{aligned} [H^0 + V'(t)] \psi(t) &= i\hbar \frac{\partial \psi}{\partial t}, \\ H^0 &= -(\hbar^2/2M) \nabla^2 + V(\mathbf{x}). \end{aligned} \right\} \quad (3.2)$$

In particular, the function $f(t)$ should be appreciably different from zero only over a certain time interval.

Consider first a potential well with center at the origin. If the potential $V(\mathbf{x})$ is chosen to be spherically symmetric, then the solutions to (3.2) may be written as

$$\psi_{nlm} = f_n(t) u_n(r) Y_l^m(\vartheta, \varphi) \exp -i(E_n/\hbar)t, \quad (3.3)$$

in which the u_n are the normalized radial parts of the energy eigenfunctions of the unperturbed Hamiltonian H^0 . The Y_l^m are chosen to be normalized so that their square integral over all angles is unity.

Now we return to our original problem of the two nucleons. Consider two different potential wells, one with center at \mathbf{x} , and with particle states which have a maximum amplitude at time x^0 , and the other with a center at \mathbf{y} , and a maximum state amplitude at time y^0 . We denote the wave functions of the nucleon in the first well by ψ^1 , and those of the nucleon in the second well by ψ^2 . Then the S -matrix element for a transition in which the nucleon in the first well goes from state nlm to $n'l'm'$, and nucleon 2 goes from $n'l'm'$ to nlm , will be proportional to the integral

$$\left. \begin{aligned} I(x, y) = \int d^4x' d^4y' \psi_{nlm}^{2*}(y') \psi_{n'l'm'}^2(y') \\ \times \Delta'_F(y' - x') \psi_{n'l'm'}^{1*}(x') \psi_{nlm}^1(x'). \end{aligned} \right\} \quad (3.4)$$

Here, $\Delta'_F(y' - x')$ is some sort of Green's function describing the propagation of the meson from the point x' to the point y' . It may be assumed to contain the effects of a non-local interaction between the meson field and the nucleon source density. To the lowest order in the coupling constant for the meson-nucleon interaction, $\Delta'_F(y' - x')$ becomes just a non-local modification of the usual local Green's function; we write it as

$$\Delta'_F(x) = (2\pi)^{-2} \int d^4k \Delta'_F(k) |g(k^2)|^2 \exp i k \cdot x, \quad (3.5)$$

with $g(k^2)$ some form factor in momentum space.

Obviously, we have

$$\left. \begin{aligned} \psi_{nlm}^1(x') &= \psi_{nlm}(x' - x), \\ \psi_{nlm}^2(y') &= \psi_{nlm}(y' - y), \end{aligned} \right\} \quad (3.6)$$

where $\psi_{nlm}(x)$ is the nlm wave function for a particle in a state centered about the origin in both space and time. As usual, it is most convenient to work in momentum space. We prefer spherical polar to rectangular coordinates, both for convenience in handling spherical potentials and, more important, because the causality condition only involves the separation of events, not their relative angular orientation. Accordingly, we also introduce spherical coordinates in momentum space, writing the product of two wave functions as

$$\left. \begin{aligned} \psi_{nlm}^*(x) \psi_{n'l'm'}(x) &= \sum_{L, M} C_{l'l'; L}^{mm'; M} Y_L^M(\vartheta, \varphi) (-i)^L / \pi \\ &\quad \times \int_{-\infty}^{\infty} dk^0 \zeta(k^0) \exp -ik^0 x^0 \int_0^{\infty} k^2 dk j_L(kr) v_{nn'}^L(k), \\ \zeta(k^0) &= (2\pi)^{-\frac{1}{2}} c \int_{-\infty}^{\infty} dt \left\{ \exp i [k^0 c + (E_n - E_{n'})/\hbar] t \right\} f_n^*(t) f_{n'}(t), \\ v_{nn'}^L(k) &= (2/\pi)^{\frac{1}{2}} \int_0^{\infty} r^2 dr j_L(kr) u_n^*(r) u_{n'}(r), \end{aligned} \right\} \quad (3.7)$$

and expanding the function $\Delta'_F(k)$ as

$$\Delta'_F(k) = \sum_{lm} Y_l^m(\vartheta_k, \varphi_k) \Delta'_{Flm}(k, k^0). \quad (3.8)$$

Substituting (3.7) and (3.8) in (3.4), and using (3.5), we finally obtain

$$\left. \begin{aligned} I(x-y) &= 16\pi^3 \sum C_{l'l'; L}^{mm'; M} C_{l'l'; L}^{m'm; M'} C_{L'L'''; L}^{M'M''m; M} i^L Y_L^M(\vartheta, \varphi) I_{LM}(x-y), \\ I_{LM}(x-y) &= \int_0^{\infty} k^2 dk j_L(kr) \int_{-\infty}^{\infty} dk^0 \exp \\ &\quad - ik^0 (x^0 - y^0) \varrho(k, k^0) \Delta'_{Flm}(k, k^0) \end{aligned} \right\} \quad (3.9)$$

with

$$\left. \begin{aligned} \varrho(k, k^0) &= \zeta(k^0)^* \zeta(k^0) v_{nn'}^{L'} v_{nn''}^{L''} (k)^* |g(k^2 - k^{02})|^2 \\ r &\equiv |\mathbf{x} - \mathbf{y}|. \end{aligned} \right\} \quad (3.10)$$

The coefficients C appearing in (3.7) and (3.10) are defined by

$$\left. \begin{aligned} Y_l^{m*} Y_{l'}^{m'} &= \sum_{L'M'} C_{l'l'; L'}^{mm'; M'} Y_{L'}^M \\ Y_{L'}^M Y_{L''}^{M''} Y_{L'''}^{m''} &= \sum_{LM} C_{L'L'''; L}^{M'M''m''; M} Y_L^M, \end{aligned} \right\} (3.11)$$

and the summation in (3.9) extends over $L, L', L'', l'', M, M', M'', m''$.

If the function $f(t)$ which limits the wave function in time is not chosen to decrease to zero too sharply, then $\varrho(k, k^0)$ will have a strong maximum at $k^0 = (E_{n'} - E_n)/\hbar c$. To see this, we need only recognize that $\zeta(k^0) = \bar{\zeta}[k^0 + (E_n - E_{n'})/\hbar c]$, where $\bar{\zeta}(k^0)$ is the Fourier integral transform of $f_n(t)^* f_{n'}(t)$. If the energy of the state n, E_n , is much greater than $E_{n'}$, then we may consider that a meson of positive energy $\sim -\hbar k^0/c$ is created at or about x , and destroyed near y . Therefore, the causality condition requires that, if $\varrho(k, k^0)$ is different from zero essentially only for $k^0 < 0$, $I_{LM}(x - y)$ should be different from zero only if y is essentially within or on the forward light cone of x . This is just the sort of condition Fierz obtains.

Of course, the better we define the time of the meson creation or destruction, the less well-defined is the energy $-\hbar k^0/c$. The extent of the uncertainty in our condition may be estimated by choosing a particular form for $f(t)$, for example, a Gaussian in time:

$$f(t) = \exp -\frac{1}{2} \gamma^2 t^2. \tag{3.12}$$

Then, $\zeta(k^0)$ becomes

$$\zeta(k^0) = (1/2 \gamma) \exp -\frac{1}{4} \gamma^{-2} [k^0 + (E_n - E_{n'})/\hbar c]^2, \tag{3.13}$$

which is also a Gaussian function. Assuming that $E_n - E_{n'}$ is much greater than mc^2 , the meson energy is fairly well defined as positive if $\gamma \sim mc^2$. With this value of γ , the uncertainty in the time at which the meson is created, as measured by the width of the maximum in $f(t)^* f(t)$, is of the order of \hbar/mc^2 . Thus, the causality condition cannot restrict the propagation properties of the meson to within a distance any smaller than $\sim c\hbar/mc^2 = \hbar/mc$. This is a rather reasonable result, since we frequently think of the Compton wavelength as some sort of extension of the meson.

The uncertainty in spatial location of the points of meson creation and destruction does not play a role in the above discussion, since this may in principle be reduced indefinitely by decreasing the range and increasing the depth of the potential well. For example, for a squarewell potential, of range R and depth V_0 , the nucleon wave function for energy E_n is appreciable only for $r < R + \sqrt{-\hbar^2/2ME_n}$. For an s -state, this distance is much less than the meson Compton wavelength if $V_0 \gg (m/M)mc^2$.

Although the previous measuring process contains the essential elements necessary to ascertain the causal or acausal behaviour, a major objection may be raised to it. This is that the nucleon was not described by a quantized field, but rather was assumed to obey a non-relativistic Schrödinger equation. The main reason for doing this was that we wished to consider nucleons in bound states, but still avoid some of the difficulties which occur in present-day treatments of bound-state problems. Particular difficulties may be encountered in applying theories with non-local interaction to bound states.⁽⁷⁾ On the other hand, our principal goal is to investigate the properties of a non-local interaction between two quantized fields, thus replacing one of the fields by an effective "source distribution", for the other field certainly limits the scope of our discussion.

Instead of arguing, as previously, that the non-local effects may be described completely by an altered meson Green's function, we may propose a second process in which both nucleon and meson are treated as quantized fields. Accordingly, a scattering problem involving nucleons in states of energy greater than Mc^2 will now be considered. As remarked previously, it is necessary to introduce an additional interaction to permit the emission and absorption of non-virtual mesons. We shall choose this additional interaction to be with the electromagnetic field, thus involving only the nucleons and not the neutral mesons. The electromagnetic field will not be treated as an external field, but rather as being quantized according to the usual theory. It is necessary, however, to assume that this nucleon-photon interaction is local, to avoid difficulties with both the gauge invariance and the construction of the S -matrix.

The particular measuring experiment is illustrated schematically in Fig. 1. We consider that initially we have two

nucleons and one photon, each described by wave packets containing only positive frequencies. The packets of nucleon 1 and the photon appear to intersect ("collide") in a region R_1 in space and time. The packet of the other nucleon, nucleon 2, passes through a second region, R_2 , well separated from R_1 . We

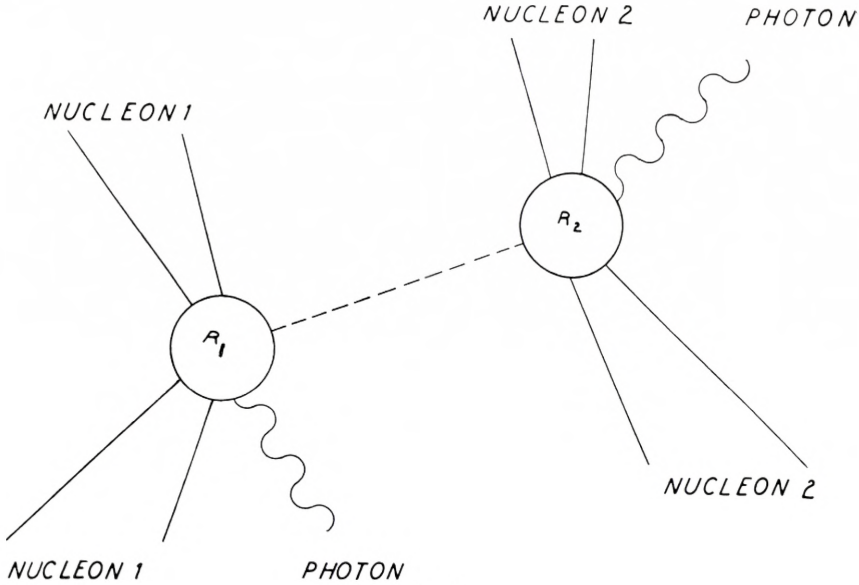


Fig. 1.

look for transitions to a final state in which we again have two nucleons and a photon, but with nucleon 2 and the photon now coming from R_2 , and nucleon 1 from R_1 . The interpretation is then that nucleon 1 has absorbed the photon, transferring this energy to the other nucleon by the exchange of a meson, the energy of this meson finally appearing in the photon emitted by nucleon 2. If all the wave packets are chosen to be minimum packets in either R_1 or R_2 , and if the photons and corresponding nucleons do not have approximately the same direction of motion, then the photon absorption and emission must take place in and around R_1 and R_2 , respectively. An analysis of the Compton effect shows then that the nucleon must lose its excitation energy by meson or photon emission within a region of dimensions of the order of magnitude of \hbar/Mc . This is also ensured if the initial and final state wave packets of nucleons

1 and 2 are chosen so that they only overlap in regions R_1 and R_2 , respectively. Then to the extent to which the regions of intersection, R_1 and R_2 , are well defined, the emission of the meson and its subsequent absorption occur in R_1 and R_2 . But if the energies of both the photons are positive, then the meson going from R_1 to R_2 must have a positive energy, and our causality condition requires that the region R_2 must lie on or within the forward light cone of R_1 .

Now let us turn to a description of the process by our field theory. We choose as the action I

$$I = \int d^4x \mathcal{L}_0(x) + \int d^4x \mathcal{L}_{EM}(x) + \int d(123) \mathcal{L}_M(123), \quad (3.14)$$

where \mathcal{L}_0 is the usual free-field Lagrangian density for a system of mesons, nucleons, and the electromagnetic field, described by operators φ ; ψ , ψ^+ ; A_μ , respectively. The meson-nucleon interaction density is taken as

$$\mathcal{L}_M(123) = -g/2 [\psi^+(1) \varphi(2) \psi(3) - \tilde{\psi}(1) \varphi(2) \tilde{\psi}^+(3)] F(123), \quad (3.15)$$

and the interaction of the nucleon with the electromagnetic field is described by

$$\mathcal{L}_{EM}(x) = ie/2 [\psi^+(x) \gamma_\mu A_\mu(x) \psi(x) - \tilde{\psi}(x) A_\mu \hat{\gamma}_\mu \tilde{\psi}^+(x)]. \quad (3.16)$$

A perturbation expansion for the S -matrix element for the process may be found by introducing a type of interaction representation, in which only the nucleon-photon interaction is chosen for H_{int} . That is, the state vector in our interaction representation, Ψ_I , is related to that vector in the Heisenberg representation with which it coincides at t_0 , Ψ_H , by

$$\Psi_I(t) = P \left[\exp -i \int_{t_0}^t dt' \int d^3x' H_{EM}(x') \right] \Psi_H, \quad (3.17)$$

with P denoting the time-ordered product. We put $\hbar = c = 1$. The S -matrix expressed in terms of operators in this representation may be found by the method of KÄLLÉN⁽⁸⁾ and YANG and FELDMAN⁽⁹⁾. It is then possible to write down the S -matrix in the Heisenberg representation, remembering that the Green's

function transforms as the product of two field operators at different space-time points. In the perturbation expansion, the lowest order terms which have non-vanishing matrix elements

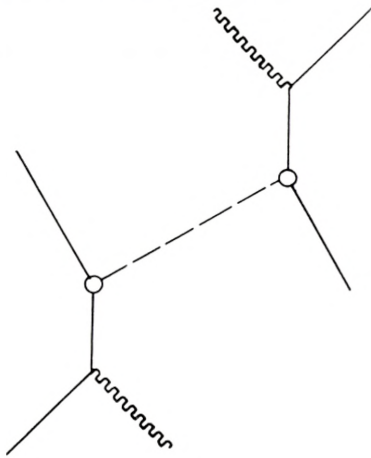


Fig. 2.

between the states considered (each with two nucleons and one photon) will be of order e^2 or e^2g^2 in the coupling constants. The terms of order e^2g^2 in the matrix element are of two types,

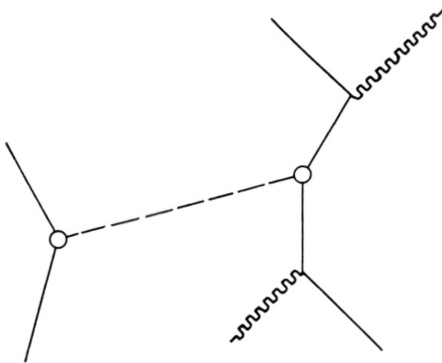


Fig. 3.

depending on whether the two photons interact with different or with the same nucleon. Sample graphs corresponding to these two types are shown in Figs. 2 and 3. The other graphs differ only in regard to which one or two of the particular nucleon line or lines the photon line is attached. An exception to this

are the disconnected graphs, which correspond to no meson exchange; these give a contribution only because the initial and final states chosen for a particular nucleon are not orthogonal. These contributions, which include all those from terms of order e^2 , will be essentially negligible if the change in the mean momentum of one of the nucleons is large compared to the spread of momenta in the nucleon wave packet. Similarly, terms corresponding to graphs of the type shown in Fig. 3 refer to processes in which the meson involved is virtual. Contributions from these may also be shown to be negligible unless R_1 and R_2 are separated by a distance less than \hbar/mc . In fact, with the restricted type of form factor in which we are particularly interested, these terms are identically zero. We are thus left only with graphs such as shown in Fig. 2. One part of the matrix element for the particular graph illustrated is

$$I = e^2 g^2 / 8 \int d(1 \dots 8) F(123) F(456) \psi_d^+(7) A_{\nu f}(7) \gamma_\nu \bar{S}(7-1) \left. \begin{array}{l} \\ \times \Delta_F(2-5) \psi_b(3) \psi_c^+(4) \bar{S}(6-8) A_{\mu e}(8) \gamma_\mu \psi_a(8), \end{array} \right\} \quad (3.18)$$

in which ψ_a and ψ_b are the initial state wave functions of nucleons 1 and 2, and ψ_c and ψ_d are the final state wave functions. The other parts differ only by permutations of the initial and final state wave functions. The initial and final state potentials of the electromagnetic field are denoted by $A_{\mu e}$ and $A_{\nu f}$. Here again $\Delta_F(x)$ is the Feynman Green's function for the meson field. The essential propagation properties of the meson field are rooted in Δ_F and in the form factors.

The wave functions ψ_a , ψ_c , and $A_{\mu e}$ refer to particles which pass through region R_1 , whereas ψ_b , ψ_d , and $A_{\nu f}$ describe particles passing through R_2 . If we denote by x_1 the midpoint of the region R_1 , and by x_2 the midpoint of R_2 , then we may define new translated wave functions ψ' by the conditions

$$\left. \begin{array}{ll} \psi'_a(x) \equiv \psi_a(x + x_1) & \psi'_e(x) \equiv \psi_b(x + x_2) \\ \psi'_c(x) \equiv \psi_c(x + x_1) & \psi'_d(x) \equiv \psi_d(x + x_2) \\ A'_{\mu e}(x) \equiv A'_{\mu e}(x + x_1) & A'_{\nu f}(x) \equiv A'_{\nu f}(x + x_2). \end{array} \right\} \quad (3.19)$$

Then, the primed wave functions should all be in the form of packets passing through the origin; that is, at time $t = 0$ they

should be minimum packets with center at $x = 0$. The matrix element (3.18) may be written more simply in terms of the Fourier transforms of the wave packets and Green's functions. The wave functions are expanded as

$$\left. \begin{aligned} \psi'_a(x) &= (2\pi)^{-2} \int d^4k v_a(k) \frac{1+e(k)}{2} \delta(k^2 + M^2) \exp i k \cdot x, \\ A'_{\mu e}(x) &= (2\pi)^{-2} \sum_{r=1,2} \int d^4k N_\mu^r(k) a_{re}(k) \frac{1+e(k)}{2} \delta(k^2) \exp i k \cdot x, \end{aligned} \right\} (3.20)$$

with similar formulas holding for the other functions. Here, $N_\mu^r(k)$ is a unit vector in the direction of polarization r , and, as a consequence of the supplementary condition on the potentials,

$$k_\mu N_\mu^r(k) = 0, \quad r = 1, 2, \quad (3.21)$$

for transverse polarizations $r = 1, 2$. The functions v_a must satisfy

$$\delta(k^2 + M^2) (\gamma_\mu k_\mu + iM) v_a = 0. \quad (3.22)$$

Using the expansions (1.2) and (3.20) for the form function and the wave functions, we obtain

$$I = e^2 g^2 / 8 \int d^4k M_1(k) M_2(k) \Delta_F(k) \exp i k \cdot (x_2 - x_1), \quad (3.23)$$

with

$$\left. \begin{aligned} M_1(k) &= (2\pi)^{-3} \int d^4k_1 d^4\kappa_1 \sum_s N_\mu^s v_c^+(k_1 + \kappa_1 - k) \gamma_\mu \frac{(k_1 + \kappa_1 + iM)}{(k_1 + \kappa_1)^2 + M^2} \\ &\times v_a(k_1) a_{se}(\kappa_1) \frac{1+e(k_1)}{2} \frac{1+e(\kappa_1)}{2} \frac{1+e(k_1 + \kappa_1 - k)}{2} \\ &\times \delta(k_1^2 + M^2) \delta(\kappa_1^2) \delta[(k_1 + \kappa_1 - k)^2 + M^2] G(k_1 + \kappa_1 - k, -k_1 - \kappa_1); \end{aligned} \right\} (3.24)$$

$$\left. \begin{aligned} M_2(k) &= (2\pi)^{-3} \int d^4k_2 d^4\kappa_2 \sum_r N_\nu^r v_d^+(k_2) \gamma_\nu \frac{(k_2 + \kappa_2 + iM)}{(k_2 + \kappa_2)^2 + M^2} \\ &\times v_b(k_2 + \kappa_2 - k) a_{rf}(\kappa_2) \frac{1+e(k_2)}{2} \frac{1+e(\kappa_2)}{2} \frac{1+e(k_2 - k + \kappa_2)}{2} \\ &\times \delta(k_2^2 + M^2) \delta(\kappa_2^2) \delta[(k_2 - k + \kappa_2)^2 + M^2] G(k_2 + \kappa_2 - k, -\kappa_2 + k); \end{aligned} \right\} (3.25)$$

and

$$\Delta_F(k) = -2i(2\pi)^{-2} [k^2 + M^2 - ie]^{-1}. \quad (3.26)$$

In general, the form of $M_1(k)$ and $M_2(k)$ will depend upon the particular choice of the form factor in momentum space, $G(l_1, l_3)$, and on the form of the wave packets selected. However, two properties of considerable importance for our purposes may be deduced without further specialization. The first of these is that

$$M_1(k) = M_2(k) = 0 \quad \text{for} \quad \left. \begin{array}{l} k^2 < 0 \\ k^0 < 0, \end{array} \right\} \quad (3.27)$$

which means that only the positive frequency components of $\Delta_F(k)$ need enter into our analysis. Of course, (3.27) does not eliminate contributions from space-like vectors k with $k^0 < 0$, but such vectors may all be transformed into vectors with positive frequency components by proper Lorentz transformations. We shall in fact later require that the propagation Green's function be such that the virtual particles described by $k^2 > 0$ give only short-range effects.

Consider the definition (3.24) for $M_1(k)$. The integrals contain a factor

$$\left. \begin{aligned} & \delta(k_1^2 + M^2) \delta(\alpha_1^2) \delta[(k_1 + \alpha_1 - k)^2 + M^2] \frac{1 + e(k_1)}{2} \frac{1 + e(\alpha_1)}{2} \frac{1 + e(k_1 + \alpha_1 - k)}{2} \\ & = \delta(k_1^2 + M^2) \delta(\alpha_1^2) \delta[k^2 + 2 k_1 \cdot \alpha_1 - 2 k \cdot (k_1 + \alpha_1)] \\ & \quad \times \frac{1 + e(k_1)}{2} \frac{1 + e(\alpha_1)}{2} \frac{1 + e(k_1 + \alpha_1 - k)}{2}. \end{aligned} \right\} \quad (3.28)$$

But if a and b are two time-like vectors, $a \cdot b$ is positive if a^0 and b^0 are of opposite signs, and negative if they are of the same sign. Hence,

$$k^2 + 2 k_1 \cdot \alpha_1 - 2 k \cdot (k_1 + \alpha_1) < 0 \quad (3.29)$$

for all vectors k such that $k^2 < 0$, $k^0 < 0$. Thus, for these vectors the δ -function is always zero, and the integral vanishes identically. A similar argument holds for $M_2(k)$. Therefore, our integration in (3.23) only need go over space-like vectors k , and over time-like vectors with $k^0 > 0$.

The second general property of $M_1(k)$ and $M_2(k)$ deals with their smoothness when considered as functions of the vector k ; that is, the continuity of their derivatives of a given order with respect to k . It may be shown that, if $G(l_1, l_3)$ and the various

functions $v(k)$, $a_r(\alpha)$ are sufficiently smooth, and n is any finite positive integer, then the derivatives of $M_1(k)$ and $M_2(k)$ with respect to k and of n th order are continuous everywhere, except possibly at $k^2 = 0$. This is not a completely trivial property, for the presence of the product of the various δ -functions might be thought to introduce discontinuities in some higher order. For example, the integral

$$I(\alpha) = \int_0^1 dx \int_0^1 dy \delta(x + y - \alpha) \tag{3.30}$$

does not possess a continuous first derivative $I'(\alpha)$ everywhere. In our case, the integral $M_1(k)$ is actually an integral over a five-dimensional surface embedded in the eight-dimensional space spanned by $k_{1\mu}$, $\alpha_{1\mu}$. This surface is formed by the intersection of the surfaces

$$\left. \begin{aligned} k_1^2 + M^2 &= 0, & \alpha_1^2 &= 0, \\ (k_1 + \alpha_1 - k)^2 + M^2 &= 0, \end{aligned} \right\} \tag{3.31}$$

and depends upon k as a parameter. The desired smoothness results from the fact that the vectors $k_{1\mu}$ and $\alpha_{1\mu}$ depend upon the five independent variables of the surface and on the parameter k in a continuous manner, a condition which is not met for (3.30). For the proof, it is necessary, among other points, to show that the equations (3.31) have a solution for all values of $k^2 > 0$ and of $k^2 < 0$, $k^0 > 0$. This means that mesons of all momenta are to be involved in the matrix element (3.23).

With these properties in mind, and with reference to the matrix element (3.23), we see that our causality condition takes a particularly simple form. It is: if $\varrho(k) \equiv M_1(k) M_2(k)$ vanishes for $k^2 < 0$, $k^0 < 0$, and possesses only discontinuities in its derivatives corresponding to those of the form factors entering into its definition, then the integral

$$I = e^2 g^2 / 8 \int d^4k \varrho(k) \Delta_F(k) \exp i k \cdot (x_2 - x_1)$$

must be essentially different from zero only if x_2 is on or within the forward light cone of x_1 . The relation of this condition to

that obtained from our previous measuring process, expressed in (3.9), is now apparent.

We are fairly sure of the validity of the use of a perturbation expansion to describe the interaction of the nucleon with the electromagnetic field, but it is a much more doubtful technique for treating the meson-nucleon interaction. It would certainly be desirable to know the effect of terms of higher order in g^2 on the matrix element, in the very least. Some of these terms will refer to processes such as the creation and annihilation of virtual nucleon-anti-nucleon pairs by the meson field. Neglecting the possibility of an interaction of these nucleons with the electromagnetic field, these pairs may presumably be removed by some sort of renormalization. In any case, their only effect will be to modify somewhat the propagation function $\Delta_F(k)$ appearing in (3.23). Since it introduces no more difficulty, we shall henceforth anticipate this modification, and replace $\Delta_F(k)$ by some effective Green's function $\Delta'_F(k)$. Other terms will refer to nucleon self-energy effects and may involve the electromagnetic field in a rather complicated manner. Nevertheless, it is easy to see that such effects do not in essence change the argument. However, one type of term which is definitely not included in our considerations is the meson analogue of the radiative corrections to scattering. These essentially replace the meson-nucleon vertices in Figs. 2 and 3 by some complicated vertex parts. We shall not discuss the effects of such processes here, save to remark that in a certain sense, for our purposes, they may be equivalent to modifying the form factor $F(123)$ somewhat. Whether or not they affect the causality properties depends to a certain extent upon the conditions which we obtain for $F(123)$.

4. Asymptotic Expansion of the Integral.

We have seen that our causality condition requires a knowledge of the behaviour of the integral

$$I(x) = \int d^4k \varrho(k) \Delta'_F(k) \exp i k \cdot x \quad (4.1)$$

for $|\mathbf{x}| \gg 1/m$. In this section, we shall determine the properties of this integral in terms of the properties of $\Delta'_F(k)$ and the func-

tion $\varrho(k)$. It should be noted first that the singularities of the integrand can be of two major types. First, the function $\Delta'_F(k)$ may introduce either poles or distributed singularities culminating in branch points. Thus the zeroth order term in a perturbation expansion of Δ'_F , which is just Feynman's Δ_F , has simple poles at $k^0 = \pm \sqrt{\mathbf{k}^2 + m^2} \mp i\epsilon, \epsilon > 0$. Furthermore, the function $\varrho(k)$ may have discontinuities in either itself, or in its derivatives. We introduce here the requirement that $G(l_1, l_3)$ may possess such discontinuities only along the surfaces $l_1^2 = 0, l_3^2 = 0, \text{ or } (l_1 + l_3)^2 = 0$. Then the discontinuities of $\varrho(k)$ will be limited to the surface $k^2 = 0$.

It is possible to separate these two types of singularities into different terms. For example, the function $\varrho(k) (k^2 + m^2 - i\epsilon)^{-1}$ may be written as

$$\frac{\varrho(\mathbf{k}, k^0)}{k^2 + m^2 - i\epsilon} = \left[\frac{\varrho(\mathbf{k}, k^0)}{k^2 + m^2 - i\epsilon} - \frac{\varrho(\mathbf{k}, k_-^0)}{(k^0 - k_-^0)(k_+^0 - k_-^0)} - \frac{\varrho(\mathbf{k}, k_+^0)}{(k^0 - k_+^0)(k_-^0 - k_+^0)} \right] + \frac{\varrho(\mathbf{k}, k_-^0)}{(k^0 - k_-^0)(k_+^0 - k_-^0)} + \frac{\varrho(\mathbf{k}, k_+^0)}{(k^0 - k_+^0)(k_-^0 - k_+^0)} \quad (4.2)$$

where

$$k_{\pm}^0 = \pm \sqrt{\mathbf{k}^2 + m^2} \mp i\epsilon. \quad (4.3)$$

Then the term in brackets in (4.2) no longer possesses the poles at $k^0 = k_+^0$ or k_-^0 , while the second and third terms do not have the discontinuities of $\varrho(k)$. Distributed singularities may be handled in the same manner, save that now the coefficients of the subtracted terms should be otherwise analytic functions which coincide with $\varrho(k) \Delta'_F(k)$ along the branch cut. After this is performed, the function $\varrho(k) \Delta'_F(k)$ may be written as the sum of two functions, $f(k)$ and $g(k)$, in which $f(k)$ has no singular points other than the discontinuities of $\varrho(k)$, and $g(k)$ has only poles and branch points corresponding to those of $\Delta'_F(k)$. Furthermore, $g(k)$ can have no singularities in the region $k^2 < 0, k^0 < 0$, for here $\varrho(k) \equiv 0$, and the coefficients of the subtracted terms must be zero. We now may consider the Fourier transforms of the two functions $f(k)$ and $g(k)$ separately.

Consider first the integral

$$I^1(x) = (2\pi)^{-2} \int d^4k f(k) \exp ik \cdot x. \quad (4.4)$$

It is convenient to expand $I^1(x)$ in spherical harmonics, obtaining

$$I^1(x) = i/(2\pi^3) \sum_{lm} i^l Y_l^m(\vartheta, \varphi) I_{lm}^1(r, x^0), \quad (4.5)$$

where

$$\left. \begin{aligned} I_{lm}^1(r, x^0) &= \int_0^\infty dk k^{l+1} j_l(kr) \int_{-\infty}^\infty dk^0 f_{lm}(k, k^0) \exp -ik^0 x^0, \\ f(k) &= \sum_{lm} Y_l^m(\vartheta_k, \varphi_k) f_{lm}(k, k^0) k^{l-1}. \end{aligned} \right\} \quad (4.6)$$

An asymptotic expansion for $I_{lm}^1(r, x^0)$ may be obtained by a method which is a slight generalization of that given by WILLIS⁽¹⁰⁾. If $f_{lm}(k, k^0)$ is square integrable, then we may write

$$\left. \begin{aligned} I_{lm}^1(r, x^0) &= L \int_{\alpha_1 \rightarrow 0}^\infty dk k^{l+1} j_l(kr) \exp -\alpha_1 k \\ &\quad \times \int_{-\infty}^\infty dk^0 f_{lm}(k, k^0) \exp [-ik^0 x^0 - \alpha_2 |k^0|]. \end{aligned} \right\} \quad (4.7)$$

We know that, save on the surface $\mathbf{k}^2 = k^{02}$, $f(k, k^0)$ possesses continuous derivatives of order $N+1$, for any finite N . Then we have

$$\left. \begin{aligned} f_{lm}(k, k^0) &= \sum_{n=0}^{N-1} \frac{1}{n!} \sum_{\nu=0}^n \binom{n}{\nu} f_+^{n-\nu\nu}(0,0) k^{n-\nu} k^{0\nu} + R_+^N, & k^2 > k^{02}; \\ &= \sum_{n=0}^{N-1} \frac{1}{n!} \sum_{\nu=0}^n \binom{n}{\nu} f_{-+}^{n-\nu\nu}(0,0) k^{n-\nu} k^{0\nu} + R_{-+}^N, & \left. \begin{aligned} k^2 < k^{02}; \\ k^0 > 0 \end{aligned} \right\} \\ &= \sum_{n=0}^{N-1} \frac{1}{n!} \sum_{\nu=0}^n \binom{n}{\nu} f_{--}^{n-\nu\nu}(0,0) k^{n-0} k^{0\nu} + R_{--}^N, & \left. \begin{aligned} k^2 < k^{02}; \\ k^0 < 0 \end{aligned} \right\} \end{aligned} \right\} \quad (4.8)$$

where

$$\left. \begin{aligned} f_+^{n-\nu\nu}(0,0) &= L \int_{k^2 \rightarrow k^{02} +} L \int_{k \rightarrow 0} \frac{\partial^{n-\nu}}{\partial k^{n-\nu}} \frac{\partial^\nu}{\partial k^{0\nu}} f(k, k^0), \\ f_{-+}^{n-\nu\nu}(0,0) &= L \int_{k^2 \rightarrow k^{02} -} L \int_{k^0 \rightarrow 0 +} \frac{\partial^{n-\nu}}{\partial k^{n-\nu}} \frac{\partial^\nu}{\partial k^{0\nu}} f(k, k^0), \\ f_{--}^{n-\nu\nu}(0,0) &= L \int_{k^2 \rightarrow k^{02} -} L \int_{k^0 \rightarrow 0 -} \frac{\partial^{n-\nu}}{\partial k^{n-\nu}} \frac{\partial^\nu}{\partial k^{0\nu}} f(k, k^0). \end{aligned} \right\} \quad (4.9)$$

The use of the subscript plus and minus signs is in cognizance of the fact that the derivatives of the function $f(k, k^0)$ may be discontinuous across the surface $\mathbf{k}^2 \equiv k^{02}$. The remainders in (4.8) may be written as

$$R^N = \frac{1}{N!} \sum_{\nu=0}^N \binom{N}{\nu} f^{N-\nu\nu}(\beta k, \beta k^0) k^{N-\nu} k^{0\nu}, \quad 0 < \beta < 1. \quad (4.10)$$

If we introduce

$$\left. \begin{aligned} \varphi_{++}(\alpha_1\alpha_2) &= \int_0^\infty dk k^{l+1} j_l(kr) \exp -\alpha_1 k \int_{-k}^k dk^0 \exp [-ik^0 x^0 - \alpha_2 |k^0|], \\ \varphi_{-+}(\alpha_1\alpha_2) &= \int_0^\infty dk k^{l+1} j_l(kr) \exp -\alpha_1 k \int_k^\infty dk^0 \exp [-ik^0 x^0 - \alpha_2 k^0], \\ \varphi_{--}(\alpha_1\alpha_2) &= \int_0^\infty dk k^{l+1} j_l(kr) \exp -\alpha_1 k \int_\infty^{-k} dk^0 \exp [-ik^0 x^0 + \alpha_2 k^0]; \end{aligned} \right\} \quad (4.11)$$

and denote $\frac{\partial^{n-\nu}}{\partial \alpha_1^{n-\nu}} \frac{\partial^\nu}{\partial \alpha_2^\nu} \varphi(\alpha_1\alpha_2)$ by $\varphi^{n-\nu\nu}(\alpha_1\alpha_2)$,

we have

$$\left. \begin{aligned} I_{lm}^1(r, x^0) &= L \int_{\alpha_1 > 0} L \int_{\alpha_2 > 0} \left\{ \sum_{n=0}^{N-1} \frac{(-)^n}{n!} \sum_{\nu=0}^n \binom{n}{\nu} [f_{++}^{n-\nu\nu}(0,0) \varphi_{++}^{n-\nu\nu}(\alpha_1\alpha_2) \right. \\ &\quad \left. + f_{-+}^{n-\nu\nu}(0,0) \varphi_{-+}^{n-\nu\nu}(\alpha_1\alpha_2) + f_{--}^{n-\nu\nu}(0,0) \varphi_{--}^{n-\nu\nu}(\alpha_1\alpha_2)] + R_N \right\}. \end{aligned} \right\} \quad (4.12)$$

The remainder here is given by

$$R^N = \sum_{\nu=0}^N [C_+ \varphi_+^{N-\nu\nu}(\alpha_1\alpha_2) + C_{-+} \varphi_{-+}^{N-\nu\nu}(\alpha_1\alpha_2) + C_{--} \varphi_{--}^{N-\nu\nu}(\alpha_1\alpha_2)]; \quad (4.13)$$

the coefficients C may be shown to be finite if $f^{N-\nu\nu}$ is of bounded variation. We shall henceforth make this assumption. All that remains in order to obtain an asymptotic expansion for $I_{lm}^1(r, x^0)$ is to evaluate the coefficients $\varphi^{n-\nu\nu}(\alpha_1\alpha_2)$. In general, this can be done only in terms of an infinite series in either r/x^0 or x^0/r , according as r is less than or greater than $|x^0|$. We find, for $r > |x^0|$,

$$\left. \begin{aligned}
 \varphi_{-+}^{n-\nu\nu} &= 2^{l+1} (-i)^{n+1} r^{-n-l-3} + S_{n\nu}, \\
 \varphi_{--}^{n-\nu\nu} &= 2^{l+1} (+i)^{n+1} (-)^{\nu} r^{-n-l-3} + S_{n\nu}, \\
 \varphi_{+}^{n-\nu\nu}(\alpha_1\alpha_2) &= -\varphi_{-+}^{n-\nu\nu}(\alpha_1\alpha_2) - \varphi_{--}^{n-\nu\nu}(\alpha_1\alpha_2), \\
 S_{n\nu} &\equiv \sum_{\sigma \geq \frac{1}{2}(n+1)}^{\infty} \frac{(l+\sigma)!(2\sigma)!}{(2\sigma-n+\nu)\sigma!(2\sigma-n-1)!} (x^0/r)^{2\sigma-n-1},
 \end{aligned} \right\} (4.14)$$

in which only terms of order α_1^0, α_2^0 have been retained. If I_{lm}^1 is rewritten as

$$\left. \begin{aligned}
 I_{lm}^1(r, x^0) &= L \underset{\alpha_1 \rightarrow 0}{L} \underset{\alpha_2 \rightarrow 0}{\sum_{n=0}^{N-1}} \frac{(-)^n}{n!} \sum_{\nu=0}^n \binom{n}{\nu} \left\{ \varphi_{-+}^{n-\nu\nu}(\alpha_1\alpha_2) [f_{-+}^{n-\nu\nu}(0,0) \right. \\
 &\quad \left. - f_{+}^{n-\nu\nu}(0,0)] + \varphi_{--}^{n-\nu\nu}(\alpha_1\alpha_2) [f_{--}^{n-\nu\nu}(0,0) - f_{+}^{n-\nu\nu}(0,0)] \right\} + R_N,
 \end{aligned} \right\} (4.15)$$

we see that $I_{lm}^1(r, x^0)$ decreases in a space-like direction more rapidly than r^{-n-l-3} if $f^{n-\nu\nu}(k, k^0)$ is continuous across the surface $k^2 = k^{02}$. The coefficient of the term of order r^{-n} in an asymptotic expansion is thus of the order of magnitude of the discontinuity in the n -th derivative of $\varrho(k)$. This agrees with a simple calculation of the effect of a discontinuous form factor upon the propagation of signals.

Similarly, if $|x^0| > r$, we have

$$\left. \begin{aligned}
 \varphi_{-+}^{n-\nu\nu} &= 2^{l+1} (-)^l (+i)^{n+1} x^{0-n-l-3} (r/x^0)^l S_{n\nu}, \\
 \varphi_{--}^{n-\nu\nu} &= 2^{l+1} (-)^{l-\nu} (-i)^{n+1} x^{0-n-l-3} (r/x^0)^l S_{n\nu}, \\
 \varphi_{+}^{n-\nu\nu}(\alpha_1\alpha_2) &= -\varphi_{-+}^{n-\nu\nu}(\alpha_1\alpha_2) - \varphi_{--}^{n-\nu\nu}(\alpha_1\alpha_2), \\
 S_{n\nu} &\equiv \sum_{\sigma=0}^{\infty} \frac{(l+\sigma)!(2\sigma+2l+n+1)!}{(2\sigma+2l+n-\nu+2)(\sigma)!(2\sigma+2l+1)!} (r/x^0)^{2\sigma}.
 \end{aligned} \right\} (4.16)$$

In this case, $I_{lm}^1(r, x^0)$ decreases in a time-like direction more rapidly than $x^{0-n-l-3}$ if $f^{n-\nu\nu}(k, k^0)$ is continuous across the light cone.

The case of $r = |x^0|$, that is, on the light cone itself, requires special attention. For $r = |x^0|$, neither the infinite series in (4.14), nor that in (4.16), converges, and hence our method for obtaining the asymptotic expansion breaks down. We might argue on physical grounds that the indeterminacy of the behaviour

on the exact surface $r = x^0$, which is of zero measure, should introduce no difficulty. A more careful analysis, however, requires that we examine the behaviour of the integral of $I(r, x^0)$ taken over some small volume element spanning the light cone, in the limit in which this element is located far from the origin. If this is done, we see immediately that at worst the decrease with distance from the origin goes only as r^{-n-2} , for functions with discontinuities in the n th derivative. Thus no real problem is presented by this singular case.

The continuity of the derivatives of $\varrho(k)$, and hence of $f(\mathbf{k}, k^0)$, may be related to the continuity of the derivatives of $G(l_1, l_3)$ with respect to $(l_1 + l_3)^2 = k^2$. We are particularly interested in the case where $G(l_1, l_3)$ vanishes for $(l_1 + l_3)^2$ greater than zero. For this type of form factor, $\varrho(k)$ will have derivatives of order $2n$ continuous across the surface $k^2 = 0$, if $G(l_1, l_3)$ has derivatives with respect to $(l_1 + l_3)^2$ of order n which are continuous across $(l_1 + l_3)^2 = 0$. The factor two arises from the fact that $\varrho(k)$ contains the product of two form factors. The discontinuities in the derivatives of the other factors in $M_1(k)$ and $M_2(k)$ will play no part if the first n derivatives of $G(l_1, l_3)$ with respect to $(l_1 + l_3)^2$ are zero at $(l_1 + l_3)^2 = 0$, as they must be if G is to vanish identically for $l_1 + l_3$ space-like.

Thus far we have been concerned only with the integral I^1 . The discussion of the Fourier transform of $g(k)$,

$$I^2(x) = (2\pi)^{-2} \int d^4k g(k) \exp i k \cdot x, \tag{4.17}$$

is fortunately very simple. We have already remarked that $g(k)$ contains only singularities in the regions $k^2 < 0$, $k^0 > 0$, and $k^2 > 0$. If these singularities all lie in the lower half of the complex k^0 plane, then $I^2(x)$ vanishes for $x^0 < 0$. Similarly, if they lie in the upper half plane, then $I^2(x)$ vanishes for $x^0 > 0$. This follows directly from an evaluation of I^2 as a contour integral in the complex k^0 plane, a procedure justified by the meromorphic nature of $g(k)$. Thus, in order that $I^2(x_2 - x_1)$ give contributions only for x_2 within or on the forward light cone of x_1 , it is necessary that $g(k)$ should have poles only at points $k^0 = K^0$, where $Im K^0 < 0$ if $Re K^0 > 0$. If we had arranged conditions so that the meson absorption occurred at x_1 and its emission at x_2 , then

the requirement would have been $Im K^0 > 0$ if $Re K^0 < 0$. However, since the sign of k^0 may be changed by a Lorentz transformation only if $|k^0| < |\mathbf{k}|$, then our requirements also become sufficient if we demand further that no singularities exist with $Re K^0 < |\mathbf{k}|$. Since poles a finite distance from the real axis give rise to terms which are damped exponentially, the above restriction should only involve those poles near this axis.

The results of the analysis presented in this section may be summarized as follows. Suppose that the singularities of the propagation function $\Delta'_F(k)$ lie in the second and fourth quadrants of the complex k^0 plane, and at least a distance k from the imaginary axis, and that the function $\varrho(k)$ has continuous derivatives of the first n orders. Then the integral $I(x_2 - x_1)$ is composed of two terms, one of which is different from zero only for $(x_2 - x_1)^2 < 0$, $x_2^0 - x_1^0 > 0$, and the other of which decreases in any space-like direction or time-like direction more rapidly than the inverse $n + 4$ power of $|\mathbf{x}_1 - \mathbf{x}_2|$ or $x_1^0 - x_2^0$, respectively. Furthermore, the decrease of this second term along the surface $|x^0| = r$ is sufficiently rapid so that its integral with respect to x_2 over some small region centered at $\langle x_2 \rangle$ decreases as $|\mathbf{x}_1 - \langle \mathbf{x}_2 \rangle|^{n+3}$.

5. Discussion.

The results of the previous section point out rather clearly the distinction between the work of Fierz, and that of Bloch and of Chrétien and Peierls. The basis of the argument of Fierz is that, save for a part which damps out rather rapidly, the positive frequency part of the Feynman Green's function Δ_F propagates only into the forward light cone. The part which damps out is unobservable due to the complementarity existing between time and energy. This result is essentially dependent upon the location of the poles of the propagation function in the complex k^0 plane. By the analysis given here, we find that our integral I^2 , which is obtained from a process selecting only positive frequency components of the propagation function, also represents a signal propagating only into the forward light cone. The difference between the analysis of Fierz and ours is that the unobservable damped-out term he obtains is, in our case, included in the integral I^1 .

The analyses of Bloch and Chrétien and Peierls, on the other hand, are mainly concerned with the effect of discontinuities in the form factor. We have found it convenient to include such discontinuities in the integral I^1 . It might be suspected, then, that their analyses are in some way comparable to that which we gave for I^1 . This is true in a formal sense if we generalize the interpretation given to the "source function" introduced by Chrétien and Peierls. The physical interpretation given to their integral containing the form function is considerably different from that which we have attached to ours, however. A type of connection between the two may be established, nonetheless. For this purpose we define a four-point "form factor", $F(1346)$, by

$$F(1346) = \int d(25) F(123) \Delta_F''(2-5) F(456), \quad (5.1)$$

in which $\Delta_F''(2-5)$ is just that part of the propagation function remaining after subtracting off the singularities, in the manner of the last section. Then we may say that our demonstration that $I^1(x_2-x_1)$ decreases rapidly with increasing distance $|\mathbf{x}_2-\mathbf{x}_1|$ or $x_2^0-x_1^0$ is somewhat equivalent to showing that $F(1346)$ decreases rapidly as the distance from the points 1 and 3 to the points 4 and 6 increases. More exactly, and following the notation of Chrétien and Peierls, we show that, for functions $\varphi(46)$ which are appreciably different from zero only when 4 and 6 are near the origin, $\hat{\varphi}(13)$ decreases as a certain inverse power of the distance of 1 and 3 from the origin, where $\hat{\varphi}(13)$ is defined by

$$\hat{\varphi}(13) = \int d(46) F(1346) \varphi(46). \quad (5.2)$$

We found that the power of decrease of $\hat{\varphi}(13)$ depended upon the degree of smoothness of the Fourier transform of $F(1346)$. Written in this manner, the similarity between our investigation of I^1 and the investigation by Chrétien and Peierls of the function

$$\tilde{\varphi}(13) = \int d(2) F(123) \varphi(2) \quad (5.3)$$

is rather obvious. The different methods used for obtaining conditions on the asymptotic expansions is purely a matter of preference. In view of this similarity, it is not surprising that sub-

stantially the same condition is obtained here as was obtained by Chrétien and Peierls.

It seems fairly clear that, for a field theory with non-local interaction, two rather different types of conditions are obtained, both of which must be satisfied for causal behaviour. The first relates to the location of singularities, demanding that they occur only in the second and fourth quadrants in the k^0 plane, and at least a distance $|\mathbf{k}|$ from the imaginary axis. This type of condition must also be satisfied for a local theory. In practice it restricts the particular choice of a Green's function.

The presence of a non-local interaction, however, introduces an additional amount of freedom into the theory, by means of the form function $G(l_1, l_3)$, which is not completely determined. This in turn creates the possibility for introducing discontinuous factors into the integrands of the integrals giving matrix elements for certain processes. These discontinuities will in general give rise to a type of acausal behaviour, unless the function $G(l_1, l_3)$, considered as a function of the variables $l_1^2, l_3^2, (l_1 + l_3)^2$, is sufficiently smooth. The probability for observing signals transmitted with velocities greater than that of light decreases essentially more rapidly than an inverse 4 + 6 power of the spatial distance between the points of observation, if the G function has continuous derivatives of the n th order.

The particular problem which we encounter in practice is that we wish, for reasons of convergence, to use form factors which vanish if either l_1^2, l_3^2 or $(l_1 + l_3)^2$ is greater than zero. Certainly then G may not be an analytic function of these variables. On the other hand, we may construct a G fulfilling these conditions, and yet possessing continuous derivatives of any pre-assigned finite order. Thus we may require the "acausal signals" to decrease more rapidly than as any pre-assigned finite inverse power. This is the extent to which causality may be preserved in our theory with non-local interaction.

The author is deeply indebted to Professor C. MØLLER, mag. scient. P. KRISTENSEN, and Dr. R. HAAG for many helpful discussions and suggestions on this problem. He wishes to express his gratitude to Professor NIELS BOHR for extending the hospitality of his institute during the time this work was performed.

References.

- (1) P. KRISTENSEN and C. MØLLER, Dan. Mat. Fys. Medd. **27**, no. 7 (1952).
 - (2) C. BLOCH, Dan. Mat. Fys. Medd. **27**, no. 8 (1952).
 - (3) P. KRISTENSEN, private communication.
 - (4) W. CHRÉTIEN and R. E. PEIERLS, Nuovo Cimento **10**, 668 (1953).
 - (5) M. FIERZ, Helv. Phys. Acta **23**, 731 (1950).
 - (6) N. VAN KAMPEN, Phys. Rev. **89**, 1072; **91**, 1267 (1953).
 - (7) W. ZIMMERMANN, Zs. f. Phys. **135**, 473 (1953).
 - (8) C. KÄLLÉN, Ark. f. Fys. **2**, 371 (1951).
 - (9) C. N. YANG and D. FELDMAN, Phys. Rev. **76**, 972 (1950).
 - (10) H. F. WILLIS, Phil. Mag. **39**, 455 (1948).
-

Det Kongelige Danske Videnskabernes Selskab

Matematisk-fysiske Meddelelser, bind **29**, nr. 3

Dan. Mat. Fys. Medd. **29**, no. 3 (1954)

EXCITATION OF
NUCLEAR ROTATIONAL STATES
IN μ -MESONIC ATOMS

BY

LAWRENCE WILETS



København 1954

i kommission hos Ejnar Munksgaard

Printed in Denmark
Bianco Lunos Bogtrykkeri A-S

I. Introduction.

X-radiations from μ -mesonic atoms have been detected by CHANG (1949) in cosmic ray studies, and more recently by FITCH and RAINWATER (1953) working with artificially produced mesons. The mesons are captured in the outer Bohr orbits and cascade inward toward the nucleus, transferring energy by radiative and Auger transitions. The mesons arrive in the lower atomic states, for the most part, with $l = n - 1$ and proceed to decay by radiative transitions, with $\Delta l = \Delta n = -1$, to the ground state. It is the $2p$ to $1s$ transition which has been studied the most.

In the low quantum states, atomic electrons do not affect the meson and the system may be treated as a hydrogen-like atom, with due regard to the characteristic effects of the mesonic mass. The level structure of the mesonic atom has been calculated for various nuclei by WHEELER (1949, 1953), FITCH and RAINWATER, and COOPER and HENLEY (1953). Only electrical forces are considered, since the μ -meson interacts only weakly with nuclear matter. The meson is treated as a Dirac particle with spin $1/2$ and magnetic moment $e\hbar/2\mu c$. The mass μ of the μ -meson is 207* times the mass of the electron, and the Bohr orbits are proportionately smaller; in *Pb*, for example, the first mesonic Bohr orbit is 3.12×10^{-13} cm compared with a nuclear radius $R \approx 7.7 \times 10^{-13}$ cm. Nuclear structure effects, small in electronic atoms, become very pronounced in the mesonic atom. Indeed, the finite extension of the nucleus (which gives rise to isotope shifts in electronic spectra) becomes a dominant consideration in the mesonic atom; in *Pb*, for example, it accounts for the reduction of the $1s$ state energy from 21.3 MeV for a point nucleus to 10.1 MeV. This also results in a reduction of the fine structure splitting of the $2p$ doublet from 0.55 MeV to 0.2 MeV in *Pb*.

* C. f. SMITH, BIRNBAUM, and BARKAS (1953).

Nuclear moment splittings, analogous to hyperfine structure in electronic atoms, depend in general upon the expectation value of r^{-3} and are proportionately much greater in mesonic atoms. WHEELER (1953) has shown that, in the case of heavy nuclei with large distortions, the quadrupole splittings of the $2p_{3/2}$ level may be of the same order of magnitude as the fine structure. Magnetic h. f. s. splittings are not so greatly enhanced, since they also depend upon the mesonic magnetic moment which varies inversely as the mesonic mass; these splittings are perhaps two orders of magnitude smaller than the fine structure.

For the effects mentioned above, the meson is considered in the *static* field of the nucleus and the nucleus unaffected by the meson. COOPER and HENLEY have discussed the polarization of the nucleus by the meson—an effect treated earlier by BREIT, ARFKEN, and CLENDENIN (1950) for the electronic case—but estimated this effect to contribute not more than 3 per cent of the transition energy. Their estimate is based upon the $1s$ mesonic level where the induced monopole effect dominates; higher multipole interactions (e.g., dipole, quadrupole, etc.) for the $1s$ state involve non-diagonal matrix elements connecting mesonic states with principal quantum numbers n greater than one, and which are thus distant in energy.

In mesonic states with $n > 1$, however, the higher multipole interactions may be realized between mesonic states with the same principal quantum number, and when the nuclear excitation energy is also small, the interaction may become large. It is known from experiments on radiative lifetimes (cf. BOHR and MOTTELSON, 1953) and Coulomb excitation (cf. HUUS and ZUPANČIČ, 1953) that in nuclei with large deformations there exist low-lying excited states which have very large quadrupole transition probabilities to the ground state. For these nuclei, the excitation matrix elements are comparable in magnitude with the static quadrupole interactions discussed above, and in many cases are larger than the nuclear excitation energies. The non-static meson-nuclear quadrupole interaction must thus be expected to have a major influence on the “fine structure” of the mesonic X-rays. It also provides a large probability that, after the meson reaches the atomic ground state, the nucleus be left in an excited state and subsequently emit a nuclear γ -ray.

These effects occur for even-even as well as for odd nuclei, since, although the quadrupole interaction vanishes in the ground state of even-even nuclei ($I = 0$), it does not vanish generally in the excited states, and non-zero matrix elements connect the ground state with excited states.

The effects of the interaction are of interest not only in understanding the spectra, but especially in providing another method of obtaining information about the magnitude and sign of nuclear deformations and nuclear charge distributions. The mesonic atom may, in fact, provide the first method of determining the sign of intrinsic quadrupole moments in even-even nuclei.

II. Description of the Model.

The low-lying states which interact especially strongly with the meson follow a very regular pattern and have been rather accurately described in terms of rotational states of intrinsically deformed nuclei (BOHR, 1952, 1954; BOHR and MOTTELSON, 1953). The theory of these states accounts for their nuclear energy spectra and also predicts many simple relations between matrix elements connecting the rotational states. These relations make it possible to greatly reduce the parameters entering into the calculations of the effects of the meson-nuclear interaction, and to interpret the empirical data of these effects in terms of simple nuclear properties. In the following, we shall describe the effects of the interaction of the meson with the excited nuclear states in terms of the model of the rotational states, even though the considerations involved in the calculation of the interaction are more generally valid.

Rotational spectra are expected in nuclei with large deformations, and have been observed to occur with considerable regularity in nuclei with $155 < A < 185$ and $A > 255$. Such nuclei may be described as possessing an intrinsic deformation which is usually symmetric about some nuclear axis. The rotation of the deformed nucleus is generated by a collective motion of the nucleons, which is similar to the classical motion of an irrotational fluid. The rotation leaves the nuclear shape unaltered and affects only the orientation of the nuclear axis. The state of the nucleus may be specified by quantum numbers I , M_I and K —the total

nuclear angular momentum, the projection along the z -axis, and the projection along the symmetry axis. In the low-lying rotational states, K is a constant and is just equal to the projection of the angular momenta of the individual nucleons along the symmetry axis; for the ground state, $I_0 = K$ except when $K = 1/2$.*

The rotational spectrum is given by

$$H_{ROT} = \frac{\hbar^2}{2\mathfrak{I}} [I(I+1) - I_0(I_0+1)]. \quad (1)$$

For odd- A or odd-odd nuclei, the sequence of states is $I = I_0, I_0 + 1, I_0 + 2, \dots$ while for even-even nuclei, where $I_0 = K = 0$, the reflection symmetry of the nuclear shape implies that only even integral values of I occur.

The moment of inertia, \mathfrak{I} , of such a system may be shown to be proportional to the square of the deformation, and the wave functions to be the properly symmetrized (with respect to the sign of K) symmetric top functions. The symmetrization depends upon the nucleonic configurations, and plays no essential role in the present discussion. For our present purposes**, it is thus sufficient to consider the unsymmetrized nuclear wave functions

$$\psi_{M_I K}^I = \sqrt{\frac{2I+1}{8\pi^2}} \mathfrak{D}_{M_I K}^I(\theta i), \quad (2)$$

where the θi are the three Eulerian angles (θ, φ, ψ) describing the orientation of the nuclear axes. For even-even nuclei, we have $K = 0$, and the wave functions are then given more simply by

$$\psi_{M_I 0}^I = \sqrt{\frac{2I+1}{8\pi^2}} \mathfrak{D}_{M_I 0}^I(\theta i) = \frac{1}{\sqrt{2\pi}} Y_{M_I}^I(\theta, \varphi). \quad (2a)$$

The nuclear distortion is characterized by an intrinsic quadrupole moment, Q_0 , oriented along the symmetry axis. It is related

* In the case $K = 1/2$, the spectrum is modified by the inclusion of terms which depend upon the nucleonic structure (cf. BOHR and MOTTELSON, 1953, eq. II. 24). The wave functions are, however, still of the form (2) and the discussion here does not depend upon the form of eq. (1).

** In section IV, where strong coupling of the meson to the nucleus is discussed, we will require an expression for the symmetrized wave functions. Equation (16) is thus analogous to (2) where the mesonic wave functions replace the nucleonic wave functions implied in (2). Cf. BOHR and MOTTELSON for a complete discussion.

to the spectroscopically observed quadrupole moment Q by the relation

$$Q = \frac{3K^2 - I(I+1)}{(I+1)(2I+3)} Q_0, \quad (3)$$

which vanishes for $K = I = 0$ or $1/2$.

The interaction of the meson with the rotational states arises from the deviation of the nuclear field from spherical symmetry due to the deformation. The most important interaction is due to the quadrupole coupling and may be written in the form

$$H' = -\frac{1}{2} Q_0 e^2 f(r) P_2(\cos \widehat{\mu N}), \quad (4)$$

where $\widehat{\mu N}$ is the angle between the meson radius vector and the symmetry axis of the nucleus. The function $f(r)$, where r is the radial coordinate of the meson, contains the radial dependence of the interaction, and is given in general form by

$$Q_0 f(r) = r^{-3} \int_0^r \varrho^{(2)}(\vec{r}') dv' + r^2 \int_r^\infty r'^{-5} \varrho^{(2)}(\vec{r}') dv', \quad (5)$$

where the primed coordinates refer to the nucleus and $\varrho^{(2)}(\vec{r}') = (3z'^2 - r'^2)$ is the quadrupole part of the nuclear charge distribution and is oriented along the nuclear symmetry axis. The first integral in (5) gives just Q_0 when extended over the entire charge of the nucleus. If the quadrupole distribution were concentrated at the surface, the radial function could be written as

$$f(r) = \begin{cases} r^{-3} & \text{if } r > R \\ r^2 R^{-5} & \text{if } r < R, \end{cases} \quad (6)$$

where R is the nuclear radius. This may also be used as an approximation for a uniformly charged ellipsoidal nucleus (cf. WHEELER, 1953).

III. Treatment of Coupled System of Meson and Rotating Nucleus.

The energy of the coupled system is given by

$$H = H_0(\vec{x}, \vec{\sigma}) + H_{ROT}(\theta i) + H'(\vec{x}, \theta_i), \quad (7)$$

where \vec{x} and $\vec{\sigma}$ are the mesonic space and spin coordinates, and $H_0(\vec{x}, \vec{\sigma})$ is the meson energy in the nuclear monopole field (i. e. the electrostatic potential averaged over all angles). This energy includes the fine structure splittings, and is characterized by the quantum numbers n , l (approximately), and j .

We shall consider the equations of motion in the uncoupled representation. We thus choose as basis vectors products of the nuclear wave functions $\Psi_{M_I K}^I$ and the meson eigenfunctions of the monopole potential. The total wave functions of the system characterized by F , the total angular momentum and M , the projection along the z -axis, may then be denoted by

$$|IK, j; FM\rangle = \sum_{M_I m} (IjM_I m | IjFM) \psi_{M_I K}^I(\theta_i) \varphi_m^j(\vec{x}, \vec{\sigma}), \quad (8)$$

where $(IjM_I m | IjFM)$ is the Clebsch-Gordon coefficient for adding angular momenta. Both H_0 and H_{ROT} are diagonal in this representation.

The Legendre polynomial $P_2(\cos \widehat{\mu N})$ which appears in H' may be written as a scalar product of spherical harmonics of order two in the meson and nuclear orientation angles:

$$P_2(\cos \widehat{\mu N}) = \frac{4\pi}{5} \sum_{q=-2}^2 (-1)^q Y_{2q}(\theta_N \varphi_N) Y_{2-q}(\theta_\mu \varphi_\mu). \quad (9)$$

The matrix elements for the interaction may then be written in the form (cf. RACAHA (1942) whose notation we follow)

$$\left. \begin{aligned} \langle IK' j'; F' | H' | IK j; F \rangle &= -\frac{1}{2} Q_0 e^2 \frac{4\pi}{5} (-1)^{I-j'-F} W(IjI'j'; F 2) \\ &\times \langle IK \| Y_N^{(2)} \| I'K \rangle \langle j \| Y_\mu^{(2)} \| j' \rangle \langle j \| f(r) \| j' \rangle \delta_{FF'} \delta_{KK'} \end{aligned} \right\} \quad (10)$$

The dependence of the matrix elements on F is contained only in the Racah coefficients, which may be evaluated from tables*. The double-bar matrix elements depend only on the nuclear or mesonic configurations. The nuclear matrix elements are given by

$$\langle IK \| Y_N^{(2)} \| I'K \rangle = \sqrt{\frac{5}{4\pi}} (2I' + 1) (2I'OK | 2I'IK) \quad (11)$$

from which it is clear that $|I - I'| \leq 2$.

The meson matrix elements depend implicitly upon other quantum numbers, in particular n and l . The element $\langle j \| Y_\mu^{(2)} \| j' \rangle$ vanishes for $j = j' = 1/2$, and since $Y_\mu^{(2)}$ is of even parity, it can only connect mesonic states of the same parity. States with different values of n are too far away in energy to mix. Thus the $1s_{\frac{1}{2}}$ and $2s_{\frac{1}{2}}$ states are unaffected by the interaction, and $2p$ states can mix only among themselves. With increasing n , the effect of the interaction rapidly decreases and is already rather small for $n = 3$ (cf. footnote on p. 14). The non-vanishing angular matrix elements for the p -states are given by

$$\left. \begin{aligned} \langle 3/2 \| Y_\mu^{(2)} \| 1/2 \rangle &= -\langle 1/2 \| Y_\mu^{(2)} \| 3/2 \rangle \\ &= -\langle 3/2 \| Y_\mu^{(2)} \| 3/2 \rangle = (\pi)^{-1/2}. \end{aligned} \right\} \quad (12)$$

The radial double-bar matrix elements

$$\langle j \| f(r) \| j' \rangle = \int_0^\infty \mathfrak{R}_{2pj}(r) f(r) \mathfrak{R}_{2pj'}(r) dr \quad (13)$$

must be evaluated from a knowledge of radial wave functions. WHEELER (1953) approximates the integral from hydrogenic Schroedinger wave functions for the $2p$ states, $\mathfrak{R}_{2p} = c^2 r^2 \exp(-Z\mu e^2 r / 2\hbar^2)$, normalized so that $\int \mathfrak{R}_{2p}^2 dr = 1$, and using (5) for $f(r)$. He then finds

$$e^2 \int \mathfrak{R}_{2p}^2 f(r) dr = 5 (Z/237)^3 f_q \text{ Mev/barn}, \quad (14)$$

where the form factor $f_q \approx (1 + 0.1x^2)^{-2}$ and the dimensionless parameter $x = RZ\mu e^2/\hbar^2$. Although the hydrogenic Schroedinger

* Cf., for example, BIEDENHARN (1952); BIEDENHARN, BLATT, and ROSE (1952), or SIMON, VAN DER SLUIS, and BIEDENHARN (1954).

wave functions may be considered poor approximations for a $2p$ meson and a Pb nucleus (the second Bohr orbit is 12.3×10^{-13} cm compared with $R \sim 7.7 \times 10^{-13}$ cm for Pb), the wave functions published by FITCH and RAINWATER for Pb do yield a form factor only 6 per cent smaller than that predicted by WHEELER.

Because F is a good quantum number, the energy matrix is reducible to submatrices in which F is a constant. When these submatrices are diagonalized, the new eigenfunctions are linear combinations of the functions given in (8); we may write them in the form

$$|\alpha, K; FM\rangle = \sum_{IJ} |IK, j; FM\rangle \langle IK, j; F | \alpha, K; F\rangle, \quad (15)$$

where a designates the other quantum numbers necessary to specify the particular state.

As will be shown in Section V, the only states which are populated with appreciable intensity are those which contain a component having the nucleus in its ground states. The number of these states is given in Table 1.

TABLE 1.

Even-Even Nuclei		Odd Nuclei	
F	No. of levels	F	No. of levels
1/2	2	$I_0 - 3/2$	1 ($I_0 \geq 3/2$)
3/2	3	$I_0 - 1/2$	3
		$I_0 + 1/2$	5
		$I_0 + 3/2$	6

This is to be contrasted with the case of no non-diagonal interactions, where only a single state for each of the listed F -values is populated.

The number of states for each value of F indicates the order of the matrix which must be diagonalized. The procedure for diagonalization is straightforward, but in the case of matrices of order 5 and 6 numerical approximation methods must be used.

The rotational spectra of the simple type (1) represent a limiting case realized for very deformed nuclei. For less deformed nuclei, the excitation spectrum is less regular but, provided the

essential non-diagonal coupling results from the interaction with one or a few low-lying states, its effect can be analyzed in a somewhat similar manner as above. The result will depend on certain matrix elements which represent partly the average quadrupole coupling of the meson with the nucleus in its ground state and excited states, and partly the quadrupole transition elements which are similar to those which determine the electric quadrupole radiative transitions between the states in question. In general, however, one can expect no simple relationship between the various matrix elements such as characterizes the rotational spectrum.

IV. Strong Coupling Approximation.

For sufficiently strong meson-nuclear quadrupole interaction, it is possible to obtain a simple solution to the coupled equations. Such a strong coupling treatment has been developed by BOHR and MOTTELSON (1953) for coupling nucleons to a deformed nucleus, and the methods are applicable also to a meson in the nuclear quadrupole field.

In the strong coupling treatment, one considers the meson as moving relatively to the deformed nucleus, and the appropriate basis vectors are thus given by

$$|K, j\Omega_\mu; FM\rangle_s = \left. \begin{aligned} & \sqrt{\frac{2F+1}{16\pi^2}} [\mathfrak{D}_{MK+\Omega_\mu}^F(\theta_i) \varphi_{\Omega_\mu}^j(\vec{x}', \vec{\sigma}') \\ & + (-1)^{F-j} \mathfrak{D}_{M-(K+\Omega_\mu)}^F(\theta_i) \varphi_{-\Omega_\mu}^j(\vec{x}', \vec{\sigma}')], \end{aligned} \right\} \quad (16)$$

in which the mesonic wave functions are described in terms of coordinates relative to the nuclear symmetry axis. The quantum number Ω_μ represents the component of j along this symmetry axis. The sign of the symmetrization is that appropriate to a meson coupled to an even-even nucleus. For odd-A or odd-odd nuclei, the symmetrization is of no significance in the present context.

The matrix elements of the quadrupole interaction H' (4) become very simple in this representation since H' is equivalent to the interaction of a meson in a fixed quadrupole field (or to

a meson in the field of a nucleus with $I = \infty$). The elements are given by

$$\left. \begin{aligned} \langle K, j\Omega_\mu; F | H' | K', j'\Omega'_\mu; F' \rangle &= -\frac{1}{2} Q_0 e^2 \langle j || f(r) || j' \rangle \\ &\times \frac{\sqrt{4\pi}}{5} (-1)^{j'-\Omega_\mu} (jj'\Omega_\mu - \Omega_\mu | jj' 20) \langle j || Y_\mu^{(2)} || j' \rangle \delta_{FF'} \delta_{KK'} \delta_{\Omega_\mu\Omega'_\mu} \end{aligned} \right\} \quad (17)$$

and are seen to be diagonal in Ω_μ .

The rotational energy of the system possesses non-diagonal as well as diagonal matrix elements in Ω_μ . The diagonal terms are given by (cf. BOHR and MOTTELSON, 1953, Eq. II. 24)

$$(H_{ROT})_0 = \left. \begin{aligned} \frac{\hbar^2}{2\mathfrak{I}} \{ F(F+1) + j(j+1) - I_0(I_0+1) - 2\Omega_\mu(K + \Omega_\mu) \\ - (-1)^{F-j} (j+1/2)(F+1/2) \delta_{\Omega_\mu, \frac{1}{2}} \delta_{K, 0} \} \end{aligned} \right\} \quad (18)$$

The last term in (18), which is to be included only for a meson coupled to an even-even nucleus, arises from symmetrization of the wave function (16), which introduces additional diagonal terms.

The matrix elements of the rotational energy which are non-diagonal in Ω_μ tend to decouple the meson from the nuclear axis, and the strong coupling approximation is the neglect of these terms. This approximation is valid when the rotational energies are small compared with the quadrupole energies (17).

The strong coupling Hamiltonian, $H_0 + (H_{ROT})_0 + H'$, is thus diagonal in Ω_μ as well as in F , K and M , and the eigenfunctions are linear combinations (with respect to j) of functions of the type (16),

$$| \alpha, K, \Omega_\mu; FM \rangle_s = \sum_j | K, j\Omega_\mu; FM \rangle_s \langle K, j\Omega_\mu; F | \alpha, K, \Omega_\mu; F \rangle_s. \quad (19)$$

If we consider the $2p$ states, the sum in (19) for $\Omega_\mu = \pm 3/2$ contains just one state with $j = 3/2$, while for $\Omega_\mu = \pm 1/2$ it contains two states with $j = 1/2$ and $3/2$. Thus, the diagonalization procedure involves at most matrices of order two. It is convenient (e.g. when discussing line intensities) also to express the strong coupling wave functions (19) in the form of the uncoupled representation (15). This transformation is given by

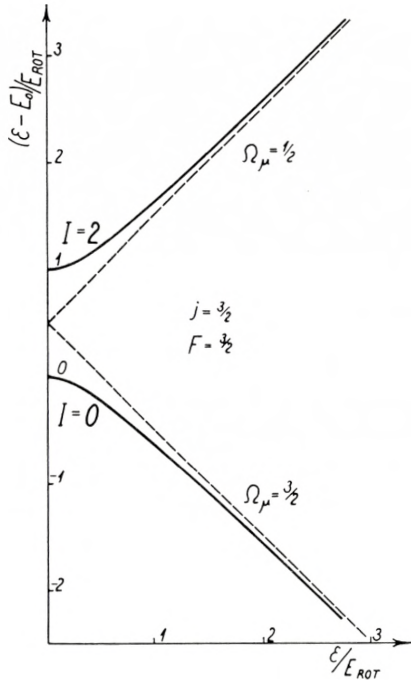


FIGURE 1.

A comparison is made between the energies given by the strong coupling approximation and the "exact" treatment for an even-even nucleus. It is assumed that the meson is in a $2p$ state, and that the fine structure splitting is large (j is a good quantum number), in which case, for the $F = 1/2$ levels and the $F = 3/2$, $j = 1/2$ level, the strong coupling approximation reduces to the exact treatment. The solid curves give the "exact" energies and the dashed curve the strong coupling limit for the levels $F = 3/2$, $j = 3/2$. E_0 is the energy in the absence of quadrupole coupling and E_{ROT} is the excitation energy of the first rotational state ($I = 2$). The quadrupole coupling is expressed in terms of

$$\epsilon = -\frac{1}{10} Q_0 e^2 \langle j || f(r) || j' \rangle.$$

In the region of weak coupling, $(\epsilon/E_{ROT} \ll 1)$, the nuclear spin I is approximately a good quantum number, while in the region of strong coupling $(\epsilon/E_{ROT} \gg 1)$, the component of the meson angular momentum along the nuclear symmetry axis, Ω_μ , is approximately a good quantum number.

$$\left. \begin{aligned} |\alpha, K, \Omega_\mu; FM\rangle_s &= \sum_{Ij} |IK, j; FM\rangle \langle K, j \Omega_\mu; F | \alpha, K, \Omega_\mu; F \rangle_s \\ &\times (IjK \Omega_\mu | Ij FK + \Omega_\mu) \sqrt{\frac{2I+1}{2F+1}} \times \begin{cases} 1 & \text{for odd-}A \text{ or odd-odd nuclei} \\ 0 & \text{for } I \text{ odd} \\ \sqrt{2} & \text{for } I \text{ even} \end{cases} \begin{matrix} \text{even-even} \\ \text{nuclei.} \end{matrix} \end{aligned} \right\} (20)$$

A measure of the error in the energy eigenvalues of the $2p$ levels is given by

$$\delta E \approx \frac{1}{8} \frac{(E_{ROT})^2}{\frac{1}{2} Q_0 e^2 \langle 1/2 \| f(r) \| 3/2 \rangle}, \quad (21)$$

where E_{ROT} is the energy of the first rotational state; the numerical coefficient refers to even-even nuclei. Fig. 1 compares the strong coupling and exact energies for $F = j = 3/2$ levels in an even-even nucleus; the fine structure splittings are assumed to be very large so that j is a good quantum number and thus the three other levels are given exactly in strong coupling.

Although the error in the energy is quadratic in E_{ROT} (cf. Eq. (21)), the error in the wave function is linear in E_{ROT} . Thus, the strong coupling approximation should be used with reservation when wave functions are required (e.g. for line intensities). The exact treatment is always available and offers no fundamental difficulties.

V. Line Intensities.

The question of the X-ray line intensities for the $2p-1s$ mesonic transitions involves an investigation of two points: (1) the relative (rate of) population of the $2p$ levels, and (2) the relative transition probabilities from the $2p$ states to the $1s$ ground states.

The radiative transitions of interest are of the *atomic* electric dipole type. The nuclear transitions, which are $M1$ or $E2$, are several orders of magnitude slower. If I were a good quantum number, we would therefore have the restriction $\Delta I = 0$. When I is not a good quantum number, the electric dipole matrix element vanishes between those components of the wave function for which $I_i \neq I_f$.

The $2p$ states are populated from higher states which interact only weakly with the nuclear quadrupole field and are, therefore, very nearly pure $I = I_0^*$. The populations of the $2p$ states (i. e. summed over M) can be shown to be proportional to

$$(2F+1) \sum_j \langle I_0 K, j; FM | \alpha, K; FM \rangle^2, \quad (22)$$

where the $\langle IK, j; FM | \alpha, K; FM \rangle$ are defined by (15).

* Of these, the $3d$ states are most responsible for feeding the $2p$ states, and also interact the most with the nucleus. Mixing of excited nuclear states becomes appreciable for $n = 3$ only for the nuclei with large deformations beyond Pb , and then may affect the intensities by around 20 per cent. The effect of mixing in the $3d$ states may be included in a straightforward manner.

In the mesonic ground state, $1s_{1/2}$, there is no interaction with the nuclear quadrupole field, and F , I and $j = 1/2$ are all good quantum numbers; the energy depends only upon I . The relative transition probabilities from the $2p$ level $|\alpha, K; F\rangle$ to the ground level with spin I are proportional to

$$\sum_j \langle IK, j; FM | \alpha, K; FM \rangle^2. \quad (23)$$

From (22) and (23), the line intensities can be computed. An atom which finds itself in the ground state, but with $I > I_0$, will emit a nuclear γ -ray. For nuclei with large deformations, the probability for this may be of the order of $1/2$.

What might be called the "center of population" of the $2p$ states is left unchanged by the inclusion of the quadrupole interaction. However, the possibility of making transitions to the atomic ground states with an excited nucleus tends to shift the center of gravity of the spectral lines to smaller energies, and this shift is just given by weighting the nuclear rotational energies with number of transitions to these final states. Such shifts will be less than about 1 per cent of the transition energies.

VI. Numerical Examples.

It is to be noted that the quadrupole moment enters only in the combination $Q_0 \langle j || f(r) || j' \rangle$. In working out numerical examples, we shall select values for this combination which are consistent with other estimates of nuclear quadrupole moments and with the assumptions that the double-far matrix element may be approximated by (14). The fine structure splittings are roughly interpolated from the numerical values of FIRCH and RAINWATER. The other parameters which enter are indicated in the particular cases.

A. *Even-Even Nuclei.* The ground state of an even-even nucleus has $I = 0$ and the first rotational level is $I = 2$, $K = 0$. No higher levels enter for the $2p$ states, and the Hamiltonian is reducible to the submatrices given below.

FIGURES 2.

Energy levels and spectra are given for even-even isotopes. All energies are given in MeV. In each of the three examples are three diagrams which give, beginning at the top,

(I) *2p energy level scheme in the absence of non-diagonal interactions.* The triplet of numbers above each line designates (IjF) , all of which are good quantum numbers when the non-diagonal interactions are neglected. The solid lines represent the levels where the nucleus is in the ground state and give the usual fine structure doublet; these are the only levels which are populated when no "mixing" is present. The dashed lines represent atomic levels in which the first nuclear rotational level ($I = 2$) is excited, and includes diagonal (static) quadrupole interactions. The height of the lines is proportional to the statistical weight $(2F + 1)$. The zero of energy is taken at the "center of gravity" of the fine structure doublet ($I = 0$).

(II) *2p energy level scheme including non-diagonal as well as diagonal quadrupole interactions.* The height of each line is proportional to its population. The only good quantum number which remains after "mixing" is F , which is denoted under each line.

(III) *The line spectrum.* Each of the $2p$ states may make transitions to the atomic ground states, $1s_{1/2}$ with $I = 0$ or 2 . This leads to the ten spectral lines represented by the solid lines. The height of the lines is proportional to the intensity. The dashed lines represent the spectrum which would be observed in the absence of non-diagonal interactions; the zero point of energy is taken at the center of gravity of this doublet. The arrow points to the center of gravity of the actual spectrum.

The values of the parameters represent estimates which contain considerable uncertainty, but are expected to exhibit the salient features of the spectra. The fine structure energies (E_{fs}) are rough extrapolations of the values given by FITCH and RAINWATER. The rotational energies (E_{ROT}) are either experimental values or consistent with the energies of neighbouring isotopes. The quadrupole interaction energy

$$\varepsilon = -\frac{1}{10} Q_0 e^2 \langle j || f(r) || j' \rangle \approx -\frac{1}{2} Q_0 (Z/237)^3 f_q \text{ MeV}$$

is based upon Q_0 consistent with spectroscopic data (from neighbouring odd isotopes), nuclear rotational energies, and Coulomb excitation. The form factor f_q is given by Wheeler's approximation. The actual parameters are given below each example.

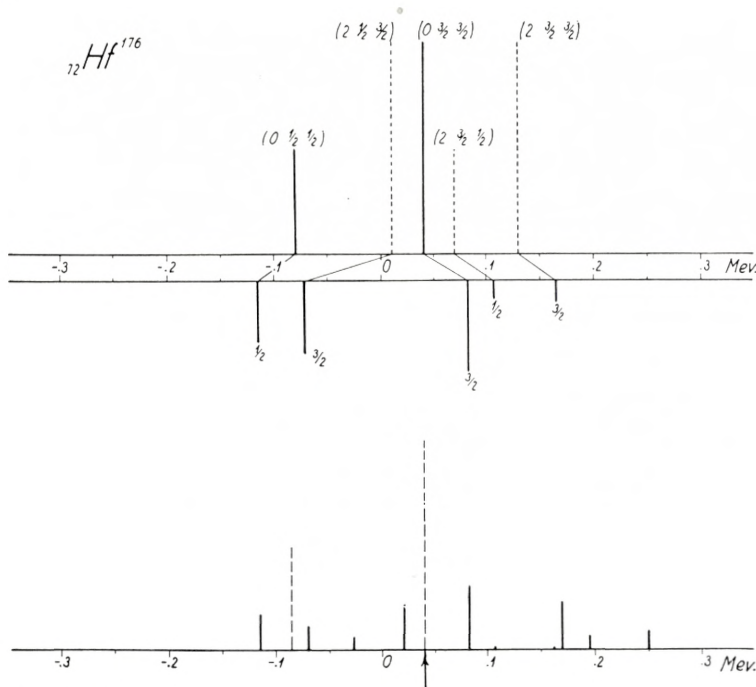


FIG. 2 a, ${}_{72}\text{Hf}^{176}$:

$$\begin{aligned}
 E_{fs} &= 0.119 \text{ MeV}, \\
 E_{ROT} &= 0.089 \text{ MeV}, \\
 \varepsilon &= 0.0579 \text{ MeV} \quad (Q_0 \approx 9 \text{ barns}, f_q \approx 0.457).
 \end{aligned}$$

Probability that the nucleus be left in the state $I = 2$ is 0.47.

$$\left. \begin{pmatrix} H_{11} & \sqrt{2} \varepsilon \\ \sqrt{2} \varepsilon & H_{22} \end{pmatrix} \cdots \begin{matrix} |00, 1/2, 1/2 M\rangle \\ |20, 3/2, 1/2 M\rangle \end{matrix} \right\} \quad (24)$$

and

$$\left. \begin{pmatrix} \bar{H}_{11} & -\varepsilon & \varepsilon \\ -\varepsilon & \bar{H}_{22} & \varepsilon \\ \varepsilon & \varepsilon & \bar{H}_{33} \end{pmatrix} \cdots \begin{matrix} |00, 3/2; 3/2 M\rangle \\ |20, 1/2; 3/2 M\rangle \\ |20, 3/2; 3/2 M\rangle \end{matrix} \right\} \quad (25)$$

where

$$\begin{aligned}
 H_{11} &= H_{00} - \frac{2}{3} E_{fs} \\
 H_{22} &= H_{00} + \frac{1}{3} E_{fs} + E_{ROT} + \varepsilon \\
 \bar{H}_{11} &= H_{00} + \frac{1}{3} E_{fs} \\
 \bar{H}_{22} &= H_{00} - \frac{2}{3} E_{fs} + E_{ROT} \\
 \bar{H}_{33} &= H_{00} + \frac{1}{3} E_{fs} + E_{ROT}
 \end{aligned}$$

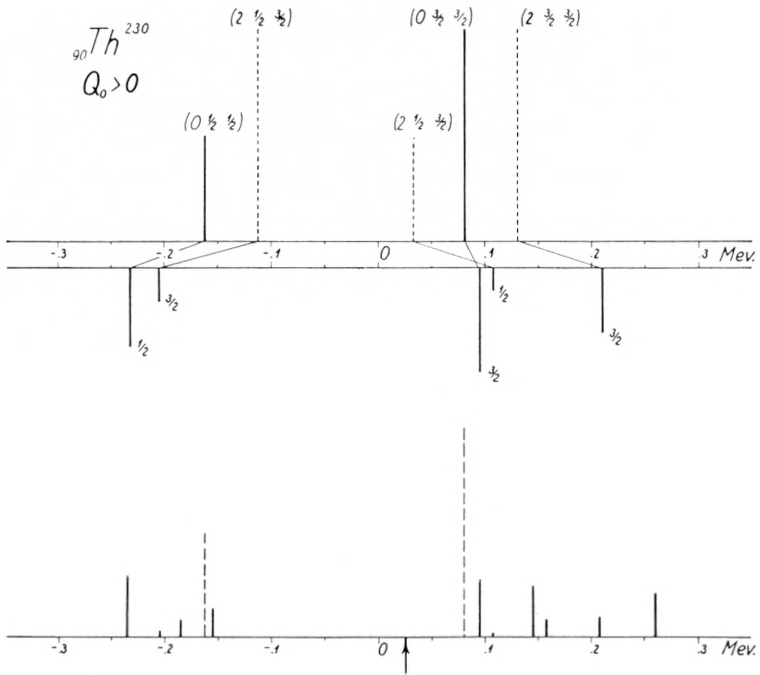


FIG. 2b, ${}_{90}\text{Th}^{230}$, $Q_0 > 0$:

$$\begin{aligned}
 E_{fs} &= 0.242 \text{ MeV}, \\
 E_{ROT} &= 0.050 \text{ MeV}, \\
 \varepsilon &= 0.0986 \text{ MeV} \quad (Q_0 \approx 12.6 \text{ barns}, f_q \approx 0.286).
 \end{aligned}$$

Probability that the nucleus be left in the state $I = 2$ is 0.52.

and $H_{00} =$ "center of gravity" of the unperturbed $2p$ doublet

$$\begin{aligned}
 E_{fs} &= \text{fine structure splitting } 2p_{3/2} - 2p_{1/2} \\
 E_{ROT} &= \text{energy of first rotational nuclear level} \\
 \varepsilon &= -\frac{1}{10} Q_0 e^2 \langle j || f(r) || j' \rangle \approx -\frac{1}{2} Q_0 (Z/237)^3 f_q \text{ MeV}.
 \end{aligned}$$

In Figs. 2, the level structure and line intensities are given for even-even isotopes Hf and Th . The parameters assumed are described in the captions. The spectra are quite different from those which are anticipated without inclusion of the non-diagonal interaction, even if the individual lines are not resolvable. Of particular interest is the way in which the spectra clearly distinguish the sign of the intrinsic quadrupole moment. In the Th example, the negative sign leads to three well-separated groups of lines, the positive sign to two.

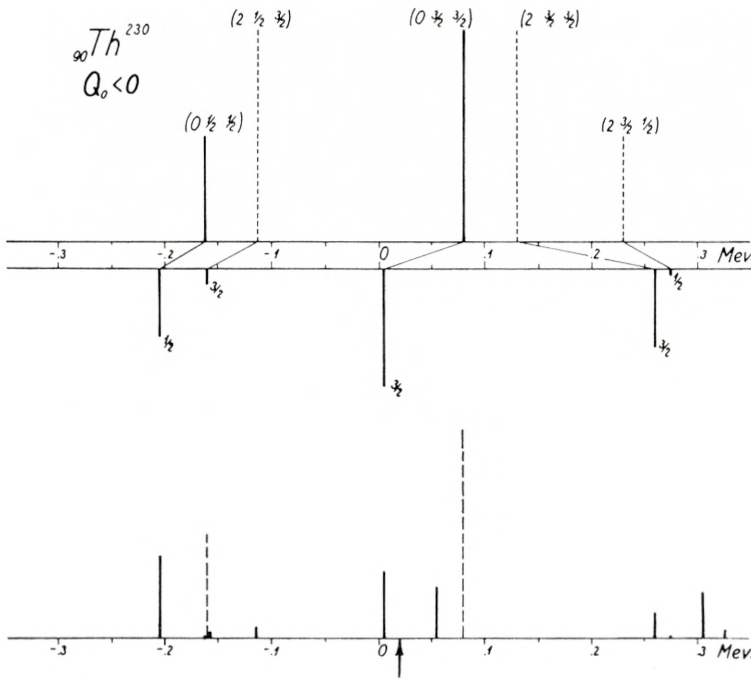


FIG. 2c, ${}_{90}\text{Th}^{230}$, $Q_0 < 0$:

All parameters are the same as for (2b), except that Q_0 and hence ε are negative. Probability that the nucleus be left in the state $I = 2$ is 0.42.

B. Odd Nuclei. As is indicated in Table 1, the odd nuclei will, in general, lead to 15 levels and require, for calculation, the diagonalization of matrices of order up to six. Although this is straightforward, we choose, for the numerical example, to use the strong coupling approximation and select a nucleus for which it is likely to be valid, U^{235} ($I = 5/2$).

Since $H_0 + (H_{ROT})_0 + H'$ is reducible in Ω_μ , the states with $\Omega_\mu = \pm 1/2$ are obtained by diagonalizing the 2×2 matrices

$$\left. \begin{pmatrix} H_{11} & \sqrt{2} \varepsilon \\ \sqrt{2} \varepsilon & H_{22} \end{pmatrix} \dots \begin{matrix} |5/2, 1/2 \pm 1/2; FM\rangle_s \\ |5/2, 3/2 \pm 1/2; FM\rangle_s, \end{matrix} \right\} \quad (26)$$

where

$$H_{11} = H_{00} - \frac{2}{3} E_{fs} + \frac{\hbar^2}{2\mathfrak{I}} \{F(F+1) - 17/2 \mp 5/2\}$$

$$H_{22} = H_{00} + \frac{1}{3} E_{fs} + \varepsilon + \frac{\hbar^2}{2\mathfrak{I}} \{F(F+1) - 11/2 \mp 5/2\}$$

and ε is defined as in expressions (24) and (25).

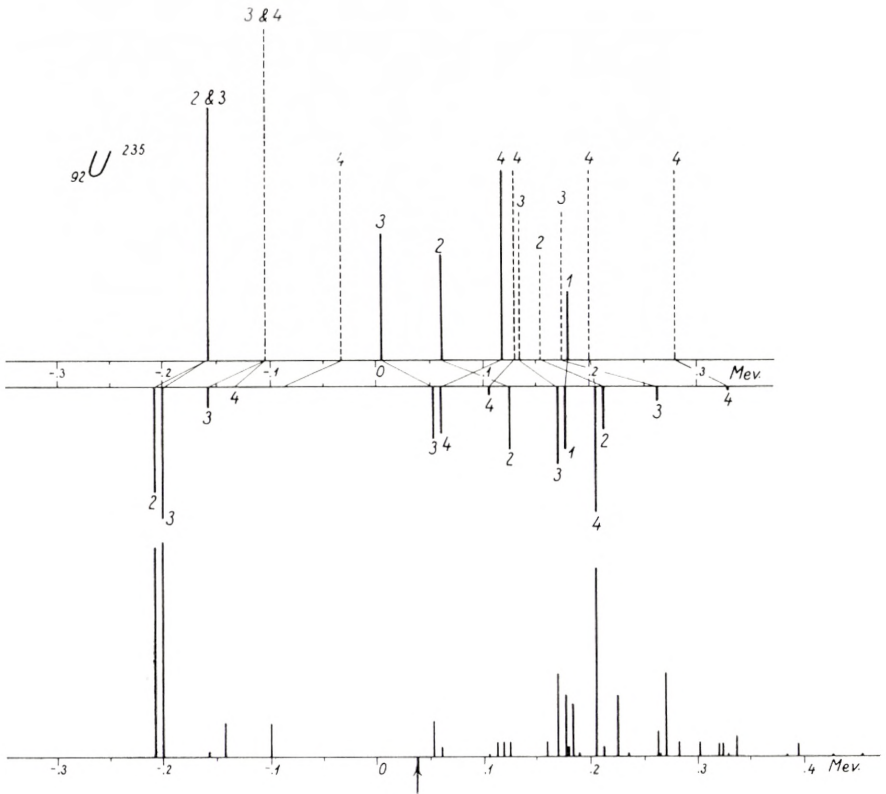


FIGURE 3.

Energy levels and spectrum for the odd isotope ${}_{92}\text{U}^{235}$.

The diagrams are essentially the same as those in Fig. 2 (the triplet of quantum numbers (IjF) is replaced by simply F in the first diagram for reasons of simplicity. The dashed lines in the first diagram represent those states with excited nuclei which can mix with the states which have $I = I_0$. The energies in the first diagram include the diagonal (static) quadrupole interactions, but not the non-diagonal interaction, which are included in the second diagram. The scale for the length of the lines in the spectrum is expanded to twice the scale used in the energy level diagrams. The energies were calculated in the strong coupling approximation, using the same parameters as for ${}_{90}\text{Th}^{230}$, except for the ground state nuclear spin:

$$\begin{aligned}
 E_{fs} &= 0.242 \text{ Mev,} \\
 E_{ROT} &= \frac{0.050}{6} [I(I+1) - I_0(I_0+1)]^{\text{Mev.}}, \quad I_0 = 5/2, \\
 \varepsilon &= 0.0986 \text{ Mev} \quad (Q_0 \approx 2.6 \text{ barns, } f_q \approx 0.286).
 \end{aligned}$$

Probability that the nucleus be left in the state $I = 7/2$ is 0.45, $I = 9/2$ is 0.06, and $I = 11/2$ is 0.02.

The states with $\Omega_\mu = \pm 3/2$ are given simply by

$$\left(H_{00} + \frac{1}{3} E_{fs} - \varepsilon + \frac{\hbar^2}{2\mathfrak{I}} \{ F(F+1) - 17/2 \mp 15/2 \} \right) \cdots |5/2, 3/2 \pm 3/2; FM\rangle_s. \quad (27)$$

In Fig. 3, the level structure and line intensities are given for U^{235} ; the parameters are described in the caption. Perhaps the most striking feature of the spectrum is its complexity. It is to be noted, however, that there appear to be two major components of the spectrum and that the separation of these components is a measure of the interaction.

VI. Conclusions.

For nuclei with large deformations, such as are encountered for $155 < A < 185$ and $A > 225$, the interaction of a μ -meson with the rotational states of a nucleus produces splittings of the $2p$ atomic levels which are comparable in size with the mesonic fine structure splittings. The effect increases the number of lines observed and influences the general pattern of the spectrum even when individual lines are not resolvable. There is a large probability that the nucleus be left in an excited rotational level after the meson reaches the atomic ground state, with the subsequent emission of a nuclear γ -ray.

Experimental studies of these effects yield directly (for nuclei with large deformations) the quantity $Q_0 \langle j || f(r) || j' \rangle$ which is a weighted integral of the quadrupole charge density of the nucleus. This gives information about the magnitude and sign of intrinsic nuclear quadrupole moments and nuclear charge distributions. In particular, it provides a method of determining the sign of the intrinsic quadrupole moments of even-even nuclei, a quantity not available previously from other experiments.

VII. Acknowledgments.

It gives me great pleasure to thank Dr. AAGE BOHR for suggesting this problem. I am grateful to Dr. BOHR, Dr. BEN R. MOTTELSON, and Dr. A. R. EDMONDS for many helpful discussions, suggestions and comments.

I wish to express my appreciation to the National Science Foundation which has made my stay at the Institute for Theoretical Physics possible through the grant of a postdoctoral fellowship, and to Professor NIELS BOHR for extending to me the hospitality of the Institute.

*Institute for Theoretical Physics
Copenhagen, Denmark.*

References.

- L. C. BIEDENHARN (1952), Tables of the Racah Coefficients, U. S. Atomic Energy Commission, ORNL-1098.
- L. C. BIEDENHARN, J. M. BLATT, and M. E. ROSE (1952), *Rev. Mod. Phys.* **25**, 729.
- A. BOHR (1952), *Dan. Mat. Fys. Medd.* **26**, no. 14.
- A. BOHR (1954), Nuclear Rotational States, Dissertation, Copenhagen.
- A. BOHR and B. R. MOTTELSON (1953), *Dan. Mat. Fys. Medd.* **27**, no. 16.
- G. BREIT, G. B. ARFKEN, and W. W. CLENDENIN (1950), *Phys. Rev.* **78**, 390.
- W. Y. CHANG (1949), *Rev. Mod. Phys.* **21**, 166; *Phys. Rev.* **75**, 1315.
- L. N. COOPER and E. M. HENLEY (1953), *Phys. Rev.* **92**, 801.
- V. L. FITCH and J. RAINWATER (1953), *Phys. Rev.* **92**, 789.
- T. HUUS and C. ZUPANČIČ (1953), *Dan. Mat. Fys. Medd.* **28**, no. 1.
- G. RACAH (1942), *Phys. Rev.* **62**, 438.
- A. SIMON, J. H. VAN DER SLUIS, and L. C. BIEDENHARN (1954), Tables of the Racah Coefficients, U. S. Atomic Energy Commission, ORNL-1679.
- F. M. SMITH, W. BIRNBAUM, and W. H. BARKAS (1953), *Phys. Rev.* **91**, 765.
- J. A. WHEELER (1949), *Rev. Mod. Phys.* **21**, 133.
- J. A. WHEELER (1953), *Phys. Rev.* **92**, 812.

Det Kongelige Danske Videnskabernes Selskab

Matematisk-fysiske Meddelelser, bind 29, nr. 4

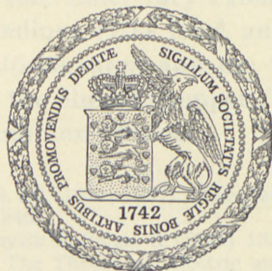
Dan. Mat. Fys. Medd. 29, no. 4 (1954)

STUDIES OF ABSORPTION SPECTRA II

Theory of Copper (II)-Spectra

BY

C. J. BALLHAUSEN



København 1954

i kommission hos Ejnar Munksgaard

Det Kongelige Danske Videnskabs Selskab

Meddelelse fra det kemiske Institut, Band 23, Nr. 4

1927

STUDIES OF ABSORPTION SPECTRA II

Theory of Copper (II) Spectra

C. J. KALLHAUS



Printed in Denmark
Bianco Lunos Bogtrykkeri A-S

Most of the theoretical work concerning the constitution and the magnetic behaviour of the complexes of the transition elements has been done on the basis of Pauling's theory, developed in his famous paper and book.¹ While this theory naturally accounts for the stereochemistry of these as well as for many other chemical compounds, it does not tell anything directly about the very characteristic absorption spectra of complex ions in solution. These features, being connected with the low excited electronic states of the cation, may be described by a perturbation treatment, in which it is investigated how the different states of the ion will split up under the influence of the outer field created by the surrounding radicals, the so-called ligands.

Already in 1929, BETHE² had evaluated the splittings of different orbits due to the influences of various outer fields, and VAN VLECK and his school³ had used this view to account for different properties of crystals. The idea of using this crystal-field theory on complex ions in aqueous solution is due to HARTMANN and ILSE,⁴ who applied it to explain the absorption spectrum of the titanium (III) ion. Later they extended the theory to the spectrum of the vanadium (III) ion,⁵ and in a recent paper⁶ BJERRUM, KLIXBÜLL JÖRGENSEN, and the present author on the same basis discussed the simpler copper (II) complexes, particularly their spectra and constitution.

¹ PAULING, L.: J.A.C.S. **53**, (1931) 1367; "The Nature of the Chemical Bond", Cornell University Press 1940.

² BETHE, H.: Ann. Physik 5 Folge, **3** (1929) 133.

³ VAN VLECK, J. H.: The Theory of Electric and Magnetic Susceptibilities. Oxford 1932.

⁴ HARTMANN, H., and ILSE, F. E.: Z. physik. Chem. **197** (1951) 239.

⁵ HARTMANN, H., and ILSE, F. E.: Z. Naturforschg. **6a**, (1951) 751.

⁶ BJERRUM, J. BALLHAUSEN, C. J., and KLIXBÜLL JÖRGENSEN, C.: Acta Chem. Scand. **8** (1954), 1275.

In the present paper, the detailed calculations underlying the results quoted in ref. 6 are given. It is possible in a very simple way to obtain the formulae determining the absorption spectra of those first transition group elements whose cations have one "effective" d -electron. In general the five-fold degenerate ground electronic level will split up, the splittings determining e. g. the magnetic susceptibility of the complex⁷ as well as the spectrum, which results from transitions between the different levels.

The titanium (III) ion was treated in this way.⁴ The electronic configuration of Ti^{+++} is $1s^2 2s^2 2p^6 3s^2 3p^6 3d^1$, the ion in solution being surrounded by six water molecules arranged octahedrally. The cubic field resulting from the six water dipoles will split the level of the $3d$ electron into two, thus producing one band. The spectra and complexes of the titanium (III) ion are not well-known, however, but all the spectra of the complexes $[Cu(NH_3)_n(H_2O)_{N-n}]^{++}$ have been reported.⁸ (N is the coordination number, and n takes the integral values 0 to N). As the electronic configuration of the cupric ion is $1s^2 2s^2 2p^6 3s^2 3p^6 3d^9$ we can use the so-called hole formalism,⁹ a description of missing electrons stating that for most purposes the holes in a shell behave as positive electrons. This is equivalent to the well-known rule that the number and type of terms are the same, e. g. for the atomic configurations d^n and d^{10-n} . We shall therefore treat the copper (II) ion as having one $3d$ positron besides the closed zinc (II) ion configuration.

We consider a cupric ion surrounded by N ligands, and as the models of the complexes the following configurations are used: the square-planar, the tetrahedral, the square-pyramidal and the octahedral configuration (Fig. 1). The choice of these particular models follows from considerations given in ref. 6. We shall first treat the octahedral configuration, as the square planar and square pyramidal configurations are included in this calculation.

We neglect the spin-orbit interaction since it is weak as compared with the ligand field, and as the unperturbed eigenfunctions for the $3d$ positron we take the hydrogen-like wave functions:

⁷ PENNEY, W. G., and SCHLAPP, R.: Phys. Rev. **42** (1932) 666.

⁸ BJERRUM, J.: Dan. Mat. Fys. Medd. **11** (1932) no. 10. *ibid.* **12** (1934) no. 15.

⁹ CORSON, E. M.: Perturbation Methods in Quantum Mechanics. (Blackie & Son 1951.)

$$\left. \begin{aligned} \psi_0 &= R \bar{Y}_2^0(\theta, \varphi) \\ \psi_1 &= R \bar{Y}_2^1(\theta, \varphi) \\ \psi_{-1} &= R \bar{Y}_2^{-1}(\theta, \varphi) \\ \psi_2 &= R \bar{Y}_2^2(\theta, \varphi) \\ \psi_{-2} &= R \bar{Y}_2^{-2}(\theta, \varphi) \end{aligned} \right\} \quad (1)$$

Here $\bar{Y}_n^m(\theta, \varphi)$ are the surface spherical harmonics normalized to unity, defined by $\bar{Y}_n^m = \bar{P}_n^m(\cos \theta) \frac{e^{im\varphi}}{\sqrt{2\pi}}$, $\bar{P}_n^m(\cos \theta)$ are the associated Legendre polynomials normalized to unity, R is the function $R = \sqrt{\frac{8}{45}} \left(\frac{Z}{3a_0}\right)^{3/2} r^2 e^{-\frac{Z}{3a_0}r}$, also normalized to unity, a_0 is the Bohr radius, and Z is the effective charge on the nucleus. We are especially interested in the first-order perturbations resulting from dipoles, but this result is most easily obtained after the calculation of the perturbations resulting from charges $-q$ placed on the sites of the dipoles has been performed.

The Hamiltonian operator becomes:

$$\mathbf{H} = -\frac{\hbar^2}{2m} \nabla^2 + \frac{Ze^2}{r} - e^2 \left(\frac{q_1}{r_1} + \frac{q_2}{r_2} + \frac{q_3}{r_3} + \frac{q_4}{r_4} + \frac{q_5}{r_5} + \frac{q_6}{r_6} \right)$$

or in terms of atomic units (used in this paper) we have for the perturbation term:

$$\mathbf{H}^{(1)} = -\left(\frac{q_1}{r_1} + \frac{q_2}{r_2} + \frac{q_3}{r_3} + \frac{q_4}{r_4} + \frac{q_5}{r_5} + \frac{q_6}{r_6} \right)$$

This quantity can be expanded in terms of the surface spherical harmonic as

$$\left. \begin{aligned} \mathbf{H}^{(1)} &= -\sum_{n=0}^{\infty} \sum_{m=-n}^n \sum_{N=1}^4 q_N \frac{4\pi}{2n+1} \cdot \frac{r_{<}^n}{r_{>}^{n+1}} \bar{Y}_n^m \left(\bar{Y}_n^m \left(\frac{\pi}{2}, N \right) \right)^* \\ &\quad - (q_5 + q_6) \sum_{n=0}^{\infty} \frac{r_{<}^n}{r_{>}^{n+1}} \sqrt{\frac{4\pi}{2n+1}} \bar{Y}_n^0 \end{aligned} \right\} \quad (2)$$

(A proof of this is given in ref. 10.) The first term in (2) is due to the charges in the plane, the second to the two charges placed

¹⁰ EYRING, H., WALTER, J., and KIMBALL, G. E.: Quantum Chemistry. (John Wiley & Sons 1944.)

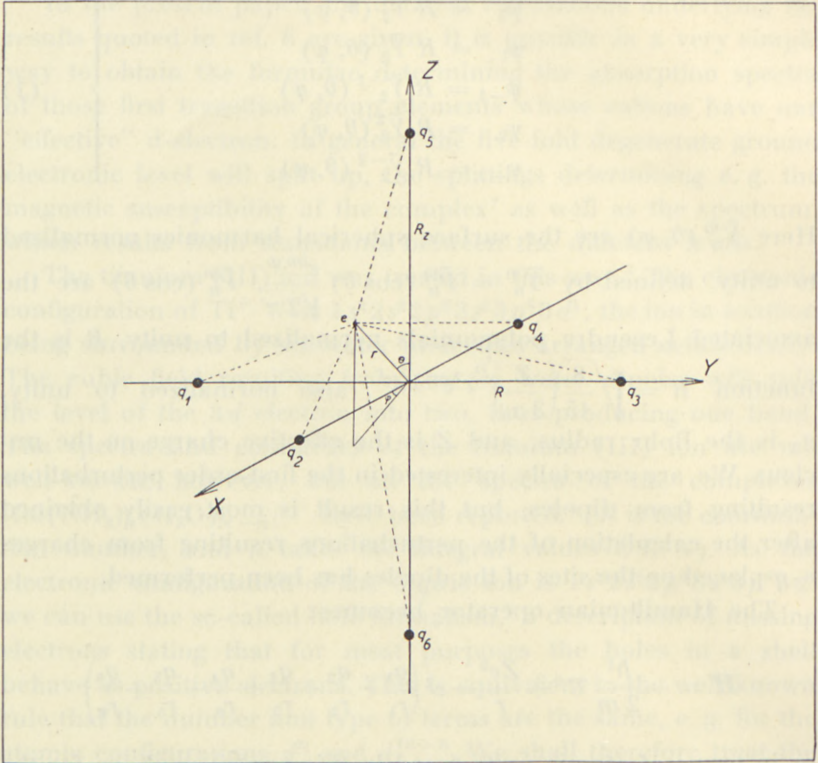


Fig. 1. Model of various types of configurations. The positions labelled 1—4 represent the square, 1—5 the square pyramid, and 1—6 the octahedron (or tetragonal bipyramid). Distances $r_1 - r_6$ from the ligands to the electron. Dipoles $\mu_1 - \mu_6$, and charges $q_1 - q_6$.

on the Z -axis. First we shall treat the perturbations due to the first term and obtain e. g. for $q_1 \neq q_2$ and $q_2 = q_3 = q_4$

$$\begin{aligned}
 \mathbf{H}^{(1)} = & -q_1 \sum_{n=0}^{\infty} \sum_{m=-n}^n \frac{4\pi}{2n+1} \frac{r_{<}^n}{r_{>}^{n+1}} \bar{Y}_n^m \bar{Y}_n^{*m} \left(\frac{\pi}{2}, 0 \right) \\
 & -q_2 \sum_0^{\infty} \sum_{-n}^n \frac{4\pi}{2n+1} \frac{r_{<}^n}{r_{>}^{n+1}} \bar{Y}_n^m \bar{Y}_n^{*m} \left(\frac{\pi}{2}, \frac{\pi}{2} \right) \\
 & -q_2 \sum_0^{\infty} \sum_{-n}^n \frac{4\pi}{2n+1} \frac{r_{<}^n}{r_{>}^{n+1}} \bar{Y}_n^m \bar{Y}_n^{*m} \left(\frac{\pi}{2}, \pi \right) \\
 & -q_2 \sum_0^{\infty} \sum_0^n \frac{4\pi}{2n+1} \frac{r_{<}^n}{r_{>}^{n+1}} \bar{Y}_n^m \bar{Y}_n^{*m} \left(\frac{\pi}{2}, \frac{3\pi}{2} \right).
 \end{aligned}$$

Remembering that $\bar{Y}_n^m(\theta, \varphi) = e^{im\varphi} \bar{Y}_n^m(\varphi, 0)$ and $(\bar{Y}_n^m)^* = (-1)^m \bar{Y}_n^{-m}$ we have:

$$\mathbf{H}^{(1)} = -[q_1 + g(m)q_2] \sum_0^\infty \sum_{-n}^n \frac{4\pi}{2n+1} \frac{r_{<}^n}{r_{>}^{n+1}} \bar{Y}_n^m \bar{Y}_n^{*m} \left(\frac{\pi}{2}, 0 \right)$$

or

$$\mathbf{H}^{(1)} = -[q_1 + g(m)q_2] \frac{1}{\sqrt{2\pi}} \sum_0^\infty \sum_{-n}^n \frac{4\pi}{2n+1} \frac{r_{<}^n}{r_{>}^{n+1}} \bar{Y}_n^m \bar{P}_n^m(0),$$

where $g(m) = 3$ for $m = 0$ and ± 4
 $g(m) = -1$ for $m = \pm 1, \pm 2, \pm 3$.

In the general case we have for the first term in (2):

$$\mathbf{H}^{(1)} = -D(m, q) \frac{1}{\sqrt{2\pi}} \sum_{n=0}^\infty \sum_{m=-n}^n \frac{4\pi}{2n+1} \frac{r_{<}^n}{r_{>}^{n+1}} \bar{Y}_n^m(\theta, \varphi) \bar{P}_n^m(0) \quad (3)$$

in which expression $D(m) = q_1 \cdot f(m) + q_2 \cdot g(m)$.

The different terms $H_{NN'}^{(1)} = \int \psi_N \mathbf{H}^{(1)} \psi_{N'}^* d\tau$, must now be evaluated in order to get the secular equation.

We get

$$\left. \begin{aligned} \mathbf{H}_{NN'}^{(1)} &= \int R^2 \bar{Y}_2^{m'} (\bar{Y}_2^{m''})^* \mathbf{H}^{(1)} d\tau \\ &= \int R^2 [A \bar{Y}_4^m + B \bar{Y}_2^m + C \bar{Y}_0^m] \mathbf{H}^{(1)} d\tau, \end{aligned} \right\} \quad (4)$$

where

$$m = m' - m'',$$

and A, B and C are constants, related to the Wigner coefficients. (See CONDON and SHORTLEY¹¹ for the nomenclature and formulae of the Wigner coefficients.) The values of A, B and C are

$$A = \int \bar{Y}_2^{m'} (Y_4^m)^* (\bar{Y}_2^{m''})^* d\Omega = (-1)^{m''} \sqrt{\frac{5}{14\pi}} (22m' - m'' | 224m)$$

$$B = \int \bar{Y}_2^{m'} (\bar{Y}_2^m)^* (\bar{Y}_2^{m''})^* d\Omega = (-1)^{m''} \left(-\sqrt{\frac{5}{14\pi}} \right) (22m' - m'' | 222m)$$

$$C = \int \bar{Y}_2^{m'} (\bar{Y}_0^m)^* (\bar{Y}_2^{m''})^* d\Omega = (-1)^{m''} \sqrt{\frac{5}{4\pi}} (22m' - m'' | 2200).$$

¹¹ CONDON, E. U., and SHORTLEY, G. H.: The Theory of Atomic Spectra, p. 73. (Cambridge 1953).

Further we have:

$$\left. \begin{aligned} \int \bar{Y}_n^m (\bar{Y}_{n'}^{m'})^* d\Omega &= \delta_{nn'} \delta_{mm'} \\ \delta_{nn'} &= \begin{cases} 0 & \text{for } n \neq n' \\ 1 & \text{for } n = n' \end{cases} \quad \delta_{mm'} = \begin{cases} 0 & \text{for } m \neq m' \\ 1 & \text{for } m = m' \end{cases} \end{aligned} \right\} \quad (5)$$

Now, from this it is seen that in

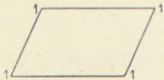
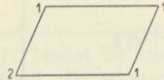
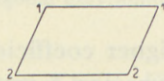
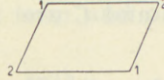
$$H_{NN'}^{(1)} = -D(m, q) \frac{1}{\sqrt{2\pi}} \int R^2 (A\bar{Y}_4^m + B\bar{Y}_2^m + C\bar{Y}_0^m) \sum_0^{\infty} \sum_{-n}^n \frac{4\pi}{2n+1} \frac{r_{>}^n}{r_{>}^{n+1}} \bar{Y}_n^m \bar{P}_n^m(0) dt$$

n can only be 4, 2 and 0 if $H_{NN'}^{(1)} \neq 0$.

As $\bar{P}_n^m = 0$ for $|m| = n - 1, n - 3, n - 5 \dots$ it also follows that $|m| = 0, 2, 4$.

The following table gives the values of $D(m)$ for different m :

TABLE 1.

Configuration	$ m $	$D(m, q)$
	0 and 4	$4 q_1$
	2	0
	0 and 4	$3 q_1 + q_2$
	2	$-q_1 + q_2$
	0 and 4	$2 q_1 + 2 q_2$
	2	0
	0 and 4	$2 q_1 + 2 q_2$
	2	$-2 q_1 + 2 q_2$

The secular equation is then:

$$\begin{vmatrix} H_{-2-2}^{(1)} - E^{(1)} & 0 & H_{20}^{(1)} & 0 & H_{-22}^{(1)} \\ 0 & H_{-1-1}^{(1)} - E^{(1)} & 0 & H_{-11}^{(1)} & 0 \\ H_{0-2}^{(1)} & 0 & H_{00}^{(1)} - E^{(1)} & 0 & H_{02}^{(1)} \\ 0 & H_{1-1}^{(1)} & 0 & H_{11}^{(1)} - E^{(1)} & 0 \\ H_{2-2}^{(1)} & 0 & H_{20}^{(1)} & 0 & H_{22}^{(1)} - E^{(1)} \end{vmatrix} = 0 \quad (6)$$

From the definition of $(\bar{Y}_n^m)^* = (-1)^m \bar{Y}_m^{-m}$ it is seen that when the indices are even

$$H_{NN'}^{(1)} = H_{-N-N'}^{(1)} \text{ and } H_{N-M}^{(1)} = H_{-NM}^{(1)} = H_{-MN}^{(1)}.$$

Using these relations, and by applying row and column additions and subtractions, it is possible to reduce the determinant to a diagonal form with the solutions

$$\left. \begin{aligned} E^{(1)} &= H_{11}^{(1)} + H_{1-1}^{(1)} \\ E^{(1)} &= H_{11}^{(1)} - H_{1-1}^{(1)} \\ E^{(1)} &= H_{22}^{(1)} - H_{2-2}^{(1)} \\ (E^{(1)})^2 - (H_{2-2}^{(1)} + H_{22}^{(1)} + H_{00}^{(1)})E^{(1)} + (H_{00}^{(1)}H_{2-2}^{(1)} + H_{00}^{(1)}H_{22}^{(1)} - 2(H_{20}^{(1)})^2) &= 0. \end{aligned} \right\} (7)$$

If we now look at the second term of (2), it is seen that for this term $m = 0$. This means that after (5) only the diagonal terms in (6) are affected, and we have in general

$$H_{NN'}^{(1)} = - \int R^2 (A \bar{Y}_n^m + B \bar{Y}_2^m + C \bar{Y}_0^m) \left[\frac{D(m, q)}{\sqrt{2\pi}} \sum_0^\infty \sum_{-n}^n \frac{4\pi}{2n+1} \frac{r_{>}^n}{r_{>}^{n+1}} \bar{Y}_n^m \bar{P}_n^m(0) \right. \\ \left. + (q_5 + q_6) \sum_0^\infty \frac{r_{>}^n}{r_{>}^{n+1}} \sqrt{\frac{4\pi}{2n+1}} \bar{Y}_n^0 \right] d\tau.$$

The evaluation of $H_{NN'}^{(1)}$, is now simple, the results being for ion-ion complexes: (the values of the G 's are determined individually by corresponding sets of R and q)

$$\left. \begin{aligned} H_{00}^{(1)} &= -D(0, q) \frac{8}{45} f \left[G_0 - \frac{1}{7} G_2 + \frac{3}{38} G_4 \right] \\ &\quad - \frac{8}{45} f(q_5 + q_6) \left[G_0 + \frac{2}{7} G_2 + \frac{2}{7} G_4 \right] \\ H_{11}^{(1)} &= -D(0, q) \frac{8}{45} f \left[G_0 - \frac{1}{14} G_2 - \frac{1}{14} G_4 \right] \\ &\quad - \frac{8}{45} f(q_5 + q_6) \left[G_0 + \frac{1}{7} G_2 - \frac{4}{21} G_4 \right] \\ H_{22}^{(1)} &= -D(0, q) \frac{8}{45} f \left[G_0 + \frac{1}{7} G_2 + \frac{1}{56} G_4 \right] \\ &\quad - \frac{8}{45} f(q_5 + q_6) \left[G_0 - \frac{2}{7} G_2 + \frac{1}{21} G_4 \right] \end{aligned} \right\} (8)$$

$$\left. \begin{aligned} H_{20}^{(1)} &= -D(2, q) \frac{8}{45} f \left[-\frac{5}{28\sqrt{6}} G_4 - \frac{3}{7\sqrt{6}} G_2 \right] \\ H_{2-2}^{(1)} &= -D(4, q) \frac{8}{45} f \frac{5}{24} G_4 \\ H_{1-1}^{(1)} &= -D(2, q) \frac{8}{45} f \left[\frac{5}{42} G_4 - \frac{3}{14} G_2 \right], \end{aligned} \right\} \quad (8)$$

where

$$G_n = \int_0^R f^6 r^6 e^{-2fr} \frac{r^n}{R^{n+1}} dr + \int_R^\infty f^6 r^6 e^{-2fr} \frac{R^n}{r^{n+1}} dr$$

and $f = \frac{Z}{3}$, using the nomenclature of Hartmann and Ilse.

Evaluating these integrals, we get

$$\begin{aligned} G_0 &= \frac{45}{8x} - \left(\frac{45}{8x} + \frac{75}{8} + \frac{15}{2}x + \frac{15}{4}x^2 + \frac{5}{4}x^3 + \frac{1}{4}x^4 \right) e^{-2x} \\ G_2 &= \frac{315}{4x^3} - \left(\frac{315}{4x^3} + \frac{315}{2x^2} + \frac{315}{2x} + 105 + \frac{105}{2}x + \frac{165}{8}x^2 + \frac{25}{4}x^3 + \frac{5}{4}x^4 \right) e^{-2x} \\ G_4 &= \frac{14175}{8x^5} - \left(\frac{14175}{8x^5} + \frac{14175}{4x^4} + \frac{14175}{4x^3} + \frac{4725}{2x^2} + \frac{4725}{4x} + \frac{945}{2} + \frac{315}{2}x \right. \\ &\quad \left. + 45x^2 + \frac{45}{4}x^3 + \frac{9}{4}x^4 \right) e^{-2x} \end{aligned}$$

when $x = fR$.

A few values of G_2 and G_4 are tabulated in Table 2.

TABLE 2.
Values of radial functions.

$x = fR$	G_2	G_4
7	0.2241	0.09533
8	0.1527	0.05200
9	0.1080	0.02960
10	0.0788	0.01772
11	0.0592	0.01100
12	0.0456	0.00712

$$x = \frac{Z}{3} \cdot R = fR \quad (R \text{ in a. u.})$$

For numerical calculations on copper (II) complexes Z is taken as 7.85 (cf. SLATER, Phys. Rev., 36, (1930) 57.)

With the help of Table 1, (7) and (8) we can now estimate the maxima of the absorption spectra of a cation — anion complex.

The ions CuCl_4^{--} and CuBr_4^{--} are of this type, even if according to the discussion in ref. 6, one might predict the composition to be $[\text{CuCl}_4(\text{H}_2\text{O})_2]^{--}$ in aqueous solution. It is not easy, however, to estimate the values of the parameters in the formula for the absorption of this complex, since the perturbation is due both to the charge of the halide ion and the induced dipole moment of the latter, caused by the influence of the cupric ion.

Both the chloro- and bromo-complexes have an absorption in the infrared. Now the distance $\text{Cu}^{++} - \text{Br}^-$ must be greater than the distance $\text{Cu}^{++} - \text{Cl}^-$, which means that the perturbation is smaller in the bromo-complex, and the absorption maximum is thus displaced towards the red in accordance with observation of the infrared band. (From $\lambda = 960 \text{ m}\mu$ in 13 M. HCl to $\lambda = 1100 \text{ m}\mu$ in 9 M. HBr.)

However, CuCl_4^{--} also has a very strong absorption in the ultraviolet passing into the violet, and the solution is therefore yellow.¹² CuBr_4^{--} has an absorption in the blue, passing into the infrared band; the solution is therefore red.

Thus the situation is more complicated than the simple description indicated before. There must be electron exchange between the anion and the cation of these complexes as the non-existence of copper (II) iodide seems to suggest.¹³ The strong absorption in the ultraviolet and visible regions may therefore be electron transfer spectra due to this exchange.

The spectra of the dipole — cation complexes are more interesting from the standpoint of this theory, since they have no absorption in the near ultraviolet. The absorption maxima for such complexes can be found in the following way:

We place a charge $-q$ at a distance R and a charge $+q$ at a distance $R + \Delta R$ from the cupric ion. As $\Delta X = f\Delta R$

$$\begin{aligned} H_{NN'}^{(1)} &= -D(m, q) \frac{8}{45} f \left[\sum_s K_s G_s(x) - \sum_s K_s G_s(x + \Delta x) \right] \\ &= D(m, q) \frac{8}{45} f \Delta x \sum_s K_s \frac{dG_s}{dx} = D(m, \mu) \frac{8}{45} f^2 \sum_s K_s B_s, \end{aligned}$$

¹² BJERRUM, J.: Dan. Mat. Fys. Medd. **22** (1946) no. 18.

¹³ FAJANS, K.: Naturwiss. **11** (1923) 165.

where μ is the point dipole equal to $eq\Delta R$. Then

$$\left. \begin{aligned} H_{00}^{(1)} &= D(0, \mu) \frac{8}{45} f^2 \left[B_0 - \frac{1}{7} B_2 + \frac{3}{28} B_4 \right] \\ &\quad + \frac{8}{45} f^2 (\mu_5 + \mu_6) \left[B_0 + \frac{2}{7} B_2 + \frac{2}{7} B_4 \right] \\ H_{11}^{(1)} &= D(0, \mu) \frac{8}{45} f^2 \left[B_0 - \frac{1}{14} B_2 - \frac{1}{14} B_4 \right] \\ &\quad + \frac{8}{45} f^2 (\mu_5 + \mu_6) \left[B_0 + \frac{1}{7} B_2 - \frac{4}{21} B_4 \right] \\ H_{22}^{(1)} &= D(0, \mu) \frac{8}{45} f^2 \left[B_0 + \frac{1}{7} B_2 + \frac{1}{56} B_4 \right] \\ &\quad + \frac{8}{45} f^2 (\mu_5 + \mu_6) \left[B_0 - \frac{2}{7} B_2 + \frac{1}{21} B_4 \right] \\ H_{20}^{(1)} &= D(2, \mu) \frac{8}{45} f^2 \left[-\frac{5}{28\sqrt{6}} B_4 - \frac{3}{7\sqrt{6}} B_2 \right] \\ H_{2-2}^{(1)} &= D(4, \mu) \frac{8}{45} f^2 \frac{5}{24} B_4 \\ H_{1-1}^{(1)} &= D(2, \mu) \frac{8}{45} f^2 \left[\frac{5}{42} B_4 - \frac{3}{14} B_2 \right] \end{aligned} \right\} (9)$$

q_1 and q_2 in the formula for $D(m)$ are altered to μ_1 and μ_2 , the values of the B 's are determined by corresponding sets of R and μ , and the functions used are:

$$\begin{aligned} \frac{dG_n}{dx} &= B_n \\ B_0 &= -\frac{45}{8x^2} \left[+\frac{45}{8x^2} + \frac{45}{4x} + \frac{45}{4} + 6x + \frac{15}{4}x^2 + \frac{3}{2}x^3 + \frac{1}{2}x^4 \right] e^{-2x} \\ B_2 &= -\frac{945}{4x^4} + \left[\frac{945}{4x^4} + \frac{945}{2x^3} + \frac{945}{2x^2} + \frac{315}{x} + \frac{315}{2} + \frac{255}{2}x + \frac{90}{4}x^2 \right. \\ &\quad \left. + \frac{15}{2}x^3 + \frac{5}{2}x^4 \right] e^{-2x} \\ B_4 &= -\frac{70875}{8x^6} + \left[\frac{70875}{8x^6} + \frac{70875}{4x^5} + \frac{70875}{4x^4} + \frac{23625}{2x^3} + \frac{23625}{4x^2} \right. \\ &\quad \left. + \frac{4725}{2x} + \frac{1575}{2} + 225x + \frac{225}{4}x^2 + \frac{27}{2}x^3 + \frac{9}{2}x^4 \right] e^{-2x} \end{aligned}$$

The functions are tabulated in Table 3. A graphical representation is given in Fig. 2.

TABLE 3.
Values of derived radial functions.

$x = fR$	$-B_0$	$-B_2$	$-B_4$
3.0	0.2213	0.1054	0.0500
3.5	0.2527	0.2118	0.1619
4.0	0.2414	0.2489	0.2050
4.5	0.2203	0.2420	0.2012
5.0	0.1957	0.2136	0.1740
6.0	0.1491	0.1437	0.1067
7.0	0.1132	0.08980	0.05779
8.0	0.08754	0.05585	0.03022
9.0	0.06937	0.03563	0.01596
10.0	0.05625	0.02356	0.008859
11.0	0.04649	0.01614	0.005001
12.0	0.03906	0.01139	0.002967
13.0	0.03328	0.008272	0.001836
14.0	0.02868	0.006152	0.001177

With the aid of Table 1, (7), and (9), we are able to calculate the maximum of absorption for various types of ammine-cupric ions.

First, the square planar configuration, equal distances R and equal dipole moments: (The Γ notation is the notation of Bethe²)

$$\left. \begin{aligned} E(\Gamma_{3(t1)}) &= \mu f^2 \frac{8}{45} \left[4 B_0 - \frac{4}{7} B_2 + \frac{3}{7} B_4 \right] && \text{1-fold degenerate.} \\ E(\Gamma_{3(t3)}) &= \mu f^2 \frac{8}{45} \left[4 B_0 + \frac{4}{7} B_2 + \frac{19}{21} B_4 \right] && \text{1-fold degenerate.} \\ E(\Gamma_{5(t4)}) &= \mu f^2 \frac{8}{45} \left[4 B_0 + \frac{4}{7} B_2 - \frac{16}{21} B_4 \right] && \text{1-fold degenerate.} \\ E(\Gamma_{5(t5)}) &= \mu f^2 \frac{8}{45} \left[4 B_0 - \frac{2}{7} B_2 - \frac{2}{7} B_4 \right] && \text{2-fold degenerate.} \end{aligned} \right\} (10)$$

Next, the square pyramidal ($\alpha = 1$) and the distorted octahedron ($\alpha = 2$). R and μ the same in the plane, and perpendicular to the plane one or two dipoles μ_z at a distance R_z : (also here corresponding μ and R are to be taken together):

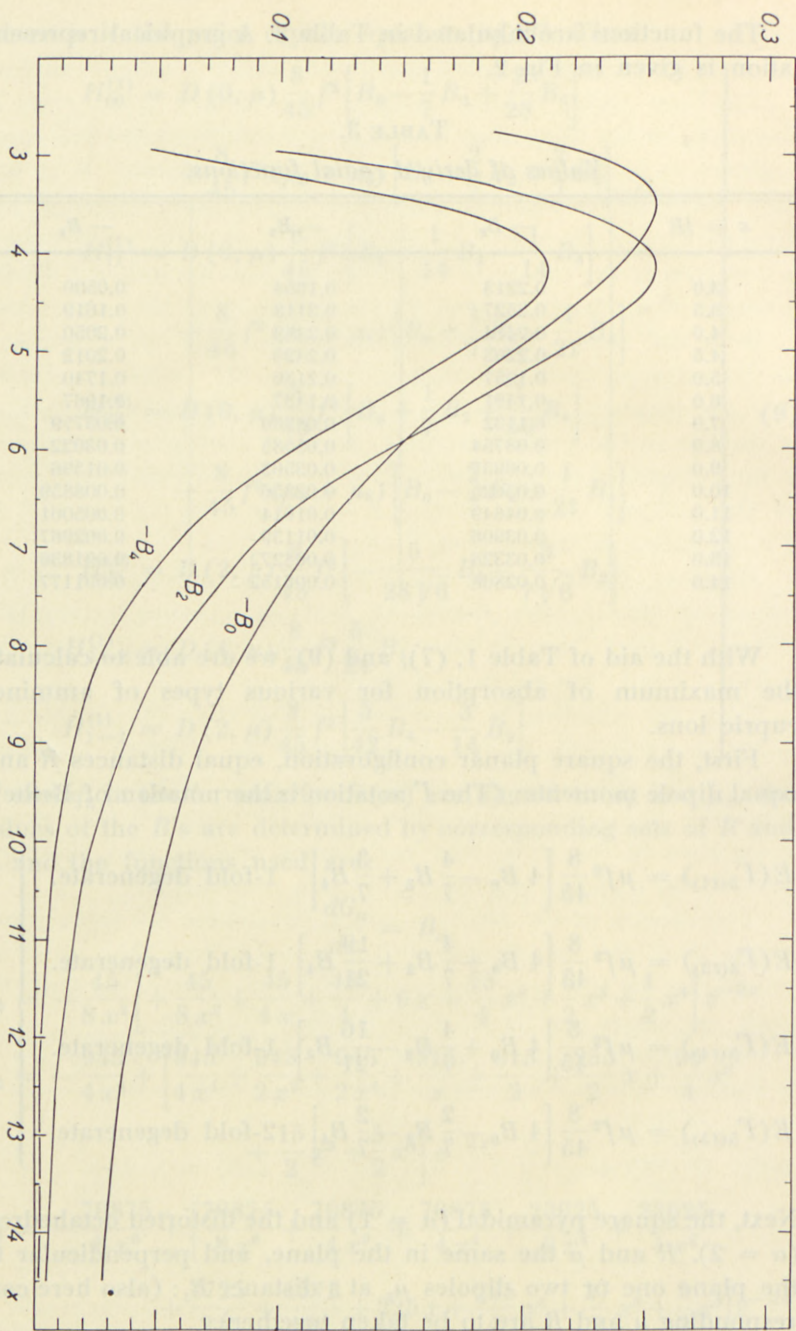


Fig. 2. Graphical representation of $-B_0$, $-B_2$ and $-B_4$ $x = r/R$ a. u.

$$\left. \begin{aligned}
 E(\Gamma_{3(t1)}) &= \mu f^2 \frac{8}{45} \left[4 B_0 - \frac{4}{7} B_2 + \frac{3}{7} B_4 \right] + \mu_z f^2 \frac{8}{45} \alpha \left[B_0 + \frac{2}{7} B_2 + \frac{2}{7} B_4 \right] \\
 E(\Gamma_{3(t3)}) &= \mu f^2 \frac{8}{45} \left[4 B_0 + \frac{4}{7} B_2 + \frac{19}{21} B_4 \right] + \mu_z f^2 \frac{8}{45} \alpha \left[B_0 - \frac{2}{7} B_2 + \frac{1}{21} B_4 \right] \\
 E(\Gamma_{5(t4)}) &= \mu f^2 \frac{8}{45} \left[4 B_0 + \frac{4}{7} B_2 - \frac{16}{21} B_4 \right] + \mu_z f^2 \frac{8}{45} \alpha \left[B_0 - \frac{2}{7} B_2 + \frac{1}{21} B_4 \right] \\
 E(\Gamma_{5(t5)}) &= \mu f^2 \frac{8}{45} \left[4 B_0 - \frac{2}{7} B_2 - \frac{2}{7} B_4 \right] + \mu_z f^2 \frac{8}{45} \alpha \left[B_0 + \frac{1}{7} B_2 - \frac{4}{21} B_4 \right]
 \end{aligned} \right\} (11)$$

The configuration of $\text{Cu}(\text{H}_2\text{O})_6^{++}$ is shown in ref. 6 to be a distorted octahedron. For this complex $\Gamma_{t3} < \Gamma_{t1} < \Gamma_{t4} < \Gamma_{t5}$.

If $\mu = \mu_z$ and $R = R_z$ (the regular octahedron) we obtain:¹⁴

$$\left. \begin{aligned}
 E(\Gamma_3) &= \frac{8}{45} f^2 \mu [6 B_0 + B_4] \quad \text{2-fold degenerate.} \\
 E(\Gamma_5) &= \frac{8}{45} f^2 \mu \left[6 B_0 - \frac{2}{3} B_4 \right] \quad \text{3-fold degenerate.} \\
 \Delta E &= \frac{8}{27} f^2 \mu B_4 \qquad E(\Gamma_5) > E(\Gamma_3)
 \end{aligned} \right\} (12)$$

It is seen that the distorted octahedral configuration will give three bands, the frequency of the maxima of the bands given

by: $h\nu_n = \Gamma_{t3} \rightarrow \begin{cases} \Gamma_{t5} \\ \Gamma_{t4} \\ \Gamma_{t1} \end{cases}$ if we look at $\text{Cu}(\text{H}_2\text{O})_6^{++}$. For the first

two bands in this complex we shall have:

$$\frac{\nu_1}{\nu_2} = \frac{E(\Gamma_{t5}) - E(\Gamma_{t3})}{E(\Gamma_{t4}) - E(\Gamma_{t3})}$$

In this relation we have a connection between the absorption maxima and the values of the dipoles at the different sites. This

¹⁴ This result is identical with that of HARTMANN and ILSE.⁴ However, we disagree with their formula for G_0 and that for $E(B_{2g})$ on p. 242. For the coefficient to $H(4)$ we obtain $\frac{128}{945}$.

formula and the experimentally estimated ratio $\nu_1/\nu_2 = 1.33$ is used in ref. 6 to show that the configuration of $\text{Cu}(\text{H}_2\text{O})_6^{++}$ can only be slightly distorted. If the configuration is distorted much, it would be necessary to have $\mu_z > \mu$ in order to get the right absorption maximum, but it is known from chemical considerations that this is not the case. It is shown in ref. 6 that a good agreement between the experimentally known facts and the theory is obtained by using $N = 6$ for $\text{Cu}(\text{H}_2\text{O})_N^{++}$ in a slightly distorted octahedral configuration, where $R = 1.95 \text{ \AA}$ and $R_z = 2.00 \text{ \AA}$.

The formulae for the absorption of the mixed complexes are not written out because of their great length, but they are easily obtained with the help of Table 1, (7) and (9). Numerical calculations of the maxima of the first band for the various cupric ammine complexes are tabulated in ref. 6. The agreements between the known and calculated absorption maxima are remarkable.

If we treat the tetrahedral configuration with $N = 4$ and equal dipoles μ we similarly obtain:

$$\left. \begin{aligned} E(\Gamma_3) &= \mu f^2 \frac{8}{45} \left[4 B_0 - \frac{4}{9} B_4 \right] \quad \text{2-fold degenerate.} \\ E(\Gamma_5) &= \mu f^2 \frac{8}{45} \left[4 B_0 + \frac{8}{27} B_4 \right] \quad \text{3-fold degenerate.} \\ E(\Gamma_3) &> E(\Gamma_5). \end{aligned} \right\} \quad (13)$$

These results agree with those of BETHE,² who has proved that under the influence of a cubic field, such as that provided by the regular octahedral and tetrahedral configurations, the five fold $(2L + 1)$ degenerate 2D level will split up into two. The more unsymmetrical a field we put on the 2D level, the more splittings we get, until at last the degeneracy is completely removed. It follows from the above discussion that in the distorted octahedral complexes $[\text{Cu}(\text{NH}_3)_n(\text{H}_2\text{O})_{6-n}]^{++}$ the number of bands will depend only on the ligands in the co-planar positions 1 — 4. Four identical ligands ($\mu_1 = \mu_2 = \mu_3 = \mu_4$) or cis-placing of two identical ligands ($\mu_1 = \mu_2 \mp \mu_3 = \mu_4$) leads to 3 bands; the introduction of one different ligand ($\mu_1 \mp \mu_2 = \mu_3 = \mu_4$), or trans-placing ($\mu_1 = \mu_3 \mp \mu_2 = \mu_4$) will give 4 bands.

The ground level for nine d-electrons in the regular octahedron is 2-fold degenerate, but in the tetrahedral case this level is 3-fold degenerate. If we multiply the functions for the different levels by their degeneracy number and then add up the resulting terms, all the B 's except B_0 vanish. This means that the "centre of gravity" of the levels is not altered by applying a perturbation to the system (cf. ref. 2).

We may conclude from the calculations on dipole-cation complexes that electronic exchange between the ligands and the central ion cannot be very important for the absorption spectra of such complexes. Now it has been pointed out by ORGEL¹⁵ that the theories of PAULING and VAN VLECK are closely connected. In this respect it may be noted that the ground energy of the planar configuration given by (10) is lower than that of the tetrahedral configuration calculated in the same way (14) even when the electrostatic interaction of the ligands is taken into account.

A difficulty of the present theory is that dipole transitions between different levels are forbidden. The occurrence of "forbidden" transitions in such complicated systems as those we are dealing with can, however, have many reasons.¹⁶ Furthermore, there seems to be experimental evidence for the assumption that the intensity of the spectra (a rough measure of which is given by $\epsilon_{\max} \cdot \nu_{1/2}$, where ϵ_{\max} is the molar extinction coefficient of the maxima and $\nu_{1/2}$ the half-width of the band in cm^{-1}) is connected with the symmetry of the perturbing field. The intensity of e. g. the $[\text{Ni}(\text{NH}_3)_n(\text{H}_2\text{O})_{6-n}]^{++}$ complexes, which can be seen from the spectra computed by BJERRUM,¹⁷ is greatest for $n = 3$.

The spectra of high intensity ($\epsilon_{\max} \sim 2000$) we shall call electron transfer spectra, these being due to transfer of electrons from the ligands to the metal ion. The spectra due to the influence of ligands on the energy terms of the partially filled electron shells in the central atom we shall call transition group spectra, because they only occur in the transition groups of the periodic system. These latter spectra are mainly of two kinds, the first having a molar extinction coefficient $\epsilon \sim 10$, the second having $\epsilon \sim 0.1$. The ultraviolet spectrum of CuCl_4^{--} is an electron transfer spectrum;

¹⁵ ORGEL, L. E.: J. Chem. Soc. **1952**, 4756.

¹⁶ HERZBERG, C: Spectra of Diatomic Molecules. (D. VAN NOSTRAND 1950.)

¹⁷ BJERRUM, J.: Metal Ammine Formation in Aqueous Solution, p. 196. (Copenhagen 1941.)

the bands of the cupric amines are transition group spectra of the first kind, while all the bands of Mn^{++} are transition group spectra of the second kind. It is hoped that further investigations will throw more light on these questions.

I wish to express my sincere thanks to Professor J. BJERRUM for suggesting this problem, and for his great interest and constant encouragement during the work. My thanks are further due to Mr. AAGE WINTHER for many helpful discussions.

*Chemistry Department A,
Technical University of Denmark,
Copenhagen.*

Det Kongelige Danske Videnskabernes Selskab

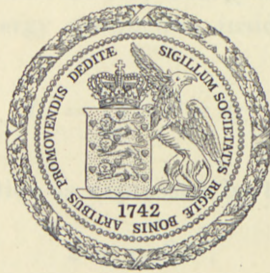
Matematisk-fysiske Meddelelser, bind 29, nr. 5

Dan. Mat. Fys. Medd. 29, no. 5 (1954)

THE ENERGY
PRODUCTION IN CONVECTIVE
CORES IN STARS

BY

PETER NAUR



København 1954

i kommission hos Ejnar Munksgaard

Det Kongelige Danske Videnskabsnyttelskab

Astronomisk Observatorium, Kbhvn S, no. 5

1964, 100 s., 16.00 kr.

THE ENERGY
PRODUCTION IN CONVECTIVE
CORES IN STARS

BY
M. J. P. C. M. VAN DEN HART



Printed in Denmark
Bianco Lunos Bogtrykkeri A-S

1. The following tables give the functions

$$I_m(\xi) = \int_0^{\xi} [\theta(\xi')]^{m+3} \xi'^2 d\xi' \quad (1)$$

and

$$W_m(\xi) = \xi^3 [\theta(\xi)]^{m+3} / I_m(\xi) \quad (2)$$

where θ is the Lane-Emden function of index $n = 3/2$. The functions have been calculated for all integral values of the parameter m from 1 to 23 inclusive.

2. The tables of $I_m(\xi)$ will facilitate the calculation of the energy production in convective cores in stars. The structure of the convective core is described by:

Distance from center, $r = \alpha\xi$

Temperature, $T = T_c\theta$

Density, $\varrho = \varrho_c\theta^{3/2}$

where α is a scale factor, and T_c and ϱ_c the central temperature and density. The energy production inside a sphere of radius r , L_r , will be

$$L_r = \int_0^r 4\pi r^2 \varrho \varepsilon dr. \quad (3)$$

If the energy production is expressed by the power law

$$\varepsilon = \varepsilon_0 \varrho^\delta T^\nu, \quad (4)$$

we get

$$L_{r(=\alpha\xi)} = 4\pi\alpha^3 \varepsilon_0 \varrho_c^{1+\delta} T_c^\nu I_m(\xi) \quad (5)$$

with $m = \nu + 3(\delta - 1)/2$.

3. The function W is the homology invariant quantity corresponding to I . The tables are primarily calculated as an aid to starting calculations of the interior structure of stars where homology invariant quantities are used as the primary variables. Such a choice will be convenient whenever the energy production and the opacity can be expressed with sufficient accuracy by power expressions, such as (4) above for ϵ and

$$\kappa = \kappa_0 \rho^{1-\alpha} T^{-3-s} \quad (6)$$

for the opacity, and the radiation pressure can be neglected. In this case we can choose the variables

$$\left. \begin{aligned} V &= -\frac{d \log P}{d \log r} \\ U &= \frac{d \log M_r}{d \log r} \\ W &= \frac{d \log L_r}{d \log r} \\ H &\equiv \frac{V}{n+1} = -\frac{d \log T}{d \log r} \end{aligned} \right\} \quad (7)$$

where we have used the usual notation: P is the pressure, M_r is the mass within the sphere of radius r , and n is the polytropic index.

In terms of these variables the usual four differential equations governing the internal structure of a star in radiative equilibrium reduce themselves to the following three differential equations

$$\left. \begin{aligned} \frac{dU}{dV} &= \frac{U(3-V+H-U)}{V(U+H-1)} \\ \frac{dW}{dV} &= \frac{W(3-(1+\delta)V-(v-1-\delta)H-W)}{V(U+H-1)} \\ \frac{dH}{dV} &= \frac{H((9+s-\alpha)H-(2-\alpha)V+W-1)}{V(U+H-1)} \end{aligned} \right\} \quad (8)$$

and the quadrature

$$\log r/r_0 = \int \frac{dV}{V(U+H-1)} \quad (9)$$

Inside the convective core the functions U , V , and H are independent of the opacity and energy production. U and V are tabulated in British Association Tables, Vol. II. The variable H follows immediately as $2V/5$. The remaining variable, W , is the function tabulated in the present publication. Contrary to what is the case of V , U and H , W depends on the energy production law. The present tables cover the ground where a law of the form (4), with $1 < \nu + 3(\delta - 1)/2 < 23$, is concerned.

The tables of W have been calculated only with the argument ξ . The applications to integrations of stellar structure require V to be the independent variable. Therefore an auxiliary table, which gives U and ξ as functions of V , has been provided.

4. In a recent paper by OSTERBROCK and the present author¹ it has been shown how an upper limit to the extent of the convective core in a star where (4) and (6) are valid can be derived. This limit has the following form: A convective core, extending to the point in the star where $V = V_0$, is only possible if

$$U_0 - W_0 - (1.2 + 0.4s + 0.6\alpha) V_0 > 0 \quad (10)$$

or

$$s + \frac{3}{2}\alpha < \frac{5(U_0 - W_0)}{2V_0} - 3. \quad (11)$$

If ε is of the form (4), the quantity on the right hand side of (11) depends only on V_0 and $\nu + 3(\delta - 1)/2$. It has been plotted in figure 1.

It is of considerable interest to know the behaviour of the convective core in a star where two energy sources, each with an output of the form (4), are active. There would be no difficulties in evaluating the W functions for such mixtures and then plotting the corresponding curves in the diagram. Since, however, the most important feature of the curve is its intersection with the $s + 3\alpha/2$ axis, we shall confine our attention to the evaluation of the position of this point. For this purpose, let us write the total energy production rate as

$$\varepsilon = \varepsilon_c (\gamma \theta^{m_1} + (1 - \gamma) \theta^{m_2}) \theta^{3/2}. \quad (12)$$

¹ Ap. J., 117, 306, 1953.

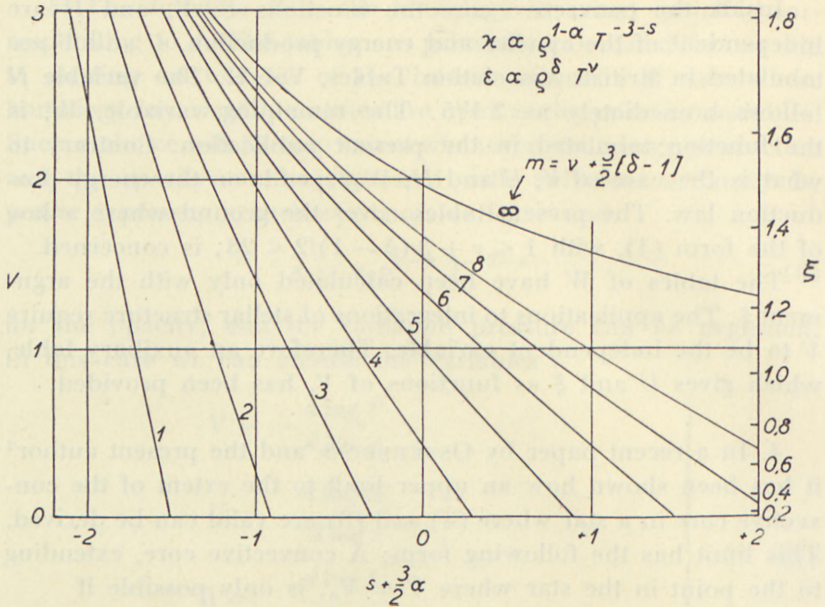


Figure 1. The curves give the upper limit to the extent of the convective core as a function of the opacity and energy production laws.

Thus ϵ_c is the total energy production rate at the center while γ measures the relative contribution to this total from the reaction characterized by the subscript 1. Using the power expansions of the Lane-Emden function it is easy to find the value of the relevant function at $V = 0$:

$$\left[\frac{5(U-W)}{2V} \right]_{V \rightarrow 0} - 3 = 0.6 \gamma m_1 + 0.6 (1-\gamma) m_2 - 2.1. \quad (13)$$

Thus the abscissa of the required intersection on the horizontal axis is a mean of the values of m for the two reactions, the weighing factor being the contribution from the particular process to the total energy production at the center.

The tables.

The tables giving ξ and U as functions of V have been obtained by interpolation of the tables given in British Association Tables, Vol. II. The second difference, Δ'' , or the modified second difference, $M'' = \Delta'' - 0.184 \Delta^{iv}$, has been given. Thus interpolation to the fraction n follows from Everett's formula:

$$f(x_i + n\Delta x) = (1 - n)f(x_i) + nf(x_{i+1}) \\ + E_0''\Delta''(x_i) + E_1''\Delta''(x_{i+1})$$

or the same expression with M'' replacing Δ'' . The coefficients E_0'' and E_1'' have been tabulated with argument n in Interpolation and Allied Tables, H. M. Stationary Office (reprinted from the Nautical Almanac for 1937). For small values of V the table for ξ becomes unmanageable. This difficulty is avoided if one works with the function $\sqrt{6V/5} - \xi$.

The tables of I and W are based on the values of θ given in British Association Tables, Vol. II. The calculations were carried out to seven decimals and only in the copy prepared for printing the functions were rounded to five and four decimals. For interpolation to arbitrary values of ξ the modified second differences have been given. Most of the work of calculating these functions was done by means of the IBM 602-A calculators at the IBM Watson Scientific Computing Laboratory, New York City.

The author is grateful to Dr. W. J. ECKERT for placing the facilities of the Watson Computing Laboratory at his disposal. He also wishes to thank the International Astronomical Union and Ole Rømer Fondet, Copenhagen, for grants while the work was carried out, and the United States Educational Foundation in Denmark for a Fulbright Travel Grant.

V	ξ	M''	U	A''
0.0	0.00000	—	3.00000	+ 30
0.1	0.34606	—	2.96414	30
0.2	0.48888	—	2.92858	30
0.3	0.59811	—1567	2.89332	29
0.4	0.68986	1065	2.85835	30
0.5	0.77040	776	2.82368	31
0.6	0.84294	601	2.78932	31
0.7	0.90936	477	2.75527	31
0.8	0.97093	396	2.72153	31
0.9	1.02850	333	2.68810	32
1.0	1.08271	291	2.65499	33
1.1	1.13401	251	2.62221	32
1.2	1.18280	224	2.58975	33
1.3	1.22935	200	2.55762	32
1.4	1.27390	180	2.52581	34
1.5	1.31665	163	2.49434	33
1.6	1.35777	149	2.46320	33
1.7	1.39740	139	2.43239	33
1.8	1.43564	128	2.40191	34
1.9	1.47260	118	2.37177	34
2.0	1.50838	111	2.34197	34
2.1	1.54305	105	2.31251	35
2.2	1.57667	97	2.28340	33
2.3	1.60932	93	2.25462	34
2.4	1.64104	87	2.22618	34
2.5	1.67189	83	2.19808	35
2.6	1.70191	80	2.17033	34
2.7	1.73113	75	2.14292	35
2.8	1.75960	71	2.11586	33
2.9	1.78736	70	2.08913	34
3.0	1.81442	66	2.06274	35
3.1	1.84082	63	2.03670	33
3.2	1.86659	61	2.01099	34
3.3	1.89175	58	1.98562	34
3.4	1.91633	57	1.96059	33
3.5	1.94034	55	1.93589	34
3.6	1.96380	— 53	1.91153	+ 33

ξ	I_6	M''	I_7	M''	I_8	M''	I_9	M''	I_{10}	M''
0.0	.00000	0	.00000	0	.00000	0	.00000	0	.00000	0
0.1	.00033	+197	.00033	+197	.00033	+197	.00033	+196	.00033	+196
0.2	.00257	360	.00256	356	.00255	351	.00254	347	.00253	343
0.3	.00830	461	.00823	446	.00816	433	.00809	419	.00802	406
0.4	.01851	485	.01822	456	.01794	428	.01767	402	.01740	376
0.5	.03342	434	.03263	389	.03187	346	.03112	306	.03040	269
0.6	.05257	322	.05083	263	.04916	210	.04756	162	.04602	+119
0.7	.07488	174	.07161	+109	.06851	+52	.06558	+4	.06281	-37
0.8	.09890	+16	.09347	-46	.08841	-95	.08369	-134	.07929	164
0.9	.12311	-127	.11492	175	.10741	209	.10052	232	.09420	245
1.0	.14612	237	.13468	264	.12439	278	.11512	280	.10675	276
1.1	.16682	306	.15189	309	.13869	301	.12700	285	.11662	264
1.2	.18455	333	.16607	313	.15004	286	.13609	256	.12390	226
1.3	.19901	324	.17718	287	.15858	248	.14265	210	.12894	176
1.4	.21028	290	.18546	242	.16466	198	.14712	159	.13223	126
1.5	.21867	243	.19134	190	.16877	146	.15000	111	.13425	83
1.6	.22465	190	.19530	140	.17141	102	.15175	73	.13541	51
1.7	.22872	141	.19786	97	.17301	66	.15276	44	.13604	29
1.8	.23136	99	.19942	64	.17394	40	.15330	25	.13636	16
1.9	.23300	65	.20033	39	.17444	23	.15358	14	.13652	8
2.0	.23398	41	.20083	23	.17470	12	.15372	7	.13659	4
2.1	.23452	24	.20109	12	.17483	6	.15378	3	.13662	2
2.2	.23482	14	.20122	6	.17488	3	.15380	1	.13663	-1
2.3	.23496	7	.20128	3	.17491	1	.15381	-1	.13663	0
2.4	.23503	4	.20131	1	.17492	-1	.15382	0		
2.5	.23507	2	.20132	-1	.17492	0	.15382	0		
2.6	.23508	-1	.20132	0						
2.7	.23508	0								

ξ	I_{11}	M''	I_{12}	M''	I_{13}	M''	I_{14}	M''	I_{15}	M''
0.0	.00000	0	.00000	0	.00000	0	.00000	0	.00000	0
0.1	.00033	+196	.00033	+195	.00033	+195	.00033	+195	.00033	+194
0.2	.00252	338	.00251	334	.00250	330	.00249	326	.00248	322
0.3	.00795	393	.00788	380	.00781	368	.00774	355	.00767	343
0.4	.01713	352	.01687	328	.01662	305	.01637	283	.01612	263
0.5	.02970	234	.02901	202	.02835	172	.02771	+144	.02708	+118
0.6	.04454	+80	.04312	+45	.04176	+14	.04045	-14	.03919	-38
0.7	.06019	-71	.05770	-100	.05534	-124	.05310	144	.05098	160
0.8	.07518	187	.07134	203	.06776	214	.06441	221	.06127	224
0.9	.08839	251	.08305	252	.07814	248	.07361	241	.06942	232
1.0	.09918	265	.09233	252	.08611	236	.08046	219	.07532	201
1.1	.10739	242	.09915	218	.09178	195	.08518	173	.07924	152
1.2	.11322	197	.10382	169	.09552	144	.08817	122	.08164	103
1.3	.11709	145	.10680	119	.09781	97	.08993	78	.08300	63
1.4	.11951	99	.10857	77	.09912	59	.09090	45	.08370	35
1.5	.12092	62	.10956	46	.09981	33	.09138	24	.08404	18
1.6	.12169	36	.11008	25	.10015	17	.09161	12	.08420	8
1.7	.12209	19	.11033	13	.10031	8	.09171	5	.08426	3
1.8	.12228	10	.11044	6	.10038	4	.09175	2	.08428	-1
1.9	.12237	4	.11049	3	.10040	1	.09176	-1	.08429	0
2.0	.12240	2	.11051	-1	.10041	-1	.09177	0	.08429	0
2.1	.12242	-1	.11051	0	.10042	0	.09177	0		
2.2	.12242	0	.11052	0	.10042	0				
2.3			.11052	0						

ξ	I_{16}	M''	I_{17}	M''	I_{18}	M''	I_{19}	M''	I_{20}	M''
0.0	.00000	0	.00000	0	.00000	0	.00000	0	.00000	0
0.1	.00033	+194	.00033	+193	.00033	+193	.00033	+193	.00033	+192
0.2	.00247	317	.00246	313	.00245	309	.00244	305	.00243	301
0.3	.00761	332	.00754	320	.00748	309	.00741	298	.00735	287
0.4	.01588	243	.01564	223	.01541	205	.01518	188	.01496	171
0.5	.02647	+ 93	.02588	+ 71	.02530	+ 50	.02474	+ 31	.02420	+ 13
0.6	.03798	- 60	.03682	- 79	.03571	- 95	.03463	-110	.03360	-122
0.7	.04897	172	.04706	181	.04524	188	.04352	193	.04188	196
0.8	.05834	224	.05559	222	.05301	218	.05059	212	.04832	205
0.9	.06556	221	.06199	210	.05869	197	.05562	184	.05278	172
1.0	.07064	184	.06635	167	.06244	151	.05885	136	.05556	121
1.1	.07389	132	.06907	116	.06469	101	.06073	87	.05712	75
1.2	.07582	86	.07061	72	.06593	60	.06172	49	.05791	40
1.3	.07686	50	.07141	40	.06655	31	.06219	25	.05828	19
1.4	.07738	26	.07179	20	.06683	15	.06240	11	.05843	8
1.5	.07762	12	.07196	9	.06695	6	.06248	5	.05849	3
1.6	.07772	5	.07203	4	.06699	2	.06251	2	.05851	- 1
1.7	.07776	2	.07205	- 1	.06701	- 1	.06252	- 1	.05852	0
1.8	.07777	- 1	.07206	0	.06701	0	.06252	0	.05852	0
1.9	.07778	0	.07206	0						
2.0	.07778	0								

ξ	I_{21}	M''	I_{22}	M''	I_{23}	M''
0.0	.00000	0	.00000	0	.00000	0
0.1	.00033	+192	.00033	+191	.00033	+191
0.2	.00242	297	.00242	293	.00241	289
0.3	.00728	277	.00722	266	.00716	256
0.4	.01473	+155	.01452	+139	.01431	+125
0.5	.02367	- 4	.02315	- 19	.02265	- 33
0.6	.03261	133	.03165	142	.03073	149
0.7	.04033	197	.03885	197	.03744	195
0.8	.04619	198	.04418	190	.04230	181
0.9	.05014	159	.04769	147	.04541	135
1.0	.05253	108	.04975	96	.04718	85
1.1	.05383	64	.05083	55	.04808	47
1.2	.05447	33	.05134	27	.04849	22
1.3	.05475	15	.05155	12	.04865	9
1.4	.05486	6	.05164	5	.04871	3
1.5	.05490	2	.05167	- 2	.04873	- 1
1.6	.05492	- 1	.05167	0	.04874	0
1.7	.05492	0			.04874	0

ξ	W_{16}	M''	W_{17}	M''	W_{18}	M''	W_{19}	M''	W_{20}	M''
0.0	3.0000	-764	3.0000	-804	3.0000	-845	3.0000	-885	3.0000	-926
0.1	2.9621	748	2.9601	786	2.9581	825	2.9561	864	2.9542	902
0.2	2.8501	698	2.8423	731	2.8345	764	2.8268	796	2.8190	828
0.3	2.6689	614	2.6521	638	2.6353	661	2.6187	683	2.6021	704
0.4	2.4269	495	2.3987	505	2.3708	514	2.3431	522	2.3156	528
0.5	2.1361	336	2.0956	329	2.0557	320	2.0162	308	1.9773	294
0.6	1.8122	-144	1.7602	-117	1.7092	-88	1.6593	-55	1.6104	-20
0.7	1.4743	+ 69	1.4133	+114	1.3542	+162	1.2970	+212	1.2416	+265
0.8	1.1432	279	1.0777	336	1.0151	394	0.9555	452	0.8986	511
0.9	0.8392	452	0.7747	509	0.7143	564	0.6578	616	0.6051	665
1.0	0.5793	557	0.5212	599	0.4681	636	0.4198	667	0.3758	692
1.1	0.3735	573	0.3259	591	0.2837	602	0.2465	605	0.2137	602
1.2	0.2236	509	0.1883	501	0.1581	488	0.1324	469	0.1106	445
1.3	0.1237	394	0.1000	370	0.0806	342	0.0648	313	0.0519	283
1.4	0.0630	268	0.0487	238	0.0375	209	0.0288	181	0.0220	155
1.5	0.0295	162	0.0217	135	0.0159	112	0.0116	91	0.0084	74
1.6	0.0126	86	0.0088	68	0.0061	53	0.0042	41	0.0029	31
1.7	0.0049	41	0.0032	30	0.0021	22	0.0014	16	0.0009	11
1.8	0.0018	17	0.0011	12	0.0007	8	0.0004	5	0.0002	4
1.9	0.0006	7	0.0003	4	0.0002	3	0.0001	+ 2	0.0001	+ 1
2.0	0.0002	2	0.0001	+ 1	0.0000	+ 1	0.0000	0	0.0000	0
2.1	0.0000	+ 1	0.0000	0	0.0000	0				
2.2	0.0000	0								

ξ	W_{21}	M''	W_{22}	M''	W_{23}	M''
0.0	3.0000	-966	3.0000	-1007	3.0000	-1048
0.1	2.9522	940	2.9502	978	2.9482	1017
0.2	2.8113	859	2.8036	891	2.7959	921
0.3	2.5855	724	2.5690	743	2.5526	761
0.4	2.2883	532	2.2612	535	2.2343	536
0.5	1.9389	-277	1.9010	-258	1.8636	-237
0.6	1.5625	+ 18	1.5157	+ 59	1.4699	+ 102
0.7	1.1880	319	1.1362	375	1.0861	432
0.8	0.8445	569	0.7930	626	0.7441	682
0.9	0.5559	710	0.5102	750	0.4677	786
1.0	0.3359	710	0.2998	723	0.2672	730
1.1	0.1849	593	0.1597	579	0.1377	561
1.2	0.0922	419	0.0767	391	0.0637	362
1.3	0.0415	253	0.0331	224	0.0263	197
1.4	0.0168	131	0.0128	110	0.0097	92
1.5	0.0061	59	0.0044	47	0.0032	37
1.6	0.0020	23	0.0014	17	0.0009	13
1.7	0.0006	8	0.0004	5	0.0002	4
1.8	0.0002	2	0.0001	+ 2	0.0001	+ 1
1.9	0.0000	+ 1	0.0000	0	0.0000	0
2.0	0.0000	0				

Det Kongelige Danske Videnskabernes Selskab

Matematisk-fysiske Meddelelser, bind **29**, nr. 6

Dan. Mat. Fys. Medd. **29**, no. 6 (1955)

A SIX GAP
 β -RAY SPECTROMETER

BY

O. B. NIELSEN AND O. KOFOED-HANSEN



København 1955

i kommission hos Ejnar Munksgaard

Printed in Denmark.
Bianco Lunos Bogtrykkeri A-S.

1. Introduction.

The theory of a new type of β -ray spectrometer has been developed previously¹⁾ for the purpose of more efficiently utilizing a radioactive source than has been possible so far. In principle, this can be accomplished by letting several double focusing spectrometers of a conventional type operate on the same source, and preferably having the same focus. However, a more suitable solution was found in a design where the individual spectrometers consist of a number of air gaps in the same electro-magnet. Source and focus are situated in field-free space, and the gaps are arranged symmetrically around the line connecting them.

A preliminary investigation of a spectrometer consisting of a single air gap has also been described.

Since then we have constructed a spectrometer with six air gaps. The instrument is characterized by a large transmission and is especially well suited for coincidence experiments with scintillation counters, as the operation of the multiplier tubes is undisturbed by magnetic fields.

The present paper gives a description of some experience with this spectrometer which has now been operating for more than a year. In addition, a few possible new applications of the focusing principle will be mentioned.

2. The electron-optical system.

Let us first repeat the most essential features of the principle of focusing.

The instrument is shown in Figs. 1a and 1b. The electro-magnet consists of six segments placed as slices of an orange, each occupying 40° of the entire circle around the symmetry

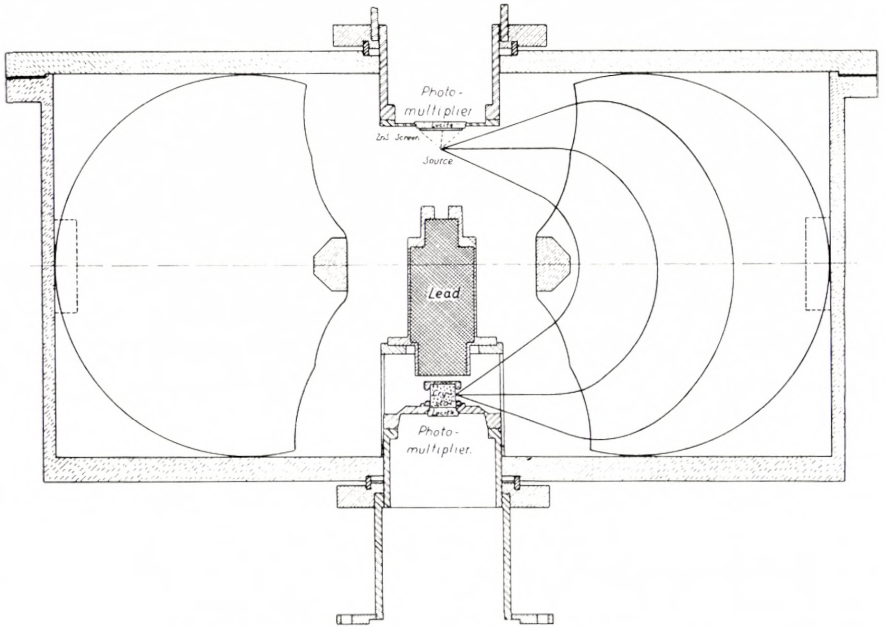


Fig. 1a. Vertical section through the spectrometer.

axis. The magnetic field is localized within the six wedge-shaped air gaps, the angle between the pole faces thus being 20° . If fringing field effects are neglected, all the lines of force will be circular.

It is evident that such a magnetic field is focusing along its own direction. Any particle starting from the source will stay in a plane containing the symmetry axis and, after sufficient deflection in the field, will return to the axis.

In the vertical plane (Fig. 1a), focusing can be obtained by choosing a suitable limiting curve for the pole pieces. It was shown theoretically (ref. 1) that a double infinity of such curves exists corresponding to a fixed position of the source and the counter. If symmetry around a plane perpendicular to the axis is demanded, only a single infinity remains.

The possibility of obtaining the ideal focusing is limited only by effects from fringing fields which cause deviations from the theoretically assumed field shape.

The existence of a fringing field, which the particles have to pass before entering the gap, has no serious disadvantages for

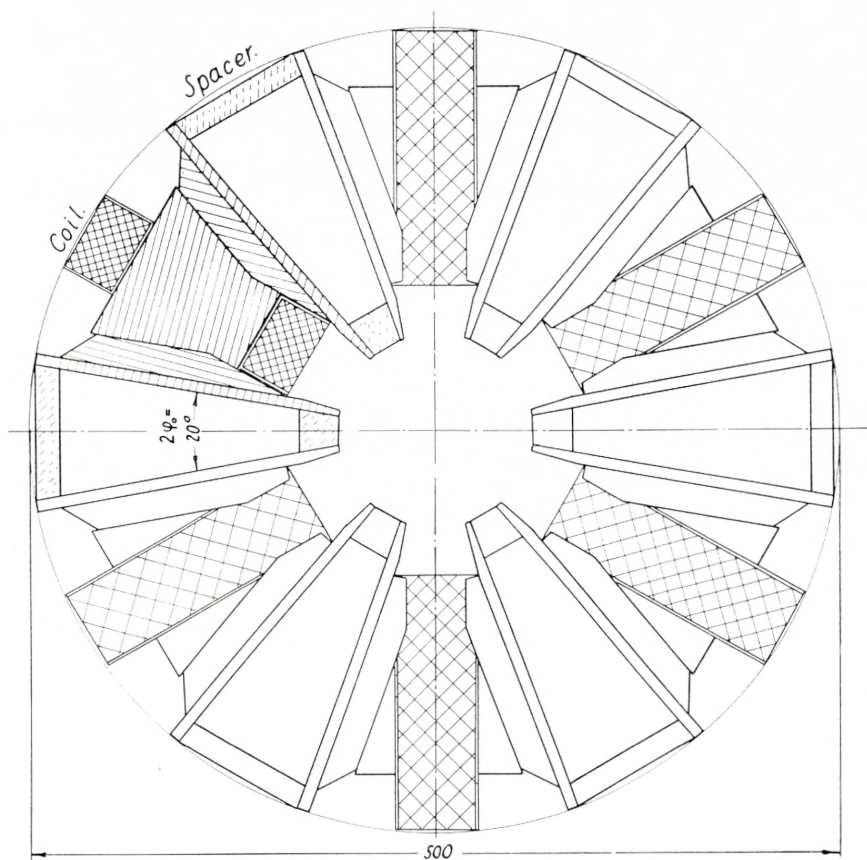


Fig. 1b. Horizontal section through the spectrometer.

the focusing in the plane of Fig. 1a, because it can be corrected for by shaping the pole pieces. In Section 6, a practical method for this correction is described.

Outside the central plane in each wedge-shaped gap the rays will be influenced by the fringing field as by a cylindrical lens²⁾³⁾ with the focal distance

$$f \sim \frac{\varrho}{\operatorname{tg} \psi}, \quad (1)$$

where ψ is the angle between the ray and the edge of the pole piece (Fig. 2) and ϱ the radius of curvature for the electron immediately inside the edge.

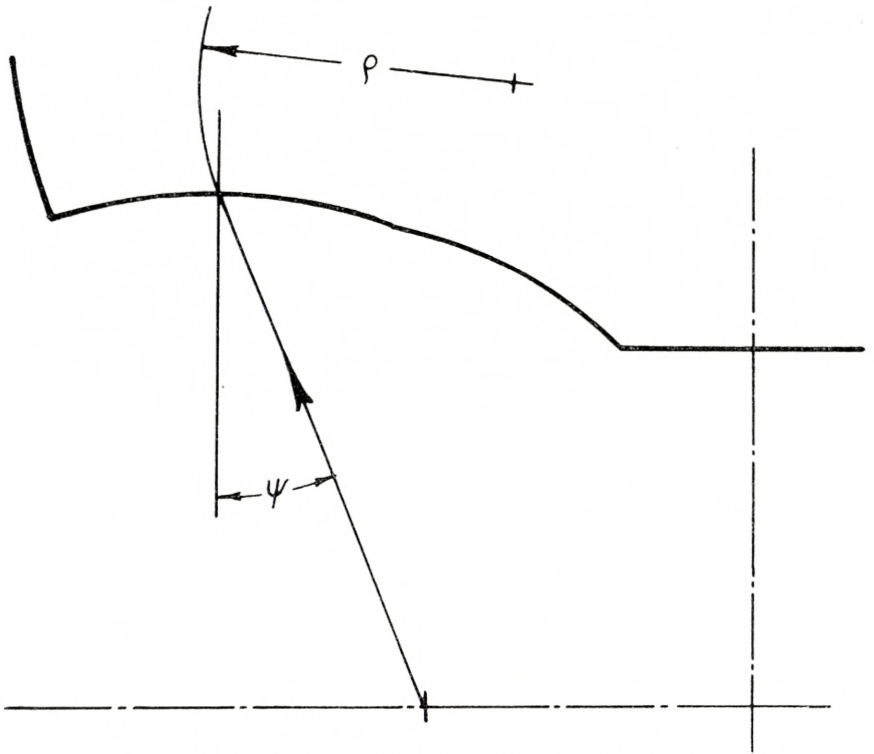


Fig. 2. Entrance of β -ray into the magnetic field.

We have made an attempt to reduce this effect by choosing the boundary of the pole plates approximately as circles with centers near the source and the focus. However, ψ , and hence f , cannot be entirely constant along the limiting curve. Thus, the image of the source has a certain extension along the direction of the magnetic field. This has no direct bearing on the resolving power, but the counter must of course be constructed so as to accept a bundle of rays with finite width.

In the present instrument, practically the entire gap is used with an entrance diaphragm to the counter of 10 mm height.

Another deviation from the ideal field shape is due to the finite radial extension of the pole plates, which causes the field to be stronger at the surface of the iron than in the central plane of the gap. This constitutes the essential limit for the resolution in the present construction. In principle, the effect can be reduced by employing more extended pole pieces or by shimming.

3. The magnet.

From the theory of focusing it followed that three parameters may vary within certain limits, as far as the construction of the pole pieces is concerned. The three parameters are: the quantity b defined in eq. (2) of ref. 1, the relative distance between source and focus, and the function ζ (a) defined by eq. (9) of ref. 1. Furthermore, when constructing the spectrometer, one has to decide on the number of gaps and the angle covered by each of them. The final design must represent a compromise between the partly opposing demands of transmission, resolving power, maximum β -momentum measurable, and economy.

The magnet with the corrected pole shape is shown in Fig. 1. As mentioned before, the individual segments have some similarity in shape with the slices of an orange. Each consists of five parts of iron screwed together. The spacers fixing their relative positions are of aluminium. For ease of machining, the limiting curves for the pole pieces are built up of circles.

The iron is of Swedish origin and has a low coercive force. The magnetic circuit is designed so as to avoid local saturation, which might influence the shape of the field. Because of the large air gaps the effect of hysteresis is small, and the field can be reproduced to within .1 per cent by adjusting the current only, provided that a suitable magnetization procedure is followed.

Each of the six coils consists of about 900 turns of 1.2 mm dia. copper wire with glass insulation, the resistance being approximately 6 ohms. The coil forms are water-cooled, but the thermal conductivity through the coils is poor since they are placed in vacuum. They cannot continuously carry more than 3 amps. corresponding to focusing of 1.5 MeV β -particles, although saturation of the iron first takes place at 5 amps. Hence, the present construction is not quite satisfactory*.

The current is furnished by a servo-controlled generator. At 1.5 MeV the power consumption amounts to about 500 Watts.

The total weight of the magnet and the coils is only about 110 kg.

* A spectrometer of the same type is now under construction by C. A. MALLMANN (Buenos Aires) who places the coils in closed containers filled with oil.

4. The vacuum system.

The cylindrical vacuum container is cast in aluminium alloy. No troubles with vacuum leaks have been encountered. The pumping system consists of one 2" oil diffusion pump and a mechanical forepump.

5. Counter equipment.

Originally we used a GM counter with six mica windows of 12 mm dia. It has now been replaced by a scintillation counter arranged as shown in Fig. 1a. The diameter of the anthracene crystal is 15 mm, and the entrance slit can be varied from 1 to 9 mm. Due to the absence of a magnetic field, the multiplier tube can be placed immediately below the crystal.

It is evident that the fringing fields from the different gaps tend to eliminate each other, so that they are relatively less extended than in a one-gap spectrometer. From the symmetry it follows that the axis is field-free, and the multipliers can be shielded by iron without any effect on the focusing.

The only disadvantage of the scintillation counter is its higher background when low energy β -particles are to be counted. We hope to reduce this effect considerably by replacing the present multiplier tube type EMI 6260 by an EMI 6094, which has a photo-cathode of only 10 mm dia.

6. Investigation of a single gap.

a. Empirical determination of the shape of the pole pieces.

The necessary corrections to the shape of the pole pieces were found by measurements similar to those carried out on the single-gap model of ref. 1.

The aperture was subdivided into a series of regions which were investigated individually. The corresponding openings in the entrance diaphragms are shown in Fig. 3. For each diaphragm the magnetization current required to focus the F line from ThB was measured. Source and counter could be moved along the

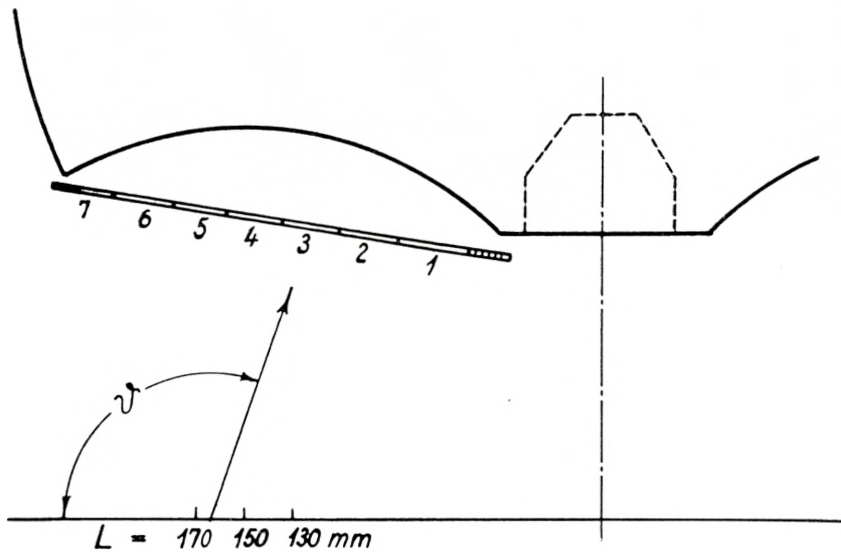


Fig. 3. Entrance diaphragms used in the investigation of the pole shape corrections.

axis from outside the vacuum, and the measurements were repeated for a set of different positions, all being symmetrical about the central plane.

The results of a series of such measurements are shown in Fig. 4. The magnetization current I_m is given as a function of the diaphragm no., i. e. of the angle ϑ . Each curve represents a value of the distance L between source and counter.

Changes in L influence the focusing current less in the outer part of the gap than in the inner part. This is due to the variation of the dispersion with ϑ , as found theoretically in ref. 1. As a consequence, the curves show maxima or minima when the distance L is within certain limits.

Around such maxima the aberration is at most of second order. The condition for first order focusing is thus fulfilled. Even considerable deviations from the theoretical field shape will not prevent the occurrence of such extrema.

After the choice of a certain L the aberration can be reduced by working the pole pieces in the regions where the deflection is too great. We have chosen $L = 165$ mm, and after the final correction the focusing current for a line is constant to within one per cent. A further reduction of the aberration was not con-

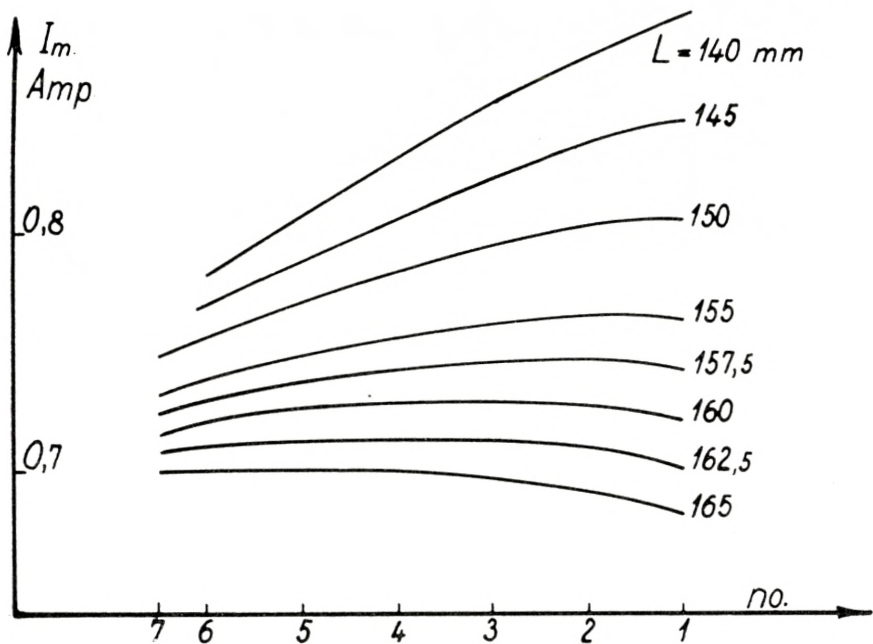


Fig. 4. The focusing current for the F line as a function of the diaphragm no. Each curve corresponds to a certain distance between source and counter.

sidered necessary because other contributions to the line width are of the same order of magnitude.

b. Some practically important properties of the electron orbits.

Curves like those drawn in Fig. 4 can also be represented in a diagram where I_m is plotted as a function of L for each diaphragm. Ideal focusing means that all curves have to pass through a common point. For the corrected pole pieces the case is illustrated in Fig. 5.

In a symmetric spectrometer ($\zeta(a) = 0$) an image is formed with magnification of unity, as shown theoretically in ref. 1. This implies that a small shift in the position of the source introduces the same shift in the focus. This effect was verified by observing that a simultaneous displacement of source and focus by 10 mm in the same direction caused only small changes of the curves in Fig. 5.

The slope of the lines in Fig. 5 determines the dispersion D for the corresponding part of the gap, since

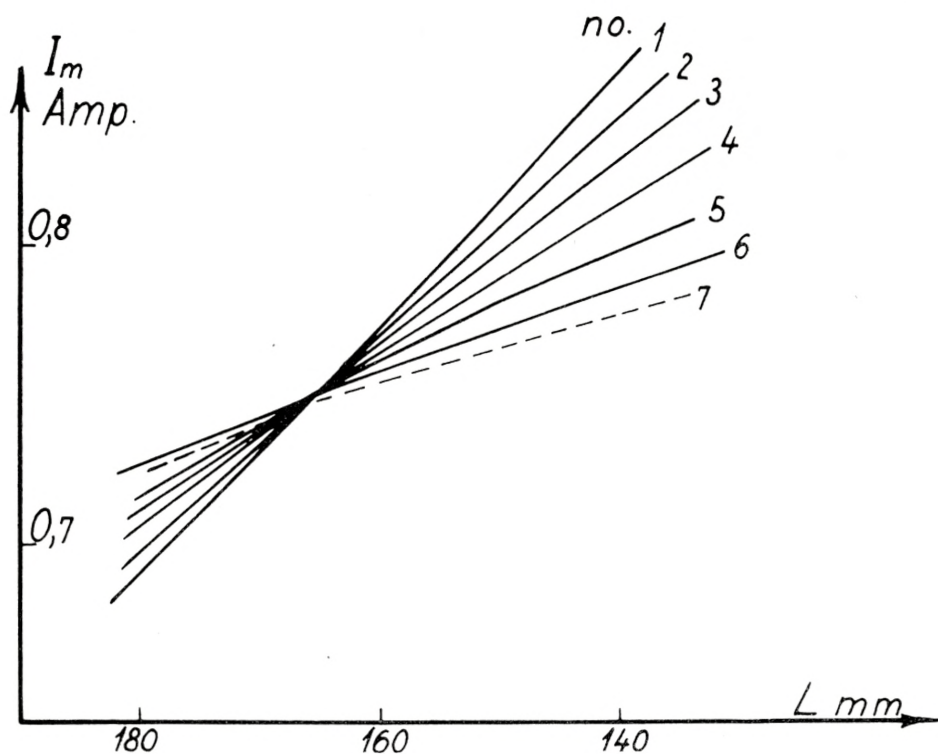


Fig. 5. The focusing current as a function of the distance between source and counter. Each curve corresponds to a diaphragm as numbered in Fig. 3. Results obtained with corrected pole pieces.

$$D = \Delta L \frac{p}{\Delta p} \quad \approx \quad \frac{\Delta L}{\Delta I_m} I_m.$$

The mean value of D is 310 mm or 1.9 times the distance L .

The variation of D causes a smearing out of the image when the magnetization current deviates from the focusing value (Fig. 6). However, at the same time a contraction in the pencil of rays appears outside the axis of symmetry. In fact, a focus line exists which represents a surface on which a portion of the spectrum is focused with good resolution. Each point on this line is characterized by a curve like those in Fig. 4 with a broad maximum in the central part.

By moving the entrance slit to the counter along the focus line, a resolution of $I_m/I_m \lesssim$ two per cent was found over an

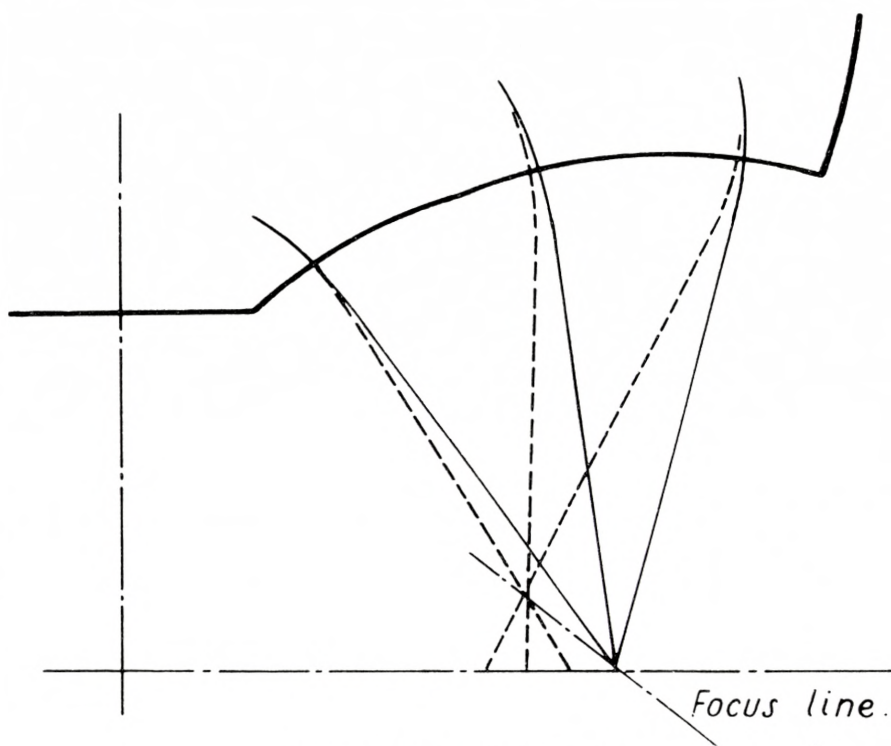


Fig. 6. Position of the focus line.

interval covering 15 per cent change in electron momentum. The existence of the line of focus leaves some freedom in the choice of the counter diameter.

Image formation outside the axis of symmetry is accompanied by a moderate increase in the height of the image, corresponding to a divergence of 20° for the bunch of rays in the direction of the lines of force.

c. The aberration across the gap.

The shape of the F line was measured through diaphragm no. 4 with apertures corresponding to three different values of the angle φ . The results are shown in Fig. 7. The contributions to the line width from the extension of the source and the entrance slit of the counter amount to $\sim .5$ per cent. It is seen that the particles passing close to the surface of the iron reach the counter for a slightly lower current than those moving in the central plane

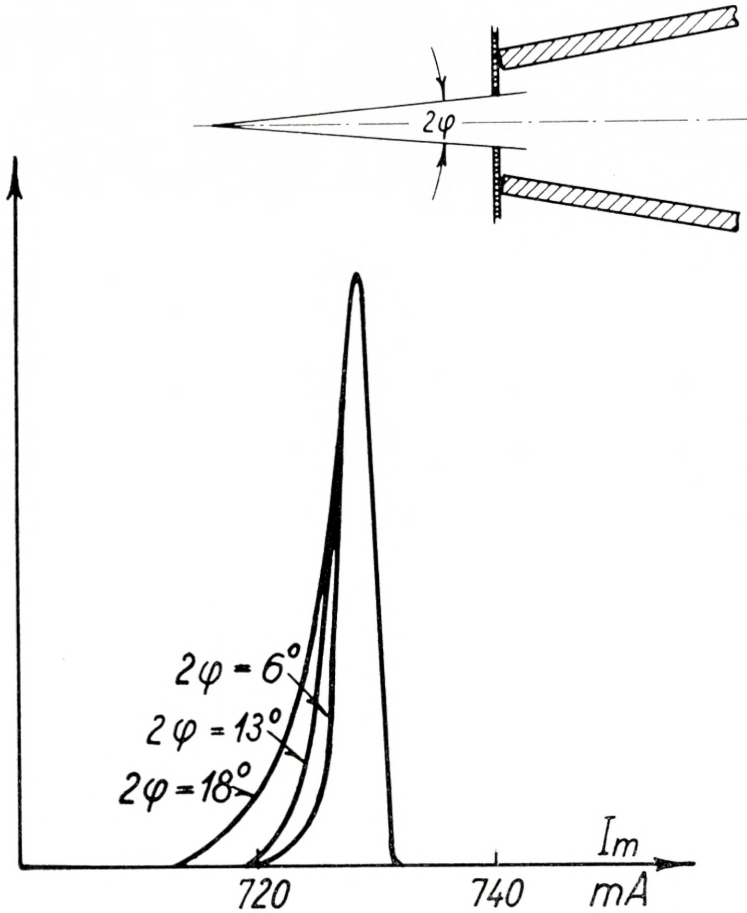


Fig. 7. Line shape measured with different opening angles φ in diaphragm no. 4. The curves are normalized at the maximum point.

of the gap. This contribution is of the order $\sim .3 \times \varphi^2$ in the part of the gap considered. As mentioned previously, this aberration depends upon the construction of the magnet and can be reduced in principle.

d. The transmission from a point source.

As in other spectrometers, the resolving power depends on the utilized solid angle. We have carried out an experimental determination of the relationship between the resolution $R = \frac{P}{\Delta p}$

and the transmission T , defined as the fraction of particles emitted from a mono-energetic source, which are counted at the peak of the line.

The total emission was found by a measurement of the line (F line from ThB) through a small hole in a diaphragm. The

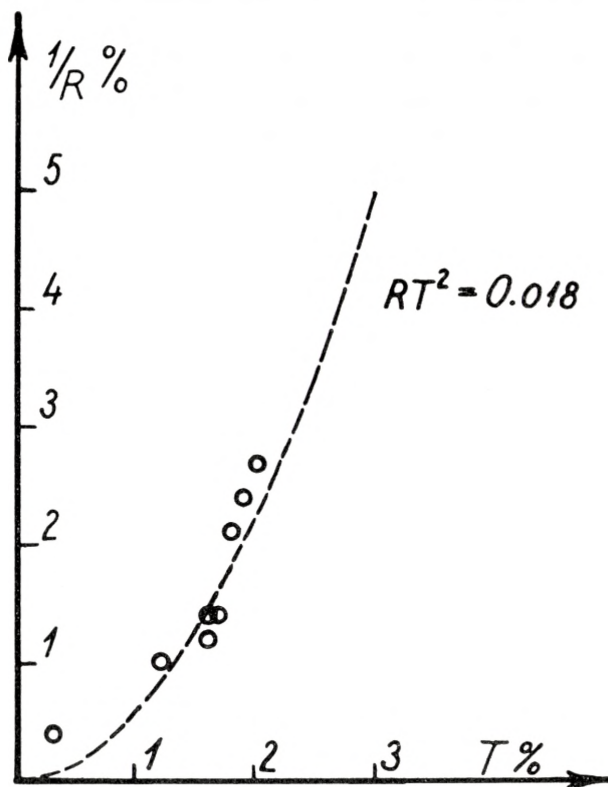


Fig. 8. Transmission versus resolution.

counter slit was so wide that the height of the line represented the solid angle defined by the diaphragm.

The transmission could then easily be determined for a number of different combinations of entrance diaphragms and counter slits. In each case, the latter were adjusted to approximate the same magnitude as the image. During these experiments the source dimensions were so small that their influence on the shape could be neglected.

Some of the results are seen in Fig. 8. The curve $RT^2 = .018$ gives a reasonable fit to the measurements. The maximum transmission of 2.0 per cent for a single gap may be compared with the total opening for each gap of 2.3 per cent of 4π .

e. Extended source.

The mean dispersion 310 mm can be used for an evaluation of the influence on the line shape of the dimensions of source and counter slit. In practice, a source area of 5×10 mm can be used at a resolution of 2.5 per cent.

7. The use of several gaps.

The use of the same source with several gaps demands of course a more detailed analysis.

It is mainly the same magnetic flux which has to pass through the entire magnetic circuit. Therefore, mechanical and electrical differences in the construction of the parts of the magnet have only a minor influence on the magnetic properties of the individual gaps. The maximum difference in field strength was reduced to less than .5 per cent by small corrections to the number of turns in some of the coils.

At present the entire spectrometer is used with a resolution of all six gaps of $1/R \sim 1.6$ per cent without any appreciable effect on the line shape from the differences in field strength in the gaps. The corresponding transmission amounts to 9 per cent of 4π .

In a measurement of the maximum energy of the continuous β -spectrum of P^{334} , the resolution was reduced to 2.5 per cent in order to obtain higher intensity. The spectrum could then be measured with a total activity of 5×10^4 source disintegrations per minute. The background counting rate in the GM tube was 10 counts per minute.

When high resolution is desired, only one gap is employed. Only three gaps can be used when the energy of the spectrum is so low that the passage of particles through the supporting foil must be avoided.

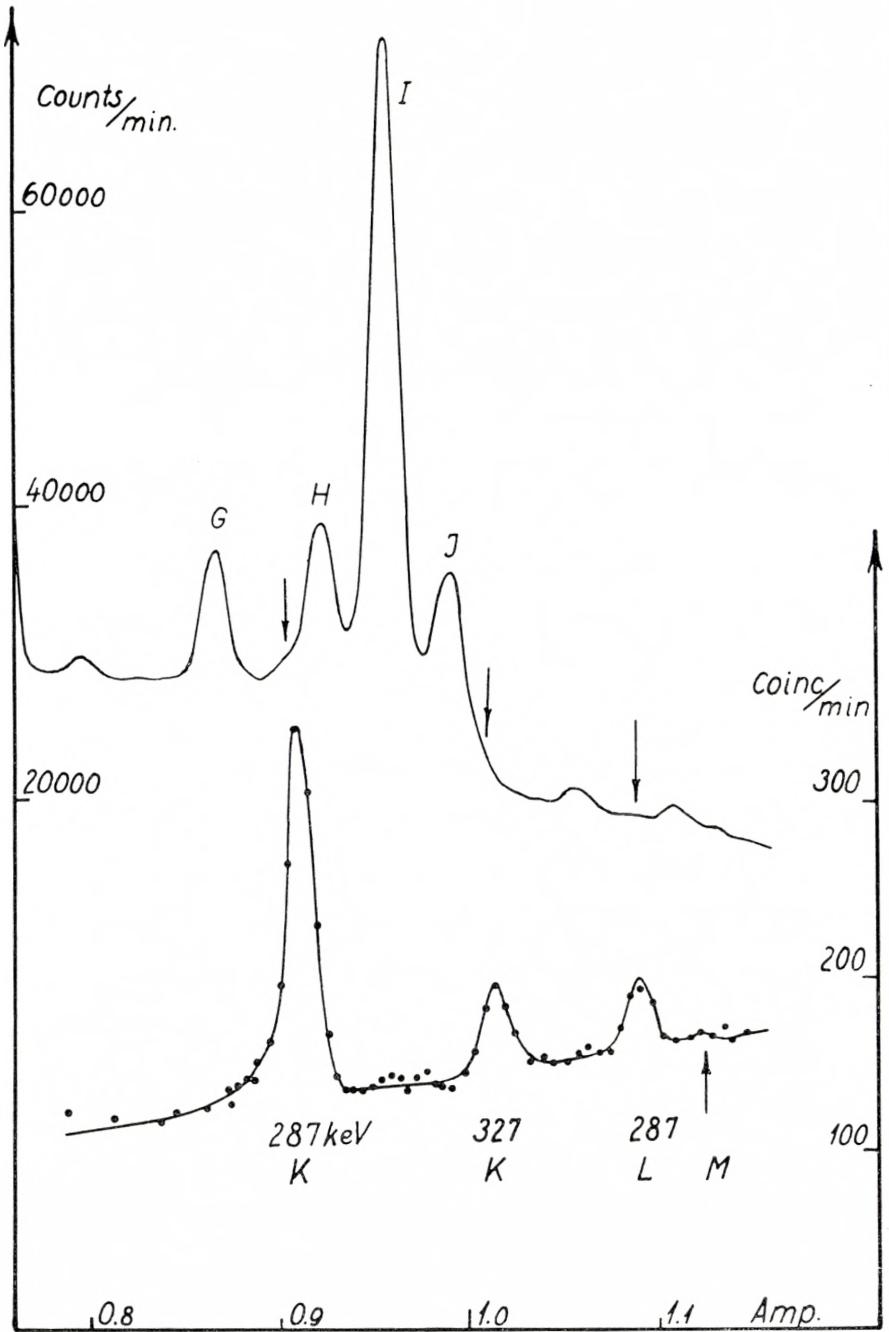


Fig. 9. Above: A part of the complex β -spectrum of $Th(B + C + C')$. The lines are given with the notation of Ellis. — Below: The corresponding α - β coincidence spectrum. Random coincidences subtracted.

8. Application as coincidence spectrometer.

The field-free space around the axis implies that the spectrometer is especially well suited for coincidence investigations. In Fig. 1a is shown the position of a ZnS-screen and a multiplier tube immediately behind the source. Since the ZnS-screen covers 30 per cent of the total solid angle, the transmission for β -lines is ~ 3 per cent in the coincident spectrum.

The upper part of Fig. 9 shows a portion of the complex $Th(B + C + C')$ β -spectrum; below we see the corresponding spectrum for coincidences between electrons and α -particles. The weak lines following the α -decay of $ThC^{5)}$ can hereby be studied without any disturbance from the extremely strong neighbouring lines. The continuous background is due to β -particles from ThC in coincidence with the α -group from ThC'' , the half life of which, 3×10^{-7} sec., is of the order of magnitude of the resolving time of the coincidence circuit.

Instead of the ZnS-screen we can of course use an anthracene crystal for β - β -coincidences or a NaI crystal for β - γ -coincidences. It is our intention in the near future to insert one further multiplier with a crystal where the lead screen is now situated (Fig. 1a). This will imply, on the one hand, a doubling of the efficiency and, on the other hand, will make possible triple coincidence investigations of decays where three particles are emitted in cascade.

9. Further applications of the focusing principle.

C. A. MALLMANN⁶⁾⁷⁾ has shown the possibility of constructing a double spectrometer for β - β -coincidences by placing two magnets above each other. The β -rays can be focused simultaneously in two spectrometers when the gaps are limited to accept particles at angles $\vartheta > 90^\circ$.

A spectrometer with pole pieces shaped as sketched in Fig. 10 can be used as a pair spectrometer, since positive and negative particles can be focused simultaneously. Focusing is achieved by shaping of the two outer boundaries, while the central limiting curve can be kept symmetrical and close to a circle.

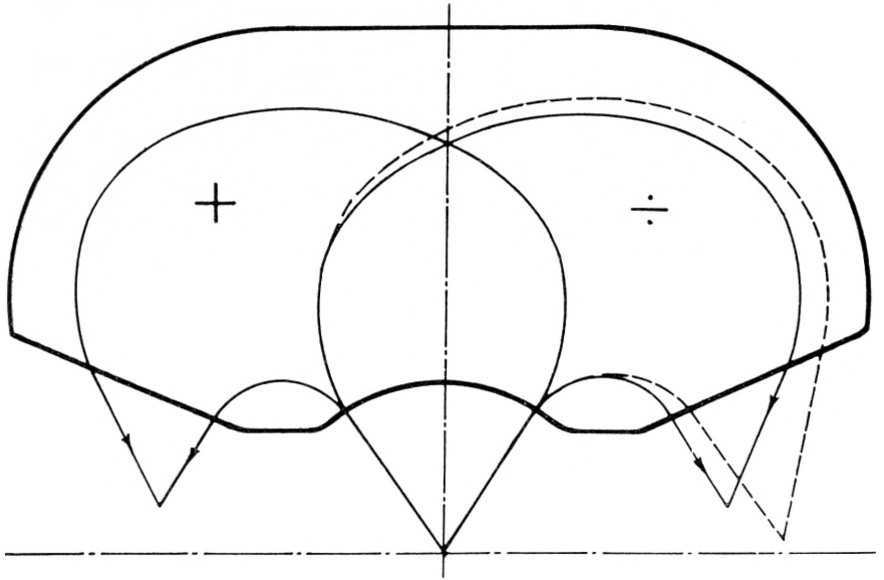


Fig. 10. Pole shape for proposed pair spectrometer.

A better relation between R and T will be obtained in this wedge-shaped field than in a homogeneous field. Furthermore, the efficiency is multiplied by the number of gaps. Also some of the advantages gained in the spectrometer developed by McDANIEL and WALKER⁸⁾ are obtained. Thus, the existence of the focal line makes it possible to work with, say, up to 2×4 counters placed close to each other. The extension of the converter is of relatively minor importance, since the sum of the momenta of electron and positron to the first approximation depends only on the relative distance between the two struck counters.

A magnet with a wedge-shaped field in a single air gap will be advantageous as double focusing spectrometer for heavy particles. In such instruments, the utilization of the theoretical solid angle demands very large magnets. In this respect, the proposed design is cheaper than the type used at present⁹⁾. This results from the fact that the magnetic field should exist only in the space occupied by the beam of particles, whereas the conventional types utilize only the central part of the field in full height.

We wish to express our gratitude to Professor NIELS BOHR for his interest in our work and for the excellent working conditions at his institute. We are also indebted to Mr. J. LINDHARD for theoretical discussions.

Summary.

A β -spectrometer is described. It is constructed according to a new principle developed previously¹⁾. A transmission of 9 per cent is obtained at a resolution of 1.6 per cent. The instrument is especially well suited for coincidence investigations with scintillation counters.

Some of the properties of the spectrometer are discussed from a practical point of view. A few new applications for the focusing principle are suggested.

*Institute for Theoretical Physics,
University of Copenhagen, Denmark.*

References.

- 1) O. KOFOED-HANSEN, J. LINDHARD and O. B. NIELSEN: Dan. Mat. Fys. Medd. **25**, no. 16, 1950.
- 2) M. CAMAC: Rev. Sci. Instr. I, **22**, 197, 1951.
- 3) M. KORSUNSKI: J. of Phys. URSS. IX. 1, 7, 1945.
- 4) B. ELBEK, K. O. NIELSEN and O. B. NIELSEN: Phys. Rev., **95**, 96, 1954.
- 5) O. B. NIELSEN: To be published.
- 6) C. A. MALLMANN: Physica XVIII, 1139, 1952.
- 7) — Publicaciones de la Comisión Nacional de la Energía Atómica, Buenos Aires, Serie Física, Vol. 1, no. 1.
- 8) B. D. McDANIEL and L. WALKER: Phys. Rev. **74**, 315, 1948.
- 9) C. W. SNYDER, S. RUBIN, W. A. FOWLER and C. C. LAURITSEN: Rev. Sci. Instr. I. **21**, 855, 1950.

Det Kongelige Danske Videnskabernes Selskab

Matematisk-fysiske Meddelelser, bind 29, nr. 7

Dan. Mat. Fys. Medd. 29, no. 7 (1955)

STUDIES OF ABSORPTION SPECTRA VI

Actinide Ions with two 5 *f*-Electrons

BY

CHR. KLIXBÜLL JØRGENSEN



København 1955

i kommission hos Ejnar Munksgaard

The Royal Danish University of Science
Copenhagen
1958

STUDIES OF ABSORPTION SPECTRA VI

BY
CHRISTIAN HANSEN

CHRISTIAN HANSEN



Printed in Denmark.
Bianco Lunos Bogtrykkeri A-S.

Introduction.

The absorption spectrum of uranium (IV) ions is interpreted as the atomic spectrum of the free ion with little influence from crystal fields. It is compared with the theoretical predictions of CONDON and SHORTLEY for systems with two f -electrons. The identification is supported by the behaviour of the spectrum of different complexes and by a new band in the ultraviolet. The energy levels are related to the actinide hypothesis, and chemical conclusions drawn from the absence of very strong absorption bands.

The absorption spectra of the lanthanide and actinide ions consist of narrow bands, which are not much influenced by chemical changes in the complexes. They are supposed to be practically the same as the atomic spectra of the free ions in vacuo, while the ordinary transition group ions have absorption spectra that are strongly dependent on the crystal field perturbations of the ligands.

The theoretical interpretation of the lanthanide spectra has been successful in simple cases. According to Pauli's equivalence theorem of electrons and holes, f^n gives the same number of terms as f^{14-n} . Thus, f^2 and f^{12} both correspond to two effective electrons, as found in Pr^{+++} and Tm^{+++} . The absorption spectrum of the praseodymium ion is discussed by ELLIS,¹ GOBRECHT,² LANGE,³ and SPEDDING,⁴ while BETHE and SPEDDING⁵ interpreted the thulium ion spectrum. Recently, the 3-electron system Nd^{+++} has been described by SATTEN.⁶ Besides this, only the ground-levels and some few other levels of the complicated lanthanide ions have been identified.

The atomic spectra of $4f^2$ are best known from La^+ , studied by RUSSELL and MEGGERS.⁷ Later the $5f^2$ -system Th^{++} was

studied by DE BRUIN, KLINKENBERG and SCHUURMANS.⁸ Of the 5 f^2 -systems of chemical interest U^{+4} is perhaps the best known. The absorption spectra of uranium (IV) complexes are the main subject of the following discussion.

Theoretical Predictions.

CONDON and SHORTLEY⁹ give a general treatment of the interaction between a few electrons by different coupling-schemes, which are idealized simplifications of the observed distribution of energy levels. In particular, the intermediate cases between (L, S) coupling (the Russell-Saunders case) and (j, j) coupling are discussed. Although (j, j) coupling is most prominent in the heavy atoms, particularly at the ends of the periods, (L, S) coupling will presumably be predominant in U^{+4} .

The electrostatic interaction of two equivalent f -electrons is given⁹ as functions of the integrals F_0 , F_2 , F_4 , and F_6 , which are determined by the electric field of the kernel, in this case the emanation configuration. SATTEN⁶ points out that the inequalities

$$F_4 \leq 0.202 F_2 \text{ and } F_6 \leq 0.0306 F_2 \quad (1)$$

are valid from the definition of these integrals⁹ (The inequality $F_6 \leq 0.00306 F_2$ is erroneously given in Satten's paper).

In the cases* La^+ , Pr^{+++} , and Th^{++} (ref. 7, 4, and 8, respectively) these integrals are given in the energy unit cm^{-1} .

	F_2	F_4	F_6
La^+	93.3 cm^{-1}	21.6 cm^{-1}	0.26 cm^{-1}
Pr^{+++}	232	47	
Th^{++}	208	42	4.6

It is most probable that the ratio F_4/F_2 has nearly the maximum value, i. e. 0.2.

The possibility of F_6 being approximately $0.03 F_2$ is very important for the position of some of the terms. Table 1 in the first two columns gives the electrostatic interaction of f^2 in the two

* RACAH⁴¹ has later given the parameters $F_2 = 193$, $F_4 = 36$, and $F_6 = 3.4 \text{ cm}^{-1}$ for Th^{++} , while KLINKENBERG⁴² gives the values 200, 55, and 4.3 cm^{-1} , respectively.

cases ($F_4 = 0.2 F_2$ and $F_6 = 0$) and ($F_4 = 0.2 F_2$ and $F_6 = 0.02 F_2$). The energy $2 F_0$, which is constant for all the given terms, is not considered.

The next column of Table 1 gives the interval splitting, expressed⁹ by the Landé interval factor ζ . This energy is added to the electrostatic interaction to give the energy of the level relative to the other levels of f^2 .

Only in the limiting case where $\zeta = 0$ the Russell-Saunders (L, S) coupling is completely in concordance with the experimental data. For increasing values of ζ the atom will approximate to (j, j) coupling, and eventually L and S will no longer have physical significance, but only the vector sum J from the j of the individual electrons. The intermediate coupling cases can be quantitatively treated by the perturbation theory, e. g. as applied by SPEDDING.⁴ For the values of J where only one level is represented in the configuration (as in the case of f^2 , with odd J values), no perturbation is predicted. In the cases where two ($J = 0$ and 6) or three ($J = 2$ and 4) levels exist with the same J , the perturbation energy is given as a function of ζ and the distances between the levels which perturb each other. The secular determinants producing these functions are given by SPEDDING.⁴ In the simple case with only two levels the energies are thus:

$$E_6 = \frac{I + H + 5 \zeta}{2} \pm \left\{ \left(\frac{I - H - 5 \zeta}{2} \right)^2 + 6 \zeta^2 \right\}^{\frac{1}{2}}$$

and

$$E_0 = \frac{S + P - 2 \zeta}{2} \pm \left\{ \left(\frac{S - P + 2 \zeta}{2} \right)^2 + 48 \zeta^2 \right\}^{\frac{1}{2}},$$

where S, P, H , and I are the electrostatic energies of the terms. The negative sign of the square root is used for the energy of the lower of the two perturbed levels, and the positive sign for the higher energy.

The last column of Table 1 gives the sign of the perturbation energy. In the cases of $J = 2$ and 4 the outermost levels are perturbed to greater distances, and the displacement of the middle one is determined by the position of the two other levels.

This theory does not consider the perturbation from electron configurations other than f^2 (see ref. 9, chapter 15). This con-

TABLE 1. The Condon-Shortley energies of f^2 .

Level	Electrostatic interaction energy		Multiplet splitting due to (L, S) interaction	Sign of perturbation energy
	$F_4 = 0.2 F_2$ $F_6 = 0$	$F_4 = 0.2 F_2$ $F_6 = 0.02 F_2$		
3H_4	$-35.2 F_2$	$-35.5 F_2$	-6ζ	—
3H_5	-35.2	-35.5	-1	0
3H_6	-35.2	-35.2	$+5$	—
3F_2	-16.6	-22.3	-4	—
3F_3	-16.6	-22.3	-1	0
3F_4	-16.6	-22.3	$+3$	$+ \text{ or } -$
1G_4	-10.4	-9.0	0	$+$
1D_2	-0.8	$+13.5$	0	$+ \text{ or } -$
1I_6	$+26.8$	$+26.8$	0	$+$
3P_0	$+51.6$	$+25.0$	-2	—
3P_1	$+51.6$	$+25.0$	-1	0
3P_2	$+51.6$	$+25.0$	$+1$	$+$
1S_0	$+99.6$	$+133.9$	0	$+$

figuration interaction takes place between terms with the same L, S and parity. Thus all configurations $[Em] 6d^2$, $[Em] 5g 7s$, and $[Em] 5f 7p$ are able to interact with some terms of $[Em] 5f^2$. In many cases, the configuration interactions in heavy atoms will remove the physical significance of electron configurations. The wave-functions of the individual terms will be mixtures of the corresponding hydrogen-like wave-functions of the pure electron configurations. It is almost impossible to predict the direction of the displacement of the levels, due to configuration interaction, before the atomic spectrum of e. g. U^{+4} is analyzed. This refinement cannot be expected yet, since the very complicated line spectra of the actinide elements are extremely difficult to disentangle. The chemical absorption spectroscopy may here give information to atomic spectroscopists about the terms of the lowest configuration of the given ion.

Experimental.

Most absorption spectra of dissolved uranium (IV) salts have been measured on the sulphate, chloride or bromide. While ÅHRLAND and LARSSON¹⁰ in the two last cases have shown that

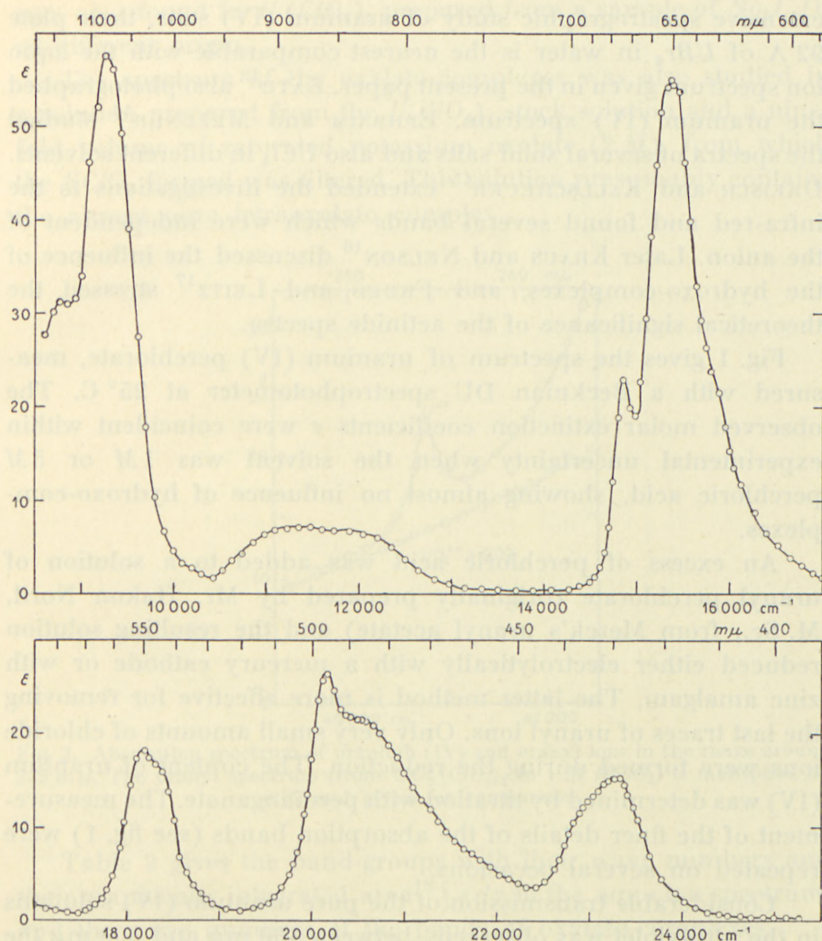


Fig. 1. Absorption spectrum of aquo uranium (IV) ions from measurements in 1 *M* and 5 *M* $HClO_4$ at 25° C. The molar extinction coefficient $\epsilon = \frac{\log_{10} I_0 - \log_{10} I}{cl}$ is given as a function of the wave number in the range 8500—25500 cm^{-1} . The path width l is 1 cm and the concentration c of U^{+4} is 0.1 *M* and 0.02 *M*.

the halide complexes are not very strong, the aquo ion can best be studied in uranium (IV) perchlorate with enough perchloric acid added to suppress formation of hydroxo compounds.

Among the spectra given in the literature FORMANEK¹¹ investigated solutions in hydrochloric acid, which also clearly showed uranium (III) bands. JONES and STRONG¹² made a very

extensive spectrographic study of uranium (IV) salts, their plate 92 A of $U\text{Br}_4$ in water is the nearest comparable with the aquo ion spectrum given in the present paper. KATO¹³ also photographed the uranium (IV) spectrum. EPHRAIM and MEZENER¹⁴ studied the spectra of several solid salts and also $U\text{Cl}_4$ in different solvents. DREISCH and KALLSCHEUER¹⁵ extended the investigations to the infra-red and found several bands which were independent of the anion. Later KRAUS and NELSON¹⁶ discussed the influence of the hydroxo-complexes, and FREED and LEITZ¹⁷ stressed the theoretical significance of the actinide spectra.

Fig. 1 gives the spectrum of uranium (IV) perchlorate, measured with a Beckman DU spectrophotometer at 25° C. The observed molar extinction coefficients ϵ were coincident within experimental uncertainty when the solvent was 1M or 5M perchloric acid, showing almost no influence of hydroxo-complexes.

An excess of perchloric acid was added to a solution of uranyl perchlorate (originally prepared by Mr. Hakon Nord, M. Sc., from Merck's uranyl acetate) and the resulting solution reduced either electrolytically with a mercury cathode or with zinc amalgam. The latter method is more effective for removing the last traces of uranyl ions. Only very small amounts of chloride ions were formed during the reduction. The content of uranium (IV) was determined by titration with permanganate. The measurement of the finer details of the absorption bands (see fig. 1) were repeated on several occasions.

Considerable transmission of the pure uranium (IV) solutions in the ultraviolet was observed—between 400 $m\mu$ and 300 $m\mu$ the molar extinction coefficient is well below 1. When further measurement with the hydrogen lamp were performed at shorter wave lengths it was evident that uranyl ions formed by oxidation were the most prominent absorbing material. However, a new band appeared at 245 $m\mu$, narrow and with a moderate extinction coefficient, maximally about 20. This band resembles the other bands found in the visible spectrum. Fig. 2 shows that it cannot reasonably be attributed to oxidation, since the uranyl spectrum increases in the interesting range without the faintest sign of a peak. The background in the uranium (IV) spectrum is presumably only partially due to the uranyl impurities. The narrow band

was also found in $U(ClO_4)_4$ prepared from a sample of $Na_2U_2O_7$ of different origin.

The spectrum of the oxalato-complexes was also studied in a solution prepared from the $U(ClO_4)_4$ stock solution and a nine-fold volume of saturated potassium oxalate (2 M), from which the $KClO_4$ formed was filtered. This solution presumably contains the almost pure tetraoxalato complex.

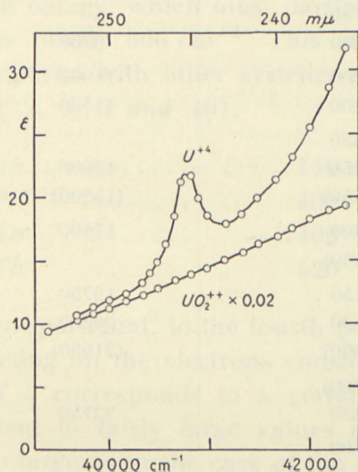


Fig. 2. Absorption spectrum of uranium (IV) and uranyl ions in the range around 245 m μ . The uranyl spectrum (from $UO_2(ClO_4)_2$ in 1 M $HClO_4$) is multiplied by 0.02 and given for comparison.

Table 2 gives the band-groups with their wave numbers and their graphically integrated area¹⁸ $\int \epsilon d\nu$ in the aquo ion spectrum, and the wave numbers of the bands of oxalato-complexes.

Since the spectrum of uranium (IV) complexes is not highly influenced by complex formation, the crystal field perturbations are small as compared with the multiplet splitting determined by the Landé factor ζ . Since the thermal energy is small as compared with ζ (kT at room temperature corresponding to 210 cm^{-1}) the higher levels of ground-term 3H are only negligibly populated, and all the narrow absorption bands must be due to transitions from 3H_4 .

It appears from Table 2 that the bands of oxalato-complex are displaced on the average 400 cm^{-1} towards lower wave numbers as compared with the aquo ion spectrum. Presumably

TABLE 2. The uranium (IV) bands observed.

Band group no.	Wave numbers of maxima in cm^{-1} (shoulders in parenthesis)		Area = $\int \epsilon d\nu$
	Uaq_N^{+4}	Uox_4^{-4}	Uaq_N^{+4}
1.....	{ 6550 } { (6900) } (ref. 15)		
2.....	{ (8750) } { 9300 }	9200	} $5 \cdot 10^4 \text{ cm}^{-1}$
3.....	{ 11200 } { 12000 }	11000 11500	} 1.3 ·
4.....	{ 14850 } { 15350 } { (15850) }	15000 15000 (15800)	} 4.8 ·
5.....	{ 18200 } { (18350) }	17800	} 1.2 ·
6.....	{ 20150 } { 20500 } { (21300) }	19750 20300 (21000)	} 3.6 ·
7.....	{ (23000) } { 23350 }	22750	} 1.5 ·
8.....	40800		} ~ 1 ·

the lowest of the levels into which 3H_4 is split by the crystal field from the ligands is some hundred cm^{-1} lower in the aquo ion than in the oxalato complex (cf. the theory of BETHE¹⁹). The symmetry of the uranium (IV) complexes discussed here seems to be cubic or nearly cubic. MARCHI and McREYNOLDS²⁰ maintain that the tetraoxalato complex most probably has the Archimedean anti-prism configuration.

All the uranium (IV) bands have relatively large half widths of about four hundred cm^{-1} (as in Pr^{+++}), while no observed band is very narrow, as e. g. the band at 427μ of Nd^{+++} . Thick layers of concentrated uranium (IV) solutions transmit light in such narrow parts of the visible spectrum between the absorption bands that they can be used for optical filters in some cases.

Identification of the Uranium (IV) Bands.

In a following section the arguments will be given for the electron configuration in uranium (IV) complexes being $[Em] 5f^2$. Under this assumption the theoretical predictions are compared with the observed spectra: One of the most certain identifications of the band groups in Table 2 is the very strong group 2 as ${}^3H_4 - {}^3H_6$. According to Table 1, the energy difference is 11ζ besides some perturbation energy, which must partially cancel. Thus the Landé factor ζ is nearly 800 cm^{-1} . This is a very reasonable value if it is compared with other systems with two effective f -electrons (see ref. 7, 4, 5 and 40):

La^+	$\zeta \sim 140 \text{ cm}^{-1}$
Pr^{+++}	400
Tm^{+++}	-1400
Th^{++}	520

ζ is formally proportional⁹ to the fourth power of the effective nuclear charge acting on the electrons considered.

This value of ζ corresponds to a certain amount of (j, j) coupling, equivalent to fairly large values of the perturbation energy, but not so large as in the case of the thulium ion (which has a nearly closed shell and correspondingly inverted multiplets with a highly negative Landé factor). It is predicted that the selection rule of S will be obeyed in some degree, giving higher intensities, *inter alia* to the triplet transitions, than to the singlets from the triplet ground-state. The intensities are presumably increasing with the value of J , but configuration interaction may cause peculiar intensity values.

The electrostatic interaction parameter F_2 can next be determined to 380 cm^{-1} from the identification of the ultraviolet band (no. 8 in Table 2) with ${}^3H_4 - {}^3P_2$. If the first column of Table 1 is chosen, the energy of this transition corresponds to

$$\{ 86.8 F_2 + 7 \zeta + \text{some perturbation energy} \}.$$

The alternative possibility of representing 3P_2 by band No. 7 would give a much more compressed* energy scale with F_2 only

* Good agreement is obtained, if F_6 is large ($\sim 10 \text{ cm}^{-1}$). But then a band is masked by others in the visible part of the spectrum, presumably 1I_6 , and the other identifications are not altered much.

about 180 cm^{-1} . This would not agree well with F_2 in Th^{++} , which is⁸ 208 cm^{-1} , since F_2 is roughly proportional to $Z + 1$, where Z is the external charge of the ion (cf. the discussion of the first transition group by CONDON and SHORTLEY⁹). From Table 1 it follows that 3F_2 and 3H_5 must be placed at essentially smaller wave numbers than one is able to measure on the Beckman *DU* spectrophotometer. The bands of lower intensity than 3H_6 , which were discovered in the infra-red by DREISCH and KALLSCHEUER¹⁵ are presumably due to these transitions. The low band group 3 is due to 3F_3 and the four other band groups in the visible, Nos. 4, 5, 6 and 7, can tentatively be assigned to the transitions from 3H_4 to 3F_4 , 1D_2 , 1G_4 , and 1I_6 , respectively. Then no observed band-group remains unidentified and predicted bands are only missed at about 36000 cm^{-1} (3P_0) and 38000 cm^{-1} (3P_1) in addition to the unobservable 1S_0 at 58000 cm^{-1} .

When the perturbation energies are found from the determinantal equations given by SPEDDING,⁴ curious consequences are found if $F + 3\zeta$ is nearly equal to G , where F and G are the electrostatic interaction energies found from the Condon-Shortley theory (see Table 1) for the terms 3F and 1G . The difference between two of the three roots of the equation for $J = 4$ will then be approximately 7.7ζ (in this case 6160 cm^{-1}) while the lowest root is placed 750 cm^{-1} below $H - 6\zeta$ by the perturbation. The former difference agrees reasonably well with the difference found between the two strong band groups Nos. 4 and 6, although the average wave number calculated is too low.

The question which of the two highest levels with $J = 4$ is 3F_4 and which is 1G_4 has no physical significance. The wave functions will be intermixed with nearly equal coefficients, and the triplet character transferred so much to both states that the intensity can be nearly equal. This is often the case, e. g., in the heavy atoms of the inert gases.²¹

This identification is supported by the shapes of the band groups, whose fine structure is due to the crystal field splitting of the excited state and the ground-state, 3H_4 . According to the theory of BETHE¹⁹ these weak crystal field perturbations will only depend on J . The bands identified here as being due to transitions to states with $J = 6$ thus have very similar structures with a

satellite towards lower wave numbers. The two band groups with $J = 4$ have the complicated structure with three or more partial bands in the spectrum of uranium (IV) aquo ion (see fig. 1). The case of $J = 3$ has another structure.

The succession of 1D_2 and 1G_4 has been inverted in the identification, due to the fine structure. The weakest point is the position of 1I_6 , which further has too small an intensity. But it is necessary to assume that it is the last band before 3P . The energy of 1I_6 seems also to be depressed⁸ in Th^{++} and is perhaps affected by configuration interactions.

It is remarkable that the Condon-Shortley theory, which has not met with very great success in dealing with the heavy atoms, is in so good agreement with the experimental data for the uranium (IV) spectrum. Table 3 gives the results with $F_2 = 380 \text{ cm}^{-1}$, $F_4 = 76 \text{ cm}^{-1}$, $F_6 = 0 \text{ cm}^{-1}$ (which seems to be the best approximation), $\zeta = 800 \text{ cm}^{-1}$, and the perturbation energies calculated by the method of SPEDDING,⁴ as compared with the observed wave number of the centre of gravity of the band group in the aquo ion spectrum.

TABLE 3. Calculated and observed levels of U^{+4} .

	Calculated	Observed
3H_5	4750 cm^{-1}	—
3H_6	9350	9200 cm^{-1}
3F_2	7700	6600 (ref. 15)
3F_3	11800	11600
3F_4 (1G_4)	12050	15400
1D_2	19500	18250
1G_4 (3F_4)	18700	20500
1I_6	29350	23200
3P_0	35500	—
3P_1	37700	—
3P_2	40000	40800
1S_0	58200	—

The average value of the absolute deviation $|v_{\text{obs}} - v_{\text{calc}}|$ is thus 1800 cm^{-1} for the 8 observed bands. The calculations of SPEDDING⁴ show the average deviation 440 cm^{-1} for the 10 bands of Pr^{+++} and of BETHE and SPEDDING⁵ 1170 cm^{-1} for the 7 observed bands of Tm^{+++} .

The Other Actinide Elements.

The suggestion that uranium is an ordinary transition element without f -electrons was rejected by KIESS, HUMPHREYS and LAUN,²² who proved that the ground-state is 5L_6 from the configuration $[Em] 5f^3 6d 7s^2$. SCHUURMANS²³ demonstrated that the lowest configuration of U^+ is $[Em] 5f^3 7s^2$ closely followed by $[Em] 5f^3 6d 7s$. Since in the transition groups the electrons with the highest principal quantum numbers are removable by ionization, it is almost certain that the fourth ionization state of uranium has the configuration $[Em] 5f^2$. There is no contradiction in the fact* that $[Em] 5f 6d$ has lower energy (15000 cm^{-1}) in Th^{++} than $[Em] 5f^2$, since f -electrons have steeply decreasing energies with increasing atomic number in the lanthanide and actinide elements.

Experimentally, attention has been concentrated on the magnetic properties. HUTCHINSON and ELLIOT²⁴ and HOWLAND and CALVIN²⁵ concluded that all the ions of the elements with atomic numbers from 92 to 95 have the general configuration $[Em] 5f^n$. But some evidence for $[Em] 6d^2$ has been found in the case of solid uranium (IV) compounds. While $5f^2$ in (L, S) coupling should give a magnetic moment of 3.58 Bohr magnetons and in (j, j) coupling 3.84 B.m., $6d^2$ is presumed to have its orbital moment quenched and to give the value 2.83 B.m. calculated from spin moment only. DAWSON²⁶ measured solid solutions of UF_4 in ThF_4 and (analogous to TRZEBIATOWSKI and SELWOOD²⁷) UO_2 in ThO_2 , and found decreasing magnetic moment by dilution with the diamagnetic thorium compounds, varying from 3.3 to 2.9 B.m. The $5f$ -electrons are not so effectively shielded in the actinides as the $4f$ -electrons in the lanthanides. If the levels of 3H_4 split by crystal fields are not equally populated, magnetic effects may be produced. According to NYHOLM,²⁸ the magnetic moment of sodium plutonyl acetate measured by DAWSON²⁹ is not a definite proof of the configuration $[Em] 6d^2$ of PuO_2^{++} .

Spectroscopic evidence is strongly against the possibility of $[Em] 6d^2$ for U^{+4} , which would give very broad bands as the ordinary transition group complexes. The green UF_4 according

* The configuration $[Em] 6d^2$ seems⁴¹ to be placed 810 cm^{-1} below $[Em] 5f 6d$ in Th^{++} .

to EPHRAIM and MEZENER¹⁴ has a reflection spectrum composed of bands at nearly same places as the aquo ion. An interesting case is the brown UO_2 , which has not the usual colour of U^{+4} (compare e. g. the lanthanide sesquioxides which are coloured by the trivalent lanthanide ions alone). Recently, GRUEN³⁰ has studied solid solutions of UO_2 in ThO_2 . While pure UO_2 has a steeply increasing absorption below 600 $m\mu$ besides an absorption band at 670 $m\mu$, the mixtures with much ThO_2 have narrow bands (as other U^{+4} salts have) at 655, 600, 540, and 515 $m\mu$, while the strong absorption begins here at 460 $m\mu$. The molecular spectrum below 460 $m\mu$ may be due to admixtures of higher oxidation states, analogous to the change of colour of CeO_2 by the presence of very small impurities. GRUEN³⁰ mentions the analogous change of absorption spectrum and electrical conductivity of olive-green nickel (II) oxide by admittance of some 10^{-4} molar excess of oxygen.

The absorption spectra of the actinide ions can further illustrate the problems discussed in SEABORG's famous paper.³¹ The spectrum of uranium (IV) ions seems not only to indicate that the $5f$ -electrons have lower energy than the $6d$ -electrons, but also that there must be a considerable energy difference. If this were not the case, transitions $5f^2-5f6d$ should occur in the spectrum. These would correspond to very strong bands, since the two combining terms are even and odd in contrast to the usual bands, which are forbidden as free dipole radiation *qua* transitions between even terms. The strong bands are known in the ultraviolet cerium (III)³² solutions, which must be caused by $[Xe]4f \rightarrow [Xe]5d$ or $[Xe]6s$. They are very broad and have molar extinction coefficients near 500. The ultraviolet part of the uranium (IV) spectrum shows no sign of such bands above the steep absorption limit at $\sim 230 m\mu$. As pointed out by SEABORG,³¹ the ordinary bands of the actinide ions are about ten times intenser than those of the lanthanide ions,³² which is in good agreement with the present results. No molecular spectrum is observed in the aquo uranium (IV) ion either. This is presumably due to the low electron affinity of U^{+4} , which shows no great tendency to transfer electrons from the ligands.³³

Uranium (III) salts do not exhibit very strong absorption bands, at least over 400 $m\mu$ (from preliminary measurements in

10 M HCl after reduction with zinc amalgam). The terms originating from $[Em] 5f^2 6d$ are thus probably considerable higher than the terms from $[Em] 5f^3$ which produce the many bands in the visible spectrum.

Two other systems with two electrons outside the emanation shell are quinevalent neptunium and sexavalent plutonium, best known as the oxo-complexes NpO_2^+ and PuO_2^{++} . These ions have each a very high, narrow band in the infra-red, and a large number of small bands with extinction coefficients near 10 (see ref. 31, p. 1042 and pp. 560, 592, respectively). The high bands at $983 m\mu$ in neptunium (V) and $833 m\mu$ in plutonium (VI) can tentatively be identified as ${}^3H_4-{}^3H_6$ giving the Landé factor ζ the probable values 900 and 1000 cm^{-1} . The number of bands in neptunium (V) in the visible is remarkably large. Measurements by HINDMAN, MAGNUSSON and LA CHAPELLE (ref. 31, p. 1042) give the wave numbers ν and maximum extinction coefficients ϵ for 1 M HCl solutions:

No.	ν	ϵ	No.	ν	ϵ
1	9759 cm^{-1}	3.5	7	16180 cm^{-1}	23.5
2	10170	325	8	16610	4.5
3	10900	2.8	9	16830	5.5
4	13000	5 (broad)	10	21000	8.5
5	14530	5.2	11	23250	8.5
6	15900	9.0	12	27400	7

The group Nos. 6—9 resemble the ${}^3H_4-{}^3F_4$ (1G_4) and the three last bands the singlet transitions for 1D_2 , 1G_4 (3F_4), and 1I_6 of the uranium (IV) ion. But the vibrational structure³⁴ imparted by the two firmly bound oxygen atoms may disturb the identification. The electrostatic interaction F_2 seems to be slightly larger than in U^{+4} , as is also to be expected if the hypothesis of $[Em] 5f^2$ is correct. Recently, GRUEN and HUTCHINSON³⁵ have given magnetochemical evidence for this electron configuration of neptunium (V). The values of ζ are larger *inter alia* for the actinide ions than for the lanthanide ions, as also found from magnetic properties of americium (III).²⁵

Uranium (V) in UO_2^+ has no absorption bands in the range $360-1000 m\mu$ ³⁶. The configuration $[Em] 5f$ would only show one band in the far infra-red, since $\frac{7}{2}\zeta$ is so small an energy. In

contrast to this, systems such as $[Xe] 4f^{13}$ in ytterbium (III) have so large a (negative) Landé factor that the internal doublet splitting of 2F is 10200 cm^{-1} . BOUSSIÈRES and HAISSINSKY³⁷ give no absorption spectrum of their protactinium (IV) compounds. Neptunium (VI) in NpO_2^{++} has a larger number of low bands³⁴ which, analogous to the uranyl ion spectrum, are not yet explained by the atomic spectra.*

The absorption spectra discussed here show that the $5f$ -electrons seem to have considerably lower energy than the $6d$ -electrons, when two electrons are considered in atoms with atomic numbers of at least 92. It is hoped to investigate later the systems with more $5f$ -electrons, e. g. U^{+++} , encouraged by the success of the Condon-Shortley theory.⁹ The actinide hypothesis of SEABORG³¹ seems to be valid to a higher degree than is often concluded from chemical evidence. The higher oxidation states found in the actinide elements are only a continued development of the tendency, also found in cerium and praseodymium in the beginning of the lanthanide series.

Acknowledgment.

I am very much indebted to Professor Jannik Bjerrum for interesting discussions.

* If the electron transfer theory of molecular spectra can be applied to the uranyl ion, the bands $\sim 22000 \text{ cm}^{-1}$ of low intensity are perhaps due to transitions of less probability to f -states in contrast to the high bands $\sim 45000 \text{ cm}^{-1}$ caused by d -states.

Additional Note.

Recently, two papers have been published on the $[Em] 5f^2$ -systems of chemical interest. SANCIER and FREED³⁸ have directly compared the reflection spectra of anhydrous $PrCl_3$ and UCl_4 . While the experimental results of these authors are very valuable (e. g. the continuous absorption³⁹ below $400 m\mu$ of UCl_3), the identification of most of the visible bands of UCl_4 with ${}^3H_4-{}^1I_6$ does not seem convincing without further proof. For this purpose, solid salts of U^{+4} (and especially the chloride with the strongly split bands¹⁴) are not so useful as the aquo ion in solution. The crystal field in the liquid state is averaged over the contributions of low symmetry, while strong deviations from cubic symmetry can occur in the rigid crystal. The continuous absorption at $300 m\mu$ of UCl_4 is presumably³⁸ a molecular spectrum which can also be obtained in concentrated HCl -solutions of uranium (IV).

GRUEN⁴⁰ calculates the spectra of NpO_2^+ and PuO_2^{++} from given values of ζ and the known terms of Th^{++} ^{41, 42} after addition of about ten per cent. It might seem more reasonable to use this experimentally determined electrostatic interaction in the place of the Condon-Shortley parameters which only are a first-order approximation. But there is a possibility of transferring configuration interactions from Th^{++} to the heavier atoms which are not necessarily similar.

It may be inquired whether the electrostatic interaction is really proportional to $Z-58$ in the actinides⁴⁰ and $Z-34$ in the lanthanides,⁶ where Z is the atomic number. The strong increase of F_2 from La^+ to Pr^{+++} corresponds rather to proportionality to the external charge $+1$, thus in this case $Z-55$. Also in the actinides evidence can be found for increasing electrostatic interaction: The isoelectronic species Np^{+++} and Pu^{+4} ($[Em] 5f^4$) have a nearly biunique correspondance between their absorption bands:

Np^{+++} (ref. 31, p. 1053)		Pu^{+4} (ref. 16)	
ν	ϵ_{\max}	ν	ϵ_{\max}
10000 cm^{-1}	29	12200 cm^{-1}	21
11700	23	13700	14
12700	46	15300	35
15100	29	18100	14
16600	25	19800	11
18100	41	21300	54

On an average 19 per cent higher wave numbers are observed among the band maxima of Pu^{+4} , as compared with Np^{+3} . This is of course partially due to the increased Landé interval factor ζ , which also causes larger perturbations. But the electrostatic interaction seems definitely to have increased more than three per cent found from the strong-shielding theory. The deviation may be connected with the strong dependence of the ionic radius on the external charge.

If the Gruen hypothesis⁴⁰ is applied to U^{+4} , the identifications of the band-groups of Table 2 would be: No. 2 3H_6 , No. 3 uncertain, No. 4 most of 3P and 1G_4 , No. 5 perhaps 3P_1 , No. 6 1I_6 , No. 7 1D_2 , and No. 8 1S_0 . It is interesting to note that a very large ζ (over 1100 cm^{-1}) also could explain some features of the observed spectrum: Band group No. 2 now being 3F_4 , No. 4 3H_6 and some 3P -levels, No. 6 1G_4 , and No. 8 1S_0 . But the primary hypothesis, the relatively low energy of 3P and high 1D , does not seem totally justifiable. As also given by RACAH⁴¹ for Th^{++} , it corresponds to a large value of F_6 and relatively small value of F_2 .

Chemistry Department A,
Technical University of Denmark, Copenhagen.

References.

1. ELLIS, C. B. *Phys. Rev.* **49** (1936) 875.
2. GOBRECHT, H. *Ann. d. Physik* [5] **28** (1937) 673.
3. LANGE, H. *Ann. d. Physik* [5] **31** (1938) 609.
4. SPEDDING, F. H. *Phys. Rev.* **58** (1940) 255.
5. BETHE, H. and SPEDDING, F. H. *Phys. Rev.* **52** (1937) 454.
6. SATTEN, R. A. *J. Chem. Phys.* **21** (1953) 637.
7. RUSSELL, N. H. and MEGGERS, W. F. *J. Res. Nat. Bur. Stand.* **9** (1932) 625.
8. BRUIN, T. L. DE, KLINKENBERG, P. F. A. and SCHUURMANS, PH. *Z. Physik* **118** (1941—42) 58.
9. CONDON, E. U. and SHORTLEY, G. H. *The Theory of Atomic Spectra*, Cambridge 1953.
10. AHLRAND, S. and LARSSON, R. *Acta Chem. Scand.* **8** (1954) 137.
11. FORMANÉK, J. *Die qualitative Spektralanalyse*. Berlin 1905.
12. JONES, H. C. and STRONG, W. W. *A Study of the Absorption Spectra . . .*, Carnegie Inst. Publ. **130** Washington 1910.
13. KATO, S. *Scient. Paper Inst. Phys. Chem. Res.* **13** (1930) 49.
14. EPHRAIM, F. and MEZENER, M. *Helv. Chim. Acta* **16** (1933) 1260.
15. DREISCH, TH. and KALLSCHEUER, O. *Z. Physik. Ch. B* **45** (1939) 19.
16. KRAUS, K. A. and NELSON, F. *The Hydrolytic Behaviour . . . U.S. Atomic Energy Comm. Doc. 1888* (1948).
17. FREED, S. and LEITZ, F. J. *The Absorption Spectra . . . U.S. Atomic Energy Comm. Doc. 1890* (1948).
18. JØRGENSEN, C. KLIXBÜLL, *Acta Chem. Scand.* **8** (1954) 1495.
19. BETHE, H. *Ann. d. Physik* [5] **3** (1929) 133.
20. MARCHI, L. E. and McREYNOLDS, J. P. *J. Am. Chem. Soc.* **65** (1943) 333 and MARCHI, L. E. *ibid.* **65** (1943) 2257.
21. RASMUSSEN, E. *Serier i de ædle Luftarters Spektre . . .* Thesis. Copenhagen 1932.
22. KIESS, C. C., HUMPHREYS, C. J. and LAUN, D. D. *J. Res. Nat. Bur. Stand.* **37** (1946) 57.
23. SCHUURMANS, PH. *Physica* **11** (1946) 419.
24. HUTCHINSON, C. A. and ELLIOT, N. J. *Chem. Phys.* **16** (1947) 920.
25. HOWLAND, J. J. and CALVIN, M. J. *Chem. Phys.* **18** (1950) 239.
26. DAWSON, J. K. *J. Chem. Soc.* **1952**, 1185.
27. TRZEBIATOWSKI, W. and SELWOOD, R. W. *J. Am. Chem. Soc.* **72** (1950) 4504.

28. NYHOLM, R. S. Quarterly Rev. **7** (1953) 377.
 29. DAWSON, J. K. J. Chem. Soc. **1952** 2705.
 30. GRUEN, D. M. J. Am. Chem. Soc. **76** (1954) 2117.
 31. SEABORG, G. T. The Transuranium Elements. Nat. Nuclear Energy Ser. Div IV, **14 B** (1949) 1492.
 32. STEWART, D. C. Light Absorption . . . U.S. Atomic Energy Comm. Doc. **2389** (1948).
 33. JØRGENSEN, C. KLIXBÜLL. Acta Chem. Scand. **8** (1954) 1502.
 34. SJOBLOM, R. and HINDMAN, J. C. J. Am. Chem. Soc. **73** (1951) 1744 and JONES, L. H. and PENNEMAN, R. A. J. Chem. Phys. **21** (1953) 542.
 35. GRUEN, D. M. and HUTCHINSON, C. A. J. Chem. Phys. **22** (1954) 386.
 36. KRAUS, K. A., NELSON, F. and JOHNSON, G. L. J. Am. Chem. Soc. **71** (1949) 2510.
 37. HAISSINSKY, M. and G. BOUSSIÈRES. J. Chem. Soc. **1949** S. 256.
 38. SANCIER, K. M. and FREED, S. J. Chem. Phys. **20** (1952) 349.
 39. FREED, S. and SANCIER, K. M. J. Chem. Phys. **22** (1954) 928.
 40. GRUEN, D. M. J. Chem. Phys. **20** (1952) 1818.
 41. RACAH, G. Physica **16** (1950) 651.
 42. KLINKENBERG, P. F. A. Physica **16** (1950) 618.
-

Det Kongelige Danske Videnskabernes Selskab

Matematisk-fysiske Meddelelser, bind 29, nr. 8

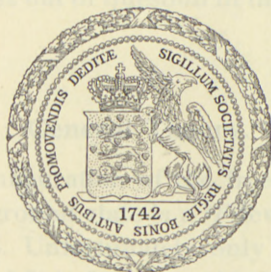
Dan. Mat. Fys. Medd. 29, no. 8 (1955)

STUDIES OF ABSORPTION SPECTRA V

The Spectra of Nickel (II) Complexes

BY

C. J. BALLHAUSEN



København 1955

i kommission hos Ejnar Munksgaard

Det Kongelige Danske Videnskabskabernes Selskab

Meddelelse fra Videnskabsrådets Sekretariat, Nr. 11

Udgivet den 15. April 1955

STUDIES OF ABSORPTION SPECTRA V

The Spectra of Nickel(II) Complexes

by

C. J. BALLHAUS



Printed in Denmark
Bianco Lunos Bogtrykkeri A-S

Various properties of the absorption spectra of the complexes of the first transition group elements have been discussed in the previous papers of this series.¹⁻⁴ The basis of these considerations was the crystal-field theory, a theory in which the assumption is made that the main properties of e. g. a complex, are determined by the electrical field originating from the ligands. It was shown that a simple perturbation treatment could account quantitatively for the absorption bands in the copper (II) complexes.

The present paper is intended to give an account of the information that may be obtained about the Ni(II)-complexes when using the crystal field theory. For this purpose the necessary quantitative results for eight equivalent *d*-electrons (or two positrons) will be derived. The derivation will be carried out in the most straightforward manner on the analogy of the method in ref. 2. The formulae derived will be utilized in the numerical calculations of the spectra of the simple para- and diamagnetic Ni(II)-ammines. Further it is shown that a strong hybridization using *3d* orbitals seems out of question in the discussed octahedral Ni(II)-complexes.

General Theory.

The electronic configuration of the free Ni(II) ion is $1s^2 2s^2 2p^6 3s^2 3p^6 3d^8$, the ground state is a 3F level. The lowest excited states are: $^1D^3P^1G^1S$. Unfortunately only the 3P term value is known with accuracy.⁵ It is found at 17000 cm^{-1} . The "normal" bands with a molar extinction coefficient $\epsilon \sim 10$ are due to transitions between states with the same multiplicity.^{2, 4} Therefore it is the splittings of the 3F and 3P terms which determine

the spectra of the paramagnetic complexes, and the splittings of the 1D , 1G and 1S terms which determine the spectra of the diamagnetic Ni(II) complexes.

We assume that the perturbing field originating from the ligands is so strong that the $(L-S)$ coupling can be neglected. The value of L and the symmetry of the field then determine the number of states into which a given term splits up. We shall use the hole-formalism² and treat the eight $3d$ electrons as equivalent to two $3d$ positrons. The unperturbed wave functions $\Psi_{L,M}$ with angular momentum L and the magnetic quantum number $M = -L, -L+1 \dots L$ are constructed by combinations of the single particle wave functions $\psi(1)$ and $\psi(2)$ of the two $3d$ positrons.

The wave functions $\Psi_{3,M}$ for the 3F state can be found by the method of CONDON and SHORTLEY.⁶ Leaving out the spin-functions we find:

$$\left. \begin{aligned}
 \Psi_{3,3} &= \sqrt{\frac{1}{2}} (\psi_2(1) \psi_1(2) - \psi_1(1) \psi_2(2)) \\
 \Psi_{3,2} &= \sqrt{\frac{1}{2}} (\psi_2(1) \psi_0(2) - \psi_0(1) \psi_2(2)) \\
 \Psi_{3,1} &= \sqrt{\frac{3}{10}} (\psi_2(1) \psi_{-1}(2) - \psi_{-1}(1) \psi_2(2)) \\
 &\quad + \sqrt{\frac{1}{5}} (\psi_1(1) \psi_0(2) - \psi_0(1) \psi_1(2)) \\
 \Psi_{3,0} &= \sqrt{\frac{1}{10}} (\psi_2(1) \psi_{-2}(2) - \psi_{-2}(1) \psi_2(2)) \\
 &\quad + \sqrt{\frac{2}{5}} (\psi_1(1) \psi_{-1}(2) - \psi_{-1}(1) \psi_1(2)) \\
 \Psi_{3,-1} &= \sqrt{\frac{3}{10}} (\psi_1(1) \psi_{-2}(2) - \psi_{-2}(1) \psi_1(2)) \\
 &\quad + \sqrt{\frac{1}{5}} (\psi_0(1) \psi_{-1}(2) - \psi_{-1}(1) \psi_0(2)) \\
 \Psi_{3,-2} &= \sqrt{\frac{1}{2}} (\psi_0(1) \psi_{-2}(2) - \psi_{-2}(1) \psi_0(2)) \\
 \Psi_{3,-3} &= \sqrt{\frac{1}{2}} (\psi_{-1}(1) \psi_{-2}(2) - \psi_{-2}(1) \psi_0(2))
 \end{aligned} \right\} (1)$$

The indices on the $3d$ single-particle wave functions refer to the magnetic quantum numbers.

The perturbation term of the Hamiltonion is the same as the one used in ref. 2, equation (3)

$$\mathbf{H}^{(1)} = \mathbf{H}^{(1)}(1) + \mathbf{H}^{(1)}(2)$$

$$\mathbf{H}^{(1)}(1) = -D(m) \frac{1}{\sqrt{2\pi}} \sum_{n=0}^{\infty} \sum_{m=-n}^n \frac{4\pi}{2n+1} \frac{r^n}{r^{n+1}} \bar{Y}_n^m(\theta_1 \varphi_1) \bar{P}_n^m(0)$$

The different terms $H_{MM'}^{(1)} = \int \Psi_{3M} \mathbf{H}^{(1)} (\Psi_{3M'})^* d\tau$ in the secular equation now have to be evaluated. On the analogy of the argument in ref. 2, it is seen that in the single electron integrals n must be 4, 2, and 0. $H_{MM'}^{(1)}$ is then different from zero only for $m = 4, 2$ and 0, which means that $M - M'$ must be even.

The secular equation is then:

$$\begin{vmatrix} H_{33}^{(1)} - E^{(1)} & 0 & H_{31}^{(1)} & 0 & H_{3-1}^{(1)} & 0 & H_{3-3}^{(1)} \\ 0 & H_{22}^{(1)} - E^{(1)} & 0 & H_{20}^{(1)} & 0 & H_{2-2}^{(1)} & 0 \\ H_{13}^{(1)} & 0 & H_{11}^{(1)} - E^{(1)} & 0 & H_{1-1}^{(1)} & 0 & H_{1-3}^{(1)} \\ 0 & H_{02}^{(1)} & 0 & H_{00}^{(1)} - E^{(1)} & 0 & H_{0-2}^{(1)} & 0 \\ H_{-13}^{(1)} & 0 & H_{-11}^{(1)} & 0 & H_{-1-1}^{(1)} - E^{(1)} & 0 & H_{-1-3}^{(1)} \\ 0 & H_{-22}^{(1)} & 0 & H_{-20}^{(1)} & 0 & H_{-2-2}^{(1)} - E^{(1)} & 0 \\ H_{-33}^{(1)} & 0 & H_{-31}^{(1)} & 0 & H_{-3-1}^{(1)} & 0 & H_{-3-3}^{(1)} - E^{(1)} \end{vmatrix} = 0 \quad (2)$$

By means of the symmetry conditions of the matrix and by row and column operations we get the four equations:

$$\left. \begin{aligned} E^{(1)} &= H_{22}^{(1)} - H_{-22}^{(1)} \\ (H_{22}^{(1)} + H_{-22}^{(1)} - E^{(1)}) (H_{00}^{(1)} - E^{(1)}) - 2(H_{20}^{(1)})^2 &= 0 \\ (H_{33}^{(1)} \pm H_{-33}^{(1)} - E^{(1)}) (H_{11}^{(1)} \pm H_{-11}^{(1)} - E^{(1)}) - (H_{13}^{(1)} \pm H_{-13}^{(1)})^2 &= 0 \end{aligned} \right\} (3)$$

The different $H_{MM'}^{(1)}$ are now evaluated. We get e. g. for $H_{00}^{(1)}$:

$$H_{00}^{(1)} = \int \Psi_0 \mathbf{H}^{(1)} (\Psi_0)^* d\tau$$

$$H_{00}^{(1)} = \int \left| \sqrt{\frac{1}{10}} (\psi_2^{(1)} \psi_{-2}^{(2)} - \psi_{-2}^{(1)} \psi_2^{(2)}) + \sqrt{\frac{2}{5}} (\psi_1^{(1)} \psi_{-1}^{(2)} - \psi_{-1}^{(1)} \psi_1^{(2)}) \right|^2$$

$$(\mathbf{H}^{(1)}(1) + \mathbf{H}^{(1)}(2)) d\tau_1 d\tau_2 = \frac{2}{5} \int |\psi_2|^2 \mathbf{H}^{(1)}(1) d\tau_1 + \frac{8}{5} \int |\psi_1|^2 \mathbf{H}^{(1)}(1) d\tau_1.$$

The question of obtaining the solutions of a two particle problem has then been reduced to the evaluation of the single-particle integrals. These integrals are tabulated in ref. 2, equation (9). Leaving out the common factor $\frac{8}{45} \cdot f^2$, we get:

$$H_{00}^{(1)} = D(0, \mu) \left[2 B_0 - \frac{2}{35} B_2 - \frac{3}{28} B_4 \right] + (\mu_5 + \mu_6) \left[2 B_0 + \frac{4}{35} B_2 - \frac{2}{7} B_4 \right]$$

Similarly we obtain:

$$\left. \begin{aligned} H_{11}^{(1)} &= D(0, \mu) \left[2 B_0 - \frac{3}{70} B_2 - \frac{1}{56} B_4 \right] + (\mu_5 + \mu_6) \left[2 B_0 + \frac{3}{35} B_2 - \frac{1}{21} B_4 \right] \\ H_{22}^{(1)} &= D(0, \mu) \left[2 B_0 + \frac{1}{8} B_4 \right] + (\mu_5 + \mu_6) \left[2 B_0 + \frac{1}{3} B_4 \right] \\ H_{33}^{(1)} &= D(0, \mu) \left[2 B_0 + \frac{1}{14} B_2 - \frac{3}{56} B_4 \right] + (\mu_5 + \mu_6) \left[2 B_0 - \frac{1}{7} B_2 - \frac{3}{21} B_4 \right] \\ H_{-22}^{(1)} &= D(4, \mu) \left[-\frac{5}{24} B_4 \right] \\ H_{20}^{(1)} &= D(2, \mu) \left[-\frac{5}{28} \sqrt{\frac{1}{30}} B_2 - \frac{3}{7} \sqrt{\frac{1}{30}} B_4 \right] \\ H_{-33}^{(1)} &= 0 \\ H_{-11}^{(1)} &= D(2, \mu) \left[-\frac{5}{42} B_4 - \frac{3}{35} B_2 \right] \\ H_{13}^{(1)} &= D(2, \mu) \left[\frac{15}{28} \sqrt{\frac{1}{15}} B_4 - \frac{3}{14} \sqrt{\frac{1}{15}} B_2 \right] \\ H_{13}^{(1)} &= D(4, \mu) \cdot \left(-\frac{5}{8 \sqrt{15}} B_4 \right). \end{aligned} \right\} (4)$$

The first order perturbation energies of the Ni(II) complex are obtained by inserting (4) into (3) and solving the equations

with respect to $E^{(1)}$. Because of the complexity of the final formulae for the general case, these will not be written out. Calculations for some definite cases are given below.

From the 3P term we get analogously:

$$\left. \begin{aligned} \Psi_{11} &= \sqrt{\frac{2}{10}} \psi_{-1}^{(1)} \psi_2^{(2)} - \sqrt{\frac{3}{10}} \psi_0^{(1)} \psi_1^{(2)} + \sqrt{\frac{3}{10}} \psi_1^{(1)} \psi_0^{(2)} - \sqrt{\frac{2}{10}} \psi_2^{(1)} \psi_{-1}^{(2)} \\ \Psi_{1,0} &= \sqrt{\frac{4}{10}} \psi_{-2}^{(1)} \psi_2^{(2)} - \sqrt{\frac{1}{10}} \psi_{-1}^{(1)} \psi_1^{(2)} + \sqrt{\frac{1}{10}} \psi_1^{(1)} \psi_{-1}^{(2)} - \sqrt{\frac{4}{10}} \psi_2^{(1)} \psi_{-2}^{(2)} \\ \Psi_{1,-1} &= \sqrt{\frac{2}{10}} \psi_{-2}^{(1)} \psi_1^{(2)} - \sqrt{\frac{3}{10}} \psi_{-1}^{(1)} \psi_0^{(2)} + \sqrt{\frac{3}{10}} \psi_0^{(1)} \psi_{-1}^{(2)} - \sqrt{\frac{2}{10}} \psi_1^{(1)} \psi_{-2}^{(2)} \end{aligned} \right\} (5)$$

The secular equation is

$$\begin{vmatrix} H_{-1-1}^{(1)} - E^{(1)} & 0 & H_{1-1}^{(1)} \\ 0 & H_{00}^{(1)} - E^{(1)} & 0 \\ H_{-11}^{(1)} & 0 & H_{11}^{(1)} - E^{(1)} \end{vmatrix} = 0,$$

i. e.

$$\left. \begin{aligned} E^{(1)} &= H_{00}^{(1)} \\ E^{(1)} &= H_{11}^{(1)} \pm H_{1-1}^{(1)}, \end{aligned} \right\} (6)$$

where

$$H_{00}^{(1)} = D(0_1\mu) \left[2B_0 + \frac{1}{5}B_2 \right] + (\mu_5 + \mu_6) \left[2B_0 - \frac{2}{5}B_2 \right]$$

$$H_{11}^{(1)} = D(0_1\mu) \left[2B_0 - \frac{1}{10}B_2 \right] + (\mu_5 + \mu_6) \left[2B_0 + \frac{1}{5}B_2 \right]$$

$$H_{1-1}^{(1)} = 0.$$

The Hexa-Coordinated Ni(II)-Complexes.

The energy levels of Ni(II) complexes, with six equal point dipoles placed in a regular octahedron around the cation, are obtained from (3) and (6):

The 3F state splits up into three levels:

$${}^3F \left\{ \begin{array}{ll} \frac{8}{45} f^2 \mu [12 B_0 - B_4] & \Gamma_4 \\ \frac{8}{45} f^2 \mu \left[12 B_0 + \frac{1}{3} B_4 \right] & \Gamma_5 \\ \frac{8}{45} f^2 \mu [12 B_0 + 2 B_4] & \Gamma_2 \end{array} \right\} \quad (7)$$

The Γ notation is the nomenclature of BETHE.⁷

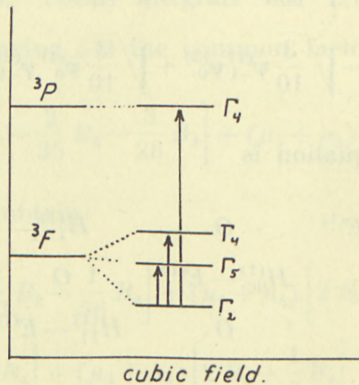


Fig. 1.

The term scheme of the paramagnetic octahedral Ni(II) complexes with cubic symmetry.

For the 3P state, which does not split up in a cubic crystal-field, we get:

$${}^3P: \frac{8}{45} f^2 \mu \cdot 12 B_0 \quad \Gamma_4.$$

The energy levels for one d -positron is²:

$$\left. \begin{array}{l} E_1 = \frac{8}{45} f^2 \mu [6 B_0 + B_4] \\ E_2 = \frac{8}{45} f^2 \mu \left[6 B_0 - \frac{2}{3} B_4 \right] \end{array} \right\} \quad (8)$$

A combination of (8) and (7) in the notation of HARTMANN and ILSE⁸ gives

$${}^3F: \left\{ \begin{array}{ll} \frac{1}{5} E_1 + \frac{9}{5} E_2 & \Gamma_4 \\ E_1 + E_2 & \Gamma_5 \\ 2 E_1 & \Gamma_2 \end{array} \right\} \quad (9)$$

$${}^3P: \frac{4}{5} E_1 + \frac{6}{5} E_2 \quad \Gamma_4 \quad (10)$$

Between these four levels three transitions from the ground state ${}^3F\Gamma_2$ are possible. (See Fig. 1). The frequencies of the three absorption bands are:

$$\left. \begin{array}{l} \nu_1 = (E_2 - E_1) \text{ cm}^{-1} \\ \nu_2 = \frac{9}{5} (E_2 - E_1) \text{ cm}^{-1} \\ \nu_3 = 17000 + \frac{6}{5} (E_2 - E_1) \text{ cm}^{-1}. \end{array} \right\} \quad (11)$$

From these is obtained the simple rule that $\nu_2/\nu_1 = 1.8$.

The spectra of Ni aq_6^{++} and Ni en_3^{++} are given in Fig. 2. As abscissa the wave number ν is taken and as ordinate the molar extinction coefficient ϵ . Inserting $(E_2 - E_1)_{\text{aq}} = 7600 \text{ cm}^{-1}$ and $(E_2 - E_1)_{\text{en}} = 10500 \text{ cm}^{-1}$ into (11), we find the absorption maxima given in Table 1.

TABLE 1.

*Comparison of experimental and calculated absorption maxima.
Wave numbers in cm^{-1} .*

	$\text{Ni (H}_2\text{O)}_6^{++}$		Ni en_3^{++}	
	obs.	calc.	obs.	calc.
ν_3	25300	26000	29000	29500
ν_2	14000	13700	18350	18900
ν_1	8000	7600	11200	10500
ν_2/ν_1	1.75	1.80	1.64	1.80

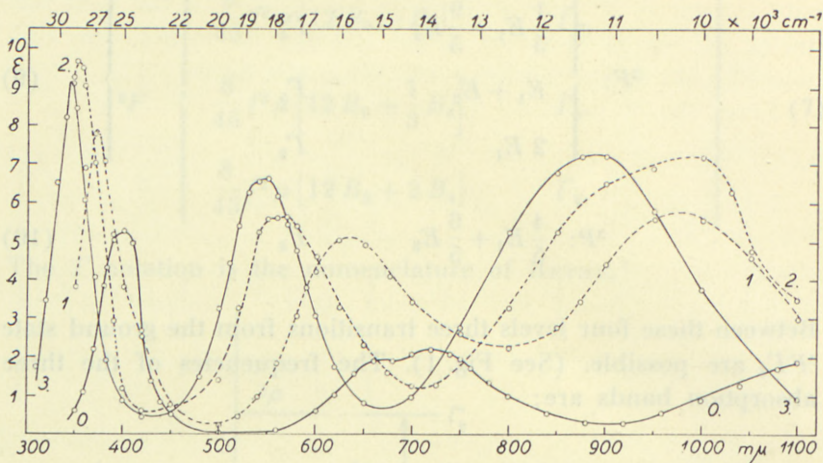


Fig. 2.

The absorption spectra of nickel-ethylenediamine complexes in aqueous solutions at 25° C. Curve (0): $\text{Ni}(\text{aq})_6^{++}$ Curve (1) $\text{Ni}(\text{en})_2\text{aq}_2^{++}$ Curve (2) $\text{Ni}(\text{en})_2\text{aq}_2^{++}$ Curve (3) $\text{Ni}(\text{en})_3^{++}$ Solutions of the composition: $C_{\text{Ni}(\text{NO}_3)_2} = 0.05M$, $C_{\text{KCl}} = 0.15M$, $C_{\text{HNO}_3} = 0.05M$ with varying concentrations of ethylenediamine were measured on a Beckman D. U. Curve (0) is obtained from solutions with $C_{\text{en}} \lesssim 0.05$. Curve (3) from solutions with $C_{\text{en}} \lesssim 0.30$. For solutions with intermediate ethylenediamine concentrations curves (1) and (2) are computed by means of the method of BJERRUM.¹³ The consecutive constants were determined to be: $\log K_1 = 7.17$, $\log K_2 = 6.07$ and $\log K_3 = 4.27$.

In Fig. 2 it is seen that the second band ν_2 in the spectrum of $\text{Ni}(\text{aq})_6^{++}$ is not symmetrical. A closer analysis³ shows that it is actually composed of two adjacent bands with a $\Delta\nu \sim 2000\text{ cm}^{-1}$. A slightly tetragonal field may produce such an effect. However, a tetragonal field would also turn ν_3 into a double band, which has not been observed. The second band in the spectrum of $\text{Ni}(\text{en})_3^{++}$ is seen to be Gaussian-shaped. Therefore, a possible explanation of the double band in the spectrum of $\text{Ni}(\text{aq})_6^{++}$ may rather be that the splitting due to the ($L-S$) coupling in the 3F state⁵ ($\sim 2200\text{ cm}^{-1}$) is not totally quenched by the weak water ligand field. This is possibly the case for the stronger field produced by the ethylenediamine.

The formulae (9) and (10) can also be applied to the spectrum of $\text{V}(\text{aq})_6^{+++}$. The energy levels of the 3F state are here placed in the opposite order of that in the hexaquo $\text{Ni}(\text{II})$ complex,

and the 3P state is situated at 13200 cm^{-1} . Experiments⁹ show that this complex has two bands placed in the visible region of the spectrum, the first at 17200 cm^{-1} , the second at 25000 cm^{-1} , so that $\nu_2/\nu_1 = 1.46$. It seems improbable that the bands can be due to transitions between the 3F levels only, since the ratio ν_2/ν_1 in this case would be $2.25^{1,8}$ (cf. (11)). On the other hand, if we assume that the term scheme is that given by ORGEL,¹⁰ the bands are due to: ${}^3F\Gamma_4 \rightarrow {}^3F\Gamma_5$ and ${}^3F\Gamma_4 \rightarrow {}^3P\Gamma_4$, i. e. $\nu_2/\nu_1 = 1.56$. This predicts a third band in Vaq_6^{+++} placed at $37000\text{ cm}^{-1} \sim 270\text{ m}\mu$ and due to ${}^3F\Gamma_4 \rightarrow {}^3F\Gamma_2$.

Mixed Ni(II) Complexes.

The complexes Nienaq_4^{++} and $\text{cis-Nien}_2\text{aq}_2^{++}$ have both the same formal configuration, i. e. two dipoles μ_2 placed in a cis-position to each other. Assuming all distances to be equal, the energy levels for the 3F state (leaving out the factor $\frac{8}{45}f^2$) is:

$$\left. \begin{aligned}
 E(\Gamma_{2(t3)}) &= \mu_1 \left[8 B_0 + \frac{4}{3} B_4 \right] + \mu_2 \left[4 B_0 + \frac{2}{3} B_4 \right] \quad (\text{ground level}) \\
 E(\Gamma_{5(t4)}) &= \mu_1 \left[8 B_0 + \frac{1}{2} B_4 \right] + \mu_2 \left[4 B_0 - \frac{1}{6} B_4 \right] \\
 E(\Gamma_{5(t5)}) &= \mu_1 \left[8 B_0 - \frac{1}{35} B_2 - \frac{11}{42} B_4 \right] + \mu_2 \left[4 B_0 + \frac{1}{35} B_2 - \frac{1}{14} B_4 \right] \\
 &+ \frac{1}{2} \sqrt{\left[\mu_1 \left(-\frac{8}{35} B_2 - \frac{11}{42} B_4 \right) + \mu_2 \left(\frac{8}{35} B_2 - \frac{1}{14} B_4 \right) \right]^2 + (\mu_1 + \mu_2)^2 \cdot \frac{5}{12} (B_4)^2} \\
 E(\Gamma_{4(t2)}) &= \mu_1 \left[8 B_0 + \frac{4}{35} B_2 - \frac{11}{14} B_4 \right] + \mu_2 \left[4 B_0 - \frac{4}{35} B_2 - \frac{3}{14} B_4 \right] \\
 E(\Gamma_{4(t5)}) &= \mu_1 \left[8 B_0 - \frac{1}{35} B_2 - \frac{11}{42} B_4 \right] + \mu_2 \left[4 B_0 + \frac{1}{35} B_2 - \frac{1}{14} B_4 \right] \\
 &- \frac{1}{2} \sqrt{\left[\mu_1 \left(-\frac{8}{35} B_2 - \frac{11}{42} B_4 \right) + \mu_2 \left(\frac{8}{35} B_2 - \frac{1}{14} B_4 \right) \right]^2 + (\mu_1 + \mu_2)^2 \cdot \frac{5}{12} (B_4)^2}
 \end{aligned} \right\} \quad (12)$$

and for the 3P term:

$$\left. \begin{aligned} E(\Gamma_{4(t2)}) &= \mu_1 \left[8 B_0 - \frac{2}{5} B_2 \right] + \mu_2 \left[4 B_0 + \frac{2}{5} B_2 \right] \\ E(\Gamma_{4(t5)}) &= \mu_1 \left[8 B_0 + \frac{1}{5} B_2 \right] + \mu_2 \left[4 B_0 - \frac{1}{5} B_2 \right]. \end{aligned} \right\} (13)$$

The formulae for the levels of the trans-Nien₂aq₂⁺⁺ complex, in which the two water dipoles μ_2 are placed in trans-position to each other, is for the ³F state:

$$\left. \begin{aligned} E(\Gamma_{2(t3)}) &= \mu_1 \left[8 B_0 + \frac{4}{3} B_4 \right] + \mu_2 \left[4 B_0 + \frac{2}{3} B_4 \right] \quad (\text{ground level}) \\ E(\Gamma_{5(t4)}) &= \mu_1 \left[8 B_0 - \frac{1}{3} B_4 \right] + \mu_2 \left[4 B_0 + \frac{2}{3} B_4 \right] \\ E(\Gamma_{5(t5)}) &= \mu_1 \left[8 B_0 + \frac{2}{35} B_2 - \frac{1}{7} B_4 \right] + \mu_2 \left[4 B_0 - \frac{2}{35} B_2 - \frac{4}{21} B_4 \right] \\ &+ \frac{1}{2} \sqrt{\left[\mu_1 \left(-\frac{16}{35} B_2 + \frac{1}{7} B_4 \right) + \mu_2 \left(\frac{16}{35} B_2 + \frac{4}{21} B_4 \right) \right]^2 + \frac{5}{3} \mu_1^2 (B_4)^2} \\ E(\Gamma_{4(t2)}) &= \mu_1 \left[8 B_0 - \frac{8}{35} B_2 - \frac{3}{7} B_4 \right] + \mu_2 \left[4 B_0 + \frac{8}{35} B_2 - \frac{4}{7} B_4 \right] \\ E(\Gamma_{4(t5)}) &= \mu_1 \left[8 B_0 + \frac{2}{35} B_2 - \frac{1}{7} B_4 \right] + \mu_2 \left[4 B_0 - \frac{2}{35} B_2 - \frac{4}{21} B_4 \right] \\ &- \frac{1}{2} \sqrt{\left[\mu_1 \left(-\frac{16}{35} B_2 + \frac{1}{7} B_4 \right) + \mu_2 \left(\frac{16}{35} B_2 + \frac{4}{21} B_4 \right) \right]^2 + \frac{5}{3} \mu_1^2 (B_4)^2} \end{aligned} \right\} (14)$$

and for the ³P state:

$$\begin{aligned} E(\Gamma_{4(t5)}) &= \mu_1 \left[8 B_0 - \frac{2}{5} B_2 \right] + \mu_2 \left[4 B_0 + \frac{2}{5} B_2 \right] \\ E(\Gamma_{4(t2)}) &= \mu_1 \left[8 B_0 + \frac{4}{5} B_2 \right] + \mu_2 \left[4 B_0 - \frac{4}{5} B_2 \right]. \end{aligned}$$

For the numerical evaluation we insert all the distances R equal to 2.0 Å (see ref. 1, 11 and 14) and $Z = 7.20$ according to SLATER,¹² i. e. $x = \frac{7.20}{3} \cdot 3.78 = 9.1$. From Table 3 in ref. 2

$B_2/B_4 = 2.26$. Further, we assume that the values of the dipole moments are the same both in the "mixed" and in the "unmixed" complexes. Then

$$\left. \begin{aligned} (E_2 - E_1)_{\text{lig.}} &= \left(\frac{8}{45} f^2 \mu B_4 \right) \cdot \frac{5}{3} = \left(\frac{8}{45} f^2 \mu B_2 \right) \cdot \frac{5}{3} \cdot \frac{1}{2.26} \text{ i. e.} \\ \frac{8}{45} f^2 \mu B_4 &= 0,60 (E_2 - E_1)_{\text{lig.}} \\ \frac{8}{45} f^2 \mu B_2 &= 1,35 (E_2 - E_1)_{\text{lig.}} \end{aligned} \right\} \quad (15)$$

The results of the calculation are shown in Table 2. The observed absorption spectra of Nienaq_4^{++} and $\text{Nien}_2\text{aq}_2^{++}$ are shown in Fig. 2; the maxima of the bands are tabulated in Table 3.

TABLE 2.

Calculated absorption maxima. Wave lengths in $m\mu$.

Nienaq_4^{++}	cis- $\text{Nien}_2\text{aq}_2^{++}$	trans $\text{Nien}_2\text{aq}_2^{++}$
1230	1150	1140
1100	1100	950
650	590	580
640	580	570
360	360	380
350	330	330

TABLE 3.

Experimentally found absorption maxima. Wave lengths in $m\mu$.

Nienaq_4^{++}	$\text{Nien}_2\text{aq}_2^{++}$
980	900, 1000
640	550, 570
370	340

The calculated absorption maxima are nearly identical with those found by experiments. However, it is only in a few cases that the adjacent bands can be distinguished from one another

on the measured absorption curves. It is seen that the spectra of the cis- and trans-Nien₂aq₂⁺⁺ complexes are nearly equal.

The spectra of the [Ni(NH₃)_n(H₂O)_{6-n}]⁺⁺ complexes can be treated analogously. Taking $(E_2 - E_1)_{NH_3} = 10100 \text{ cm}^{-1}$, e. g. the band of Nickel monoquo pentammine, which BJERRUM¹² found to have a maximum at 17200 cm^{-1} , is placed at 17300 cm^{-1} . It is instructive to compare the absorption curves in Fig. 13, ref. 13, of the nickel ammines with the absorption curves in Fig. 2 of the nickel ethylenediamine complexes. It is observed that the spectra of the [Ni(NH₃)₂(H₂O)₄]⁺⁺ and [Ni(NH₃)₄(H₂O)₂]⁺⁺ complexes show a slight displacement towards the red as compared with the corresponding ethylenediamine complexes. This is also to be expected, as $(E_2 - E_1)_{NH_3} = 10100 \text{ cm}^{-1}$ is slightly lower than $(E_2 - E_1)_{en} = 10500 \text{ cm}^{-1}$.

The dipole moments for the distance 2.0 \AA and for $Z = 7.20$ are calculated to be:

$$\begin{aligned}\mu_{H_2O} &= 3.45 \text{ Debye} \\ \mu_{NH_3} &= 4.55 \text{ —} \\ \mu_{en} &= 4.74 \text{ —}\end{aligned}$$

Thus both the chemical evidence, as shown by BJERRUM,¹³ and the model developed here seem to verify that the hexacoordinated Ni(II) complexes are built very nearly as regular octahedrons.

The Four-Coordinated Ni (II) Complexes.

It has been shown by X-ray examinations that the diamagnetic four-coordinated Ni(II) complexes have a square-planar configuration. (For a review, see ref. 14). According to the magnetic evidence the ground level must be a singlet.

In order to investigate which state could possibly be the ground state we shall first consider the splittings of the levels in a distorted octahedron. The lowest level of the ¹G term in a distorted octahedron (¹G *F*_{4(t2)} in the nomenclature of BETHE⁷) is:

$$E^{(1)} = \frac{8}{45} f^2 \mu_1 [8 B_0 + \frac{8}{7} B_2 + \frac{1}{7} B_4] + \frac{8}{45} f^2 \mu_2 [4 B_0 - \frac{8}{7} B_2 + \frac{4}{21} B_4].$$

This is the level which splits up the most in a tetragonal field, and as none of the other states has this symmetry, the level can cross these. Taking $B_2/B_4 = 2.26$ and $\mu_2 = 0$, we get for the square-planar complex

$$E^{(1)} = \frac{8}{45} f^2 \mu_1 [8 B_0 + 2.72 B_4].$$

For relatively strong ligand fields this level can be the ground state, and the complex thus diamagnetic. However, paramagnetic

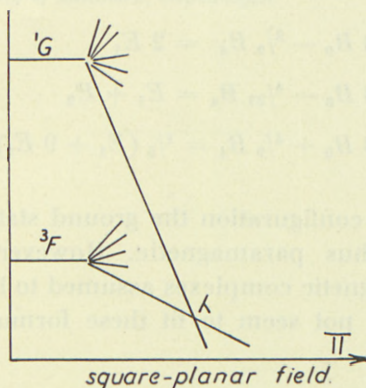


Fig.3.

Fig. 3. The term splittings in the square-planar configuration. The ground level is changed from a triplet to a singlet at the point λ .

complexes with square-planar configuration seem also to be possible (Fig. 3).

The 1G state is estimated by CONDON and SHORTLEY⁶ to be placed at $\sim 22000 \text{ cm}^{-1}$, and a reasonable value of the splitting of the 3F level in a square-planar field is $\sim 12000 \text{ cm}^{-1}$. If ${}^1G ({}^1G_{4(12)})$ is the ground state, $\frac{8}{45} f^2 \mu \cdot 2.72 B_4 > 34000 \text{ cm}^{-1}$, i. e. $\frac{8}{45} f^2 \mu B_4 > 12500 \text{ cm}^{-1}$, which in fact corresponds to a rather strong crystal-field.

Even if our calculations are only valid for small ligand-fields, we can e. g. try to calculate the first absorption band of Nistien₂⁺⁺. (stien = C, C-di(phenyl)ethylenediamine). If we use $\frac{8}{45} f^2 \mu B_4 = 13000 \text{ cm}^{-1}$, this band ${}^1G ({}^1G_{4(12)}) \rightarrow {}^1D ({}^1D_{3(11)})$ is placed at $550 m\mu$. Experiments show only one band situated

at $450 m\mu$. Another possibility is that second order effects have already depressed the 1D ($\Gamma_{3(t1)}$) level beneath the 1G ($\Gamma_{4(t2)}$) level. It is known that in strong crystal fields this level is placed below the former.

The splittings in a regular tetrahedron are similar, but the inverse of the splittings in a regular octahedron.¹⁷ It turns out that the coefficients to B_4 obtained in the octahedral case are to be multiplied by the factor $-4/9$, e. g. for the 3F state: (the factor $\frac{8}{45}f^2\mu$ is omitted)

$${}^3F \left\{ \begin{array}{ll} 8 B_0 - \frac{8}{9} B_4 = 2 E_1 & \Gamma_2 \\ 8 B_0 - \frac{4}{27} B_4 = E_1 + E_2 & \Gamma_5 \\ 8 B_0 + \frac{4}{9} B_4 = \frac{1}{5} (E_1 + 9 E_2). & \Gamma_4 \end{array} \right.$$

In the tetrahedral configuration the ground state is a triplet and the complex is thus paramagnetic. However, the absorption spectra of paramagnetic complexes assumed to have a tetrahedral configuration¹⁴ do not seem to fit these formulae.

General Remarks.

As demonstrated in the above sections the simple crystal-field theory is able to account for most of the experimental material. Thus it seems unlikely that the overlap-integrals between the ligands and the metal-ion can be of much importance. This seems to be in accordance with recent calculations by CRAIG, MACCOLL, NYHOLM, ORGEL and SUTTON.¹⁵ The hybridization $3d^2 4s 4p^3$ would produce two $4d$ electrons, predicting a level order inversed to the one found and with a ratio $\nu_2/\nu_1 = 2.25$ (cf. formula (9)). However, the actual ratio $\nu_2/\nu_1 = 1.64$ of the $\text{Ni}_{3^{++}}$ bands is, as we have seen, in fair agreement with the picture of an unchanged electronic configuration of the metal ion.

VAN VLECK¹⁶ pointed out that complexes are held together more by polarization forces than by true valence forces. This seems to be true for the Ni(II) complexes discussed here.

In later publications the theory will be extended to the simpler cobalt and chromium complexes and to their poly-nuclear compounds.

I am much indebted to Professor J. BJERRUM for his great interest in my work, and for many valuable suggestions. My thanks are further due to Mr. KLIXBÜLL JØRGENSEN for interesting discussions.

*Chemistry Department A,
Technical University of Denmark, Copenhagen.*

Literature.

1. BJERRUM, J., BALLHAUSEN, C. J., and KLIXBÜLL JØRGENSEN, C. Acta Chem. Scand. 8 (1954) 1275.
2. BALLHAUSEN, C. J. Dan. Mat. Fys. Medd. 29, no. 4 (1954).
3. KLIXBÜLL JØRGENSEN, C. Acta Chem. Scand. 8 (1954) 1495.
4. KLIXBÜLL JØRGENSEN, C. Acta Chem. Scand. 8 (1954) 1502.
5. Atomic Energy Levels. (National Bureau of Standards 467 (1949)).
6. CONDON, E. V. and SHORTLEY, G. H. The Theory of Atomic Spectra (Cambridge 1953).
7. BETHE, H. Ann. Physik 5 Folge 3 (1929) 133.
8. HARTMANN, H. and ILSE, F. E. Z. Naturforschg. 6a (1951) 751.
9. HARTMANN, H. and SCHLÄFER, H. L. Z. Naturforschg. 6a (1951) 754.
10. ORGEL, L. E. J. Chem. Soc. 1952, 4756.
11. MUKHERJEE, P. L. Z. Krist. 91 (1935) 504.
12. SLATER, J. C. Phys. Rev. 36 (1930) 57.
13. BJERRUM, J. Metal Ammine Formation in Aqueous Solution. Thesis. Copenhagen (1941).
14. NYHOLM, R. S. Quart. Rev. 1953, 7 No. 4, 398.
15. CRAIG, D. P., MACCOLL, A., NYHOLM, R. S., ORGEL, L. E., SUTTON, L. E. J. Chem. Soc. 1954 332.
16. VAN VLECK, J. H.: The Theory of Electric and Magnetic Susceptibilities (Oxford 1932) p. 293.
17. GORTER, C. J. Phys. Rev. 42, 437 (1932).

Det Kongelige Danske Videnskabernes Selskab

Matematisk-fysiske Meddelelser, bind **29**, nr. 9

Dan. Mat. Fys. Medd. **29**, no. 9 (1955)

INTENSITY RULES
FOR BETA AND GAMMA TRANSITIONS
TO NUCLEAR ROTATIONAL
STATES

BY

G. ALAGA, K. ALDER, A. BOHR, AND B. R. MOTTELSON



København 1955

i kommission hos Ejnar Munksgaard

CONTENTS

	Page
I. Introduction	3
II. Spectra of Strongly Deformed Nuclei.....	3
III. Classification of β - and γ -Transitions in Strongly Deformed Nuclei....	8
IV. Branching Ratios.....	9
V. Effect of Perturbations.....	14
a) <i>K</i> -forbiddenness.....	17
b) Rotational admixtures.....	19
References	21

I. Introduction.

The systematic occurrence of rotational spectra in strongly deformed nuclei implies many simple relations within the decay schemes of these nuclei. The great regularity in the properties of these states makes it possible to predict with considerable accuracy their energies and sequence of spins¹. Moreover, the close relationship between the wave functions of the different states in a rotational sequence implies that the relative strengths of the transitions from a given nuclear state to the various members of a rotational family are governed by simple rules. In many cases, one obtains general quantitative relationships similar to the intensity rules for the fine structure and hyperfine structure of atomic spectra. These relationships may often be a valuable tool in the classification of decay schemes.

We shall here consider the intensity rules that apply to β - and γ -transitions in the deformed nuclei². The available empirical evidence appears to be consistent with these rules and thus to lend further support to the assumed coupling scheme for these nuclei.

II. Spectra of Strongly Deformed Nuclei.

For nuclei whose equilibrium shape deviates strongly from spherical symmetry, one can distinguish approximately between two essentially different modes of excitation, rotational and intrinsic. The former is associated with a collective motion which

¹ BOHR and MOTTELSON, 1953a, 1953b, 1953c (the latter to be referred to in the following as BM); FORD, 1953; ASARO and PERLMAN, 1953. For a recent discussion of the theory and summary of the empirical data on nuclear rotational states, cf. A. BOHR, 1954; BOHR and MOTTELSON, 1954; NEWTON, 1954.

² Similar intensity rules governing transitions to the different members of a rotational sequence can also be given for the α -decay process (BOHR, FRÖMAN, and MOTTELSON, 1955) and the stripping reaction (SATCHLER, 1955).

affects only the orientation in space while preserving the internal structure of the nucleus; the latter may be associated with the excitation of individual particles or with collective vibrations of the nuclear shape.

The rotational spectrum depends essentially on the nuclear equilibrium shape, and is especially simple for axially symmetric nuclei. The rotational motion can then be characterized by

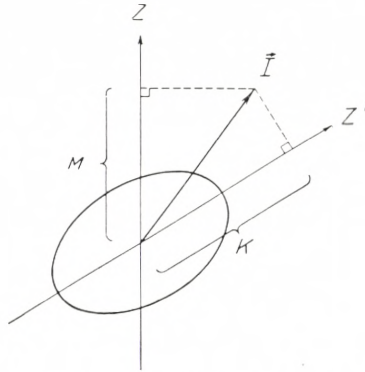


Fig. 1. Angular momentum quantum numbers for a strongly deformed nucleus. For strongly deformed nuclei possessing axial symmetry, the coupling scheme is characterized by the three constants of the motion: the total angular momentum, I , its projection, M , on an axis fixed in space (the z -axis in the figure), and its projection, K , on the nuclear symmetry axis, z' .

the quantum numbers I , K , M , representing the total angular momentum, its projection on the nuclear symmetry axis, and its projection on the space fixed axis, respectively (cf. Fig. 1).

The separation of the nuclear motion into rotational and intrinsic modes corresponds to the existence of approximate solutions of the nuclear wave equation of the simple product type

$$\Psi = \sqrt{\frac{2I+1}{8\pi^2}} \varphi_{\tau K} \mathfrak{D}_{MK}^I(\theta_i), \quad (1)$$

where φ represents the intrinsic structure characterized by K , and the additional set of quantum numbers, τ . For some purposes, one may attempt to describe the intrinsic wave function in greater detail in terms of the binding states of the individual nucleons in the deformed field and the collective vibrations of the nuclear shape (cf. the quantum numbers Ω_p , Ω , n_β , and n_γ employed in BM; more detailed calculations of single particle

states in deformed potentials have been performed by NILSSON (1955) and by GOTTFRIED (1955)). Since, however, the intensity rules discussed below are independent of the intrinsic nuclear structure, it suffices in the present context to characterize this structure by the unspecified set of quantum numbers, τ .

The rotational wave functions $\mathfrak{D}(\theta_i)$, depending on the Eulerian angles θ_i of the nuclear coordinate system, are the proper functions for the symmetric top normalized so as to give a unitary transformation from the space fixed to the nuclear coordinate system. Due to the reflection symmetry of the nuclear shape, the complete wave function must be symmetrized by adding the term obtained from (1) by a rotation of 180° about an axis perpendicular to the nuclear symmetry axis (cf. BM, eq. II. 15).

The states in a rotational band are characterized by the same intrinsic wave function $\varphi_{\tau K}$ and are labeled by different values of I . In an odd-A nucleus, where K is a positive half integer number, I may take on the values

$$I = K, K + 1, K + 2, \dots \left. \begin{array}{l} \text{all same parity as the} \\ \text{intrinsic structure.} \end{array} \right\} \quad (2)$$

In an even-even nucleus, the ground state has $K = 0$ and the symmetrization of the wave function limits the rotational band to

$$I = 0, 2, 4, 6, \dots \text{ even parity.} \quad (3)$$

In an odd-odd nucleus or in excited intrinsic states of even-even nuclei with $K \neq 0$, the rotational sequence is again given by (2).

The energies of the states in a rotational band are given, apart from a constant, by the expression

$$E_I = \frac{\hbar^2}{2\mathfrak{J}} \left\{ I(I + 1) + a(-)^{I+1/2} (I + 1/2) \delta_{K, 1/2} \right\}, \quad (4)$$

where the moment of inertia \mathfrak{J} depends on the nuclear deformation and is thus expected to vary fairly smoothly with A , increasing as one moves away from closed shell configurations. The second term in (4), which occurs only for odd-A nuclei with $K = 1/2$, is associated with the symmetrization of (1). The parameter, a , can be expressed in terms of the properties of the intrinsic wave function (cf., e. g., BOHR and MOTTELSON, 1954, eq. 5 a).

Rotational spectra of the type (4), characteristic of axially symmetric nuclei, are found to occur systematically in certain regions of elements (especially for $155 < A < 185$ and $A > 225$; for an example, cf. Fig. 2). The intensity rules discussed below thus apply particularly to these nuclei¹.

The energies associated with the excitation of individual particles depend on the level spacings for particle motion in the deformed field which are on the average a few hundred keV for a heavy nucleus. Intrinsic excitations of a collective vibrational character are in general expected to have somewhat higher energies, of the order of one or a few MeV.

Although intrinsic particle excitations and rotational excitations may have comparable energies, the two types of excitations can be rather easily distinguished, partly on the basis of the regularities in spins and energies in a rotational band, and partly on the basis of their essentially different transition probabilities.

The γ -transitions within a rotational family are of $E2$ and $M1$ type (cf. (2) and (3)). The $E2$ transition probabilities are strongly enhanced as compared with those corresponding to the transitions of a single proton; the enhancement which results from the collective nature of the nuclear quadrupole field increases with the nuclear deformation and is observed in some cases to exceed a factor of one hundred (BOHR and MOTTELSON, 1953a, 1954; BM, Chapter VII). The $M1$ rotational transition probability is related to the static magnetic moment of the nucleus and is of the order of magnitude of estimates for single-particle transitions, since the gyromagnetic ratio for the collective motion is of the same order of magnitude as that for single-particle motion (BM, Chapter VII).

In contrast, the transition probabilities for β - and γ -transitions between different particle configurations are usually smaller than those corresponding to single-particle transitions in a fixed spherical potential. Thus, the observed $M4$ γ -transitions and the allowed β -transitions are found to be retarded

¹ Outside these regions of elements, other regularities in the nuclear spectra have been observed, also suggestive of collective excitations (SCHARFF-GOLDHABER and WENESER, 1955; cf. also HEYDENBURG and TEMMER, 1954a). The spectra observed, however, differ essentially from (3) and (4), and exhibit features characteristic of collective vibrations about a spherical equilibrium shape.

by a factor (the unfavoured factor) in the range 10^{-1} to 10^{-2} . Such a retardation may result partly from the modification of the individual-particle wave functions implied by the non-spherical potential, and partly from a collective adjustment of the nuclear shape (BM, Chapters VII and VIII). A further retarda-

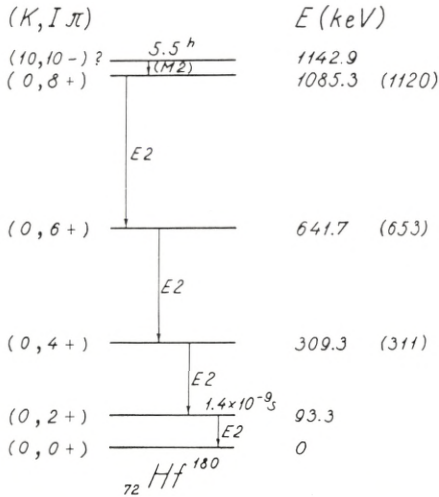


Fig. 2. Decay scheme for 5.5 h isomeric state in Hf^{180} . The empirical data are taken from MIHELICH, SCHARFF-GOLDHABER, and MCKEOWN (1954). The internal conversion and angular correlation data are consistent with the spins and multiplicities shown in the figure. The states are labeled by the quantum numbers $(K, I \pi)$.

The observed excitation energies are listed in keV, and the values obtained from (3) and (4) with the moment of inertia adjusted to the first excited state are given in parenthesis. The small deviations from these calculated values are negative and have just the $I^2(I + 1)^2$ dependence expected from the rotation-vibration interaction (BOHR and MOTTELSON, 1954).

The experimental evidence regarding the multipolarity of the 5.5 h isomeric transition is not conclusive. The very high degree of K -forbiddenness of this transition (cf. p. 17 below) implies that it should be many orders of magnitude slower than a single-particle transition of the same multipole order. While the observed lifetime may suggest an $M3$ or $E4$ classification on the basis of single-particle estimates, the expected retardation therefore suggests a lower multipole order. Thus, if the transition were $M2$, the retardation would amount to a factor of about 10^{-9} , which seems not excessive.

tion may result if the transition involves configurations of more than one particle (MOSZKOWSKI, 1953).

The simple separation between intrinsic excitations and collective rotations is realized in the limit of large deformations, where the rotational motion is so slow that it does not disturb

the nucleonic configuration or distort the nuclear shape. With decreasing deformation, and increasing rotational frequency, the intrinsic nuclear structure is excited by the rotational motion, and the quantum numbers K , τ are no longer exact constants of the motion. This implies a modification in the rotational spectrum (4), which may often be described by a term proportional to $I^2(I+1)^2$, as is characteristic of the rotation-vibration interaction in molecules. The magnitude of this correction term provides a measure of the adequacy of the rotational description. In the regions of the especially well developed rotational spectra ($155 < A < 185$ and $A > 225$), these correction terms in the energy amount to one per cent or less for the lowest rotational excitations (cf. Fig. 2, and also BOHR and MOTTELSON, 1954, especially Fig. 6 and Table II). More specific perturbations, associated with the particle-rotation coupling, may occur if the particle structure possesses a low lying state which is strongly excited by the rotational motion (cf. footnote on p. 16 below).

III. Classification of β - and γ -Transitions in Strongly Deformed Nuclei.

It is convenient to characterize β - and γ -transitions by their multipolarity, L , and their parity, π , representing the angular momentum and parity of the emitted radiation (cf., e. g., ROSE, 1954).

For γ -transitions, this classification just corresponds to the usual classification in terms of electric and magnetic multipole orders (EL and ML). The parity is

$$\pi = \left\{ \begin{array}{ll} (-)^L & \text{for } EL \\ (-)^{L+1} & \text{for } ML. \end{array} \right\} \quad (5)$$

For β -transitions, the classification of the various transition operators in multipole orders is given in Table I. The number in parenthesis is the order of forbiddenness, which is often used in the analysis of ft -values, but which may differ from the multipole order.

The selection rules on L and π for a transition from a state with quantum numbers (K_i, I_i, π_i) to a state with (K_f, I_f, π_f) are

$$|I_i - I_f| \equiv \Delta I \leq L \leq I_i + I_f \quad \pi = \pi_i \pi_f \quad (6)$$

$$|K_i - K_f| \equiv \Delta K \leq L. \quad (6a)$$

While the selection rules involving I and π are rigorous, that involving K depends on the adequacy of the wave function (1). Small deviations from the rotational wave functions, of the type discussed at the end of Section II, will relax this latter selection rule, which then acts to retard, rather than completely forbid the corresponding multipole transition. We shall refer to such transitions as K -forbidden and characterize the degree of this forbiddenness by the number ν , where

$$\nu = \Delta K - L. \quad (7)$$

The consequences of K -forbiddenness are discussed further in Section V.

IV. Branching Ratios.

The strength of a nuclear β - or γ -transition of multipole order, L , between an initial state, i , and a final state, f , may be characterized by the reduced transition probability

$$B(L, I_i \rightarrow I_f) = \sum_{\mu M_f} |\langle I_i M_i | \mathfrak{M}(L, \mu) | I_f M_f \rangle|^2, \quad (8)$$

where $\mathfrak{M}(L, \mu)$ is the μ -component of the transition operator of multipole order L . For γ -emission of frequency ω , the transition probability per second is

$$T = \frac{8\pi(L+1)}{L[(2L+1)!!]^2} \frac{1}{\hbar} \left(\frac{\omega}{c}\right)^{2L+1} B(L). \quad (9)$$

Similarly, the cross section for Coulomb excitation is simply proportional to $B(L)$. For β -transitions of a given multipole order, the ft -value is inversely proportional to the reduced transition probability for the corresponding multipole operator (cf. Table I).

TABLE I.

		$\pi = +$		$\pi = -$		
L	{	0	1	(0)	$\vec{\sigma} \cdot \vec{r}, \beta\gamma_5$	(1)
		1	$\vec{\sigma}$	(0)	$\vec{r}, \vec{r} \times \vec{\sigma}, \alpha$	(1)
		2	R_{ij}, A_{ij}, T_{ij}	(2)	B_{ij}	(1)
		3	B_{ijk}	(2)	$R_{ijk}, A_{ijk}, T_{ijk}$	(3)

Beta decay transition operators, classified according to multipole order, L , and parity, π .

The transition operators are written in the notation of KONOPINSKI and UHLENBECK (1941). The number in parenthesis gives the degree of forbiddenness.

For transitions between two states which can be represented by pure wave functions of the type (1), it is convenient to express the multipole operators in the coordinate system fixed in the nucleus

$$\mathfrak{M}(L, \mu) = \sum_{\nu} \mathfrak{D}_{\mu\nu}^L(\theta_i) \mathfrak{M}'(L, \nu), \quad (10)$$

where $\mathfrak{M}'(L, \nu)$ has the same form as $\mathfrak{M}(L, \nu)$ but is a function of the nucleon coordinates in the primed coordinate system (cf. Fig. 1).

The reduced transition probability then takes the form

$$B(L, I_i \rightarrow I_f) = \sum_{\mu, M_f} |\langle \tau_i K_i I_i M_i | \sum_{\nu} \mathfrak{D}_{\mu\nu}^L \mathfrak{M}'(L, \nu) | \tau_f K_f I_f M_f \rangle|^2. \quad (11)$$

The integration over the Eulerian angles, θ_i , appearing in the matrix element (11) can be performed explicitly and only the term with $\nu = K_i - K_f$ gives a non-vanishing contribution. The reduced transition probability can thus be written as a product of a geometrical factor, depending only on the angular momenta I , K , and L , and a factor involving integrations over the intrinsic wave function of the initial and final states and thus depending only on τ , K , and L .

For transitions between two members of a rotational family, the intrinsic wave functions of initial and final states are the same, and the intrinsic part of the matrix element reduces to an expectation value. The absolute transition probabilities can then be directly expressed in terms of the intrinsic nuclear moments (cf. BM, § VIIc. ii).

In transitions involving a change of the intrinsic nuclear state, the absolute value of the matrix elements depends on more specific features of the intrinsic nuclear structure. However, when one compares the reduced transition probability for the emission of a given multipole radiation from a state, i , to different members f, f', \dots of a rotational family, the factor involving the intrinsic wave functions is the same. One thus obtains a ratio which depends only on the geometrical factors and can be written

$$\frac{B(L, I_i \rightarrow I_f)}{B(L, I_i \rightarrow I_{f'})} = \frac{\langle I_i L K_i K_f - K_i | I_i L I_f K_f \rangle^2}{\langle I_i L K_i K_f - K_i | I_i L I_{f'} K_f \rangle^2}, \quad (12)$$

where $\langle I_i L K_i K_f - K_i | I_i L I_f K_f \rangle$ is the vector addition coefficient for the addition of the angular momenta I_i and L to form the resultant I_f (cf., e. g., CONDON and SHORTLEY, 1935). The relation (12), of course, also holds where the states i and f, f' belong to the same rotational family.

In special cases, where $L \geq K_i + K_f$, the symmetrization of (1) may imply that the transition matrix elements become a sum of two products of geometrical and intrinsic factors. The ratio of reduced transition probabilities can then be written in the form

$$\left. \begin{aligned} & \frac{B(L, I_i \rightarrow I_f)}{B(L, I_i \rightarrow I_{f'})} = \\ & \frac{\langle I_i L K_i K_f - K_i | I_i L I_f K_f \rangle + b(-)^{I_f + K_f} \langle I_i L K_i, -K_f - K_i | I_i L I_f - K_f \rangle}{\langle I_i L K_i K_f - K_i | I_i L I_{f'} K_f \rangle + b(-)^{I_{f'} + K_f} \langle I_i L K_i, -K_f - K_i | I_i L I_{f'} - K_f \rangle} \end{aligned} \right\} \quad (13)$$

where b is a parameter depending on the intrinsic wave function (cf. the similar parameter a in (4)). When either K_i or K_f is zero, (13) reduces to (12) regardless of L . A case of interest in which the parameter b enters significantly in the transition probabilities is that of $M1$ γ -radiation within a rotational sequence with $K = 1/2$ ¹.

The recent extensive use of the Coulomb excitation reaction for the study of nuclear rotational states has provided a number

¹ For collective $E2$ transitions within such a rotational sequence with $K = 1/2$, the quantity b vanishes.

TABLE II.

Nucleus	I_0	$E_{I_0+1} - E_{I_0}$	$E_{I_0+2} - E_{I_0}$	$\frac{B(E2; I_0 \rightarrow I_0+2)}{B(E2; I_0 \rightarrow I_0+1)}$	$\frac{B(M1; I_0+2 \rightarrow I_0+1)}{B(M1; I_0+1 \rightarrow I_0)}$	References
$^{45}\text{Rh}^{103}$	1/2	295	357	1.8 (1.5)	—	a)
$^{47}\text{Ag}^{107}$	1/2	320	415	1.7 (1.5)	—	a)
$^{47}\text{Ag}^{109}$	1/2	306	405	1.8 (1.5)	—	a)
$^{63}\text{Eu}^{153}$	5/2	84	195 (192)	0.4 (0.35)	~ 2 (1.45)	b) c)
$^{65}\text{Tb}^{159}$	3/2	58	138 (139)	0.3 (0.56)	—	b) c)
$^{67}\text{Ho}^{165}$	7/2	94	209 (209)	0.26 (0.26)	~ 2 (1.53)	b) c)
$^{71}\text{Lu}^{175}$	7/2	114	248 (252)	—	~ 1 (1.53)	b) c)
$^{72}\text{Hf}^{177}$	(7/2) ¹	113	250 (251)	0.20 (0.26)	—	b) c) d)
$^{73}\text{Ta}^{181}$	7/2	136	303 (304)	0.21 (0.26)	—	b) e) f)
$^{74}\text{W}^{183}$	1/2	46	99	~ 1 (1.5)	—	c) f) g)
$^{79}\text{Au}^{197}$	3/2	277	555 (665)	2 (0.56)	—	b) h) i)

¹ The spin of Hf^{177} is given as 7/2, as indicated by the observed rotational level spacings and the observed relative intensities. Earlier spectroscopic evidence (RASMUSSEN 1935) had tentatively indicated a spin value 1/2 or 3/2.

- a) HEYDENBURG and TEMMER (1954).
- b) HEYDENBURG and TEMMER (1954a).
- c) HUUS et. al. (1955).
- d) MARMIER and BOEHM (1955).
- e) HUUS and ZUPANČIČ (1953).
- f) McCLELLAND, MARK, and GOODMAN (1955).
- g) MURRAY et al. (1955).
- h) COOK, CLASS, and EISINGER (1954).
- i) GOLDBURG and WILLIAMSON (1954).

Relative transition intensities from Coulomb excitation data.

In the Coulomb excitation of odd-A nuclei, one strongly excites the two lowest members of the ground state rotational band, having spins $I_0 + 1$ and $I_0 + 2$, where I_0 is the ground state spin. The energies of the states so populated are given in columns three and four, and the value of $E_{I_0+2} - E_{I_0}$ calculated by means of (4) from the observed $E_{I_0+1} - E_{I_0}$ is listed in parenthesis in column four. The nuclei with $I_0 = K = 1/2$ exhibit the effect of the second term in (4). From the observed cross sections for the excitation of the two states in question, one may obtain the ratio of the $E2$ reduced transition probabilities listed in column five; the theoretical ratio (12) is listed in parenthesis. The study of the radiative de-excitation has permitted in some cases an estimate of reduced $M1$ transition probabilities; the observed ratios are listed in column six, together with the theoretical value (12) (in parenthesis). For a discussion of the derivation of the reduced transition probabilities from the Coulomb excitation cross section, cf. the forthcoming review article by ALDER et al. (1955).

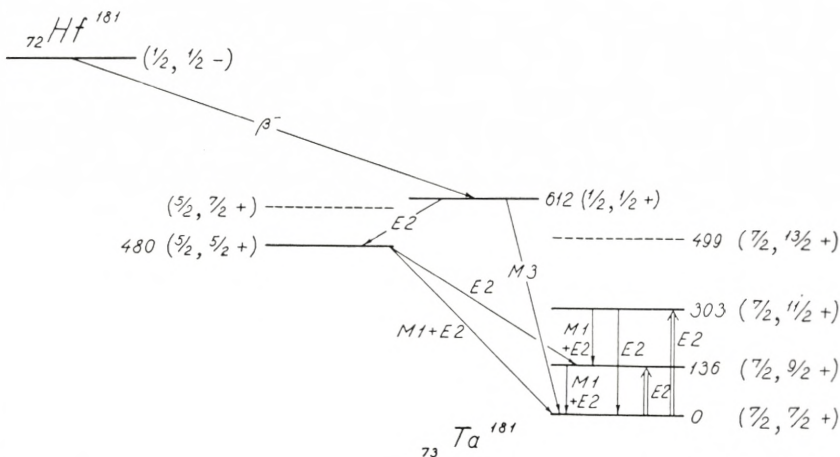


Fig. 3. Level scheme for Ta^{181} . The figure illustrates the information on the level structure of Ta^{181} obtained from the analysis of the β -decay of Hf^{181} (McGOWAN, 1954) and of the Coulomb excitation (double arrows) (HUUS and ZUPANČIČ, 1953; HUUS and BJERREGÅRD, 1953; EISINGER, COOK, and CLASS, 1954). These reactions appear to populate states belonging to three different rotational bands, and this is indicated by drawing members of the same bands (having same K and π) above each other, while the different bands are displaced sideways. The excitation energies are listed in keV, and the states are labeled by the quantum numbers $(K, I \pi)$. The absolute parity is uncertain, and the value relative to that of the ground state is given. The levels drawn dotted are not populated in these reactions, but their position is inferred from formulae (2) and (4). The spin assignments for the 480 keV and 612 keV levels tentatively suggested here differ from those of McGOWAN (1954), but are consistent with the angular correlation and conversion data given in this reference and, in addition, seem more compatible with the long lifetime for the 612 keV γ -transition which is here assigned the multipolarity $M3$, rather than $M1$.

In this level scheme, one may compare in a number of cases relative transition probabilities to two different members of the ground state rotational band.

a) The relative cross sections for the population of the $(7/2, 9/2+)$ and $(7/2, 11/2+)$ levels in the Coulomb excitation process depend on the ratio of the two $E2$ reduced transition probabilities, $B(E2; 7/2, 7/2 \rightarrow 7/2, 11/2)$ and $B(E2; 7/2, 7/2 \rightarrow 7/2, 9/2)$, which according to (12) should be 0.26. The observed value for this ratio is about 0.2.

b) The $M1$ transition probability in the $(7/2, 11/2+) \rightarrow (7/2, 9/2+)$ transition can be determined from the data discussed in a), together with the observed branching ratio for this transition in competition with the $(7/2, 11/2+) \rightarrow (7/2, 7/2+)$ $E2$ cross-over transition. By means of (12) one can then calculate the $M1$ transition probability for the $(7/2, 9/2+) \rightarrow (7/2, 7/2+)$ transition, and one finds that this transition should have an $E2$ intensity of 10–20%. From the angular correlation data of McGOWAN (1954), interpreted in terms of the spin assignments given in the figure, one obtains an $E2$ admixture in this transition of about 7%; attenuation effects due to quadrupole coupling may somewhat increase this value. The K -shell internal conversion coefficient is also consistent with an $E2$ admixture of the order of 10%.

A knowledge of the amount of $E2$ radiation in the $(7/2, 11/2+) \rightarrow (7/2, 9/2+)$ transition would make possible a further test of the intensity rules, by comparison with the transitions discussed under a).

c) The relative strength of the $E2$ transitions from the 480 keV level with $K = 5/2$ to the two first members of the ground state rotational band give the

ratio $B(E2; 5/2, 5/2 \rightarrow 7/2, 7/2):B(E2; 5/2, 5/2 \rightarrow 7/2, 9/2)$. The value calculated from (12) is 1.25 while the observed ratio is about 1.1, assuming the 480 keV transition to be 85 % $E2$ and 15 % $M1$, as indicated by the angular correlation data.

The large $E2:M1$ ratio in the 480 keV transitions may be ascribed to a coupling between the two rotational bands, which results in a small admixture of $(5/2, 7/2+)$ to the Ta ground state, with a consequent great enhancement of the $E2$ transitions. While in general such rotational admixtures may affect the intensity rules, in the present case of $\Delta K = 1$ and $E2$ radiation, the rules are not affected, provided one assumes that the intrinsic quadrupole moment is about the same in the two rotational bands (cf. pp. 19 ff.). From the observed lifetime of the 480 keV level one can estimate the squared amplitude of admixture to be about 10^{-3} .

of tests of the intensity rules (12) as applied to the transitions within a rotational band. Some of the general features of the decay schemes studied in this manner are illustrated in Figs. 3 and 4, and a summary of the available data from this source is given in Table II. The intensity rule has also been tested by the evidence on the relative lifetimes of the $2+$ and $4+$ rotational states in ${}_{88}\text{Ra}^{226}$ as deduced from the relative attenuation of the $\alpha-\gamma$ correlation associated with the two states (FALK-VAIRANT, TEILLAC, VALADAS, and BENOIST, 1954).

The intensity rules (12) applied to transitions involving a change in the intrinsic structure are illustrated by the β -decay branching ratios of the odd-odd nuclei ${}_{69}\text{Tm}^{170}$ (cf. Fig. 5), ${}_{45}\text{Rh}^{106}$, and ${}_{47}\text{Ag}^{106}$ (cf. Fig. 6), and by the γ -transition branching ratios in the even-even nucleus ${}_{74}\text{W}^{182}$ (cf. Fig. 7).

V. Effect of Perturbations.

Although the evidence on rotational spectra suggests that in the regions of the strongly deformed nuclei the wave functions (1) give a good representation of the nuclear states, the expected small deviations from this description may sometimes be significant.

Such deviations may be described by a wave function of the form

$$\Psi = \sqrt{\frac{2I+1}{8\pi^2}} \left\{ \varphi_{\tau K} \mathfrak{D}_{MK}^I + \sum_{\tau' K'} e_{\tau' K'} \varphi_{\tau' K'} \mathfrak{D}_{MK'}^I \right\}, \quad (14)$$

where the expansion amplitudes $e_{\tau' K'}$ can be estimated from the effect of the perturbation terms, representing the partial decoupling of the rotational from the intrinsic motion (cf. A. BOHR,

1952, eq. 96). Thus, the decoupling of the last odd particle gives rise, in first order ($K' = K \pm 1$), to terms in (14) with

$$\left. \begin{aligned} e_{\tau' K \pm 1} &= \frac{1}{E_{\tau KI} - E_{\tau' K'I}} \langle \tau KI | -\frac{\hbar^2}{\mathfrak{I}} (I_{x'} j_{x'} + I_{y'} j_{y'}) | \tau' K \pm 1 I \rangle \\ &= -\frac{1}{\Delta E} \frac{\hbar^2}{2\mathfrak{I}} \sqrt{(I \mp K)(I \pm K + 1)} \langle \tau K | j_{x'} \mp i j_{y'} | \tau' K \pm 1 \rangle, \end{aligned} \right\} \quad (15)$$

where $\Delta E = E_{\tau KI} - E_{\tau' K'I}$ is the energy difference between the unperturbed states. The x' and y' axes are perpendicular to the intrinsic nuclear symmetry axis (cf. Fig. 1) and \vec{j} is the angular momentum of the particle.

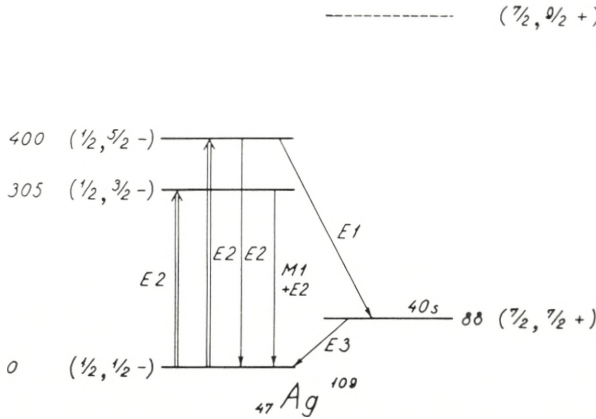


Fig. 4. Level scheme for Ag^{109} . The figure illustrates the information on the level structure of Ag^{109} obtained from Coulomb excitation (HUUS and LUNDÉN, 1954; HEYDENBURG and TEMMER, 1954). The notation is similar to that of Fig. 3.

The negative parity levels provide an example of a rotational series with $K = 1/2$, in which the second term in (4) gives rise to anomalous spacings. The decoupling parameter a deduced from the observed levels has the value 0.67.

The relative cross sections for the population of the $(1/2, 3/2^-)$ and $(1/2, 5/2^-)$ levels in the Coulomb excitation yield the ratio $B(E2; 1/2, 1/2 \rightarrow 1/2, 5/2^-) : B(E2; 1/2, 1/2 \rightarrow 1/2, 3/2^-) = 1.8$ to be compared with the value 1.50 obtained from (12).

The 88 keV level belongs to the well-known class of $7/2^+$ isomeric states found in this region of elements. It is populated in the Coulomb excitations by a weak $E1$ branch from the 400 keV level. The observed branching ratio from this level to the ground state and the isomeric state can be combined with the cross section for Coulomb excitation to yield a value for the reduced transition probability for the $E1$ γ -ray of $B(E1; 5/2^- \rightarrow 7/2^+) = 2 \times 10^{-32} e^2 \text{ cm}^2$. This value is smaller by a factor of about 10^6 than the value corresponding to a single-particle $E1$ transition (cf., e.g., BLATT and WEISSKOPF, 1952, p. 627). The reduction may be, at least partly, ascribed to the K -forbiddenness of the transition.

Similar level structures have been observed for Ag^{107} and Rh^{103} (HEYDENBURG and TEMMER, 1954); cf. Table II.

The intrinsic matrix element appearing in the final expression (15) is of similar type as those which enter in the probabilities for nuclear transitions involving a change in the particle configuration. While a quantitative evaluation is difficult, such matrix elements are known to involve unfavoured factors (cf. p. 7

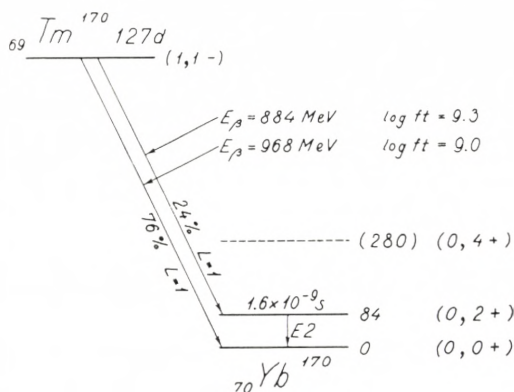


Fig. 5. Beta decay of Tm^{170} . The experimental data for the Tm^{170} decay are taken from GRAHAM, WOLFSON, and BELL (1952). The notation in the figure is the same as in Fig. 3. The 84 keV level in Yb^{170} can be identified as the first rotational excitation on the basis of its short lifetime.

The experimental ratio of 1.9 ± 0.2 for the ft -values of the two branches of the β -decay is in good agreement with the value 2.0 obtained from (12), assuming Tm^{170} to have $I = 1$ and the β -transitions to be of multipole order $L = 1$ (cf. Table I).

In the region of the well developed rotational spectra, similar branching ratios have been observed in the decays of Ho^{164} (BROWN and BECKER, 1954), Re^{186} (METZGER and HILL, 1951; STEFFEN, 1951; KOERTS, 1954) and Np^{236} (PASSELL, 1954). In two additional cases (Lu^{176} (GOLDHABER and HILL, 1952) and Ta^{180} (BROWN, BENDEL, SHORE, and BECKER, 1951)), there is some evidence for an odd-odd nucleus of spin 1 which β -decays to the ground state and first excited state of the neighbouring even-even nucleus, but with an ft -ratio appreciably smaller than the expected value of 2; in these cases, however, the assignments seem not to have been definitely established.

above) which may imply a rather small value for e ($e^2 \sim 10^{-1}$ to 10^{-2}) even in cases where ΔE is of the order of rotational energies¹.

¹ Note added in proof:

The recent high precision measurements on the W^{183} level structure (MURRAY, SNELGROVE, MARMIER, and DuMOND, 1954; MURRAY, BOEHM, MARMIER, and DuMOND, 1955) have revealed deviations from the rotational spectrum (4) of the magnitude of a few per cent. The observed deviations cannot be accounted for in terms of a rotation-vibration interaction and indicate a relatively large coupling to an excited particle configuration. The inclusion of a particle-rotation coupling of the type (15), acting between the ground state band and the first excited band, has made possible an interpretation of these effects (KERMAN, 1955). The squared amplitudes of the admixed states are found to be of the order of ten per cent and their unusually large magnitude in this case affects in an important way the transition intensities.

Higher order terms involving $|K - K'| > 1$ will be appreciably smaller, decreasing rather rapidly with the change in K .

The admixed states in (14) have an especially important effect on the intensity rules if either the unperturbed matrix element is very small (as is, for instance, often the case with low energy $E1$ radiation) or even vanishes (as for the K -forbidden transitions; cf. below), or if the admixed amplitude is associated with an especially large matrix element (cf. the rotational admixtures discussed below).

a) K -forbiddenness.

The above estimate of the deviations from the wave function (1) indicates that K -forbidden transitions (cf. p. 9) may be appreciably retarded, but that this retardation is usually not large enough to alter the predominant multipole order of a nuclear transition (cf., however, the γ -transitions in W^{182} between the $K = 2-$ and $K = 0+$ rotational bands (Fig. 7)). It will, however,

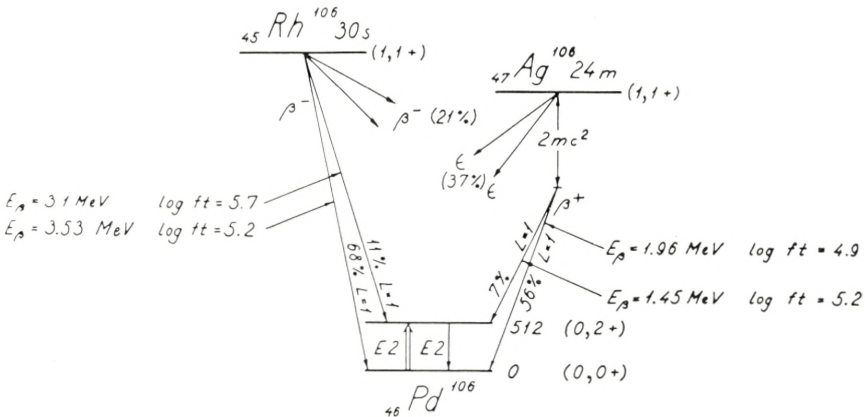


Fig. 6. Rotational branchings in the β -decay of Rh^{106} and of Ag^{106} . The notation in the figure is the same as used in Fig. 3. The experimental data for the Rh^{106} decay are taken from ALBURGER (1952) and for the Ag^{106} decay from BENDEL, SHORE, BROWN, and BECKER (1953), who besides the transitions shown have also found evidence for β -transitions from Rh^{106} and electron capture transitions from Ag^{106} to higher states in Pd^{106} . We here only consider the branching between transitions to the ground state and the 512 keV first excited $2+$ state. Assuming the quantum numbers indicated in the figure, the ratio of $|f|$ -values for the transitions to the first excited state and the ground state should be 2.0 (cf. (12)), which is in fairly good agreement with the measured ratios of about 2 for the Ag^{106} decay and about 3 for the Rh^{106} decay. There is, however, evidence from the higher excited states in Pd^{106} that the coupling scheme may be rather different from that of Fig. 1 (cf. footnote on p. 6).

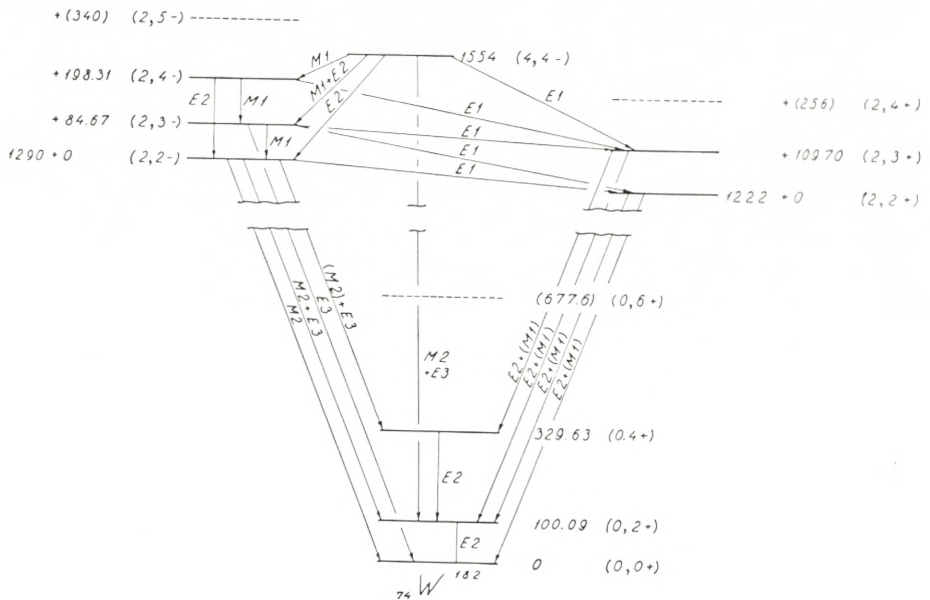


Fig. 7. Level scheme for W^{182} . The notation is the same as that used in Fig. 3. The experimental data, which are obtained from a study of the radiation following the β -decay of Ta^{182} , is taken from BOEHM, MARMIER, and DUOND (1954) (cf. also MIHELICH, 1954; FOWLER, KRUSE, KESHISHIAN, KLOTZ, and MELLOR, 1954). Apart from the indicated levels, there is evidence for two very weakly populated states at energies of about 1255 keV and 1437 keV. Otherwise, the level scheme drawn above differs from that given by BOEHM et. al. only in the spin assignments of the 1331 keV and 1554 keV levels; the assignments suggested here are, however, also in agreement with the data in this reference.

The level scheme is interpreted as involving primarily states associated with four rotational series. The first series, comprising the three lowest levels, is the systematically occurring $K = 0+$ ground state rotational band of even-even nuclei. (For lifetime and Coulomb excitation of the 100 keV level, cf. SUNYAR, 1954; HUUS and BJERREGÅRD, 1953; MCCLELLAND, MARK, and GOODMAN, 1954). The calculated energy of the $6+$ member of this band includes a small correction for the rotation-vibration interaction, as deduced from the observed energies of the $2+$ and $4+$ states.

The second series, beginning with the 1222 keV level, has $K = 2+$ and a moment of inertia rather close to that of the ground state band, although a little smaller. The third series, beginning with the 1290 keV level, has $K = 2-$ and a moment of inertia again of the same order of magnitude as that of the ground state, but in this case somewhat larger. This larger moment is in agreement with a general tendency observed for configurations, as in odd-A nuclei, having particles in addition to those filled in pairs. (Cf. BOHR and MOTTELSON, 1954; BOHR, FRÖMAN, and MOTTELSON, 1955). In this view, the somewhat smaller moment of inertia for the $2+$ series might indicate an intrinsic excitation of collective vibrational type leaving the particles in a paired configuration (cf. further below).

The β -decay of Ta^{182} further populates a level at 1554 keV, which seems to be the lowest member of a fourth rotational band.

The measured γ -intensities provide a number of tests of the intensity rules (12):

a) The branching ratio of the 1222 keV level to the ground state and 100 keV levels yields $B(E2; 2,2 \rightarrow 0,0) : B(E2; 2,2 \rightarrow 0,2) = 0.62$, assuming pure $E2$ radia-

tions for both transitions. The ratio calculated from (12) is 0.70. The amount of $M1$ radiation observed in these high energy transitions appears small, but is difficult to determine quantitatively. According to (12), the intensity of the 893 keV $E2$ transition from the 1222 keV level to the 329 keV level, which has so far not been observed, should be 1.5 % of the ground state transition.

b) The branching ratio of the transitions from the $(2,3+)$ level to the 100 keV and 329 keV levels gives $B(E2; 2,3 \rightarrow 0,2):B(E2; 2,3 \rightarrow 0,4) = 2.1$, to be compared with the theoretical value 2.5.

The observation of rather pure $E2$ radiation in the $\Delta I = 1$ transitions between the $K = 2+$ and $K = 0+$ rotational bands may be understood in terms of the K -forbiddenness for $M1$ radiation. The $K = 2+$ band may possibly represent vibrational excitations of the ground state; such an interpretation would account for the strength of these transitions, as reflected in the fact that the $(2,3+) \rightarrow (2,2+)$ rotational transition is too weak to be observed. A crucial test of the vibrational character of these levels would be provided by a determination of the cross section for Coulomb excitation of the $(2,2+)$ level.

c) The ratio of the intensities of the $E1$ transitions from the $(2,3-)$ level to the $(2,3+)$ and $(2,2+)$ levels is calculated from (12) and (9) to be 0.031:1. While the low energy transition has been detected, its weak intensity has so far prevented a quantitative determination of this branching ratio.

d) The assignment of quantum numbers in the figure also provides an interpretation of the observation that the $\Delta I = 0$ and 1 transitions between the $K = 2-$ and $K = 0+$ rotational bands appear to be mainly of $M2$ or $E3$ type, rather than $E1$, which is K -forbidden.

Such a K -forbiddenness may also account for the fact that no β -transitions are observed directly to the members of the $K = 0+$ ground state rotational band.

lead to increased admixtures of higher multipole components, which may be especially significant in the so-called parity unfavoured transitions (γ -transitions with $\pi = (-)^{\Delta I + 1}$ and β -transitions with $\pi = (-)^{\Delta I}$ ($\Delta I = 0$ excepted)), where mixed multipole transitions are most likely to occur.

An example of a highly K -forbidden transition ($\nu = 8$) where a large retardation factor is expected is provided by the 5.5 h isomeric transition in Hf^{180} (cf. Fig. 2). Another such example is the β -decay of Lu^{176} , where the high order of K -forbiddenness ($\nu = 5$ or 6) suggests the interpretation of the observed $\log ft = 18.9$ as a second forbidden transition with an unfavoured factor of the order of 10^{-7} .

b) Rotational admixtures.

In the calculation of nuclear transition probabilities, small admixtures in the wave functions (1) may be significant, even where there is no K -forbiddenness, if the associated transition matrix element is large. Thus, the large transition matrix element for $M1$ and $E2$ radiation within a rotational family (cf. p. 6) implies that, in a transition involving a change in the particle

structure, special significance attaches to the admixtures to one of the combining states of a wave function belonging to the rotational family of the other. Especially for $E2$ radiation, these rotational admixtures are expected to contribute a significant, and in many cases a dominant part of the transition matrix element (especially for $\Delta K = 1$, where the admixed amplitudes are largest (cf. pp. 14 ff.)).

Since the γ -transitions within a rotational family are generally of mixed $E2 + M1$ character for $\Delta I = 1$, the rotational admixtures may lead to mixed multipole radiation also for transitions associated with a change in the intrinsic nuclear structure and having $\Delta I = 0$ or 1 and $\pi = +$.

Another consequence of the rotational admixtures may be to modify the relative intensity rules (12) and (13) for $M1$ and $E2$ γ -radiation. In certain cases, the modified rules may be derived by considering the I -dependence of the admixed amplitudes.

For $\Delta K = 1$, however, it is found that the intensity rules for the $E2$ radiation are not affected if the nuclear deformations for the two states are approximately the same. An interesting example is provided by the decay of the 480 keV state in Ta^{181} (cf. Fig. 3). The squared amplitude of the rotational admixture is here of the order of 10^{-3} , but is nevertheless mainly responsible for the $E2$ radiation as evidenced by the strong admixture of $E2$ in the 480 keV $\Delta I = 1$ transition.

We wish to acknowledge stimulating contacts with Professor J. W. M. DUMOND and Drs. N. HEYDENBURG, G. TEMMER, and T. HUUS. We are also indebted to these authors for communicating experimental results prior to publication. One of us (G. A., on leave from the University of Zagreb) is indebted to the Institute Rudjer Bošković for a grant.

*Institute for Theoretical Physics
University of Copenhagen
and
CERN (European Organization for Nuclear Research)
Theoretical Study Division.*

References.

- D. E. ALBURGER (1952), *Phys. Rev.* **88**, 339.
- K. ALDER, A. BOHR, T. HUUS, B. R. MOTTELSON, A. WINTHER, and C. ZUPANČIČ (1955), to be submitted to *Rev. Mod. Phys.*
- F. ASARO and I. PERLMAN (1953), *Phys. Rev.* **91**, 763.
- W. L. BENDEL, F. W. SHORE, N. H. BROWN, and R. A. BECKER (1953), *Phys. Rev.* **90**, 888.
- J. M. BLATT and V. F. WEISSKOPF (1952), *Theoretical Nuclear Physics*, John Wiley and Sons, N. Y.
- F. BOEHM, P. MARMIER, and J. W. M. DUMOND (1954), *Phys. Rev.* **95**, 864.
- A. BOHR (1952), *Dan. Mat. Fys. Medd.* **26**, no. 14.
- A. BOHR (1954), *Rotational States of Atomic Nuclei*, Ejnar Munksgaard, Copenhagen.
- A. BOHR, P. O. FRÖMAN, and B. R. MOTTELSON (1955), *Dan. Mat. Fys. Medd.* **29**, no. 10.
- A. BOHR and B. R. MOTTELSON (1953a), *Phys. Rev.* **89**, 316.
(1953b), *Phys. Rev.* **90**, 717.
(1953c), *Dan. Mat. Fys. Medd.* **27**, no. 16.
(1954), Chapter 17 of "Beta and Gamma Ray Spectroscopy", ed. by K. SIEGBAHN, North Holland Publishing Co.
- H. N. BROWN, W. L. BENDEL, F. J. SHORE, and R. A. BECKER (1951), *Phys. Rev.* **84**, 292.
- H. N. BROWN and R. A. BECKER (1954), *Phys. Rev.* **96**, 1372.
- E. U. CONDON and G. H. SHORTLEY (1935), *The Theory of Atomic Spectra*. The University Press, Cambridge.
- C. F. COOK, C. M. CLASS, and J. T. EISINGER (1954), *Phys. Rev.* **96**, 658.
- J. T. EISINGER, C. F. COOK, and C. M. CLASS (1954), *Phys. Rev.* **94**, 735.
- P. FALK-VAIRANT, J. TEILLAC, G. VALADAS, and P. BENOIST (1954), *C. R.* **238**, 1409 and 1656.
- K. W. FORD (1953), *Phys. Rev.* **90**, 29.
- C. M. FOWLER, H. W. KRUSE, V. KESHISHIAN, R. J. KLOTZ, and G. P. MELLOR (1954), *Phys. Rev.* **94**, 1082.
- W. I. GOLDBURG and R. M. WILLIAMSON (1954), *Phys. Rev.* **95**, 767.
- M. GOLDHABER and R. D. HILL (1952), *Rev. Mod. Phys.* **24**, 179.
- K. GOTTFRIED (1955), private communication.
- R. L. GRAHAM, J. L. WOLFSON, and R. E. BELL (1952), *Can. J. Phys.* **30**, 459.

- N. P. HEYDENBURG and G. M. TEMMER (1954), Phys. Rev. **95**, 861.
N. P. HEYDENBURG and G. M. TEMMER (1954a), private communication;
cf. also the review article by ALDER et al. (1955).
T. HUUS and J. BJERREGÅRD (1953), Phys. Rev. **92**, 1579.
T. HUUS and A. LUNDÉN (1954), Phil. Mag. **45**, 966.
T. HUUS and C. ZUPANČIČ (1953), Dan. Mat. Fys. Medd. **28**, no. 1.
T. HUUS, J. H. BJERREGÅRD, and B. ELBEK (1955), to be published in
Dan. Mat. Fys. Medd.
A. K. KERMAN (1955), to be published.
L. KOERTS (1954), Phys. Rev. **95**, 1358.
E. J. KONOPINSKI and G. E. UHLENBECK (1941), Phys. Rev. **60**, 308.
P. MARMIER and F. BOEHM (1955), Phys. Rev. **97**, 103.
C. L. McCLELLAND, H. MARK, and C. GOODMAN (1954), Phys. Rev.
93, 904.
C. L. McCLELLAND, H. MARK, and C. GOODMAN (1955), Phys. Rev. **97**,
1191.
F. K. MCGOWAN (1954), Phys. Rev. **93**, 471 and Phys. Rev. **93**, 163.
F. R. MEZTGER and R. D. HILL (1951), Phys. Rev. **82**, 646.
J. W. MIHELICH (1954), Phys. Rev. **95**, 626 (A).
J. W. MIHELICH, G. SCHARFF-GOLDHABER, and M. McKEOWN (1954).
Phys. Rev. **94**, 794 (A).
S. A. MOSZKOWSKI (1953), Phys. Rev. **89**, 474.
J. J. MURRAY, F. BOEHM, P. MARMIER, and J. W. M. DUMOND (1955),
Phys. Rev. **97**, 1007.
J. J. MURRAY, P. SNELGROVE, P. E. MARMIER, and J. W. M. DUMOND
(1954) Phys. Rev. **96**, 858 (A).
J. O. NEWTON (1954), Nuclear Properties of the Very Heavy Elements.
Contribution to Progress in Nuclear Physics, vol. 4; ed. by O. R.
FRISCH.
S. G. NILSSON (1955), Dan. Mat. Fys. Medd. **29**, no. 16, in the press.
T. O. PASSELL (1954), thesis. University of California, Berkeley.
E. RASMUSSEN (1935), Naturwiss. **23**, 69.
M. E. ROSE (1954), Proc. Phys. Soc. **67**, 239.
G. R. SATCHLER (1955), Phys. Rev. **97**, 1416.
G. SCHARFF-GOLDHABER and J. WENESER (1955), Phys. Rev. **98**, 212.
R. M. STEFFEN (1951), Phys. Rev. **82**, 827.
A. W. SUNYAR (1954), Phys. Rev. **93**, 1122.

Det Kongelige Danske Videnskabernes Selskab

Matematisk-fysiske Meddelelser, bind **29**, nr. 10

Dan. Mat. Fys. Medd. **29**, no. 10 (1955)

ON THE FINE STRUCTURE IN ALPHA DECAY

BY

A. BOHR, P. O. FRÖMAN, AND B. R. MOTTELSON



København 1955

i kommission hos Ejnar Munksgaard

Printed in Denmark
Bianco Lunos Bogtrykkeri A/S

The coupling scheme associated with large nuclear deformations, and appropriate to the very heavy nuclei, suggests that the preferred mode of α -decay involves nucleons in paired orbits. For the even-even nuclei, the strongest transition thus goes to the ground state of the daughter, and the fine structure populates predominantly the rotational band associated with this configuration; for odd-A nuclei, the favoured α -decays populate the rotational band for which the orbit of the last odd nucleon remains unchanged. From this interpretation one also obtains a number of correlations between energies and lifetimes of the favoured α -decays in even-even and odd-A nuclei. Moreover, it is possible to estimate the intensity ratios in the favoured α -decays of odd-A nuclei on the basis of those observed in the even-even nuclei.

Many striking regularities have been observed in the α -decay fine structure of the heavy elements, especially for the even-even nuclei, and it has been shown that these regularities are related to the fact that the α -decay process primarily populates states in the daughter belonging to a rotational band (ASARO and PERLMAN, 1953, 1954; FALK-VAIRANT, TEILLAC, VALLADAS, and BENOIST, 1954; MILSTED, ROSENBLUM, and VALADARES, 1954; cf. also the review article by NEWTON, 1954).

In the present paper, we shall consider a simple picture of the α -particle formation, related to the coupling scheme of these strongly deformed nuclei, which makes possible a further discussion of the regularities in the α fine structure. This interpretation also implies a number of relationships between the α -decay of even-even and odd-A nuclei.

In nuclei whose equilibrium shape possesses a large deformation, one expects a band of rotational states associated with each configuration of the particles¹. In most cases, the nuclear

¹ For a more detailed discussion of nuclear rotational states, cf. BOHR and MOTTELSON, 1953, 1954; and A. BOHR, 1954.

shape is expected to possess axial symmetry, and the rotational spectrum is then given by

$$E = \frac{\hbar^2}{2\mathfrak{I}} \{I(I+1) + a(-1)^{I+1/2}(I+1/2)\delta_{K,1/2}\} \quad (1)$$

apart from a constant depending on the intrinsic nuclear structure. The quantum number K represents the projection of the total angular momentum along the nuclear symmetry axis and is constant for all the states in a given rotational band. The effective moment of inertia which depends on the nuclear deformation is denoted by \mathfrak{I} , and the quantity a is a decoupling parameter which occurs only in the rotational spectra for configurations with $K = 1/2$.

The independent particle motion in axially symmetric deformed potentials may be characterized by the quantum number Ω_p representing the projection of the total angular momentum of the particle along the nuclear symmetry axis. States differing only in the sign of Ω_p are degenerate, and the lowest state of a nucleus is thus obtained by filling the particles pairwise in states of opposite Ω_p .

In an even-even nucleus, the ground state configuration therefore has $K = (\sum_p \Omega_p) = 0$, and the associated rotational band contains the levels

$$I = 0, 2, 4, 6 \dots \text{(even parity)}. \quad (2)$$

In an odd-A nucleus, K is equal to $|\Omega_p|$ for the last odd nucleon, and for each binding state of this particle there is a rotational band containing the states

$$I = K, K+1, K+2, \dots \left. \begin{array}{l} \text{(all same parity as} \\ \text{the orbit of the last} \\ \text{odd nucleon).} \end{array} \right\} \quad (3)$$

Particles occupying states which differ only in the sign of Ω_p interact especially strongly due to the large overlap of their wave functions. Thus, the formation of an α -particle from an independent particle system of this structure is expected to take place most easily from two such pairs of protons and neutrons. This type of α -decay, which is characterized by the selection

rules $\Delta K = 0$ and no change of parity, will be referred to as the favoured α -transitions.

A further consequence of the non-spherical field of the nucleus is the exchange of angular momentum between α -particle and daughter nucleus, which implies that in general several

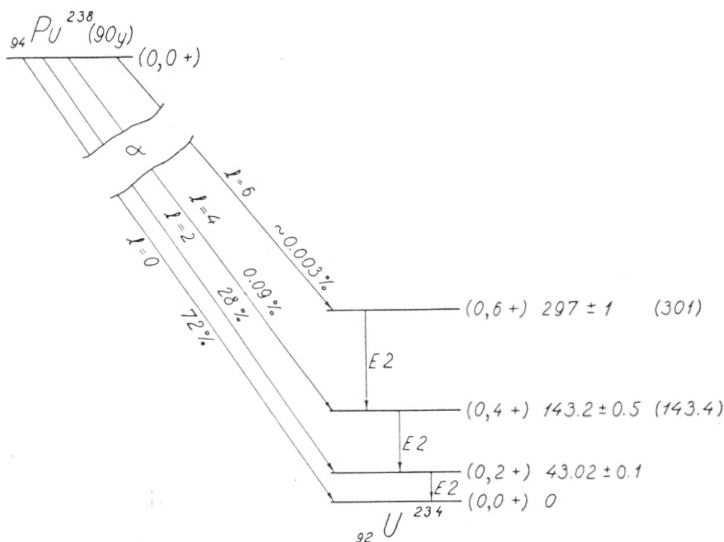


Fig. 1. *Alpha-decay of Pu^{238} .* The experimental data is taken from NEWTON and ROSE, 1953, and from ASARO and PERLMAN, 1954 a. The states are labeled by the quantum numbers $(K, I\pi)$, where π is the parity.

The α -decay of Pu^{238} , which illustrates the typical pattern observed in the even-even α -emitters with $A > 220$, populates the rotational sequence associated with the ground state configuration $(0, I+)$ of the daughter nucleus. The observed energies are given in keV; the values shown in parenthesis are calculated from (1) by adjusting the moment of inertia to give the observed energy of the first excited state. The small deviations between the calculated and measured values have a negative sign and increase with I , as is expected for the correction terms to (1) resulting from the rotation-vibration interaction (cf. BOHR and MOTTELSON, 1953, 1954). This correction has the form $-R I^2 (I + 1)^2$. The value of R , estimated from the observed energies, is $R \approx 2 \times 10^{-3}$ keV, which is of the expected order of magnitude.

members of each rotational band are populated with comparable intensity.

In an even-even nucleus, the α -decay should thus take place primarily to the lowest $K = 0$ band of the daughter, i. e. the ground state and its rotational excitations. This pattern has indeed been observed as a systematic feature of the α fine structure in even-even nuclei possessing large deformations ($A > 220$)

(ASARO and PERLMAN, 1953; NEWTON, 1954); for an example, cf. Fig. 1. The spins and energies of the populated excited states are in agreement with (2) and (1). The rotational character of the excitations is further supported by the $E2$ transition probabilities which are several orders of magnitude greater than for single-particle transitions (cf. NEWTON, 1954; TEMMER and HEYDENBURG, 1954).

The great similarity in the decay process for the different even-even nuclei in this region is exhibited by the marked regularity in the lifetime energy relations for the ground state transitions (PERLMAN, GHIORSO, and SEABORG, 1950; KAPLAN, 1951). With relatively good accuracy (within about a factor of two), the transition probability per second, P_0 , for all these transitions can be represented by the simple Geiger-Nuttall law

$$\log_{10} P_0 = C - \frac{D}{\sqrt{E}}, \quad (4)$$

where E is the kinetic energy of the α -particle, while C and D are constants for each element and vary regularly with Z . The relationship (4) as well as the order of magnitude of C and D can be obtained from the theory of barrier penetration (cf., e. g., GAMOW and CRITCHFIELD, 1949). The values of C and D , determined by a recent analysis (FRÖMAN, 1955) of the empirical data, are listed in Table I.

TABLE I.

Z	C	D
84	50.15	128.8
86	50.94	132.7
88	51.51	136.2
90	51.94	139.4
92	52.55	143.1
94	53.35	147.4
96	53.97	151.3
98	54.40	154.7

The table lists the coefficients appearing in the empirical Geiger-Nuttall relation (Eq. (4)) for even-even ground state transitions. The units employed are such that, when the α -energy is measured in MeV, the transition probability is given in sec^{-1} . The coefficients are listed as functions of the charge number Z of the parent nucleus.

There is also a considerable regularity in the intensities of the α fine structure, leading to the rotational excitations of the ground state configurations. The observed transition probabilities to the $(2+)$ levels are of the order of (4), while those to the $(4+)$ and $(6+)$ levels are systematically smaller (ASARO and PERLMAN, 1953). This hindrance, which shows a regular variation with A , amounting in the heaviest elements to a factor of about a hundred, can be ascribed only partly to the centrifugal barrier encountered by the α -particle.

A detailed theory of the intensity rules for the population of the rotational band in the daughter nucleus would involve, in the first place, a consideration of the α formation process and of the boundary conditions it implies at the non-spherical nuclear surface. In the second place, there would be involved a treatment of the penetration problem for the α -wave through the anisotropic Coulomb barrier (HILL and WHEELER, 1953). Due to the exchange of angular momentum between the α -particle and the residual nucleus, this latter part of the α decay process is described by a system of coupled differential equations (RASMUSSEN, 1954a; FRÖMAN, 1955).

The problem is simplified, however, by the fact that the formation of the α -particle and its passage through the region close to the nuclear surface, in which appreciable exchange of angular momentum may occur, takes place in a time short compared to the nuclear rotational period. It is, therefore, possible to a first approximation to consider the nucleus as fixed in space during the α -particles' traversal of this region¹. We shall later exploit this simplification in the comparison between the α -decay of even-even and odd- A nuclei.

The α fine structure pattern in even-even nuclei so far discussed has included only the favoured transitions in which the α -particle is formed from nucleons in paired orbits, and thus leaves the daughter even-even nucleus in the ground state rotational band². It is of course also possible for the α -decay to populate

¹ For a more detailed discussion of this approximation and of the solutions obtained, cf. FRÖMAN, 1955.

² Favoured transitions may also be expected to take place to excited configurations with $K = 0$, representing either the excitation of a pair of particles or a collective vibration. Such states may, however, have a rather high excitation energy (~ 1 MeV) and, in fact, such transitions seem not so far to have been observed.

excited particle configurations in the daughter nucleus; examples of such unfavoured transitions have been observed in the α -spectrum of Th^{230} (α_{255}) (BOUSSIERES et al., 1953; RASETTI and BOOTH, 1953; VALLADAS and BERNAS, 1953) and Th^{228} (α_{217}) (BOUSSIERES et al., 1953; ASARO, STEPHENS, and PERLMAN,

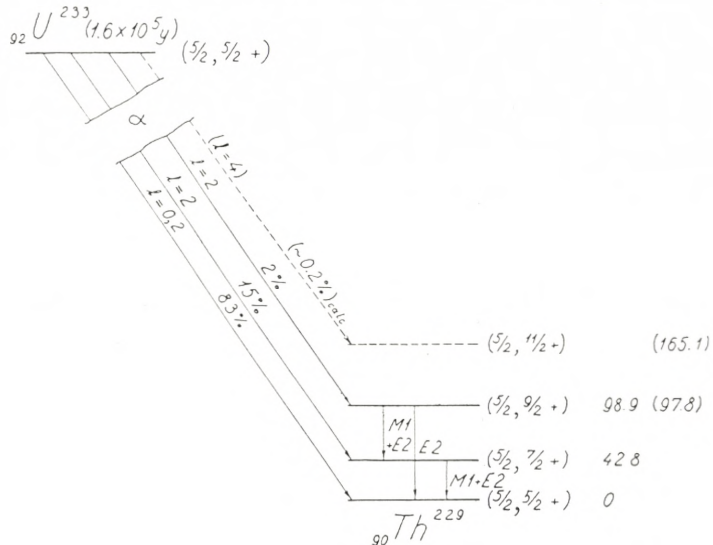


Fig. 2. *Alpha-decay of U^{233} .* The decay scheme is based on experimental data given in the references found in Table III. The notation is the same as in Fig. 1.

The α -decay is interpreted as taking place to the ground state rotational band in Th^{229} . The value of K for this band is deduced, by means of (1) and (3), from the measured energies of the first and second excited states, and is found to equal the known spin of the parent nucleus, as is expected for the favoured α -transitions. The interpretation of the transitions as of the favoured type is further supported by the reduced transition probability for the ground state transition (cf. Table II). For a theoretical estimate of the relative intensities of the fine structure components, cf. Table IV.

The position of the expected, but so far not observed, third excited state is deduced from (1), and the intensity of the α -group populating this state is calculated from (5) (cf. Table IV). The parities in the figure represent values relative to that of the U^{233} ground state, and are based on the interpretation of the α -transitions as favoured, which implies no change of parity.

1953; NEWTON and ROSE, 1954). As expected, the transition probabilities are appreciably smaller than for the favoured transitions given by (4).¹

¹ Note added in proof: Recently, similar transitions have been identified in the α -spectra of other neighbouring nuclei, and evidence has been provided for the (1-) character of the excited states in question (STEPHENS, ASARO, and PERLMAN, 1954). It has been suggested (R. F. CHRISTY, private communication) that these excitations may be of collective type associated with a nuclear shape containing deformations of odd multipole type.

In an odd-A nucleus, the favoured α -decays leave the last odd particle moving in the same orbital in the daughter as in the parent¹. If this configuration is that of the ground state band of the daughter nucleus, the expected fine structure pattern is much the same as in even-even nuclei with the most intense transition going to the ground state and regularly decreasing intensities of the branchings to the rotational excitations of this configuration. An example of such a decay is provided by U^{233} (cf. Fig. 2).

If the orbital of the last odd particle in the parent corresponds to an excited particle configuration in the daughter the transitions to the ground state band are hindered and the decay is expected to take place predominantly to the rotational band associated with the excited configuration in question (provided its excitation energy is not too great).

As an example of such a pattern in an odd-A nucleus, the α -decay of Am^{241} is shown in Fig. 3 (RASMUSSEN, 1954; ASARO and PERLMAN, 1954; MILSTED, ROSENBLUM, and VALADARES, 1954).

If the favoured transitions leave the daughter with appreciable excitation energy ($\gtrsim 1/2$ MeV), these transitions, although intrinsically preferred, may be relatively weak. In this case, the α fine structure may be somewhat more complex with no single transitions dominating. The α -decays of Th^{227} and Pa^{231} appear to provide examples of this type (FRILLAY, ROSENBLUM, VALADARES, and BOUSSIERES, 1954; ROSENBLUM, COTTON, and BOUSSIERES, 1949).

The similarity between the favoured α -transitions in odd-A and even-even nuclei implies a number of simple relations between the two classes of transitions, as regards energy systematics, lifetimes, and fine structure intensities.

In particular, a close correspondence is expected between the even-even ground state transitions and the favoured odd-A transitions to the head of the daughter band (i. e. having $\Delta I = 0$). The decay energies of the two types of transitions should exhibit similar trends, and the odd-A transitions in question should also follow approximately the same Geiger-Nuttal law (4) as the even-even ground state transitions.

¹ A similar interpretation of the α fine structure in odd-A nuclei has recently been discussed by NEWTON, 1954, and by RASMUSSEN, private communication.

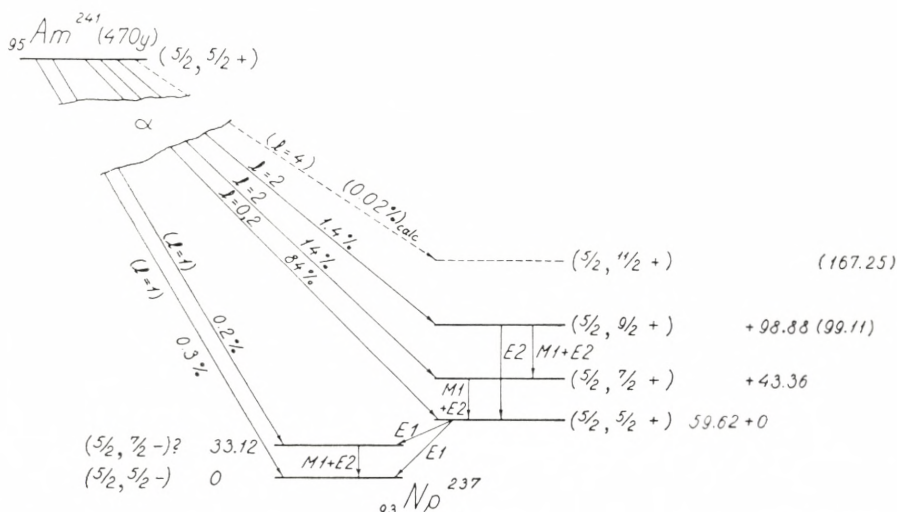


Fig. 3. Alpha-decay of Am^{241} . The decay scheme is based on experimental data given in the references found in Table III. The states are labeled as in Fig. 1. Parities are relative to that of the Am^{241} ground state. Levels which are interpreted as belonging to the same rotational band in Np^{237} are drawn above each other, while the two different rotational bands are displaced sideways.

The favoured α -transitions take place to the 60 keV level and its rotational excitations. The accurately measured energies in this series show the K -value to be $5/2$. The very small difference between the observed value for the $(5/2, 9/2+)$ level and the value calculated from (1) (shown in parenthesis) is just of the sign and magnitude expected from the rotation-vibration interaction, as observed in U^{234} (cf. Fig. 1). (For Np^{237} , one finds $R \approx 1.5 \times 10^{-3}$ keV, which agrees with the value obtained from U^{234} , considering the expected variation of R with $\left(\frac{h^2}{2\mathcal{I}}\right)^3$ (cf. BOHR and MOTTELSON, 1953, p. 91)). The α -intensity to the expected $(5/2, 11/2+)$ level has been estimated from (5) (cf. Table IV).

From (5), one also estimates that the α -transition to the $(5/2, 5/2+)$ level should be 80% $l = 0$ and 20% $l = 2$. Evidence on this mixture may be obtained from the α - γ correlation between this α -group and the 60 keV E1 γ -ray. From the calculated mixture and the spin values given in the figure, one estimates

$$W(\theta) = 1 \pm .35 P_2(\cos \theta). \text{ An angular anisotropy of } A = \frac{W(\pi)}{W(\pi/2)} - 1 = -0.21$$

has been found (FRASER and MILTON, 1954) to decay with a lifetime of 5.5×10^{-9} sec. However, as evidenced by the α - γ correlations in even-even nuclei, one expects for these strongly deformed nuclei, attenuations from quadrupole couplings acting over times appreciably shorter than those studied. The observed anisotropy which is about half that estimated therefore appears consistent with the present interpretation of the decay.

The α -decay to the ground state of Np^{237} is strongly hindered ($F \sim 10^{-3}$). If one tentatively assumes the 33 keV level to be a rotational excitation of the ground state, and the α -decays to both these states to be predominantly $l = 1$, one estimates from (5) the relative intensities 1:0.25, in favour of the ground state transition. This interpretation of the first excited state would also imply a branching ratio of 1:0.035 for the E1 γ -rays from the $(5/2, 5/2+)$ level to the $(5/2, 5/2-)$ and $(5/2, 7/2-)$ levels (cf. ALAGA, ALDER, BOHR, and MOTTELSON, 1955). The observed ratio is 1:0.07 (BELING, NEWTON, and ROSE, 1952).

Thus, the observed transition probabilities may be used to identify the favoured odd-A transitions in a given decay scheme. The α -transitions in odd-A nuclei, tentatively classified in this manner as favoured and having $\Delta I = 0$, are listed in Table II, together with the even-even ground state transitions.

The table gives the α -energy and reduced transition probability F , which is the ratio of the observed transition probability to that given by (4). Although the classification of the odd-A transitions is in some cases rather uncertain, there are seen to exist for almost all the odd-A α -emitters groups with transition probabilities comparable to those of the even-even ground state transitions¹. The fluctuation in F for the odd-A and even-even transitions seem to be comparable, apart from a few uncertain cases, but there appears to be a systematic tendency for the odd-A F -values to be somewhat smaller than unity, on the average by a factor of about two. As will be seen below, there are a number of such small systematic differences between the odd-A and even-even favoured transitions.

The α -energies of the favoured $\Delta I = 0$ transitions are plotted in Fig. 4. It is seen that the odd-A and even-even transitions exhibit closely parallel trends with, however, a systematic tendency for the odd-A energies to be smaller, by about 200 keV, than those interpolated between the even-even nuclei.

Such an effect may be understood in terms of the change of the kinetic energy of the last odd particle associated with the small shrinking of the nuclear volume. Thus, if one assumes the nuclear radius to be proportional to $A^{1/3}$, the difference in radius between the parent and daughter nuclei implies an energy shift of just a few hundred keV.

In cases where a rotational fine structure has been observed in the favoured odd-A decays, more detailed tests of the present interpretation can be made. These cases are listed in Table III, which gives the observed level spacings in columns four and five.

The ratios of spacings of successive states are seen to agree well with those given by (1). Moreover, as expected, the moments of inertia are similar to those in neighbouring even-even nuclei.

¹ In a quantitative comparison between odd-A and even-even transition probabilities for these $\Delta I = 0$ favoured transitions, a small correction, of the order of 20 per cent, should be made for the $l = 2$ contribution to the odd-A decay (cf. (5)).

TABLE II. *Favoured α -transitions with $\Delta I = 0$.*

Parent element	Even-even isotopes ground state transitions			Odd-A isotopes $\Delta I = 0$ favoured transitions		
	A	E (MeV)	F	A	E (MeV)	F
$_{88}\text{Ra}$	220	7.43	0.6	219	8.0	0.3
	222	6.51	1.3	221	6.71	0.3
	224	5.681	1.0	223	5.596	0.2
	226	4.779	0.8
$_{89}\text{Ac}$	223	6.64	0.3
	225	5.80	0.3
	227	4.942	0.2
$_{90}\text{Th}$	224	7.13	1.3	223	7.55	0.5
	226	6.30	1.3	225	6.57	0.4
	228	5.421	0.8	227	5.704	0.2
	230	4.682	0.6	229	4.85	0.5
	232	3.98	1.6
$_{91}\text{Pa}$	227	6.46	0.6
	231	4.722	0.4
$_{92}\text{U}$	228	6.67	0.8	227	6.8	2.0
	230	5.85	1.3	229	6.42	0.3
	232	5.318	0.6	233	4.823	0.5
	234	4.763	0.8	235	4.20	0.3
	236	4.50	1.0
	238	4.18	1.0
$_{93}\text{Np}$	231	6.28	25.1
	233	5.53	2.0
	235	5.06	0.5
	237	4.77	0.4
$_{94}\text{Pu}$	232	6.58	0.1	235	5.85	0.4
	234	6.19	0.6	239	5.150	0.3
	236	5.75	1.0	241	4.893	1.3
	238	5.495	0.6
	240	5.162	0.8
	242	4.898	0.8
$_{95}\text{Am}$	237	6.01	0.1
	239	5.75	0.2
	241	5.476	0.6
	243	5.267	0.8

TABLE II. *Favoured α -transitions with $\Delta I = 0$ (continued).*

Parent element	Even-even isotopes ground state transitions			Odd-A isotopes $\Delta I = 0$ favoured transitions		
	A	E (MeV)	F	A	E (MeV)	F
${}_{96}\text{Cm}$	238	6.50	1.6	241	5.89	0.1
	240	6.26	1.0	243	5.777	0.5
	242	6.110	0.6	245	5.34	0.3
	244	5.798	0.8
${}_{97}\text{Bk}$	243	6.20	0.1
	245	5.90	0.3
${}_{98}\text{Cf}$	244	7.15	0.8	249	5.82	0.3
	246	6.75	0.8
	248	6.26	1.3
	250	6.05	0.6
	252	6.15	1.3

Table II. *Favoured α -transitions with $\Delta I = 0$.*

Most of the investigated odd-A α -decays contain a single component, or a group of components, having transition probabilities of the order of magnitude (4), characteristic of the even-even ground state transitions. These components are interpreted as the favoured transitions which leave the configuration of the last odd particle unchanged. The most energetic of these favoured transitions is expected to have $\Delta I = 0$, and to be very similar to the even-even ground state transitions.

The table lists the α -energies of these favoured $\Delta I = 0$ transitions in the even-even and odd-A nuclei, together with the reduced transition probabilities F , which give the ratio between the observed transition probability for the group in question and that calculated from (4) and Table I. (For odd-Z elements, the appropriate coefficients C and D have been obtained by interpolation in Table D).

Included in the table are odd-A nuclei for which α -groups have been observed with $F \geq 0.1$. A more detailed test of the classification of these transitions as of the favoured type can be made in cases where the rotational fine structure has been observed (cf. Tables III and IV).

The empirical data is taken from the review articles by HOLLANDER, PERLMAN, and SEABORG, 1953, and by SEABORG, 1954 and, in addition, from GHIORSO et al., 1954, (Cf^{249} and Cf^{250}), and THOMPSON et al., 1954 (Cf^{252}). The table includes only nuclei with $Z \geq 88$, which are sufficiently far removed from the closed-shell region around Pb^{208} that one may expect the simple features associated with the coupling scheme of strongly deformed nuclei.

The tendency toward somewhat larger moments of inertia for these odd-A nuclei as compared with the even-even neighbours continues a trend previously observed in other regions of the periodic table (BOHR and MOTTELSON, 1954).

The value of K for the rotational band in the daughter

nucleus, as obtained from the observed rotational energies, is listed in column seven of Table III. As is expected for the favoured α -transitions, it is seen to agree with the K -values for the parent nucleus in all the cases where the spin of this nucleus has been measured.

The present interpretation of the favoured α -decays further

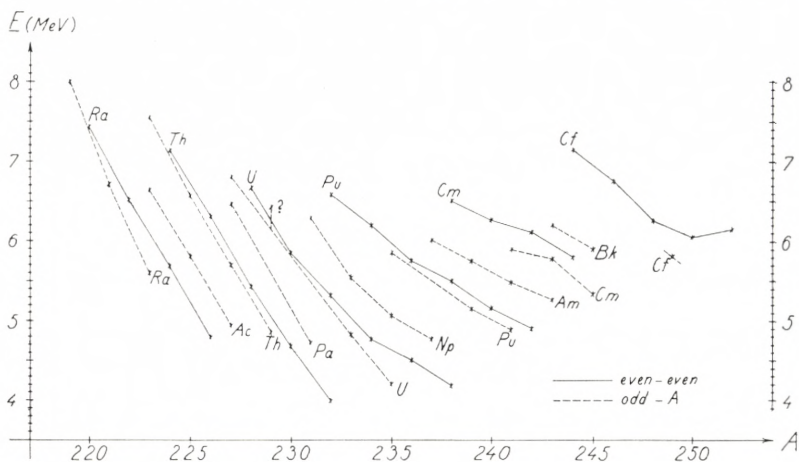


Fig. 4. Energy systematics for favoured α -transitions. The figure shows the α -energies for even-even ground state transitions and for the odd-A transitions tentatively classified as favoured and $\Delta I = 0$ (cf. Table II). As expected, the two types of transitions exhibit closely parallel trends, with the odd-A energies systematically smaller by about 200 keV than those obtained by interpolation between the even-even energies. The most conspicuous deviation is that of U^{229} , where the classification of the listed group as favoured is rather uncertain, due to the uncertainty in the intensity of the electron capture branch of this decay.

implies that the ground state rotational band in the parent nucleus should have energy spacings very similar to that populated in the daughter. Thus, it is of interest, for example, that in the β -decay of Np^{239} , leading to Pu^{239} , γ -rays are observed (cf. HOLLANDER, PERLMAN, and SEABORG, 1953) with energies 13 and 49 keV, which are very close to the fine structure separations observed in the α -decay of Pu^{239} (cf. Table III). In addition, the suggestion (ASARO and PERLMAN, 1952) that the predominant mode of the α -decay of Pu^{231} ($I = 1/2$; cf. Table III) does not lead to the ground state of U^{235} ($I = 5/2$; STUKENBROEKER and McNALLY Jr., 1950) is in agreement with the present interpretation.

The similarity between the favoured transitions in even-even and odd-A nuclei makes possible an estimate of the relative

TABLE III.

Parent nucleus	$I_i = K_i$	E_0	$E_1 - E_0$	$E_2 - E_0$	$E_3 - E_0$	K_f	$\left(\frac{3\hbar^2}{\mathfrak{I}}\right)$	$\left(\frac{3\hbar^2}{\mathfrak{I}}\right)_{e-e}$	References
${}_{96}\text{Cm}^{243}$..	278	44.2	102 (101)	(170)	5/2	38	44	a)
${}_{95}\text{Am}^{243}$	5/2	75	43	97 (98)	(166)	5/2	37	45	b) c)
${}_{95}\text{Am}^{241}$	5/2	60	43.3	98.9 (99.0)	(167)	5/2	37	45	b) d)
${}_{94}\text{Pu}^{239}$	1/2	?	13.5	52.0	(83)	1/2	37	43	e)
${}_{92}\text{U}^{233}$	5/2	0	43	99 (98)	(166)	5/2	37	58	f)
${}_{91}\text{Pa}^{231}$	3/2	331	68	?	..	68	..

- a) F. ASARO (private communication)
- b) ASARO and PERLMAN (1954).
- c) CONWAY and McLAUGHLIN (1954).
- d) MILSTED, ROSENBLUM, and VALADARES (1954).
- e) VAN DEN BERG, KLINKENBERG, and REGNAUT (1954).
- f) VAN DER SLUIS and McNALLY (1954).

Table III. *Rotational fine structure in favoured odd-A α -transitions.*

The table collects the data on the rotational bands populated by the favoured α -decays of odd-A elements. The empirical evidence is taken from the review article by HOLLANDER, PERLMAN, and SEABORG, 1953, except where otherwise noted.

Column two lists the spin of the parent nucleus, where measured. Column three gives the excitation energy E_0 of the state in the daughter, which corresponds to the ground state of the parent, and is populated by the most energetic of the favoured α -transitions (cf. Table II). The rotational excitations of this state are populated with regularly decreasing intensities and the observed energy spacings $E_1 - E_0$ and $E_2 - E_0$ are listed in columns four and five. These states have the spins $K_f + 1$ and $K_f + 2$ (cf. (3)), where K_f is the spin of the E_0 level. The value of K_f can be determined by means of (1) from the observed energy ratio $E_2 - E_0$: $E_1 - E_0$, and is listed in column seven. It is seen that, as expected, the values of K_f are the same as those of K_i (column two). The energies $E_2 - E_0$ and $E_3 - E_0$, calculated from (1) by adjusting the moment of inertia to the observed value of $E_1 - E_0$, are given in parenthesis in columns five and six. The last columns, eight and nine, provide a comparison between the observed moments of inertia for these rotational series and those of the ground state band in the neighbouring even-even nucleus, obtained by removing the last odd nucleon. The irregular fine structure intervals observed for the favoured α -decays of Pu²³⁹ suggests $K_f = 1/2$, in agreement with the measured value $K_i = 1/2$; the decoupling parameter deduced from the observed energies is $a = -0.26$ (cf. (1)).

intensities in the fine structure pattern in odd-A nuclei on the basis of those observed in even-even elements. The principal difference between the two cases is that, in an even-even nucleus, an α -particle with a given angular momentum, l , can populate only a single member of a rotational family in the daughter while, for odd-A nuclei, several such states can be populated (except for $l = 0$). Thus, the total emission probability for

α -particles of a given l in odd-A nuclei is shared among several fine structure components in each rotational band. A simple comparison of the relative intensity patterns for even-even and odd-A nuclei can be obtained in the approximation, discussed above, in which the nucleus may be considered as fixed in space during the traversal of the α -particle through the non-spherical part of the Coulomb barrier. In this case, the total emission probability for a given l is the same for the favoured transitions in the even-even and odd-A nuclei, assuming the nuclear deformation to be approximately the same in the two cases. Moreover, the probability that an α -particle of given l leaves the daughter in a particular state of the rotational band is given in terms of a vector addition coefficient¹.

Thus, for a favoured α -transition from a parent in a state I_i, K_i to a daughter in a state $I_f, K_f = K_i$, one obtains approximately

$$P = P_0(Z, E) \sum_l c_l \langle I_i l K_i 0 | I_f l I_f K_f \rangle^2 \quad (5)$$

for the transition probability per second². The quantity P_0 is given by (4) and is a function of Z and of the energy E of the fine structure component in question. The coefficient c_l which determines the total reduced transition probability for a given l may be obtained from the observed intensities in the even-even nuclei. The value of c_0 is unity by the definition of P_0 ; the coefficient c_2 is relatively constant for the even-even α -emitters with $A > 220$ and is on the average about 0.7³; the values of c_4 vary rather strongly with A , becoming quite small at the very heaviest elements; values of less than 0.01 having been reported (ASARO and PERLMAN, 1953). Only even values of l are involved, since favoured α -transitions leave the nuclear parity unaltered. The final factor in (5) is the vector addition coefficient for the addition of the angular momenta I_i and l to form the resultant I_f .

In Table IV, the relative fine structure intensities in the favoured odd-A α -transitions are compared with those calculated

¹ Similar relative intensity rules apply to β - or γ -transitions of a given multipole order, populating different members of a rotational band (ALAGA, ALDER, BOHR, and MOTTELSON, 1955).

² In (5), the small energy dependence of the centrifugal barrier effect is neglected.

³ Cf. p. 18 for note added in proof.

TABLE IV.

Parent nucleus	I_i	Obs. rel. intensities			Calc. rel. intensities				Assumed c_4
		$I = K_f, K_f + 1, K_f + 2$			$I = K_f, K_f + 1, K_f + 2, K_f + 3$				
${}_{96}\text{Cm}^{243}$	(5/2)	100	16	~ 4	100	15	2.2	0.03	0.01
${}_{95}\text{Am}^{243}$	5/2	100	15	~ 3	100	14	2.1	0.03	0.01
${}_{95}\text{Am}^{241}$	5/2	100	17	1.7	100	14	2.2	0.03	0.01
${}_{94}\text{Pu}^{239}$	1/2	100	29	16	100	23	19	0.4	0.03
${}_{92}\text{U}^{233}$	5/2	100	18	2.4	100	13	1.8	0.2	0.1
${}_{91}\text{Pa}^{231}$	3/2	100	~ 20		100	11			

Table IV. *Relative intensities of fine structure components in favoured odd-A α -transitions.*

The empirical data is taken from the references given in Table III. The spins of the parent nuclei are listed in column two. (For Cm^{243} , the I_i -value is deduced from the data in Table III). The observed relative intensities of the favoured α -transitions leading to the states with spins $I_f = K_f, K_f + 1, K_f + 2$ are listed in column three. In column four are given the relative intensities calculated from (5) and (4). The coefficient c_2 has been taken to be 0.7, which represents an average value of those measured for the $l = 2$ transitions in even-even nuclei in this region of elements. The assumed values of c_4 , which are listed in the last column and which only appreciably affect the calculated $I = K_f + 3$ intensities, are taken from $l = 4$ transitions in neighbouring even-even nuclei.

from (5). The rather good agreement lends some further support to the present interpretation of these transitions.

The published data test the expression (5) only for transitions involving $l = 0$ and 2; due to the smallness of c_4 as observed in even-even nuclei, one expects in odd-A nuclei weak transitions populating the higher members of the rotational band in the daughter (cf. Table IV). Thus, for the $l = 4$ transition from Am^{241} to the expected 11/2 state at 226 keV in Np^{237} (cf. Fig. 3), one estimates, using $c_4 = 0.01$ as determined from the Pu^{238} decay, an intensity of about .03 %. Recently, an α -group of the corresponding energy and with an intensity of this order of magnitude has been tentatively reported (ROSENBLUM and VALADARES, private communication).

Expression (5) can also be used for the unfavoured α -decays, but its application is in such cases more restricted, since the coefficients c_l are unknown¹. It may, however, be used to estimate

¹ In unfavoured transitions with $l \geq K_i + K_f (K_i \neq 0; K_f \neq 0)$, the expression for P may contain extra terms, similar to the decoupling term in (1), associated with the symmetrization of the wave function describing the nuclear rotational motion.

relative transition probabilities to different members of a rotational series if only a single value of l enters significantly (for an example, cf. Fig. 3).

A further test of (5) can be provided by α - γ correlations which may be employed in the case of α -transitions of mixed l to yield the relative intensity of the different l -components. (For an example, cf. Fig. 3).

The authors wish to acknowledge stimulating discussions with Drs. R. F. CHRISTY, S. ROSENBLUM, M. VALADARES, as well as with the members of the "Institut du Radium" in Paris.

*Institute for Theoretical Physics
University of Copenhagen
and
CERN (European Organization for Nuclear Research)
Theoretical Study Division, Copenhagen.*

Note added in proof (cf. p. 16):

Recent studies of the α fine structure of Cf^{250} and Cf^{252} (L. B. MAGNUSSON et al., Phys. Rev. **96**, 1576, 1954) and of 100^{254} (F. ASARO, F. STEPHENS, and I. PERLMAN, Bul. Am. Phys. Soc. **29**, no. 8, G4) indicate somewhat smaller values for c_2 (~ 0.25) and larger values for c_4 (~ 0.03) for these new isotopes.

References.

- G. ALAGA, K. ALDER, A. BOHR, and B. R. MOTTELSON (1955), *Dan. Mat. Fys. Medd.* **29**, no. 9.
- F. ASARO and I. PERLMAN (1952), quoted in HOLLANDER, PERLMAN, and SEABORG (1953).
- F. ASARO and I. PERLMAN (1953), *Phys. Rev.* **91**, 763.
- F. ASARO and I. PERLMAN (1954), *Phys. Rev.* **93**, 1423.
- F. ASARO and I. PERLMAN (1954a), *Phys. Rev.* **94**, 381.
- F. ASARO, F. STEPHENS, Jr., and I. PERLMAN (1953), *Phys. Rev.* **92**, 1495.
- J. K. BELING, J. O. NEWTON, and B. ROSE (1952), *Phys. Rev.* **86**, 797.
- M. VAN DEN BERG, P. F. A. KLINKENBERG, and P. REGNAUT (1954), *Physica* **20**, 37.
- A. BOHR (1954), *Rotational States in Atomic Nuclei*. Ejnar Munksgaard, Copenhagen.
- A. BOHR and B. R. MOTTELSON (1953), *Dan. Mat. Fys. Medd.* **27**, no. 16.
- A. BOHR and B. R. MOTTELSON (1954), Chapter 17 of "Beta and Gamma Spectroscopy", ed. by K. SIEGBAHN, North Holland Publ. Co.
- G. BOUISSIERES, P. FALK-VAIRANT, M. RIOU, J. TEILLAC, and C. VICTOR, (1953), *C. R.* **236**, 1874.
- J. G. CONWAY and R. D. McLAUGHLIN (1954), *Phys. Rev.* **94**, 498.
- P. FALK-VAIRANT, J. TEILLAC, G. VALLADAS, and P. BENOIST (1954), *C. R.* **238**, 1409 and 1656.
- J. S. FRASER and J. C. D. MILTON (1954), *Phys. Rev.* **94**, 795 (A).
- M. FRILLAY, S. ROSENBLUM, M. VALADARES, and G. BOUISSIERES (1954), *Journ. Phys. et Rad.* **15**, 45.
- P. O. FRÖMAN (1955), to be published.
- G. GAMOW and C. L. CRITCHFIELD (1949), *Theory of Atomic Nucleus and Nuclear Energy-Sources*. Clarendon Press, Oxford.
- A. GHIORSO, S. G. THOMPSON, G. R. CHOPPIN, and B. G. HARVEY (1954), *Phys. Rev.* **94**, 1081.
- D. L. HILL and J. A. WHEELER (1953), *Phys. Rev.* **89**, 1102.
- J. M. HOLLANDER, I. PERLMAN, and G. T. SEABORG (1953), *Rev. Mod. Phys.* **25**, 469.
- I. KAPLAN (1951), *Phys. Rev.* **81**, 962.
- J. MILSTED, S. ROSENBLUM, and M. VALADARES (1954), *C. R.* **239**, 259 and 700 (1954).

- J. O. NEWTON (1954), Nuclear Properties of the Very Heavy Elements. Contribution to Progress in Nuclear Physics, vol. 4; ed. by O. R. FRISCH.
- J. O. NEWTON and B. ROSE (1953), private communication. Cf. also Report of Birmingham Conference, July 1953.
- J. O. NEWTON and B. ROSE (1954), Phil. Mag. **45**, 58.
- I. PERLMAN, A. GHIORSO, and G. T. SEABORG (1950), Phys. Rev. **77**, 26.
- F. RASETTI and E. C. BOOTH (1953), Phys. Rev. **91**, 315.
- J. O. RASMUSSEN, Jr. (1954), Ark. f. Fysik, **7**, 185.
- J. O. RASMUSSEN, Jr. (1954a), UCRL 2431.
- S. ROSENBLUM, E. COTTON, and G. BOUSSIÈRES (1949), C. R. **229**, 825.
- G. T. SEABORG (1954), Chapters 7, 11, and 13 in "The Actinide Elements". Ed. by G. T. SEABORG and J. J. KATZ. National Nuclear Energy Series IV, 14 A, McGraw-Hill, New York.
- K. L. VAN DER SLUIS and J. R. McNALLY, Jr. (1954), J. Opt. Soc. Am. **44**, 87.
- F. STEPHENS, Jr., F. ASARO, and I. PERLMAN (1954), Phys. Rev. **96**, 1568.
- G. L. STUKENBROEKER and J. R. McNALLY, Jr. (1950), J. Opt. Soc. Am. **40**, 336.
- G. M. TEMMER and N. P. HEYDENBURG (1954), Phys. Rev. **93**, 351 and 906, and private communication.
- S. G. THOMPSON, A. GHIORSO, B. G. HARVEY, and G. R. CHOPPIN (1954), Phys. Rev. **93**, 908.
- G. VALLADAS and R. BERNAS (1953), C. R. **236**, 2230.

Det Kongelige Danske Videnskabernes Selskab

Matematisk-fysiske Meddelelser, bind **29**, nr. 11

Dan. Mat. Fys. Medd. **29**, no. 11 (1955)

STUDIES OF ABSORPTION SPECTRA VII

Systems with three and more *f*-Electrons

BY

CHR. KLIXBÜLL JØRGENSEN



København 1955

kommission hos Ejnar Munksgaard

Printed in Denmark
Bianco Lunos Bogtrykkeri A-S

Introduction.

The sixth paper of this series discussed systems with two $5f$ -electrons¹ and a preliminary note² mentioned some features of the absorption spectra of lanthanide and actinide ions containing more f -electrons. The present paper is an attempt to identify the energy levels of these systems.

In the first transition group, the energy levels of the free ion in vacuo are usually well known and the influence from the surrounding molecules determining the observed spectra.^{3, 4, 5, 6} In contrast to this behaviour the lanthanide and actinide ions show relatively small chemical effects in the spectra, but the terms of the free ion are not known from atomic spectroscopy.

Thus, the most important part of the identification is the calculation of the energies of the different terms originating from the electron configuration $[Xe] 4f^n$ in the lanthanides and $[Em] 5f^n$ in the actinides. CONDON and SHORTLEY⁷ have presented a very extensive theory of the electrostatic interaction between the electrons in partially filled shells.

The calculation of the energy levels proceeds in three steps of refinement: First, the electrostatic interaction can be expressed in terms of the parameters F_2 , F_4 , and F_6 (F_0 is disregarded in the present paper, since its contribution is invariant within the same configuration), as outlined in ref. 7, p. 174. But in the case where two or more terms of the given configuration present the same set of quantum numbers L and S , only the average energy of these terms can be obtained directly. Next, these cases can be treated by construction of the appropriate eigen-functions and by finding the different eigen-values. RACAH⁸ has developed very useful group-theoretical methods for calculating the energies of especially f^n -configurations. If q terms present the same combination of L and S , the energy of the terms can be found as

the eigen-values of a matrix of the order q , while the results are independent of all other terms (in the Condon-Shortley theory it is necessary to calculate all the energy levels in a certain order). The third achievement of a first-order calculation is the introduction of the intermediate coupling-scheme, where the mutual perturbations between the levels in the pure Russell-Saunders' case are given as functions of the Lande interval factor ζ . For instance, ISHIZU and OBI⁹ have given the corresponding matrices for f^3 -systems. The values of ζ in the individual multiplets, expressed in terms of ζ_{4f} or ζ_{5f} can also be found by the two first steps of the Condon-Shortley method mentioned above.

f^3 -systems.

The first Condon-Shortley treatment of any f^3 -system was given by SATTEN¹⁰ for Nd^{+++} in crystals of $Nd(BrO_3)_3 \cdot 9 H_2O$. He pointed out that the energy differences between the quartet terms are multiples of $5 F_2 + 6 F_4 - 91 F_6$. It is very convenient for purposes of identification that the ratio between the single parameters in this case is unimportant. The strong bands observed in Nd^{+++} imply most certainly $5 F_2 + 6 F_4 - 91 F_6 = 1400 \text{ cm}^{-1}$ and $\zeta_{4f} = 900 \text{ cm}^{-1}$, which can also be extrapolated* from Pr^{+++} . ζ in the quartets equals $\frac{1}{3} \zeta_{4f}$, while f^2 -systems have $\zeta = \frac{1}{2} \zeta_{nf}$.

But the relative values of F_2 , F_4 and F_6 are important for the positions of the doublet terms. From the definition of the parameters, SATTEN implies the inequalities $F_4 < 0.203 F_2$ and $F_6 < 0.00306 F_2$, but the correct value⁷ in the last case is $F_6 < 0.0306 F_2$, as is also given by SATTEN in the fraction in eq. 11. Whenever F_6 is negligibly small and $F_4 = 0.2 F_2$, the doublets do not give as good agreement with experimental results as do the quartet terms. Rather, a value of $F_6 = 0.02 F_2$ can be used² as a tentative proposal. Table 1 gives the centre of gravity for each term in the two cases.

In the cases where the doublet terms are represented twice

* As also from $\zeta_{4f} = 644 \text{ cm}^{-1}$ in Ce^{+++} , known from atomic spectroscopy⁵⁵. Nevertheless, the quite small splitting of the multiplet 4D might support ζ_4 considerably $< 900 \text{ cm}^{-1}$ in Nd^{+++} .

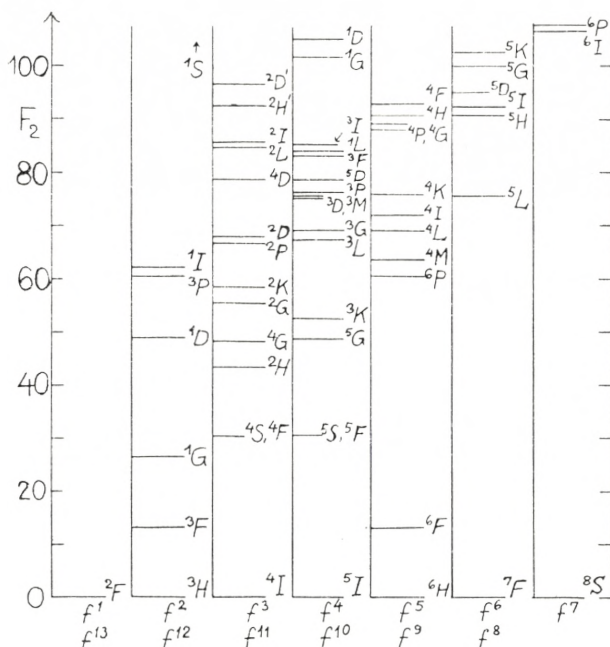


Fig. 1. Centres of gravity of multiplets in f^n -systems, expressed in the Condon-Shortley parameter F_2 , assuming $F_4 = 0.2 F_2$ and $F_6 = 0.02 F_2$.

(in the righthand column), the complicated energy expressions are not linear in F_6 , while they are so in the other terms.

Fig. 1 gives the terms of the f^n -systems with the second choice of parameters $F_4 = 0.2 F_2$ and $F_6 = 0.02 F_2$, and with the lowest term at 0 F_2 .

TABLE 1. Electrostatic interaction of f^3 for selected values of the Condon-Shortley parameters.

	$F_4 = 0.2 F_2$ $F_6 = 0$	$F_4 = 0.2 F_2$ $F_6 = 0.02 F_2$		$F_4 = 0.2 F_2$ $F_6 = 0$	$F_4 = 0.2 F_2$ $F_6 = 0.02 F_2$
4I	— 93.2 F_2	— 97.6 F_2	2H	— 62.0 F_2	— 54.2 F_2
4F	— 49.8	— 67.0	$^2H'$	— 2.6	— 5.1
4S	— 49.8	— 67.0	2G	— 39.7	— 40.8
4G	— 25.0	— 49.4	$^2G'$	+ 63.5	+ 39.8
4D	+ 18.4	— 18.8	2F	+ 7.8	+ 20.6
2L	— 12.6	— 13.0	$^2F'$	+ 124.4	+ 113.6
2K	— 39.8	— 39.0	2D	— 40.3	— 30.5
2I	— 6.2	— 12.3	$^2D'$	+ 13.7	— 1.2
2P	— 33.8	— 30.9			

TABLE 2. Doublet term levels for Nd^{+++} .

	Without intermediate coupling	With approx. intermediate coupling	Observed ¹¹
${}^2H_{9/2}$	17300 cm^{-1}	16600 cm^{-1}	15700 cm^{-1}
${}^2H_{11/2}$	17900	17600	16000
${}^2G_{7/2}$	21300	21500	20800
${}^2G_{9/2}$	22400	24000	21000
${}^2K_{13/2}$	21400	21300	21300
${}^2K_{15/2}$	23500	23200	21700
${}^2P_{1/2}$	25100	24500	23400
${}^2P_{3/2}$	25100	25900	23900
${}^2D_{3/2}$	23300	21700	23100
${}^2D_{5/2}$	26400	26000	26300
${}^2L_{15/2}$	30000	30500	..
${}^2L_{17/2}$	31900	31900	30400
${}^2I_{11/2}$	30900	30900	31800
${}^2I_{13/2}$	31400	31500	..
${}^2H'_{9/2}$	32200	32400	33500
${}^2H'_{11/2}$	34700	34700	34400
${}^2D'_{3/2}$	35000	35700	..
${}^2D'_{5/2}$	34600	35000	..
${}^2F_{5/2}$	40600	41100	38500
${}^2F_{7/2}$	42700	42600	39900
${}^2G'_{7/2}$	48700	49200	..
${}^2G'_{9/2}$	47800	47900	..
${}^2F'_{5/2}$	72600	72700	..
${}^2F'_{7/2}$	71500	71500	..

Table 2 gives the doublet levels for the f^3 -system Nd^{+++} , if $F_2 = 325 \text{ cm}^{-1}$, $F_4 = 65 \text{ cm}^{-1}$, $F_6 = 6,5 \text{ cm}^{-1}$, $\zeta_{4f} = 900 \text{ cm}^{-1}$ and the centre of ${}^4I = 3300 \text{ cm}^{-1}$.

There are calculated levels in two cases: (1) without intermediate coupling effects and (2) an approximate treatment of the perturbations given by ISHIDZU and OBL.⁹ If the secular determinant is written

$$\begin{vmatrix} a_{11} & a_{12} & \dots & a_{1n} \\ a_{21} & a_{22} & \dots & a_{2n} \\ \dots & \dots & \dots & \dots \\ a_{n1} & a_{n2} & \dots & a_{nn} \end{vmatrix} = 0, \quad (1)$$

where $a_{pq} = a_{qp}$, and especially $a_{qq} = E_q - E$ and $a_{pq} = k_{pq} \zeta_{4f} (p \neq q)$. E_q is the energy of the unperturbed level and k_{pq}

the non-diagonal elements;⁹ then different roots of E are the perturbed levels. If one of the unperturbed levels, E_q , has a larger distance from all the other E_p than the order of magnitude of $k_{pq} \zeta_{4f}$, it is a good approximation to write one of the roots

$$E = E_q + \sum_{p \neq q} \frac{k_{pq}^2 \zeta_{4f}^2}{E_q - E_p}. \quad (2)$$

When $|E_q - E_p|$ decreases, the formula gives too large perturbations, and in the limit $E_p = E_q$ the mutual repulsion of the levels are given by

$$E = E_q \pm k_{pq} \zeta_{4f}. \quad (3)$$

If only two levels coincide, their centre of gravity can be used as a level and be perturbed by all the contributions, acting separately on them.

The third column of Table 2 gives the wave numbers of the bands, observed by STEWART¹¹ in the spectrum of aqueous solutions of neodymium perchlorate. In some cases, e. g. the weak bands in the blue due to 2G and 2K , the aquo ion in solution shows the four predicted bands more distinctly than the crystal. The absorption spectrum of the solid is very valuable for investigations of the fine structure,¹⁰ but is not so useful for detection of the atomic level, which is split more by crystal fields of lower symmetry in the rigid crystal.

The single band at $427.5 \text{ m}\mu$ (23400 cm^{-1}) is presumably due to the transition to ${}^2P_{1/2}$, which is the state with $J = \frac{1}{2}$ sought for by SATTEN.

Fig. 2 shows the observed spectra of the f^3 - and f^4 -systems; in the case of Nd^{+++} the measurements by STEWART¹¹ are given.

The electron configuration $[Em] 5f^3$ is exemplified by U^{+++} , Np^{+4} , PuO_2^+ , and AmO_2^{++} . The absorption spectrum of U^{+++} in aqueous solution has been reported by KATO,¹² SEABORG,¹³ and is extensively discussed by STEWART.¹⁴ The infra-red part of the spectrum has been investigated by ROHMER et al.¹⁵ These authors found two weak bands at 7070 and 10320 cm^{-1} , and two strong bands at 8230 and $11240 - 11490 \text{ cm}^{-1}$, whereas the band at 9430 cm^{-1} presumably¹⁵ is due to impurities of U^{+4} , while STEWART¹⁴ assigns the band to U^{+3} . The reflection spectrum of solid UCl_3 has been studied among others by FREED and

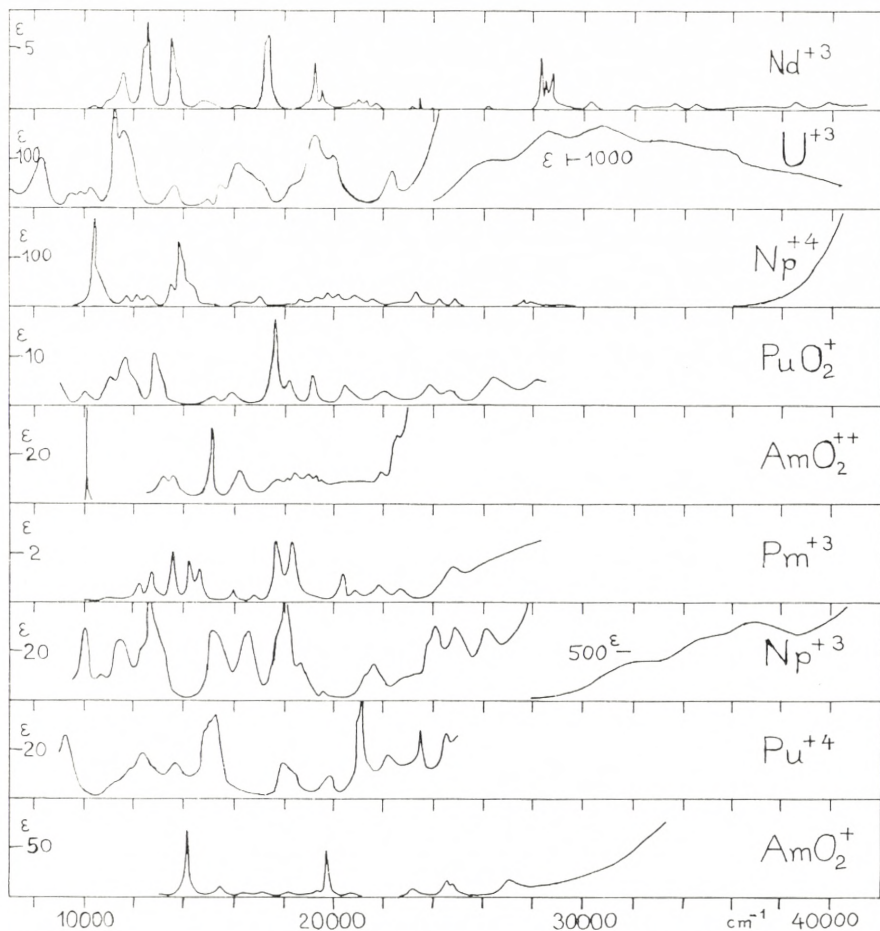


Fig. 2. Observed spectra of f^3 - and f^4 -systems in aqueous solution. Neodymium (III),¹¹ uranium (III),¹⁴ neptunium (IV),¹⁷ plutonium (V),¹³ americium (VI),^{18, 56} promethium (III),²¹ neptunium (III),¹⁷ plutonium (IV),²² and americium (V).¹⁸

SANCIER.¹⁶ Np^{+4} was studied by SJOBLÖM and HINDMAN¹⁷ in 1 M HCl and 1 M H_2SO_4 , giving evidence for the pure aquo ion in solution, while PuO_2^+ in 0.5 M HCl was studied by CONNICK, KASHA, McVEY and SHELIN (ref. 13, p. 559). AmO_2^{++} was investigated* by STEPHANAU, NIGON and PENNEMAN.¹⁸

If the transition is $^4I_{9/2} - ^4I_{15/2}$, then $\zeta_{5f} = 1700\text{ cm}^{-1}$, 2100 cm^{-1} and 2700 cm^{-1} can be implied from the strong bands with centres at 11300 cm^{-1} (U^{+3}), 13800 cm^{-1} (Np^{+4}) and 17600 cm^{-1}

* ASPREY, STEPHANAU and PENNEMAN⁵⁶ found a high, narrow band at 10100 cm^{-1} .

(PuO_2^+). This is in good agreement with the value of $\zeta_{5f} = 1600 \text{ cm}^{-1}$ in U^{+4} (ref. 1). The bands at 8200 cm^{-1} (U^{+3}), 10400 cm^{-1} (Np^{+4}), and 11700 cm^{-1} or 12900 cm^{-1} (PuO_2^+) are then probably ${}^4I_{9/2} - {}^4I_{13/2}$. The identification of the higher terms is rendered difficult by the large value of ζ_{5f} . The three bands with increasing intensity at 13800 , 16400 , and 19100 cm^{-1} in U^{+3} and 16800 , ~ 20000 , and 23300 cm^{-1} in Np^{+4} are perhaps due to ${}^4F_{5/2}$, ${}^4F_{7/2}$, and ${}^4F_{9/2}$, respectively. This gives the distance between the centre of gravity ${}^4F - {}^4I$ equal to $16400 - 6000 = 10400 \text{ cm}^{-1}$ in U^{+3} and $20000 - 7400 = 12600 \text{ cm}^{-1}$ in Np^{+4} . This is slightly larger than the 10000 cm^{-1} of Nd^{+3} , and the displacement towards higher wave numbers in the actinides is thus mainly due to larger values of ζ . The other bands, on the basis of this theory, are due to levels of 2H , 4G , ${}^2K \dots$, but the observed bands over 20000 cm^{-1} cannot be identified with certainty as yet. In U^{+3} only one such band at 22200 cm^{-1} , which is weak and narrow, is observed.

Table 3 illustrates the choice of parameters $\zeta_{5f} = 1700 \text{ cm}^{-1}$, $F_2 = 340 \text{ cm}^{-1}$, $F_4 = 68 \text{ cm}^{-1}$, and $F_6 = 6.8 \text{ cm}^{-1}$ for U^{+3} . The second column gives the approximate influence (within an accuracy of $\sim 200 \text{ cm}^{-1}$) of intermediate coupling, cf. eq. 2 and ref. 9. The ground-state ${}^4I_{9/2}$ is decreased 1200 cm^{-1} by the perturbations of other levels with $J = \frac{9}{2}$.

The wave numbers of Table 3, when multiplied by 1.2, apply quite well to Np^{+4} and they explain the large number of bands observed between 19000 and 25000 cm^{-1} in this spectrum. Over 24000 cm^{-1} in U^{+3} appears the broad and intense absorption due to the transitions¹ $[Em] 5 f^3 \rightarrow [Em] 5 f^2 6 d$ with maxima* at

* Measured in $10 M HCl$ by Messrs. K. G. POULSEN, M. Sc., and F. WOLDBYE, M. Sc., using the new Cary spectrophotometer. The scarlet colour, produced by reduction with zinc, disappears at room temperature in less than a minute. Solutions in $6 M HClO_4$ are reduced much more slowly under formation of traces of chloride by metals, but the bluish grey solutions are of more prolonged stableness. FONTANA⁵³ measured the reaction rate with water in perchlorate medium and found it strongly increasing with the ionic strength, but not dependent *inter alia* on the hydrogen ion concentration. The colour change with HCl is peculiar, since no particular effect on the uranium (III) spectrum could be observed. It is perhaps connected with the shift of the uranium (IV) bands in chloro complexes, which cause different overlappings of the absorption bands. Mixtures of trivalent and quadrivalent uranium in concentrated hydrochloric acid are olive-brown, because only light in a narrow range about $560 m\mu$ contributes to the visual impression. Cf. the observations of SOMEYA.⁶⁰

TABLE 3. Calculated and observed levels of U^{+++} .

	Calc. without intermediate coupling	With approx. intermediate coupling	Observed
${}^4J_{11/2}$	3100 cm^{-1}	4100 cm^{-1}	—
${}^4I_{13/2}$	6900	7800	8200 cm^{-1}
${}^4I_{15/2}$	11100	11700	11300
${}^4F_{3/2}$	13100	12600	—
${}^4F_{5/2}$	14500	15000	13800
${}^4S_{3/2}$	16500	16600	15700
${}^4F_{7/2}$	16500	17300	16400
${}^4G_{5/2}$	18200	18800	19100
${}^4F_{9/2}$	19100	18100	19800
${}^2H_{9/2}$	20100	19700	—
${}^4G_{7/2}$	20200	20900	22200
${}^2H_{11/2}$	21200	22200	..
${}^4G_{9/2}$	22800	23200	..
${}^2K_{13/2}$	23900	25100	..
${}^2G_{7/2}$	24400	26500	..
${}^4G_{11/2}$	25900	26300	..

25800, 28500, and 31000 cm^{-1} with molar extinction coefficients ~ 1000 .

Np^{+4} does not show this type of absorption¹⁷ below 40000 cm^{-1} , which shows the increasing energy difference between 5 *f*- and 6 *d*-electrons with increasing atomic number by the same oxidation state, i. e. state of ionization. PuO_2^+ also has quite weak bands in the measured range (10000—28500 cm^{-1}), and there seems to be a tendency towards lower intensities with higher oxidation state. This was likewise observed for the iso-electronic sequence $Np^{+3} - Pu^{+4} - AmO_2^+$ discussed in the next section. The high narrow bands^{18, 56} of AmO_2^{++} at 10100 and 15100 cm^{-1} and the weaker bands at 13200, 13700, and 16200 cm^{-1} are presumably due to f^n -transitions, while the absorption at higher wave numbers is a molecular spectrum of the UO_2^{++} -type.¹

f^4 -systems.

The electrostatic interaction is for the quintet terms:

$$\left. \begin{array}{l} {}^5I \quad - 95 F_2 \quad - 240 F_4 \quad - 1079 F_6 \\ {}^5G \quad - 40 \quad - 174 \quad - 2080 \\ {}^5F \quad - 60 \quad - 198 \quad - 1716 \\ {}^5D \quad - 5 \quad - 132 \quad - 2717 \\ {}^5S \quad - 60 \quad - 198 \quad - 1716 \end{array} \right\} (4)$$

It is seen in all cases that the energy is $30 F_2 + 99 F_4 + 858 F_6$ lower than the quartet terms of f^3 with the same L , and especially, the energies of 5F and 5S are equal. The interval factor ζ for all the quintet terms equals $\frac{1}{4} \zeta_{nf}$. Two of the triplet terms are represented only once in f^4 :

$$\left. \begin{array}{l} {}^3M \quad - 55 F_2 \quad - 150 F_4 \quad - 211 F_6 \quad \zeta = \frac{1}{6} \zeta_{nf} \\ {}^3L \quad - 70 \quad - 105 \quad - 316 \quad \zeta = \frac{5}{24} \zeta_{nf} \end{array} \right\} (5)$$

while the others are represented twice or more times. RAO¹⁹ has calculated the matrices of electrostatic interaction in these cases by Slater's method.⁷ REILLY²⁰ recalculated these matrices by means of Racah's method⁸ and corrected several errors. Their elements are given in the parameter system of RACAH as the linear combinations

$$e_0 E^0 + e_1 E^1 + e_2 E^2 + e_3 E^3,$$

$$\left. \begin{array}{l} \text{where } E^0 = F_0 - 10 F_2 - 33 F_4 - 286 F_6 \\ E^1 = \frac{1}{9} \{ 70 F_2 + 231 F_4 + 2002 F_6 \} \\ E^2 = \frac{1}{9} \{ F_2 - 3 F_4 + 7 F_6 \} \\ E^3 = \frac{1}{3} \{ 5 F_2 + 6 F_4 - 91 F_6 \}. \end{array} \right\} (6)$$

It is valid⁸ for all the terms of the configuration f^n ($n \leq 7$)

$$e_0 = \frac{n(n-1)}{2}, \quad (7)$$

and $e_0 E^0$ can thus be used for convenience as zero-point of the energy-scale. e_1 is given as function of n , the seniority number⁸ v (which can be n , $n-2$, $n-4$ or $n-6$ and at least 0) and the total spin S :

$$e_1 = \frac{9(n-v)}{2} + \frac{v(v+2)}{4} - S(S+1). \quad (8)$$

The non-diagonal elements contain only $e_2 E^2 + e_3 E^3$ contributions. Since $e_2 E^2$ and $e_3 E^3$ are of the same order of magnitude and mostly smaller than E^1 , it is seen that the terms are divided into groups with the same v and S (and the highest values of S and v have the lowest energy *inter alia*), whose structure is determined by the $e_2 E^2 + e_3 E^3$ values.

The matrices of REILLY²⁰ are used with the assumptions that $F_4 = 0.2 F_2$ and $F_6 = 0.02 F_6$ (giving $E^1 = 17.36 F_2$, $E^2 = 0.06 F_2$, and $E^3 = 1.46 F_2$) and $E^0 = 0$. The energies below $60 F_2$ are then:

$$\left. \begin{array}{ll} {}^5_4I_{20} & - 30.7 F_2 & {}^3_4D_{20} & 42.9 F_2 \\ {}^5_4S_{00} & 0 & {}^3_4M_{30} & 44.7 \\ {}^5_4F_{10} & 0 & {}^3_4P_{11} & 45.7 \\ {}^5_4G_{20} & 17.5 & {}^5_4D_{20} & 48.2 \\ {}^3_4K_{30} & 21.6 & {}^3_4F_{30} & 52.3 \\ {}^3_4L_{21} & 36.6 & {}^1_4L_{22} & 52.9 \\ {}^3_4G_{21} & 38.5 & {}^3_4I_{20} & 54.1 \end{array} \right\} \quad (9)$$

The superscript is as usual the multiplicity $2S+1$, the left subscript the seniority number v and the right subscript the quantum numbers U , which can be found in ref. 8, Table 1. They denote a group-theoretical classification of the terms in f^n -systems.

It is seen that f^3 - and f^4 -systems are likely to have their strong absorption bands in the visible spectrum at nearly the same places. Really, Pm^{+++} has, according to LANTZ and PARKER,²¹ a group of strong bands between 12000 and 22000 cm^{-1} as also Nd^{+++} . The continuous absorption given at the higher wave numbers can perhaps be ascribed to the influence of the strong radioactivity on the solvent. The molar extinction coefficients in the figures are erroneously multiplied by 1000.

The electron configuration $[Em] 5f^4$ is exhibited by ions

Np^{+3} , Pu^{+4} , and AmO_2^+ . Fig. 2 gives the spectra measured of the neptunium (III) aquo ion¹⁷ and of americium (V).¹⁸ The monomer aquo ion of plutonium (IV) was studied by HINDMAN.²²

The broad bands at ~ 32000 , 34500 , 37500 , and 42000 cm^{-1} of Np^{+++} are due to transitions $[Em] 5f^4 \rightarrow [Em] 5f^3 6d$ with the excited states 5L , ${}^5K \dots$. In contrast to this atomic spectrum, the strong bands of plutonium (IV) complexes in the ultraviolet are presumably due to electron transfer, i. e. internal redox processes.^{2, 5} Chloro complexes of U^{+4} have their "electron transfer spectrum" over 34000 cm^{-1} , but this is found below 25000 cm^{-1} in chloro complexes²² of Pu^{+4} , since the latter ion is a stronger oxidizing agent, i. e. has greater electron affinity.

The narrow bands of Pu^{+4} have an average of 19 per cent higher wave numbers¹ than Np^{+3} . Similar results were obtained above for Np^{+4} and U^{+3} . Thus, the external charge seems to have a strong influence on the screening of the f -electrons. The screening constant is presumed to be quite constant 34 in the trivalent lanthanides²³ and 58 in the actinides.²⁴ But the f -electrons seem not screened much in ions of low charge,* e. g. ζ_{4f} is -0.1 cm^{-1} in neutral cesium and 64 cm^{-1} in Ba^+ , and ζ_{5f} is only 81 cm^{-1} in Ra^+ while it is 1236 cm^{-1} in Th^{+3} . The hydrogen-like f -wave functions are only smaller than the kernel in ions with high external charge. Even in the trivalent ions, "external screening" prevents very large energy decrease of the f -electrons.

The strong bands at 12700 cm^{-1} (Np^{+3}), 15200 cm^{-1} (Pu^{+4}), and 19700 cm^{-1} (AmO_2^+) are presumably due to ${}^5I_4 - {}^5I_8$, thus giving $\zeta_{5f} = 1900$, 2300 , and 3000 cm^{-1} , respectively, if intermediate coupling effects are not considered. The bands at 10000 cm^{-1} (Np^{+3}), 12300 cm^{-1} (Pu^{+4}), and 14100 cm^{-1} (AmO_2^+) are possibly due to 5I_7 . The values of $J = 2, 3, 4$, and 5 are represented in both 5F and 5G and give intermediate coupling effects. The high values of $J (= 6, 7 \text{ and } 8)$ in 3K will also give strong bands. It is not possible to identify them, until methods for determination of J from crystal field studies are developed, cf. SATTEN.¹⁰

* Cf. MEISSNER and WEINMANN⁶¹, RASMUSSEN⁶², ⁶³ KLINKENBERG and LANG³⁸.

f^5 -systems.

By direct use of Condon-Shortley's method the following energies can be determined:*

$$\left. \begin{array}{l} {}^6H \quad - 115 F_2 \quad - 348 F_4 \quad - 2587 F_6 \\ {}^6F \quad - 100 \quad - 330 \quad - 2860 \\ {}^6P \quad - 45 \quad - 264 \quad - 3861 \\ {}^4M \quad - 105 \quad - 231 \quad - 1089 \end{array} \right\} \begin{array}{l} \zeta = \frac{1}{5} \zeta_{nf} \\ \zeta = \frac{1}{9} \zeta_{nf} \end{array} \quad (10)$$

It is seen that the sextet terms are displaced $9 E^0$ below the corresponding f^2 -triplets. By Racah's method (using $10 E^0$ as zero-point for the energy-scale) it is possible to calculate the following diagonal elements for the matrices:

TABLE 4. Diagonal elements for electrostatic interaction in f^5

$$\left(S = \frac{5}{2} \text{ and } \frac{3}{2}, v = 5 \right).$$

${}^6_5H_{11}$	—	$9 E^3$		
${}^6_5F_{10}$		0		
${}^6_5P_{11}$	+	$33 E^3$		
${}^4_5M_{30}$	$5 E^1$ —	$50 E^2$ —	$23 E^3$	
${}^4_5L_{21}$	5 +	85	—	23
${}^4_5K_{21}$	5 —	219	—	$13/3$
${}^4_5K_{30}$	5 +	188	+	$16/3$
${}^4_5J_{20}$	5 +	40	—	2
${}^4_5J_{30}$	5 —	50	—	11
${}^4_5H_{11}$	5 +	0	—	2
${}^4_5H_{21}$	5 +	197	+	26
${}^4_5H_{30}$	5 —	176	+	14
${}^4_5G_{20}$	5 —	$1040/7$	+	$8/7$
${}^4_5G_{21}$	5 +	$1089/7$	+	$11/21$
${}^4_5G_{30}$	5 +	104	+	$22/3$
${}^4_5F_{10}$	5 +	0	+	0
${}^4_5F_{21}$	5 —	65	+	3
${}^4_5F_{30}$	5 —	76	+	42
${}^4_5D_{20}$	5 +	$1144/7$	+	$22/7$
${}^4_5D_{21}$	5 —	$1781/7$	+	$202/7$
${}^4_5P_{11}$	5 +	0	+	$44/3$
${}^4_5P_{30}$	5 +	104	—	$14/3$

* SCHUURMANS⁵⁴ has calculated the energies of quintet terms of f^4 and sextet terms of f^5 and f^7 by means of Condon and Shortley's method.

The seniority numbers 3 and 1 are not considered here. For instance the quartet terms with $\nu = 3$ have $9 E^1$, thus much higher energy levels than the ($\nu = 5$) cases. The non-diagonal elements can be calculated individually from Racah's theory. Some cases of interest for the low-lying energy levels are:

$$\left. \begin{aligned}
 ({}^4_5K_{21} \parallel {}^4_5K_{30}) &= 8\sqrt{17} E^2 + \frac{8}{3}\sqrt{17} E^3 \\
 ({}^4_5I_{20} \parallel {}^4_5I_{30}) &= -120\sqrt{3} E^2 + 2\sqrt{3} E^3 \\
 ({}^4_5H_{11} \parallel {}^4_5H_{30}) &= -10\sqrt{39} E^2 - \frac{5}{3}\sqrt{39} E^3 \\
 ({}^4_5G_{20} \parallel {}^4_5G_{21}) &= -\frac{16}{7}\sqrt{2145} E^2 + \frac{5}{21}\sqrt{2145} E^3 \\
 ({}^4_5F_{10} \parallel {}^4_5F_{21}) &= -\frac{1}{3}\sqrt{165} E^3 \\
 ({}^4_5P_{11} \parallel {}^4_5P_{30}) &= 130\sqrt{11} E^2 - \frac{5}{3}\sqrt{11} E^3
 \end{aligned} \right\} \quad (11)$$

With the same assumption ($E^1 = 17.36 F_2$, $E^2 = 0.06 F_2$, and $E^3 = 1.46 F_2$) the levels given in Fig. 1 are obtained from these values. Fig. 3 gives the observed spectra of the systems with five and more f -electrons.

The distribution of the sextet terms agrees with Sm^{+++} . The many strong bands in the infra-red are due to levels of 6H and 6F , and the only other strong band at 24800 cm^{-1} is due to ${}^6H_{5/2} - {}^6P_{7/2}$. Thus, E^3 is increased only ten per cent as compared with Pr^{+++} , if intermediate coupling or configuration interaction⁷ effects can be excluded. From the spectrum in the infra-red and fluorescence spectra GOBRECHT²³ found $\zeta_{4f} = 1200 \text{ cm}^{-1}$ in Sm^{+++} .

Since Sm^{+++} has¹¹ weak bands distributed at wave numbers over 17900 cm^{-1} , some quartet terms must occur at slightly lower energies than expected from the parameter ratio $F_4 = 0.2 F_2$ and $F_6 = 0.02 F_2$, as also in Pr^{+++} , where E^1 (or F_6) is relatively small. The calculations show that 4M with the J -values $\frac{15}{2}$, $\frac{17}{2}$, $\frac{19}{2}$, and $\frac{21}{2}$ should be the lowest quartet term. The positions

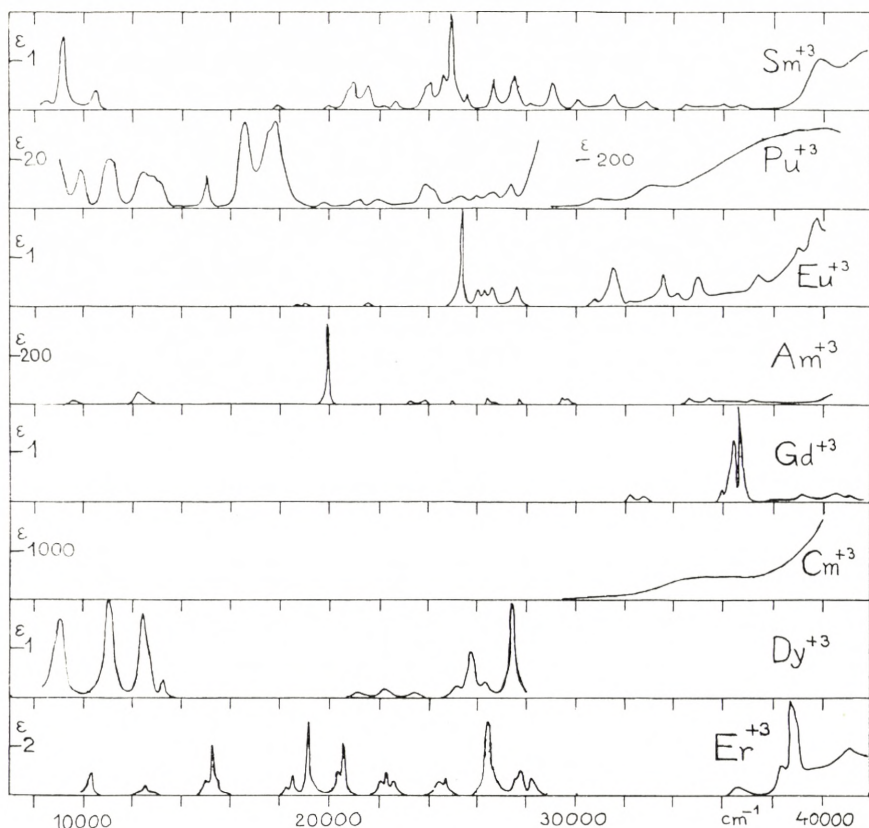


Fig. 3. Observed spectra of f^5 -, f^6 -, f^7 -, f^9 - and f^{11} -systems in aqueous solution. Samarium (III),¹¹ plutonium (III),^{14, 22} europium (III),¹¹ americium (III),¹⁸ gadolinium (III),¹¹ curium (III),³⁵ dysprosium (III),⁴⁷ and erbium (III).^{48, 49}

of the different levels of the multiplet can be found from the general formula:

$$E = E_0 + \frac{\zeta}{2} \{ J(J+1) - L(L+1) - S(S+1) \}, \quad (12)$$

where E_0 is the centre of gravity of the term and ζ is ζ_{nf} multiplied by a constant characteristic of the term. These constants have been calculated for many f^n -cases by RAO.²⁵

HINDMAN²² has given the absorption spectrum of plutonium (III) aquo ions (cf. ref. 13, p. 574). Table 5 gives the results for the two low sextets 6H and 6F , if their centres of gravity are assumed to have the distance $9 E^3 = 6000 \text{ cm}^{-1}$ and $\zeta_{5f} = 2500$

TABLE 5. Calculated and observed sextet levels of Pu^{+++} .

	Calc.	Obs.
${}^6H_{13/2}$	10000 cm^{-1}	9900 cm^{-1}
${}^6F_{5/2}$	10500	11100
${}^6F_{7/2}$	12250	122—13200
${}^6H_{15/2}$	13750	15000
${}^6F_{9/2}$	14500	16600
${}^6F_{11/2}$	17250	17900
$({}^6P_{7/2})$	36750	—

cm^{-1} (as extrapolated from the other trivalent actinide ions). The bands at 19800, 21200, and 21900 cm^{-1} have only intensities about ten per cent of the strong bands and they are due to quartet levels. At the limit of the measured range, 28500 cm^{-1} , an absorption begins which is either a strong f^5 -band (6P) or the much stronger $[Em] 5 f^5 \rightarrow [Em] 5 f^4 6 d$ transitions. STEWART¹⁴ gives shoulders at 31000 and 33500 cm^{-1} before a broad band at 40000 cm^{-1} (see Fig. 3), but no definite conclusion can be drawn.

No information has been given on the absorption spectrum of Am^{+4} , which probably occurs in solid AmO_2 or AmF_4 .

f^6 -systems.

By direct diagonalization according to CONDON and SHORTLEY can be found:

$$\left. \begin{array}{l} {}^7F \quad - 150 F_2 \quad - 495 F_4 \quad - 4290 F_6 \quad \zeta = \frac{1}{6} \zeta_{nf} \\ {}^5L \quad - 140 \quad - 336 \quad - 2582 \quad \zeta = \frac{1}{16} \zeta_{nf} \end{array} \right\} \quad (13)$$

It is seen that 7F has the energy $-15 E^0$. Using Racah's method, the terms with $S = 2$ and the seniority number $\nu = 6$ have the energies in Table 5, when $-15 E^0$ is used as zero-point of the energy scale.

TABLE 6. Diagonal elements of electrostatic interaction of $f^6(S = 2, v = 6)$.

$$\begin{aligned}
 {}^5_6P_{11} &= 6 E^1 + 0 E^2 + 11 E^3 \\
 {}^5_6D_{20} &= 6 + 858/7 + 11 \\
 {}^5_6D_{21} &= 6 - 1131/7 + 18 \\
 {}^5_6F_{21} &= 6 - 195 + 15 \\
 {}^5_6G_{20} &= 6 - 780/7 + 4 \\
 {}^5_6G_{21} &= 6 + 1683/7 + 11 \\
 {}^5_6H_{11} &= 6 + 0 - 3 \\
 {}^5_6H_{21} &= 6 - 21 + 6 \\
 {}^5_6I_{20} &= 6 + 30 - 7 \\
 {}^5_6K_{21} &= 6 + 135 - 7 \\
 {}^5_6L_{21} &= 6 - 105 - 15
 \end{aligned}$$

Some non-diagonal elements are:

$$\left. \begin{aligned}
 ({}^5_6H_{11} \parallel {}^5_6H_{21}) &= -12 \sqrt{455} E^2 \\
 ({}^5_6G_{20} \parallel {}^5_6G_{21}) &= -\frac{24}{7} \sqrt{4290} E^2 \\
 ({}^5_6D_{20} \parallel {}^5_6D_{21}) &= \frac{234}{7} \sqrt{132} E^2
 \end{aligned} \right\} \quad (14)$$

These values are used for the f^6 -levels in Fig. 1. Fig. 3 gives the observed spectra of $Eu^{+++11,18}$ and Am^{+++18} .

GOBRECHT²³ found $\zeta_{4f} = 1450 \text{ cm}^{-1}$ in Eu^{+++} from fluorescence studies. The band of Am^{+++} at 12300 cm^{-1} , identified as ${}^7F_0 - {}^7F_6$, gives $\zeta_{5f} = 3500 \text{ cm}^{-1}$ when no intermediate coupling effects are considered. The most characteristic features of the two spectra are the extremely weak bands (compared with the other lanthanides and actinides, respectively) due to the change of S from 3 to 2. But the bands at 25300 cm^{-1} in Eu^{+++} and 19900 cm^{-1} in Am^{+++} have quite normal intensities.

The latter case is presumably due to the transition ${}^7F_0 - {}^5L_6$. Since the distance between the two levels with $J = 6$ is not much greater than ζ_{5f} , the excited state intermixes strongly¹ with 7F_6 . The only difficulty is the great change of J by the transition, since usually only $|\Delta J| \leq 4$ are allowed with reasonable probability.²⁶ 5I_4 and 5H_4 are thus also possible explanations of the band in Eu^{+++} .

The extremely narrow and weak bands of Eu^{+++} at 19000 and 21500 cm^{-1} have been investigated by SPEDDING, MOSS, and WALLER²⁷ and by FREED, WEISSMAN, and FORTRESS.²⁸ According to HELLWEGE and KAHLE²⁹ the bands are due to transitions to 5D_1 and 5D_2 , while the very strongly forbidden transition to 5D_0 has been observed at 17250 cm^{-1} . FREED³⁰ assumes the two first bands to be due to levels with $J = 2$ and 3 . The occurrence of 5D seems peculiar; compare Table 5. It can be connected with strong interaction with the 5D -term with seniority number 4, which has the diagonal element of energy $9E^1 + 143/7E^3$. The non-diagonal elements with the two other terms are rather large:

$$({}^5D_{20} \parallel {}^5D_{20}) = \frac{22}{7} \sqrt{14} E^3 \quad \text{and} \quad ({}^5D_{20} \parallel {}^5D_{21}) = \frac{12}{7} \sqrt{462} E^3.$$

Nevertheless, none of the 5D -terms should pass below 5L . The multiplet splitting of the term is strong, $\zeta \simeq \zeta_{4f}$, as is often the case with the lowest of the two interacting multiplets with the same L and S ⁹, and the interaction with the levels of the ground-state can be rather high, due to the low values of J .

The isoelectronic species Sm^{++} was studied by BUTEMENT and TERRY.³¹ BUTEMENT³² later discussed this and other divalent lanthanides and assumed that the broad and intense bands, giving the orange-red colour of samarium (II) salts, are due to $[Xe] 4f^6 \rightarrow [Xe] 4f^5 5d$. As shown in the next section, divalent ions will have considerably less energy differences for this type of process than the trivalent ions.

f^7 -systems.

By direct diagonalization according to CONDON and SHORTLEY was found:

$$\left. \begin{array}{l} {}^8S \quad - 210 F_2 \quad - 693 F_4 \quad - 6006 F_6 \\ {}^6I \quad - 175 \quad \quad - 504 \quad \quad - 4291 \quad \zeta = 0 \text{ for all sextet terms.} \end{array} \right\} (15)$$

If the energy of 8S , $-21E^0$, is used as zero-point of the energy-scale, the following energies of the sextet terms are obtained by Racah's method:

$$\left. \begin{aligned}
 {}^6_7J_{20} &= 7 E^1 - 70 E^2 - 7 E^3 \\
 {}^6_7G_{20} &= 7 \quad + 260 \quad + 4 \\
 {}^6_7D_{20} &= 7 \quad - 286 \quad + 11 \\
 {}^6_5H_{11} &= 9 E^1 + 9 E^3 \\
 {}^6_5F_{10} &= 9 E^1 \\
 {}^6_5P_{11} &= 9 E^1 - 33 E^3
 \end{aligned} \right\} (16)$$

It is seen that analogously to the positions of d^2 - and d^5 -terms (ref. 8, p. 1363) the energies of 8S , 6I , 6G , 6D , 6H , 6F , and 6P in f^7 -systems are exactly opposite in value to 1S , 1I , 1G , 1D , 3H , 3F , and 3P in f^2 -systems. Thus, the relative position of 6I and 6P will depend¹ on F_6/F_2 (or E^1/E^3), but they will be the lowest terms highly over the ground-state 8S . The spectrum¹¹ of Gd^{+++} has bands only at wave numbers over 32000 cm^{-1} , and the most prominent of the weak, ΔS -forbidden bands are the group at 39000 cm^{-1} , which presumably is due to the high J -values of 6I . Since $\zeta = 0$, all multiplet splitting is due to intermediate coupling effects. If the assumptions of Fig. 1 are used, the energy difference ${}^6I - {}^8S$ correspond to $106.7 F_2$, thus F_2 is 365 cm^{-1} , which agrees well with $F_2 = 325 \text{ cm}^{-1}$ in Nd^{+++} under the same assumptions.

The information on the absorption spectrum of Cm^{+++} has been quite divergent. WERNER and PERLMAN^{33,34} investigated solution in $0.5 M HCl$, having a high (ϵ maximally 483^{33} or 1140^{34}) and broad band at 28400 cm^{-1} and a weak shoulder at 21700 cm^{-1} . The strong α -activity of the solution is liable to produce absorbing impurities, e. g. chlorine. CRANE and PERLMAN³⁵ give the spectrum of $0.0013 M Cm(ClO_4)_3$ as a steep absorption limit at 40000 cm^{-1} , a shoulder ($\epsilon \sim 400$) at 35000 cm^{-1} , and nearly no absorption below 29000 cm^{-1} (Fig. 3). It would be very interesting to know the reflection spectrum of curium (III) fluoride or another compound (oxide, sulphate) without the tendency of a molecular spectrum. The narrow bands of $[Em]5f^7$ in the ultraviolet of Cm^{+++} have not yet been detected.

FREED and KATCOFF³⁶ studied the absorption spectrum of Eu^{++} in crystals. These authors concluded that the strong bands with vibrational structure in the range $25000\text{--}34000 \text{ cm}^{-1}$ are

due to $[Xe]4f^7 \rightarrow [Xe]4f^6 5d$ or even to transfer of electrons out in the crystal lattice, the opposite direction of the usual "electron transfer spectra". The real f^7 -bands of Eu^{++} are presumably masked by the strong bands near 30000 cm^{-1} .

On the analogy of the transition groups, it can be predicted that the energy difference between d - and f -electrons in a given

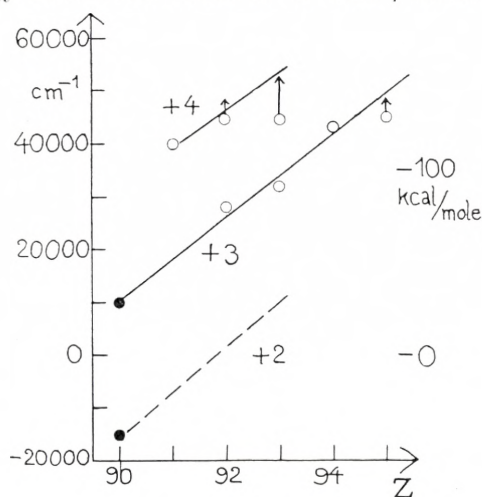


Fig. 4. The energy difference between the lowest terms of the electron configurations $[Em] 5f^{n-1} 6d$ and $[Em] 5f^n$. Filled circles from atomic spectroscopy.^{37, 38} Upward arrows by minimum values from chemical absorption spectra (no transition observed in measured range of wave lengths).

lanthanide or actinide element will decrease with decreasing oxidation state. Fig. 4 shows the energy difference between the lowest term of $[Em] 5f^{n-1} 6d$ and of $[Em] 5f^n$ in the actinides. The filled circles represent measurements from atomic spectroscopy (for Th^{++} of KLINKENBERG³⁷ and for Th^{+++} of KLINKENBERG and LANG³⁸). Open circles represent the results obtained from chemical absorption spectra discussed above. Upward arrows represent minimum values for the energy difference. The value for protactinium (IV) is derived from the measurements of R. E. ELSON.³⁹ This oxidation state* has broad bands at 35000 and 40000 cm^{-1} in $1\text{ M H}_2\text{SO}_4$ and at 40000 cm^{-1} 2 M HClO_4 .

It is seen from Fig. 4 that divalent actinides most probably will have strong absorption bands in the visible part of the

* Cf. the recent measurements by FRIED and HINDMAN.⁶⁴

spectrum, due to the relatively small energy necessary to excite a $5f$ -electron to a $6d$ -state.

The internal f^n -transitions are possible only because some states with opposite parity are slightly intermixed in the real states, which have no absolutely pure electron configuration.^{7,26} These interactions are due to fields with no centre of symmetry²⁶ acting on the excited electron configurations of which the $f^{n-1}d$ discussed above are the nearest to the ground-state. It is remarkable that the intensities of the narrow f^n -bands generally decrease with increasing distance between $f^{n-1}d$ and f^n , e. g. in the series Pr^{+++} , Nd^{+++} , Pm^{+++} , Sm^{+++} . In the actinides, a similar trend is not only found at increasing atomic number, but especially with increasing ionization state. This corresponds strictly to the energy difference between $6d$ - and $5f$ -electrons, as shown by Fig. 4. If this configuration interaction is the most important cause of intensity, it can be predicted that values of L which do not occur in the $f^{n-1}d$ -configuration, would exhibit weaker bands *inter alia*. This is perhaps the explanation of the anomalously low intensity of 1I_6 in Pr^{+++} as compared with Tm^{+++} .

f^9 -systems.

The electrostatic interaction in f^{14-n} -systems is completely equivalent to the f^n -systems. Since the intermediate coupling effects are quite important in the heavy end of the lanthanides, only some remarks will be made here about f^9 - and f^{11} -systems, which show some recognizable features. All the work done on these ions has been concentrated on the actions of crystal fields — MEEHAN and NUTTING⁴⁰ studied the sulphates of dysprosium, holmium, erbium, and thulium, SPEDDING⁴¹ the erbium (III) ion; SEVERIN has measured the fine structure of several holmium (III)⁴² and erbium (III) salts,⁴³ and ROSA⁴⁴ dysprosium. Recently, HELLWEGE⁴⁵ has treated the crystal field problems theoretically,** and GIESEKUS⁴⁶ especially the conditions in

* This band is not yet observed in Pr^{+3} , if HELLWEGE⁴⁵ is correct in assigning 1D_2 to the band at 16900 cm^{-1} . F_6 seems to be 64 times too small in the calculations of TREFFTZ.⁶⁶ As will be discussed elsewhere, the corrected value ($F_6 = 0.0152 F_2$) satisfies the observed data. The supposed⁵² 1I_6 of Tm^{+3} at 28000 cm^{-1} has been measured 12 times less intense than given by HOOGSCHAGEN.²⁶

** The influence of unsymmetrical crystal fields of citrate, ethylenediamine-tetraacetate and many other complexes of lanthanides has been investigated among others by HOLLECK and ECKHARDT⁶⁷.

TABLE 7. Calculated and observed sextet levels of Dy^{+++} .

	Calc.	Obs. (ref. 47)
${}^6H_{13/2}$	2700 cm^{-1}	—
${}^6H_{11/2}$	5000	—
${}^6F_{11/2}$	6500	—
${}^6H_{9/2}$	7000	7600 cm^{-1}
${}^6H_{7/2}$	8600	8100
${}^6F_{9/2}$	8500	9100
${}^6H_{5/2}$	9900	—
${}^6F_{7/2}$	10100	11000
${}^6F_{5/2}$	11400	12400
${}^6F_{3/2}$	12300	13200
${}^6F_{1/2}$	12800	—
${}^6P_{7/2}$	25400	25100
${}^6P_{5/2}$	26700	25800, 26300
${}^6P_{3/2}$	27600	27400

crystals of bromate enneahydrates. However, the atomic energy levels have not received much attention.

The dysprosium (III) aquo ion in solution was studied by HOOGSCHAGEN, SCHOLTE, and KRUYER⁴⁷ (see Fig. 3). The spectrum has strong bands below 13200 cm^{-1} , due to 6H and 6F , three weak bands at 21100, 22100, and 23400 cm^{-1} , presumably due to 4M , and strong bands in the range 25100—27400 cm^{-1} due to 6P . Table 7 gives the calculated and observed sextet levels of Dy^{+++} with $E^3 = 520 \text{ cm}^{-1}$ and $\zeta_{4f} = 1800 \text{ cm}^{-1}$ (cf. GOBRECHT²³). No measurements of californium (III) have been published, but the 6F -bands must be distributed over most of the visible spectrum with ζ_{5f} about 4500 cm^{-1} .

The absorption bands of Dy^{+++} also resemble those of Sm^{+++} by their width, which can even compete with Pr^{+++} and Tm^{+++} . In contrast to this, the bands of Eu^{+++} and Tb^{+++} are very narrow. These similarities between f^n - and f^{14-n} -systems are connected with the sensitivity to crystal field perturbations.⁴⁶

f^{11} -systems.

These systems, which are equivalent to f^3 -systems, are exemplified by Er^{+++} (a spectrophotometric study was made by HOOGSCHAGEN and GORTER⁴⁸ and by MOELLER and BRANTLEY⁴⁹). The absorption spectrum of centurium (III) has not yet been reported.

TABLE 8. The lowest levels of Er^{+++} .

	Without intermediate coupling	Approx. inter- mediate coupling (eq. 2, 3)	Observed
${}^4I_{13/2}$	6000 cm^{-1}	6500 cm^{-1}	6500 cm^{-1} (ref. 50)
${}^4I_{11/2}$	11200	11400	10300 (ref. 48)
${}^4I_{9/2}$	15600	14300	12500
${}^4F_{9/2}$	15800	14500	15300
${}^4F_{7/2}$	19400	19600	18300, 19100
${}^4G_{11/2}$	21700	21000	20400
${}^4F_{5/2}$	22600	21600	22200
${}^2H_{11/2}$	23900	25000	26500 (ref. 49)
${}^2H_{9/2}$	25400	23200	24600
${}^4G_{9/2}$	26100	27500	27500
${}^2K_{15/2}$	27900	27800	28100

GOBRECHT²³ identified the band at 15300 cm^{-1} in Er^{+++} with ${}^4I_{15/2} - {}^4I_{9/2}$ giving $\zeta_{4f} = 2350 \text{ cm}^{-1}$ (while the f^{13} -system Yb^{+++} has $\zeta_{4f} = 2950 \text{ cm}^{-1}$). In opposition to most other spectroscopic evidence, GOBRECHT maintained that transitions with decreasing values of J had the highest probability, thus giving the strongest bands. In the author's opinion, it is rather difficult to find the highest levels of these inverted multiplets (from more than seven f -electrons), because they have the lowest values of J . The high value of ζ_{4f} gives strong perturbations between the levels with the same J . These will distribute the levels of 4F , 4G , and 2H , which are responsible for most of the visible bands of erbium (III) in a rather irregular way. Table 8 illustrates a reasonable choice of parameters, $F_2 = 400$, $F_4 = 80$, $F_6 = 8 \text{ cm}^{-1}$, and $\zeta_{4f} = 2400 \text{ cm}^{-1}$. Approximate calculations of intermediate coupling are also given. ${}^4I_{15/2}$ is then decreased 800 cm^{-1} . The levels with $J = 9/2$ intermix strongly.

Table 9 gives the found values of the electrostatic interaction parameter $E^3 = \frac{5}{3}F_2 + 2F_4 - \frac{91}{3}F_6$, which determines the distance between the multiplets of highest multiplicity. The values for Pr^{+++} and Tm^{+++} are given in ref. 51 and 52, for Nd^{+++} in ref. 10, and for U^{+4} in ref. 1.

Besides crystal field studies,^{10, 45, 46} further identification of the lanthanide and actinide terms will be promoted by atomic

TABLE 9. The electrostatic interaction parameter E^3 .

f^2	Pr^{+++}	460 cm^{-1}		U^{+4}	$\sim 780 \text{ cm}^{-1}$
f^3	Nd^{+++}	480	U^{+++}	500 cm^{-1}	Np^{+4} 610
f^4	Pm^{+++}	~ 500	Np^{+++}	~ 550	Pu^{+4} ~ 650
f^5	Sm^{+++}	480	Pu^{+++}	~ 670	
f^9	Dy^{+++}	520			
f^{11}	Er^{+++}	580			
f^{12}	Tm^{+++}	630			

spectroscopy, if a light-source can be constructed which ionizes the metal atoms strongly, at least to triply charged ions, but which does not excite them very much over their respective ground-states. Then, the transitions from $f^{n-1}s$, $f^{n-1}d$ and $f^{n-1}g$ to f^n will give strong emission lines, and the selection rules and Zeeman effect can be used for identification of the values of J .

Additional Note.

SATTEN⁵⁸ has commented on the note.² He is correct in pointing out that $F_4 = 0.2 F_2$ implies $F_6 = 0.03 F_2$. It might be preferred to use the ratio $F_4 = 0.17 F_2$ and $F_6 = 0.02 F_2$, which give slightly decreasing F^k integrals, as RACAH⁵⁹ found in Th^{++} . But such a change from the set $F_4 = 0.02 F_2$, $F_6 = 0.02 F_2$ used here would have almost no significance for the numerical results derived here. The most important difference, in the author's opinion, is between F_6 being negligibly small, as really found in the strongly perturbed⁷ La^+ and probably¹ also in U^{+4} , and F_6 being considerably over half its maximum value, as in⁵⁹ Th^{++} and in the author's opinion in most other lanthanides* and actinides. The influence on the Racah parameters⁸ discussed above can be seen from this table:

F_4/F_2	F_6/F_2	E^1	E^2	E^3	E^1/E^3
0.20	0.03	19.58 F_2	0.068 F_2	1.12 F_2	17.5
0.20	0.02	17.36	0.060	1.46	11.9
0.17	0.02	16.60	0.070	1.40	11.8
0.15	0.02	16.08	0.077	1.36	11.8
0.15	0.01	13.85	0.069	1.66	8.3
0.15	0.00	11.62	0.061	1.97	5.9

* also in Pr^{+3} , see the note p. 22.

Since the energy differences between terms with the same multiplicity and seniority number are mainly determined by E^3 , while the differences between such groups are multiples of E^1 (see eq. 8), the weak bands due to lower multiplicity will be displaced towards higher wave numbers, compared to the strong bands of the highest multiplicity, by increasing ratio E^1/E^3 .

The statement of SATTEN⁵⁸ that ${}^2P_{1/2}$ of Nd^{+++} cannot be placed so high as at 23400 cm^{-1} with any choice of F_k parameters, seems objectionable. The set $F_2 = 340\text{ cm}^{-1}$ $F_4 = 55\text{ cm}^{-1}$ and $F_6 = 7\text{ cm}^{-1}$ is adjusted to SATTEN's¹⁰ quartet terms and gives with $\zeta_{4f} = 900\text{ cm}^{-1}$ the energy ${}^2P_{1/2} - {}^4I_{9/2} = 24630\text{ cm}^{-1}$ without intermediate coupling. The interaction with ${}^4D_{1/2}$ will then depress the energy $\sim 600\text{ cm}^{-1}$. The interesting suggestion of SATTEN⁵⁸ that crystal fields intermix states as ${}^2G_{9/2}$ and ${}^2P_{1/2}$ is made somewhat uncertain by the fact that the wave number of the 4273 \AA -line seems only to shift in different complexes due to change of the energy of the ground-state ${}^4I_{9/2}$ and its crystal field splittings. The two last arguments have been accepted by SATTEN in a private communication.

Acknowledgment.

I am very much indebted to Professor Jannik Bjerrum for his interest in the work.

Summary.

The atomic energy levels causing the narrow bands of lanthanide and actinide elements are investigated. The case of Nd^{+++} , studied by SATTEN, is discussed with particular respect to the doublet terms, and the other systems with three effective f -electrons are considered. The electrostatic interaction of 4, 5, 6, and 7 f -electrons is computed from RACAH's and simpler cases from CONDON and SHORTLEY's theory. The relative positions of the multiplets agree well with the observed spectra, while the certain identification of the different levels is difficult, due to effects of intermediate coupling. In most of the actinide ions, the Lande interval factor ζ_{5f} is found to be rather more than 2

ζ_{4f} in the corresponding lanthanide ions. The electrostatic interaction, which separates the terms, seems to be quite similar in the two cases, except for an increase with increasing oxidation state, due to variations in effective charge. The transitions $[Em] 5f^n \rightarrow [Em] 5f^{n-1}6d$, causing broad and intense absorption bands, are used to estimate the very high energy difference between 6 *d*- and 5 *f*-electrons in the actinide ions (see Fig. 4). Some spectra due to molecular transfer of electrons are discussed and the spectrum of Cm^{+++} is shown not to be the predicted f^7 -spectrum. Observed spectra of Dy^{+++} and Er^{+++} are compared with the theory. Several tables give numerical results, and especially Table 9 gives the values of electrostatic interaction in the investigated cases of lanthanide and actinide ions.

*Chemistry Department A,
Technical University of Denmark, Copenhagen.*

References.

1. JØRGENSEN, C. KLIXBÜLL *Dan. Mat. Fys. Medd.* **29** (1955) No. 7.
2. JØRGENSEN, C. KLIXBÜLL *J. Chem. Phys.* **23** (1955).
3. BJERRUM, J., BALLHAUSEN, C. J. and JØRGENSEN, C. KLIXBÜLL *Acta Chem. Scand.* **8** (1954) 1275.
4. BALLHAUSEN, C. J. *Dan. Mat. Fys. Medd.* **29** (1954) No. 4.
5. JØRGENSEN, C. KLIXBÜLL *Acta Chem. Scand.* **8** (1954) 1502.
6. BALLHAUSEN, C. J. *Dan. Mat. Fys. Medd.* **29** (1955) No. 8.
7. CONDON, E. U. and SHORTLEY, G. H. *Theory of Atomic Spectra.* Cambridge 1953.
8. RACAH, G. *Phys. Rev.* **76** (1949) 1352.
9. ISHIDZU, T. and OBI, SHIN-YA *J. Phys. Soc. Japan* **5** (1950) 145.
10. SATTEN, R. A. *J. Chem. Phys.* **21** (1953) 637.
11. STEWART, D. C. *Light Absorption, I*, AECD-2389.
12. KATO, S. *Scient. Paper, Inst. Phys. Chem. Res.* **13** (1930) 49.
13. SEABORG, G. T., KATZ, J. J. and MANNING, W. M. *The Transuranium Elements.* *Nat. Nucl. En. Ser. Vol. 14 B.*
14. STEWART, D. C. *Light Absorption, II*, AECD-3351 (ANL-4812).
15. ROHMER, R., FREYMANN, R., CHEVET, A. and HAMON, P. *Bull. soc. chim. France* **1952** 603.

16. FREED, S. and SANCIER, K. M. *J. Chem. Phys.* **22** (1954) 928.
17. SJOBLUM, R. K. and HINDMAN, J. C. *J. Am. Chem. Soc.* **73** (1951) 1744.
18. STEPHANAU, S. E., NIGON, J. P. and PENNEMAN, R. A. *J. Chem. Phys.* **21** (1953) 42.
19. RAO, K. SURYANARAYANA *Indian J. Phys.* **24** (1950) 51, *ibid.* **26** (1952) 427.
20. REILLY, E. F. *Phys. Rev.* **91** (1953) 876.
21. PARKER, G. W. and LANTZ, P. M. *J. Am. Chem. Soc.* **72** (1950) 2834.
22. HINDMAN, J. C. *Ionic Species . . .* AECD-1893.
23. GOBRECHT, H. *Ann. Physik* [5] **31** (1938) 755.
24. GRUEN, D. M. *J. Chem. Phys.* **20** (1952) 1818.
25. RAO, K. SURYANARAYANA *Indian J. Phys.* **24** (1950) 296.
26. BROER, L. J. F., GORTER, C. J. and HOOGSCHAGEN, J. *Physica* **11** (1945) 231.
27. SPEDDING, F. H., MOSS, C. C. and WALLER, R. C. *J. Chem. Phys.* **8** (1940) 908.
28. FREED, S., WEISSMAN, S. I. and FORTRESS, F. E. *J. Am. Chem. Soc.* **63** (1941) 1079.
29. HELLWEGE, K. H. and KAHLE, H. G. *Z. Physik* **129** (1951) 62 and 85.
30. FREED, S. *Rev. Mod. Phys.* **14** (1942) 105.
31. BUTEMENT, F. D. S. and TERREY, H. *J. Chem. Soc.* **1937** 1112.
32. BUTEMENT, F. D. S. *Trans. Faraday Soc.* **44** (1948) 617.
33. WERNER, L. B. and PERLMAN, I. *The preparation . . .* AECD-1898.
34. WERNER, L. B. and PERLMAN, I. *J. Am. Chem. Soc.* **73** (1951) 5215.
35. CRANE, W. W. T. and PERLMAN, I. AECD-2911.
36. FREED, S. and KATCOFF, S. *The Absorption . . .* MDDC-1228.
37. KLINKENBERG, P. F. A. *Physica* **16** (1950) 618.
38. KLINKENBERG, P. F. A. and LANG, R. J. *Physica* **15** (1949) 774.
39. SEABORG, G. T. and KATZ, J. J. *The Actinide Elements. Nat. Nucl. En. Ser. Vol. 14 A.*
40. MEEHAN, E. J. and NUTTING, G. C. *J. Chem. Phys.* **7** (1939) 1002.
41. SPEDDING, F. H. *J. Chem. Phys.* **5** (1937) 316.
42. SEVERIN, H. *Z. Physik* **125** (1949) 455.
43. SEVERIN, H. *Ann. Physik* [6] **1** (1947) 41.
44. ROSA, A. M. *Ann. Physik* [5] **43** (1943) 161.
45. HELLWEGE, K. H. *Ann. Physik* [6] **4** (1948) 95, 127, 136, 143, 150 and 357.
46. GIESEKUS, H. *Ann. Physik* [6] **8** (1951) 350.
47. HOOGSCHAGEN, J., SCHOLTE, TH. G. and KRUYER, S. *Physica* **11** (1946) 504.
48. HOOGSCHAGEN, J. and GORTER, C. J. *Physica* **14** (1948) 197.
49. MOELLER, TH. and BRANTLEY, J. C. *Anal. Chem.* **22** (1950) 433.
50. STAIR, R. and FAICK, C. A. *J. Res. Nat. Bur. Stand.* **38** (1947) 95.
51. SPEDDING, F. H. *Phys. Rev.* **58** (1940) 255.
52. BETHE, H. and SPEDDING, F. H. *Phys. Rev.* **52** (1937) 454.

53. FONTANA, B. J. Kinetics of the Decomposition . . . MDDC-1453.
 54. SCHUURMANS, PH. *Physica* **11** (1946) 475.
 55. LANG, R. J. *Phys. Rev.* **49** (1936) 552.
 56. ASPREY, L. B., STEPHANAU, S. E. and PENNEMAN, R. A. *J. Am. Chem. Soc.* **73** (1951) 5715.
 57. HOLLECK, L. and ECKHARDT, D. *Z. Naturforschg.* **9 a** (1954) 347.
 58. SATTEN, R. A. *J. Chem. Phys.* **23** (1955).
 59. RACAH, G. *Physica* **16** (1950) 651.
 60. SOMEYA, K. *Z. anorg. Chem.* **161** (1927) 46.
 61. MEISSNER, K. W. and WEINMANN, W. *Ann. Physik* [5] **29** (1937) 758.
 62. RASMUSSEN, E. *Z. Physik* **83** (1933) 404.
 63. RASMUSSEN, E. *Z. Physik* **86** (1933) 24.
 64. FRIED, S. and HINDMAN, J. C. *J. Am. Chem. Soc.* **76** (1954) 4863.
 65. HELLWEGE, A. M. and HELLWEGE, K. H. *Z. Physik* **130** (1951) 549.
 66. TREFFTZ, E. *Z. Physik* **130** (1951) 561.
-

Det Kongelige Danske Videnskabernes Selskab

Matematisk-fysiske Meddelelser, bind **28**, nr. 12

Dan. Mat. Fys. Medd. **28**, no. 12 (1954)

CONFIGURATION SPACE
REPRESENTATION FOR NON-LINEAR
FIELDS

BY

P. KRISTENSEN



København 1954

i kommission hos Ejnar Munksgaard

CONTENTS

	Page
Introduction	3
1. The field equations including coupling to external sources	5
2. Generating functionals for ordered products of field operators	11
i) The time ordered product	11
ii) Matrix elements of normal products	16
3. Properties of matrix elements of N -products	21
4. The equations of motion	26
i) The equations of motion in the functional representation	26
ii) The η -functions	28
iii) The equations of motion in the configuration space representation ..	32
5. The equations for the one and two nucleon problems	35
i) The one-nucleon equation	36
ii) The two-nucleon equation	41
Summary	45
Appendix I. The sources of the spinor fields	46
Appendix II. Reformulation of a theorem due to Wick	48
Appendix III. The equations of motion for the $T\psi$ -functions	51
References	53

Introduction.

In the theory of nucleons and mesons we deal with a situation in which the coupling between the two fields is not small. It is, therefore, of importance for the treatment of such problems to develop methods more powerful than perturbation theory. The divergence difficulties inherent in current field theory necessitate a formulation of the non-perturbation approaches which allow for an incorporation of the idea of renormalization of mass and charge. In practice, this implies as a necessary condition that the formalism must be covariant.

The method proposed by SALPETER and BETHE [1], [10] for the treatment of the two-body problem is an example of such an approach. A general theory of a similar kind has been initiated by SCHWINGER [2]. In this theory, one starts from the consideration of certain combinations of vacuum expectation values of time ordered products of field operators, the so-called Green's functions. In general such quantities obey inhomogeneous equations of motion. It can be seen that the study of the oscillating solutions of the corresponding homogeneous equations provides information about the energy and momentum values of stationary states of the system. According to Schwinger, these homogeneous equations apply to scattering problems as well. By his method, equations of the Bethe-Salpeter type can be established without reference to the limit of no interaction. However, it seems rather difficult by means of this kind of approach to obtain a clear understanding of the nature of the wave functions which obey the homogeneous equation.

Partly to overcome this problem, HEISENBERG [5] and FREESE [4] have proposed to start directly from a definition of the wave function for the problem. In the general formalism

developed by Freese it is shown how, for each state of the system, one can construct an infinite set of wave functions from free field Green's functions and matrix elements of time ordered products of field operators. The construction is such that the discontinuities in the matrix elements are compensated by corresponding discontinuities in the free field Green's functions. Consequently, Freese's wave functions obey homogeneous equations of motion. The infinite set of wave functions constitutes a generalization of the Fock representation in the configuration space for free fields to the case of interacting fields. For some problems one can substitute the infinite set of wave functions by essentially one function, only. The equation obtained for this function is of a similar structure as the equation of the Bethe-Salpeter type following from Schwinger's theory, but is in general not identical with Schwinger's equation. One reason for this may be found in the fact that free field concepts enter in Freese's representation.

In the present paper, an attempt is made at modifying the ideas of Heisenberg and Freese so as to unify their theory with that of Schwinger, and thus to combine the advantages of both formalisms. To this purpose, we employ the technique of variation of external sources developed by PEIERLS and SCHWINGER [6]. In Section 1, a survey of this method is given in a form which is convenient for our purpose. In Section 2, we relate to any state of the system a functional of the sources. The variational derivatives of this functional with respect to the sources define an infinite set of amplitudes. These are shown in Section 3 to generalize the Fock representation to non-linear fields. No reference to free field concepts is made in the definition of the state vector amplitudes. Several simple properties of the Fock representation are maintained in the non-linear case.

The problem of the construction of the scalar product of two states given in this configuration space representation has not been solved. Until further progress is made one must, therefore, use the term representation with some reservation. The equations of motion, in the configuration space representation, are derived in Section 4. Finally, in Section 5, a preliminary discussion is given of the one-nucleon problem and of the two-nucleon problem.

The corresponding equations of motion become identical with those following from Schwinger's theory.

Much of the discussion given by Freese can directly be taken over to the present formalism and is not repeated here. In particular for the discussion of scattering problems, the reader may be referred to Freese's paper.

All considerations below are of a highly formal character in so far as we have completely neglected the divergence difficulties. However, the renormalization theory, for instance in the form given by KÄLLÉN [8], can easily be incorporated in the present formalism.

The author wishes to express his gratitude to Professor C. Møller for much encouragement and many stimulating discussions during the performance of the present work. He has also profited greatly from numerous discussions with the members of the CERN Study group and the guests of the Institute for Theoretical Physics, University of Copenhagen. In particular, it is a pleasure to thank drs. R. Haag and N. Hugenholtz for their kind interest and helpful comments on the subject of the present paper. Finally, financial support from "Statens almindelige videnskabsfond" is gratefully acknowledged.

1. The field equations including coupling to external sources.

With the aim to illustrate the general method we consider the example of a spin one-half field (nucleons) coupled to a scalar neutral meson field. With a suitable symmetrization of the interaction terms, the equations of motion are

$$\left. \begin{aligned} (\partial + M) \psi_0(x) + (\lambda/2) \{ u_0(x), \psi_0(x) \} &= 0, \\ (\bar{\partial} + M) \bar{\psi}_0(x) + (\lambda/2) \{ u_0(x), \bar{\psi}_0(x) \} &= 0, \\ (-\square + m^2) u_0(x) + (\lambda/2) [\bar{\psi}_0(x), \psi_0(x)] &= 0. \end{aligned} \right\} \quad (1.1)$$

Here, λ is the coupling parameter, and ∂ and $\bar{\partial}$ denote

$$\partial = \gamma_\mu \partial / \partial x_\mu, \quad \bar{\partial} = -\gamma_\mu^T \partial / \partial x_\mu,$$

where γ_μ^T is the transposed of the matrix γ_μ . The index μ runs from one to four and $x_\mu = (x_1, x_2, x_3, x_4)$, $x_4 = it$. As usual, $\bar{\psi}_0$ is defined in terms of ψ_0^* , the Hermitian conjugate of ψ_0 , as $\bar{\psi}_0 = \psi_0^\dagger \gamma_4$. The units chosen are such that $\hbar = c = 1$.

As mentioned in the introduction, we employ the method of variation of external sources developed by PEIERLS and SCHWINGER [6]. Therefore, we introduce external sources for all three kinds of fields and thus modify the equations (1.1) to

$$\left. \begin{aligned} (\partial + M) \psi(x) + (\lambda/2) \{ u(x), \psi(x) \} + \varphi(x) &= 0, \\ (\bar{\partial} + M) \bar{\psi}(x) + (\lambda/2) \{ u(x), \bar{\psi}(x) \} + \bar{\varphi}(x) &= 0, \\ (-\square + m^2) u(x) + (\lambda/2) [\bar{\psi}(x), \psi(x)] + I(x) &= 0. \end{aligned} \right\} \quad (1.2)$$

By omitting in these equations the subscript attached to the field operators in (1.1) we distinguish the source-dependent field variables from the usual ones describing the closed system. In the following, we assume that the sources vanish for both $|\vec{x}|$ and $|t|$ tending to infinity. With this restriction the equations (1.2) can be supplemented by a boundary condition which requires that the source-dependent field operators become identical with the usual source-free fields in the infinite past. Considering such solutions only we can regard the field variables as functionals of the sources. As no other solutions of the equations (1.2) will be considered in the following, it is superfluous to discriminate by any label this retarded solution from other possible ones.

We take $I(x)$, the external source of the meson field, as a c-number. Of course, one could also treat the external spinor sources as c-numbers. However, this is not what we shall do. In order that the external sources be useful, one should take the spinor sources as the analogue of c-numbers for the fermion case, i. e. as quantities such that

$$\{ \varphi(x), \varphi(x') \} = \{ \varphi(x), \bar{\varphi}(x') \} = \{ \bar{\varphi}(x), \bar{\varphi}(x') \} = 0, \quad (1.3)$$

and

$$\left. \begin{aligned} \{ \varphi(x), \psi_0(x') \} &= \{ \bar{\varphi}(x), \psi_0(x') \} = 0 \\ \{ \varphi(x), \bar{\psi}_0(x') \} &= \{ \bar{\varphi}(x), \bar{\psi}_0(x') \} = 0, \end{aligned} \right\} \quad (1.4)$$

while φ and $\bar{\varphi}$ commute with I (and of course with any other c-number). For the further specification of the manifold of pairs of spinor sources it is advantageous to write φ and $\bar{\varphi}$ in the form

$$\left. \begin{aligned} \varphi(x) &= \Theta_0 f(x), \\ \bar{\varphi}(x) &= \Theta_0 g(x), \end{aligned} \right\} \quad (1.5)$$

where Θ_0 is a constant operator which commutes with f and g and anticommutes with ψ_0 and $\bar{\psi}_0$. Hence, due to (1.4) and (1.3), f and g commute with ψ_0 and $\bar{\psi}_0$ and satisfy

$$\{f(x), f(x')\} = \{f(x), g(x')\} = \{g(x), g(x')\} = 0. \quad (1.6)$$

As is well known, essentially only one such quantity Θ_0 exists, viz. the parity of the difference ΔN between the number of nucleons and the number of anti-nucleons. In terms of the field operators, ΔN is

$$\Delta N = \frac{1}{2} \int [\psi_0^*(\vec{x}, t), \psi_0(\vec{x}, t)] d^3 \vec{x}. \quad (1.7)$$

We choose Θ_0 as

$$\Theta_0 = (-1)^{\Delta N} = \text{parity of } \Delta N, \quad (1.8)$$

thereby normalizing Θ_0 so that $\Theta_0^2 = 1$ and $\Theta_0 |0\rangle = |0\rangle$, where $|0\rangle$ is the vacuum state of the source-free system.

Corresponding to any pair f, g , we define the domain of pairs of sources obtained by allowed variations as the totality of pairs of the form $f + \delta f, g + \delta g$, where δf and δg are infinitesimal and anti-commute with f and g , i. e.

$$\left. \begin{aligned} \{\delta f(x), f(x')\} &= \{\delta g(x), f(x')\} = 0, \\ \{\delta f(x), g(x')\} &= \{\delta g(x), g(x')\} = 0. \end{aligned} \right\} \quad (1.9)$$

It should be noted that (1.9) is not a consequence of (1.6). For any pair f, g we now require the manifold of allowed variations to be so large that we, from a relation of the type

$$\int [\delta f(x) K(x) + \delta g(x) L(x)] d^4 x = 0, \quad (1.10)$$

holding for all pairs of allowed variations, can conclude that $K(x)$ and $L(x)$ vanish identically. In (1.10), K and L are considered as quantities of the same nature as f and g .

This last mentioned property of the spinor sources, together with (1.6), is all we need for the formal calculations below. The consistency of all requirements is demonstrated in Appendix I by the construction of an example of a possible domain of pairs f, g . As shown there, one can imagine the quantities f, g , or as we shall say, the f-number pairs, to be infinite matrices. It should, however, be emphasized that the f-number pairs will be treated as a kind of numbers and not as operators. In other words, all matrix elements are matrix elements in the space of the source-free operators only, and are, for the rest, quantities of the same nature as the f-number pairs. Thus, corresponding to (1.5) and the fact that the parity of the vacuum state of the source-free system is unity, we write

$$\langle 0 | \varphi(x) | \Psi \rangle = f(x) \langle 0 | \Theta_0 | \Psi \rangle = f(x) \langle 0 | \Psi \rangle. \quad (1.11)$$

In this relation $|\Psi\rangle$ can be any state.

By means of the field equations one can easily see that the spinor sources anticommute with the source-dependent spinor fields and commute with u . This statement is based on the essential property of the source-dependent fields that ψ and $\bar{\psi}$ are odd functionals of quantities which anticommute with the spinor sources, while u is an even functional of such quantities. Thus

$$\left. \begin{aligned} \{\varphi(x), \psi(x')\} = \{\bar{\varphi}(x), \psi(x')\} = 0, \\ \{\varphi(x), \bar{\psi}(x')\} = \{\bar{\varphi}(x), \bar{\psi}(x')\} = 0. \end{aligned} \right\} \quad (1.12)$$

Similarly, it can be verified that allowed variations $\delta\varphi$ and $\delta\bar{\varphi}$ anticommute with ψ and $\bar{\psi}$ and commute with u . By allowed variations we here understand variations of the form $\delta\varphi = \Theta_0\delta f$ and $\delta\bar{\varphi} = \Theta_0\delta g$, where δf and δg satisfy (1.9).

Conversely, we could also have started from (1.12) instead of (1.4), as (1.4) follows from (1.12), the field equations (1.2) and the retarded boundary condition.

One further remark may be useful here. It can easily be verified from (1.2) and the boundary condition that the canonical commutation relations

$$\left. \begin{aligned} \{ \psi_\alpha(\vec{x}, t), \bar{\psi}_\beta(\vec{x}', t) \} &= (\gamma_4)_{\alpha\beta} \delta(\vec{x} - \vec{x}') \\ [u(\vec{x}, t), \dot{u}(\vec{x}', t)] &= i \delta(\vec{x} - \vec{x}') \end{aligned} \right\} \quad (1.13)$$

hold in the source-dependent case also.

We can now formulate the following main theorem as regards the dependence of the fields on the sources. For any infinitesimal variation δI of the meson field source, and for any pair of allowed variations $\delta\varphi$ and $\delta\bar{\varphi}$ of the spinor sources, the corresponding variations of the fields are given by

$$\left. \begin{aligned} \delta\psi(x) &= i \left[\int_{-\infty}^t \delta W(x') d^4 x', \psi(x) \right], \\ \delta\bar{\psi}(x) &= i \left[\int_{-\infty}^t \delta W(x') d^4 x', \bar{\psi}(x) \right], \\ \delta u(x) &= i \left[\int_{-\infty}^t \delta W(x') d^4 x', u(x) \right], \end{aligned} \right\} \quad (1.14)$$

where the infinitesimal operator δW is

$$\delta W(x) = \delta\bar{\varphi}(x) \psi(x) + \bar{\psi}(x) \delta\varphi(x) + u(x) \delta I(x). \quad (1.15)$$

The statement (1.14) is included in the general variation principle for quantized systems formulated by SCHWINGER [6]. It is, however, quite easy to prove (1.14) directly from the field equations. Evidently, (1.14) is in accordance with the boundary condition. Therefore, we only need to show that the variations (1.14) satisfy the varied field equations. For instance, from the first equation (1.14), we get

$$\begin{aligned} (\partial + M) \delta\psi(x) &= i \left[\int_{-\infty}^t \delta W(x') d^4 x', (\partial + M) \psi(x) \right] \\ &+ \left[\int d^3 \vec{x}' \delta W(\vec{x}', t), \gamma_4 \psi(x) \right], \end{aligned}$$

which by the field equations, the properties of the sources, and the canonical commutators becomes

$$(\partial + M) \delta\psi(x) + (\lambda/2) \{u(x), \delta\psi(x)\} \\ + (\lambda/2) \{\delta u(x), \psi(x)\} + \delta\varphi(x) = 0.$$

This is precisely the equation one would have obtained by varying the first equation (1.2). In a similar manner one obtains the other varied field equations, and this verifies (1.14).

In concluding this section we shall reexpress the contents of the variational equations (1.14), using the notion of variational derivatives. Consider a functional, $\Phi[\varphi, \bar{\varphi}, I]$ say, of the sources. Assume, that one can write the variation of this functional in the form

$$\delta\Phi[\varphi, \bar{\varphi}, I] = \int (\delta f(x)A(x) + \delta g(x)B(x) + \delta I(x)C(x)) d^4x = 0,$$

holding for any infinitesimal allowed variations of the sources. Then, the quantities A , B , and C are uniquely determined. This follows from the conclusion drawn from (1.10). We can thus define A , B , and C as the variational derivatives of the functional Φ corresponding to variations of f , g , and I , respectively. It is convenient to introduce the notation

$$A(x) = \delta\Phi[\varphi, \bar{\varphi}, I]/\delta f(x), \\ B(x) = \delta\Phi[\varphi, \bar{\varphi}, I]/\delta g(x), \\ C(x) = \delta\Phi[\varphi, \bar{\varphi}, I]/\delta I(x).$$

It should be emphasized that, for instance, $\delta f(x)$ and $A(x)$ do not commute in general. The variational derivatives introduced here are thus left-hand derivatives. In a similar way, one could introduce right-hand variational derivatives.

As above, let $|0\rangle$ be the vacuum state of the source-free system and let $|\Psi\rangle$ be any other source-independent state. From (1.14) we get

$$\delta\langle 0|\psi(x)|\Psi\rangle = i \int_{-\infty}^{\infty} \frac{1 - \varepsilon(x' - x)}{2} \\ \times \langle 0|[\bar{\varphi}(x')\delta\varphi(x') + \delta\bar{\varphi}(x')\cdot\psi(x') + \delta I(x')\cdot u(x'), \psi(x)]|\Psi\rangle d^4x'.$$

As usual, $\varepsilon(x' - x)$ is the step function $(t' - t)/|t' - t|$. From this equation we infer, using the properties of allowed variations and relations like

$$\langle 0 | \delta\varphi(x) = \delta f(x) \langle 0 | \Theta_0 = \delta f(x) \langle 0 |, \quad (1.16)$$

that

$$\left. \begin{aligned} i \frac{\delta \langle 0 | \psi(x) | \Psi \rangle}{\delta g(x')} &= - \frac{1 - \varepsilon(x' - x)}{2} \langle 0 | \{ \psi(x'), \psi(x) \} | \Psi \rangle, \\ -i \frac{\delta \langle 0 | \psi(x) | \Psi \rangle}{\delta f(x')} &= - \frac{1 - \varepsilon(x' - x)}{2} \langle 0 | \{ \bar{\psi}(x'), \psi(x) \} | \Psi \rangle, \\ i \frac{\delta \langle 0 | \psi(x) | \Psi \rangle}{\delta I(x')} &= - \frac{1 - \varepsilon(x' - x)}{2} \langle 0 | [u(x'), \psi(x)] | \Psi \rangle. \end{aligned} \right\} (1.17)$$

In a similar manner, one may obtain expressions for the variational derivatives of matrix elements of the other field variables. The minus sign on the left-hand side of the second equation originates from the reordering $\bar{\psi} \delta\varphi = -\delta\varphi \bar{\psi}$ necessary to obtain the left-hand variational derivative with respect to f .

2. Generating functionals for ordered products of field operators.

The ordered products considered in this section can all be constructed from one operator \mathbf{T} which, as we shall see, is the generator of the time ordered product as defined by Wick [9].

i) *The time ordered product.*

We introduce an operator \mathbf{T} by the variational equation

$$\delta \mathbf{T} = -i \mathbf{T} \int_{-\infty}^{\infty} \delta W(x) dx \quad (2.1)$$

and the boundary condition $\mathbf{T} = 1$ in the limit of vanishing

sources*. The infinitesimal operator δW , defined by (1.15), is closely connected to the total variation of the operator

$$W(x) = \bar{\varphi}(x) \varphi(x) + \bar{\psi}(x) \psi(x) + I(x) u(x). \quad (2.2)$$

It follows from the properties of the sources that

$$[\delta W(x'), \varphi(x)] = [\delta W(x'), \bar{\varphi}(x)] = [\delta W(x'), I(x)] = 0, \quad (2.3)$$

whence, by (1.14),

$$\delta_{\text{total}} W(x) = \delta W(x) + i \int_{-\infty}^x [\delta W(x'), W(x)] dx'. \quad (2.4)$$

We shall verify in detail that the solution of the variational equation (2.1) is given by

$$\left. \begin{aligned} \mathbf{T} &= \bar{P} \exp \left\{ -i \int_{-\infty}^{\infty} W(x) dx \right\} \\ &= \sum_{n=0}^{\infty} \frac{(-i)^n}{n!} \int_{-\infty}^{\infty} dx' \cdots \int_{-\infty}^{\infty} dx^{(n)} \bar{P} \{ W(x') \cdots W(x^{(n)}) \}, \end{aligned} \right\} \quad (2.5)$$

where \bar{P} orders the W -factors in the reverse sense of DYSON'S [3] chronologically ordering operator. Thus, if $x^{(\mu)}$ antedates $x^{(\nu)}$, then $W(x^{(\nu)})$ appears to the right of $W(x^{(\mu)})$ in the \bar{P} -ordered product. To prove (2.5) we first consider the variation of an ordinary product of W -factors. By (2.4) we get

$$\left. \begin{aligned} \delta \{ W(x') W(x'') \dots W(x^{(n)}) \} \\ &= i \left(\int_{-\infty}^{x'} \delta W(x) dx \right) W(x') W(x'') \dots W(x^{(n)}) \\ &+ i W(x') \left(\int_{x'}^{x''} \delta W(x) dx \right) W(x'') \dots W(x^{(n)}) \\ &+ \dots \\ &+ i W(x') W(x'') \dots W(x^{(n)}) \left(\int_{x^{(n)}}^{\infty} \delta W(x) dx \right) + \end{aligned} \right\} \quad (2.6)$$

* For a more general discussion it might be of advantage to consider another solution of the variational equation (2.1) corresponding to the boundary condition $\mathbf{T} = S$ for $\varphi = \bar{\varphi} = I = 0$, where S is the S -matrix for the closed system. All considerations in the following remain valid for this choice of solution.

$$\left. \begin{aligned}
 &+ \delta W(x') \cdot W(x'') \dots W(x^{(n)}) \\
 &+ \dots \\
 &+ W(x') W(x'') \dots \delta W(x^{(n)}) \\
 &- i W(x') W(x'') \dots W(x^{(n)}) \cdot \int_{-\infty}^{\infty} \delta W(x) dx,
 \end{aligned} \right\} \quad (2.6)$$

where we have collected the contributions from the commutators between δW and W in an obvious manner. The complete symmetry of the \bar{P} -ordered product allows us to write the variation of the general term in series (2.5) in the somewhat simpler form

$$\left. \begin{aligned}
 &\delta \int_{-\infty}^{\infty} dx' \dots \int_{-\infty}^{\infty} dx^{(n)} \bar{P} \{ W(x') W(x'') \dots W(x^{(n)}) \} \\
 &= i \int_{-\infty}^{\infty} dx' \dots \int_{-\infty}^{\infty} dx^{(n)} \int_{-\infty}^{\infty} dx \bar{P} \{ \delta W(x) W(x') \dots W(x^{(n)}) \} \\
 &- i \int_{-\infty}^{\infty} dx' \dots \int_{-\infty}^{\infty} dx^{(n)} \bar{P} \{ W(x') \dots W(x^{(n)}) \} \cdot \int_{-\infty}^{\infty} \delta W(x) dx \\
 &+ n \int_{-\infty}^{\infty} dx' \dots \int_{-\infty}^{\infty} dx^{(n)} \bar{P} \{ \delta W(x') \cdot W(x'') \dots W(x^{(n)}) \}.
 \end{aligned} \right\} \quad (2.7)$$

If we introduce this expression into the variation of \mathbf{T} obtained from (2.5), we see that the contributions from the first and the third term on the right-hand side of (2.7) cancel, and that the sum of the remaining terms equals the right-hand side of (2.1). This verifies (2.5) as this expression obviously is in accordance with the boundary condition.

All allowed variations commute with W . Thus, by (2.5), also \mathbf{T} commutes with these variations and we can write (2.1) in the form

$$\delta \mathbf{T} = - i \int_{-\infty}^{\infty} dx \{ \delta \bar{\varphi} \mathbf{T} \psi - \delta \varphi \mathbf{T} \bar{\psi} + \delta I \mathbf{T} u \}. \quad (2.8)$$

Consequently, for any source-independent state $|\Psi\rangle$, we have by (1.16)

$$\left. \begin{aligned} i \frac{\delta \langle 0 | \mathbf{T} | \Psi \rangle}{\delta I(x)} &= \langle 0 | \mathbf{T} u(x) | \Psi \rangle \\ i \frac{\delta \langle 0 | \mathbf{T} | \Psi \rangle}{\delta g(x)} &= \langle 0 | \mathbf{T} \psi(x) | \Psi \rangle \\ -i \frac{\delta \langle 0 | \mathbf{T} | \Psi \rangle}{\delta f(x)} &= \langle 0 | \mathbf{T} \bar{\psi}(x) | \Psi \rangle. \end{aligned} \right\} \quad (2.9)$$

From (2.8) and the variational equations (1.14) we get for the variation of, for instance, the right-hand side of the second equation (2.9)

$$\begin{aligned} \delta \langle 0 | \mathbf{T} \psi(x) | \Psi \rangle &= \\ -i \left[\int_x^{\infty} \delta I(x') \langle 0 | \mathbf{T} u(x') \psi(x) | \Psi \rangle + \int_{-\infty}^x \delta I(x') \langle 0 | \mathbf{T} \psi(x) u(x') | \Psi \rangle \right] \\ -i \left[\int_x^{\infty} \delta g(x') \langle 0 | \mathbf{T} \psi(x') \psi(x) | \Psi \rangle - \int_{-\infty}^x \delta g(x') \langle 0 | \mathbf{T} \psi(x) \psi(x') | \Psi \rangle \right] \\ +i \left[\int_x^{\infty} \delta f(x') \langle 0 | \mathbf{T} \bar{\psi}(x') \psi(x) | \Psi \rangle - \int_{-\infty}^x \delta f(x') \langle 0 | \mathbf{T} \psi(x) \bar{\psi}(x') | \Psi \rangle \right], \end{aligned}$$

whence

$$\left. \begin{aligned} i \frac{\delta \langle 0 | \mathbf{T} \psi(x) | \Psi \rangle}{\delta I(x')} &= \langle 0 | \mathbf{T} T(u(x') \psi(x)) | \Psi \rangle \\ i \frac{\delta \langle 0 | \mathbf{T} \psi(x) | \Psi \rangle}{\delta g(x')} &= \langle 0 | \mathbf{T} T(\psi(x') \psi(x)) | \Psi \rangle \\ -i \frac{\delta \langle 0 | \mathbf{T} \psi(x) | \Psi \rangle}{\delta f(x')} &= \langle 0 | \mathbf{T} T(\bar{\psi}(x') \psi(x)) | \Psi \rangle, \end{aligned} \right\} \quad (2.10)$$

where $T(\dots)$ designates Wick's time-ordered product. The expressions (2.9) and (2.10) are special cases of the general formula

$$\left. \begin{aligned} i \frac{\delta}{\delta I(x')} \cdots i \frac{\delta}{\delta I(x^{(k)})} i \frac{\delta}{\delta g(y')} \cdots i \frac{\delta}{\delta g(y^{(l)})} \\ \times \left(-i \frac{\delta}{\delta f(z')} \right) \cdots \left(-i \frac{\delta}{\delta f(z^{(m)})} \right) \langle 0 | \mathbf{T} | \Psi \rangle = \\ \langle 0 | \mathbf{T} T(u(x') \cdots u(x^{(k)}) \psi(y') \cdots \psi(y^{(l)}) \bar{\psi}(z') \cdots \bar{\psi}(z^{(m)})) | \Psi \rangle, \end{aligned} \right\} \quad (2.11)$$

which reveals \mathbf{T} as the generator of the T -product. To prove (2.11) denote, for fixed values of the space time points, $x' \cdots x^{(k)}$ $y' \cdots y^{(l)}$ $z' \cdots z^{(m)}$, the chronologically ordered sequence of the same points by $x_1, x_2, \cdots x_n$, $n = k + l + m$. Further, let χ denote any of the field variables $\psi, \bar{\psi}$, and u . With this notation, we have

$$\begin{aligned} & \delta \langle 0 | \mathbf{T} \chi(x_1) \cdots \chi(x_n) | \Psi \rangle = \\ & - i \langle 0 | \mathbf{T} \int_{x_1}^{\infty} \delta W(x) dx \chi(x_1) \cdots \chi(x_n) | \Psi \rangle, \\ & - i \langle 0 | \mathbf{T} \chi(x_1) \int_{x_2}^{x_1} \delta W(x) dx \cdots \chi(x_n) | \Psi \rangle, \\ & - i \cdots \\ & - i \langle 0 | \mathbf{T} \chi(x_1) \cdots \chi(x_n) \int_{-\infty}^{x_n} \delta W(x) dx | \Psi \rangle, \end{aligned}$$

in virtue of (2.1) and the variational equations (1.14). If we displace all source variations to the extreme left we get

$$\left. \begin{aligned} & \delta \langle 0 | \mathbf{T} \chi(x_1) \cdots \chi(x_n) | \Psi \rangle = \\ & - i \int_{-\infty}^{\infty} \delta g(x) (\pm) \langle 0 | \mathbf{T} P \{ \psi(x) \chi(x_1) \cdots \chi(x_n) \} | \Psi \rangle dx, \\ & + i \int_{-\infty}^{\infty} \delta f(x) (\pm) \langle 0 | \mathbf{T} P \{ \bar{\psi}(x) \chi(x_1) \cdots \chi(x_n) \} | \Psi \rangle dx, \\ & - i \int_{-\infty}^{\infty} \delta I(x) \langle 0 | \mathbf{T} P \{ u(x) \chi(x_1) \cdots \chi(x_n) \} | \Psi \rangle dx, \end{aligned} \right\} \quad (2.12)$$

where P is Dyson's chronologically ordering operator. The (\pm) factor in the two first terms on the right-hand side of (2.12) is the parity of the number of permutations between the nucleon operators and the variations of the spinor field sources. Evidently, the number of these permutations equals the number of permutations of spinor fields required to bring the field variables ψ and $\bar{\psi}$, respectively, from the place indicated in (2.12) to the position required by the P -operator. Thus, (\pm) is the change of sign characterizing Wick's T -product as compared with Dyson's P -product and, hence,

$$\left. \begin{aligned}
 & i \delta \langle 0 | \mathbf{T} T (u(x') \cdots \bar{\psi}(z^{(m)})) | \Psi \rangle = \\
 & \left. \begin{aligned}
 & \int_{-\infty}^{\infty} \delta g(x) \langle 0 | \mathbf{T} T (\psi(x) u(x') \cdots \bar{\psi}(z^{(m)})) | \Psi \rangle dx, \\
 & - \int_{-\infty}^{\infty} \delta f(x) \langle 0 | \mathbf{T} T (\bar{\psi}(x) u(x') \cdots \bar{\psi}(z^{(m)})) | \Psi \rangle dx, \\
 & + \int_{-\infty}^{\infty} \delta I(x) \langle 0 | \mathbf{T} T (u(x) u(x') \cdots \bar{\psi}(z^{(m)})) | \Psi \rangle dx.
 \end{aligned} \right\} (2.13)
 \end{aligned}$$

The minus sign is due to the occurrence of $\delta\varphi$ to the right of $\bar{\psi}$ in the expression for δW . The proof of (2.11) is now easily completed by an induction argument.

ii) *Matrix elements of normal products.*

The formula (2.11) demonstrates the convenience of Schwinger's formalism for the introduction of ordered products of field operators, but adds nothing new. The normal product*, however, is not defined for non-linear fields and it is, therefore, more interesting that we by this formalism can give a general definition of the normal product. The detailed discussion of the normal product as introduced here, and in particular the proof that this product is a generalization of that introduced by Wick for free fields, will be given in the following section.

The generator for the N -product is the operator \mathbf{N} which is connected with the \mathbf{T} -operator by

$$\mathbf{N} = \langle 0 | \mathbf{T} | 0 \rangle^{-1} \mathbf{T}. \quad (2.14)$$

We shall regard

$$\left. \begin{aligned}
 \Psi(x' \cdots x^{(k)} | y' \cdots y^{(l)} | z' \cdots z^{(m)}) &= i \frac{\delta}{\delta I(x')} \cdots i \frac{\delta}{\delta I(x^{(k)})} \\
 i \frac{\delta}{\delta g(y')} \cdots i \frac{\delta}{\delta g(y^{(l)})} \left(-i \frac{\delta}{\delta f(z')} \right) \cdots \left(-i \frac{\delta}{\delta f(z^{(m)})} \right) &\langle 0 | \mathbf{N} | \Psi \rangle
 \end{aligned} \right\} (2.15)$$

as the matrix element between the states $\langle 0 |$ and $| \Psi \rangle$ of the N -ordered product of the field variables corresponding to the

* By Wick [9] denoted as the S -product. To avoid the use of the letter S for too many purposes we shall, henceforward, use the term N -product.

space-time points indicated¹. The relation (2.14) implies

$$\langle 0 | \mathbf{N} | \Psi \rangle = \langle 0 | \mathbf{T} | 0 \rangle^{-1} \langle 0 | \mathbf{T} | \Psi \rangle \quad (2.16)$$

and

$$\langle 0 | \mathbf{T} | 0 \rangle \langle 0 | \mathbf{N} | \Psi \rangle = \langle 0 | \mathbf{T} | \Psi \rangle. \quad (2.17)$$

From these two expressions two relations originate between the matrix elements of N -products and the matrix elements of T -products. To express these relations in a compact form we introduce some conventions about notation.

Let $\xi', \xi'', \dots, \xi^{(\kappa)}$, $\kappa \leq k$ denote some of the space-time points $x', x'', \dots, x^{(k)}$. By

$$x', x'', \dots, x^{(k)}; \xi', \xi'', \dots, \xi^{(\kappa)} \quad (2.18)$$

we denote the sequence of space-time points obtained by omitting the space-time points $\xi', \xi'', \dots, \xi^{(\kappa)}$ from the sequence $x', x'', \dots, x^{(k)}$. Thus, for example, $x', x'', x''', x''''; x'', x'''' = x', x''''$. In the same way, we introduce symbols such as $y', y'', \dots, y^{(l)}$; $\eta', \eta'', \dots, \eta^{(\lambda)}$ and $z', z'', \dots, z^{(m)}$; $\zeta', \zeta'', \dots, \zeta^{(\mu)}$.

We also introduce a notation for matrix elements of T -products similar to that we use for matrix elements of N -products. For instance, we write the right-hand side of (2.11) as

$$T_{\Psi}(x' \dots x^{(k)} | y' \dots y^{(l)} | z' \dots z^{(m)}). \quad (2.19)$$

If $|\Psi\rangle$ is the vacuum state, we denote the vacuum expectation value of the T -product by

$$T_0(x' \dots x^{(k)} | y' \dots y^{(l)} | z' \dots z^{(m)}). \quad (2.20)$$

For completeness, we note that, in the special case $k = l = m = 0$, we write

$$\left. \begin{aligned} \langle 0 | \mathbf{T} | \Psi \rangle &= T_{\Psi}(| |), \\ \langle 0 | \mathbf{N} | \Psi \rangle &= \Psi(| |). \end{aligned} \right\} \quad (2.21)$$

¹ It is evident how to generalize this definition and the formula (2.11) to matrix elements of the N - and T -products, respectively, between any two (source-independent) states of the system.

Also, with the notation (2.20), we have

$$\langle 0 | \mathbf{T} | 0 \rangle = T_0(| |). \quad (2.22)$$

As mentioned in Section 1, matrix elements of field operators are in general not c -numbers. This introduces some minor complications in the following considerations, but is the price we have to pay in order that all three kinds of sources appear in a symmetric manner in the variational equations (1.14).

Still, any T_0 -function with an even total number of spinor space-time points is effectively a c -number in the theory. Any f -number commutes with such "even" T_0 -functions. The general relation for, for instance, δf is

$$\left. \begin{aligned} & \delta f T_0(x' \cdots | y' \cdots y^{(l)} | z' \cdots z^{(m)}) \\ & = (-1)^{l+m} T_0(x' \cdots | y' \cdots y^{(l)} | z' \cdots z^{(m)}) \delta f, \end{aligned} \right\} \quad (2.23)$$

and is easily proved by the use of (1.16) and the anti-commutativity of $\delta \varphi$ with all spinor fields. A similar relation holds for δg , f , and g . Hence, even T_0 -functions commute with any functional of f and g and, in particular, with any other T_0 -function. Thus,

$$[T_0(x' \cdots | y' \cdots y^{(l)} | z' \cdots z^{(m)}), T_0(x_1 \cdots | y_1 \cdots y_\lambda | z_1 \cdots z_\mu)] = 0$$

if $\lambda + \mu$ is even. The variational derivative of this equation with respect to $g(y)$ gives, for the case of $l + m$ being odd,

$$\begin{aligned} & [T_0(x' \cdots | y y' \cdots y^{(l)} | z' \cdots z^{(m)}), T_0(x_1 \cdots | y_1 \cdots y_\lambda | z_1 \cdots z_\mu)] \\ & - \{T_0(x' \cdots | y' \cdots y^{(l)} | z' \cdots z^{(m)}), T_0(x_1 \cdots | y y_1 \cdots y_\lambda | z_1 \cdots z_\mu)\} = 0. \end{aligned}$$

The appearance of an anti-commutator is a consequence of the anti-commutativity of δg with odd T_0 -functions. The first term vanishes and we infer that two T_0 -functions, both having an odd total number of spinor space-time points, anti-commute. In particular, $T_0(| |)$ commutes with all matrix elements and

$$\left. \begin{aligned} \{T_0(|y|), T_0(|y'|)\} &= 0, \\ \{T_0(|y|), T_0(|z|)\} &= 0, \\ \{T_0(|z|), T_0(|z')\} &= 0. \end{aligned} \right\} \quad (2.24)$$

We are now prepared to prove the first of the relations mentioned above. From (2.17) follows

$$\left. \begin{aligned} &T_{\psi}(x' \cdots x^{(k)} | y' \cdots y^{(l)} | z' \cdots z^{(m)}) \\ &= \sum_{\kappa \lambda \mu} \frac{1}{\kappa!} \sum_{\xi' \cdots \xi^{(\kappa)}} \frac{1}{\lambda!} \sum_{\eta' \cdots \eta^{(\lambda)}} \frac{1}{\mu!} \sum_{\zeta' \cdots \zeta^{(\mu)}} \\ &\times (\pm) T_0(\xi' \cdots \xi^{(\kappa)} | \eta' \cdots \eta^{(\lambda)} | \zeta' \cdots \zeta^{(\mu)}) \\ &(x' \cdots x^{(k)}; \xi' \cdots \xi^{(\kappa)} | y' \cdots y^{(l)}; \eta' \cdots \eta^{(\lambda)} | z' \cdots z^{(m)}; \zeta' \cdots \zeta^{(\mu)}), \end{aligned} \right\} \quad (2.25)$$

where the summation is taken over $\kappa = 0, 1, \cdots, k$, $\lambda = 0, 1, \cdots, l$, and $\mu = 0, 1, \cdots, m$ while the ξ 's run independently over all the space-time points $x' \cdots x^{(k)}$, etc. The factorials take into account that we sum over all permutations of the sets $\xi' \cdots$, $\eta' \cdots$ and $\zeta' \cdots$. Apart from the factor (\pm) in front of the general term, (2.25) is easily recognized as the usual formula for the iterated derivative of a product, viz. the product on the left-hand side of (2.17). Thus, (2.25) is correct if we interpret the sign factor (\pm) correctly. From (2.23) it follows, however, that the factor (\pm) is the parity of the permutation of spinor space-time points involved in the substitution

$$\left. \begin{aligned} &(x' x'' \cdots x^{(k)} | y' y'' \cdots y^{(l)} | z' z'' \cdots z^{(m)}) \rightarrow \\ &(\xi' \cdots \xi^{(\kappa)} | \eta' \cdots \eta^{(\lambda)} | \zeta' \cdots \zeta^{(\mu)}) \\ &x' \cdots x^{(k)}; \xi' \cdots \xi^{(\kappa)} | y' \cdots y^{(l)}; \eta' \cdots \eta^{(\lambda)} | z' \cdots z^{(m)}; \zeta' \cdots \zeta^{(\mu)}. \end{aligned} \right\} \quad (2.26)$$

To illustrate (2.25) we note a few examples which also later will serve for reference:

$$T_{\Psi}(x'x''|) = T_0(|) \Psi(x'x''|) + T_0(x'|) \Psi(x''|) \left. \begin{array}{l} \\ + T_0(x''|) \Psi(x'|) + T_0(x'x''|) \Psi(|) \end{array} \right\} \quad (2.27)$$

$$T_{\Psi}(x|y) = T_0(|) \Psi(x|y) + T_0(x|) \Psi(|y) \left. \begin{array}{l} \\ + T_0(|y) \Psi(x|) + T_0(x|y) \Psi(|) \end{array} \right\} \quad (2.28)$$

$$T_{\Psi}(x|z) = T_0(|) \Psi(x|z) + T_0(x|) \Psi(|z) \left. \begin{array}{l} \\ + T_0(|z) \Psi(x|) + T_0(x|z) \Psi(|), \end{array} \right\} \quad (2.29)$$

and, finally, to illustrate the (\pm) factor,

$$T_{\Psi}(|y'y''|) = T_0(|) \Psi(|y'y''|) + T_0(|y'|) \Psi(|y''|) \left. \begin{array}{l} \\ - T_0(|y''|) \Psi(|y'|) + T_0(|y'y''|) \Psi(|). \end{array} \right\} \quad (2.30)$$

The formula (2.25) may be looked upon as a recursion formula which implicitly expresses the Ψ -functions in terms of matrix elements of T -products. The resulting formula may, however, be obtained directly from (2.16) if we introduce the functions

$$C(x' \cdots x^{(k)} | y' \cdots y^{(l)} | z' \cdots z^{(m)}) = i \frac{\delta}{\delta I(x')} \cdots i \frac{\delta}{\delta I(x^{(k)})} \left. \begin{array}{l} \\ i \frac{\delta}{\delta g(y')} \cdots i \frac{\delta}{\delta g(y^{(l)})} \left(-i \frac{\delta}{\delta f(z')} \right) \cdots \left(-\frac{\delta}{\delta f(z^{(m)})} \right) C(|), \end{array} \right\} \quad (2.31)$$

where

$$C(|) = \langle 0 | \mathbf{T} | 0 \rangle^{-1}. \quad (2.32)$$

By an argument similar to that by which (2.25) was obtained, we get from (2.16)

$$\left. \begin{array}{l} \Psi(x' \cdots x^{(k)} | y' \cdots y^{(l)} | z' \cdots z^{(m)}) \\ = \sum_{\kappa\lambda\mu} \frac{1}{\kappa!} \sum_{\xi' \cdots \xi^{(\kappa)}} \frac{1}{\lambda!} \sum_{\eta' \cdots \eta^{(\lambda)}} \frac{1}{\mu!} \sum_{\zeta' \cdots \zeta^{(\mu)}} \\ (\pm) C(\xi' \cdots \xi^{(\kappa)} | \eta' \cdots \eta^{(\lambda)} | \zeta' \cdots \zeta^{(\mu)}) \\ T_{\Psi}(x' \cdots x^{(k)}; \xi' \cdots \xi^{(\kappa)} | y' \cdots y^{(l)}; \eta' \cdots \eta^{(\lambda)} | z' \cdots z^{(m)}; \zeta' \cdots \zeta^{(\mu)}). \end{array} \right\} \quad (2.$$

An important property of the Ψ -functions follows from (2.14). In the special case where $|\Psi\rangle$ is the vacuum state of the source-free system, we have $\langle 0 | \mathbf{N} | 0 \rangle = 1$, independent of the sources. Hence, all Ψ -functions vanish, except the one corresponding to $k = l = m = 0$. Thus, in this case, (2.33) reduces to

$$\left. \begin{aligned} & \sum_{\kappa\lambda\mu} \frac{1}{\kappa!} \sum_{\xi' \dots \xi^{(\kappa)}} \frac{1}{\lambda!} \sum_{\eta' \dots \eta^{(\lambda)}} \frac{1}{\mu!} \sum_{\zeta' \dots \zeta^{(\mu)}} \\ & (\pm) C(\xi' \dots \xi^{(\kappa)} | \eta' \dots \eta^{(\lambda)} | \zeta' \dots \zeta^{(\mu)}) \\ & {}_0 \langle x' \dots x^{(k)}; \xi' \dots \xi^{(\kappa)} | y' \dots y^{(l)}; \eta' \dots \eta^{(\lambda)} | z' \dots z^{(m)}; \zeta' \dots \zeta^{(\mu)} \rangle \\ & = \delta_{0k} \delta_{0l} \delta_{0m}, \end{aligned} \right\} \quad (2.34)$$

and this is a recursion formula expressing the C -functions in terms of vacuum expectation values of T -products¹.

In the following, the formulas (2.25), (2.33), and (2.34) will serve as a basis for the discussion of the properties of the matrix elements of N -products. It will be shown that these expressions generalize the algebraic relations between T - and N -products for free fields to the case of non-linear fields.

3. Properties of matrix elements of N -products.

In the Fock representation [7] in configuration space for free fields, one characterizes a state of the system by an infinite set of many-particle wave functions. As long as one considers free fields, this representation may in a trivial way be extended to a multiple time representation. If we use the notion of a normal product, we can write the many-time wave functions, or as we prefer to say here, the state vector amplitudes, in the form

$$\left. \begin{aligned} & \Psi(x' \dots x^{(k)} | y' \dots y^{(l)} | z' \dots z^{(m)}) \\ & = \langle 0 | N(u(x') \dots u(x^{(k)}) \psi(y') \dots \psi(y^{(l)}) \bar{\psi}(z') \dots \bar{\psi}(z^{(m)})) | \Psi \rangle. \end{aligned} \right\} \quad (3.1)$$

The results of Wick's discussion of the properties of T - and N -products of free field operators are expressed in the Appendix

¹ The formula (2.34) could also have been obtained directly from the identity $C(|) T_0(|) = 1$.

II with the aid of a notation which is convenient for our purpose. In Section 2, we derive relations connecting matrix elements of the normal product of field operators for non-linear fields with matrix elements of T -products. If we compare the formula (2.25) with Wick's formula (Ap. II. 11), we see that the N -product for non-linear fields, as defined by (2.15), is a generalization of the N -product for free fields, as the formula (2.25) in the limit $\varphi = \bar{\varphi} = I = \lambda = 0$ reduces to the corresponding formula for free fields given in the Appendix II.

The equation (2.15) may, therefore, be taken as the general definition, valid also for non-linear fields, of the state vector amplitudes which represent any given state $|\Psi\rangle$. After a discussion, in this section, of some of the simplest properties of the state vector amplitudes, we shall in the following section derive the equations of motion in this new representation. It will then be seen that the state vector amplitudes are closely connected to the "wave functions" which enter in the homogeneous equations of motion following from Schwinger's theory.

The following simple properties of the state vector amplitudes are independent of the magnitude of the coupling constant.

i) The ground state of the source-free system has the representation $\Psi(|) = 1$, while all other amplitudes vanish. As already remarked at the end of the last section, this follows in a trivial way from the definitions (2.15) and (2.14). The fact that the simplest state of the system has the simplest possible representation is in accordance with the expectation that the present formalism provides us with a convenient description of the lowest lying levels of the system.

ii) It is easily verified from (2.25), by means of well-known properties of T -products, that the state vector amplitudes are symmetric functions in all meson coordinates and anti-symmetric in as well all nucleon coordinates as all anti-nucleon coordinates. So far we have not introduced \mathcal{P} -functions such that we can speak about symmetry properties when interchanges of, for instance, nucleons and anti-nucleons are involved. It is, however, evident how one could generalize (2.15) to cover such cases also. One would then obtain state vector amplitudes which,

in the general case, possess all the well-known symmetry properties of the free field wave function (3.1). The most direct way to see this is to observe that we formally can use the relations

$$\left. \begin{aligned} \left\{ i \frac{\delta}{\delta g(y')}, i \frac{\delta}{\delta g(y'')} \right\} &= 0, \\ \left\{ i \frac{\delta}{\delta g(y')}, -i \frac{\delta}{\delta f(z')} \right\} &= 0, \\ \left\{ -i \frac{\delta}{\delta f(z')}, -i \frac{\delta}{\delta f(z'')} \right\} &= 0, \end{aligned} \right\} \quad (3.2)$$

and commutativity of $i\delta/\delta I$ with all variational derivative operators when the objects of operation are matrix elements of T - and N -products. To this remark we shall come back in the next section. To illustrate (3.2) we evaluate

$$\left. \begin{aligned} \left(-i \frac{\delta}{\delta f(z)} \right) \langle 0 | \mathbf{T} T(\psi(y') \cdots \psi(y^{(l)})) | \Psi \rangle \\ = \langle 0 | \mathbf{T} T(\bar{\psi}(z) \psi(y') \cdots \psi(y^{(l)})) | \Psi \rangle \\ = (-1)^l T_{\Psi}(|y' \cdots y^{(l)}|z). \end{aligned} \right\} \quad (3.3)$$

Here we have used (2.13) and the symmetry properties of T -products.

iii) The state vector amplitudes are continuous functions of the coordinates. This is not quite trivial, because matrix elements of T -products are, in general, discontinuous functions. The discontinuous character of the T_{Ψ} -functions is made apparent by the δ -terms in the equations of motion for these functions (Ap. III. 3, 4 and 5). It can, however, be seen that the application of the differential operators occurring in the field equations to Ψ -functions does not give rise to such δ -functions. This can, for instance, be proved by induction using (2.25). In the following section, we find that the Ψ -functions satisfy homogeneous equations of motion, and this constitutes another verification of the continuity of these functions¹.

¹ The first derivative of the Ψ -functions with respect to a meson coordinate is also continuous. This difference between spinor field variables and meson field variables reflects the difference in the equations of motion for the two kinds of fields, the nucleon equations being of the first order, while the meson equation is of the second order.

iv) If the state $|\Psi\rangle$ represented by the infinite set of state vector amplitudes is a stationary state, corresponding to the eigenvalues P_μ for the total energy momentum vector of the closed system, then, in the source-free limit, the Ψ -functions oscillate according to

$$\Psi(x' \cdots | y' \cdots | z' \cdots) \sim \exp i P_\mu X_\mu. \quad (3.4)$$

Here, the X_μ 's are any "center of gravity" coordinate. For instance, one can take X_μ as the average value of the coordinates $x'_\mu, \cdots y'_\mu, \cdots z'_\mu, \cdots$.¹ This follows immediately from (2.33) and the fact that T_Ψ -functions possess this property. The property (3.4) is of course the basis for the application of the present formalism to bound state problems.

v) The configuration space representation. The state vector amplitudes corresponding to a state $|\Psi\rangle$ provide us with a generalization of the Fock representation for free fields. As we have seen above, several of the simple properties of the Fock representation are maintained in the general case. One might, therefore, consider the set of state vector amplitudes as a representation of the state $|\Psi\rangle$. We shall take such a point of view in the following, and speak of this representation as the configuration space representation. Alternatively, we can also consider the functional $\Psi(|\cdot|)$ which generates the state vector amplitudes as representing the state in question. In this way we speak of the functional representation. For the sake of convenience, we denote these two representations by the CSR and the FR, respectively.

To make full use of the CSR one should know, at least in principle, how to construct the scalar product of two states represented by their state vector amplitudes. This problem could not be solved and we have not even been able to prove that the CSR is a complete representation. Until further progress is

¹ Cf. FREESE [4]. As mentioned by FREESE, the most general definition of X_μ is

$$X_\mu = \alpha' x'_\mu + \cdots + \beta' y'_\mu + \cdots + \gamma' z'_\mu + \cdots,$$

where the α, β , and γ 's are subject to the condition

$$\alpha' + \cdots + \beta' + \cdots + \gamma' + \cdots = 1.$$

made, application of the present formalism must therefore be based on an assumption of the completeness of the representation.

A comparison of the CSR with other better known representations might offer a possibility of discussing the completeness problem. The fact that $\langle 0 |$ is the vacuum state of the source-free system has been used in the discussion of the oscillating behaviour of the amplitudes representing stationary states. It is easily seen that all other considerations remain valid for any choice of $\langle 0 |$ if only this state coincides with the free-field vacuum in the limit of no coupling. An example of another possible choice of this state is provided by the vacuum state $\langle 0, \sigma |$ for the free fields $u(x, \sigma), \psi(x, \sigma)$ which coincide with the source independent fields on a space-like surface σ . Moreover, it can be seen that one can choose different states in the definition of the functional $\Psi(| |)$. Thus, instead of (2.15), we could have defined

$$\Psi_{\sigma'}^{\sigma''}(| |) = \frac{\langle 0, \sigma'' | \mathbf{T} | \Psi \rangle}{\langle 0, \sigma' | \mathbf{T} | 0, \sigma' \rangle},$$

where $|0, \sigma''\rangle$ and $|0, \sigma'\rangle$ may be different.

The choice

$$\Psi_{\sigma}^{\sigma}(| |) = \frac{\langle 0, \sigma | \mathbf{T} | \Psi \rangle}{\langle 0, \sigma | \mathbf{T} | 0, \sigma \rangle} \tag{3.5}$$

leads to a representation in which the state vector amplitudes for all space-time points on σ coincide with the Tamm-Dancoff representation.

As is well known, one can consider the state $|0\rangle$ as the limit of $|0, \sigma\rangle$ in the sense of a certain limiting process, usually referred to as the adiabatic switching-on of the coupling at $t = -\infty$. In the sense of the same limiting process, one can regard the CSR representation as the limit of the representation based on (3.5) for $\sigma \rightarrow -\infty$. The coincidence of the representation (3.5) with the Tamm-Dancoff representation on σ tells us that (3.5) is a complete representation. There might, therefore, be a possibility of discussing the completeness of the CSR by a comparison with the Tamm-Dancoff representation. The complexity of the limiting process involved, however, does not make this a very promising prospect.

Another representation could be based on the functional

$$\Psi_{\sigma}(|\rangle) = \frac{\langle 0 | \mathbf{T} | \Psi \rangle}{\langle 0, \sigma | \mathbf{T} | 0, \sigma \rangle}. \quad (3.6)$$

The corresponding state vectors can be seen to coincide on σ with the representation given by DYSON [12].

4. The equations of motion.

In the preceding section, we have introduced two new representations, the functional representation and the configuration space representation. The simplest way to obtain the equations of motion in these two representations is first to derive the equations of motion in the FR. As we shall see, the equations of motion in the CSR can be obtained from those in the FR by a simple procedure.

i) The equations of motion in the FR. To determine the dependence of the functional Ψ on the sources we must try to set up variational equations making use of the field equations. The Ψ -functions depending on one space-time point only are given by the expressions

$$\left. \begin{aligned} \Psi(x|\rangle) &= T_0(|\rangle)^{-1} T_{\Psi}(x|\rangle) - T_0(|\rangle)^{-1} T_0(x|\rangle) T_0(|\rangle)^{-1} T_{\Psi}(|\rangle), \\ \Psi(|y|\rangle) &= T_0(|\rangle)^{-1} T_{\Psi}(|y|\rangle) - T_0(|\rangle)^{-1} T_0(|y|\rangle) T_0(|\rangle)^{-1} T_{\Psi}(|\rangle), \\ \Psi(|z|\rangle) &= T_0(|\rangle)^{-1} T_{\Psi}(|z|\rangle) - T_0(|\rangle)^{-1} T_0(|z|\rangle) T_0(|\rangle)^{-1} T_{\Psi}(|\rangle). \end{aligned} \right\} \quad (4.1)$$

These equations are special cases of the formula (2.33), but can also easily be verified directly from the definition (2.15). As shown in the Appendix II, the T_{Ψ} -functions depending on one space-time point satisfy

$$\left. \begin{aligned} (-\square_x + m^2) T_{\Psi}(x|\rangle) - \lambda T_{\Psi}(|x|x) + I(x) T_{\Psi}(|\rangle) &= 0, \\ (\partial_y + M) T_{\Psi}(|y|\rangle) + \lambda T_{\Psi}(y|y) + f(y) T_{\Psi}(|\rangle) &= 0, \\ (\bar{\partial}_z + M) T_{\Psi}(|z|\rangle) + \lambda T_{\Psi}(z|z) + g(z) T_{\Psi}(|\rangle) &= 0. \end{aligned} \right\} \quad (4.2)$$

These equations are of course also satisfied in the special case of $|\Psi\rangle$ being the vacuum state, i. e. for T_0 -functions. Combining (4.1) and (4.2) we get

$$\left. \begin{aligned}
 (-\square_x + m^2) \Psi(x||) - \lambda T_0(||)^{-1} T_{\Psi}(|x|x) \\
 + \lambda T_0(||)^{-1} T_0(|x|x) \Psi(||) = 0, \\
 (\partial_y + M) \Psi(|y|) + \lambda T_0(||)^{-1} T_{\Psi}(y|y|) \\
 - \lambda T_0(||)^{-1} T_0(y|y|) \Psi(||) = 0, \\
 (\bar{\partial}_z + M) \Psi(||z) + \lambda T_0(||)^{-1} T_{\Psi}(z||z) \\
 - \lambda T_0(||)^{-1} T_0(z||z) \Psi(||) = 0,
 \end{aligned} \right\} (4.3)$$

where the sources do no longer explicitly appear. To express (4.3) as linear equations in Ψ and the variational derivatives of Ψ , we eliminate the T_{Ψ} -functions by use of expressions of the type (2.28), (2.29). The resulting equations contain as factors certain combinations of T -functions for which we introduce the notation

$$\left. \begin{aligned}
 \eta(x||) &= T_0(||)^{-1} T_0(x||), \\
 \eta(|y|) &= T_0(||)^{-1} T_0(|y|), \\
 \eta(||z) &= T_0(||)^{-1} T_0(||z).
 \end{aligned} \right\} (4.4)$$

By the aid of these η -functions we can write the resulting linear differential variational equations for Ψ in the form

$$\left. \begin{aligned}
 (-\square_x + m^2) \Psi(x||) - \lambda \eta(|x|) \Psi(||x) \\
 + \lambda \eta(||x) \Psi(|x|) - \lambda \Psi(|x|x) = 0, \\
 (\partial_y + M) \Psi(|y|) + \lambda \eta(y||) \Psi(|y|) \\
 + \lambda \eta(|y|) \Psi(y||) + \lambda \Psi(y|y|) = 0, \\
 (\bar{\partial}_z + M) \Psi(||z) + \lambda \eta(z||) \Psi(||z) \\
 + \lambda \eta(||z) \Psi(z||) + \lambda \Psi(z||z) = 0.
 \end{aligned} \right\} (4.5)$$

Thus, for any state $|\Psi\rangle$, the corresponding functional Ψ satisfies (4.5). The problem which restrictions (if any) must be imposed on the solutions of (4.5) to guarantee that the functional obtained represents a state of the system has not been solved in general. Hereto we shall return later.

ii) The η -functions. By a similar method we obtain equations of motion for the η -functions. Combining (4.2) and (4.4) we get

$$\left. \begin{aligned} (-\square_x + m^2) \eta(x||) - \lambda T_0(||)^{-1} T_0(|x|x) + I(x) &= 0, \\ (\partial_y + M) \eta(|y|) + \lambda T_0(||)^{-1} T_0(y|y) + f(y) &= 0, \\ (\bar{\partial}_z + M) \eta(||z) + \lambda T_0(||)^{-1} T_0(z||z) + g(z) &= 0. \end{aligned} \right\} \quad (4.6)$$

It is convenient to introduce a functional η by

$$\eta(||) = \log \langle 0 | \mathbf{T} | 0 \rangle. \quad (4.7)$$

The η -functions (4.4) are contained as special cases in the following general definition of η -functions:

$$\left. \begin{aligned} &\eta(x' \cdots | y' \cdots | z' \cdots) \\ &= i \frac{\delta}{\delta I(x')} \cdots i \frac{\delta}{\delta g(y')} \cdots \left(-i \frac{\delta}{\delta f(z')} \right) \cdots \eta(||). \end{aligned} \right\} \quad (4.8)$$

Thus, for instance, η -functions depending on two space-time points are given by

$$\left. \begin{aligned} \eta(|y|z) &= T_0(||)^{-1} T_0(|y|z) - \eta(|y|) \eta(||z), \\ \eta(x|y) &= T_0(||)^{-1} T_0(x|y) - \eta(x||) \eta(|y|), \\ \eta(x||z) &= T_0(||)^{-1} T_0(x||z) - \eta(x||) \eta(||z). \end{aligned} \right\} \quad (4.9)$$

With the aid of these formulas we can eliminate the T_0 -functions in (4.6) and obtain

$$\left. \begin{aligned} (-\square_x + m^2) \eta(x||) - \lambda \eta(|x|) \eta(||x) - \lambda \eta(|x|x) + I(x) &= 0, \\ (\partial_y + M) \eta(|y|) + \lambda \eta(y||) \eta(|y|) + \lambda \eta(y|y) + f(y) &= 0, \\ (\bar{\partial}_z + M) \eta(||z) + \lambda \eta(z||) \eta(||z) + \lambda \eta(z||z) + g(z) &= 0. \end{aligned} \right\} \quad (4.10)$$

These equations are variational differential equations satisfied by the η -functional in the FR.

Contrary to the \mathcal{Y} -functional which depends on the particular state considered, the η -functional is uniquely determined in the theory. We must, therefore, supplement the η -equations by

boundary conditions characterizing the particular solution of (4.10) which enters in the equations of motion for the Ψ -functional.

For the discussion of this problem we need an interpretation of the operator \mathbf{T} . Let $\mathbf{T}(t)$ be the transformation which connects the source-free fields and the source-dependent fields according to

$$\left. \begin{aligned} u(x) &= \mathbf{T}(t)^{-1} u_0(x) \mathbf{T}(t), \\ \psi(x) &= \mathbf{T}(t)^{-1} \psi_0(x) \mathbf{T}(t). \end{aligned} \right\} \quad (4.11)$$

As may be seen from (1.14), $\mathbf{T}(t)$ satisfies the variational equation

$$\delta \mathbf{T}(t) = -i \mathbf{T}(t) \int_{-\infty}^t \delta W(x') dx', \quad (4.12)$$

and the boundary condition $\mathbf{T}(t) = 1$ in the limit of vanishing sources. Hence, we see that the operator \mathbf{T} , as defined by (2.1), can be interpreted as the transformation which connects the source-independent fields with the complete source-dependent fields in the infinite future, i. e.

$$\lim_{t \rightarrow \infty} (\mathbf{T}^{-1} u_0(x) \mathbf{T} - u(x)) = 0,$$

and similar relations for the two other fields. We shall use these relations in the form

$$\left. \begin{aligned} \lim_{t \rightarrow \infty} (u_0(x) \mathbf{T} - \mathbf{T} u(x)) &= 0, \\ \lim_{t \rightarrow \infty} (\psi_0(x) \mathbf{T} - \mathbf{T} \psi(x)) &= 0, \\ \lim_{t \rightarrow \infty} (\bar{\psi}_0(x) \mathbf{T} - \mathbf{T} \bar{\psi}(x)) &= 0. \end{aligned} \right\} \quad (4.13)$$

Assume now, as we already tacitly have done in the previous considerations, that the source-independent system by a suitable renormalization has been cast into a form such that a state of lowest energy, the vacuum state, exists and that the energy and momentum of this state is zero. It follows that any stationary state of the system corresponds to an energy momentum vector lying inside the half cone in momentum space characterized by $p_\mu p_\mu < 0$ and $p_0 > 0$. Evidently, time-like momenta corresponding to negative energy are excluded by the assumption made. How-

ever, also space-like momenta are excluded since, by a suitable Lorentz transformation, any space-like momentum vector might be brought into a form with $p_0 < 0$, i. e. with negative energy. Corresponding to the invariant decomposition of momentum space into the three subspaces: the positive frequency part (or the (+)-part) characterized by $p_\mu p_\mu < 0, p_0 > 0$, the negative frequency part (or the (−)-part) characterized by $p_\mu p_\mu < 0, p_0 < 0$, and the (0)-part with $p_\mu p_\mu > 0$, we can split any field variable into three parts, the (+)- the (−)- and the (0)-part. For instance, if we define $u(p)$ by

$$u(x) = (2\pi)^{-2} \int u(p) e^{ipx} dp, \quad (4.14)$$

we have

$$\left. \begin{aligned} u^{(+)}(x) &= (2\pi)^{-2} \int_{p^2 < 0, p_0 > 0} u(p) e^{ipx} dp, \\ u^{(-)}(x) &= (2\pi)^{-2} \int_{p^2 < 0, p_0 < 0} u(p) e^{ipx} dp, \\ u^{(0)}(x) &= (2\pi)^{-2} \int_{p^2 > 0} u(p) e^{ipx} dp. \end{aligned} \right\} \quad (4.15)$$

From our assumption it follows that

$$u_0(x) |0\rangle = u_0^{(-)}(x) |0\rangle. \quad (4.16)$$

Hence also, as $\lim_{t \rightarrow -\infty} (u(x) - u_0(x)) = 0$,

$$\lim_{t \rightarrow -\infty} (u(x) - u_0^{(-)}(x)) |0\rangle = 0, \quad (4.17)$$

i. e. $u(x) |0\rangle$ contains only negative frequencies in the infinite past. The corresponding statement about the asymptotic behaviour of the field variables when multiplied by $\langle 0 | \mathbf{T}$ from the left follows from (4.13). By the same kinds of arguments as those leading to (4.17) we get

$$\lim_{t \rightarrow +\infty} \langle 0 | \mathbf{T} (u(x) - u_0^{(+)}(x)) = 0. \quad (4.18)$$

Thus, $\langle 0 | \mathbf{T} u(x)$ contains only positive frequencies in the in-

finite future. The same result applies to the two other kinds of field variables.

Consider any T_0 -function

$$T_0(x' \cdots x^{(v)} \cdots x^{(k)} | y' \cdots | z' \cdots),$$

say. In the limit where one of the space-time points, for instance $x^{(v)}$, tends to $-\infty$, we have, considering all other space-time points as fixed,

$$\left. \begin{aligned} & \lim_{x_0^{(v)} \rightarrow -\infty} [T_0(x' \cdots x^{(v)} \cdots x^{(k)} | y' \cdots | z' \cdots) \\ & - \langle 0 | \mathbf{T} T(u(x') \cdots u(x^{(v-1)}) u(x^{(v+1)}) \cdots u(x^{(k)}) \cdots) \\ & \quad \times u(x^{(v)} | 0 \rangle] = 0. \end{aligned} \right\} (4.19)$$

Hence, we infer from (4.17) that in the limit $x_0^{(v)} \rightarrow -\infty$ the T_0 -function contains only negative frequencies in a Fourier decomposition with respect to $x^{(v)}$. The same property holds for any other space-time point occurring in a T_0 -function. In the opposite limit, we get by a similar argument that T_0 contains only positive frequencies corresponding to any space-time point approaching the infinite future. Using a terminology which is suggestive in connection with the discussion, given by STUECKELBERG, FEYNMAN and FIERZ [11], of the properties of the causal Green's functions, we say that T_0 -functions obey causal boundary conditions. The possibility of expressing the η -functions in terms of T_0 -functions (as, for instance, expressed by (4.8) and (4.7)) implies that also η -functions satisfy causal boundary conditions.

The equations for the η -functions (4.10) are of the second order in the variational derivatives. We must therefore supplement the boundary conditions with the value of the functional η and its first variational derivative in the limit of vanishing sources. In this limit, however, $\mathbf{T} = 1$. Hence, $\eta(x||) = \langle 0 | u_0(x) | 0 \rangle = 0$, in virtue of (4.16). Similarly, in the same limit, $\eta(|y) = \eta(|z) = 0$. Finally, by the definition (4.7) we have chosen $\eta(|) |_I = \bar{\varphi} = 0 = 0$.

Similar considerations apply to the state vector amplitudes in the infinite future. This is obvious from (2.33) or alternatively from the definition (2.15). Hence, Ψ -functions obey causal

boundary conditions in the infinite future. In the infinite past, however, the behaviour of the Ψ -functions depend on the particular state considered. One more information about the Ψ -functions follows from the considerations in Section 3, iv). If we consider the Ψ -functions for all time variables equal, then, in the source-free limit, only positive frequencies are allowed with respect to this common time.

It is not known whether more conditions must be imposed on the state vector amplitudes to guarantee that a solution of the equations of motion (4.5) actually represents a state of the system. The solution of this problem is of course connected with the likewise unsolved problem of the completeness of the CSR.

iii) The equations of motion in the CSR. Having thus obtained the equations of motion in the FR it becomes a simple matter to derive the equations of motion in the CSR. As mentioned in the Appendix III, in connection with the derivation of the equations of motion of the time ordered products, the differential operators occurring in the field equations commute with all variational operators. We can, therefore, obtain an infinite set of linear differential equations for the Ψ -functions by variational derivation of the equations (4.5). For instance, by applying the variational operator $i \delta/\delta I(x')$ to the first equation (4.5), we get

$$\left. \begin{aligned} (-\square_x + m^2) \Psi(x x' ||) - \lambda \eta(|x|) \Psi(x' ||x) \\ + \lambda \eta(|x) \Psi(x' |x) - \lambda \eta(x' |x) \Psi(|x) \\ + \lambda \eta(x' ||x) \Psi(|x) - \lambda \Psi(x' |x|x) = 0. \end{aligned} \right\} (4.20)$$

Similarly, from the second equation (4.5), we infer

$$\left. \begin{aligned} (\partial_y + M) \Psi(x' |y) + \lambda \eta(y ||) \Psi(x' |y) \\ + \lambda \eta(|y) \Psi(x' y ||) + \lambda \eta(y x' ||) \Psi(|y) \\ + \lambda \eta(x' |y) \Psi(y ||) + \lambda \Psi(x' y |y) = 0. \end{aligned} \right\} (4.21)$$

Proceeding, and taking variational derivatives, one can construct equations involving Ψ -functions with an arbitrary number of meson space-time coordinates. Equations involving one more

nucleon space time point and one more anti-nucleon space time point are obtained by applying the operators $i\delta/\delta g(y')$ and $-i\delta/\delta f(z')$, respectively. Only, when varying the spinor sources, one should remember the anti-commutativity (3.2) of the nucleon variational operators. Thus,

$$\begin{aligned}
 i \frac{\delta}{\delta g(y')} (\eta(y||) \Psi(|y|)) &= \eta(y|y') \Psi(|y|) - \eta(y||) \Psi(|yy'|), \\
 i \frac{\delta}{\delta g(y')} (\eta(|y|) \Psi(y||)) &= -\eta(|yy'|) \Psi(y||) - \eta(|y|) \Psi(y|y'), \\
 i \frac{\delta}{\delta g(y')} \Psi(y|y|) &= -\Psi(y|yy').
 \end{aligned}$$

Observing this, we get by applying $i\delta/\delta g(y')$ to the second equation (4.5)

$$\left. \begin{aligned}
 (\partial_y + M) \Psi(|yy'|) + \lambda \eta(y||) \Psi(|yy'|) + \lambda \Psi(y|yy'|) \\
 - \lambda \eta(y|y'|) \Psi(|y|) + \lambda \eta(|yy'|) \Psi(y||) \\
 + \lambda \eta(|y|) \Psi(y|y') = 0.
 \end{aligned} \right\} (4.22)$$

By a similar procedure one obtains equations connecting the various η -functions. For later reference we note a few examples:

$$\left. \begin{aligned}
 (-\square_x + m^2) \eta(xx'|) - \lambda \eta(x'|x|) \eta(|x|) - \lambda \eta(|x|) \eta(x'|x) \\
 - \lambda \eta(x'|x|x) + i \delta(x - x') = 0,
 \end{aligned} \right\} (4.23)$$

$$\left. \begin{aligned}
 (\partial_y + M) \eta(|y|z) + \lambda \eta(y||) \eta(|y|z) - \lambda \eta(y||z) \eta(|y|) \\
 + \lambda \eta(y|y|z) + i \delta(y - z) = 0,
 \end{aligned} \right\} (4.24)$$

$$\left. \begin{aligned}
 (\bar{\partial}_z + M) \eta(|y|z) + \lambda \eta(z||) \eta(|y|z) + \lambda \eta(z|y|) \eta(|z|) \\
 + \lambda \eta(z|y|z) + i \delta(y - z) = 0,
 \end{aligned} \right\} (4.25)$$

and, finally, an equation involving three space time points

$$\left. \begin{aligned} (\partial_y + M) \eta(x|y|z) + \lambda \eta(y||) \eta(x|y|z) + \lambda \eta(xy|y|z) \\ + \lambda \eta(xy||) \eta(|y|z) - \lambda \eta(xy||z) \eta(|y|) \\ - \lambda \eta(y||z) \eta(x|y) = 0. \end{aligned} \right\} (4.26)$$

The last equation can, for instance, be obtained by operating with $i\delta/\delta I(x)$ on the equation (4.24).

In the CSR it would seem most natural to represent the state under consideration by the state vector amplitudes taken in the limit of vanishing sources. There is, however, as emphasized by SCHWINGER [2], some advantage of postponing the limiting process $I(x) \rightarrow 0$ to a later stage in the considerations. If we, instead of considering meson theory, had taken electrodynamics as an example of illustrating the general scheme developed here, we would have had an obvious reason for doing this, as in electrodynamics the external source of the electromagnetic field has a direct interpretation in terms of a classical distribution of current and charge interacting with the system. Such a justification can hardly be found in our case. Still, we shall find it mathematically convenient in the following considerations to keep the meson field source in the theory.

We, thus, consider the limit of vanishing spinor sources. In this case, simplifications arise due to the fact that the difference ΔN between the total number of nucleons and the total number of anti-nucleons is then a constant of the motion. This implies a selection rule for T_0 -functions. Only those T_0 -functions are different from zero which contain the same number of nucleon and anti-nucleon space time points. If no \mathbf{T} operator appeared in the definition

$$T_0(x' \cdots | y' \cdots | x' \cdots) = \langle 0 | \mathbf{T} \cdot T(u(x') \cdots \psi(y') \cdots \bar{\psi}(z') \cdots) | 0 \rangle,$$

this selection rule would follow in the usual way from $\Delta N | 0 \rangle = 0$. However, it is easily seen from (2.5), remembering that in the limit considered we have $W = Iu$, that ΔN commutes with \mathbf{T} and, thus, the selection rule is not influenced by the presence of the \mathbf{T} -operator.

With this result, we can write (4.5) in the simpler form

$$\left. \begin{aligned} &(-\square_x + m^2) \Psi(x||) - \lambda \Psi(|x|x) = \bar{0}, \\ &(\partial_y + M) \Psi(|y|) + \lambda \eta(y||) \Psi(|y|) + \lambda \Psi(y|y|) = 0, \\ &(\bar{\partial}_z + M) \Psi(|z|) + \lambda \eta(z||) \Psi(|z|) + \lambda \Psi(z||z) = 0, \end{aligned} \right\} (4.27)$$

the limit $\varphi = \bar{\varphi} = 0$ being understood in these equations. It may be of some interest in the following to compare these equations with the equations obtained from (4.23), (4.24), and (4.25), taking the same limit, viz.

$$\left. \begin{aligned} &(-\square_x + m^2) \eta(x x' ||) - \lambda \eta(x' | x | x) + i \delta(x - x') = 0, \\ &\partial_y + M) \eta(|y|z) + \lambda \eta(y||) \eta(|y|z) + \lambda \eta(y|y|z) + i \delta(y - z) = 0, \\ &\bar{\partial}_z + M) \eta(|y|z) + \lambda \eta(z||) \eta(|y|z) + \lambda \eta(z|y|z) + i \delta(y - z) = 0. \end{aligned} \right\} (4.28)$$

These two sets of equations are of very much the same structure. The main difference is that the equations for the state vector amplitudes are homogeneous equations, while those for the η -functions are inhomogeneous ones. We shall discuss the relations between these two sets of equations more closely in the next section. Here, we only mention that the second equation (4.27) and the second equation (4.28) may be written as

$$\left. \begin{aligned} &\left(\partial_y + M + \lambda \eta(y||) + i \lambda \frac{\delta}{\delta I(y)} \right) \Psi(|y|) = 0, \\ &\left(\bar{\partial}_y + M + \lambda \eta(y||) + i \lambda \frac{\delta}{\delta I(y)} \right) \eta(|y|z) = -i \delta(y - z), \end{aligned} \right\} (4.29)$$

respectively. Thus, we see that, in a certain sense, $\Psi(|y|)$ obey the homogeneous equation of motion corresponding to the equation for $\eta(|y|z)$.

5. The equations for the one- and two-nucleon problems.

As mentioned in the Introduction, the present formalism combines the theory of Schwinger with that of Heisenberg and Freese. To illustrate this we shall briefly discuss the formal properties of the one- and two-nucleon equations from the point of view of the CSR. For the sake of completeness, and in order

to introduce some convenient notations, we first summarize the derivation of the one-nucleon equation given by SCHWINGER [2].

i) *The one-nucleon equation.*

In the limit of vanishing spinor sources the simplest η -functions satisfy, according to (4.10) and (4.28), the equations of motion

$$\left. \begin{aligned} (-\square + m^2) \eta(x||) - \lambda \eta(|x|x) + I(x) &= 0, \\ (-\square + m^2) \eta(xx' ||) - \lambda \eta(x'|x|x) + i\delta(x-x') &= 0, \\ (\partial_y + m + \lambda \eta(y||)) \eta(|y|z) + \lambda \eta(y|y|z) + i\delta(y-z) &= 0. \end{aligned} \right\} (5.1)$$

To simplify the notation, and also to distinguish the η -functions in this limit from the general ones, we introduce

$$\left. \begin{aligned} U(x) &= \eta(x||), \\ \Delta'_c(x, x') &= i\eta(xx' ||), \\ S'_c(x, x') &= -i\eta(|x|x'), \end{aligned} \right\} (5.2)$$

and, consequently, write the equations (5.1) in the form

$$\left. \begin{aligned} (-\square + m^2) U(x) - i\lambda S'_c(x, x) + I(x) &= 0, \\ (-\square + m^2) \Delta'_c(x, x') + i\lambda \frac{\delta}{\delta I(x')} S'_c(x, x) &= \delta(x-x'), \\ (\partial + M + \lambda U(x)) S'_c(x, x') + i\lambda \frac{\delta}{\delta I(x)} S'_c(x, x') &= -\delta(x-x'). \end{aligned} \right\} (5.3)$$

As discussed in Section 4.ii, the η -functions satisfy causal boundary conditions. Hence, in the limit $I = \lambda = 0$, we have

$$\left. \begin{aligned} \Delta'_c(x, x') &= \Delta_c(x-x'), \\ S'_c(x, x') &= S_c(x-x'), \end{aligned} \right\} (5.4)$$

where Δ_c and S_c are the well-known causal solutions of

$$\left. \begin{aligned} (-\square + m^2) \Delta_c(x-x') &= \delta(x-x'), \\ (\partial + M) S_c(x-x') &= -\delta(x-x'). \end{aligned} \right\} (5.5)$$

The equations (5.3) are, for our case of nucleons interacting with scalar neutral mesons, the analogue of the equations for the Green's functions in electrodynamics studied in Schwinger's paper. Following his method we substitute the variational derivative operators in (5.3) by polarization operators Π_c^* and Σ_c^* defined by

$$\left. \begin{aligned} i \lambda \frac{\delta}{\delta I(x')} S'_c(x, x) &= \Pi_c^*(x, 1) A'_c(1, x') \\ i \lambda \frac{\delta}{\delta I(x)} S'_c(x, x') &= \Sigma_c^*(x, 1) S'_c(1, x'). \end{aligned} \right\} \quad (5.6)$$

Here, and in the following, numbers occurring twice denote variables of integration. Thus, for instance,

$$\Sigma_c^*(x, 1) S'_c(1, x') = \int \Sigma_c^*(x, \xi') S'_c(\xi', x') d\xi'. \quad (5.7)$$

By (5.6) the equations (5.3) take the form

$$\left. \begin{aligned} (-\square + m^2) U(x) - i \lambda S'_c(x, x) &= -I(x), \\ (-\square + m^2) A'_c(x, x') + \Pi_c^*(x, 1) A'_c(1, x') &= \delta(x - x'), \\ (\partial + M + \lambda U(x)) S'_c(x, x') + \Sigma_c^*(x, 1) S'_c(1, x') &= -\delta(x - x'). \end{aligned} \right\} \quad (5.8)$$

Operating on the last of these equations with $i \lambda \delta / \delta I(x'')$ we get, after integration and taking into account the causal boundary conditions,

$$i \lambda \frac{\delta}{\delta I(x'')} S'_c(x', x''') = S'_c(x', 1) \Phi(1, 2, 3) A'_c(2, x'') S'_c(3, x'''). \quad (5.9)$$

The kernel Φ depending on three space time points is given by

$$\left. \begin{aligned} &\Phi(x', x'', x''') \\ &= -i \lambda^2 \delta(x' - x'') \delta(x'' - x''') - i \lambda \frac{\delta \Sigma_c^*(x', x''')}{\delta U(x'')} \end{aligned} \right\} \quad (5.10)$$

In the derivation of (5.9) use has been made of the fact that I does not appear explicitly in the last equation (5.8), whence

$$\frac{\delta}{\delta I(x)} \Sigma_c^* (x', x'') = - \frac{\delta \Sigma_c^* (x', x''')}{\delta U(2)} \Delta'_c (2, x''). \quad (5.11)$$

On comparison of (5.6) and (5.9) we infer integro variational equations characterizing the polarization operators, viz.

$$\left. \begin{aligned} \Pi_c^* (x, x') &= S'_c (x, 1) \Phi (1, x', 3) S'_c (3, x), \\ \Sigma_c^* (x, x') &= S'_c (x, 1) \Phi (1, 2, x') \Delta'_c (2, x). \end{aligned} \right\} \quad (5.12)$$

For later reference we mention that, from the equation conjugate to the last equation (5.1), viz.

$$(\bar{\partial}_z + M + \lambda \eta (z|)) \eta (|y|z) + \lambda \eta (z|y|z) + i \delta (y - z) = 0, \quad (5.13)$$

we get by arguments similar to those leading to (5.8) an equation of the form

$$(\bar{\partial}' + M + \lambda U (x')) S'_c (x, x') + S'_c (x, 1) \bar{\Sigma}_c^* (1, x') = - \delta (x - x'). \quad (5.14)$$

The polarization operator in this equation is given by

$$\bar{\Sigma}_c^* (x, x') = \Phi (x, 2, 3) \Delta'_c (2, x') S'_c (3, x'). \quad (5.15)$$

According to Schwinger, the one-nucleon equation is obtained as the homogeneous equation of motion corresponding to the inhomogeneous equation (5.8) for the Green's function S'_c . Thus, denoting the one-nucleon "wave function" by χ , the equation reads

$$(\partial + M + \lambda U (x)) \chi (x) + \Sigma_c^* (x, 1) \chi (1) = 0. \quad (5.16)$$

As shown in the previous section, the equation of motion for the state vector amplitude depending on one nucleon coordinate is

$$(\partial_y + M + \lambda U (y)) \Psi (|y|) + i \lambda \frac{\delta}{\delta I(y)} \Psi (|y|) = 0. \quad (5.17)$$

The similarity between this equation and the inhomogeneous equation for the Green's function S'_c makes it natural to investigate under which conditions solutions of (5.16) also satisfy (5.17). For this to be true we must have

$$i \lambda \frac{\delta}{\delta I(x)} \chi(x) = \Sigma_c^* (x, 1) \chi(1). \quad (5.18)$$

By derivation of (5.16) with respect to $I(x')$ we get, after integration, an expression for the variational derivative of χ , viz.

$$i \lambda \frac{\delta \chi(x)}{\delta I(x')} = \chi^{(0)}(x'; x) + S'_c(x, 1) \Phi(1, 2, 3) A'_c(2, x') \chi(3). \quad (5.19)$$

The function $\chi^{(0)}$ is a so far undetermined solution of

$$(\partial + M + \lambda U(x)) \chi^{(0)}(x'; x) + \Sigma_c^* (x, 1) \chi^{(0)}(x'; 1) = 0. \quad (5.20)$$

Comparing (5.18) with (5.19) we see that χ is a solution of (5.17), provided that $\chi^{(0)}$ vanishes.

We thus have the result that any solution of the coupled equations

$$\left. \begin{aligned} (\partial_y + M + \lambda U(y)) \Psi_{(1)}(|y|) + \Sigma_c^* (y, 1) \Psi_{(1)}(|1|) &= 0, \\ \Psi_{(1)}(x|y|) &= \lambda^{-1} S'_c(y, 1) \Phi(1, 2, 3) A'_c(2, x) \Psi_{(1)}(|3|) \end{aligned} \right\} \quad (5.21)$$

also satisfies (5.17). The reverse statement is of course not true. We have, therefore, attached a subscript to the state vector amplitudes in these equations to indicate that a solution in the form (5.21) is possible for a restricted class of states only, the one-nucleon states.

From (5.17) we get by variational derivation an infinite system of coupled equations for the state vector amplitudes. The first of the equations derived from (5.17) reads

$$\left. \begin{aligned} (\partial_y + M + \lambda U(y)) \Psi(x|y|) - i \lambda A'_c(x, y) \Psi(|y|) \\ + \lambda \Psi(xy|y|) &= 0. \end{aligned} \right\} \quad (5.22)$$

Let us now follow, in the present version of the CSR, the suggestion by Freese and try to eliminate all amplitudes depending on one or more meson coordinates from the infinite set of equations. The states for which this elimination process is possible might, alternatively, be called the one-nucleon states. To get an idea how the resulting equation will look we convert the infinite system of equations into a finite one by the approximation assumption that $\Psi(xy|y|)$ can be neglected in (5.22). We can then solve (5.22) by the aid of the Green's function satisfying

$$(\partial_y + M + \lambda U(y)) S_c^{(U)}(y, y') = -\delta(y - y'), \quad (5.23)$$

and causal boundary conditions. The approximate solution of (5.22) is then

$$\Psi(x|y) = \varphi^{(0)}(x; y) - i\lambda S_c^{(U)}(y, 1) \Delta'_c(1, x) \Psi(|1|), \quad (5.24)$$

where $\varphi^{(0)}$ is a solution of

$$(\partial_y + M + \lambda U(y)) \varphi^{(0)}(x; y) = 0. \quad (5.25)$$

To obtain an equation of the form (5.16) we choose $\varphi^{(0)} = 0$. With this choice we get, instead of (5.17),

$$(\partial_y + M + \lambda U(y)) \Psi(|y|) - i\lambda^2 S_c^{(U)}(y, 1) \Delta'_c(1, y) \Psi(|1|) = 0. \quad (5.26)$$

In the next approximation one would keep all amplitudes with less than two meson space time points. Proceeding in this way one can, in principle, construct an exact equation of the form (5.16), provided that the procedure converges. The polarization operator $'\Sigma_c^*$, say, obtained in this way is characterized by the requirement that the resulting equation

$$(\partial_y + M + \lambda U(y)) \Psi(|y|) + '\Sigma_c^*(y, 1) \Psi(|1|) = 0$$

is consistent with (5.17), i. e. that

$$'\Sigma_c^*(y, 1) \Psi(|1|) = i\lambda \frac{\delta}{\delta I(y)} \Psi(|y|).$$

By arguments similar to those above it can easily be verified that $'\Sigma_c^*$ is, in fact, identical with Σ_c^* . Thus the resulting one-nucleon equation is identical with Schwinger's equation.

The advantage of the equations (5.21) as compared with the infinite system of equations obtained from (5.17) becomes obvious when we pass to the physically interesting limit of vanishing external sources. For $I = 0$, the second equation (5.21) and the equations obtained therefrom by variational derivation become explicit expressions for the state vector amplitudes with one and more meson space time coordinates. Therefore, for $I = 0$, any solution of the one-nucleon equation provides us

with a corresponding solution of the equations of motion in the configuration space representation.

ii) *The two-nucleon equation.*

According to Schwinger, the two-nucleon Green's function is defined by

$$G(y, y'; z, z') = \frac{\delta}{\delta f(z')} \frac{\delta}{\delta f(z)} \frac{T_0(|yy'|)}{T_0(|)} \Big|_{\varphi=\bar{\varphi}=0} \quad (5.27)$$

Using the formulas in Section 4, it is easily verified that

$$G(y, y'; z, z') = \left. \begin{aligned} &G(y, y'; z, z') \\ &= \eta(|yy'|zz') - \eta(|y|z) \eta(|y'|z') + \eta(|y|z') \eta(|y'|z), \end{aligned} \right\} \quad (5.28)$$

the limit $\varphi = \bar{\varphi} = 0$ being understood in this formula. An equation of motion for $\eta(|yy'|zz')$ can be obtained from (4.10) by taking appropriate variational derivatives. From the equation obtained in this way, and by (5.3), we get

$$\left. \begin{aligned} &(\partial_y + M + \lambda U(y)) G(y, y'; z, z') + i\lambda \frac{\delta}{\delta I(y)} G(y, y'; z, z') \\ &= -\delta(y-z) S'_c(y', z') + \delta(y-z') S'_c(y', z). \end{aligned} \right\} \quad (5.29)$$

Using (5.3) we see that

$$\left. \begin{aligned} &(\partial_{y'} + M + \lambda U(y) + \lambda \frac{\delta}{\delta I(y)}) (\partial_y + M + \lambda U(y') + i\lambda \frac{\delta}{\delta I(y')}) G(y, y'; z, z') \\ &= \delta(y-z) \delta(y'-z') - \delta(y-z') \delta(y'-z). \end{aligned} \right\} \quad (5.30)$$

Following Schwinger, we introduce an interaction operator W by

$$\left. \begin{aligned} &F(y) F(y') G(y, y'; z, z') - W(y, y'; 1, 2) G(1, 2; z, z') \\ &= \delta(y-z) \delta(y'-z') - \delta(y-z') \delta(y'-z). \end{aligned} \right\} \quad (5.31)$$

The symbol F is an abbreviation of the integral differential operator entering in the equation for the one-nucleon Green's function, i. e.

$$F(y) \xi(y) = (\partial_y + M + \lambda U(y)) \xi(y) + \Sigma_c^*(y, 1) \xi(1). \quad (5.32)$$

As G satisfies causal boundary conditions we can integrate (5.31) by means of S'_c . Combining the resulting equation, viz.

$$\left. \begin{aligned} F(y) G(y, y'; z, z') + S'_c(y', 2) W(y, 2; 3, 4) G(3, 4; z, z') \\ = -\delta(y - z) S'_c(y', z') + \delta(y - z') S'_c(y', z), \end{aligned} \right\} (5.33)$$

with (5.29) we infer a condition on the interaction operator:

$$\left. \begin{aligned} i \lambda \frac{\delta}{\delta I(y)} G(y, y'; z, z') = \Sigma_c^*(y, 1) G(1, y'; z, z') \\ + S'_c(y', 2) W(y, 2; 3, 4) G(3, 4; z, z'). \end{aligned} \right\} (5.34)$$

Integrating (5.33) once more, we find that

$$\left. \begin{aligned} G(y, y'; z, z') - S'_c(y, 1) S'_c(y', 2) W(1, 2; 3, 4) G(3, 4; z, z') \\ = S'_c(y, z) S'_c(y', z') - S'_c(y, z') S'_c(y', z). \end{aligned} \right\} (5.35)$$

From this equation one gets an expression for the variational derivative of G with respect to $I(y)$ which, together with (5.34), gives Schwinger's characterization of the interaction operator, viz.

$$\left. \begin{aligned} W(y, y'; 1, 2) G(1, 2; z, z') \\ = \Phi(y', 1, 2) A'_c(1, y) G(y, 2; z, z') \\ + S'_c(y, 1) i \lambda \frac{\delta}{\delta I(y)} [W(1, y'; 3, 4) G(3, 4; z, z')]. \end{aligned} \right\} (5.36)$$

For W we shall use another equation which does not depend explicitly on the variational derivative of the two-nucleon Green's function. From (5.35) one gets, using (5.9),

$$\left. \begin{aligned} i \lambda \frac{\delta}{\delta I(x)} G(y, y'; z, z') \\ = \frac{1}{2} \lambda G(y, y'; 1, 2) \left[i \frac{\delta}{\delta I(x)} W(1, 2; 3, 4) \right] G(3, 4; z, z') \\ + G(y, y'; 1, 2) \Phi(1, 3, 4) A'_c(3, x) S'_c(4, 5) F(5) F(2) G(5, 2; z, z'). \end{aligned} \right\} (5.37)$$

The combination of this expression with (5.34) gives the alternative characterization of W , viz.

$$\left. \begin{aligned}
 & (\Sigma_c^* (y, z) \delta (y' - z') - \Sigma_c^* (y, z') \delta (y' - z)) + S'_c (y', 2) W (y, 2; z, z') \\
 &= \frac{1}{2} \lambda G (y, y'; 1, 2) i \frac{\delta}{\delta I(y)} W (1, 2; z, z') \\
 &- \frac{1}{2} \bar{F} (z') G (y, y'; 1, z') \Phi (1, 2, z) \Delta'_c (2, y) \\
 &- \frac{1}{2} \bar{F} (z) G (y, y'; z, 1) \Phi (1, 2, z') \Delta'_c (2, y).
 \end{aligned} \right\} (5.38)$$

Here, \bar{F} denotes the operator entering in the equation of motion for the one-nucleon Green's function in the form given by (5.14), i. e.

$$\bar{F} (z) \zeta (z) = (\bar{\partial}_z + M + \lambda U (z)) \zeta (z) + \zeta (1) \bar{\Sigma}_c^* (1, z). \quad (5.39)$$

The equations of motion for the state vector amplitude depending on two nucleon space time points obtained from the equation (4.22) by passing to the limit of vanishing spinor sources read

$$\left. \begin{aligned}
 & (\partial_y + M + \lambda U (y)) \Psi (|y y'|) + \lambda \Psi (y |y y'|) = 0, \\
 & (\partial_{y'} + M + \lambda U (y')) \Psi (|y y'|) + \lambda \Psi (y' |y y'|) = 0,
 \end{aligned} \right\} (5.40)$$

whence also

$$\left(\partial_y + M + \lambda U (y) + i \lambda \frac{\delta}{\delta I(y)} \right) \left(\partial_{y'} + M + \lambda U (y') + i \lambda \frac{\delta}{\delta I(y')} \right) \Psi (|y y'|) = 0. \quad (5.41)$$

This equation is a homogeneous equation of motion corresponding to (5.30) in the same sense as the equation (5.17) for the one-nucleon amplitude is the homogeneous equation corresponding to the equation for the one-nucleon Green's function (5.3).

According to Schwinger, the two-nucleon equation is the homogeneous equation corresponding to the equation (5.31), i. e.

$$F (y) F (y') \chi (y, y') - W (y, y'; 1, 2) \chi (1, 2) = 0. \quad (5.42)$$

It seems to be difficult to establish any general connection between the solutions of this equation and the solutions of (5.41). If, however, we take instead of (5.42) the two integrated equations

$$\left. \begin{aligned} F(y) \chi(y, y') + S'_c(y', 2) W(y, 2; 3, 4) \chi(3, 4) &= 0, \\ F(y') \chi(y, y') + S'_c(y, 1) W(1, y'; 3, 4) \chi(3, 4) &= 0, \end{aligned} \right\} (5.43)$$

where the inhomogeneous terms have been dropped, then one can rather easily find the connection between the solutions of these equations and the solutions of (5.40). Evidently, the condition for compatibility of (5.43) and (5.40) is that

$$\left. \begin{aligned} \Sigma_c^*(y, 1) \chi(1, y') + S'_c(y', 2) W(y, 2; 3, 4) \chi(3, 4) \\ = i\lambda \frac{\delta}{\delta I(y)} \chi(y, y'), \\ \Sigma_c^*(y', 2) \chi(y, 2) + S'_c(y, 1) W(1, y'; 3, 4) \chi(3, 4) \\ = i\lambda \frac{\delta}{\delta I(y')} \chi(y, y'). \end{aligned} \right\} (5.44)$$

By integration of (5.43) we get

$$\chi(y, y') - S'_c(y, 1) S'_c(y', 2) W(1, 2; 3, 4) \chi(3, 4) = \varphi(y, y'), \quad (5.45)$$

where φ is any solution of

$$F(y) \varphi(y, y') = F(y') \varphi(y, y') = 0, \quad (5.46)$$

i. e. φ has one-particle properties with respect to both coordinates. From this equation we infer by arguments similar to those used in the derivation of the one-particle equation that

$$\left. \begin{aligned} i\lambda \frac{\delta}{\delta I(x)} \varphi(y, y') &= \varphi^{(0)}(x; y, y') \\ + S'_c(y', 1) \Phi(1, 2, 3) \Delta'_c(2, x) \varphi(y, 3) \\ + S'_c(y, 1) \Phi(1, 2, 3) \Delta'_c(2, x) \varphi(3, y'), \end{aligned} \right\} (5.47)$$

where

$$F(y) \varphi^{(0)}(x; y, y') = F(y') \varphi^{(0)}(x; y, y') = 0. \quad (5.48)$$

Using this we find from (5.45) an expression for the variational derivative of χ with respect to $I(x)$, viz.

$$\left. \begin{aligned} i\lambda \frac{\delta}{\delta I(x)} \chi(y, y') &= \frac{1}{2} \lambda G(y, y'; 1, 2) \left[i \frac{\delta}{\delta I(x)} W(1, 2; 3, 4) \right] \chi(3, 4) \\ - (\bar{F}(4) G(y, y'; 1, 4)) \Phi(1, 2, 3) \Delta'_c(2, x) \chi(3, 4) &+ R^{(0)}, \end{aligned} \right\} (5.49)$$

where $R^{(0)}$ is a contribution which vanishes for $\varphi^{(0)}$ equal to zero. On comparison with (5.44) and using (5.38) we find that χ satisfies (5.40), provided that $\varphi^{(0)}$ vanishes.

Hence, corresponding to (5.21), we have the result for the two-nucleon system: Any solution of the coupled equations

$$\left. \begin{aligned} \mathcal{U}_{(2)}(|yy'|) - S'_c(y, 1) S'_c(y', 2) W(1, 2; 3, 4) \Psi_{(2)}(|34|) = \varphi(y, y') \\ \lambda \frac{\delta}{\delta I(x)} \Psi_{(2)}(|yy'|) = \frac{1}{2} \lambda G(y, y'; 1, 2) \left[i \frac{\delta}{\delta I(x)} W(1, 2; 3, 4) \right] \Psi_{(2)}(|34|) \\ - (\bar{F}(4) G(y, y'; 1, 4)) \Phi(1, 2, 3) \Delta'_c(2, x) \Psi_{(2)}(|34|), \end{aligned} \right\} (5.50)$$

where $\varphi(y, y')$ satisfies (5.46), is a solution of (5.40). In particular, passing to the limit $I = 0$, the second equation (5.50) and its variational derivatives become explicit expressions for the state vector amplitudes depending on one and more meson coordinates besides the two nucleon space time coordinates. It is thus possible in a unique way to relate to any solution of the Bethe-Salpeter equation a solution of the equations of motion in the configuration space representation.

Summary.

A reformulation of quantum field theory is given, in which any state of the system considered is represented by a functional depending on external sources. The variational derivatives of this functional provide us with a generalization of the Fock representation in configuration space to the case of non-linear fields. The representing amplitudes can be expressed entirely in terms of matrix elements of time ordered products of field operators and possess several simple properties which are independent of the magnitude of the coupling constant. It is shown that these amplitudes satisfy homogeneous equations of motion which can be derived in a simple manner. The equations of the Bethe-Salpeter type following herefrom become identical with those following from Schwinger's theory of Green's functions. Our representation has many properties in common with that given by Freese.

Appendix I.

The sources of the spinor fields.

In Section 1 we have assumed that the domain of the external sources can be chosen so large that variational derivatives with respect to allowed variations of f and g can be defined in a unique way. This property together with the anti-commutativity (1.6) is all we need for the development of the configuration space representation. It is, maybe, not quite trivial that the requirements to the sources are consistent. We shall, therefore, construct an example of a possible domain of allowed f -number pairs.

Let a_n and b_n , $n = 1, 2, \dots$ be two sets of infinite matrices which satisfy the commutation rules

$$\left. \begin{aligned} \{ a_n, a_m^\dagger \} &= \delta_{nm} \\ \{ a_n, a_m \} &= \{ a_n^\dagger, a_m^\dagger \} = 0, \\ \{ b_n, b_m^\dagger \} &= \delta_{nm} \\ \{ b_n, b_m \} &= \{ b_n^\dagger, b_m^\dagger \} = 0, \end{aligned} \right\} \text{(Ap. I. 1)}$$

while all the a 's anti-commute with all the b 's. As is well known, there exists a matrix which anti-commutes with all the a 's and with all the b 's and with their adjoints. This matrix Ω , say, is the parity of the matrix $\Sigma (a_n^\dagger a_n + b_n^\dagger b_n)$. We choose Ω hermitian and unitary, i. e.

$$\Omega^\dagger = \Omega, \quad \Omega^2 = 1. \quad \text{(Ap. I. 2)}$$

For the construction of the f -number pairs we further need two complete orthonormal sets of functions in four-dimensional space, $f_n(x)$ and $g_n(x)$, such that any function, $\xi(x)$ say, can be expanded in either of the forms

$$\xi(x) = \Sigma \xi_n^{(f)} f_n(x)$$

or

$$\xi(x) = \Sigma \xi_n^{(g)} g_n(x).$$

Let c_1 and c_2 be complex numbers. Then,

$$\left. \begin{aligned} f(x) &= c_1 \sum a_n f_n(x) \\ g(x) &= c_2 \sum b_n g_n(x), \end{aligned} \right\} \text{(Ap. I. 3)}$$

is a possible allowed f -number pair. In fact, due to (Ap. I. 1)

$$\{f(x), f(x')\} = \{f(x), g(x')\} = \{g(x), g(x')\} = 0. \quad \text{(Ap. I. 4)}$$

A domain of f -number pairs can be obtained from the particular pair (Ap. I. 3) by unitary transformations in the a, b -space. In particular we are interested in infinitesimal unitary transformations such that the corresponding variations of the f -number pair form a pair of allowed variations in the sense of Section 1, i. e. such that

$$\left. \begin{aligned} \{\delta f(x), f(x')\} &= \{\delta f(x), g(x')\} = 0, \\ \{\delta g(x), f(x')\} &= \{\delta g(x), g(x')\} = 0. \end{aligned} \right\} \text{(Ap. I. 5)}$$

Such variations can be obtained by means of the matrix

$$A = \sum (a_n^\dagger \Omega a_n - a_n^* \Omega a_n + b_n^\dagger \Omega b_n - b_n^* \Omega b_n), \quad \text{(Ap. I. 6)}$$

where the a_n 's and the b_n 's are infinitesimal complex numbers. By the properties of Ω , A is anti-hermitian, whence $1 + A$ is unitary. By this transformation the a_n 's and the b_n 's vary according to

$$\left. \begin{aligned} \delta a_n &= -[A, a_n] = \Omega a_n, \\ \delta b_n &= -[A, b_n] = \Omega b_n. \end{aligned} \right\} \text{(Ap. I. 7)}$$

The corresponding variation of the f -number pairs is

$$\left. \begin{aligned} \delta f(x) &= c_1 \Omega \sum a_n f_n(x), \\ \delta g(x) &= c_2 \Omega \sum b_n g_n(x). \end{aligned} \right\} \text{(Ap. I. 8)}$$

Obviously we have here an example of a pair of allowed variations for any set of infinitesimal a_n 's and b_n 's. Thus, all variations of the form

$$\left. \begin{aligned} \delta f(x) &= \Omega \delta \xi(x), \\ \delta g(x) &= \Omega \delta \eta(x), \end{aligned} \right\} \text{(Ap. I. 9)}$$

where $\delta\xi$ and $\delta\eta$ are infinitesimal functions are included among the allowed variations. Therefore, if an expression of the form (1.10) holds for an arbitrary pair of allowed variations, we have in particular

$$\Omega \int (\delta\xi(x) K(x) + \delta\eta(x) L(x)) \delta x = 0, \quad (\text{Ap. I. 10})$$

with arbitrary $\delta\xi$ and $\delta\eta$. As Ω is non-singular we conclude that $K(x)$ as well as $L(x)$ vanish identically.

Appendix II.

Reformulation of a theorem due to Wick.

Let $u(x)$ be the field operator of a free scalar neutral meson field. We shall use Dyson's notation

$$N(u(x') u(x'') \cdots u(x^{(n)})) \quad (\text{Ap. II. 1})$$

to designate the product of the u 's ordered such that all absorption operators stand to the right of all emission operators. This product we call the normal product of the u 's indicated. As shown by Wick [9], any time ordered product can be decomposed into a sum of normal constituents according to

$$T(u(x') u(x'') \cdots u(x^{(n)})) = \sum_{\nu=0}^n N^{(\nu)}. \quad (\text{Ap. II. 2})$$

For ν odd $N^{(\nu)}$ vanishes. For ν even, $N^{(\nu)}$ is a sum of terms, one term for each possible pairing of ν factors u . Let for ν even, $\xi', \xi'', \cdots, \xi^{(\nu)}$ be some of the space time points $x', x'', \cdots, x^{(n)}$. For a definite pairing $(\xi', \xi''), (\xi''', \xi''''), \cdots, (\xi^{(\nu-1)}, \xi^{(\nu)})$ the contribution to $N^{(\nu)}$ is

$$\left. \begin{aligned} &\langle 0 | T(u(\xi') u(\xi'')) | 0 \rangle \langle 0 | T(u(\xi''') u(\xi'''')) | 0 \rangle \cdots \\ &\quad \times \langle 0 | T(u(\xi^{(\nu-1)}) u(\xi^{(\nu)})) | 0 \rangle \\ &\quad \times N(u(x') u(x'') \cdots u(x^{(n)}); \xi', \xi'', \cdots, \xi^{(\nu)}). \end{aligned} \right\} (\text{Ap. II. 3})$$

Here, $N(\cdots)$ denotes the normal product of the unpaired u 's. For instance,

$$N(u(x') u(x'') u(x''') u(x'''')); x'' x'''' \equiv N(u(x') u(x''')).$$

To obtain $N^{(v)}$ from terms of the form (Ap. II. 3) one must add all contributions from possible pairings of the space time points $\xi', \xi'', \dots \xi^{(v)}$ and, further, sum over all subsets of v field operators u . Hence, we can write $N^{(v)}$ in the form

$$\left. \begin{aligned} N^{(v)} &= \sum_{\xi', \xi'', \dots \xi^{(v)}} C(\xi', \xi'', \dots \xi^{(v)}) \\ N(u(x') u(x'') \dots u(x^{(n)}); \xi', \xi'', \dots \xi^{(v)}), \end{aligned} \right\} \text{(Ap. II. 4)}$$

where the C 's are certain c -number functions not depending on n . The summation runs over all subsets $\xi', \xi'', \dots \xi^{(v)}$. In particular, we note that, for n even,

$$N^{(n)} = C(x', x'', \dots x^{(n)}). \quad \text{(Ap. II. 5)}$$

Combining (Ap. II. 4) and (Ap. II, 2) we have

$$\left. \begin{aligned} T(u(x') \dots u(x^{(n)})) &= \\ \sum_{v=0}^n \sum_{\xi' \dots \xi^{(v)}} C(\xi', \dots \xi^{(v)}) N(u(x') \dots u(x^{(n)}); \xi', \dots \xi^{(v)}). \end{aligned} \right\} \text{(Ap. II. 6)}$$

We include formally odd v 's in the summation and choose vanishing corresponding C 's.

The vacuum expectation value of any N -product is zero. Thus, from (Ap. II. 6) for n even, we get explicit expressions for the C 's, viz.

$$C(x', x'', \dots x^{(n)}) = T_0(x', x'', \dots x^{(n)}). \quad \text{(Ap. II. 7)}$$

As in (2.20), $T_0(x', \dots)$ stands for the vacuum expectation value of the T -product. Wick's theorem now takes the form

$$\left. \begin{aligned} T(u(x') \dots u(x^{(n)})) &= \\ \sum_{v=0}^n \sum_{\xi' \dots \xi^{(v)}} T_0(\xi', \dots \xi^{(v)}) N(u(x') \dots u(x^{(n)}); \xi', \dots \xi^{(v)}). \end{aligned} \right\} \text{(Ap. II. 8)}$$

It should be noted that (Ap. II. 7) also holds for v odd as the vacuum expectation value of the product of an odd number of free field operators vanishes.

In case also other types of fields are considered, the definition of the N -product is slightly modified. Each term in the N -product

should now be multiplied by a factor (\pm) which has the value $+1$ if the permutation of spinor operators involved in the ordering process is even, and -1 if this permutation is odd.

Consider the case of a free meson field u and a free spinor field described by the field operators $\bar{\psi}$ and ψ . Similar to (Ap. II. 8) one can write Wick's theorem for this case in the form

$$\left. \begin{aligned} & T(u(x') \cdots u(x^{(k)}) \psi(y') \cdots \psi(y^{(l)}) \bar{\psi}(z') \cdots \bar{\psi}(z^{(m)})) = \\ & \sum_{\alpha\lambda\mu} \sum_{\xi' \dots \xi^{(\alpha)}} \sum_{\eta' \dots \eta^{(\lambda)}} \sum_{\zeta' \dots \zeta^{(\mu)}} (\pm) T_0(\xi' \dots \xi^{(\alpha)} | \eta' \dots \eta^{(\lambda)} | \zeta' \dots \zeta^{(\mu)}) \\ & \times N(u(x') \cdots u(x^{(k)}); \xi' \dots \xi^{(\alpha)} | \psi(y') \cdots \psi(y^{(l)}); \eta' \dots \eta^{(\lambda)} | \\ & \quad \bar{\psi}(z') \cdots \bar{\psi}(z^{(m)}); \zeta' \dots \zeta^{(\mu)}), \end{aligned} \right\} \text{(Ap. II. 9)}$$

where (\pm) is the parity of the permutation

$$\left\{ \begin{array}{l} (\xi' \dots \xi^{(\alpha)} | \eta' \dots \eta^{(\lambda)} | \zeta' \dots \zeta^{(\mu)}) \\ (x' \dots x^{(k)}; \xi' \dots \xi^{(\alpha)} | y' \dots y^{(l)}; \eta' \dots \eta^{(\lambda)} | z' \dots z^{(m)}; \zeta' \dots \zeta^{(\mu)}) \\ \rightarrow (x' \dots x^{(k)} | y' \dots y^{(l)} | z' \dots z^{(m)}). \end{array} \right\}$$

We introduce the notation

$$\Psi(x' \cdots | y' \cdots | z' \cdots) = \langle 0 | N(u(x') \cdots \psi(y') \cdots \bar{\psi}(z') \cdots) | \Psi \rangle. \quad \text{(Ap. II. 10)}$$

If, further, we use the notation of Section 2 (p. 17), we get from (Ap. II. 9)

$$\left. \begin{aligned} & T_{\Psi}(x' \cdots x^{(k)} | y' \cdots y^{(l)} | z' \cdots z^{(m)}) = \\ & \sum_{\alpha\lambda\mu} \frac{1}{\alpha!} \sum_{\xi' \dots \xi^{(\alpha)}} \frac{1}{\lambda!} \sum_{\eta' \dots \eta^{(\lambda)}} \frac{1}{\mu!} \sum_{\zeta' \dots \zeta^{(\mu)}} (\pm) T_0(\xi' \dots \xi^{(\alpha)} | \eta' \dots \eta^{(\lambda)} | \zeta' \dots \zeta^{(\mu)}) \\ & \times \Psi(x' \cdots x^{(k)}; \xi' \dots \xi^{(\alpha)} | y' \dots y^{(l)}; \eta' \dots \eta^{(\lambda)} | z' \dots z^{(m)}; \zeta' \dots \zeta^{(\mu)}). \end{aligned} \right\} \text{(Ap. II. 11)}$$

The factorials take into account that we now perform the summation such that the ξ 's, η 's, and ζ 's run independently over the x 's, y 's, and z 's, respectively.

As is well known, the functions Ψ are the representing amplitudes for the state $|\Psi\rangle$ in the Fock representation in the configuration space. We can thus regard (Ap. II. 11) as a re-

cursion formula expressing the Fock amplitudes in terms of matrix elements of time ordered products.

Appendix III.

The equations of motion for the T_{Ψ} -functions.

The equations of motion for the T_{Ψ} -functions depending on one space time point only are easily obtained from the field equations (1.2). One finds¹

$$\left. \begin{aligned} (-\square_x + m^2) T_{\Psi}(x||) - \lambda T_{\Psi}(|x|x) + I(x) T_{\Psi}(|) &= 0, \\ (\partial_y + M) T_{\Psi}(|y|) + \lambda T_{\Psi}(y|y|) + f(y) T_{\Psi}(|) &= 0, \\ (\bar{\partial}_z + M) T_{\Psi}(|z) + \lambda T_{\Psi}(z||z) + g(z) T_{\Psi}(|) &= 0. \end{aligned} \right\} \text{(Ap. III. 1)}$$

From the variational equations (1.14) and the canonical commutators it follows that

$$(\partial_y + M) \delta \psi(y) = \delta [(\partial_y + M) \psi(y)],$$

and similar relations for the other field variables. Hence, the differential operators appearing in the field equations commute with all variational derivative operators. We can thus obtain equations of motion for T_{Ψ} -functions depending on more than one space time point simply by taking variational derivatives of the equations (Ap. III. 1). For instance, applying $-i \delta/\delta f(z)$ to the second of these equations, we get

$$\left. \begin{aligned} (\partial_y + M) T_{\Psi}(|y|z) + \lambda T_{\Psi}(y|y|z) \\ + f(y) T_{\Psi}(|z) + i \delta(y-z) T_{\Psi}(|) &= 0. \end{aligned} \right\} \text{(Ap. III. 2)}$$

One should note that, for instance,

$$-i \frac{\delta}{\delta f(z)} T_{\Psi}(|y|) = - T_{\Psi}(|y|z).$$

¹ The T -product of $\psi(x)$ and $\bar{\psi}(x')$ for $x = x'$ is chosen as

$$T(\psi(x) \bar{\psi}(x)) = \frac{1}{2} [\psi(x), \bar{\psi}(x)].$$

Hence the minus sign in the first equation (Ap. III. 1).

The following equations hold

$$\left. \begin{aligned} & (-\square_x + m^2) T_{\Psi}(x' \cdots | y' \cdots y^{(l)} | z' \cdots) \\ & - (-1)^l \lambda T_{\Psi}(x'' \cdots | x' y' \cdots y^{(l)} | x' z' \cdots) \\ & + I(x') T_{\Psi}(x'' \cdots | y' \cdots y^{(l)} | z' \cdots) \\ & + i \sum_{\xi} \delta(x' - \xi) T_{\Psi}(x'' \cdots; \xi | y' \cdots y^{(l)} | z' \cdots) = 0. \end{aligned} \right\} \text{(Ap. III. 3)}$$

$$\left. \begin{aligned} & (\partial_{y'} + M) T_{\Psi}(x' \cdots | y' \cdots | z' \cdots) \\ & + \lambda T_{\Psi}(x' \cdots y' | y' \cdots | z' \cdots) \\ & + f(y') T_{\Psi}(x' \cdots | y'' \cdots | z' \cdots) \\ & + i \sum_{\zeta} (\pm) \delta(y' - \zeta) T_{\Psi}(x' \cdots | y'' \cdots | z' \cdots; \zeta) = 0. \end{aligned} \right\} \text{(Ap. III. 4)}$$

$$\left. \begin{aligned} & (\bar{\partial}_{z'} + M) T_{\Psi}(x' \cdots | y' \cdots y^{(l)} | z' \cdots) \\ & + \lambda T_{\Psi}(x' \cdots z' | y' \cdots y^{(l)} | z' \cdots) \\ & + g(z') (-1)^l T_{\Psi}(x' \cdots | y' \cdots y^{(l)} | z'' \cdots) \\ & + i \sum_{\eta} (\pm) \delta(\eta - z') T_{\Psi}(x' \cdots | y' \cdots y^{(l)}; \eta | z'' \cdots) = 0. \end{aligned} \right\} \text{(Ap. III. 5)}$$

The (\pm) factors have the same meaning as, f. inst., in (2.25).

One can verify these formulas by induction on the number of space time points. To illustrate: if we apply $i \delta / \delta g(y)$ on (Ap. III.5), we get

$$\left. \begin{aligned} & (\bar{\partial}_{z'} + M) T_{\Psi}(x' \cdots | y y' \cdots y^{(l)} | z' \cdots) \\ & + \lambda T_{\Psi}(x' \cdots z' | y y' \cdots y^{(l)} | z' \cdots) \\ & - g(z') (-1)^l T_{\Psi}(x' \cdots | y y' \cdots y^{(l)} | z' \cdots) \\ & + i \delta(y - z') (-1)^l T_{\Psi}(x' \cdots | y' \cdots y^{(l)} | z'' \cdots) \\ & + i \sum_{\eta \neq y} (\pm) \delta(\eta - z') T_{\Psi}(x' \cdots | y y' \cdots y^{(l)}; \eta | z'' \cdots) = 0. \end{aligned} \right\} \text{(Ap. III. 6)}$$

As the number of nucleon space time points has now increased by one, the third term has the required sign factor. The factor $(-1)^l$ appearing in the fourth term is in accordance with the

convention as regards the value of the parity factor (\pm). Hence, the two last terms in (Ap. III. 6) combine to give a term of the form of the last term in (Ap. III. 5) and we see that (Ap. III. 6) is again of the form (Ap. III. 5).

The above equations have been derived by FREESE [4] for the source-free case by means of other methods.

References.

1. E. E. SALPETER and H. A. BETHE, Phys. Rev. **84**, 1232 (1951).
2. J. SCHWINGER, Proc. Nat. Acad. Sci. **37**, 452 (1951).
3. J. F. DYSON, Phys. Rev. **75**, 486 & 1736 (1949).
4. E. FREESE, Dissertation, Göttingen (1953).
5. W. HEISENBERG, Nachrichten Akad. Wiss. Göttingen **8** (1953);
Zeitschrift für Naturforschung **8 a**, 776 (1953).
6. R. PEIERLS, Proc. Roy. Soc. London A, **214**, 143 (1952).
J. SCHWINGER, Phys. Rev. **82**, 914 (1952).
7. V. FOCK, Z. Physik der Sovj. **75**, 622 (1932).
8. G. KÄLLÉN, Helv. Phys. Acta, **XXV**, 417 (1952).
9. G. C. WICK, Phys. Rev. **80**, 268 (1950).
10. M. GELL-MANN and F. LOW, Phys. Rev. **84**, 350 (1951)
11. E. C. G. STUECKELBERG, Helv. Phys. Acta. **IXX**, 242 (1946); R. P.
FEYNMAN, Phys. Rev. **76**, 749 (1949); M. FIERZ, Helv. Phys.
Acta. **23**, 731 (1950).
12. J. F. DYSON, Phys. Rev. **91**, 421 (1953).

Det Kongelige Danske Videnskabernes Selskab

Matematisk-fysiske Meddelelser, bind **29**, nr. 13

Dan. Mat. Fys. Medd. **29**, no. 13 (1955)

A THEORY OF INTERFERENCE FILTERS

BY

ALFRED HERMANSEN



København 1955

i kommission hos Ejnar Munksgaard

CONTENTS

	Page
§ 1. FRESNEL'S <i>equations for dielectrics and metals</i>	3
§ 2. FRESNEL'S <i>factors for a system of thin layers</i>	11
General equations	13-14
Recurrence formulae	15-16
General theorems	17-18
§ 3. <i>Interference filters with two systems of reflective layers</i>	18
General equations for optical properties in transmission	19-24
General equations for optical properties in reflection	25
The FABRY-PEROT filter ML_2M	26
Calculation of $R, T, \delta, \beta, \sigma, \alpha$, for silver layers	26-32
Calculation of $I(\lambda)$ for filters ML_2M and ML_4M	33-35
Calculation of $R(\lambda)$ for ML_2M and $M'L_2M''$	36-37
The ML_4M filter used as phase plate	38-39
Calculation of $I(\lambda)_s$ and $I(\lambda)_p$ at oblique incidence	39-45
The TURNER frustrated total reflection filter	46
General characteristics of the filter ML_2M	46-47
§ 4. <i>Interference filters with three systems of reflective layers</i>	47
General equations for $I(\lambda)$ and $R(\lambda)$	48-49
Conditions for only one peak in transmission	50
Equations for W_2 and W_{10}	51-52
Calculation of I_{\max}, F, W_2 , etc., for different values of λ	53
Calculation of $I(\lambda)$ for the filters $M'L_2M''L_2M', M'L_4M''L_4M'$ $M''L_2M'L_2M''$ and $M''L_2H_{\frac{1}{2}}L_2M''$	54-62
The filter $M'L_4M''L_4M'$ used as phase plate	62-63
Calculation of $R(\lambda)$ for the filters $M'L_2M''L_2M'$ and $M'L_4M''L_4M'$	64-65
§ 5. <i>Interference filters with four systems of reflective layers</i>	65
General equations for $I(\lambda)$ and $R(\lambda)$	66-68
Conditions for only one peak in transmission	69
Equations for W_2, W_{10} and W_{1000}	70
Calculation of I_{\max}, F, W_2 , etc. for different values of λ	71
Calculation of $I(\lambda)$ for the filters $M'L_2M''L_2M', M'L_4M''L_4M',$ $M''L_2M'L_2M''$ and $M''L_2H_{\frac{1}{2}}L_2H_{\frac{1}{2}}L_2M''$	72-79
The filter $M'L_4M''L_4M''L_4M'$ used as phase plate	80
Calculation of $R(\lambda)$ for the filters $M'L_2M''L_2M''L_2M'$ and $M'L_4M''L_4M''L_4M'$	80-83
§ 6. <i>Improvements of filters with silver layers by means of $\frac{\lambda}{4}$-layers L and H</i>	83
General considerations	83-85
Calculation of optical properties of filters such as $ML'H_2L'M,$ $ML'HLH_2LHL'M$, etc.	85-87
§ 7. <i>Multiple dielectric layer interference filters</i>	87
Calculation of $R_q(180^\circ), R_q(150^\circ), j = \frac{1}{2} \cdot \frac{dy}{dx}$ and W_2 for $r = 0.262$	88-90
Calculation of (λ_s, λ_p) at oblique incidence for the filters $D_6H_2D_6$ and $D_7L_2D_7$ ($\varphi = 15^\circ, 30^\circ, 45^\circ, 60^\circ, 75^\circ$)	91
Calculation of $W_2^{(s)}, W_2^{(p)}$ at $\varphi = 75^\circ$ for the filter $D_7L_2D_7$	91
Summary	92-94
References	95-96

Introduction.

This paper describes the theory of interference filters of various types (especially interference filters with three and four silver layers, § 4 and § 5).

It will be shown how all the optical properties (such as reflectivity, transmission, phase changes at reflection, transmission, etc.) of an interference filter can be exactly calculated when the indices of refraction $\nu - i\kappa$, n and the thicknesses t , d of the different thin layers are known as a function of the wavelength λ ($\nu - i\kappa$ is the index of refraction and t the thickness of a metal layer). Furthermore relations are deduced between the optical constants of the reflective layers which give optimum conditions for the different types of filters.

In a following paper, it will be discussed how it is possible to measure the thicknesses of the dielectric layers on the filter base itself with an accuracy of about 20 \AA and how such a filter can be made by means of the high-vacuum evaporation process for a filter area of $22 \times 22 \text{ cm}$.

§ 1. FRESNEL'S Equations.

Reflection of light from and transmission through a boundary (fig. 1) between two materials 0 and 1 with indices of refraction n_0 and n_1 are determined by FRESNEL'S equations derived from the MAXWELL equations of electrodynamics [1] & [2].

The following notations will be used:

φ angle of incidence, χ angle of refraction, and n index of refraction. s used as index means the component of the electric vector perpendicular to the plane of incidence and p used as index the component parallel to the plane of incidence.

χ is determined by SNELL'S law:

$$n_0 \cdot \sin \varphi = n_1 \sin \chi. \quad (1, 1)$$

If (E_s, E_p) are the components of the electric vector of the incident plane light wave, the components of the electric vector

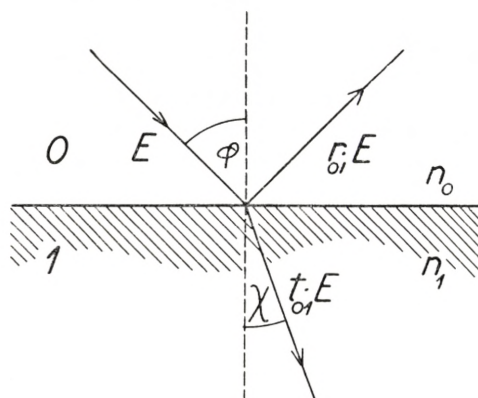


Fig. 1.

φ : Angle of incidence.

χ : Angle of refraction.

E : s or p component of electric vector of incident light wave.

of the reflected light wave $(E_s^{(R)}, E_p^{(R)})$ and of the transmitted wave $(E_s^{(T)}, E_p^{(T)})$ are determined by

$$E_s^{(R)} = E_s \cdot r_s; \quad r_s = \frac{n_0 \cos \varphi - n_1 \cos \chi}{n_0 \cos \varphi + n_1 \cos \chi} \quad (1, 2)$$

$$E_p^{(R)} = E_p \cdot r_p; \quad r_p = \frac{n_1 \cos \varphi - n_0 \cos \chi}{n_1 \cos \varphi + n_0 \cos \chi} \quad (1, 3)$$

$$E_s^{(T)} = E_s \cdot t_s; \quad t_s = 1 + r_s. \quad (1, 4)$$

$$E_p^{(T)} = E_p \cdot t_p; \quad t_p = (1 + r_p) \cdot \frac{n_0}{n_1}. \quad (1, 5)$$

The direction of the light is $0 \rightarrow 1$.

If the direction of the light is the opposite $1 \rightarrow 0$, n_0 must be interchanged with n_1 and φ with χ .

The following relations are satisfied:

$$r_{01} = -r_{10} \quad (1, 6)$$

$$t_{01} \cdot t_{10} - r_{01} \cdot r_{10} = 1 \quad (1, 7)$$

(valid either for the s or the p component).

At a normal angle of incidence ($\varphi = \chi = 0$) only one component of the electric vector is present, and the FRESNEL equations in this special case are the following:

$$r_{01} = \frac{n_0 - n_1}{n_0 + n_1}. \quad (1, 8)$$

$$t_{01} = 1 + r_{01}. \quad (1, 9)$$

Direction of the light: $0 \rightarrow 1$.

(The reason why $r_s = -r_p$ when $\varphi = 0$ is that $E_s = -E_p$ for the incident wave by definition [1]).

All these equations are also valid when the material 1 is absorbent (especially a metal). In this case the index of refraction n_1 is represented by a complex number $n_1 = \nu - i\kappa$ and χ is a complex angle determined by (1, 1).

In accordance with [3] we define $a - ib = n_1 \cos \chi$; from (1, 1) we get $a - ib = \sqrt{(\nu - i\kappa)^2 - n_0^2 \sin^2 \varphi} = i\sqrt{g + i \cdot 2\nu\kappa}$ (with $g = \kappa^2 + n_0^2 \sin^2 \varphi - \nu^2$), and from this equation we then obtain

$$b = \sqrt{\frac{1}{2}(g + \sqrt{g^2 + (2\nu\kappa)^2})}, \quad (1, 10)$$

and

$$a = \frac{\nu\kappa}{b}. \quad (1, 11)$$

By introducing $n_1 \cos \chi = a - ib$ into (1, 2) and (1, 3) the FRESNEL equations can be written as follows:

$$r_s = \varrho_s \cdot e^{i\delta_s} = \frac{1 - \frac{1}{n_0 \cos \varphi} (a - ib)}{1 + \frac{1}{n_0 \cos \varphi} (a - ib)} \quad (1, 12)$$

TABLE 1. Angle of incidence $\varphi = 45^\circ$.

<i>a</i>			<i>b</i>			
$\chi \backslash \nu$	0.1	0.2	$\chi \backslash \nu$	0.0	0.1	0.2
1.0	0.08174	0.16402	1.0	1.2247	1.2234	1.2194
1.5	.09048	.18114	1.5	1.6583	1.6578	1.6561
2.0	.09429	.18865	2.0	2.1213	2.1211	2.1203
2.5	.09623	.19249	2.5	2.5981	2.5979	2.5975
3.0	.09734	.19468	3.0	3.0822	3.0821	3.0819
3.5	.09803	.19605	3.5	3.5707	3.5707	3.5705
4.0	.09847	.19695	4.0	4.0620	4.0620	4.0619
4.5	.09879	.19759	4.5	4.5552	4.5552	4.5551
5.0	.09902	.19803	5.0	5.0498	5.0497	5.0497
5.5	.09918	.19837	5.5	5.5453	5.5453	5.5453
6.0	.09931	.19863	6.0	6.0415	6.0415	6.0415

<i>c</i>			<i>h</i>			
$\chi \backslash \nu$	0.1	0.2	$\chi \backslash \nu$	0.0	0.1	0.2
1.0	0.10893	0.21819	1.0	0.8165	0.8165	0.8166
1.5	.10690	.21378	1.5	1.3568	1.3570	1.3578
2.0	.10476	.20945	2.0	1.8856	1.8858	1.8863
2.5	.10335	.20668	2.5	2.4056	2.4057	2.4061
3.0	.10245	.20490	3.0	2.9200	2.9201	2.9203
3.5	.10185	.20372	3.5	3.4307	3.4307	3.4309
4.0	.10146	.20291	4.0	3.9389	3.9390	3.9391
4.5	.10117	.20232	4.5	4.4455	4.4455	4.4456
5.0	.10096	.20191	5.0	4.9507	4.9508	4.9508
5.5	.10080	.20159	5.5	5.4551	5.4551	5.4551
6.0	.10068	.20134	6.0	5.9588	5.9588	5.9588

$$r_p = \varrho_p \cdot e^{i\delta_p} = - \frac{\left(1 - \frac{\cos \varphi}{n_0} (c - ih)\right)}{\left(1 + \frac{\cos \varphi}{n_0} (c - ih)\right)} \quad (1, 13)$$

with

$$c - ih = \left(\frac{2b^2 - (\chi^2 - \nu^2)}{a^2 + b^2}\right) \cdot a - i \left(\frac{2a^2 + \chi^2 - \nu^2}{a^2 + b^2}\right) \cdot b. \quad (1, 14)$$

If the light wave with the angle of incidence φ coming from air ($n_0 = 1$) is first to pass under the angle of refraction ψ through

TABLE 2. Angle of incidence $\varphi = 60^\circ$.

<i>a</i>			<i>b</i>			
$\varkappa \backslash \nu$	0.1	0.2	$\varkappa \backslash \nu$	0.0	0.1	0.2
1.0	0.07569	0.15192	1.0	1.3229	1.3213	1.3165
1.5	.08664	.17349	1.5	1.7321	1.7313	1.7292
2.0	.09178	.18365	2.0	2.1794	2.1791	2.1780
2.5	.09450	.18904	2.5	2.6458	2.6456	2.6449
3.0	.09608	.19218	3.0	3.1225	3.1224	3.1220
3.5	.09708	.19416	3.5	3.6056	3.6055	3.6052
4.0	.09774	.19548	4.0	4.0927	4.0926	4.0925
4.5	.09820	.19640	4.5	4.5826	4.5825	4.5824
5.0	.09853	.19707	5.0	5.0744	5.0744	5.0743
5.5	.09878	.19756	5.5	5.5678	5.5678	5.5677
6.0	.09898	.19795	6.0	6.0622	6.0622	6.0621

<i>c</i>			<i>h</i>			
$\varkappa \backslash \nu$	0.1	0.2	$\varkappa \backslash \nu$	0.0	0.1	0.2
1.0	0.10809	0.21680	1.0	0.7559	0.7555	0.7542
1.5	.10826	.21658	1.5	1.2990	1.2992	1.2998
2.0	.10625	.21249	2.0	1.8352	1.8355	1.8361
2.5	.10461	.20920	2.5	2.3623	2.3624	2.3628
3.0	.10346	.20692	3.0	2.8823	2.8823	2.8827
3.5	.10268	.20534	3.5	3.3975	3.3976	3.3978
4.0	.10211	.20422	4.0	3.9094	3.9095	3.9096
4.5	.10170	.20341	4.5	4.4189	4.4190	4.4191
5.0	.10141	.20280	5.0	4.9266	4.9267	4.9268
5.5	.10117	.20235	5.5	5.4331	5.4331	5.4332
6.0	.10099	.20199	6.0	5.9385	5.9385	5.9385

a dielectric layer with the index of refraction n (before reaching the boundary) (a, b) and (c, h) will be unchanged as g is unchanged. ($n_0 \cdot \sin \varphi = n \cdot \sin \psi$) and in (1, 12) and (1, 13) we have only to change n_0 to n and $\cos \varphi$ to $\cos \psi$.

In Tables 1—3 (a, b) and (c, h) are given as functions of (ν, \varkappa) with angles of incidence $\varphi = 45^\circ, 60^\circ$, and 75° , respectively, and with $n_0 = 1,0$ (only to be used for silver). From these tables it is apparent that for $\nu < 0.2$ it will be sufficient in most cases to use the approximation:

TABLE 3. Angle of incidence $\varphi = 75^\circ$.

a			b			
$\begin{array}{c} \nu \\ \kappa \end{array}$	0.1	0.2	$\begin{array}{c} \nu \\ \kappa \end{array}$	0.0	0.1	0.2
1.0	0.07202	0.14457	1.0	1.3903	1.3886	1.3834
1.5	.08412	.16846	1.5	1.7841	1.7833	1.7808
2.0	.09006	.18023	2.0	2.2210	2.2206	2.2193
2.5	.09329	.18663	2.5	2.6801	2.6798	2.6791
3.0	.09519	.19041	3.0	3.1517	3.1515	3.1510
3.5	.09640	.19282	3.5	3.6308	3.6307	3.6304
4.0	.09721	.19442	4.0	4.1150	4.1149	4.1147
4.5	.09777	.19555	4.5	4.6025	4.6024	4.6023
5.0	.09819	.19637	5.0	5.0924	5.0923	5.0923
5.5	.09849	.19699	5.5	5.5842	5.5842	5.5841
6.0	.09873	.19746	6.0	6.0773	6.0772	6.0772

c			h			
$\begin{array}{c} \nu \\ \kappa \end{array}$	0.1	0.2	$\begin{array}{c} \nu \\ \kappa \end{array}$	0.0	0.1	0.2
1.0	10677	.21428	1.0	0.7193	0.7185	0.7163
1.5	.10874	.21758	1.5	1.2611	1.2612	1.2616
2.0	.10708	.21415	2.0	1.8010	1.8011	1.8017
2.5	.10538	.21076	2.5	2.3320	2.3321	2.3326
3.0	.10413	.20823	3.0	2.8556	2.8557	2.8560
3.5	.10321	.20641	3.5	3.3739	3.3739	3.3742
4.0	.10256	.20512	4.0	3.8882	3.8883	3.8885
4.5	.10208	.20416	4.5	4.3998	4.3998	4.4000
5.0	.10171	.20344	5.0	4.9092	4.9092	4.9093
5.5	.10144	.20288	5.5	5.4171	5.4171	5.4172
6.0	.10122	.20244	6.0	5.9237	5.9238	5.9238

$$\left. \begin{aligned} b = \sqrt{g}; \quad a = \frac{\nu\kappa}{\sqrt{g}}; \quad h = \frac{\kappa^2}{\sqrt{g}} \quad \text{and} \quad c = \left(2 - \frac{\kappa^2}{g}\right) a \\ (g = \kappa^2 + n_0^2 \sin^2 \varphi). \end{aligned} \right\} \quad (1, 15)$$

In the case of normal incidence ($\varphi = 0$) we obtain

$$r_{01} = \varrho_0 \cdot e^{i\delta_0} = \frac{1 - \left(\frac{\nu}{n_0} - i \frac{\kappa}{n_0}\right)}{1 + \left(\frac{\nu}{n_0} - i \frac{\kappa}{n_0}\right)}. \quad (1, 16)$$

TABLE 4. 180 — δ_0 (in degrees).

$\varkappa \backslash \nu$	0.0	0.1	0.2	0.3
1.0	90.000	89.713	88.850	87.423
1.1	84.547	84.289	83.517	82.235
1.2	79.611	79.380	78.690	77.547
1.3	75.137	74.931	74.317	73.300
1.4	71.075	70.892	70.346	69.444
1.5	67.381	67.218	66.732	65.931
1.6	64.011	63.866	63.435	62.723
1.7	60.931	60.803	60.419	59.785
1.8	58.109	57.995	57.652	57.088
1.9	55.517	55.415	55.109	54.605
2.0	53.130	53.039	52.765	52.314
2.1	50.927	50.845	50.599	50.194
2.2	48.888	48.814	48.594	48.229
2.3	46.997	46.930	46.732	46.403
2.4	45.240	45.180	45.000	44.703
2.5	43.603	43.548	43.386	43.117
2.6	42.075	42.026	41.878	41.634
2.7	40.647	40.601	40.467	40.244
2.8	39.308	39.267	39.144	38.941
2.9	38.051	38.014	37.902	37.716
3.0	36.870	36.836	36.732	36.563
3.1	35.757	35.726	35.632	35.475
3.2	34.708	34.679	34.592	34.449
3.3	33.717	33.690	33.610	33.478
3.4	32.779	32.754	32.680	32.558
3.5	31.891	31.868	31.800	31.686
3.6	31.048	31.027	30.964	30.859
3.7	30.248	30.228	29.170	29.072
3.8	29.487	29.469	29.414	29.324
3.9	28.763	28.746	28.695	28.611
4.0	28.072	28.057	28.009	27.930
4.1	27.414	27.399	27.355	27.281
4.2	26.785	26.771	26.730	26.661
4.3	26.184	26.171	26.132	26.068
4.4	25.609	25.596	25.560	25.500
4.5	25.058	25.046	25.012	24.955
4.6	24.529	24.519	24.487	24.433
4.7	24.023	24.013	23.983	24.932
4.8	23.537	23.527	23.499	23.451
4.9	23.069	23.060	23.033	22.988
5.0	22.620	22.611	22.586	22.544

TABLE 4 (continued).

$z \backslash y$	0.0	0.1	0.2	0.3
5.0	22.620	22.611	22.586	22.544
5.1	22.187	22.179	22.155	22.116
5.2	21.771	21.763	21.741	21.703
5.3	21.370	21.363	21.341	21.305
5.4	20.983	20.976	20.956	20.922
5.5	20.610	20.603	20.584	20.552
5.6	20.249	20.243	20.225	20.194
5.7	19.901	19.895	19.878	19.849
5.8	19.565	19.559	19.543	19.515
5.9	19.239	19.234	19.218	19.192
6.0	18.925	18.920	18.905	18.879

The FRESNEL equations in reflection (1, 12—13—16) are all written in the following manner: $\varrho \cdot e^{i\delta} = \frac{1 - (x - iy)}{1 + (x - iy)}$ (x and y are positive numbers).

The reflectivity is

$$R = \varrho^2 = \frac{1 + x^2 + y^2 - 2x}{1 + x^2 + y^2 + 2x} \quad (1, 17)$$

and the phase change δ at reflection is determined by

$$tg \delta = -\frac{2y}{x^2 + y^2 - 1}. \quad (1, 18)$$

To calculate (ϱ_0, δ_0) at normal incidence and (ϱ_s, δ_s) ; (ϱ_p, δ_p) at oblique incidence, mathematical tables of ϱ (1, 17) and δ (1, 18) as a function of (x, y) would have been of great value.

$$(0 < y < 20 \quad \text{and} \quad 0 < x < 2,0).$$

By calculation of ϱ intervals in x : 0.01 and in y : 0.1 and by calculation of δ intervals in x : 0.1 and in y : 0.01. However, such mathematical tables are not available.

In this paper only a small table of δ as a function of (v, z) is given (Table 4).

When once r is calculated, $t = \xi \cdot e^{i\beta}$ can most easily be calculated from (1, 4—5—9) by means of *A Table for Use in the Addition of Complex Numbers* calculated by JØRGEN RYBNER and K. STEENBERG SØRENSEN [4].

§ 2. "FRESNEL'S FACTORS" for a System of Thin Layers.

We consider a plane infinite incident wave of light; just before it reaches System I fig. 2 the s or p component of the electric vector at the point A we shall denote E_A (complex number).

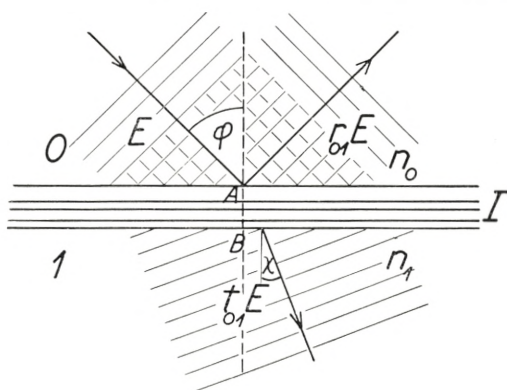


Fig. 2.

A system of thin layers I sandwiched between material 0 and material 1. System I may consist of one or more thin layers, the thickness of each being less than a few wavelengths of light.

E : s or p component of the electric vector.

After reflection from System I the component considered has now at the point A the value $E_A^{(R)}$ and after transmission through System I the value $E_B^{(T)}$ at the point B. We now define the FRESNEL factors (r, t) for the system of thin layers I by the following:

$$r_{01} = \frac{E_A^{(R)}}{E_A} \quad \text{and} \quad t_{01} = \frac{E_B^{(T)}}{E_A}.$$

Direction of light: $0 \rightarrow 1$ and s and p components still considered separately (indices not written).

When the direction of the light is the opposite: $1 \rightarrow 0$ the FRESNEL factors belonging to I are defined by

$$r_{10} = \frac{E_B^{(R)}}{E_B} \quad \text{and} \quad t_{10} = \frac{E_A^{(T)}}{E_B}.$$

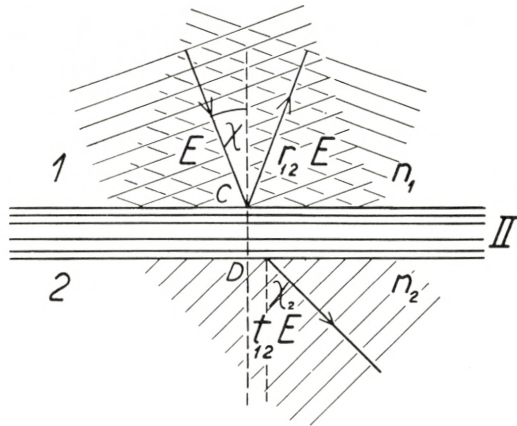


Fig. 3.

Another system of thin layers sandwiched between material 1 and material 2.

Next we consider a second system of thin layers II (fig. 3). The FRESNEL factors of this System II are defined in the same way as for System I by:

$$r_{12} = \frac{E_C^{(R)}}{E_C}; \quad t_{12} = \frac{E_D^{(T)}}{E_C} \quad (\text{direction of light: } 1 \rightarrow 2)$$

and

$$r_{21} = \frac{E_D^{(R)}}{E_D}; \quad t_{21} = \frac{E_C^{(T)}}{E_D} \quad (\text{direction of light: } 2 \rightarrow 1)$$

Now Systems I and II are combined to form a new system of thin layers I + II as shown on fig. 4.

It is now easy to express the FRESNEL factors $r_{02} = \frac{E_A^{(R)}}{E_A}$ and $t_{02} = \frac{E_D^{(T)}}{E_A}$ belonging to I + II by the FRESNEL factors r_{01} , t_{01} ; r_{10} , t_{10} and r_{12} , t_{12} ; r_{21} , t_{21} , belonging to Systems I and II, respectively.

If we consider the oscillations of the plane (infinite) wave which takes place in the layer between Systems I and II, we find by superposition of the wave systems in reflected light at point A directly from fig. 4 (by considering the plane wave front):

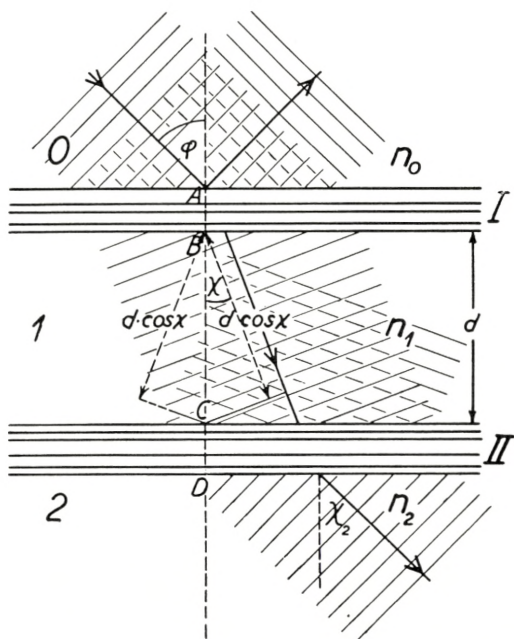


Fig. 4.

System I (fig. 2) and System II (fig. 3) combined to make a new System I + II.
 Material 1 forms a thin layer with thickness d between I and II.

$$\begin{aligned}
 E_A^{(R)} &= E_A \cdot r_{02} = E_A \cdot r_{01} + E_A \cdot t_{01} \cdot e^{-i\frac{x}{2}} \cdot r_{12} \cdot e^{-i\frac{x}{2}} \cdot t_{10} + \\
 &E_A \cdot t_{01} \cdot e^{-i\frac{x}{2}} \cdot r_{12} \cdot e^{-i\frac{x}{2}} \cdot r_{10} \cdot e^{-i\frac{x}{2}} \cdot r_{12} \cdot e^{-i\frac{x}{2}} \cdot t_{10} \\
 + E_A \cdot t_{01} \cdot e^{-i\frac{x}{2}} \cdot r_{12} \cdot e^{-i\frac{x}{2}} \cdot r_{10} \cdot e^{-i\frac{x}{2}} \cdot r_{12} \cdot e^{-i\frac{x}{2}} \cdot r_{10} \cdot e^{-i\frac{x}{2}} \cdot r_{12} \cdot e^{-i\frac{x}{2}} \cdot t_{10} \\
 + \text{etc.} &= E_A \cdot r_{01} + E_A \cdot t_{01} \cdot t_{10} \cdot r_{12} \cdot e^{-ix} \cdot \sum_{m=0}^{\infty} (r_{12} \cdot r_{10})^m \cdot e^{-imx} \\
 &= E_A \left(r_{01} + \frac{t_{01} \cdot t_{10} \cdot r_{12} \cdot e^{-ix}}{1 - r_{12} \cdot r_{10} \cdot e^{-ix}} \right).
 \end{aligned}$$

From which follows:

$$r_{02} = \frac{r_{01} - r_{12} (r_{01} \cdot r_{10} - t_{01} \cdot t_{10}) \cdot e^{-ix}}{1 - r_{12} \cdot r_{10} \cdot e^{-ix}} \quad (2, 1)$$

with

$$x = \frac{2\pi n_1}{\lambda} \cdot 2d \cos \chi = \frac{4\pi dn_1 \cos \chi}{\lambda} \quad (2, 2)$$

(derived directly from fig. 4).

In transmission we find in the same way by superposition of all the plane waves oscillating between I and II:

$$t_{02} = t_{01} \cdot t_{12} \cdot e^{-i\frac{x}{2}} \sum_{m=0}^{\infty} (r_{12} \cdot r_{10})^m \cdot e^{-imx},$$

from which follows:

$$t_{02} = \frac{t_{01} \cdot t_{12} \cdot e^{-i\frac{x}{2}}}{1 - r_{12} \cdot r_{10} \cdot e^{-ix}}. \quad (2, 3)$$

The reflectivity of System I + II (with direction of the incoming light $0 \rightarrow 2$) is

$$R_{02} = r_{02} \cdot \bar{r}_{02} \quad (2, 4)$$

(\bar{r}_{02} means the complex conjugate number of r_{02}).

The transmitted energy through I + II can be derived from POYNING'S theorem of electrodynamics [1] to be

$$T'_{02} = t_{02} \cdot \bar{t}_{02} \cdot \frac{n_2 \cos \chi_2}{n_0 \cos \varphi}, \quad (2, 5)$$

where χ_2 is the angle of refraction in material 2.

To derive r_{20} and t_{20} we only have to interchange the indices 0 and 2 in (2, 1) and (2, 3).

The following relation is valid:

$$\frac{t_{02}}{t_{20}} = \frac{t_{01} \cdot t_{12}}{t_{10} \cdot t_{21}}. \quad (2, 6)$$

The fundamental formulae (2, 1—3) have been developed by ABELÈS [5] in much the same way as here by summing an infinite system of interfering wave systems. Recently, however, ISHIGURO and KATO [6] have developed (2, 1—3) directly from the boundary conditions of electrodynamics by using a matrix representation. This rigorously proves that (2, 1—3) are valid also when material 1 is absorbent, with an index of refraction

$v - i\kappa$. In this case we have to put

$$x = \frac{4\pi}{\lambda} \cdot d(a - ib),$$

where (a, b) are determined by (1, 10–11), and we obtain

$$e^{-ix} = e^{-\frac{4\pi d \cdot b}{\lambda}} \cdot e^{-i \frac{4\pi d \cdot a}{\lambda}}.$$

First we consider a special case of the fundamental equations (2, 1–3), where System I is only a boundary (all layers in

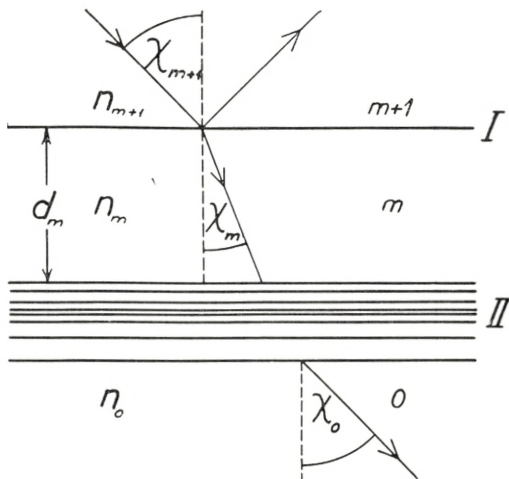


Fig. 5.

The direction of the light is the opposite of that used in fig. 4.

System I have zero thickness) and System II consists of $m - 1$ thin layers (fig. 5). In this special case we obtain from (1, 6–7)

$$r_{m+1, m} = -r_{m, m+1} \quad \text{and} \quad t_{m+1, m} \cdot t_{m, m+1} - r_{m+1, m} \cdot r_{m, m+1} = 1$$

and when this is introduced into (2, 1) and (2, 3) and when the notations $r_{12} = r_{m, 0}$ and $t_{12} = t_{m, 0}$ are used, we get the following fundamental recurrence formulae: (s or p component)

$$r_{m+1, 0} = \frac{r_{m+1, m} + r_{m, 0} \cdot e^{-ix_m}}{1 + r_{m+1, m} \cdot r_{m, 0} \cdot e^{-ix_m}} \quad (2, 7)$$

$$t_{m+1,0} = \frac{t_{m+1,m} \cdot t_{m,0} \cdot e^{-i \frac{x_m}{2}}}{1 + r_{m+1,m} \cdot r_{m,0} \cdot e^{-ix_m}} \quad (2, 8)$$

$$x_m = \frac{4\pi d_m \cdot n_m \cdot \cos \chi_m}{\lambda} \quad (2, 9)$$

$r_{m+1,m}$, $t_{m+1,m}$ are determined by (1, 2—3) (when $n_0 = n_{m+1}$, $n_1 = n_m$, $\chi_{m+1} = \varphi$ and $\chi_m = \chi$ are introduced), i. e.

$$r_{m+1,m}^{(s)} = \frac{n_{m+1} \cdot \cos \chi_{m+1} - n_m \cdot \cos \chi_m}{n_{m+1} \cdot \cos \chi_{m+1} + n_m \cdot \cos \chi_m} \quad (2, 10)$$

$$r_{m+1,m}^{(p)} = \frac{n_m \cdot \cos \chi_{m+1} - n_{m+1} \cdot \cos \chi_m}{n_m \cdot \cos \chi_{m+1} + n_{m+1} \cdot \cos \chi_m} \quad (2, 11)$$

$$t_{m+1,m}^{(s)} = 1 + r_{m+1,m}^{(s)} \quad (2, 12)$$

$$t_{m+1,m}^{(p)} = (1 + r_{m+1,m}^{(p)}) \cdot \frac{n_{m+1}}{n_m} \quad (2, 13)$$

The reflectivity of the system is determined by:

$$R_{m+1,0} = r_{m+1,0} \cdot \bar{r}_{m+1,0}; \quad (2, 14)$$

the energy transmitted through the system is:

$$T'_{m+1,0} = t_{m+1,0} \cdot \bar{t}_{m+1,0} \cdot \frac{n_0 \cos \chi_0}{n_{m+1} \cdot \cos \chi_{m+1}}, \quad (2, 15)$$

and all other optical properties (such as phase change by reflection, transmission, etc.) of a system of m thin layers (absorbent or not) can be calculated when d_m and n_m are known.

From the fundamental formulae (2, 7—15) it is now easy to show that the following relations are valid:

$$\frac{1 + r_{m+1,0}^{(s)}}{t_{m+1,0}^{(s)}} = \frac{1 + r_{m,0}^{(s)} \cdot e^{-ix_m}}{t_{m,0}^{(s)} \cdot e^{-i \frac{x_m}{2}}} \quad (s \text{ and } 0 \text{ components}) \quad (2, 16 a)$$

$$\frac{1 + r_{m+1,0}^{(p)}}{t_{m+1,0}^{(p)}} = \frac{1 + r_{m,0}^{(p)} \cdot e^{-ix_m}}{t_{m,0}^{(p)} \cdot e^{-i \frac{x_m}{2}}} \cdot \frac{n_{m+1}}{n_m} \quad (p \text{ components}) \quad (2, 16 b)$$

and

$$\frac{1 - r_{m+1,0}^{(s)}}{1 + r_{m+1,0}^{(s)}} = \frac{n_m \cdot \cos \chi_m}{n_{m+1} \cdot \cos \chi_{m+1}} \cdot \left(\frac{1 - r_{m,0}^{(s)} \cdot e^{-ix_m}}{1 + r_{m,0}^{(s)} \cdot e^{-ix_m}} \right) \quad (2, 17 a)$$

$$\frac{1 - r_{m+1,0}^{(p)}}{1 + r_{m+1,0}^{(p)}} = \frac{n_{m+1} \cdot \cos \chi_m}{n_m \cdot \cos \chi_{m+1}} \cdot \left(\frac{1 - r_{m,0}^{(p)} \cdot e^{-ix_m}}{1 + r_{m,0}^{(p)} \cdot e^{-ix_m}} \right). \quad (2, 17 b)$$

Further, if the upper layer m (with thickness d_m) is transparent (dielectric layer), we get

$$\left. \begin{aligned} n_{m+1} \cdot \cos \chi_{m+1} \cdot \frac{(1 - \bar{r}_{m+1,0} \cdot r_{m+1,0})}{\bar{t}_{m+1,0} \cdot t_{m+1,0}} = \\ n_m \cdot \cos \chi_m \cdot \frac{(1 - \bar{r}_{m,0} \cdot r_{m,0})}{t_{m,0} \cdot \bar{t}_{m,0}} \end{aligned} \right\} \quad (2, 18 a)$$

(valid both for s and p components).

By means of (2, 14–15) this can be expressed by

$$\frac{1 - R_{m+1,0}}{T'_{m+1,0}} = \frac{1 - R_{m,0}}{T'_{m,0}}, \quad (2, 18 b)$$

i. e. if to a system of thin layers (absorbent or not) is added one or more transparent layers, $\frac{1 - R}{T'}$ remains constant. This theorem has first been proved to be generally valid by F. ABELÈS [7].

For only one layer we deduce from (2, 6) and (2, 10–13)

$$t_{20} = t_{02} \cdot \frac{n_2 \cos \chi_2}{n_0 \cos \chi_0},$$

and by induction we get generally for a system of $m-1$ layers

$$t_{m,0} = t_{0,m} \cdot \frac{n_m \cdot \cos \chi_m}{n_0 \cdot \cos \chi_0}. \quad (2, 19)$$

The transmission through the system is (2, 15)

$$T'_{m,0} = t_{m,0} \cdot \bar{t}_{m,0} \cdot \frac{n_0 \cos \chi_0}{n_m \cos \chi_m} = t_{0,m} \cdot \bar{t}_{0,m} \cdot \frac{n_m \cos \chi_m}{n_0 \cos \chi_0} = T'_{0,m} \quad (2, 20)$$

i. e. at a system of thin layers the transmission remains the same if the direction of the light is reversed. (The layers can be absorbent or not, the material above and below the system of thin layers must not be absorbent). Other general proofs of this theorem have been given by MAYER [2] and ABELÈS [7].

§ 3. Interference Filters with Two Systems of Reflective Layers I and II. (Spec. two silver layers).

An interference filter can very generally be defined as a thin dielectric layer enclosed between two strong reflective systems of thin layers I and II (fig. 6).

We now make the assumption that the reflectivity and the transmission (and phase change by reflection or transmission) of each

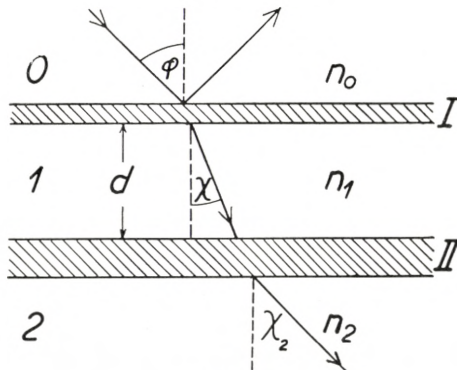


Fig. 6.

of the systems I and II considered separately, only show a small variation with the wavelength (within each spectral region of $\frac{\lambda}{10}$) or expressed more simply: I or II must not be interference filters themselves.

For this simple type of interference filters many general properties can be derived directly from (2, 1—3).

If in (2, 1—3) the following substitutions are made:

$$r_{01} = \sqrt{R_{01}} \cdot e^{i\delta_{01}} \quad r_{10} = \sqrt{R_{10}} \cdot e^{i\delta_{10}} \quad r_{12} = \sqrt{R_{12}} \cdot e^{i\delta_{12}} \quad \text{and}$$

$$t_{01} = \sqrt{T_{01}} \cdot e^{i\beta_{01}} \quad t_{10} = \sqrt{T_{10}} \cdot e^{i\beta_{10}} \quad t_{12} = \sqrt{T_{12}} \cdot e^{i\beta_{12}}$$

(δ is the phase change at reflection and β the phase change at transmission) and if we further introduce

$$\sigma \cdot e^{i\alpha} = 1 - \frac{t_{01} \cdot t_{10}}{r_{01} \cdot r_{10}} = 1 - \sqrt{\frac{T_{01} \cdot T_{10}}{R_{01} \cdot R_{10}}} \cdot e^{i(\beta_{01} + \beta_{10} - \delta_{01} - \delta_{10})}. \quad (3, 1 a)$$

$$\mathbf{R} = \sqrt{R_{10} \cdot R_{12}} \quad (3, 1 b)$$

and

$$y = x - \delta_{10} - \delta_{12}, \quad (3, 1 c)$$

we get the following general formulae:

$$r_{02} = \sqrt{R_{02}(\lambda)} \cdot e^{i\delta_{02}(\lambda)} = \frac{\sqrt{R_{01}} (1 - \sigma \mathbf{R} \cdot e^{-i(y-\alpha)}) e^{i\delta_{01}}}{(1 - \mathbf{R} \cdot e^{-iy})} \quad (3, 2)$$

$$t_{02} = \sqrt{T_{02}(\lambda)} \cdot e^{i\beta_{02}(\lambda)} = \frac{\sqrt{T_{01} \cdot T_{12}} \cdot e^{-i(\frac{x}{2} - \beta_{01} - \beta_{12})}}{(1 - \mathbf{R} \cdot e^{-iy})}. \quad (3, 3)$$

The intensity of the reflected light $R_{02}(\lambda)$ and of the transmitted light $I(\lambda)$ (in proportion to the intensity of the incident light $I_s^{(0)} = 1$ or $I_p^{(0)} = 1$; s and p components are treated separately) are from (3, 2—3) and (2, 4—5) determined to be:

$$R_{02}(\lambda) = \frac{R_{01} (1 - 2 \sigma \mathbf{R} \cdot \cos(y - \alpha) + (\sigma \mathbf{R})^2)}{(1 - 2 \mathbf{R} \cos y + \mathbf{R}^2)} \quad (3, 4)$$

(direction of light: $0 \rightarrow 2$),

and if we define

$$\mathbf{T}_1 = \frac{n_1 \cdot \cos \chi}{n_0 \cos \varphi} \cdot T_{01} \quad \text{and} \quad \mathbf{T}_2 = \frac{n_2 \cdot \cos \chi_2}{n_1 \cos \chi} \cdot T_{12}$$

we get the intensity distribution for the transmitted light

$$I(\lambda) = \frac{\mathbf{T}_1 \cdot \mathbf{T}_2}{1 - 2\mathbf{R} \cos y + \mathbf{R}^2} \quad (3, 5 \text{ a})$$

or written in a more convenient manner

$$I(\lambda) = \frac{\mathbf{T}_1 \cdot \mathbf{T}_2}{(1 - \mathbf{R})^2} \frac{1}{\left(1 + \frac{4\mathbf{R}}{(1 - \mathbf{R})^2} \cdot \sin^2 \frac{y}{2}\right)} \quad (3, 5 \text{ b})$$

($I(\lambda)$ will according to (2, 20) be the same if the direction of the light is reversed).

The wavelengths λ_m at which $I(\lambda)$ reach a maximum are determined by

$$y = 360^\circ (m - 1) \quad m = 1, 2, 3 \dots\dots$$

and the wavelengths $\lambda_{m+\frac{1}{2}}$ at which $I(\lambda)$ becomes a minimum by

$$y = 180^\circ (2m - 1) \quad m = 1, 2, 3 \dots\dots$$

The Determination of $y(\lambda)$ or of $\lambda(y)$.

This determination is important in calculating λ_m and $I(\lambda)$ in the neighbourhood of λ_m .

$$y = \frac{360}{\lambda} \cdot 2 dn_1 \cdot \cos \chi - (\delta_{10} + \delta_{12}) \left\{ \begin{array}{l} \text{(when } y \text{ is mea-} \\ \text{sured in degrees)} \end{array} \right\} \quad (3, 6 \text{ a})$$

or

$$\frac{360 + y}{360} = \frac{1}{\lambda} \cdot \left(2 dn_1 \cos \chi + \frac{(360 - (\delta_{10} + \delta_{12}))}{360} \cdot \lambda \right) \quad (3, 6 \text{ b})$$

δ_{01} and δ_{12} are dependent on the wavelength λ .

We now define

$$Z(\lambda) = \left(\frac{360 - \delta_{10}(\lambda) - \delta_{12}(\lambda)}{360} \right) \cdot \lambda. \quad (3, 7)$$

By introducing $Z(\lambda)$ and λ_m (corresponding to $y = 360 \cdot (m - 1)$) into (3, 6 b) we get the following fundamental equations:

$$m\lambda_m = 2 dn_1 \cdot \cos \chi + Z(\lambda_m) \quad (3, 8)$$

and

$$\frac{360 + y}{360} = \frac{1}{\lambda} (m \cdot \lambda_m + Z(\lambda) - Z(\lambda_m)). \quad (3, 9)$$

If I and II (fig. 6) each consist of only one silver layer, $Z(\lambda)$ will only show a small dependence upon λ (fig. 8 below). If, however, I and II consist of a combination of one silver layer and several quarter wavelength layers of dielectrics with low and high index of refraction or of $\frac{\lambda}{4}$ -dielectric layers alone, the dependence of $\delta_{10} + \delta_{12}$ upon λ in the neighbourhood of λ_m must in each case be calculated by means of (2, 7) and next $y(\lambda)$ by (3, 6 a). (The results of such calculations of $y(\lambda)$ are shown in fig. 49 p. 86 and in fig. 51 p. 90).

From (3, 5—9) we are now able to calculate $I(\lambda)$ in detail. However, it will often be sufficient to describe $I(\lambda)$ by means of the following quantities:

1. The values of λ_m (from (3, 8) or direct from (3, 6 a));
2. The values of

$$I_{\max} = I(\lambda_m) = \frac{\mathbf{T}_1(\lambda_m) \cdot \mathbf{T}_2(\lambda_m)}{(1 - \mathbf{R}(\lambda_m))^2}; \quad (3, 10)$$

3. The contrast factor

$$F = \frac{I_{\max}}{I_{\min}} = \frac{I(\lambda_m)}{I(\lambda_{m+\frac{1}{2}})} = \frac{\mathbf{T}_1(\lambda_m) \cdot \mathbf{T}_2(\lambda_m)}{\mathbf{T}_1(\lambda_{m+\frac{1}{2}}) \cdot \mathbf{T}_2(\lambda_{m+\frac{1}{2}})} \cdot \left(\frac{1 + \mathbf{R}(\lambda_{m+\frac{1}{2}})}{1 - \mathbf{R}(\lambda_m)} \right)^2. \quad (3, 11 a)$$

If R and T with sufficient accuracy are independent of λ (within the wavelength region $\lambda_{m+\frac{1}{2}} < \lambda < \lambda_{m-\frac{1}{2}}$) the contrast factor is simply expressed by

$$F = \frac{I_{\max}}{I_{\min}} = \left(\frac{1 + \mathbf{R}}{1 - \mathbf{R}} \right)^2; \quad (\mathbf{R} = \sqrt{R_{10} \cdot R_{12}}). \quad (3, 11 b)$$

4. The half intensity band width W_2 defined by

$$I\left(\lambda_m \pm \frac{W_2}{2}\right) = \frac{1}{2} \cdot I(\lambda_m)$$

and the tenth intensity band width W_{10} defined by

$$I\left(\lambda_m \pm \frac{W_{10}}{2}\right) = \frac{1}{10} \cdot I(\lambda_m).$$

If we introduce $y = 360^\circ(m-1) + \gamma_k$ (where γ_k is a small angle corresponding to the k 'th intensity band width W_k), we find (from (3, 5 b))

$$I\left(\lambda_m \pm \frac{W_k}{2}\right) = \frac{\mathbf{T}_1 \cdot \mathbf{T}_2}{(1-\mathbf{R})^2} \cdot \frac{1}{\left(1 + \frac{4\mathbf{R}}{(1-\mathbf{R})^2} \sin^2\left(\frac{\gamma_k}{2}\right)\right)}$$

and this is by definition equal to

$$\frac{1}{k} \cdot I(\lambda_m) = \frac{1}{k} \cdot \frac{\mathbf{T}_1 \mathbf{T}_2}{(1-\mathbf{R})^2}.$$

So we obtain

$$\frac{4\mathbf{R}}{(1-\mathbf{R})^2} \sin^2\left(\frac{\gamma_k}{2}\right) = k-1 \quad \text{and} \quad \sin \frac{\gamma_k}{2} = \frac{(1-\mathbf{R})\sqrt{k-1}}{2\sqrt{\mathbf{R}}} \quad (3, 12 a)$$

or approximately

$$\gamma_k = \frac{180}{\pi} \cdot \frac{(1-\mathbf{R})\sqrt{k-1}}{\sqrt{\mathbf{R}}} \quad (3, 12 b)$$

degree.

In the neighbourhood of $\lambda = \lambda_m$ we have approximately

$$y(\lambda) = 360^\circ \cdot \left(m-1-f \cdot \frac{(\lambda-\lambda_m)}{\lambda_m}\right), \quad \text{where } f = -\left(\frac{dy}{d\lambda}\right)_{\lambda=\lambda_m} \cdot \frac{\lambda_m}{360}, \quad (3, 13 a)$$

and as $y = 360 \cdot (m-1) + \gamma_k$ corresponds to $\lambda_m - \lambda = \frac{W_k}{2}$

we obtain $\frac{\gamma_k}{180} = \frac{f \cdot W_k}{\lambda_m}$, and from (3, 12 b) we finally get

$$W_k = \frac{\lambda_m}{f} \cdot \frac{(1 - \mathbf{R})}{\pi \cdot \sqrt{\mathbf{R}}} \cdot \sqrt{1 - k},$$

and in particular we get

$$W_2 = \frac{\lambda_m}{f} \cdot \frac{(1 - \mathbf{R})}{\pi \cdot \sqrt{\mathbf{R}}} \quad (3, 14)$$

and

$$W_{10} = 3 \cdot W_2. \quad (3, 15)$$

When I and II (fig. 6) are silver layers we have approximately $y(\lambda) = 360 \cdot \left(\frac{m \cdot \lambda_m}{\lambda} - 1 \right)$ according to p. 21 and in this case we simply get

$$f = m \quad (m = 1, 2, 3 \dots \dots).$$

In case of filters where I and II (fig. 6) consist of several layers f will be different from an integer.

If the mean reflectivity $\mathbf{R} = \sqrt{R_{10} \cdot R_{12}}$ is increased W_2 (3, 14) will decrease and $F = \frac{I_{\max}}{I_{\min}}$ (3, 11) will increase. However, because of absorption in I and II (fig. 6) I_{\max} (3, 10) will rapidly decrease. If we assume that the absorption in both I and II is $A = (A_{10} = A_{12})$, I_{\max} is expressed by:

$$I_{\max} = \frac{(1 - R_{10} - A)(1 - R_{12} - A)}{(1 - \sqrt{R_{10} \cdot R_{12}})^2}. \quad (3, 16)$$

It is now easy to show that for a definite (constant) value of $\mathbf{R} = \sqrt{R_{10} \cdot R_{12}}$ (i. e. for a definite value of the contrast factor) I_{\max} will reach its highest value when $R_{12} = R_{10} = (\mathbf{R})$ (i. e. when I and II have the same reflectivity; for a definite (constant) value of R_{12} , however, I_{\max} will reach its highest value when $R_{10} = R_{12} \cdot (1 - A)^2$).

From the above considerations it is obvious that one of the greatest problems in producing interference filters is that of finding a material (consisting of one or more thin layers) with a sufficiently high reflectivity R throughout a spectral region of reasonable length (as great as possible).

In most applications an interference filter is used at normal incidence ($\varphi = 0$). A small deviation $\Delta\varphi$ from parallelism of the incident light gives rise to a shift, say $\Delta\lambda_m$, towards violet according to (3, 8). If $\frac{Z(\lambda_m) - Z(\lambda_m + \Delta\lambda_m)}{m}$ is sufficiently small we get

$$5. \quad \Delta\lambda_m = \frac{1}{2} \frac{(\Delta\varphi)^2}{n_1^2} \cdot \left(\lambda_m - \frac{Z(\lambda_m)}{m} \right). \quad (3, 17)$$

However, the dependence of Z upon wavelength often makes this calculation of $\Delta\lambda_m$ more difficult.

At an oblique angle of incidence all the formulae (3, 1–16) must be written separately for s and p components. (3, 8) especially will split up into

$$m \cdot \lambda_m^{(s)} = 2 dn_1 \cos \chi + Z_s(\lambda_m^{(s)}) \quad (3, 18 a)$$

and

$$m \lambda_m^{(p)} = 2 dn_1 \cos \chi + Z_p(\lambda_m^{(p)}). \quad (3, 18 b)$$

Because of the difference in δ_s and δ_p (evident from (1, 12–14)) Z_s and Z_p will usually be unequal and result in a splitting up into two transmission peaks at $\lambda_m^{(s)}$ and $\lambda_m^{(p)}$, respectively, the one polarized perpendicular upon and the other parallel to the plane of incidence.

At an oblique angle of incidence φ a small deviation $\Delta\varphi$ in the angle of incidence will give rise to a shift in wavelength of $\Delta\lambda_m$ determined by means of the derivate of (3, 8):

$$\Delta\lambda_m = - \frac{\left(\lambda_m - \frac{Z(\lambda_m)}{m} \right) \sin 2\varphi}{2 \left(\left(\frac{n}{n_0} \right)^2 - \sin^2 \varphi \right)} \cdot \Delta\varphi \quad (3, 19)$$

(Z regarded as constant and angle of incidence φ in material with index of refraction n_0).

It should be noticed that this is a first order deviation in $\Delta\varphi$ as opposed to (3, 17) at $\varphi = 0$.

The Properties of the Filter (fig. 6) in Reflection.

If no absorption takes place in I and II we have

$$I(\lambda) + R_{02}(\lambda) = 1 \quad (\text{conservation of energy})$$

(in this special case we have $R_{02} = R_{20}$ according to (2, 20)).

From (3, 4—5 a) we get

$$I(\lambda) + R_{02}(\lambda) = \frac{(1-R_{10})(1-R_{12})}{1-2\mathbf{R}\cos y + \mathbf{R}^2} + \frac{R_{01}(1-2\sigma\mathbf{R}\cos(y-\alpha) + (\sigma\mathbf{R})^2)}{1-2\mathbf{R}\cos y + \mathbf{R}^2}$$

with $\mathbf{R} = \sqrt{R_{10} \cdot R_{12}}$.

This will only be equal to 1 if

$$\alpha = 0 \quad \text{and} \quad \sigma = \frac{1}{R_{10}} \left(= \frac{1}{R_{01}} \right) \quad (3, 20)$$

as $\sigma \cdot e^{i\alpha}$ at the same time must satisfy (3, 1 a).

With a thin metal layer (such as *Al* or *Ag*) absorption takes place in I and then α will no longer be zero, but with layers which are almost opaque α will only have a small negative value (less than one degree). In this case we get as a first approximation

$$\sigma = \frac{1-A}{R_{01}} \quad (A \text{ absorption in I}). \quad (3, 21)$$

The condition for obtaining $R_{02}(\lambda) = 0$ at a definite wavelength is (from (3, 4))

$$1 - 2\sigma\mathbf{R}\cos(y-\alpha) + (\sigma\mathbf{R})^2 = 0$$

or

$$\cos(y-\alpha) = \frac{1 + (\sigma\mathbf{R})^2}{2\sigma\mathbf{R}}.$$

This quantity is always ≥ 1 , i. e. $R_{02}(\lambda) = 0$ only if

$$\underline{\sigma\mathbf{R} = 1} \quad (\mathbf{R} = \sqrt{R_{10} \cdot R_{12}}), \quad (3, 22)$$

and this takes place at

$$y = \alpha^\circ + 360^\circ(m-1).$$

If I is not absorbent

$$\sigma R = \frac{1}{R_{10}} \cdot \sqrt{R_{10} \cdot R_{12}} = \sqrt{\frac{R_{12}}{R_{10}}};$$

in this case the condition for zero intensity of $R_{02}(\lambda)$ is $R_{12} = R_{10}$ (it is immaterial whether II is absorbent or not).

If I is absorbent and $R_{10} = R_{12}$ no value of λ exist at which $R_{02}(\lambda) = 0$; however, it is possible to find a value of R_{10} at which the equation (3, 22) is satisfied (as a first approximation we get $R_{01} = (1 - A)^2 \cdot R_{12}$). In this case $R_{02}(\lambda) = 0$ is satisfied at wavelengths determined by $y = \alpha + 360 \cdot (m - 1)$ in combination with (3, 9). The wavelength at which the maximum of transmission occurs is determined by $y = 360 \cdot (m - 1)$. Hence it follows that a small difference results between λ_{\max} in transmission and λ_{\min} in reflection. The same will be the case if $R_{10} = R_{12}$ and I is absorbent.

The FABRY-PEROT Filter $ML_{2m}M$.

The simplest of the types of interference filters treated above is the FABRY-PEROT filter which simply consists of two silver layers M with a dielectric layer L_{2m} in between. (L_{2m} means a $2m \cdot \frac{\lambda}{4}$ layer). The name of this filter originates from the fact that the filter is a Fabry-Perot interferometer with a very small spacing between the reflecting surfaces. The first production and description of filters of this type are due to GEFFCKEN [8].

It is important to note that the filter blank need not be more accurately polished than an ordinary optical surface as the different thin layers all follow the irregularities of the blank. (It is unnecessary to use an interferometer plate as filter blank).

In order to calculate the properties of this filter the first step is to make numerical calculations of R , T , δ , β , σ , α , etc., for silver layers of different thicknesses t and at different wavelengths λ .

The reflectivity R_{∞} and the phase change δ_0 at the boundary between an opaque silver layer and a dielectric with an index of refraction n_0 are determined (at normal incidence) by (1, 17—18) when we put $x - iy = \frac{\nu}{n_0} - i \frac{\nu}{n_0}$. When n_0 increases R_{∞} decreases, which means that only dielectrics with a low index

of refraction can be used for interference filters of the type $ML_{2m}M$. (L means a $\frac{\lambda}{4}$ -layer with *low* index of refraction).

In the numerical calculations (the results of which are given in Tables 6—13) it is assumed that $n = 1.36$ on both sides of the silver layer (fig. 7). In practice one side of the silver layer is bounded by glass (or cement) with $n = 1.5$; the influence upon R_{10} and T will, however, be small as compared with the experimental uncertainty in determining $\nu - i\kappa$. $n_0 = 1.36$ has been chosen because this corresponds to the index of refraction obtained by slow evaporation of cryolite. The index of refraction of MgF_2 too is only slightly higher than 1.36.

The different values of $\nu - i\kappa$ published [2] vary greatly, depending partly upon the conditions by producing the silver layers and partly upon the different optical methods by which $\nu - i\kappa$ is measured. The most reliable values of κ seem to be those published by SCHULZ [9], which were determined by measurements of δ_0 at the boundary between the air and a nearly opaque silver layer. Furthermore from accurate measurements of R and T at nearly opaque silver layers published by KUHN [10] ν can be calculated from $R_\infty = R + T$. We get

$$\nu = \frac{1.02 + \kappa^2}{2} \cdot \left(\frac{1 - R_\infty}{1 + R_\infty} \right)$$

when as a first approximation $\nu^2 = 0.02$ is adopted.

The values of $\nu - i\kappa$ employed in the following numerical calculations are given in Table 5.

TABLE 5.

λ	ν	κ	R_∞
3800	0.20	1.77	0.82
4000	0.18	1.95	0.86
4500	0.14	2.42	0.92
5000	0.14	2.89	0.94
5500	0.15	3.36	0.95
6000	0.15	3.82	0.96
6560	0.13	4.27	0.97
7100	0.14	4.68	0.97
7680	0.15	5.11	0.98

TABLE 6. $\lambda = 4000 \text{ \AA}$ $\nu - i\kappa = 0.18 - i 1.95$.

t in \AA	R	T	A	$\left(\frac{T}{1-R}\right)^2$	$\left(\frac{1+R}{1-R}\right)^2$	$180-\delta^\circ$	β°	σ	$-\alpha^\circ$
150	.1852	.7179	.0969	.7762	2.12	75°13	7°38	4.8495	11°92
200	.2881	.5956	.1163	.6999	3.27	73.44	8.79	3.0427	10.48
250	.3889	.4809	.1302	.6194	5.17	72.16	9.72	2.2145	8.98
300	.4802	.3801	.1397	.5347	8.11	71.23	10.24	1.7719	7.53
350	.5585	.2954	.1461	.4477	12.5	70.56	10.43	1.5118	6.21
400	.6231	.2266	.1503	.3615	18.6	70.11	10.36	1.3489	5.05
500	.7155	.1297	.1548	.2080	36.4	69.61	9.66	1.1706	3.25
550	.7469	.0972	.1559	.1475	47.6	69.49	9.13	1.1211	2.57
600	.7709	.0725	.1566	.1001	59.8	69.42	8.52	1.0865	2.03
∞	.8414	.00	.1586	.00		69.48			

TABLE 7. $\lambda = 4500 \text{ \AA}$ $\nu - i\kappa = 0.14 - i 2.42$.

t in \AA	R	T	A	$\left(\frac{T}{1-R}\right)^2$	$\left(\frac{1+R}{1-R}\right)^2$	$180-\delta$	β	σ	$-\alpha$
150	.2560	.6662	.0778	.8017	2.85	70.29	14.39	3.5903	7.69
200	.3838	.5266	.0896	.7304	5.04	67.08	17.40	2.3613	4.66
250	.4997	.4042	.0961	.6527	9.00	64.64	19.57	1.7997	5.18
300	.5970	.3038	.0992	.5683	15.7	62.84	21.06	1.5012	4.11
350	.6748	.2250	.1002	.4785	26.5	61.54	22.00	1.3271	3.22
400	.7351	.1649	.1000	.3876	42.9	60.62	22.53	1.2191	2.50
500	.8150	.0869	.0981	.2204	96.2	59.57	22.74	1.1031	1.47
∞	.9060	.00	.0940	.00		58.55			

TABLE 8. $\lambda = 5000 \text{ \AA}$ $\nu - i\kappa = 0.14 - i 2.89$.

t in \AA	R	T	A	$\left(\frac{T}{1-R}\right)^2$	$\left(\frac{1+R}{1-R}\right)^2$	$180-\delta$	β	σ	$-\alpha$
150	.3290	.5955	.0755	.7878	3.92	64.56	20.62	2.8009	6.21
200	.4717	.4456	.0827	.7114	7.76	60.35	24.63	1.9374	4.88
250	.5902	.3247	.0851	.6279	15.1	57.29	27.34	1.5439	3.81
300	.6825	.2328	.0847	.5375	28.1	55.12	29.12	1.3363	2.825
350	.7516	.1652	.0832	.4422	49.7	53.61	30.49	1.2160	2.119
400	.8022	.1165	.0813	.3470	83.0	52.56	31.17	1.1422	1.582
500	.8649	.0573	.0778	.1799	190.6	51.35	31.57	1.0644	0.873
∞	.9282	.00	.0718	.00		50.32			

TABLE 9. $\lambda = 5500 \text{ \AA}$ $\nu - i\kappa = 0.15 - i 3.36$.

t in \AA	R	T	A	$\left(\frac{T}{1-R}\right)^2$	$\left(\frac{1+R}{1-R}\right)^2$	$180-\delta$	β	σ	$-\alpha$
150	.4009	.5234	.0757	.7633	5.44	59.11	26.22	2.2978	5.291
200	.5495	.3713	.0792	.6792	11.8	54.29	30.83	1.6697	3.932
250	.6634	.2582	.0784	.5884	24.4	50.95	33.92	1.3847	2.872
300	.7462	.1779	.0759	.4913	47.3	48.67	35.89	1.2349	2.087
350	.8051	.1220	.0729	.3914	85.8	47.13	37.09	1.1488	1.513
400	.8463	.0834	.0703	.2976	144.3	46.10	37.76	1.0965	1.097
500	.8951	.0389	.0660	.1377	326.4	44.94	38.10	1.0422	0.575
∞	.9399	.00	.0601	.00		44.00			

TABLE 10. $\lambda = 6000 \text{ \AA}$ $\nu - i\kappa = 0.15 - i 3.82$.

t in \AA	R	T	A	$\left(\frac{T}{1-R}\right)^2$	$\left(\frac{1+R}{1-R}\right)^2$	$180-\delta$	β	σ	$-\alpha$
150	.4690	.4609	.0701	.7535	7.65	54.47	31.27	1.9771	4.222
200	.6179	.3119	.0702	.6661	17.93	49.28	36.27	1.5007	2.986
250	.7239	.2087	.0674	.5712	38.98	45.82	39.48	1.2853	2.100
300	.7965	.1392	.0643	.4681	77.93	43.54	41.48	1.1726	1.479
350	.8466	.0930	.0604	.3676	144.9	42.03	42.66	1.1082	1.045
400	.8803	.0622	.0575	.2698	246.7	41.04	43.31	1.0693	0.741
500	.9188	.0278	.0534	.1175	558.4	39.96	43.63	1.0296	0.374
∞	.9516	.00	.0484	.00		39.12			

TABLE 11. $\lambda = 6560 \text{ \AA}$ $\nu - i\kappa = 0.13 - i 4.27$.

t in \AA	R	T	A	$\left(\frac{T}{1-R}\right)^2$	$\left(\frac{1+R}{1-R}\right)^2$	$180-\delta$	β	σ	$-\alpha$
150	.5291	.4149	.0560	.7764	10.5	50.86	35.76	1.7811	2.971
200	.6748	.2709	.0543	.6937	26.5	45.40	40.96	1.3991	2.084
250	.7728	.1763	.0509	.6022	60.9	41.87	44.39	1.2265	1.386
300	.8375	.1152	.0473	.5023	127.9	39.59	46.45	1.1364	0.956
350	.8802	.0756	.0442	.3975	246.3	38.10	47.66	1.0850	0.668
400	.9084	.0498	.0418	.2956	434.1	37.14	48.36	1.0542	0.466
500	.9398	.0218	.0384	.1305	1038.3	36.09	48.80	1.0228	0.230
∞	.9654	.00	.0346	.00		35.31			

TABLE 12. $\lambda = 7100 \text{ \AA}$ $\nu - i\kappa = 0.14 - i 4.68$.

l in \AA	R	T	A	$\left(\frac{T}{1-R}\right)^2$	$\left(\frac{1+R}{1-R}\right)^2$	$180-\delta$	β	σ	$-\alpha$
150	.5711	.3739	0550	.7600	13.4	47.63	39.00	1.6518	2.669
200	.7104	.2375	0521	.6726	34.9	42.13	44.34	1.3324	1.770
250	.8004	.1517	0479	.5776	81.4	38.65	47.62	1.1881	1.187
300	.8582	.0977	0441	.4747	171.7	36.43	49.60	1.1128	.808
350	.8957	.0634	0409	.3695	330.3	35.00	50.77	1.0701	.558
400	.9202	.0414	0384	.2691	579.0	34.09	51.41	1.0445	.386
450	.9363	.0271	0366	.1810	924.0	33.50	51.70	1.0286	.269
500	.9470	.0173	.0357	.1066	1349.5	33.11	51.78	1.0180	.182
∞	.9685	.00	.0315	.00		32.38			

TABLE 13. $\lambda = 7680 \text{ \AA}$ $\nu - i\kappa = 0.15 - i 5.11$.

l in \AA	R	T	A	$\left(\frac{T}{1-R}\right)^2$	$\left(\frac{1+R}{1-R}\right)^2$	$180-\delta$	β	σ	$-\alpha$
150	.6100	.3363	.0537	.7436	17.0	44.63	42.01	1.5489	2.384
200	.7419	.2085	.0496	.6527	45.5	39.14	47.34	1.2794	1.543
250	.8241	.1310	.0449	.5544	107.5	35.75	50.54	1.1578	1.017
300	.8756	.0834	.0410	.4498	227.3	33.62	52.44	1.0944	.684
350	.9086	.0537	.0377	.3447	436.1	32.26	53.54	1.0585	.468
400	.9299	.0348	.0353	.2464	757.9	31.39	54.14	1.0370	.321
450	.9438	.0227	.0335	.1632	1196.3	30.82	54.40	1.0237	.223
500	.9530	.0148	.0322	.0997	1726.7	30.46	54.45	1.0153	.155
∞	.9713	.00	0.287	.00		29.78			

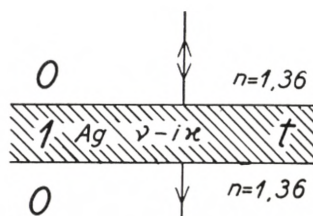


Fig. 7.

Tables 6—13 are calculated by means of (2, 7—9) and (1, 16—18), which in the special case indicated in fig. 7 become:

$$\sqrt{R} \cdot e^{i\delta} = r_{01} \frac{1 - e^{-ix}}{1 - r_{01}^2 \cdot e^{-ix}} \quad (3, 23)$$

$$\sqrt{T} \cdot e^{i\beta} = \frac{(1 - r_{01}^2) e^{-i\frac{x}{2}}}{1 - r_{01}^2 \cdot e^{-ix}} \quad (3, 24)$$

$$r_{01} = \frac{1 - \left(\frac{\nu}{n_0} - i \frac{\varkappa}{n_0} \right)}{1 + \frac{\nu}{n_0} - i \frac{\varkappa}{n_0}} \quad (3, 25)$$

and

$$e^{-ix} = e^{-\frac{4\pi\varkappa t}{\lambda}} \cdot e^{-i\frac{4\pi\nu t}{\lambda}}. \quad (3, 26)$$

To calculate $R(\lambda)$ of a FABRY-PEROT filter we must further calculate $\sigma e^{i\alpha} = 1 - \frac{T}{R} e^{i(2\beta - 2\delta)}$ from the calculated values of (R, δ) and (T, β) .

All these calculations have been carried out directly from (3, 23—26) by means of RYBNER's tables [4].

In the calculations it is assumed that $\nu - i\varkappa$ at a definite wavelength λ is independent of the thickness t of the silver layer.

The formulae (3, 23—26) depend only upon the variable quantities in the combinations $\frac{\nu(\lambda) - i\varkappa(\lambda)}{n_0}$ and $\frac{\nu(\lambda) - i\varkappa(\lambda)}{\lambda} t$.

If the index of refraction n_0 is changed to n' the tables can still be used if the λ scale is changed to λ' and the t scale to t' ; the transformation is determined by

$$\frac{\nu(\lambda') - i\varkappa(\lambda')}{n_0} = \frac{\nu(\lambda) - i\varkappa(\lambda)}{n'} \quad \text{and} \quad \frac{\nu(\lambda') - i\varkappa(\lambda')}{\lambda'} t' = \frac{\nu(\lambda) - i\varkappa(\lambda)}{\lambda} t,$$

i. e. $t' = \frac{n'}{n_0} \cdot \frac{\lambda'}{\lambda} \cdot t$, and if approximately $\nu(\lambda) - i\varkappa(\lambda) = (k_1 - ik_2) \cdot \lambda$,

then $\lambda' = \frac{n_0}{n'} \cdot \lambda$ and $t' = t$. (This will be a good approximation for δ because it only slightly depends upon ν).

From Tables 6—13 graphs of $Z(\lambda, t) = \left(\frac{180 - \delta_0(\lambda, t)}{180} \right) \cdot \lambda$ can be made for different thicknesses t of the silver layers (fig. 8).

If the filter consists of two silver layers of different thicknesses t' and t''

$$Z_{\text{res}} = \frac{360 - \delta_0(t') - \delta_0(t'')}{360} = \frac{1}{2}(Z(\lambda_1, t') + Z(\lambda_1, t'')).$$

These graphs (fig. 8) are important because it is possible when $Z(\lambda)$ is known to determine the optical thickness nd which

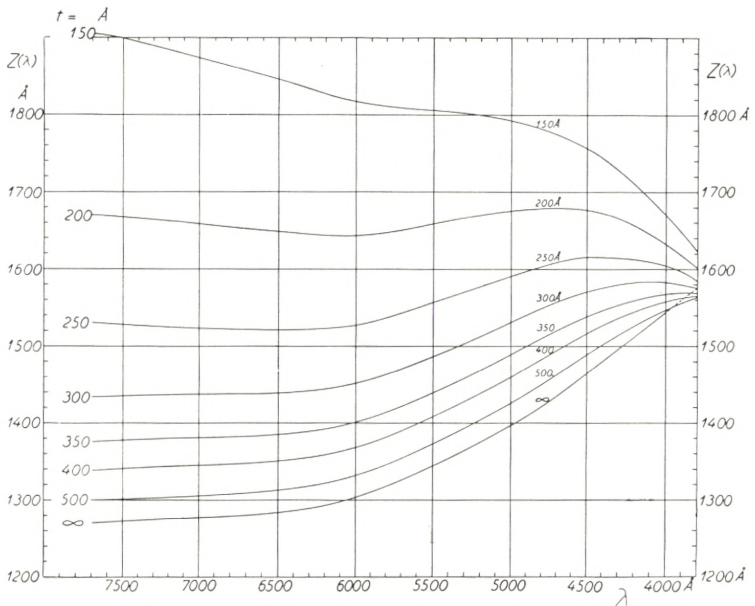


Fig. 8.

corresponds to a definite λ_m . (From (3, 8)). Inversely, if λ_m are measured spectroscopically and d is measured for one definite wavelength, $Z(\lambda)$ can be determined directly by experiment. (This has been done by SCHULZ [9]; with $n = 1$ this gives a determination of $\kappa(\lambda)$).

The half intensity band width W_2 has not been calculated in the tables for each t, λ value. For this reason a table of

$$W_2(R) = \frac{(1-R) 5500}{\pi \sqrt{R} \cdot 2}$$

is added (Table 14) corresponding to a filter with $\lambda_m = 5500 \text{ \AA}$ and $m = 2$. From this table W_2' corresponding to another λ_m

can easily be calculated by means of

$$W_2'(R) = W_2(R) \cdot \frac{\lambda_m}{m \cdot 2750}.$$

TABLE 14.

R	W_2 in Å	R	W_2 in Å	R	W_2 in Å
0.75	252.7	0.84	152.8	0.93	63.5
.76	241.0	.85	142.4	.94	54.2
.77	229.4	.86	132.2	.95	44.9
.78	218.0	.87	122.0	.96	35.7
.79	206.8	.88	112.0	.97	26.7
.80	195.7	.89	102.1	.98	17.7
.81	184.8	.90	92.3	.99	8.8
.82	174.0	.91	82.6		
.83	163.3	.92	73.0		

When R , T , $y(\lambda)$ are calculated it is possible to calculate line shapes at different wavelengths and thicknesses of the silver layers. In all the following graphs it has simply been chosen to calculate the wavelength scale by means of (3, 9) with the approx. $Z(\lambda) = Z(\lambda_m)$. If $y = 360 \cdot (m - 1) + \gamma$ (γ a small angle), we get:

$$\lambda = \frac{360 m \cdot \lambda_m}{360 m + \gamma}, \quad (3, 27 a)$$

and this combined with (3, 5 b)

$$I(\lambda) = \frac{T^2}{(1 - R)^2} \frac{1}{\left(1 + \frac{4R}{(1 - R)^2} \sin^2 \frac{\gamma}{2}\right)} \quad (3, 27 b)$$

determines the intensity distribution in the neighbourhood of a peak.

Furthermore R and T of the silver layers are regarded as constant in all the following graphs throughout the spectral region considered in the graphs. If the variation of R , T , etc., upon wavelength within the line were taken into account, the calculations would be rather tedious and only result in deviations in

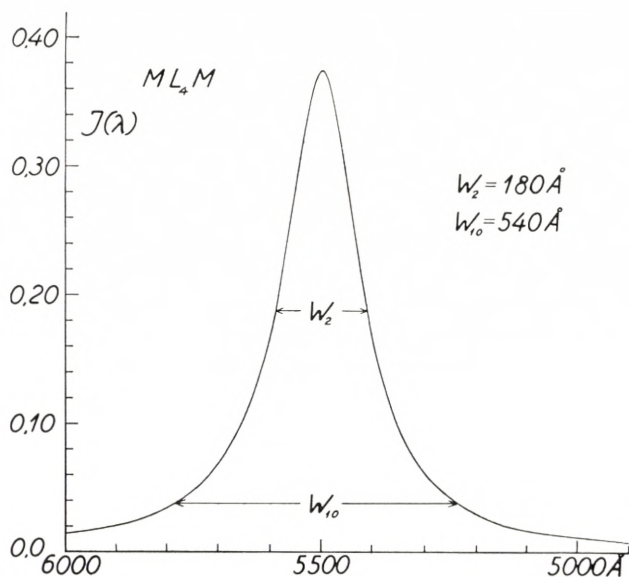


Fig. 9.

2nd order filter. W_2 calculated from (3,14) is 181 \AA and $W_{10} = 3 \cdot W_2 = 543 \text{ \AA}$
 $\nu - i\kappa = 0.15 - i 3.36$.

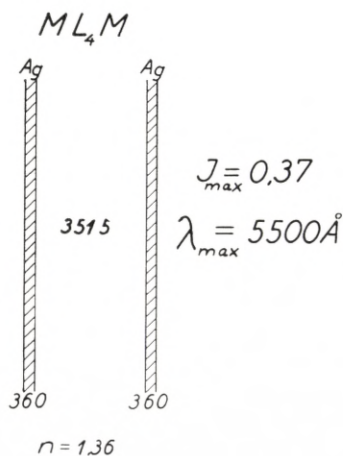


Fig. 10.

(All measures in \AA).

FABRY-PEROT filter 2nd order. The peak of the 1st order is at about 10800 \AA and the peak of the 3rd order at about 3750 \AA . The line shape (2nd order) is shown in fig. 9.

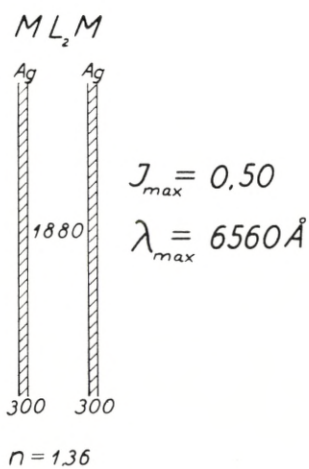
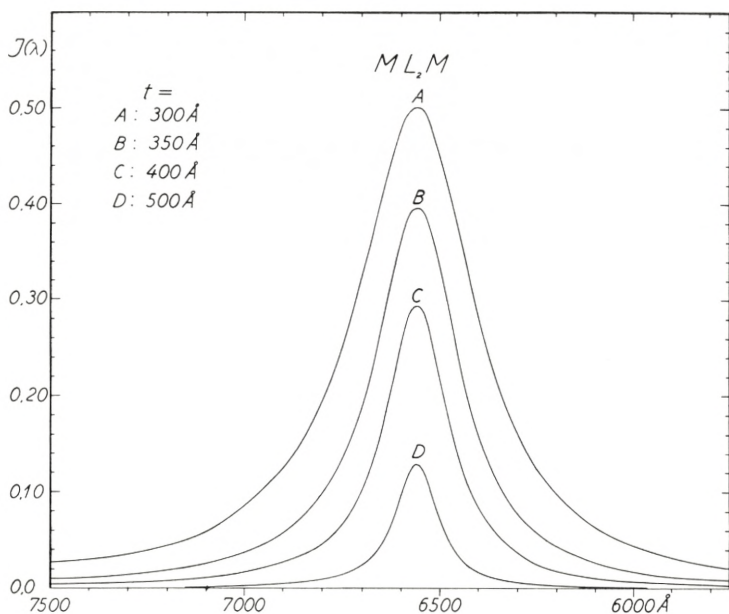


Fig. 12.
 1st order filter ($m = 1$) (the peak of the 2nd order is at 3400 Å).
 (Curve A in fig. 11).

the "wings" of the line and even here the effect is small as compared with the experimental uncertainty in $\nu - i\kappa$. The deviations will be the greatest for a filter of the first order.

In fig. 9 is shown the line shape of a FABRY-PEROT filter of the 2nd order, and fig. 10 shows the relative thicknesses of the thin layers. In fig. 11 line shapes have been calculated with different thicknesses t of the silver layers and with peak transmission at 6560 Å. The rapid decrease in I_{\max} with increasing t is apparent.

Furthermore is it possible to calculate $R(\lambda)$ for a filter of the type ML_2mM by means of (3, 2) or (3, 4). (3, 2) becomes

$$R(\lambda) = \frac{R \cdot |1 - \sigma \mathbf{R} \cdot e^{-i(y-\alpha)}|^2}{|1 - \mathbf{R} \cdot e^{-iy}|^2}; \quad (R = \mathbf{R}). \quad (3, 28)$$

The wavelength scale is calculated by means of (3, 27 a). Fig. 13 and in fig. 14 show the results of such calculations of the intensity distribution $R(\lambda)$ in reflected light (at normal incidence).

In fig. 13 the same filter is considered as in fig. 11 Curve C in transmission. (Each silver layer has a thickness of 400 Å;

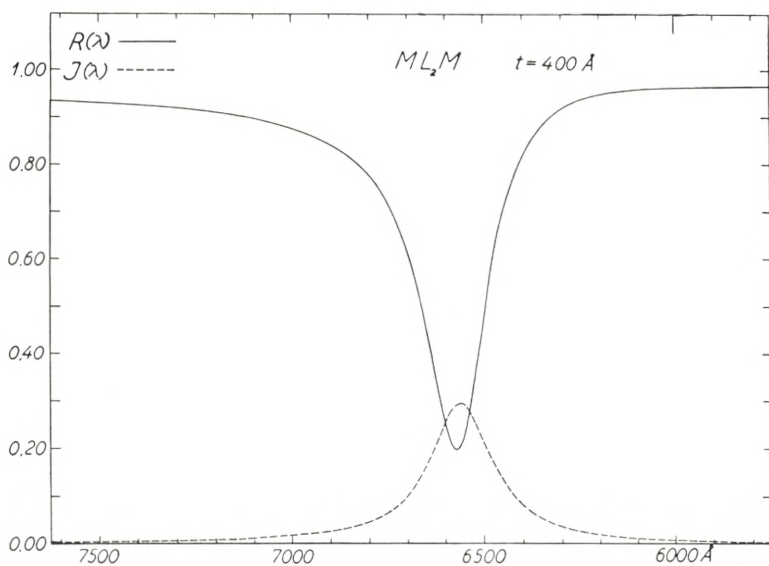


Fig. 13.
 $R(\lambda)$ and $I(\lambda)$ for a FABRY-PEROT filter with the silver layers of equal thickness ($t = 400 \text{ \AA}$).

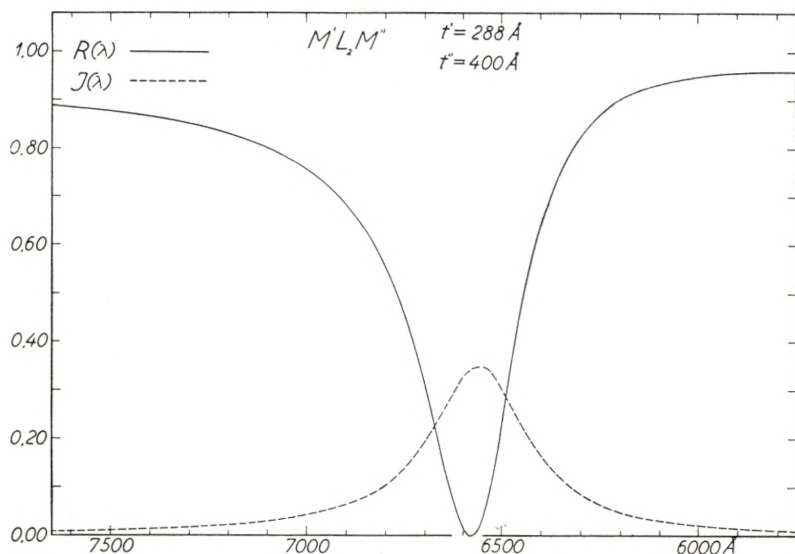


Fig. 14.

$R(\lambda)$ and $I(\lambda)$ for a FABRY-PEROT filter. The silver layers are of unequal thickness ($t'' = 400 \text{ \AA}$ and $t' = 288 \text{ \AA}$) t' is determined in such a way that $\sigma \mathbf{R} = 1$; ($\mathbf{R} = \sqrt{R' \cdot R''}$).

$R = 0.908$). The small negative value of $\alpha = -0^{\circ}.466$ (Table 11) gives rise to an asymmetric line shape of $R(\lambda)$. Furthermore it should be noted that the minimum value of $R(\lambda)$ turns out to be as high as 0.20 and the minimum is found at a wavelength a little higher than the wavelength at which $I(\lambda)$ has a maximum in transmission.

In fig. 14 a filter $M'L_2M''$ is considered with the two silver layers of unequal thickness. $t'' = 400 \text{ \AA}$ and $t' = 288 \text{ \AA}$ is determined in such a way (from Table 11) that $\sigma \mathbf{R} = 1$; $\mathbf{R} = \sqrt{R' \cdot R''} = 0.864$ (the reflection takes place from the t' side of the filter), $R(\lambda) = 0$ at $y = \alpha = -1^{\circ}.060$ (see page 25). This calculation shows that it is possible to extinguish a spectral line by means of a reflection interference filter. $I_{\max} = 0.34$ ($I_{\max} = 0.45$ of a filter with the two silver layers of equal thickness and with a reflectivity equal to the mean reflectivity of the filter in fig. 14. $R = \sqrt{R' \cdot R''} = 0.86$).

Reflection interference filters with an opaque metal layer at the bottom (e. g. aluminium) have first been treated in theory

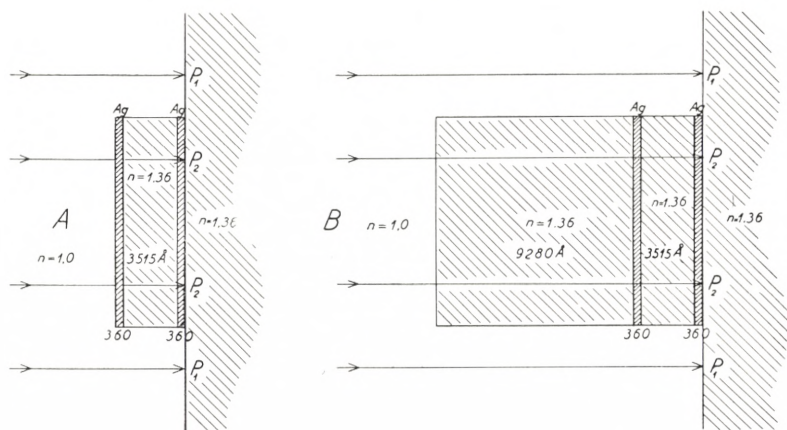
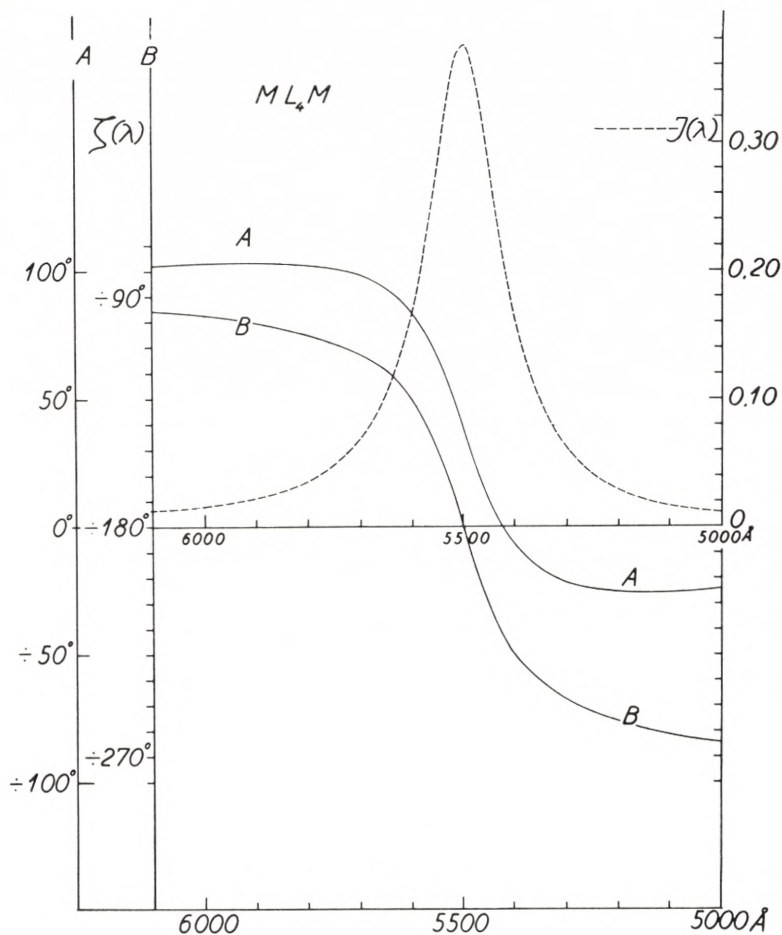


Fig. 15.

A FABRY-PEROT interference filter used as phase plate. Unbroken lines: A. The filter is on one side bounded by air. B. To the filter is added a thin dielectric layer in such a way that the phase difference at the peak is -180° . Broken line: $I(\lambda)$ for the filter (the same as the filter in fig. 10).

and practice by HADLEY and DENNISON [11]. These reflection filters have the great advantage of also being applicable to the infrared and ultraviolet spectral region, but have the disadvantage that rather broad spectral regions are reflected.

By means of (3, 2—3) and RYBNER'S tables [4] it is furthermore easy to calculate the phase change at reflection and transmission, as a function of the wavelength, in the neighbourhood of a peak. As the phase change at transmission by interference filters is of special interest in the phase contrast microscope as shown by LOCQUIN [12], a calculation has been made in the case of the filter in fig. 10. The results are given in fig. 15. In the case of *A* the phase difference between P_2 (light passing through the phase plate) and P_1 (light passing outside the phase plate) is (from (3, 3))

$$\zeta(\lambda) = \left((\beta_{01} + \beta_{12}) - \frac{360}{\lambda} \cdot nd - \varepsilon(\lambda) \right) + \frac{360}{\lambda} (2t + d); \quad (3,29)$$

t is the thickness of the silver layers and $\varepsilon(\lambda)$ is determined from $\varrho \cdot e^{i\varepsilon(\lambda)} = 1 - \mathbf{R} \cdot e^{-i\vartheta}$. — The phase changes at transmission through the silver layers are determined from Table 9. The approximations $\beta_{01} = \beta_{12} = \beta$ and $\beta = \beta_0 - k \cdot \lambda$ have been made. If, as in the case of *B* (fig. 15), a thin dielectric layer (with index of refraction n and thickness d_1) is added to the phase plate, the phase difference $-\frac{360}{\lambda} \cdot (n-1) \cdot d_1$ has to be added to $\zeta(\lambda)$ in (3, 29). In fig. 15 curve *B*, d_1 is determined in such a way that the phase difference is -180° at $\lambda_m = 5500 \text{ \AA}$. The graphs correspond very closely to those previously published by DUFOUR [13]. By the use of a combination of the type *B* (fig. 15) it is possible to change from a negative to a positive contrast of the image by a variation of wavelength.

Calculation of $I(\lambda)_s$ and $I(\lambda)_p$ at an Oblique Angle of Incidence.

When the angle of incidence φ is increased from $\varphi = 0$, a shift of λ_m towards violet, and a splitting up in two components $\lambda_m^{(s)}$ and $\lambda_m^{(p)}$ result. The first problem now is to calculate $\lambda_m^{(s)}$, $\lambda_m^{(p)}$ when $\lambda_m^{(0)}$, $n(\lambda)$ and $\nu(\lambda) - i\kappa(\lambda)$ are known. The calculation

is carried out by means of (3, 18):

$$m \cdot \lambda_m^{(s)} = 2 dn \cos \chi + Z_s(\lambda_m^{(s)}),$$

where

$$Z_s(\lambda_m^{(s)}) = \left(\frac{360 - \delta_{10}^{(s)}(\lambda_m^{(s)}) - \delta_{12}^{(s)}(\lambda_m^{(s)})}{360} \right) \cdot \lambda_m^{(s)}$$

(and analogous equations for the p component).

A first approximation of $\lambda_{\frac{p+s}{2}}^{(1)} = \frac{\lambda_m^{(s)} + \lambda_m^{(p)}}{2}$ can be calculated by means of (3, 8) $m \cdot \lambda_{\frac{p+s}{2}}^{(1)} = 2 dn \cos \chi + Z_0(\lambda_m^{(0)})$ with $2 dn = m \lambda_m^{(0)} - Z_0(\lambda_m^{(0)})$, ($\lambda_m^{(0)}$ corresponds to λ_m at $\varphi = 0$ and $Z_0(\lambda_m^{(0)})$ is determined from fig. 8) and a second approximation $\lambda_{\frac{p+s}{2}}^{(2)}$ by $m \cdot \lambda_{\frac{p+s}{2}}^{(2)} = 2 dn \cos \chi + Z_0\left(\lambda_{\frac{p+s}{2}}^{(1)}\right)$ and perhaps a third approximation has to be determined (by means of (3, 8) and fig. 8).

Now it is evident from Table 4 that δ (and $Z = \frac{180 - \delta}{180} \cdot \lambda$) only show a small dependence upon ν when as at silver $\nu < 0.2$. For this reason $\frac{Z_0(\lambda)}{\lambda}$ (fig. 8) can be regarded as a function of $\frac{\varkappa(\lambda)}{n}$ and $\frac{\varkappa(\lambda) \cdot t}{\lambda}$ only: $\frac{Z_0(\lambda, t)}{\lambda} = F\left(\frac{\varkappa(\lambda)}{n}, \frac{\varkappa(\lambda) \cdot t}{\lambda}\right)$.

At oblique incidence we have (1, 12—13)

$$\frac{Z_s(\lambda, t)}{\lambda} = F\left(\frac{b}{n \cos \chi}, \frac{b \cdot t}{\lambda}\right) \quad \text{and} \quad \frac{Z_p(\lambda, t)}{\lambda} = F\left(\frac{h \cos \chi}{n}, \frac{b \cdot t}{\lambda}\right).$$

A first approximation of Z_s and Z_p can now be determined by means of fig. 8 if (λ, t) are transformed to (λ', t') by means of the equations

$$\frac{\varkappa(\lambda'_s)}{n} = \frac{b\left(\lambda_{\frac{p+s}{2}}\right)}{n \cdot \cos \chi}; \quad \frac{\varkappa(\lambda'_s) \cdot t'_s}{\lambda'_s} = \frac{b\left(\lambda_{\frac{p+s}{2}}\right) \cdot t}{\lambda_{\frac{p+s}{2}}}$$

and

$$\frac{\varkappa(\lambda'_p)}{n} = \frac{h\left(\frac{\lambda_{p+s}}{2}\right)}{n} \cdot \cos \chi; \quad \frac{\varkappa(\lambda'_p)}{\lambda'_p} \cdot t'_p = \frac{b\left(\frac{\lambda_{p+s}}{2}\right) \cdot t}{\frac{\lambda_{p+s}}{2}};$$

(λ'_s, t'_s) are then determined by

$$\varkappa(\lambda'_s) = \frac{b(\lambda)}{\cos \chi}; \quad t'_s = \frac{\lambda'_s}{\lambda} \cdot t \cdot \cos \chi \tag{3, 30}$$

and

$$(\lambda'_p, t'_p) \text{ by } \varkappa(\lambda'_p) = h(\lambda) \cdot \cos \chi; \quad t'_p = \frac{\lambda'_p}{\lambda} \cdot \frac{b(\lambda) \cdot t}{\varkappa(\lambda'_p)} \tag{3, 31}$$

(where $\lambda = \frac{\lambda_{p+s}}{2}$).

From (λ'_s, t'_s) we now determine $Z_0(\lambda'_s, t'_s)$ from fig. 8 and we then get $Z_s\left(\frac{\lambda_{p+s}}{2}\right) = \frac{\lambda_{p+s}}{\lambda'_s} \cdot Z_0(\lambda'_s, t'_s)$. Finally λ_s is determined by $m\lambda_s = 2dn \cos \chi + Z_s\left(\frac{\lambda_{p+s}}{2}\right)$ and λ_p is determined in quite an analogous way. $b(\lambda)$, $h(\lambda)$ are determined from Tables 1—3 corresponding to $\varkappa = \varkappa\left(\frac{\lambda_{p+s}}{2}\right)$. ($\lambda_0 = \lambda_m^{(0)}$; $\lambda_s = \lambda_m^{(s)}$ and $\lambda_p = \lambda_m^{(p)}$).

Now the same calculation must be repeated with λ_s instead of λ in (3, 30) and λ_p instead of λ in (3, 31) and a further repetition may be necessary if (λ_s, λ_p) deviate more than 20 Å from the previous approximation (for a filter of the first order).

Above, the index of refraction n of the dielectric has been regarded as independent of the wavelength and equal for both the s and p component. However, dispersion as well as birefringence can easily be taken into account in the formulae (3, 30—31) if necessary.

When λ_s and λ_p have been calculated in the way mentioned above, line shapes can be calculated by (3, 27) when first the s and p components of R and T have been calculated by means of (1, 12—13) and (3, 23—24) (with $x = \frac{4\pi t}{\lambda}(a - ib)$).

To show the applicability of the above procedure calculations (for different φ) have been made in the case of a FABRY-PEROT filter (1st order) with $\lambda_0 = 6560 \text{ \AA}$, $t = 350 \text{ \AA}$ and $n = 1.36$.

(At $\varphi = 0$ the line shape of this filter is seen in fig. 11 Curve B). The different approximations before reaching the correct values of λ_s and λ_p are shown in Table 15 and the line shapes in figs. 16—18.

TABLE 15. ($\lambda_0 = 6560 \text{ \AA}$)

φ	15°	30°	45°	60°	75°	
From fig. 8	$\left\{ \begin{array}{l} \frac{\lambda_{s+p}^{(1)}}{2} \dots\dots \\ \frac{\lambda_{s+p}^{(2)}}{2} \dots\dots \\ \frac{\lambda_{s+p}^{(3)}}{2} \dots\dots \end{array} \right.$	6466	6198	5836	5375	5028 Å
		6466	6206	5833	5440	5139
		5833	5435	5120
From fig. 8 and (3,30—31)	$\left\{ \begin{array}{l} \lambda_s^{(1)} \dots\dots \\ \lambda_p^{(1)} \dots\dots \\ \lambda_s^{(2)} \dots\dots \\ \lambda_p^{(2)} \dots\dots \end{array} \right.$	5632	5106	4695
		6047	5760	5624
		5647	5135	4730
		6038	5770	5565
Directly from (3,23—24)	$\left\{ \begin{array}{l} \lambda_s^{(3)} \dots\dots \\ \lambda_p^{(3)} \dots\dots \end{array} \right.$	5642	5130	4720
		6039	5770	5580
Calculated from (3,32)	$\left. \right\} \text{“}n\text{”} \dots$	1.534	1.542	1.553	1.556	1.559

HADLEY and DENNISON [11 a] have used an approximate formula to enable a direct calculation of n from measurements of $\lambda_{\frac{p+s}{2}} = \frac{\lambda_p + \lambda_s}{2}$ at oblique incidence.

From (3, 6 a)

$$\frac{360}{\lambda_0} \cdot 2 dn - 2 \delta_0(\lambda_0) = 360 (m - 1)$$

and

$$180 \cdot \left(\frac{1}{\lambda_s} + \frac{1}{\lambda_p} \right) \cdot 2 dn \cdot \cos \chi - (\delta_s(\lambda_s) + \delta_p(\lambda_p)) = 360 (m - 1)$$

they get

$$\frac{360}{\lambda_0} \cdot 2 dn = \frac{360}{2} \left(\frac{1}{\lambda_s} + \frac{1}{\lambda_p} \right) \cdot 2 dn \cos \chi + 2 \delta_0 - (\delta_s + \delta_p).$$

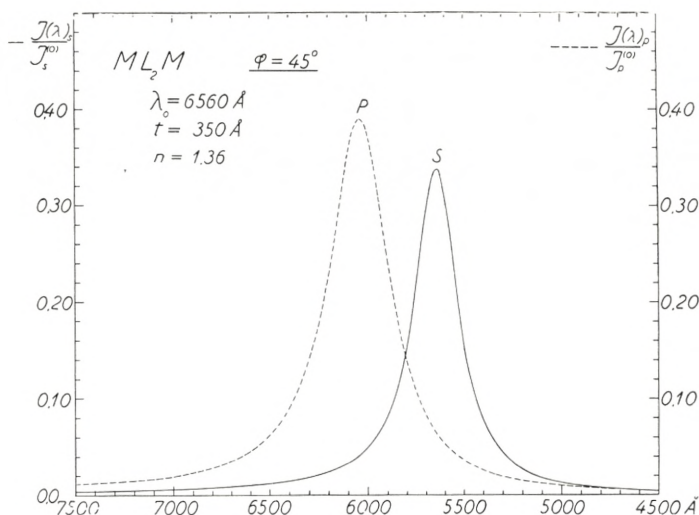


Fig. 16.

Then the approximation $2\delta_0(\lambda_0) = \delta_s(\lambda_s) + \delta_p(\lambda_p)$ is introduced and the following formula results:

$$\cos \chi = \frac{\lambda_{s+p}}{\lambda_0}$$

or

$$n = \frac{\sin \varphi}{\sqrt{1 - \left(\frac{\lambda_{p+s}}{\lambda_0}\right)^2}} \left(\text{with } \frac{1}{\frac{\lambda_{p+s}}{2}} = \frac{1}{\lambda_p} + \frac{1}{\lambda_s} \approx \frac{1}{\frac{\lambda_p + \lambda_s}{2}} \right). \quad (3, 32)$$

If this approximation should be useful then n calculated from (3, 32) by substituting the (λ_s, λ_p) values from Table 15 should turn out to be about 1.36. However, as shown below in Table 15 “ n ” calculated from (3, 32) is as high as 1.55. This shows that the approximation (3, 32) cannot be used (by filters of lower order) and this explains why HADLEY and DENNISON [11a] find values of n much too high. λ_s and λ_p are not only dependent upon λ_0 (at $\varphi = 0$), n and φ but also upon $\varkappa(\lambda)$, and this will particularly be the case for a filter of the first order ($m = 1$) as shown in figs. 16–18. At higher orders ($m \simeq 8-10$) the splitting up $\lambda_p - \lambda_s$ is m times smaller, and the error in $\frac{\lambda_{p+s}}{2}$ in using

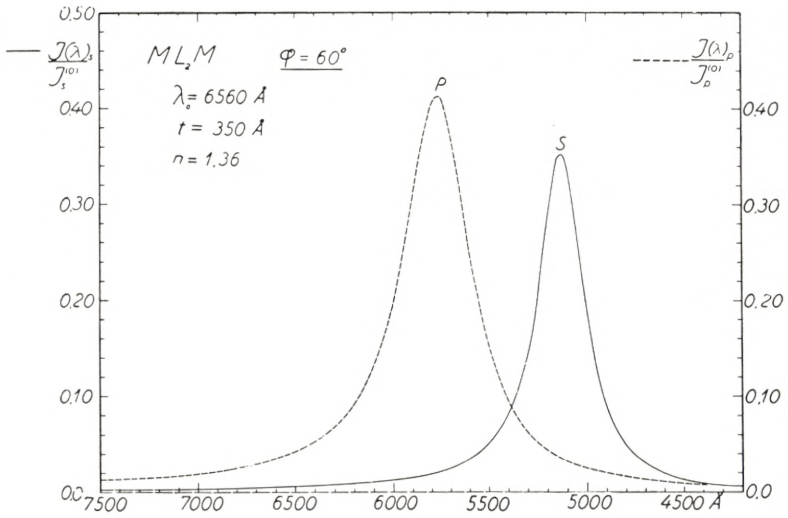


Fig. 17.

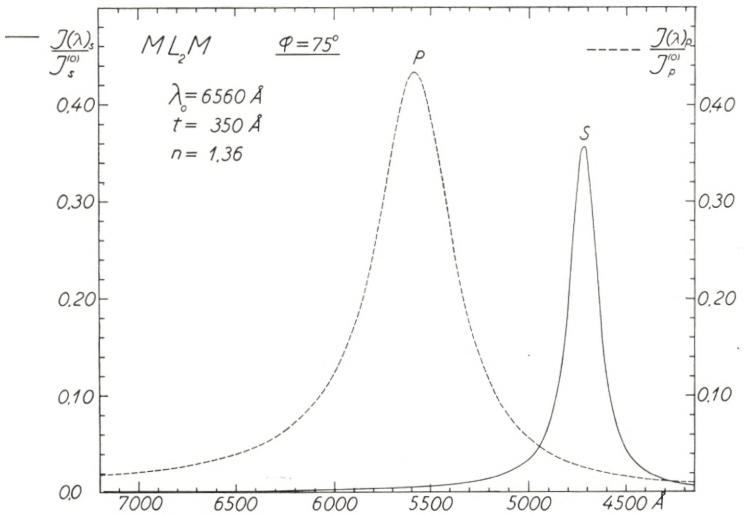


Fig. 18.

the approximation $\delta_0(\lambda_0) = \frac{\delta_s(\lambda_s) + \delta_p(\lambda_p)}{2}$ is m times smaller; in this case λ_s and λ_p will be nearly independent of $\varkappa(\lambda)$ and (3, 32) can be employed with a tolerable approximation.

(λ_s, λ_p) can easily be measured by a spectroscope at various

angles of incidence and we hereby obtain information on $n(\lambda)$ and $\varkappa(\lambda)$ (especially for a filter of the first order). Moreover, determinations of W_2 and I_{\max} by means of a spectrophotometer fix R and T of the silver layers.

If the incident light is unpolarized and has the intensity $I_0 = 2 \cdot I_s^{(0)} = 2 \cdot I_p^{(0)}$, $I(\lambda)$ of the transmitted light is

$$I(\lambda) = \frac{I_0}{2} \left(\frac{I(\lambda)_s}{I_s^{(0)}} + \frac{I(\lambda)_p}{I_p^{(0)}} \right)$$

(the ordinates of the s and p curves of figs. 16—18 have to be added together and divided by 2).

The degree of polarization (the s direction compared with the p direction) will at the wavelength λ_s be $\frac{I(\lambda_s)_s}{I(\lambda_s)_p}$ and the degree of polarization at the wavelength λ_p (the p direction compared with the s direction) $\frac{I(\lambda_p)_p}{I(\lambda_p)_s}$, this can easily be read off figs. 16—18. If the FABRY-PEROT filter should be used at oblique incidence to isolate a spectral line and simultaneously act as polarizer it would be best to use the p component.

TABLE 16.

$$\cos \chi = \sqrt{1 - \frac{\sin^2 \varphi}{n^2}}$$

φ n	5°	10°	15°	30°	45°	60°	75°	80°
1.30	0.99775	0.99104	0.97998	0.92308	0.83913	0.74580	0.66927	0.65278
1.31	.99778	.99118	.98029	.92429	.84181	.75031	.67551	.65943
1.32	.99782	.99131	.98059	.92548	.84442	.75469	.68155	.66587
1.33	.99785	.99144	.98088	.92664	.84696	.75895	.68742	.67210
1.34	.99788	.99157	.98117	.92778	.84944	.76309	.69310	.67816
1.35	.99791	.99169	.98145	.92889	.85185	.76712	.69861	.68399
1.36	.99794	.99182	.98172	.92997	.85421	.77104	.70396	.68967
1.37	.99797	.99193	.98199	.93102	.85651	.77486	.70915	.69518
1.38	.99800	.99205	.98226	.93205	.85875	.77857	.71420	.70052
1.39	.99803	.99217	.98251	.93306	.86094	.78219	.71910	.70572
1.40	.99806	.99228	.98276	.93405	.86307	.78571	.72386	.71076
1.52	.99835	.99343	.98535	.94417	.88483	.82122	.77132	.76089
2.36	.99932	.99729	.99397	.97730	.95406	.93024	.91240	.90877

Before leaving the theory of interference filters of the FABRY-PEROT type, the TURNER frustrated total reflection filter should be briefly mentioned. This ingeniously constructed filter (indicated by A.F. TURNER [14] and [15]) is based on frustrated total reflection instead of reflection from silver layers and is constructed by evaporation on the hypotenuse surface of a flint glass prism, first a low index layer, then the high index spacer layer and again another low index layer, and finally another flint glass prism is cemented to the first. As no absorption occurs, R can reach a value so close to 1 that W_2 can be as low as 10 \AA , the limit is set by the crystalline structure of the fluoride layers [16]. Because of the oblique angle of incidence (high value of χ) two components (s and p) result, each with an intensity about 0.50. The filter has the disadvantage that it is of a limited area and that a very small deviation ($\frac{1}{3}^\circ$) from parallelism of the incident light will result in a shift greater than $\frac{1}{2} W_2$ (follows from (3, 19)). Furthermore, in most applications one of the components (s or p) must be extinguished by a polarizer. However, BILLINGS [17] has tried to construct a filter of this type with a birefringent material as spacer layer to avoid a splitting up in two components at a definite angle of incidence. The theory of a TURNER filter is the same as for a FABRY-PEROT filter, but the reflectivity must be calculated by special equations deduced directly from the MAXWELL equations of electrodynamics [17] and [17 a].

Before more complicated filters are treated a short summary of the most characteristic properties of the FABRY-PEROT filter will be given. The contrast factor $F = \frac{I_{\max}}{I_{\min}}$ is determined by the reflectivity R alone, $R < 1 - A$, where A is the absorption coefficient in the silver layer, i. e. $F < \left(\frac{1 + R_\infty}{1 - R_\infty}\right)^2 = \left(\frac{2 - A}{A}\right)^2$.

The half intensity band width W_2 can be made as small as $40\text{--}50 \text{ \AA}$, when the order m is sufficiently high. However, to extinguish the neighbouring peaks it is necessary to combine the filter with another interference filter of lower order or with absorption filters, but then I_{\max} drops considerably. The most serious drawback of the FABRY-PEROT filter is that the contrast factor F (for a reasonable I_{\max}) is only about 200 (Tables 6—13),

which means that this filter cannot be used for an efficient isolation of spectral lines. Moreover the colour will be impure (with an I_{\max} as high as 0.40) on account of the spectral region far from the peak. For this reason it would be of some value to examine the possibility of making filters with higher contrast factors F consisting of three or four silver layers and two or three dielectric layers, respectively (with the same or multiple thickness).

§ 4. Interference Filters with *Three* Systems of Reflective Layers I, II, and III (e. g. three silver layers).

Three systems of thin layers are considered (fig. 19). As previously when considering two systems we make the assumption that R, T, δ, β , etc., belonging to each of the systems I, II, and III, considered separately, vary only slightly with the wavelength (within each wavelength span of about $\frac{\lambda}{10}$) or in other words I, II, and III must not be interference filters themselves (e. g. each of the systems may consist of a silver layer combined with quarter wavelength layers of dielectrics).

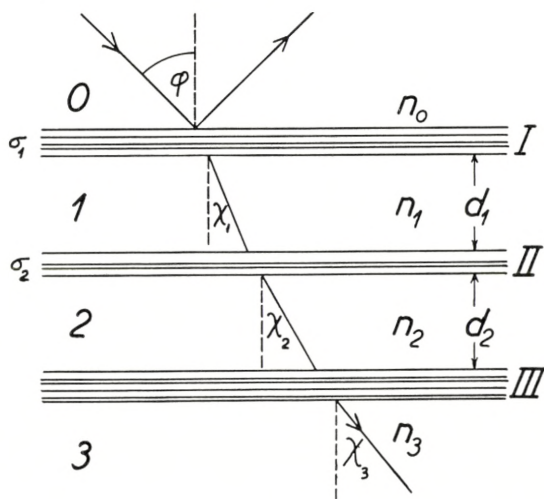


Fig. 19.

The notations used are analogous to those used in fig. 6

$$\sigma_1 \cdot e^{i\alpha_1} = 1 - \frac{t_{01} \cdot t_{10}}{r_{01} \cdot r_{10}} \quad \sigma_2 \cdot e^{i\alpha_2} = 1 - \frac{t_{12} \cdot t_{21}}{r_{12} \cdot r_{21}}$$

If now II + III is regarded as a single system (II in fig. 4) we deduce directly from the fundamental equations (2, 1—3) when Index 2 is interchanged with Index 3:

$$r_{03} = \frac{r_{01}(1 - r_{10} \cdot r_{13} \cdot \sigma_1 \cdot e^{-ix_1 + i\alpha_1})}{1 - r_{10} \cdot r_{13} \cdot e^{-ix_1}}; \quad t_{03} = \frac{t_{01} \cdot t_{13} \cdot e^{-i\frac{x_1}{2}}}{1 - r_{10} \cdot r_{13} \cdot e^{-ix_1}}$$

and once again from (2, 1—3) (now II and III in fig. 19 are equal to I and II in fig. 4) (r_{13}, t_{13}) can be expressed by

$$r_{13} = \frac{r_{12}(1 - r_{21} \cdot r_{23} \cdot \sigma_2 \cdot e^{-ix_2 + i\alpha_2})}{1 - r_{21} \cdot r_{23} \cdot e^{-ix_2}}; \quad t_{13} = \frac{t_{12} \cdot t_{23} \cdot e^{-i\frac{x_2}{2}}}{1 - r_{21} \cdot r_{23} \cdot e^{-ix_2}}$$

and when (r_{13}, t_{13}) are substituted in (r_{03}, t_{03}) we obtain:

$$r_{03} = \frac{r_{01}((1 - r_{21} \cdot r_{23} \cdot e^{-ix_2}) - e^{-ix_1 + i\alpha_1} \cdot r_{10} \cdot r_{12} \cdot \sigma_1 (1 - r_{21} \cdot r_{23} \cdot \sigma_2 \cdot e^{-ix_2 + i\alpha_2}))}{(1 - r_{21} \cdot r_{23} \cdot e^{-ix_2}) - e^{-ix_1} \cdot r_{10} \cdot r_{12} (1 - r_{21} \cdot r_{23} \cdot \sigma_2 \cdot e^{-ix_2 + i\alpha_2})}$$

and

$$t_{03} = \frac{t_{01} \cdot t_{12} \cdot t_{23} \cdot e^{-i\frac{x_1}{2} - i\frac{x_2}{2}}}{(1 - r_{21} \cdot r_{23} \cdot e^{-ix_2}) - e^{-ix_1} \cdot r_{10} \cdot r_{12} (1 - r_{21} \cdot r_{23} \cdot \sigma_2 \cdot e^{-ix_2 + i\alpha_2})}$$

or by introducing the notations

$$r_{01} = \sqrt{R_{01}} \cdot e^{i\delta_{01}} \quad r_{12} = \sqrt{R_{12}} \cdot e^{i\delta_{12}} \dots \text{etc.} \quad t_{01} = \sqrt{T_{01}} \cdot e^{i\beta_{01}} \dots \text{etc.},$$

and

$$\mathbf{R}_1 = \sqrt{R_{10} \cdot R_{12}}; \quad y_1 = x_1 - \delta_{10} - \delta_{12}; \quad x_1 = \frac{360}{\lambda} \cdot 2 d_1 n_1 \cos \chi_1 \quad (4, 1)$$

related to the dielectric layer 1 and

$$\mathbf{R}_2 = \sqrt{R_{21} \cdot R_{23}}; \quad y_2 = x_2 - \delta_{21} - \delta_{23}; \quad x_2 = \frac{360}{\lambda} \cdot 2 d_2 \cdot n_2 \cdot \cos \chi_2 \quad (4, 1)$$

related to the dielectric layer 2.

We obtain the fundamental formulae:

$$\sqrt{R_{03}(\lambda)} \cdot e^{i\delta_{03}} = \frac{\sqrt{R_{01}} \cdot e^{i\delta_{01}} \cdot ((1 - \mathbf{R}_2 \cdot e^{-iy_2}) - e^{-i(y_1 - \alpha_1)} \cdot \mathbf{R}_1 \sigma_1 (1 - \mathbf{R}_2 \cdot \sigma_2 \cdot e^{i(y_2 - \alpha_2)}))}{(1 - \mathbf{R}_1 \cdot e^{-iy_1} - \mathbf{R}_2 \cdot e^{-iy_2} + \mathbf{R}_1 \cdot \mathbf{R}_2 \cdot \sigma_2 \cdot e^{-i(y_1 + y_2) + i\alpha_2})} \quad (4,$$

$$\overline{T_{03}(\lambda)} \cdot e^{i\beta_{03}} = \frac{\sqrt{T_{01} \cdot T_{12} \cdot T_{23}} \cdot e^{i(\beta_{01} + \beta_{12} + \beta_{23}) - i\left(\frac{x_1}{2} + \frac{x_2}{2}\right)}}{(1 - \mathbf{R}_1 \cdot e^{-iy_1} - \mathbf{R}_2 \cdot e^{iy_2} + \mathbf{R}_1 \cdot \mathbf{R}_2 \cdot \sigma_2 \cdot e^{-i(y_1 + y_2) + i\alpha_2})}. \quad (4, 3)$$

The intensity distribution in transmission is given by

$$I(\lambda) = \frac{\mathbf{T}_1 \cdot \mathbf{T}_2 \cdot \mathbf{T}_3}{\left| 1 - \mathbf{R}_1 \cdot e^{-iy_1} - \mathbf{R}_2 \cdot e^{-iy_2} + \mathbf{R}_1 \cdot \mathbf{R}_2 \cdot \sigma_2 \cdot e^{-i(y_1 + y_2) + i\alpha_2} \right|^2}. \quad (4, 4)$$

When the following notations are introduced in (4, 3):

$$\mathbf{T}_1 = T_{01} \cdot \frac{n_1 \cos \chi_1}{n_0 \cos \varphi}; \quad \mathbf{T}_2 = T_{12} \cdot \frac{n_2 \cdot \cos \chi_2}{n_1 \cdot \cos \chi_1} \quad \text{and} \quad \mathbf{T}_3 = T_{23} \cdot \frac{n_3 \cos \chi_3}{n_2 \cos \chi_2}$$

(\mathbf{T}_1 , \mathbf{T}_2 , and \mathbf{T}_3 denote the energy transmitted through each of the systems I, II, or III considered separately).

$I(\lambda)$ is maximum or minimum when the denominator vice versa is minimum or maximum (as it is assumed that the numerator is almost independent of the wavelength).

The denominator is

$$\left. \begin{aligned} & (1 - \mathbf{R}_1 e^{-iy_1} - \mathbf{R}_2 \cdot e^{-iy_2} + \mathbf{R}_1 \mathbf{R}_2 \sigma_2 \cdot e^{-i(y_1 + y_2 - \alpha_2)}) \\ & \times (1 - \mathbf{R}_1 e^{iy_1} - \mathbf{R}_2 e^{iy_2} + \mathbf{R}_1 \mathbf{R}_2 \sigma_2 \cdot e^{i(y_1 + y_2 - \alpha_2)}) = \\ & 1 + \mathbf{R}_1^2 + \mathbf{R}_2^2 + (\sigma_2 \mathbf{R}_1 \mathbf{R}_2)^2 - 2 \mathbf{R}_2 \cos y_2 - 2 \mathbf{R}_1 \cos y_1 \\ & + 2 \sigma_2 \mathbf{R}_1 \mathbf{R}_2 \cos (y_1 + y_2 - \alpha_2) + 2 \mathbf{R}_1 \mathbf{R}_2 \cos (y_2 - y_1) \\ & - 2 \sigma_2 \mathbf{R}_1 \mathbf{R}_2^2 \cos (y_1 - \alpha_2) - 2 \sigma_2 \mathbf{R}_2 \mathbf{R}_1^2 \cos (y_2 - \alpha_2). \end{aligned} \right\} \quad (4, 5)$$

We now make the assumption that $y_1 = y_2$ and obtain

$$\left. \begin{aligned} & + \mathbf{R}_1^2 + \mathbf{R}_2^2 + (\sigma_2 \mathbf{R}_1 \mathbf{R}_2)^2 - 2 (\mathbf{R}_1 + \mathbf{R}_2) \cos y + 2 \sigma_2 \mathbf{R}_1 \mathbf{R}_2 \cos (2y - \alpha_2) \\ & - 2 \sigma_2 \mathbf{R}_1 \mathbf{R}_2 (\mathbf{R}_1 + \mathbf{R}_2) \cos (y - \alpha_2). \end{aligned} \right\} \quad (4, 6)$$

The minimum or maximum of the denominator is determined by the fact that the first derivative should be equal to zero, i. e.

$$+ \mathbf{R}_2) (\sin y + \sigma_2 \cdot \mathbf{R}_1 \mathbf{R}_2 \sin (y - \alpha_2)) - 2 \sigma_2 \mathbf{R}_1 \mathbf{R}_2 \sin (2y - \alpha_2) = 0. \quad (4, 7)$$

So far no approximations have been made, but now we introduce the approximation $\alpha_2 = 0$ (from Tables 6—13 it is to be expected that this will be a good approximation when the absorption is low and the reflectivity high of the central System II).

In the case of $\alpha_2 = 0$ (4, 7) simply reduces to

$$\sin y \cdot ((\mathbf{R}_1 + \mathbf{R}_2) (1 + \sigma_2 \cdot \mathbf{R}_1 \mathbf{R}_2) - 4 \sigma_2 \cdot \mathbf{R}_1 \mathbf{R}_2 \cdot \cos y) = 0.$$

Max. or min. occur when $\sin y = 0$ i.e. $y = 360^\circ \cdot (m-1)$ and when

$$\cos y = \frac{(\mathbf{R}_1 + \mathbf{R}_2) (1 + \sigma_2 \cdot \mathbf{R}_1 \cdot \mathbf{R}_2)}{4 \sigma_2 \cdot \mathbf{R}_1 \cdot \mathbf{R}_2}. \quad (4, 8)$$

This means: If the quantity (4, 8) is greater than or equal to unity, $I(\lambda)$ will only have a single maximum (for a specific order m) at $y = 360^\circ \cdot (m-1)$; $m = 1, 2, 3, \dots$

If, however, the quantity (4, 8) is less than unity, two neighbouring maxima of $I(\lambda)$ will occur at $y = \pm v + 360^\circ \cdot (m-1)$; $m = 1, 2, 3, \dots$ determined by (4, 8) and now a relative minimum at $y = 360^\circ \cdot (m-1)$.

If $R_{10} = R_{23}$ and $R_{12} = R_{21}$ (especially I and III identical), we simply have $\mathbf{R}_1 = \mathbf{R}_2 = \mathbf{R}$, and the condition of obtaining a single peak (for a specific order) is in this symmetrical case:

$$\frac{1 + \sigma_2 \mathbf{R}^2}{2 \sigma_2 \mathbf{R}} \geq 1 \quad \text{or} \quad \mathbf{R} \leq 1 - \sqrt{1 - \frac{1}{\sigma_2}}. \quad (4, 9)$$

If $\mathbf{R} = \sqrt{R_{10} \cdot R_{12}}$ and the approximation (3, 21) $\sigma_2 = \frac{1-A}{R_{12}}$ are introduced into (4, 8), we arrive at

$$\sqrt{R_{12}} \geq \frac{2(1-A)\sqrt{R_{10}}}{(1-A)R_{10} + 1}. \quad (4, 10)$$

DUFOR has in 1949 [18] developed an approximate theory for interference filters with three silver layers. He requires that $R_{20} = R_{23}$ at $y = 360^\circ \cdot (m-1)$ and from this condition a relation between R_{12} and R_{10} (similar to (4, 10)) is obtained. $R_{20} = R_{23}$ will give the highest value of I_{\max} for a definite value of $R_{20} \cdot R_{23}$

(see page 23). However, in the case of three reflecting layers as opposed to a FABRY-PEROT filter, the contrast factor is not solely dependent on $R_{20} \cdot R_{23}$, so the introduction of the condition $R_{20} = R_{23}$ seems unnatural. But when $A = 0$, DUFOUR's equation is identical with (4, 10), and when the absorption coefficient A is small, DUFOUR's equation only deviates slightly from (4, 10).

When only one peak is present ((4, 9) is satisfied) I_{\max} and $F = \frac{I_{\max}}{I_{\min}}$ are determined approximately ($\alpha_2 = 0$) directly by (4, 4) on introducing $y = 360^\circ \cdot (m-1)$ and $y = 180^\circ \cdot (2m-1)$, respectively:

$$I_{\max} = \frac{T_1 \cdot T_2 \cdot T_3}{(1 - R_1 - R_2 + \sigma_2 \cdot R_1 \cdot R_2)^2} \quad (4, 11)$$

and

$$F = \frac{I_{\max}}{I_{\min}} = \left(\frac{1 + R_1 + R_2 + \sigma_2 \cdot R_1 \cdot R_2}{1 - R_1 - R_2 + \sigma_2 \cdot R_1 \cdot R_2} \right)^2. \quad (4, 12)$$

However, when using silver layers this contrast factor will only be correct for higher order filters. For $m = 1$ or 2 , R and T will vary considerably from λ_{\max} to λ_{\min} , the true contrast factor on the red side of the peak will be greater than F calculated from (4, 12), and the true contrast factor on the violet side of the peak will be smaller than (4, 12).

Calculation of W_2 and W_{10} .

In the case of $\alpha_2 = 0$ and $y_1 = y_2 = y$ (4, 4) can conveniently be written as follows:

$$I(\lambda) = \frac{T_1 \cdot T_2 \cdot T_3}{A + B \sin^2 \frac{y}{2} + C \cdot \sin^4 \frac{y}{2}} \quad (4, 13)$$

with

$$A = (1 - R_1 - R_2 + \sigma_2 R_1 \cdot R_2)^2 \quad (4, 13 a)$$

$$B = 4 ((R_1 + R_2) (1 + \sigma_2 R_1 \cdot R_2) - 4 \sigma_2 R_1 R_2) \quad (4, 13 b)$$

and

$$C = 16 \sigma_2 R_1 \cdot R_2. \quad (14, 13 c)$$

When only one peak is present $\mathbf{B} \geq 0$ and if two peaks exist, we have $\mathbf{B} < 0$, and the wavelengths of the two peaks are determined by (4, 8) or by

$$\sin \frac{y}{2} = \pm \sqrt{\frac{\mathbf{B}}{2\mathbf{C}}}.$$

In the case of one peak the W_k defined by

$$I\left(\lambda_m \pm \frac{W_k}{2}\right) = \frac{1}{k} \cdot I(\lambda_m)$$

are determined by means of

$$(k-1)\mathbf{A} = \mathbf{B} \sin^2 \frac{\gamma_k}{2} + \mathbf{C} \sin^4 \frac{\gamma_k}{2}$$

and by

$$W_k = \frac{\gamma_k \cdot \lambda_m}{f \cdot 180}, \quad f = -\frac{\lambda_m}{360} \cdot \left(\frac{dy}{d\lambda}\right)_{\lambda = \lambda_m}$$

when $y = 360 \cdot (m-1) \pm \gamma_k$ corresponds to $\lambda_m \mp \frac{W_k}{2}$. In the case of $\mathbf{B} = 0$ (the line shape corresponds to the "limit" between one and two peaks) these equations can easily be solved; we obtain:

$$\sin \frac{\gamma_k}{2} = \sqrt[4]{\frac{(k-1) \cdot \mathbf{A}}{\mathbf{C}}}$$

and approximately

$$W_k = \frac{2\lambda_m}{\pi \cdot f} \sqrt[4]{\frac{(k-1) \cdot \mathbf{A}}{\mathbf{C}}}$$

and for $k = 2$

$$W_2 = \frac{\lambda_m \cdot \sqrt{1 - \mathbf{R}_1 - \mathbf{R}_2 + \sigma_2 \mathbf{R}_1 \mathbf{R}_2}}{\pi \cdot f \cdot \sqrt[4]{\sigma_2 \mathbf{R}_1 \cdot \mathbf{R}_2}}, \quad (4, 14)$$

and we further get the relation

$$W_{10} = \sqrt{3} \cdot W_2. \quad (4, 15)$$

Table 17 contains the results of calculations made in the special case of 3 silver layers placed in a dielectric with $n = 1.36$

TABLE 17.

λ $\nu - i \times$ l''	$R_{12}(=R'')$ $T_{12}(=T'')$ σ_2	$R_{10}(=R')$ $T_{10}(=T')$	l' l'' in Å	I_{\max}	$F =$ $\frac{I_{\max}}{I_{\min}}$	W_2 (2·order) in Å	W_{10} (2·order) in Å
4000 0.18— i 1.95 600	0.7708 0.0725 1.0865	0.6684 0.1796	449 600	0.152	580	260	450
4000 0.18— i 1.95 500	0.7155 0.1297 1.1706	0.5342 0.3217	334 500	0.297	162	357	618
4500 0.14— i 2.42 500	0.8150 0.0868 1.1031	0.5914 0.3095	297 500	0.406	420	317	549
5000 0.14— i 2.89 500	0.8649 0.0573 1.0644	0.6575 0.2577	286 500	0.404	1000	282	489
5500 0.15— i 3.36 500	0.8951 0.0389 1.0422	0.7126 0.2105	280 500	0.379	2300	252	436
6000 0.15— i 3.82 500	0.9188 0.0278 1.0296	0.7508 0.1830	269 500	0.386	4800	231	400
6560 0.13— i 4.27 500	0.9398 0.0218 1.0228	0.7702 0.1789	249 500	0.463	7700	222	385
6560 0.13— i 4.27 400	0.9084 0.0498 1.0542	0.6583 0.2872	194 400	0.585	1400	339	587
7100 0.14— i 4.68 450	0.9363 0.0271 1.0286	0.7416 0.2077	217 450	0.516	5000	268	464
7680 0.15— i 5.11 450	0.9438 0.0227 1.0237	0.7615 0.1900	212 450	0.507	7300	265	458

$R_1 = R_2 = R$ and $y_1 = y_2$ (i. e. a symmetrical filter as shown in figs. 22 and 24). The calculations are carried out by means of Tables 6—13. When the thickness of the central silver layer t'' has been chosen, R can be calculated from (4, 9)

$$\left(R = 1 - \sqrt{1 - \frac{1}{\sigma_2}}; R = \sqrt{R' \cdot R''} \right)$$

so that only one peak results. Next, R' , t' , T' and from these quantities I_{\max} and $F = \frac{I_{\max}}{I_{\min}}$ are calculated by means of (4, 11—12), and finally W_2 and W_{10} are calculated from (4, 14—15).

In practice, however, α_2 is not zero, but has some small value (Tables 6—13). To get an idea of the true intensity distribution $I(\lambda)$ in the neighbourhood of λ_m numerical calculations have been carried out for different values of t' and t'' for the silver layers, directly from (4, 4) written in the form

$$I(\lambda) = \frac{T_1^2 \cdot T_2}{\varrho_1^2 \left| 1 - \frac{\varrho_2}{\varrho_1} \cdot e^{i(\varepsilon_2 - \varepsilon_1) - iy} \right|^2} = \frac{T_1^2 \cdot T_2}{(\varrho_1 \cdot \varrho_3)^2} \quad (4, 16)$$

with

$$\varrho_1 \cdot e^{i\varepsilon_1} = 1 - R e^{-iy} \quad (4, 16 a)$$

$$\varrho_2 \cdot e^{i\varepsilon_2} = 1 - \sigma_2 R \cdot e^{-i(y - \alpha_2)} \quad (4, 16 b)$$

and

$$\varrho_3 \cdot e^{i\varepsilon_3} = 1 - \frac{\varrho_2}{\varrho_1} \cdot e^{i(\varepsilon_2 - \varepsilon_1 - y)}. \quad (4, 16 c)$$

The calculations have been carried out by means of RYBNER'S tables [4]. In fig. 20 a first order filter $M' L_2 M'' L_2 M'$ of this type is considered. The thickness of the inner silver layer is $t'' = 400 \text{ \AA}$ ($\sigma_2 = 1.0542$ and $\alpha_2 = -0.466$) for all the curves. The thicknesses of the two outer silver layers t' are A: 150 \AA , B: 200 \AA (just exceeding the value of R' at which only one peak occurs (see Table 17)) and C: 400 \AA (the three silver layers have the same thickness and two peaks appear which have somewhat different but low intensities).

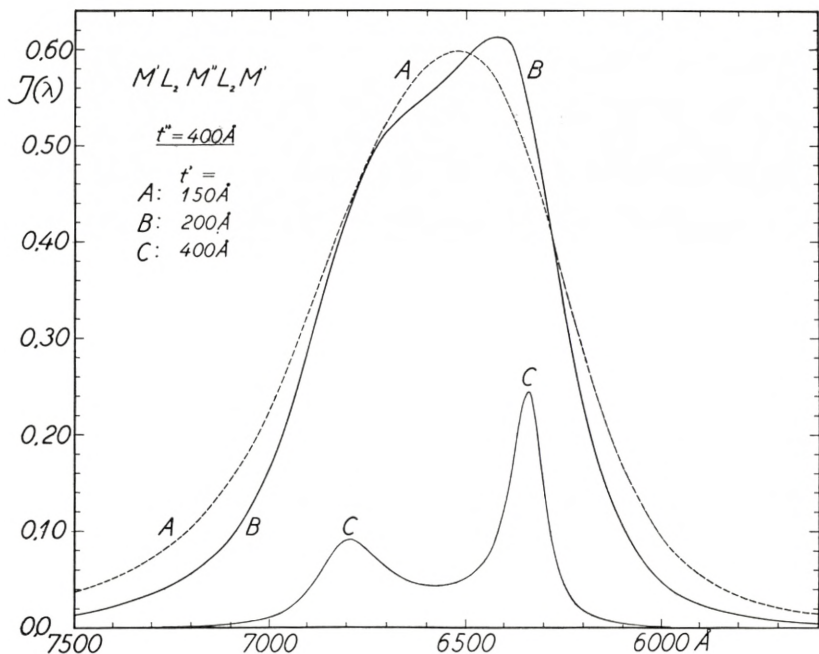


Fig. 20.

$I(\lambda)$ for filters of the type $M'L_2M''L_2M'$ the thickness of M'' is 400 Å in all cases. The thickness of M' is, A: 150 Å, B: 200 Å and C: 400 Å. The thickness of L_2 is chosen such that for $M'L_2M''$ is $\lambda_{\max} = 6560$ Å.

From fig. 20 (and from further calculations not given here) it follows that the value of R' at which I_{\max} has its highest value when R'' is constant, is very near the value of R' determined by

$$R' = \frac{1}{R''} \cdot \left(1 - \sqrt{1 - \frac{1}{\sigma_2}}\right)^2. \quad (4, 9)$$

In fig. 21 again a filter of the type $M'L_2M''L_2M'$ is considered (solid line) but here the thickness of the central silver layer is $t'' = 500$ Å ($\sigma_2 = 1.0228$ $\alpha_2 = -0.230^\circ$) and the outer silver layers has a thickness of $t' = 250$ Å. (This corresponds very closely to a value of R' which satisfies (4, 9)). For comparison an $I(\lambda)$ curve for a FABRY-PEROT filter ML_2M (fig. 11, A) has been added (fig. 21 broken line) the thickness $t = 300$ Å for the M -layers has been chosen in such a way that I_{\max} is about the same for the two filters. The advantages of the compound filter

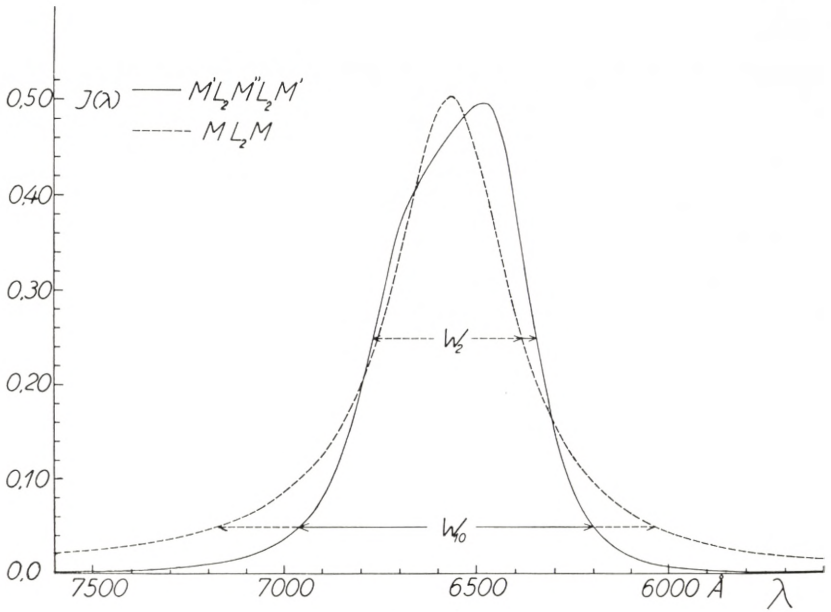


Fig. 21.

Solid line: $I(\lambda)$ for a filter $M'L_2M''L_2M'$ with $t'' = 500 \text{ \AA}$ and $t' = 250 \text{ \AA}$.
 Broken line: $I(\lambda)$ for a filter ML_2M with $t = 300 \text{ \AA}$. The thickness of the L_2 layers are determined as for fig. 20.

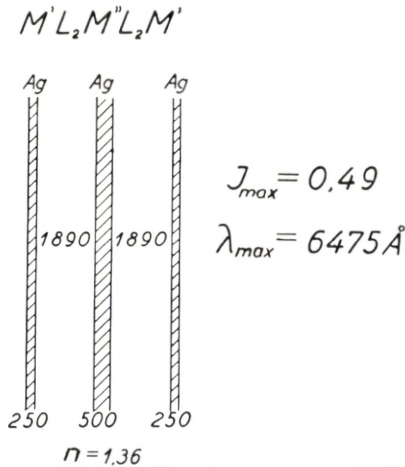


Fig. 22.

The filter the intensity curve of which is the solid line in fig. 21.

$M'L_2M''L_2M'$ is apparent from fig. 21. W_2 (for the filter $M'L_2M''L_2M'$) is (read off from fig. 21) 410 \AA and $W_{10} = 760 \text{ \AA}$ in good agreement with the values given in Table 17.

Both in fig. 20 and in fig. 21 it is assumed that $\nu - i\kappa = 0.13 - i 4.27$ (in the wavelength region considered) and the thickness d of the dielectric layers has been determined in such a way that a filter $M'L_2M''$ would have had peak transmission at $\lambda = 6560 \text{ \AA}$. The wavelength scale has been determined according to (3, 27 a) by

$$\lambda = \frac{6560}{1 + \frac{y}{360}}$$

A comparison between fig. 20 and fig. 21 shows that the thickness t'' of the central silver layer M'' has to be chosen rather great to obtain a W_2 value of about the same size as for a FABRY-PEROT filter with the same I_{\max} .

In fig. 23 $I(\lambda)$ is shown for two filters $M'L_4M''L_4M'$ green 2nd order $t'' = 500 \text{ \AA}$ ($\sigma_2 = 1.0422$; $\alpha_2 = -0.575^\circ$) in the case of both the filters. For the solid line curve $t' = 280 \text{ \AA}$ (determined such that R' satisfies (4, 9)) and for the broken curve $t' = 330 \text{ \AA}$ ((4, 8) is less than unity, i. e. two peaks and

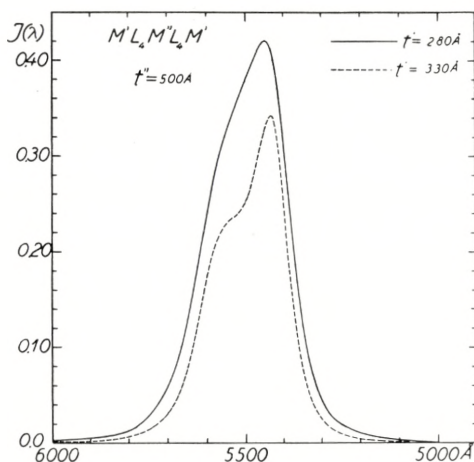


Fig. 23.

$I(\lambda)$ for two filters of the type $M'L_4M''L_4M \cdot t'' = 500 \text{ \AA}$ for both filters. Solid line: $t' = 280 \text{ \AA}$. Broken line: $t' = 330 \text{ \AA}$. d is determined such that $\lambda_{\max} = 5500 \text{ \AA}$ for the filter $M'L_4M''$.

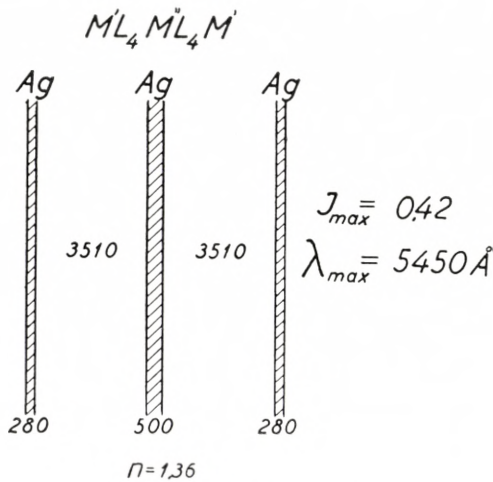


Fig. 24.

The filter $I(\lambda)$ of which is the solid line curve of fig. 23.

a lower I_{max} result). $\nu - i\kappa = 0.15 - i \cdot 3.36$ and the wavelength scale has been calculated from (3, 27 a)

$$\lambda = \frac{5500}{1 + \frac{\gamma}{720}}$$

with $\gamma = y - 360$. The thickness d of the dielectric layers L_2 is determined in accordance with (3, 8) so that a filter of the construction $M'L_4M''$ would have had λ_{max} equal to 5500 \AA .

In fig. 25 the solid line curve is the same as the solid line curve in fig. 23 (i. e. $I(\lambda)$ for the filter fig. 24). The broken line curve is the intensity

$$I(\lambda) = \frac{0.379}{1 + 2127.2 \cdot \sin^4\left(\frac{\gamma}{2}\right)}$$

calculated from (4, 13) with the approximation $\alpha_2 = 0$. The actual small value of $\alpha_2 = -0.575^\circ$ gives rise to an asymmetric line shape and a shift in λ_{max} towards violet. Another difference is that the exact calculation (with $\alpha_2 = -0.575^\circ$) predicts an I_{max} about 10 per cent. larger than obtained by the approximative theory with $\alpha_2 = 0$. (The same is apparent from fig. 20 and fig. 21 as compared with Table 17).

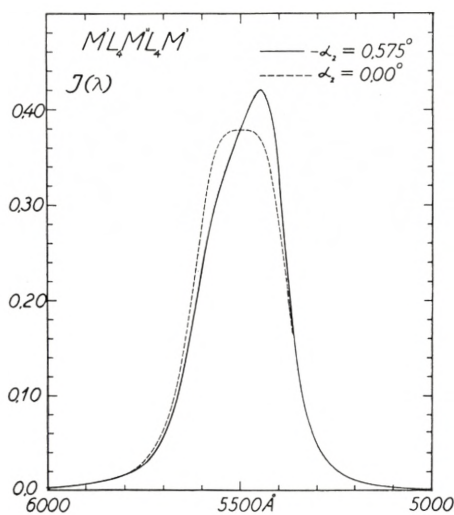


Fig. 25.

Unbroken line: $I(\lambda)$ for the filter in fig. 24. $\alpha_2 = -0.575^\circ$.

Broken line: $I(\lambda)$ calculated from (4, 13) with $\alpha_2 = 0$.

The deviations between the two curves in fig. 25 are the greatest in the very neighbourhood of the peak, but W_2 and particularly W_{10} will be very nearly equal for the two curves.

If the three silver layers have the same thickness, two widely separated peaks result (fig. 20 curve C). If the thickness of the central silver layer is now decreased, the separation between the two peaks will increase and because of the increase in α_2 (caused by the decrease in the thickness of an absorbent layer) the asymmetry will be more and more pronounced. (Fig. 27 solid line corresponding to the filter in fig. 28 a). If, however, a thin ZnS layer ($n_1 = 2.36$) is used as the central reflecting layer, we have $\alpha_2 = 0$, and in this case $I(\lambda)$ can be calculated exactly from (4, 13), and λ_{\max} is determined by (4, 8).

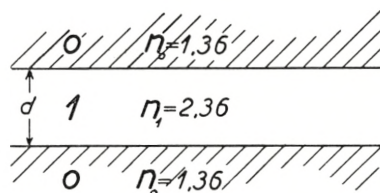


Fig. 26.

R and T for the ZnS layer (fig. 26) are determined by (3, 23—24)

$$\sqrt{R} \cdot e^{i\delta} = r_{01} \frac{(1 - e^{-ix})}{1 - r_{01}^2 \cdot e^{-ix}} \quad \text{and} \quad \sqrt{T} \cdot e^{i\beta} = \frac{(1 - r_{01}^2) \cdot e^{-i\frac{x}{2}}}{1 - r_{01}^2 \cdot e^{-ix}}$$

with

$$r_{01} = \frac{n_0 - n_1}{n_0 + n_1} \quad \text{and} \quad x = 360 \cdot \frac{2 dn_1}{\lambda}$$

From these equations follows $R + T = 1$ (conservation of energy) and

$$\frac{1}{R} = 1 + \frac{(1 - r_{01}^2)^2}{4 \cdot r_{01}^2 \sin^2 \frac{x}{2}} \quad (4, 17)$$

and

$$\sigma_2 \cdot e^{i\alpha_2} = 1 - \frac{T}{R} \cdot e^{i(2\beta - 2\delta)} = 1 + \frac{(1 - r_{01}^2)}{4 r_{01}^2 \sin^2 \frac{x}{2}} \text{ i. e. } \sigma_2 = \frac{1}{R} \text{ and } \alpha_2 = 0$$

in accordance with (3, 20).

From these formulae it is easy to calculate the intensity distribution $I(\lambda)$ for a definite value of the thickness d of the ZnS layer.

In fig. 27 solid line $I(y)$ has been calculated for $t' = 150 \text{ \AA}$

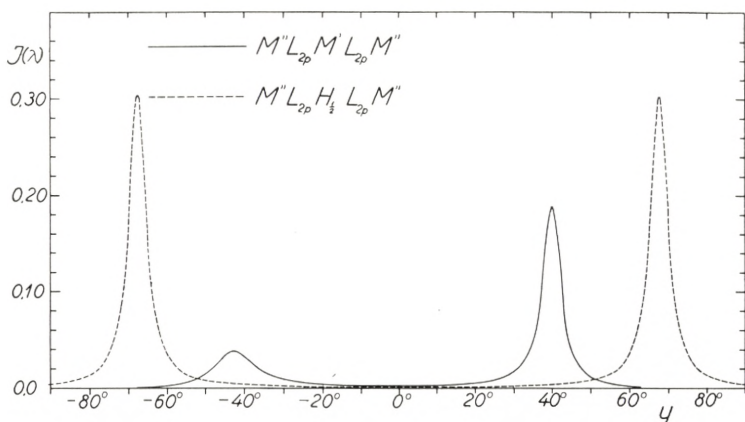


Fig. 27.

Solid line: $I(\lambda)$ for the filter $M''L_2M'L_2M''$ constructed as shown in fig. 28 a.
Broken line curve: $I(\lambda)$ for the filter $M''L_2H_{\frac{1}{2}}L_2M''$ constructed as shown in fig. 28 b.

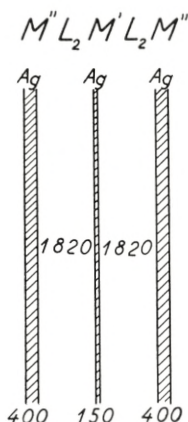


Fig. 28 a.

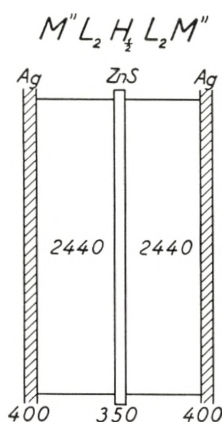


Fig. 28 b.

Fig. 28 a. The filter, $I(\lambda)$ of which is indicated in fig. 27 solid line.
 Fig. 28 b. The filter $I(\lambda)$ of which is indicated in fig. 27 broken line. The low index layers L_2 of the filters are determined in such a way that the filters $M''L_2M'$, and $M''L_2H_{\frac{1}{2}}L_2M''$ both have peak transmission at $\lambda = 6560 \text{ \AA}$.

(thickness of the central silver layer) and $t'' = 400 \text{ \AA}$ (thickness of the outer silver layers) by means of (4, 16).

In fig. 27 broken line

$$I(y) = \frac{0.002122}{1.4057 - 9.0178 \sin^2 \frac{y}{2} + 14.5352 \sin^4 \frac{y}{2}}$$

has been calculated corresponding to $x = 90^\circ$ ($\frac{\lambda}{8}$ -layer at $\lambda = 6560 \text{ \AA}$) for the ZnS layer. The thickness of both the silver layers is 400 \AA and x and $v - i\kappa = 0.13 - i.4$. 27 has been regarded as independent of the wavelength. This is only a rough approximation in the case of $p = 1$ as on figs. 28 a—b, but will be a good approximation in the neighbourhood of 6560 \AA for a filter of higher order ($p \simeq 8-10$). Fig. 29 shows the approximate distri-

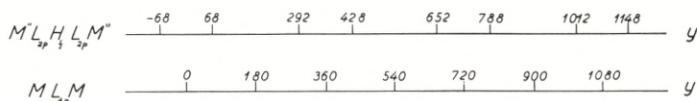


Fig. 29.

The positions of the peaks on the y scale for a higher order filter $M''L_{2p}H_{\frac{1}{2}}L_{2p}M''$ as compared with the position of the peaks for a FABRY-PEROT filter $M''L_{4p}M''$.

bution on the y -scale of the peaks for such a filter $M''L_{2p}H_{\frac{1}{2}}L_{2p}M''$ as compared with the distribution of the peaks for a FABRY-PEROT filter $M''L_{4p}M''$ (which is very nearly equally spaced). I_{\max} is the same for both filters in accordance with (2, 18 b).

The Filter $M'L_4M''L_4M'$ Used as Phase Plate.

Fig. 30 shows the phase change at transmission for a filter $M'L_4M''L_4M'$ (like that in fig. 24). The calculation is quite analogous to that on page 39 for a FABRY-PEROT filter. The phase plate is shown at the bottom of fig. 30. The phase difference between P_2 (light passing through the phase plate) and P_1 (light passing outside the phase plate) is according to (4, 3)

$$\zeta(\lambda) = \left(\beta_{01} + \beta_{12} + \beta_{23} - \frac{360}{\lambda} \cdot 2 dn - \varepsilon_3(\lambda) \right) + \left. \begin{array}{l} \\ \frac{360}{\lambda} (2t' + t'' + 2d) \end{array} \right\} \quad (4, 18)$$

making the approximations

$$\beta_{01} = \beta_{23} \quad \text{and} \quad \beta_{01} + \beta_{23} + \beta_{12} = \beta_0 - k \cdot \lambda.$$

$\varepsilon_3(\lambda)$ (the phase change from multiple reflections in the layers) is calculated from (4, 16 c). The phase change is zero in the neighbourhood of the peak and a change from negative ($+90^\circ$) to positive (-90°) contrast of the image is possible by means of a small alteration of the wavelength.

The Intensity $R(\lambda)$ in Reflection.

The intensity distribution $R(\lambda)$ in the reflected light from a filter of this type can without any approximation be calculated from (4, 2). A general analysis of the properties of the filter $M'L_{2p}M''L_{2p}M'$ in reflection has not been carried out here (as it would only be a rough approximation to place $\alpha_1 = 0$), but $R_{03}(\lambda)$ has been calculated directly from (4, 2) in three special cases of the filters the transmission curves of which are shown

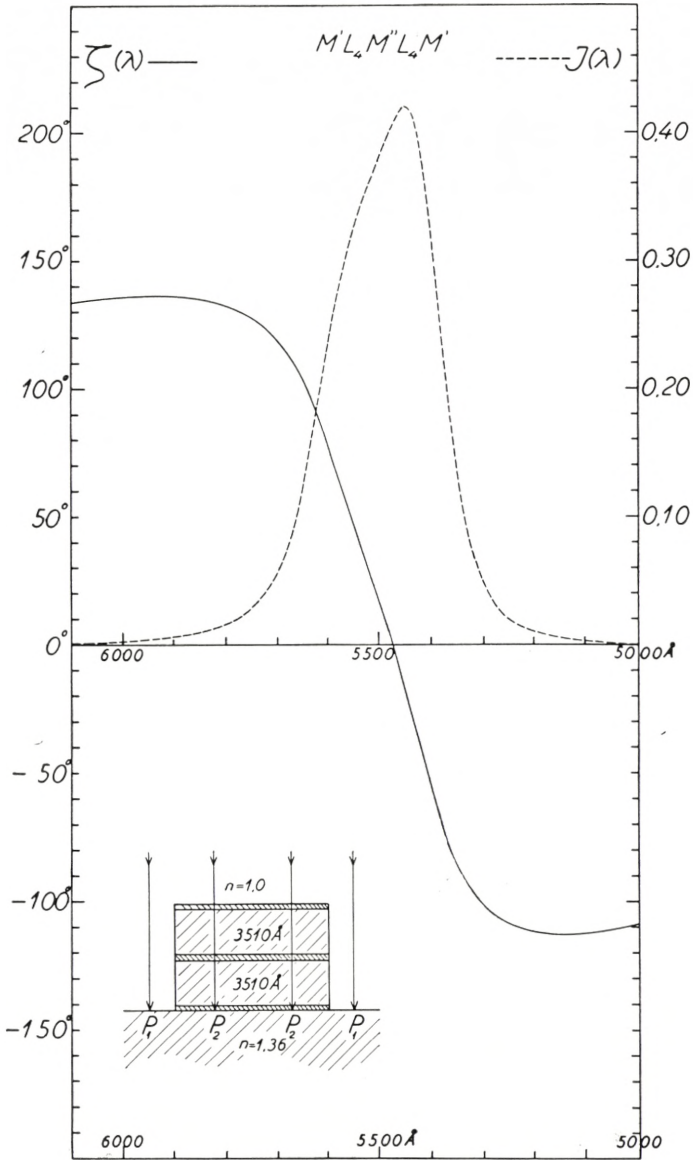


Fig. 30.

Solid line: Phase change at transmission through an interference filter of the type $M'L_4M''L_4M'$. (Phase difference between P_2 and P_1).

Broken line: $I(\lambda)$ for the same filter. (The same as the solid line curve in figs. 24 and 25). The phase plate is shown below in the left corner of fig. 30).

in fig. 20 Curve B, fig. 21 (unbroken line) and fig. 23 (unbroken line). (4, 2) can be written

$$R_{03}(\lambda) = \frac{R_{01} \cdot \left| 1 - \sigma_1 \mathbf{R} \cdot \frac{\varrho_2}{\varrho_1} \cdot e^{i(\varepsilon_2 - \varepsilon_1) - i(y - \alpha_1)} \right|^2}{\left| 1 - \mathbf{R} \cdot \frac{\varrho_2}{\varrho_1} \cdot e^{i(\varepsilon_2 - \varepsilon_1) - iy} \right|^2}$$

$$\varrho_1 \cdot e^{i\varepsilon_1} = 1 - \mathbf{R} \cdot e^{-iy}, \quad \varrho_2 \cdot e^{i\varepsilon_2} = 1 - \sigma_2 \mathbf{R} \cdot e^{-i(y - \alpha_2)}$$

and

$$\varrho_3 \cdot e^{i\varepsilon_3} = 1 - \mathbf{R} \cdot \frac{\varrho_2}{\varrho_1} \cdot e^{i(\varepsilon_2 - \varepsilon_1) - iy}$$

have been calculated above (4, 16 a-c), and if further

$$\varrho_4 \cdot e^{i\varepsilon_4} = 1 - \sigma_1 \cdot \mathbf{R} \cdot \frac{\varrho_2}{\varrho_1} \cdot e^{i(\varepsilon_2 - \varepsilon_1) - i(y - \alpha_1)}$$

is calculated, we simply get

$$R_{03}(\lambda) = R_{01} \cdot \left(\frac{\varrho_4}{\varrho_3} \right)^2.$$

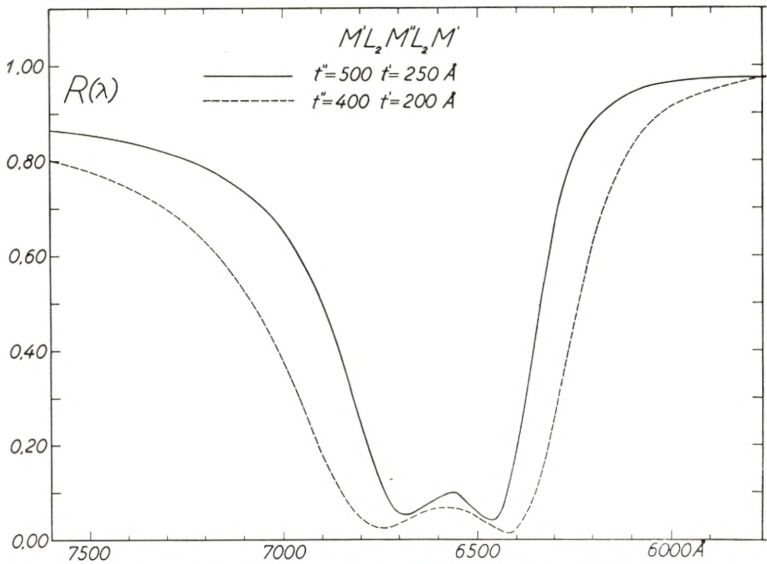


Fig. 31.

Intensity distribution in reflection from the filters of the type $M'L_2M''L_2M'$. Unbroken line: Reflection from the filter in fig. 22 and with transmission curve in fig. 21 (unbroken line) $\alpha_1 = -1.386^\circ$ and $\alpha_2 = -0.230^\circ$. Broken line: Reflection from the filter the transmission curve of which is given in fig. 20, Curve B. $\alpha_1 = -2.084^\circ$ and $\alpha_2 = -0.466^\circ$.

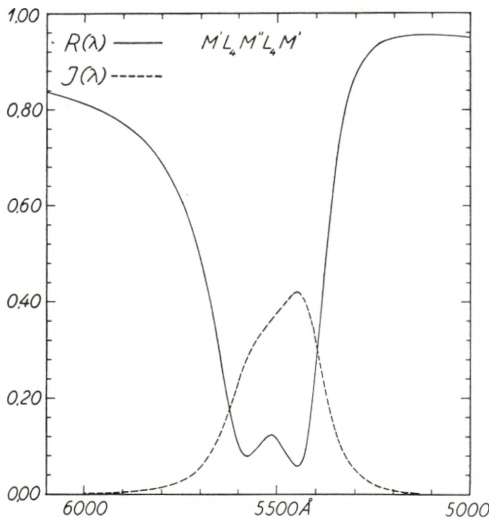


Fig. 32.

Unbroken line: Intensity distribution in reflection from the filter in fig. 24. $\alpha_1 = -2.401^\circ$ and $\alpha_2 = -0.575^\circ$. Broken line: Intensity distribution at transmission through the same filter.

The three curves of $R(\lambda)$ (fig. 31—32) have much the same trends and are characterized by having two minima and, as in the case of fig. 13, the minima do not reach zero.

Recently GEFCKEN [19] has also considered filters of this type with three silver layers.

§ 5. Interference Filters with **Four** Systems of Reflective Layers. (e. g. four silver layers).

The same assumption is adopted here, as in the previous sections, viz. that each of the systems I, II, III, and IV, when considered separately, do not act as interference filters themselves.

The treatment in this section is quite analogous to that of § 4. The following notations are used here as previously:

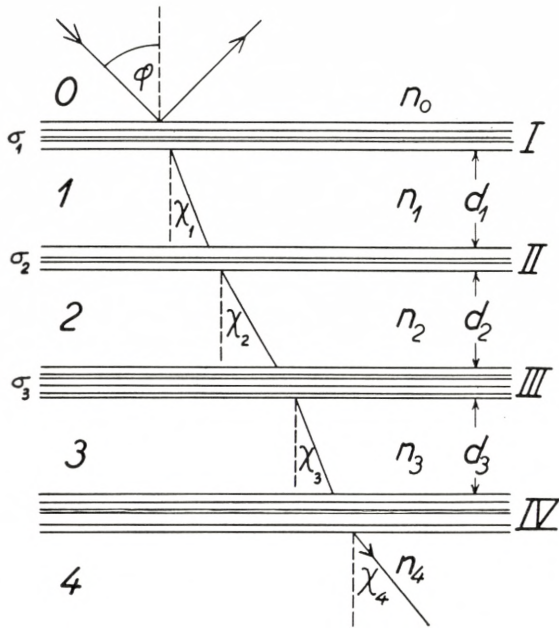


Fig. 33.

$$x_q = \frac{2 d_q \cdot n_q \cdot \cos \chi_q}{\lambda} \quad y_q = x_q - \delta_{q,q-1} - \delta_{q,q+1}$$

$$\sigma_q \cdot e^{i\alpha_q} = 1 - \frac{t_{q-1,q} \cdot t_{q,q-1}}{r_{q-1,q} \cdot r_{q,q-1}}; \quad r_{q,q-1} = \sqrt{R_{q,q-1}} \cdot e^{i\delta_{q,q-1}} \text{ etc.}$$

and

$$t_{q,q-1} = \sqrt{T_{q,q-1}} \cdot e^{i\beta_{q,q-1}} \quad \text{and} \quad \mathbf{R}_q = \sqrt{R_{q,q-1} \cdot R_{q,q+1}}$$

and from this follows

$$r_{q,q-1} \cdot r_{q,q+1} \cdot e^{-ix_q} = \mathbf{R}_q \cdot e^{-iy_q}, \quad (q = 1, 2, 3).$$

As in § 4 II + III + IV are considered as a single system (and identical with II in fig. 4) and (2, 1–3) is employed (Index 2 being changed to Index 4):

$$r_{04} = \frac{r_{01} (1 - r_{10} \cdot r_{14} \cdot \sigma_1 \cdot e^{-i(x_1 - \alpha_1)})}{1 - r_{10} \cdot r_{14} \cdot e^{-ix_1}}; \quad t_{04} = \frac{t_{01} \cdot t_{14} \cdot e^{-i \frac{x_1}{2}}}{1 - r_{10} \cdot r_{14} \cdot e^{-ix_1}}$$

and in these formulae the following substitutions are made, derived from (4, 2-3):

$$r_{12} = \frac{r_{12}((1 - \mathbf{R}_3 \cdot e^{-iy_3}) - \sigma_2 \mathbf{R}_2 \cdot e^{-iy_2 + i\alpha_2} \cdot (1 - \sigma_3 \mathbf{R}_3 \cdot e^{-iy_3 + i\alpha_3}))}{(1 - \mathbf{R}_3 \cdot e^{-iy_3}) - \mathbf{R}_2 \cdot e^{-iy_2} (1 - \sigma_3 \mathbf{R}_3 \cdot e^{-iy_3 + i\alpha_3})}$$

and

$$t_{14} = \frac{t_{12} \cdot t_{23} \cdot t_{34} \cdot e^{-i(\frac{x_2}{2} + \frac{x_3}{2})}}{(1 - \mathbf{R}_3 \cdot e^{-iy_3}) - \mathbf{R}_2 \cdot e^{-iy_2} (1 - \sigma_3 \mathbf{R}_3 \cdot e^{-iy_3 + i\alpha_3})}$$

and we arrive at

$$4 = \left. \begin{aligned} & \frac{\sqrt{R_{01}} \cdot e^{i\delta_{01}} ((1 - \mathbf{R}_3 \cdot e^{-iy_3}) (1 - \sigma_1 \mathbf{R}_1 \cdot e^{-i(y_1 - \alpha_1)}) \\ & \quad - \mathbf{R}_2 \cdot e^{-iy_2} (1 - \sigma_3 \mathbf{R}_3 \cdot e^{-i(y_3 - \alpha_3)}) (1 - \sigma_1 \cdot \sigma_2 \cdot \mathbf{R}_1 \cdot e^{-i(y_1 - \alpha_1 - \alpha_2)}))}{(1 - \mathbf{R}_3 \cdot e^{-iy_3}) (1 - \mathbf{R}_1 \cdot e^{-iy_1})} \\ & \quad - \mathbf{R}_2 \cdot e^{-iy_2} (1 - \sigma_3 \mathbf{R}_3 \cdot e^{-i(y_3 - \alpha_3)}) (1 - \sigma_2 \mathbf{R}_1 \cdot e^{-i(y_1 - \alpha_2)}) \end{aligned} \right\} (5, 1)$$

and

$$4 = \left. \begin{aligned} & \frac{\sqrt{T_{01} \cdot T_{12} \cdot T_{23} \cdot T_{34}} \cdot e^{-i(\frac{x_1}{2} + \frac{x_2}{2} + \frac{x_3}{2}) + i(\beta_{01} + \beta_{12} + \beta_{23} + \beta_{34})}}{(1 - \mathbf{R}_3 \cdot e^{-iy_3}) (1 - \mathbf{R}_1 \cdot e^{-iy_1})} \\ & \quad - \mathbf{R}_2 \cdot e^{-iy_2} (1 - \sigma_3 \mathbf{R}_3 \cdot e^{-i(y_3 - \alpha_3)}) (1 - \sigma_2 \mathbf{R}_1 \cdot e^{-i(y_1 - \alpha_2)}) \end{aligned} \right\} (5, 2)$$

We now consider the properties in transmission in the case where the filter is constructed symmetrically, i. e. when $\mathbf{R}_1 = \mathbf{R}_3 = \mathbf{R}$

$$y_1 = y_3, \quad \sigma_2 = \sigma_3 \quad \text{and} \quad n_1 = n_3.$$

In this case we obtain

$$I(\lambda) = \frac{T_1 \cdot T_2^2 \cdot T_4}{|(1 - \mathbf{R} \cdot e^{-iy_1})^2 - \mathbf{R}_2 \cdot e^{-iy_2} (1 - \sigma_2 \mathbf{R} \cdot e^{-i(y_1 - \alpha_2)})^2|^2} \quad (5, 3)$$

$$\mathbf{T}_1 = T_{01} \cdot \frac{n_1 \cdot \cos \chi_1}{n_0 \cdot \cos \varphi}; \quad \mathbf{T}_2 = \mathbf{T}_3 = T_{12} = T_{23} \quad \text{and} \quad \mathbf{T}_4 = T_{34} \cdot \frac{n_4 \cdot \cos \chi_4}{n_1 \cdot \cos \chi_1}$$

are the energies transmitted through Systems I, II, III, and IV, when each of the systems are considered separately.

The denominator P in (5, 3) can be expressed by

$$\begin{aligned}
 P = & 1 + \mathbf{R}^4 + 4\mathbf{R}^2 + \mathbf{R}_2^2 + 4(\sigma_2 \mathbf{R} \mathbf{R}_2)^2 + \mathbf{R}_2^2 \cdot (\sigma_2 \mathbf{R})^4 + 4\mathbf{R} \cdot \mathbf{R}_2 \cdot \cos(y_1 - y_2) \\
 & + 4\sigma_2 \cdot \mathbf{R}^3 \cdot \mathbf{R}_2 \cdot \cos(y_1 - y_2 + \alpha_2) - 4\mathbf{R}(\mathbf{R}^2 + 1) \cos y_1 \\
 & - 4\sigma_2 \mathbf{R} \cdot \mathbf{R}_2^2 ((\sigma_2 \mathbf{R})^2 + 1) \cdot \cos(y_1 - \alpha_2) - 2 \cdot \mathbf{R}_2 \cdot \cos y_2 \\
 & - 2\mathbf{R}_2 \sigma_2^2 \cdot \mathbf{R}^4 \cdot \cos(y_2 - 2\alpha_2) - 8\sigma_2 \mathbf{R}_2 \cdot \mathbf{R}^2 \cdot \cos(y_2 - \alpha_2) \\
 & - 2\mathbf{R}_2 \cdot \mathbf{R}^2 \cos(2y_1 - y_2) + 2 \cdot \mathbf{R}^2 \cos 2y_1 + 2(\mathbf{R}_2 \sigma_2 \mathbf{R})^2 \cos(2y_1 - 2\alpha_2) \\
 & + 4\sigma_2 \mathbf{R}_2 \mathbf{R} \cdot \cos(y_1 + y_2 - \alpha_2) + 4\mathbf{R}_2 \cdot \mathbf{R} \cdot (\sigma_2 \mathbf{R})^2 \cdot \cos(y_1 + y_2 - 2\alpha_2) \\
 & - 2\mathbf{R}_2 \cdot (\sigma_2 \mathbf{R})^2 \cos(2y_1 + y_2 - 2\alpha_2).
 \end{aligned} \tag{5, 4}$$

We now make the approximation $\alpha_2 = 0$ and consider the case $y_1 = y_2 (= y_3) = y$ in detail. It is easy to show from (5, 4) that

P in this case can be expressed by a polynomial in $\sin^2 \frac{y}{2}$:

$$P = \mathbf{A} + \mathbf{B} \sin^2 \frac{y}{2} + \mathbf{C} \sin^4 \frac{y}{2} + \mathbf{D} \sin^6 \frac{y}{2} \tag{5, 5}$$

$$\mathbf{A} = ((1 - \mathbf{R})^2 - \mathbf{R}_2 (1 - \sigma_2 \mathbf{R})^2)^2 \tag{5, 6}$$

$$\mathbf{C} = 16\mathbf{R} (2\mathbf{R}_2 (\sigma_2 \mathbf{R})^2 - \mathbf{R} (6\sigma_2^2 \mathbf{R}_2 - (\sigma_2 \mathbf{R}_2)^2 - 1) + 2\sigma_2 \mathbf{R}_2) \tag{5, 7}$$

$$\mathbf{D} = 64\mathbf{R}_2 (\sigma_2 \mathbf{R})^2 \tag{5, 8}$$

and

$$\mathbf{B} = \mathbf{M} - \mathbf{A} - \mathbf{C} - \mathbf{D} \text{ with } \mathbf{M} = ((1 + \mathbf{R})^2 + \mathbf{R}_2 (1 + \sigma_2 \mathbf{R})^2)^2. \tag{5, 9}$$

The coefficient \mathbf{A} is determined directly from (5, 3) when $y = 360^\circ \cdot (m - 1)$, and $\mathbf{M} = \mathbf{A} + \mathbf{B} + \mathbf{C} + \mathbf{D}$ is determined when $y_1 = y_2 = 180^\circ \cdot (2m - 1)$ is substituted in the denominator and simultaneously we get

$$I_{\max} = \frac{(\mathbf{T}_1 \cdot \mathbf{T}_2)^2}{\mathbf{A}} \text{ (when } \mathbf{T}_1 = \mathbf{T}_4 \text{ as is often the case)} \tag{5, 10}$$

and

$$F = \frac{I_{\max}}{I_{\min}} = \frac{\mathbf{M}}{\mathbf{A}}. \tag{5, 11}$$

The values of y at which maximum or minimum of $I(\lambda)$ occur are determined by $\frac{dP}{dy} = 0$,

$$\text{i. e.} \quad \sin \frac{y}{2} \cdot \cos \frac{y}{2} \left(\mathbf{B} + 2 \mathbf{C} \sin^2 \frac{y}{2} + 3 \mathbf{D} \sin^4 \frac{y}{2} \right) = 0.$$

Only one peak is present (for a given order m) at $y = 360^\circ \cdot (m-1)$ if there is no value of y which satisfies the equation

$$\mathbf{D} \cdot \sin^4 \frac{y}{2} + 2 \mathbf{C} \cdot \sin^2 \frac{y}{2} + \mathbf{B} = 0 \quad \text{or} \quad \sin^2 \left(\frac{y}{2} \right) = -\frac{\mathbf{C}}{3 \mathbf{D}} \pm \frac{\sqrt{\mathbf{C}^2 - 3 \mathbf{B} \mathbf{D}}}{3 \mathbf{D}}. \quad (5, 12)$$

A further investigation shows that the coefficients \mathbf{B} and \mathbf{D} are always positive numbers, from which it follows that if $\mathbf{C} > 0$, only a single peak results; if, however, $\mathbf{C} < 0$; $\mathbf{C}^2 - 3 \mathbf{B} \cdot \mathbf{D} > 0$, and three peaks result (for a given order m).

We now introduce $\mathbf{R} = \mathbf{H}$ corresponding to $\mathbf{C} = 0$, i. e. determined by

$$\underline{\mathbf{H}^2 - \mathbf{H} \left(3 - \frac{\mathbf{R}_2}{2} - \frac{1}{2 \cdot \sigma_2^2 \cdot \mathbf{R}_2} \right) + \frac{1}{\sigma_2} = 0}, \quad (5, 13)$$

and the final result is then the following:

if $\mathbf{R} < \mathbf{H}$, only one peak is present at $y = 360^\circ \cdot (m-1)$;

if $\mathbf{R} > \mathbf{H}$, three peaks result, the one at $y = 360^\circ \cdot (m-1)$

and the others at $y = \pm v + 360^\circ \cdot (m-1)$ determined by

$$\sin^2 \frac{v}{2} = -\frac{\mathbf{C}}{3 \mathbf{D}} + \frac{\sqrt{\mathbf{C}^2 - 3 \mathbf{B} \mathbf{D}}}{3 \mathbf{D}}, \quad (5, 14)$$

and the two minima between the 3 peaks at $y = \pm u + 360^\circ \cdot (m-1)$ are determined by

$$\sin^2 \frac{y}{2} = -\frac{\mathbf{C}}{3 \mathbf{D}} - \frac{\sqrt{\mathbf{C}^2 - 3 \mathbf{B} \mathbf{D}}}{3 \mathbf{D}}. \quad (5, 15)$$

Calculation of W_2 , W_{10} and W_{1000} .

The k 'th intensity band width W_k is determined in the usual way (from (5, 5)) by means of the equations

$$\left. \begin{aligned} (k-1) \mathbf{A} &= \mathbf{B} \cdot \sin^2 \frac{\gamma_k}{2} + \mathbf{C} \sin^4 \frac{\gamma_k}{2} + \mathbf{D} \sin^6 \frac{\gamma_k}{2}; \\ \gamma_k &= y - 360(m-1) \text{ and } W_k = \frac{\gamma_k \cdot \lambda_m}{180 \cdot f}. \end{aligned} \right\} (5, 16)$$

In the case of $\mathbf{R} = \mathbf{H}$ we have $\mathbf{C} = 0$, and \mathbf{B} has a small positive value, and W_{10} and still better W_{1000} can be determined approximately by

$$\sin \frac{\gamma_k}{2} = \sqrt[6]{\frac{(k-1) \mathbf{A}}{\mathbf{D}}} \quad (5, 16 a)$$

and

$$W_k = \frac{\gamma_k}{180} \cdot \frac{\lambda_m}{f} \quad (k = 10 \text{ and } 1000 \text{ respectively}).$$

In the case of W_2 , $\mathbf{B} \sin^2 \frac{\gamma_k}{2}$ has to be taken into account ($f \cong m$ for filters with silver layers).

Table 18 contains the results of calculations made in the special case of a symmetrical filter with four silver layers placed in a dielectric with $n = 1.36$. The calculations are carried out by means of Tables 6–13 and are analogous to the calculations of Table 17. When the thickness t'' of the central silver layers has been chosen, $\mathbf{R} = \sqrt{R' \cdot R''} = \mathbf{H}$ is calculated from (5, 13) so that only one peak results. Next R' , t' \mathbf{T}_1 and I_{\max} , F , W_2 , W_{10} and W_{1000} (2nd order) are calculated. For comparison I_{\max} $F = \frac{I_{\max}}{I_{\min}}$; W_2 and W_{10} for filters of the Fabry-Perot type ML_4M and for filters of the type $M'L_4M''L_4M'$ (Table 17) have been added. In Table 18, t for the Fabry-Perot filters has been chosen in such a way that I_{\max} is about the same as for filters of the type $M'L_4M''L_4M'$ treated in this section. The contrast factor F is about 10 times higher for this type of compound interference filters than for the type treated in § 4, and F for the latter type is again 10 times higher than the contrast factor F of a Fabry-

λ $\nu - i\kappa$	ML_4M				$M'L_4M'L_4M'$				$M'L_4M''L_4M''L_4M'$				
	t	R	I_{\max}/I_{\min}	$\frac{W_2}{W_{10}} \left(= 3 \cdot W_2 \right)$	t' t''	R' R''	I_{\max}/I_{\min}	$\frac{W_2}{W_{10}} \left(= W_2 \cdot 1.3 \right)$	t' t''	R' R''	I_{\max}/I_{\min}	$\frac{W_2}{W_{10}} \left(\approx 1.5 \cdot W_2 \right)$	W_{1000}
4000	550	.7469	0.11475	186 Å	449 Å	.6684	0.152	260 Å	344 Å	.5493	0.157	251 Å	1018 Å
0.18— i 1.95			0.48 · 10 ²	558	600	.7709	0.58 · 10 ³	450	600	.7709	0.79 · 10 ⁴	395	
4000	450	.6690	0.285	258	334	.5342	0.297	357	256	.3996	0.273	348	1681
0.18— i 1.95			0.25 · 10 ²	774	500	.7155	0.16 · 10 ³	618	500	.7155	0.13 · 10 ⁴	542	
4500	400	.7351	0.388	221	297	.5914	0.406	317	235	.4649	0.360	312	1184
0.14— i 2.42			0.43 · 10 ²	663	500	.8150	0.42 · 10 ³	549	500	.8150	0.59 · 10 ⁴	477	
5000	400	.8022	0.347	176	286	.6575	0.404	282	229	.5414	0.358	277	1022
0.14— i 2.89			0.83 · 10 ²	528	500	.8649	1.0 · 10 ³	489	500	.8649	2.29 · 10 ⁴	424	
5500	375	.8257	0.345	168	280	.7126	0.379	252	226	.6082	0.337	248	861
0.15— i 3.36			1.10 · 10 ²	504	500	.8951	2.3 · 10 ³	436	500	.8951	7.71 · 10 ⁴	380	
6000	350	.8466	0.368	159	269	.7508	0.386	231	218	.6567	.345	229	815
0.15— i 3.82			1.45 · 10 ²	477	500	.9188	4.8 · 10 ³	400	500	.9188	22.3 · 10 ⁴	348	
6560	350	.8802	0.3975	133	249	.7702	0.463	222	204	.6831	0.414	218	757
0.13— i 4.27			2.46 · 10 ²	399	500	.9398	7.7 · 10 ³	385	500	.9398	51.2 · 10 ⁴	332	
6560	300	.8375	0.502	185	194	.6583	0.585	339	156	.5473	0.532	337	1183
0.13— i 4.27			1.28 · 10 ²	555	400	.9084	1.4 · 10 ³	587	400	.9084	4.37 · 10 ⁴	503	
7100	300	.8582	0.475	173	217	.7416	0.516	268	178	.6478	0.466	265	915
0.14— i 4.68			1.72 · 10 ²	519	450	.9363	5.0 · 10 ³	464	450	.9363	27.3 · 10 ⁴	400	
7680	300	.8756	0.450	162	212	.7615	0.507	265	174	.6731	0.458	263	900
0.15— i 5.11			2.27 · 10 ²	486	450	.9438	7.3 · 10 ³	458	450	.9438	47.2 · 10 ⁴	395	

Perot filter with the same value of I_{\max} , and W_{10} is less for the two compound types than for the Fabry-Perot type. Furthermore these two types of interference filters make it possible (by variation of t' and t'') to vary the band width and at the same time to keep F constant. In many applications a broad band width, combined with a small intensity outside the band, is desirable.

In the formulae (5, 5–16) from which Table 18 has been calculated, the approximation $\alpha_2 = 0$ is done. Actually α_2 is not zero, but has a small negative value. However, this small value of α_2 is large enough to change the line shape considerably in the very neighbourhood of the peak (as was the case in § 4) but the “wings” of the line are almost unaltered, and W_2 and furthermore W_{10} and W_{1000} calculated from (5, 16) will be nearly the same as obtained by an exact numerical calculation.

The exact numerical calculations carried out for this type of compound interference filter are quite analogous to those carried out in § 4. The equation (5, 3) can be written in the following way:

$$I(\lambda) = \frac{(\mathbf{T}_1 \cdot \mathbf{T}_2)^2}{\varrho_1^4 \left| 1 - \mathbf{R}_2 \cdot \left(\frac{\varrho_2}{\varrho_1} \right)^2 \cdot e^{-i(y_2 - 2\varepsilon_2 + 2\varepsilon_1)} \right|^2}, \quad (5, 17)$$

With

$$\varrho_1 \cdot e^{i\varepsilon_1} = 1 - \mathbf{R} \cdot e^{-iy_1} \quad (5, 17a)$$

and

$$\varrho_2 \cdot e^{i\varepsilon_2} = 1 - \sigma_2 \mathbf{R}_2 \cdot e^{-iy_1 + i\alpha_2} \quad (5, 17b)$$

to be calculated in the first step, and the next step is to calculate

$$\varrho_3 \cdot e^{i\varepsilon_3} = 1 - \mathbf{R}_2 \cdot \left(\frac{\varrho_2}{\varrho_1} \right)^2 \cdot e^{-i(y_2 - 2\varepsilon_2 + 2\varepsilon_1)}, \quad (5, 17c)$$

and finally

$$I(\lambda) = \left(\frac{\mathbf{T}_1 \cdot \mathbf{T}_2}{\varrho_1^2 \cdot \varrho_3} \right)^2. \quad (5, 17d)$$

In the calculations y_2 is only exactly equal to y_1 at $\lambda = \lambda_m$, but chosen according to

$$y_2 - 360(m-1) = (y_1 - 360(m-1)) \cdot \frac{360m - \delta_{10} - \delta_{12}}{360m - 2\delta_{21}}, \quad (5, 18)$$

and the wavelength scale is determined by (3, 27 a) as previously.

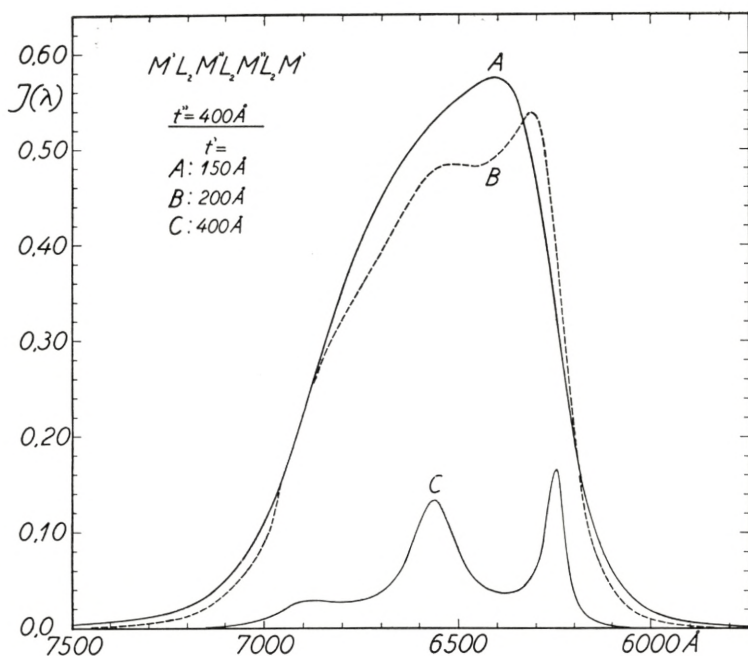


Fig. 34.

$I(\lambda)$ for filters of the type $M'L_2M''L_2M''L_2M'$ the thickness of M'' is 400 \AA in all cases. The thickness of M' is A: 150 \AA , B: 200 \AA and C: 400 \AA . The thicknesses of the L_2 layers are chosen such that λ_{\max} for $M'L_2M''$ and for $M''L_2M''$ is 6560 \AA .

In fig. 34 (analogous to fig. 20) the thickness of the two central silver layers is $t'' = 400 \text{ \AA}$ in all the graphs ($\sigma_2 = 1.0542$; $\alpha_2 = -0^\circ.466$). The thickness t' of the two outer silver layers is as follows:

A: $t' = 150$ almost corresponding to $\mathbf{R} = \mathbf{H}$ determined by (5, 13) (only one peak present).

B: $t' = 200 \text{ \AA}$ now $\mathbf{R} > \mathbf{H}$ (and $\mathbf{C} < 0$). Two neighbouring peaks result (the third peak which according to the approximate theory should have a position symmetrical to the second peak, has nearly disappeared in fig. 34).

C: $t' = 400 \text{ \AA}$. The four silver layers are all of equal thickness. Three peaks result. The positions of the peaks (along the abscissa) correspond closely to the values calculated from (5, 14); the line shapes for the two outer peaks are, however, very different from those calculated approximately from (5, 5–9). It is evident from

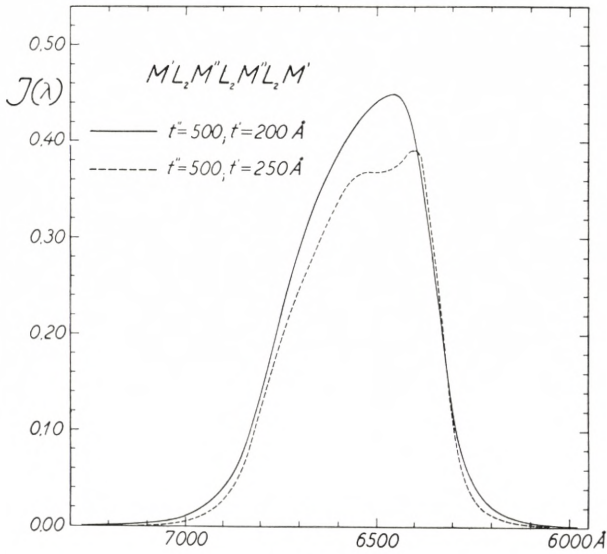


Fig. 35.

$I(\lambda)$ for two filters of the type $M'L_2M''L_2M''L_2M' \cdot t'' = 500 \text{ \AA}$ for both filters. Unbroken line: $t' = 200 \text{ \AA}$. Broken line: $t' = 250 \text{ \AA}$ d_1 and d_2 are determined such that λ_{\max} for the filters $M'L_2M''$ and $M''L_2M''$ is 6560 \AA .

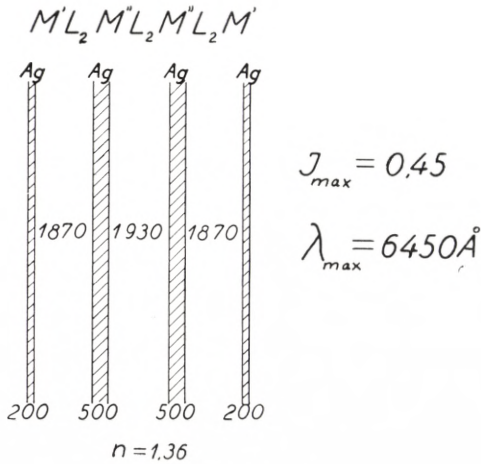


Fig. 36.

(All measures in \AA).

The relative measure for the thin layers in the compound filter, $I(\lambda)$ of which is shown in fig. 35 (unbroken line).

fig. 34 and from other numerical calculations not given here, that I_{\max} reaches its highest value if \mathbf{R} very closely corresponds to $\mathbf{R} = \mathbf{H}$ determined by (5, 13) (\mathbf{R}_2 regarded as constant). At $\mathbf{R} > \mathbf{H}$ (curve B) and for $\mathbf{R} < \mathbf{H}$ I_{\max} decreases, and at $\mathbf{R} = 0$ we have $M''L_2M''$ (i. e. the Fabry-Perot filter fig. 11 Curve C) with $I_{\max} = 0.30$. (The same data are used as in fig. 20).

In fig. 35 again a filter of the type $M'L_2M''L_2M''L_2M'$ is considered, but here the thickness of the two central silver layers is 500 \AA for both curves. The unbroken curve is $I(\lambda)$ when the thickness of the two outer silver layers is $t' = 200 \text{ \AA}$, this corresponds closely to $\mathbf{R} = \mathbf{H}$ determined by (5, 13); i. e. only one peak results. The broken curve is $I(\lambda)$ when $t' = 250 \text{ \AA}$; $\mathbf{R} > \mathbf{H}$ and an unsymmetrical line shape with two peaks results. Also here I_{\max} reaches its highest value near $\mathbf{R} = \mathbf{H}$; i. e. for $\mathbf{R} > \mathbf{H}$ and $\mathbf{R} < \mathbf{H}$ I_{\max} will decrease. For $\mathbf{R} = 0$ the filter is reduced to the Fabry-Perot filter $M''L_2M''$ (fig. 11 Curve D) with $I_{\max} = 0.12$. Both in fig. 34 and fig. 35 $\nu - i\kappa = 0.13 - i.4.27$ is regarded as constant and the wavelength scale is given by

$$\lambda = \frac{6560}{1 + \frac{y}{360}}$$

In fig. 37 $I(\lambda)$ (unbroken line) corresponding to a compound filter of the second order $M'L_4M''L_4M''L_4M'$ is shown. We get

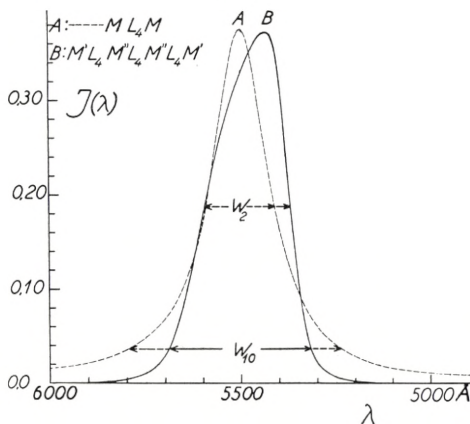


Fig. 37.

Unbroken line: $I(\lambda)$ for the filter $M'L_4M''L_4M''L_4M'$ the data of which are shown in fig. 38. Broken line: $I(\lambda)$ for a filter ML_4M with $t = 360 \text{ \AA}$. (The filter is shown in fig. 10).

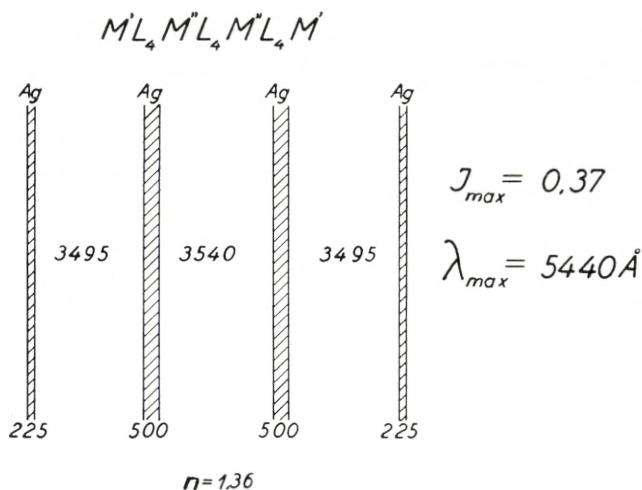


Fig. 38.

The filter $I(\lambda)$ of which is shown in fig. 37 (unbroken line). The relative dimensions are true to scale.

from fig. 37 $W_2 = 225 \text{ \AA}$ and $W_{10} = 370 \text{ \AA}$ in good agreement with the values calculated from the approximate theory with $\alpha_2 = 0$. (Table 18). Also here $I_{max} = 0.37$ is much higher than I_{max} of the Fabry-Perot filter $M''L_4M''$, which is equal to 0.14. t' has been chosen in such a manner that $R = H$ (determined by (5, 13)), and the thicknesses of the dielectric layers have been chosen in such a way that the Fabry-Perot filters $M'L_4M''$ and $M''L_4M''$ both have a peak at 5500 \AA . For comparison $I(\lambda)$ (broken line) for a Fabry-Perot filter ML_4M with the same I_{max} as for the compound filter, has been added. (The Fabry-Perot filter is the same as that shown in fig. 10). It should be noticed that W_{10} for the compound filter is considerably less than W_{10} for the Fabry-Perot filter and that $W_{10} \simeq 1.5 \cdot W_2$ for the compound filter.

In fig. 39 again $I(\lambda)$ corresponding to the filter in fig. 38 is shown (unbroken line) $\alpha_2 = -0.575^\circ$. The broken line is

$$I(\lambda) = \frac{0.337}{1 + 18.54 \sin^2\left(\frac{y}{2}\right) + 77062 \cdot \sin^6\left(\frac{y}{2}\right)}$$

calculated from (5, 5-9) with $\alpha_2 = 0$. Just as in fig. 25 the deviation between the two curves is rather great in the neigh-

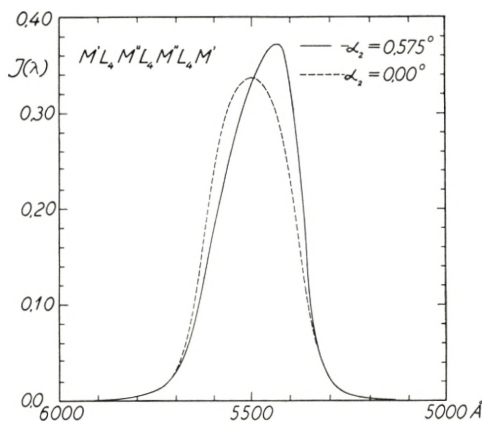


Fig. 39.

Unbroken line: $I(\lambda)$ for the filter in fig. 38 $\alpha_2 = -0.575^\circ$.
 Broken line: $I(\lambda)$ calculated from (5, 5—9) with $\alpha_2 = 0$.

bourhood of the peak. However, the deviations in W_2 and in W_{10} are small. As in case of fig. 34—35 the small negative value of α_2 gives rise to a shift in λ_{\max} towards violet (in comparison with λ_{\max} for the filters $M'L_4M''$ and $M''L_4M''$) and to an unsymmetrical line shape. Finally it should be noted that I_{\max} is raised by about 10 per cent. similarly to the filters of the type in § 4.

The thin silver layers at the outside of a filter (such as that in fig. 38) will more easily deteriorate through chemical action than the central thicker silver layers. However, the two outer silver layers can be replaced by dielectric layers as shown in fig. 40. The line shape will be almost the same as that shown in fig. 37 (unbroken line), but I_{\max} will be raised from 0.37 to 0.58 as no absorption takes place in the dielectric layers. (H in fig. 40 means a $\frac{\lambda}{4}$ -layer of ZnS with $n = 2.36$).

When the four silver layers are of the same thickness, three peaks result, with intensities lower than I_{\max} for the filter $M''L_2M''$ (fig. 34, C). If the thicknesses of the inner silver layers are smaller than that of the outer layers, the separation of the three peaks increases and as α_2 increases the difference in intensities of the three peaks will continue to increase. In fig. 41 (unbroken line) $I(\lambda)$ is indicated, calculated for a filter shown in fig. 42 a. The

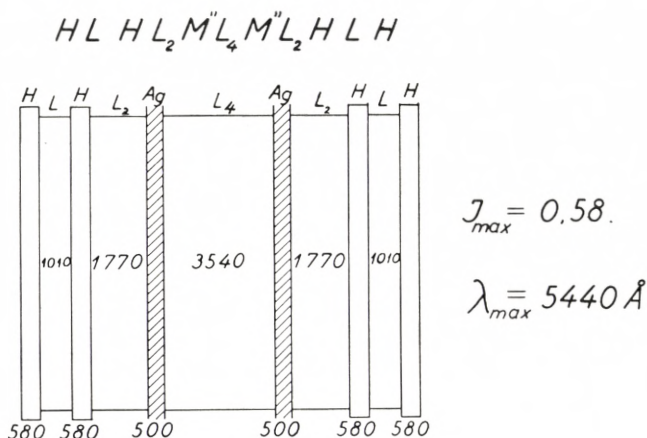


Fig. 40.

Filter of the compound type treated in this section with each of the external silver layers replaced by three dielectric layers.

$$L = \frac{\lambda}{4}\text{-layer with } n_L = 1.36$$

$$H = \frac{\lambda}{4}\text{-layer with } n_H = 2.36$$

thickness of the outer silver layers is equal to 400 \AA and of the central silver layers equal to 150 \AA . $\nu - i\kappa = 0.13 - i.4.27$ has been regarded as constant, and for this reason the calculation is only approximate for a filter of the 1st order.

If the central silver layers are replaced by two thin ZnS layers,

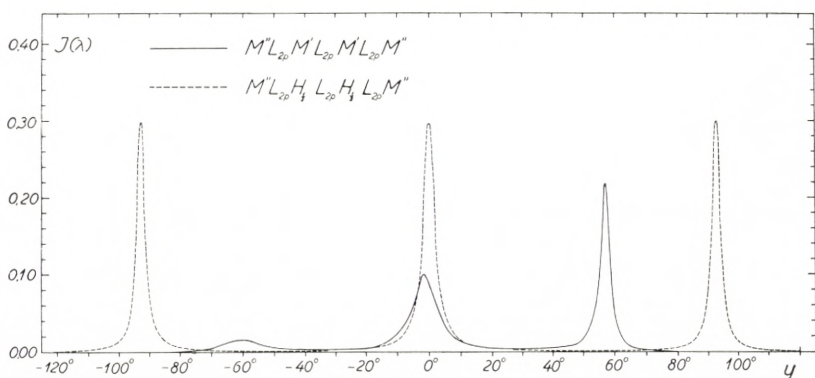


Fig. 41.

Continuous curve: $I(\lambda)$ for the filter $M''L_2M'L_2M'L_2M''$ constructed as shown in fig. 42 a. Broken line curve: $I(\lambda)$ for the filter $M''L_2H_{\frac{1}{2}}L_2H_{\frac{1}{2}}L_2M''$ constructed as shown in fig. 42 b.

$M''L_2M'L_2M'L_2M''$

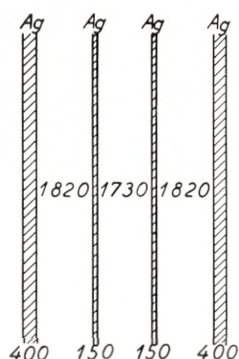


Fig. 42 a.

$M''L_2H_{\frac{1}{2}}L_2H_{\frac{1}{2}}L_2M''$

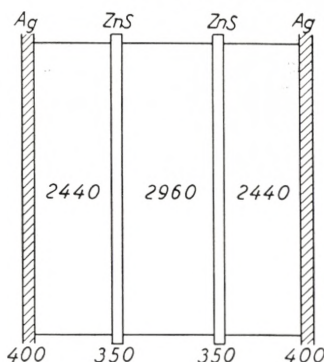


Fig. 42 b.

Fig. 42 a. The filter the $I(\lambda)$ of which is shown in fig. 41 (unbroken line).

Fig. 42 b. The filter $I(\lambda)$ of which is shown in fig. 41 (broken line).

The low index layers L_2 of the filters are determined in such a manner that the filters $M''L_2M'$, $M'L_2M'$, $M''L_2H_{\frac{1}{2}}$, and $H_{\frac{1}{2}}L_2H_{\frac{1}{2}}$ all have peak transmission at $\lambda = 6560 \text{ \AA}$.

then $a_2 = 0$ and in this case $I(\lambda)$ can be calculated by means of (5, 5—9). $I(\lambda)$ has been calculated (analogously to page 60) corresponding to a thickness of the ZnS layers equal to $\frac{\lambda}{8 n_H}$ at $\lambda = 6560 \text{ \AA}$, i. e. $x = 90^\circ$ (fig. 42 b). If $v - i\kappa = 0.13 - i.4.27$ and x are regarded as independent of the wavelength, we obtain (from (4, 17) and (5, 5—9))

$$I(\lambda) = \frac{0.001817}{0.006146 + 15.979 \sin^2 \frac{y}{2} - 60.959 \sin^4 \frac{y}{2} + 58.140 \cdot \sin^6 \frac{y}{2}}$$

$I(y)$ is shown in fig. 41 (broken line curve).

Fig. 43 shows the positions of the peaks for a higher order filter $M''L_{2p}H_{\frac{1}{2}}L_{2p}H_{\frac{1}{2}}L_{2p}M''$ as compared with the positions

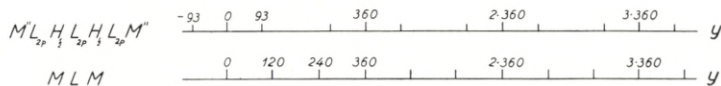


Fig. 43.

The position of the peaks on the y scale for a higher order filter $M''L_{2p}H_{\frac{1}{2}}L_{2p}H_{\frac{1}{2}}L_{2p}M''$ as compared with the position of the peaks for a Fabry-Perot filter $M''L_{6p}M''$.

of the peaks for a Fabry-Perot filter $M''L_{6\rho}M''$. (The values of I_{\max} are the same for the two filters).

The Filter $M'L_4M''L_4M''L_4M'$ Used as Phase Plate.

In fig. 44 the phase change at transmission is shown for a filter $M'L_4M''L_4M''L_4M'$ (like that in fig. 38). The phase difference between P_2 (light passing through the phase plate) and P_1 (light passing outside the phase plate) is, according to (5, 2),

$$\xi(\lambda) = \left. \begin{aligned} & \left(2\beta_1 + 2\beta_2 - \frac{360}{\lambda} \cdot n(2d_1 + d_2) - \varepsilon_3(\lambda) \right) \\ & + \frac{360}{\lambda} (2t' + 2t'' + 2d_1 + d_2). \end{aligned} \right\} \quad (5, 18)$$

β_1 is the phase change at transmission for the outer silver layers and β_2 the phase change for the central silver layers.

d_1 is the thickness of the two outer dielectric layers and d_2 for the central dielectric layer and the approximations $\beta_{01} = \beta_{34} = \beta_1$ and $2\beta_1 + 2\beta_2 = \beta_0 - k \cdot \lambda$ are made.

$\varepsilon_3(\lambda)$ (the phase change from multiple reflections in the layers) is calculated from (5, 17 c).

Calculation of $R(\lambda)$.

The intensity distribution $R(\lambda)$ in reflection from a filter of this compound type can be calculated directly from (5, 1); this equation can (in the case of symmetry) be written as follows:

$$R_{04}(\lambda) = \frac{R_{01} \varrho_4^2 \left| 1 - \mathbf{R}_2 \cdot \frac{\varrho_2}{\varrho_1} \cdot \frac{\varrho_5}{\varrho_4} \cdot e^{i(\varepsilon_2 - \varepsilon_1) + i(\varepsilon_3 - \varepsilon_4) - iy_2} \right|^2}{(\varrho_1 \varrho_3)^2},$$

where $\varrho_1 \cdot e^{i\varepsilon_1} = 1 - \mathbf{R} \cdot e^{-iy_1}$; $\varrho_2 \cdot e^{i\varepsilon_2} = 1 - \sigma_2 \cdot \mathbf{R} \cdot e^{-i(y_1 - \alpha_2)}$ ($\mathbf{R} = \sqrt{R' \cdot R_2}$) and $\varrho_3 \cdot e^{i\varepsilon_3} = 1 - \mathbf{R}_2 \cdot \left(\frac{\varrho_2}{\varrho_1} \right)^2 \cdot e^{2i(\varepsilon_2 - \varepsilon_1) - iy_2}$ have previously been calculated. If further $\varrho_4 \cdot e^{i\varepsilon_4} = 1 - \sigma_1 \mathbf{R} \cdot e^{-i(y_1 - \alpha_1)}$ and $\varrho_5 \cdot e^{i\varepsilon_5} = 1 - \sigma_1 \cdot \sigma_2 \cdot \mathbf{R} \cdot e^{-i(y_1 - \alpha_1 - \alpha_2)}$ are calculated by means of Rybner's tables [4], we finally obtain

$$R(\lambda) = R' \cdot \left(\frac{\varrho_4 \cdot \varrho_6}{\varrho_1 \cdot \varrho_3} \right)^2 \quad (\varrho_6 \text{ denote the bracket in the numerator}).$$

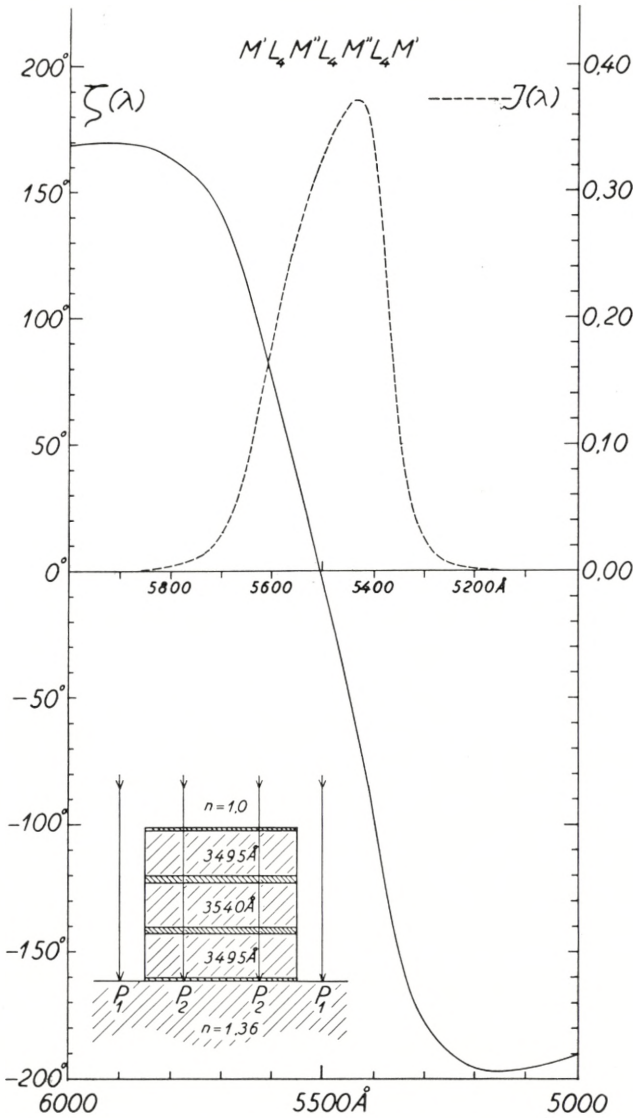


Fig. 44.

Unbroken line: Phase change at transmission through a filter of the type $M'L_4M''L_4M'L_4M'$. (Phase difference between P_2 and P_1). Broken line: $I(\lambda)$ for the same filter. The phase plate is shown below in the left corner of fig. 44.

This calculation has been done in case of three filters. (The $I(\lambda)$'s for these filters are shown in fig. 34 Curve A, fig. 35 unbroken line and fig. 37 unbroken line corresponding to $R(\lambda)$ in

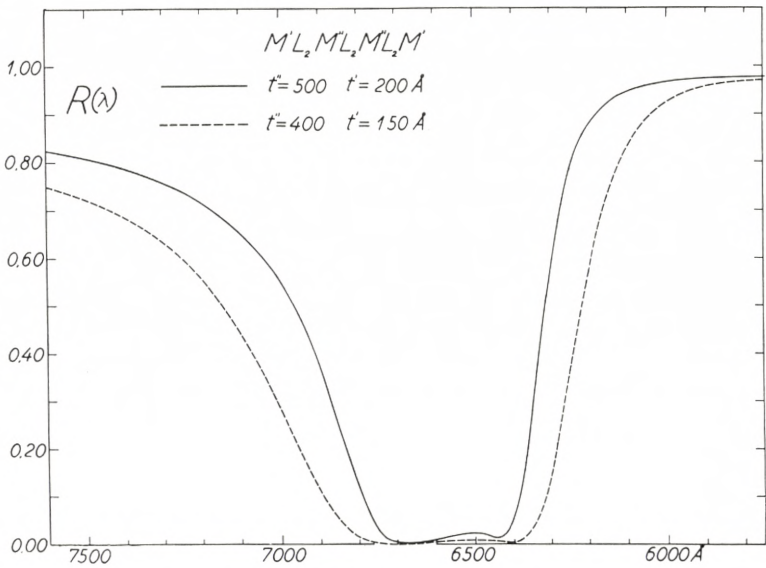


Fig. 45.

Unbroken line: $R(\lambda)$ for the filter shown in fig. 36 and the $I(\lambda)$ for the same filter is shown in fig. 35. (Unbroken line). $\alpha_1 = -2^\circ.084$; $\alpha_2 = -0^\circ.230$. Broken line: $R(\lambda)$ of a filter of the same type but with thinner silver layers. The corresponding $I(\lambda)$ curve is given in fig. 34 (Curve A) $\alpha_1 = -2^\circ.971$; $\alpha_2 = -0^\circ.466$.

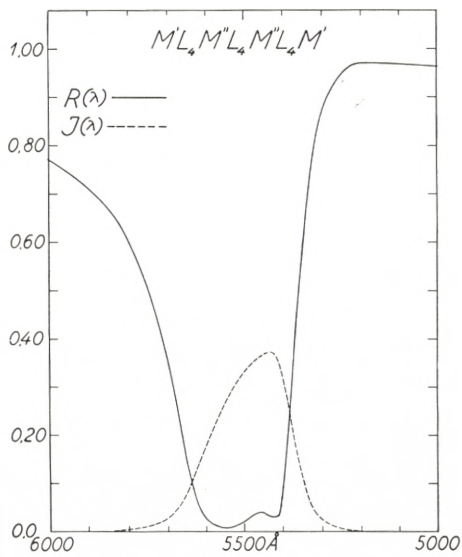


Fig. 46.

Unbroken line: $R(\lambda)$ for the compound filter constructed as shown in fig. 38. Broken line: $I(\lambda)$ for the same filter. $\alpha_1 = -3^\circ.386$; $\alpha_2 = -0^\circ.575$.

fig. 45 broken and unbroken line, and to fig. 46 unbroken line, respectively).

A general mathematical analysis has not been carried out and would be rather complicated because the value of α_1 here is essential for the shape of the $R(\lambda)$ curve.

The three curves of $R(\lambda)$ (fig. 45—46) have much the same trend (two minima). It should be noticed that the broad minimum towards longer wavelength is near zero intensity especially in the case of fig. 45.

In the previous section only the case $y_2 = y_1$ has been considered in detail. If $y_2 = m \cdot y_1$ ($m = 2, 3, 4 \dots$), the condition which expresses that only one peak must occur (at a definite order) is more complicated. However, the condition which expresses that I_{\max} should have its highest value for a definite value of R_2 is the same as in the case of $y_2 = y_1$, and in reality the only difference in the the case of $y_2 = m \cdot y_1$ is that W_2 becomes smaller than in case of $y_2 = y_1$ and satellite bands occur corresponding to the higher orders for the filter $M''L_{2m}M''$.

§ 6. Improvements of the Interference Filters $ML_{2m}M$, $M'L_{2m}M''L_{2m}M'$ and $M'L_{2m}M''L_{2p}M''L_{2m}M'$ by Means of $\frac{\lambda}{4}$ -layers with Alternately Low (L) and High (H) Index of Refraction.

The simplest improvement is to replace the L_{2m} layer with three dielectric layers $L'H_{2m-2}L'$.

From (2, 17 a) we get at normal incidence

$$\frac{1 - r_{20}}{1 + r_{20}} = \frac{n_L (1 - \sqrt{R_{10}} \cdot e^{-i(x_1 - \delta_{10})})}{n_H (1 + \sqrt{R_{10}} \cdot e^{-i(x_1 - \delta_{10})})}. \quad (6, 1)$$

The maximum value of R_{20} occurs when $x_1 = \delta_{10}$, and in this case R_{20} is determined by

$$\frac{1 - \sqrt{R_{20}}}{1 + \sqrt{R_{20}}} = \frac{n_L}{n_H} \cdot \left(\frac{1 - \sqrt{R_{10}}}{1 + \sqrt{R_{10}}} \right) = a, \quad \text{i. e.} \quad R_{20} = \left(\frac{1 - a}{1 + a} \right)^2. \quad (6, 2)$$

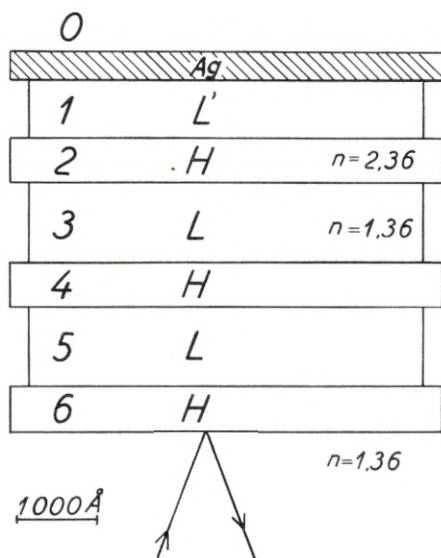


Fig. 47.

The reflective system I or II of fig. 6.

The next improvements of the filter $ML_{2m}M$ (or more correctly $ML'L_{2m-2}L'M'$) would be $ML'HL_{2m-4}HL'M$ and $ML'HLH_{2m-6}LHL'M$, etc.

Again by (2, 17 a) we get

$$\frac{1-r_{30}}{1+r_{30}} = \frac{n_H}{n_L} \left(\frac{1+\sqrt{R_{20}}}{1-\sqrt{R_{20}}} \right) = \left(\frac{n_H}{n_L} \right)^2 \left(\frac{1+\sqrt{R_{10}}}{1-\sqrt{R_{10}}} \right)$$

and in general

$$\frac{1-\sqrt{R_{q,0}}}{1+\sqrt{R_{q,0}}} = \left(\frac{n_L}{n_H} \right)^{q-1} \left(\frac{1-\sqrt{R_{10}}}{1+\sqrt{R_{10}}} \right) \quad (6, 3)$$

and

$$\delta_{q,0} = -(q-2) \cdot 180^\circ. \quad (6, 4)$$

In this way the reflectivity from each of the systems I and II of a filter like that in fig. 6 can easily be calculated. The calculation of transmission T and of $\sigma \cdot e^{i\alpha}$ is carried out by means of the following general theorem:

If two filters A and B (fig. 48) only differ in such a way that

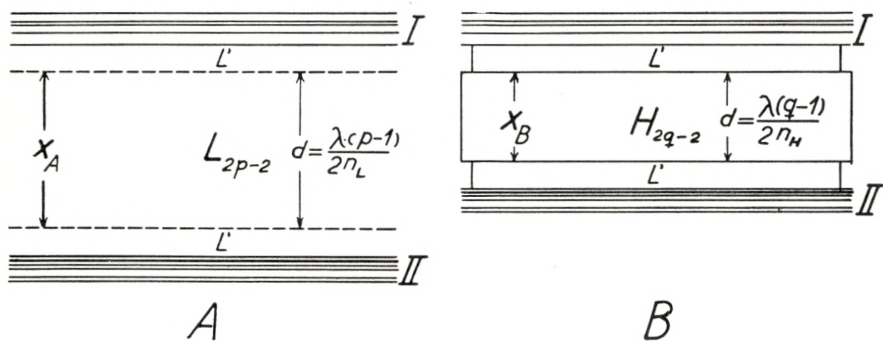


Fig. 48.

the layer L_{2p-2} at A is replaced by the layer H_{2q-2} at B, where L and H are exactly $\frac{\lambda}{4}$ -layers for a wavelength λ_1 (corresponding to $x_A = 360^\circ \cdot (p-1)$ and $x_B = 360^\circ \cdot (q-1)$), then $I(\lambda_1)$, $R(\lambda_1)$, $\zeta(\lambda_1)$, etc., are identical for the two filters (follows direct from the recurrence formulae (2,7-8)), and we get $\frac{T_A}{1-R_A} = \frac{T_B}{1-R_B}$ (which

is a special case of (2,18b)) and $\frac{1 - \sigma_A \cdot R_A \cdot e^{i\alpha_A}}{1 - R_A} \simeq \frac{1 - \sigma_B \cdot R_B \cdot e^{i\alpha_B}}{1 - R_B}$.

From these equations R_B , T_B , σ_B and α_B can easily be calculated for the wavelength λ_1 with good accuracy when $t > 350 \text{ \AA}$.

When we add more quarter wavelength layers to the silver layer, (fig. 47) R_{0q} increases according to (6, 3). This means that the absorption factor A_{0q} as well as σ_q and α_q will decrease.

To calculate $I(\lambda)$ for filters of the type § 3 when I and II of fig. 6 consist of several layers, we must first calculate $y(\lambda)$ by means of (2, 7) and (3, 6 a), and next y is substituted in (3, 5 b).

In fig. 49 $y(\lambda)$ is calculated for different numbers of dielectric layers but with the same thickness $t = 350 \text{ \AA}$ of the silver layers.

$\lambda_1 = 6560 \text{ \AA}$ $n_L = 1.38$ (MgF_2) and $n_H = 2.36$ (ZnS). From fig. 49 it is obvious that besides the main peak at 6560 \AA neighbouring peaks occur. E. g. the filter $ML'HLHL H_2 LHLHL'M$ has peaks at 5130 \AA , 4740 \AA , and 4340 \AA (where $y = 360^\circ \cdot p$) (Curve C). For comparison a Fabry-Perot filter $ML'L_8L'M$ has been added (Curve D, broken line). This filter has neighbouring peaks at 5480 \AA , 4700 \AA , and 4120 \AA (read off from fig. 49). Not only the

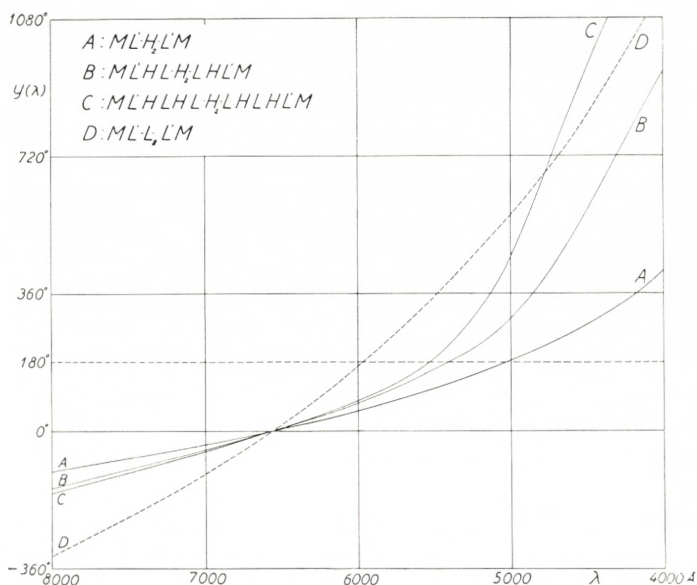


Fig. 49.

$y(\lambda)$ calculated for filters of different kinds $A-D$. $n_L = 1.38$, $n_H = 2.36$ and $t = 350 \text{ \AA}$ for the M layers.

main peak at 6560 \AA , but also the neighbouring peaks will according to (2, 18 b) have the same $I_{\max} = \left(\frac{T}{1-R}\right)^2$ for the two filters C and D . In Table 19 some characteristic properties of the filters $A-D$ have been added.

TABLE 19.

	q	R_{0q}	f	W_2	λ_{\min}	I_{\min}	$\lambda_{2(\max)}$
A	2	0.9243	1.61	102.1 \AA	5030 \AA	$4.65 \cdot 10^{-3}$	4180 \AA
B	4	0.9734	2.11	26.6	5410	$1.05 \cdot 10^{-3}$	4860
C	6	0.9908	2.33	8.2	5530	$0.49 \cdot 10^{-3}$	5130
D		0.8740	5.00	56.3	5970	$2.91 \cdot 10^{-3}$	5480

$\lambda_1 = 6560 \text{ \AA}$ and $I_{\max} = 0.398$ in all the filters $A-D$ (fig. 49)

$$f = -\left(\frac{dy}{d\lambda}\right)_{\lambda=\lambda_1} \cdot \frac{\lambda_1}{360} \quad \text{and} \quad I_{\min} = \left(\frac{T_1}{1-R_1}\right)^2 \cdot \left(\frac{1-R_{\min}}{1+R_{\min}}\right)^2.$$

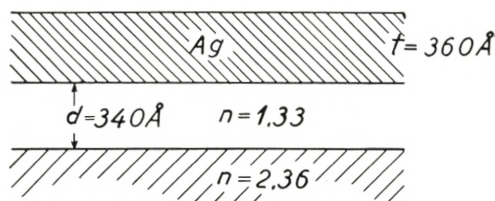


Fig. 50.

Filters of this silver multiple dielectric layer type have been described and produced by TURNER [20] and DUFOUR [21].

Calculation of $I(\lambda)$ for such a filter at oblique incidence can be carried out in an analogous way for the s and p component treated separately. (First R_{0q} , δ_{0q} from (2, 7–11) and (1, 12–13), next $y(\lambda)$ from (3, 6 a), and finally $I(\lambda)$ from (3, 5 b) are to be calculated).

The simplest filter of this type is $ML'H_{2m-2}L'M$. This filter is of interest for special purposes because the violet shift of λ_1 at oblique incidence is smaller than in the filter $ML_{2m}M$. As mentioned above, the highest value of R_{02} occurs when L' has a thickness of $\frac{\delta_{10}}{180} \cdot \frac{\lambda_1}{4 n_L}$, i. e. $x_1 = \delta_{10} \simeq 141^\circ$. If x_1 is considerably less than this value ($x_1 \simeq 60^\circ$), a calculation shows that the splitting up into two components λ_s and λ_p is small up to an angle of incidence of 60° . If $n_H = 2.36$, n_L should be below 1.34 to get the best result. (Fig. 50).

§ 7. Multiple Dielectric Layer Interference Filters.

Each of the systems I and II (in the case of filters of § 3 or I–IV in the case of filters of § 4–5) consist in this case of 3–11 quarter wavelength layers of dielectrics with alternately low (n_L) and high (n_H) index of refraction in this case beginning with a high index layer on the filter blank.

If I and II (fig. 6) each consist of q quarter wavelength layers $D_q = HLHLHLH \dots$, the reflectivity R_q of the system D_q is at the peak λ_1 (where the layers are exactly $\frac{\lambda}{4}$ -layers) determined by (6, 3) to be

$$R_q(\lambda_1) = \left(\frac{1 - \left(\frac{n_L}{n_H}\right)^q \cdot \frac{n_G}{n_H}}{1 + \left(\frac{n_L}{n_H}\right)^q \cdot \frac{n_G}{n_H}} \right)^2 \quad (7, 1)$$

n_G is the index of refraction of the filter blank (glass plate $n_G = 1.518$).

To calculate $I(\lambda)$ for filters with reflective systems of this type R_q , δ_q must be calculated by means of (2, 7) as a function of $x = 180^\circ \cdot \frac{\lambda_1}{\lambda}$ (at normal incidence). SCHRÖDER [22] has from (2, 7) developed a general mathematical expression for $1 - R_q(x)$ and made calculations for $r = 0.25$ and $r = 0.40$ ($r = \frac{n_H - n_L}{n_H + n_L}$ at $\varphi = 0$). ABELÈS [7] has expressed $R_q(x)$, $\delta_q(x)$ in terms of TCHEBYCHEFF's polynomials, and by means of an NBSMTP table $R_9(x)$ has been calculated. Further investigations concerning $R_q(x)$, $\delta_q(x)$ have been made by DUFOUR [23], DUFOUR and HERPIN [24], and VAŠÍČEK [25].

Some of these calculations have been repeated here, carried out direct from the recurrence formula (2,7) by means of RYBNER's tables [4]. All these calculations show that within a span of $2v$ in x $180 - v < x < 180 + v$ the difference $R_q(x) - R_q(180)$ will be sufficiently small to make use of D_q as a reflective coating for interference filters within the region $\lambda_0 < \lambda < \lambda_2$. λ_1 corresponds to $x = 180^\circ$; λ_0 to $x = 180^\circ + v$ and λ_2 to $x = 180^\circ - v$, $x = \frac{\lambda_1}{\lambda} \cdot 180^\circ$ and $R_q(-x) = R_q(x)$.

This wavelength region $\lambda_0 < \lambda < \lambda_2$ is almost independent of q when $q > 5$; outside this region $R_q(x)$ decreases rapidly; according to VAŠÍČEK [25] the more the greater q is.

The value of v is a function of r only. When $n_L = 1.38$ (MgF_2) and $n_H = 2.36$ (ZnS) (as in Table 20), we have $r = 0.262$ and $v \simeq 30^\circ$. When $\lambda_1 = 5500 \text{ \AA}$, this corresponds to $\lambda_0 = 4715 \text{ \AA}$ and $\lambda_2 = 6600 \text{ \AA}$, and for $\lambda_1 = 6560 \text{ \AA}$ we get $\lambda_0 = 5620 \text{ \AA}$ and $\lambda_2 = 7870 \text{ \AA}$. If $r = 0.4$, we get $v \simeq 50^\circ$, at $\lambda_1 = 6560 \text{ \AA}$ this corresponds to $\lambda_0 = 5130 \text{ \AA}$ and $\lambda_2 = 9080 \text{ \AA}$. ($r = 0.4$ corresponds closely to MgF_2 and Sb_2S_3 which according to SCHRÖDER

[22] can be employed in the red-infrared region). So with this type of filters the wavelength region covered by the filter is more restricted than by filters with silver layers.

TABLE 20.

q	R_q $x = 180^\circ$	R_q $x = 180^\circ \pm 30^\circ$	f $= \frac{1}{2} \cdot \left(\frac{dy}{dx} \right)_{x=180^\circ}$	W_2 $\lambda_1 = 6560 \text{ \AA}$
1	0.2056	0.1946	1.40	
2	0.4089	0.3671	1.74	
3	0.5962	0.5162	2.00	
4	0.7399	0.6298	2.15	294 \AA
5	0.8386	0.7134	2.25	164
6	0.9022	0.7747	2.32	92.7
7	0.9416	0.8199	2.37	53.0
8	0.9654	0.8664	2.39	30.8
9	0.9796	0.8902	2.40	17.0
10	0.9881	0.9086	2.40	10.4
11	0.9930	0.9231	2.41	6.1
12	0.9959	0.9342	—	3.6
13	0.9976	0.9436	—	2.1
14	0.9986	0.9513	—	1.2
15	0.9992	0.9577	—	0.7

In Table 20

$$f = - \left(\frac{dy}{d\lambda} \right)_{\lambda=\lambda_1} \cdot \frac{\lambda_1}{360} = \frac{1}{2} \cdot \left(\frac{dy}{dx} \right)_{x=180} \simeq \frac{y(180) - y(176)}{8}$$

and

$$W_2 = \frac{(1 - R_q) \cdot \lambda_1}{f \cdot \pi \cdot \sqrt{R_q}}$$

for filters of the type $D_q L_2 D_q$ (q uneven) or $D_q H_2 D_q$ (q even). The final f value is a function of r only and decreases when r increases. In fig. 51 $y(\lambda)$ is shown for filters of a different kind of the type in § 3. Curve A corresponds to $D_3 L_2 D_3$ which is very closely equal to $y(\lambda)$ for $ML_4 M$. Curve B corresponds to $D_7 L_2 D_7$ (or very closely to $D_6 H_2 D_6$). Curve C refers to $y(\lambda)$ for $ML_6 M$ and Curve E to $D_7 L_4 D_7$ (f for this filter is 3.37). All the filters have peak transmission at $\lambda_1 = 6560 \text{ \AA}$.

Reflective coatings D_q for FABRY-PEROT interferometers and filters of the type $D_q L_2 D_q$ with $q = 7, 9, 11$ have in recent years

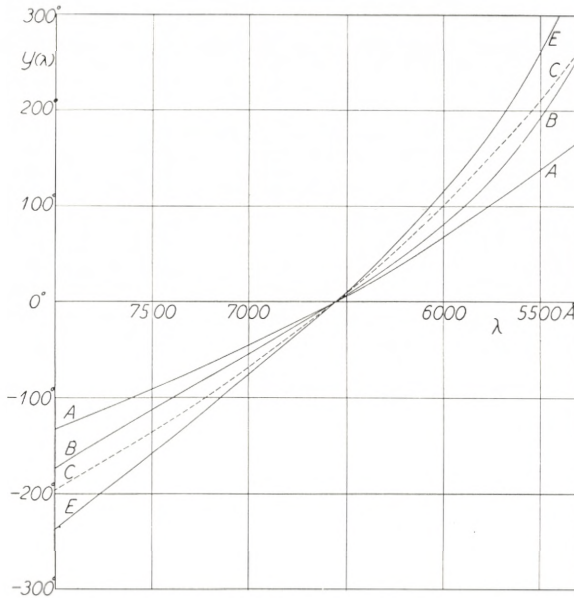


Fig. 51.

$y(\lambda)$ for filters of different kinds. A: $D_3 L_2 D_3$ ($D_3 = HLH$) or $ML_4 M$. B: $D_7 L_2 D_7$ ($D_7 = HLHLHLH$). C: $ML_6 M$ and E: $D_7 L_4 D_7$. $n_L = 1.38$, $n_H = 2.36$ (and $t = 350 \text{ \AA}$ for the M -layers).

been made in many laboratories [26–30], most of them with cryolite and ZnS as low and high index materials. Because of absorption in the ZnS layers such coatings can only be employed for $\lambda > 4000 \text{ \AA}$. From measurements of I_{\max} and W_2 at $D_7 L_2 D_7$ filters RING and WILCOCK [30] have calculated the absorption in a D_7 system of layers to be 0.017 at 4100 \AA and 0.008 at 4500 \AA . POLSTER [29] has produced filters $D_7 L_2 D_2$ with I_{\max} as high as 0.80 at $\lambda_1 = 5500 \text{ \AA}$, which corresponds to a still smaller absorption in a D_7 system of layers. Because of crystalline structure in the spacer layer L_2 and absorption in the D_q layers it has not been possible so far to obtain a value of W_2 lower than $10\text{--}15 \text{ \AA}$ [30].

At an oblique angle of incidence φ we have $x_H = \frac{\lambda_0}{\lambda} \cdot 180^\circ \cdot \cos \chi_H$ and $x_L = \frac{\lambda_0}{\lambda} \cdot 180^\circ \cdot \cos \chi_L$ (if $x_H = x_L = \frac{\lambda_0}{\lambda} \cdot 180^\circ$ at $\varphi = 0$). To obtain $I(\lambda)$, $R_q(\lambda)$ and $\delta_q(\lambda)$ must be calculated separately for the s and p component by means of the recurrence formula (2, 7) combined with (2, 10–11). To find (λ_s, λ_p) corresponding to λ_0

at $\varphi = 0$ for a filter $D_q L_2 D_q$ it is sufficient to determine x_L in such a way that $y = 2(x_L - \delta_q(x_L))$ is equal to $360 \cdot p$, ($p = 0, 1, 2, 3 \dots$). Such a calculation of $y(x_L)$ in the neighbourhood of the peak can be carried out by means of RYBNER'S tables [4] or by means of a graphical method (to be described in a following paper).

In Table 21 (λ_s, λ_p) have been calculated for two filters $D_6 H_2 D_6$ and $D_7 L_2 D_7$ with $\lambda_0 = 6560 \text{ \AA}$. It should be noticed, however, that if the dispersion of MgF_2 and ZnS is neglected, $\frac{\lambda_s}{\lambda_0}, \frac{\lambda_p}{\lambda_0}$ are independent of λ_0 .

TABLE 21. ($\lambda = 6560 \text{ \AA}$)

	φ	15°		30°		45°		60°		75°	
		<i>s</i> & <i>p</i>		<i>s</i>	<i>p</i>	<i>s</i>	<i>p</i>	<i>s</i>	<i>p</i>	<i>s</i>	<i>p</i>
$D_6 H_2 D_6$	λ_{\max}/λ_0	0.9897	0.9613	0.9605	0.9215	0.9176	0.8805	0.8702	0.8497	0.8318	
	λ_{\max}	6493	6306	6301	6045	6019	5776	5709	5574	5456	
$D_7 L_2 D_7$	λ_{\max}/λ_0	0.9866	0.9482	0.9491	0.8616	0.8958	0.8286	0.8399	0.7771	0.7968	
	λ_{\max}	6472	6220	6226	5849	5876	5436	5510	5098	5227	
	<i>r</i>	0.2620	0.2840	0.2398	0.3103	0.2124	0.3428	0.1774	0.3720	0.1448	

In Table 22 W_2 has been calculated for $\varphi = 75^\circ$ in the case of the filter $D_7 L_2 D_7$

$$f_s = - \left(\frac{dy}{d\lambda} \right)_{\lambda=\lambda_s} \cdot \frac{\lambda_s}{360} = \left(\frac{dy}{dx_L} \right)_{\lambda=\lambda_s} \cdot \frac{1}{2} \cdot \frac{\lambda_0}{\lambda_s} \cdot \cos \chi_L$$

(and analogously for the *p* component).

TABLE 22.

	<i>s</i>	<i>p</i>
λ_{\max}	5098 Å	5227 Å
<i>f</i>	1.90	3.35
R_q	0.9887	0.6618
W_2	9.7 Å	208 Å

$\varphi = 75^\circ D_7 L_2 D_7$ filter.

Calculations at oblique incidence up to $\varphi = 30^\circ$ have also been done by DUFOUR and HERPIN [24].

In Tables 20—22 $n_H d_H = n_L d_L = \frac{\lambda_0}{4}$ to obtain optimum conditions at $\varphi = 0$. However, to obtain optimum conditions at a definite angle of incidence φ and at a definite wavelength λ_1 we must require that

$$x_H = x_L = 180^\circ \text{ or } n_H d_H = \frac{\lambda_1}{4 \cdot \cos \chi_H} \text{ and } n_L d_L = \frac{\lambda_1}{4 \cos \chi_L} \quad (7, 2)$$

and in this case we have $\lambda_1 = \lambda_s = \lambda_p$ (no split-up into two components), only $W_2^{(s)}$ will be different from $W_2^{(p)}$ because r_s and r_p are different (Tables 21—22). It should further be noted that if (7, 2) is satisfied at e. g. $\varphi = 45^\circ$, $\lambda_s - \lambda_p$ in the whole region $0 < \varphi < 45^\circ$ will be very small.

Finally it should be mentioned that for special purposes it would perhaps be valuable to construct all-dielectric filters also of the types described in § 4 and § 5. If the absorption in a D_7 system is 0.01 and in a D_9 system 0.02 [28] I_{\max} for the filter $D_5 L_2 D_9 L_2 D_5$ would be 0.75, for the filter $D_3 L_2 D_7 L_4 D_7 L_2 D_3$ 0.90, and for the filter $D_3 L_2 D_9 L_2 D_9 L_2 D_3$ 0.60 (I_{\max} for the filter $D_9 L_2 D_9$ would be 0.11). Filters of a similar type have been suggested by TURNER [31].

Summary.

A general theory of interference filters has been developed concerning filters with two three and four systems of reflective layers.

In § 1 and § 2 the general equations for a system of thin layers have been developed, which are to be used at the calculation of all the optical properties of the system such as R , T , δ , β , etc. (reflectivity, transmission, phase change at reflection and transmission, etc.) when the indices of refraction (n , $\nu - i\kappa$) and the thicknesses (d , t) of all the layers in the system are known. These general equations in § 2 have been developed from FRESNEL'S equations at a boundary treated in § 1. In § 3 a

general theory has been developed for interference filters with two systems of reflective layers I and II. This theory has been used for a numerical calculation of $I(\lambda)$, $R(\lambda)$ for the FABRY-PEROT filter $ML_{2m}M$ ($M = Ag$ layer, $L = \frac{\lambda}{4}$ -layer of dielectric), and furthermore the phase change at transmission through the filter $\zeta(\lambda)$ has been calculated. (The filter used as phase plate). Next, $I(\lambda)_s$ and $I(\lambda)_p$ of the filter ML_2M have been calculated at the oblique incidence φ . ($\varphi = 45^\circ, 60^\circ, 75^\circ$). In § 4 a general theory of interference filters with three systems of reflective layers I, II, III has been developed. The condition to get only one peak (at a definite order) is

$$R < 1 - \sqrt{1 - \frac{1}{\sigma_2}}; \quad R = \sqrt{R' \cdot R''} \quad (\sigma_2 \simeq \frac{1 - A''}{R''} \quad \text{and} \quad R'')$$

refer to the centre layer II and R' to the outer layers II and III), and this condition corresponds closely to the condition of obtaining the highest value of I_{\max} at a definite value of R'' . This theory has been applied to numerical calculations of $I(\lambda)$ (and in a few cases also $R(\lambda)$) in the case of filters with three silver layers $M' L_{2m} M'' L_{2m} M'$. Also $\zeta(\lambda)$ has been calculated.

In § 5 quite an analogous theory has been developed for filters with four systems of reflective layers I—IV. Here the equation for obtaining optimum conditions is $R < H$, where H is determined by

$$H^2 - H \left(3 - \frac{R_2}{2} - \frac{1}{2 \cdot \sigma_2 \cdot R_2} \right) + \frac{1}{\sigma_2} = 0 \quad (R_2 = R'');$$

R_2 , σ_2 refer to II, III and R' to I, IV ($R = \sqrt{R' \cdot R''}$). Here again $I(\lambda)$, $\zeta(\lambda)$ and $R(\lambda)$ have been calculated for filters with four silver layers $M' L_{2m} M'' L_{2m} M'' L_{2m} M'$.

In § 6 is treated the improvement of filters with silver layers by means of quarter wavelength layers of dielectrics (L and H layers of fluoride and ZnS). The properties of filters such as $ML'H_2L'M$ and $ML'HLH_2LHL'M$ have been calculated.

In § 7 the application of multiple dielectric layer systems $D_q = HLHLHLHL \dots$ (q layers) instead of silver layers as

reflective systems I—IV has been treated. The limited wavelength region $\lambda_2 - \lambda_0$ for high reflectivity has been determined for $r = 0.26$ and $r = 0.40$. Furthermore, the properties of the filters $D_6 H_2 D_6$ and $D_7 L_2 D_2$ have been calculated at oblique incidence ($\varphi = 15^\circ, 30^\circ, 45^\circ, 60^\circ$ and 75°) as well. Filters of the types $D_5 L_2 D_9 L_2 D_5$ and $D_3 L_2 D_7 L_4 D_7 L_2 D_3$ have also been mentioned.

Acknowledgement.

These investigations have been made at the Physics Department of the Royal Veterinary and Agricultural College, Copenhagen. I wish to thank the director of the Physics Department, Professor EBBE RASMUSSEN, for the great interest he has taken in this work.

*Physics Department,
Royal Veterinary and Agricultural College, Copenhagen.*

References.

1. MAX BORN: *Optik* (1933). (Berlin, Verlag von Julius Springer)
2. HERBERT MAYER: *Physik Dünner Schichten* (1950). (Wissenschaftliche Verlagsgesellschaft, M. B. H. Stuttgart)
3. H. GEIGER & KARL SCHELL: *Handbuch der Physik*, Vol. 20, 242
4. JØRGEN RYBNER and K. STEENBERG SØRENSEN: *Table for Use in the Addition of Complex Numbers*. (Jul. Gjellerups forlag, København 1948)
5. F. ABELÈS: *Ann. de Phys.* **3**, 516 (1948)
6. KOZŌ ISHIGURO and TOSHIO KATŌ: *J. Phy. Soc. of Japan*, **8**, 77 (1953)
7. F. ABELÈS: *Theses* (Paris, 1950)
8. W. GEFFCHEN: *Ann. d. Phys.* **40**, 385 (1941) and D. R. P. No. 716154 (1942)
9. L. G. SCHULZ: *J. Opt. Soc. Am.* **41**, 1047 (1951)
10. H. KUHN: *J. Phys. et le Radium*, **11**, 422 (1950) or H. KUHN and B. A. WILSON: *Proc. Phys. Soc. B*, **63**, 745 (1950)
11. L. N. HADLEY and D. M. DENNISON: *J. Opt. Soc. Am.* **37**, 451 (1947)
— *ibid.* **38**, 483, (1948)
12. M. LOCQUIN: *Contraste de Phase et Contraste par Interference*, p. 115 (Editions de la "Revue d'Optique Théorique et Instrumentale", Paris 1952)
13. CH. DUFOUR: *ibid.* p. 109
14. A. F. TURNER: *J. Opt. Soc. Am.* **36**, 711 (A) (1946)
15. P. LEURGANS and A. F. TURNER: *ibid.* **37**, 983 (A) (1947)
16. A. E. GEE and H. D. POLSTER: *ibid.* **39**, 1044 (1949)
17. B. H. BILLINGS: *ibid.* **40**, 471 (1950)
- 17a. H. D. POLSTER: *ibid.* **39**, 1038 (1949)
18. CH. DUFOUR: *J. Phys. et le Radium* **11**, 413 (1950)
19. W. GEFFCKEN: *Zs. f. angew. Phys.*, VI, 249 (1954)
20. A. F. TURNER: *J. Phys. et le Radium* **11**, 444 (1950)
21. CH. DUFOUR: *Thèses* (Paris 1950) and *Revue d'Optique* **31**, 1 (1952)
22. H. SCHRÖDER: *Zs. f. angew. Phys.* III, 53 (1951)
23. CH. DUFOUR: *Revue d'Optique* **31**, 1 (1952) and *ibid.* **32**, 321 (1953)
24. CH. DUFOUR and A. HERPIN: *Optica Acta* **1**, 1 (1954)

25. A. VAŠÍČEK: Czechosl. J. Phys. **3**, 206 (1953)
 26. M. BANNUNG: J. Opt. Soc. Am. **37**, 792 (1947)
 27. CH. DUFOUR: Le Vide, No. 16—17, 480 (1948) or Thèses (Paris 1950)
 28. A. H. JARRET and VON KLÜBER: Nature **169**, 790 (1952) and
A. H. JARRET: *ibid.* 170, 455 (1952)
 29. H. D. POLSTER: J. Opt. Soc. Am. **42**, 21 (1952)
 30. J. RING and W. L. WILCOCK: Nature **171**, 648 (1953)
— *ibid.* **173**, 994 (1954)
 31. A. F. TURNER: J. Opt. Soc. Am. **42**, 878 (1952)
-

Det Kongelige Danske Videnskabernes Selskab

Matematisk-fysiske Meddelelser, bind **29**, nr. 14

Dan. Mat. Fys. Medd. **29**, no. 14 (1955)

STUDIES OF ABSORPTION SPECTRA X

d-Electrons in Crystal Fields of Different Symmetries

BY

C. J. BALLHAUSEN AND CHR. KLIXBÜLL JØRGENSEN



København 1955

i kommission hos Ejnar Munksgaard

Printed in Denmark.
Bianco Lunos Bogtrykkeri A-S.

BETHE¹ calculated the number of possible energy levels originating from an electron with a given l in crystal fields of any symmetry. These results apply also to an atomic term with given L in crystal fields of intermediate strength. Small letters are used in this paper to denote single electrons (l, γ_n , etc.) and capital letters to designate total systems (L, Γ_n , etc.). Quantitative calculations of the energy differences occurring in the complex ions of the first transition group were first performed by ILSE and HARTMANN.^{2,3} These authors applied the theory to Ti^{+3} and V^{+3} . Similar calculations have recently been reported for Cu^{++} , Ni^{++} , and most of the other metal ions of the first transition group.⁴⁻⁷ The theory of d^2 -levels in crystal-fields of cubic symmetry³ has been extended to d^n -levels in such fields.⁷ The present paper gives a similar treatment of d^n -levels in fields of lower symmetry (tetragonal and rhombic, the latter being the lowest symmetry of consequence for the splitting of the levels), based on the calculations^{4,5} on d and d^2 -levels in these fields.

Introduction.

The character system of a state in a crystal field of given symmetry can be considered as a p -dimensional vector, if p different numbers are given in the set, e. g. $p = 5$ in the cubic case, where the character systems C are given as the sets (e, c_2, c_3, c_4, c_5). In this five-dimensional space, five fundamental vectors are given as the "irreducible Darstellungen" of BETHE (ref. 1, Table 1). The characters are here given in the order of BETHE.¹ (In the textbook of EYRING, WALTER and KIMBALL²⁸ the characters are given in the order (e, c_5, c_2, c_3, c_4) in the cubic while BETHE's order is not changed in the tetragonal case) They correspond to the quantum numbers Γ_n :

$$\left. \begin{aligned} C(I_1) &= (1, 1, 1, 1, 1) \\ C(I_2) &= (1, 1, -1, -1, 1) \\ C(I_3) &= (2, 2, 0, 0, -1) \\ C(I_4) &= (3, -1, 1, -1, 0) \\ C(I_5) &= (3, -1, -1, 1, 0). \end{aligned} \right\} \quad (1)$$

Any non-fundamental vector C can be expressed as a linear combination of the fundamental vectors in only one way:

$$C = a_1 C(I_1) + a_2 C(I_2) + a_3 C(I_3) + a_4 C(I_4) + a_5 C(I_5). \quad (2)$$

The linear combination coefficients a_n of eq. 2 are always positive integers.

The character systems $C(L)$ found by BETHE by considerations of the single $(2L + 1)$ -dimensional rotation group can be expressed in the familiar tables of cubic term splittings:

$$\left. \begin{aligned} C(S) &= C(I_1) \\ C(P) &= C(I_4) \\ C(D) &= C(I_3) + C(I_5) \\ C(F) &= C(I_2) + C(I_4) + C(I_5) \\ C(G) &= C(I_1) + C(I_3) + C(I_4) + C(I_5) \\ C(H) &= C(I_3) + 2C(I_4) + C(I_5), \end{aligned} \right\} \quad (3)$$

where S, P, D is the usual spectroscopic notation for $L = 0, 1, 2, \dots$. This table was first given by BETHE, and extended for some higher values of L by HELLWEGE.⁸ It is periodical¹ with $L = 12$ (λ is a positive integer)

$$C(12\lambda + L) = \lambda C_{12} + C(L), \quad (4)$$

where $C_{12} = (24, 0, 0, 0, 0) = C(I_1) + C(I_2) + 2C(I_3) + 3C(I_4) + 3C(I_5)$.

An important operation is the formation of internal vector products from the vectors (e, c_2, c_3, c_4, c_5) and $(e', c'_2, c'_3, c'_4, c'_5)$, viz.

$$C = (e e', c_2 c'_2, c_3 c'_3, c_4 c'_4, c_5 c'_5). \tag{5}$$

These products C can also be expressed in the fundamental vectors of eq. 1, giving the results of Table 1. This is a multiplication table of Γ_p and Γ_q , showing the validity of the commutative law:

TABLE 1. Internal vector products in cubic symmetry.

	Γ_1	Γ_2	Γ_3	Γ_4	Γ_5
Γ_1	Γ_1	Γ_2	Γ_3	Γ_4	Γ_5
Γ_2	Γ_2	Γ_1	Γ_3	Γ_5	Γ_4
Γ_3	Γ_3	Γ_3	$\Gamma_1 + \Gamma_2 + \Gamma_3$	$\Gamma_4 + \Gamma_5$	$\Gamma_4 + \Gamma_5$
Γ_4	Γ_4	Γ_5	$\Gamma_4 + \Gamma_5$	$\Gamma_1 + \Gamma_3 + \Gamma_4 + \Gamma_5$	$\Gamma_2 + \Gamma_3 + \Gamma_4 + \Gamma_5$
Γ_5	Γ_5	Γ_4	$\Gamma_4 + \Gamma_5$	$\Gamma_2 + \Gamma_3 + \Gamma_4 + \Gamma_5$	$\Gamma_1 + \Gamma_3 + \Gamma_4 + \Gamma_5$

In crystal fields of tetragonal symmetry the character systems are also five-dimensional vectors, and there are five fundamental vectors $C(\Gamma_{t1})$, $C(\Gamma_{t2})$, $C(\Gamma_{t3})$, $C(\Gamma_{t4})$, and $C(\Gamma_{t5})$ with the coordinates given in ref. 1, Table 5. It is seen that the first coordinate, e , is 1, 1, 1, 1, 2, respectively. This is normally called the degeneracy number of the state, analogous to e in the cubic case. We shall here denote cubic quantum numbers by Γ_{cn} (or simply Γ_n where no misunderstanding is possible), tetragonal numbers by Γ_{tn} and rhombic ones by Γ_{rn} .

The tetragonal character systems of L , $C(L)$ are given in ref. 1, Table 6. On the analogy of eq. 4, $C(L)$ is periodical¹ with the period 4, i. e.

$$\left. \begin{aligned} C(4\lambda + L) &= \lambda C_4 + C(L) \\ C_4 &= C(P) + C(D) = C(S) + C(F). \end{aligned} \right\} \tag{6}$$

Since C_4 is thus expressible, all tetragonal $C(L)$ can be expressed as linear combinations of $C(S)$, $C(P)$, $C(D)$, and $C(F)$ with non-negative coefficients. This is the cause of the similar behaviour⁷ of a cubic $C(L)$ vector when the following arguments are considered.

The values of tetragonal $C(L)$ can be found from eq. 6 and 7:

$$\left. \begin{aligned} C(S) &= C(\Gamma_{t1}) \\ C(P) &= C(\Gamma_{t2}) + C(\Gamma_{t5}) \\ C(D) &= C(\Gamma_{t1}) + C(\Gamma_{t3}) + C(\Gamma_{t4}) + C(\Gamma_{t5}) \\ C(F) &= C(\Gamma_{t2}) + C(\Gamma_{t3}) + C(\Gamma_{t4}) + 2C(\Gamma_{t5}). \end{aligned} \right\} \quad (7)$$

It is now of great interest to know whether a certain cubic state Γ_{cn} can be identified with certainty as a sum of tetragonal states Γ_{tm} . This corresponds to the effects of making a cubic crystal-field very slightly tetragonal and thus forming tetragonal splittings of the cubic levels. Eq. 3 and 7 give the two only possible solutions:

$$\left. \begin{array}{ll} \text{Possibility 1} & \text{Possibility 2} \\ \Gamma_{c1} \rightarrow \Gamma_{t1} & \Gamma_{c1} \rightarrow \Gamma_{t1} \\ \Gamma_{c2} \rightarrow \Gamma_{t3} & \Gamma_{c2} \rightarrow \Gamma_{t4} \\ \Gamma_{c3} \rightarrow \Gamma_{t1} + \Gamma_{t3} & \Gamma_{c3} \rightarrow \Gamma_{t1} + \Gamma_{t4} \\ \Gamma_{c4} \rightarrow \Gamma_{t2} + \Gamma_{t5} & \Gamma_{c4} \rightarrow \Gamma_{t2} + \Gamma_{t5} \\ \Gamma_{c5} \rightarrow \Gamma_{t5} + \Gamma_{t4} & \Gamma_{c5} \rightarrow \Gamma_{t3} + \Gamma_{t5}. \end{array} \right\} \quad (8)$$

BETHE chose possibility 1, but this cannot be done exclusively on the basis of these equations.

From the internal vector products, Table 2 can be constructed by methods similar to those outlined above for Table 1:

TABLE 2. Internal vector products in tetragonal symmetry.

	Γ_{t1}	Γ_{t2}	Γ_{t3}	Γ_{t4}	Γ_{t5}
Γ_{t1}	Γ_{t1}	Γ_{t2}	Γ_{t3}	Γ_{t4}	Γ_{t5}
Γ_{t2}	Γ_{t2}	Γ_{t1}	Γ_{t4}	Γ_{t3}	Γ_{t5}
Γ_{t3}	Γ_{t3}	Γ_{t4}	Γ_{t1}	Γ_{t2}	Γ_{t5}
Γ_{t4}	Γ_{t4}	Γ_{t3}	Γ_{t2}	Γ_{t1}	Γ_{t5}
Γ_{t5}	Γ_{t5}	Γ_{t5}	Γ_{t5}	Γ_{t5}	$\Gamma_{t1} + \Gamma_{t2} + \Gamma_{t3} + \Gamma_{t4}$

Table 2 gives no reason for preferring possibility 1 of eq. 8 to possibility 2, since it is exactly symmetrical with respect to change of Γ_{t3} to Γ_{t4} et vice versa.

In the rhombic case all the four fundamental vectors have $e = 1$, i. e. they are all only once degenerate. According to BETHE,

they are connected with the tetragonal quantum numbers in the following way:

$$\left. \begin{aligned} \Gamma_{t1} &\rightarrow \Gamma_{r1} \\ \Gamma_{t2} &\rightarrow \Gamma_{r2} \\ \Gamma_{t3} &\rightarrow \Gamma_{r1} \\ \Gamma_{t4} &\rightarrow \Gamma_{r2} \\ \Gamma_{t5} &\rightarrow \Gamma_{r3} + \Gamma_{r4}. \end{aligned} \right\} \quad (9)$$

They have thus the following multiplication table:

TABLE 3. Internal vector products in rhombic symmetry.

	Γ_{r1}	Γ_{r2}	Γ_{r3}	Γ_{r4}
Γ_{r1}	Γ_{r1}	Γ_{r2}	Γ_{r3}	Γ_{r4}
Γ_{r2}	Γ_{r2}	Γ_{r1}	Γ_{r4}	Γ_{r3}
Γ_{r3}	Γ_{r3}	Γ_{r4}	Γ_{r1}	Γ_{r2}
Γ_{r4}	Γ_{r4}	Γ_{r3}	Γ_{r2}	Γ_{r1}

Crystal Fields in Co-Ordination Compounds.

From the formulae in ref. 4, it is easily shown that in octahedral complexes the crystal field energy levels are determined only by three quantities which represent the perturbations from the sets of two ligands on each of three axes in the Cartesian coordinate system. This is an extension of the equivalence of *z*-axis contributions, applied to copper (II) complexes,⁴ and in accord with the empirical observations of SUEDA,⁹ that the absorption spectrum is determined only by the influences of the three sets of ligands in *trans*-positions.

In the following calculations the distances of all the ligands are assumed to be equal, giving the same values when put in the functions⁴ B_2 and B_4 . However, the following considerations are also valid when different values of B_2 and B_4 are obtained from each of the ligands. The difference between the six ligands is expressed as differences in the effective point dipole moment μ , but the results can be applied to ionic charges q , G_2 and G_4 ,

as well. The sum of the dipoles in the direction of the x -axis and y -axis and z -axis are represented by μ_1 , μ_2 , and μ_3 .

The complex is said to have a crystal-field of cubic symmetry, if $\mu_1 = \mu_2 = \mu_3$. If two of the dipole moment sums are equal, but different from the third, e.g. $\mu_1 = \mu_2 \neq \mu_3$, the crystal field has tetragonal symmetry. Whenever all the three are different, one has rhombic symmetry, which is the lowest symmetry possible in any octahedral complex.

The energy E of a given level is expressed formally as

$$\left. \begin{aligned} E &= E(\text{free ion}) + E(\text{common pert.}) \\ &+ E(\text{cub}) + E(\text{tetr}) + E(\text{rhomb}). \end{aligned} \right\} (10)$$

E (free ion) is the energy of the corresponding atomic term, which is perturbed by the crystal field (by interaction between different terms the intermixed sum of the individual E (free ion)). E (common pert.) is the energy equal for all levels of the electron configuration due to the B_0 contributions of the perturbation. E (cub) is the energy of the corresponding cubic and E (tetr.) of the corresponding tetragonal level (see the splitting rules eq. 8 (Poss. 1) and eq. 9), and finally E (rhomb) the remaining energy, which is only different from 0 in Γ_{15} -levels, split to Γ_{r3} and Γ_{r4} , and in the interacting two Γ_{r1} states. The latter result is shown in what follows to be connected with Bethe's theorem of the centre of gravity of a group of levels whose degeneracy is removed by fields of less symmetry. B_0 is not regarded at all, because it only contributes to E (common pert.). B_2 occurs alone in E (tetr), and E (rhomb), while B_4 occurs in all the three last parts of eq. 10. In crystal fields of cubic symmetry, E (tetr) = E (rhomb) = 0.

In the complex ions with six equal molecules as ligands, the crystal field does not a priori need being of cubic symmetry since the ligands may have slightly differently induced dipole moment and distances. Eq. 10 would give decreased energy if E (tetr) and E (rhomb) can be negative, i. e. some tetragonal or rhombic splitting of the ground-state occurs. VAN VLECK¹⁰ pointed out early that the Jahn-Teller effect would only allow complex ions to be stable in which the ground-state is only once degenerate on a $(2L + 1)$ basis, i. e. $e = 1$ in the corresponding

vector. The only stable octahedral complexes of cubic symmetry thus have Γ_1 or Γ_2 as ground-states, while the others deform to tetragonal or even rhombic symmetry (in the case of Γ_{15}). However this theorem concerns only the direction of deformation, not the absolute deviation from cubic symmetry.

The ground-states in most magnetically anomalous ions (with the total spin quantum number S less than the S in the free ion) are Γ_{e1} (in $d^5\Gamma_{e5}$), while the magnetically normal ions with the maximum value of S are distributed in the following way in octahedral complexes:

$$\left. \begin{array}{l} d \text{ and } d^6 \text{ rhombic or "compressed" tetragonal} \\ d^2 \text{ and } d^7 \text{ tetragonal} \\ d^3 \text{ and } d^8 \text{ cubic} \\ d^4 \text{ and } d^9 \text{ tetragonal} \\ d^5 \text{ cubic.} \end{array} \right\} \quad (11)$$

VAN VLECK¹⁰ has maintained that systems with one d -electron have the least energy when they have rhombic symmetry. As is seen in the following section, tetragonal symmetry with $\mu_1 > \mu_2 = \mu_3$ would also give a stable once degenerate ground-state. The "compressed" tetragonal form of the complex would probably have approximately the same energy as the rhombic form. Therefore it is possible that the titanium (III) hexa-aquo ion exists in an equilibrium between the two forms. Whenever tetragonality of the type $\mu_1 = \mu_2 > \mu_3$ is stable as in d^4 - and d^9 -systems (e. g. chromium (II) or copper (II) complexes), this structure will be energetically favoured because the ligands are held in place by the steeply increasing potential of the sphere-symmetrical kernel. The tetragonality can thus be due only to weakening of some of the electrostatic bonds to the ligands. This is more likely to happen for two of the six ligands rather than for four as in the case of "compressed" tetragonality.

Two Interacting States in Crystal Fields of Intermediate Strength.

When a given combination of S and Γ_n is represented only once in an electron configuration, its energy will be linearly dependent on crystal field strength (in cubic fields $(E_1 - E_2)$, where E_1 is the energy of a γ_3 -electron and E_2 the energy of a γ_5 -electron). This dependence is found by calculations on either weak or strong crystal fields. The two latter terms are defined in the following way: In weak fields $(E_1 - E_2)$ is negligibly small, compared with the distances between terms of different L in the free ion. In the strong fields $(E_1 - E_2)$ is much larger than these distances.

When two or more levels with the same S and Γ_n occur, the weak and strong crystal fields may give totally different energy expressions. In the case of cubic symmetry the values of N in systems with n d -electrons correspond to the number of γ_3 -electrons. We define:

$$E(\text{cub}) = \left(N - \frac{2n}{5} \right) (E_1 - E_2). \quad (12)$$

In weak fields N is not always an integer and in strong fields the original terms with definite values of L can no longer be distinguished. The diagonal sum rule only ensures⁷ that the sum $N_1 + N_2 + \dots + N_q$ of the q different levels is constant for each value of the crystal field, corresponding to varying intermixing of the strong-field wave-functions.

ORGEL¹¹ determined this interaction in a very important case: the two I_4 originating in weak crystal fields from 3F and 3P in d^2 -systems, and going to γ_5^2 and γ_3^2 in strong crystal fields. The numerical result can as well be applied⁷ to the two I_4 of highest S in d^3 -, d^7 -, and d^8 -systems. In what follows, the interaction between two states is generally treated without use of Condon-Shortley parameters. The energy of the two states in intermediate crystal field strength can be found as the two roots E in the matrix of second order¹¹

$$\begin{vmatrix} E_\alpha + \left(N_\alpha - \frac{2n}{5} \right) (E_1 - E_2) - E & K \\ K & E_\beta + \left(N_\beta - \frac{2n}{5} \right) (E_1 - E_2) - E \end{vmatrix} = 0. \quad (13)$$

K is the energy of interaction between the two states considered. N_α and N_β are the integers corresponding to the strong crystal field case. In the free ion $(E_1 - E_2)$ equals 0. Here the two energy roots are E_a and E_b :

$$\left. \begin{matrix} E_a \\ E_b \end{matrix} \right\} = \frac{E_\alpha + E_\beta}{2} \pm \sqrt{\left(\frac{E_\alpha - E_\beta}{2}\right)^2 + K^2}. \quad (14)$$

It is seen that E_α and E_β always occur in the closed interval between E_a and E_b . It is thus possible to choose a parameter x , such that

$$\left. \begin{matrix} 0 \leq x \leq 1 \\ E_\alpha = (1-x)E_a + xE_b \\ E_\beta = xE_a + (1-x)E_b. \end{matrix} \right\} \quad (15)$$

Eq. 14 and 15 then gives

$$K^2 = x(1-x)(E_b - E_a)^2. \quad (16)$$

The parameters x and $(1-x)$ chosen in eq. 15 are just the intermixing coefficients¹⁶ of the strong field-states in the states in the weak field. This relation is biunique in the case of only two interacting states, found for instance in d^2 -levels in cubic fields. In d^8 -systems, $(1-x)$ is to be substituted for x in Table 4. The data are compiled in Table 4. Two interacting states have

TABLE 4. Interacting states among d^2 -levels in crystal fields of cubic symmetry.

Quantum number	E_a	E_b	x	$\left(\frac{K}{E_b - E_a}\right)^2 = x - x^2$	States in strong crystal fields
3T_4	3F	3P	$1/5$	$4/25$	$\gamma_5^2 + \gamma_5\gamma_3$
1T_1	1G	1S	$3/5$	$6/25$	$\gamma_5^2 + \gamma_3^2$
1T_3	1D	1G	$4/7$	$12/49$	$\gamma_5^2 + \gamma_3^2$
1T_5	1D	1G	$4/7$	$12/49$	$\gamma_5^2 + \gamma_5\gamma_3$

the smallest energy difference when the diagonal elements of eq. 13 are equal, and then it is $2K$. Since the interaction energy K has nearly its maximum value, $\frac{1}{2}(E_b - E_a)$, for the three d^2 -sets

with $S = 0$, their minimum distance must occur at very small crystal-field strengths, i. e. the second-order effects in $(E_1 - E_2)$ are in most cases more important than the first-order effects found in weak cubic fields. The asymptotes in strong crystal fields are given by the equations

$$E = E_\alpha + \left(N_\alpha - \frac{2n}{5}\right)(E_1 - E_2)$$

and the analogous with E_β and N_β .

One d -Electron Systems.

As mentioned above, the 2D -state of one d -electron is split up in fields of lower symmetry as shown in Fig. 1.

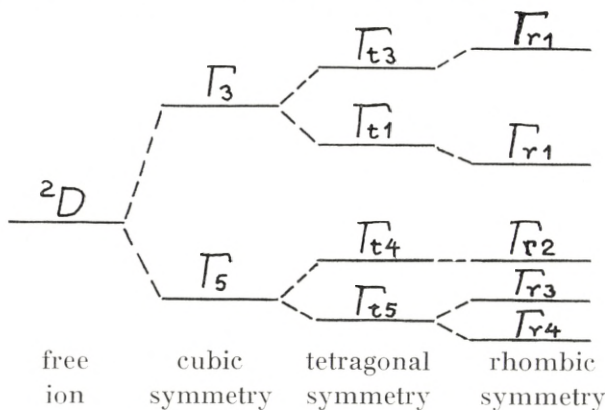


Fig. 1. States of one d -electron in octahedral complexes of decreasing symmetry.

BALLHAUSEN⁴ calculated the energies of the rhombic symmetry. (In all the following equations, the factor $\frac{8}{45}f^2$ is omitted for convenience). The three lowest states have:

$$\left. \begin{aligned} &\Gamma_{c5} \rightarrow \Gamma_{t4} \rightarrow \Gamma_{r2}: \\ &\mu_1 \left[\frac{1}{7} B_2 - \frac{4}{21} B_4 \right] + \mu_2 \left[\frac{1}{7} B_2 - \frac{4}{21} B_4 \right] + \mu_3 \left[-\frac{2}{7} B_2 + \frac{1}{21} B_4 \right] \\ &\Gamma_{c5} \rightarrow \Gamma_{t5} \rightarrow \Gamma_{r3}: \\ &\mu_1 \left[\frac{1}{7} B_2 - \frac{4}{21} B_4 \right] + \mu_2 \left[-\frac{2}{7} B_2 + \frac{1}{21} B_4 \right] + \mu_3 \left[\frac{1}{7} B_2 - \frac{4}{21} B_4 \right] \end{aligned} \right\} \quad (17)$$

$$\left. \begin{aligned} \Gamma_{c5} &\rightarrow \Gamma_{t5} \rightarrow \Gamma_{r4}: \\ \mu_1 \left[-\frac{2}{7} B_2 + \frac{1}{21} B_4 \right] &+ \mu_2 \left[\frac{1}{7} B_2 - \frac{4}{21} B_4 \right] + \mu_3 \left[\frac{1}{7} B_2 - \frac{4}{21} B_4 \right]. \end{aligned} \right\} \quad (17)$$

The affiliation to tetragonal states can be found by putting $\mu_1 = \mu_2$. In the limit, where $\mu_1 = \mu_2 = \mu_3$, the cubic states are found. The rhombic quantum numbers Γ_{r3} and Γ_{r4} are chosen arbitrarily. The energies of the two highest states are roots of the equation

$$\left. \begin{aligned} E^2 - (H_{22} + H_{2-2} + H_{00})E + (H_{22}H_{00} \\ + H_{2-2}H_{00} - 2(H_{20})^2) = 0, \end{aligned} \right\} \quad (18)$$

giving a square-root dependence. The functions H_{ab} are defined in ref. 4. Only in the case $\mu_1 = \mu_2$ is the dependence on crystal field strength linear, because H_{20} then equals 0. This represents the interaction between the two states with the same rhombic quantum number Γ_{r1} .

In the tetragonal case $\mu_1 = \mu_2$, these two states are normal, and the four possible states are:

$$\left. \begin{aligned} \Gamma_{c3} &\rightarrow \Gamma_{t3}: 2\mu_1 \left[\frac{1}{7} B_2 + \frac{19}{84} B_4 \right] + \mu_3 \left[-\frac{2}{7} B_2 + \frac{1}{21} B_4 \right] \\ \Gamma_{c3} &\rightarrow \Gamma_{t1}: 2\mu_1 \left[-\frac{1}{7} B_2 + \frac{3}{28} B_4 \right] + \mu_3 \left[\frac{2}{7} B_2 + \frac{2}{7} B_4 \right] \\ \Gamma_{c5} &\rightarrow \Gamma_{t4}: 2\mu_1 \left[\frac{1}{7} B_2 - \frac{4}{21} B_4 \right] + \mu_3 \left[-\frac{2}{7} B_2 + \frac{1}{21} B_4 \right] \\ \Gamma_{c5} &\rightarrow \Gamma_{t5}: 2\mu_1 \left[-\frac{1}{14} B_2 - \frac{1}{14} B_4 \right] + \mu_3 \left[+\frac{1}{7} B_2 - \frac{4}{21} B_4 \right]. \end{aligned} \right\} \quad (19)$$

For use of the formalism, expressed in eq. 10, the cubic contributions must be written

$$\left. \begin{aligned} \Gamma_{c3}: E(\text{cub}) &= (\mu_1 + \mu_2 + \mu_3) \frac{1}{6} B_4 \\ \Gamma_{c5}: E(\text{cub}) &= -(\mu_1 + \mu_2 + \mu_3) \frac{1}{9} B_4 \end{aligned} \right\} \quad (20)$$

and the tetragonal contributions

$$\left. \begin{aligned} \Gamma_{t3}: E(\text{tetr}) &= \left(\frac{\mu_1 + \mu_2}{2} - \mu_3 \right) \left[\frac{2}{7} B_2 + \frac{5}{42} B_4 \right] \\ \Gamma_{t1}: E(\text{tetr}) &= \left(\frac{\mu_1 + \mu_2}{2} - \mu_3 \right) \left[-\frac{2}{7} B_2 - \frac{5}{42} B_4 \right] \\ \Gamma_{t4}: E(\text{tetr}) &= \left(\frac{\mu_1 + \mu_2}{2} - \mu_3 \right) \left[\frac{2}{7} B_2 - \frac{10}{63} B_4 \right] \\ \Gamma_{t5}: E(\text{tetr}) &= \left(\frac{\mu_1 + \mu_2}{2} - \mu_3 \right) \left[-\frac{1}{7} B_2 + \frac{5}{63} B_4 \right]. \end{aligned} \right\} \quad (21)$$

The rhombic contributions of Γ_{t3} and Γ_{t1} together equal 0 and must be considered as interaction effects of the type discussed in the preceding section. The rhombic contribution of Γ_{t4} equals 0, and that of

$$\Gamma_{t5}: E(\text{rhomb}) = \pm (\mu_1 - \mu_2) \left[\frac{3}{14} B_2 - \frac{5}{42} B_4 \right]. \quad (22)$$

It is not possible to use a single parameter E_t for $E(\text{tetr})$ analogous to $(E_1 - E_2) = (\mu_1 + \mu_2 + \mu_3) \frac{5}{18} B_4$ for $E(\text{cub})$. The contributions of B_4 compared with those of B_2 in eq. 21 are $-\frac{4}{3}$ times higher in Γ_{t4} and Γ_{t5} than they are in Γ_{t3} and Γ_{t1} .

The theorem on centres of gravity¹ is valid for all the individual splittings in a given field. However, this theorem is also valid for the further splitting of a degenerate level due to fields of lower symmetry. This is of consequence for the following sections.

Two d -Electron Systems.

The energies of the d^2 -levels in tetragonal fields⁵ are compared here with results for d^n -levels in tetragonal fields, analogous to the theory of cubic fields.⁷

We shall first calculate the electron distributions in strong tetragonal fields on the quantum numbers γ_{t5} , γ_{t4} , γ_{t1} , and γ_{t3} in order of increasing energy (in fields with almost no cubic

TABLE 5. d^2 -levels in strong tetragonal fields.

Degeneracy number	Electron distribution	Levels	Energy	
γc_3^2	1	${}^1\Gamma_{11}$	$\mu_1 \left[\frac{4}{7} B_2 + \frac{19}{21} B_4 \right] + \mu_3 \left[-\frac{4}{7} B_2 + \frac{2}{21} B_4 \right]$	
		${}^1\Gamma_{13}(c3)$ ${}^3\Gamma_{13}(c2, {}^3F)$	$\mu_1 \left[\frac{2}{3} B_4 \right] + \mu_3 \left[\frac{1}{3} B_4 \right]$	
	1	γ_{11}^2	${}^1\Gamma_{11}$	$\mu_1 \left[-\frac{4}{7} B_2 + \frac{3}{7} B_4 \right] + \mu_3 \left[\frac{4}{7} B_2 + \frac{4}{7} B_4 \right]$
$\gamma c_3 \gamma c_5$	4	${}^1\Gamma_{12}(c4, {}^1G)$ ${}^3\Gamma_{12}(c4)$	$\mu_1 \left[\frac{4}{7} B_2 + \frac{1}{14} B_4 \right] + \mu_3 \left[-\frac{4}{7} B_2 + \frac{2}{21} B_4 \right]$	
		${}^1\Gamma_{15}$ ${}^3\Gamma_{15}$	$\mu_1 \left[\frac{1}{7} B_2 + \frac{13}{42} B_4 \right] + \mu_3 \left[-\frac{1}{7} B_2 - \frac{1}{7} B_4 \right]$	
	4	$\gamma_{11} \gamma_{14}$	${}^1\Gamma_{14}(c5)$ ${}^3\Gamma_{14}(c5, {}^3F)$	$\mu_1 \left[-\frac{1}{6} B_4 \right] + \mu_3 \left[\frac{1}{3} B_4 \right]$
γc_5^2	8	$\gamma_{11} \gamma_{15}$	${}^1\Gamma_{15}$ ${}^3\Gamma_{15}$	$\mu_1 \left[-\frac{3}{7} B_2 + \frac{1}{14} B_4 \right] + \mu_3 \left[\frac{3}{7} B_2 + \frac{2}{21} B_4 \right]$
		1	γ_{14}^2	${}^1\Gamma_{11}$
	6	γ_{15}^2	${}^1\Gamma_{15}(c5)$ ${}^3\Gamma_{15}(c4)$ ${}^1\Gamma_{11}$ ${}^1\Gamma_{13}(c3)$ ${}^1\Gamma_{14}(c5)$ ${}^3\Gamma_{12}(c4)$	$\mu_1 \left[\frac{1}{7} B_2 - \frac{11}{21} B_4 \right] + \mu_3 \left[-\frac{1}{7} B_2 - \frac{3}{21} B_4 \right]$ $\mu_1 \left[-\frac{2}{7} B_2 - \frac{2}{7} B_4 \right] + \mu_3 \left[\frac{2}{7} B_2 - \frac{8}{21} B_4 \right]$

contributions, the order of γ_{t_4} and γ_{t_1} is inverted). It is fortunate that the corresponding cubic quantum numbers $\gamma_5, \gamma_5, \gamma_3$, and γ_3 are then definitely fixed. Table 2 is used for the vector product $\gamma_{tp} \gamma_{tq}$ when $p \neq q$. This case is not restricted by the Pauli exclusion principle, and thus both values of $S = 1$ and 0 occurs. The case $p = q$ is more difficult. When γ_{tp} has $e = 1$, the electron pair γ_{tp}^2 is a closed shell, the term is ${}^1\Gamma_{t_1}$. When $e = 2$, as in $\gamma_{t_5}^2$, it is necessary to collect further information. The known case of d^2 -levels gives $S = 1$ for ${}^3\Gamma_{t_2}$ and $S = 0$ for the three others ${}^1\Gamma_{t_1}$, ${}^1\Gamma_{t_3}$, and ${}^1\Gamma_{t_4}$. Table 5 give the energies in strong tetragonal fields of these levels, depending on the two parameters $\mu_1 (= \mu_2)$ and μ_3 .

The levels of Table 5 can be divided as follows: In cases where more levels with the same tetragonal quantum number are present in the same of the three groups $\gamma_{c_3}^2$, $\gamma_{c_3}\gamma_{c_5}$, and $\gamma_{c_5}^2$, nothing can be said with certainty in connection with a single level in weak fields. In cases where only one level with the same tetragonal quantum number is present in a group, the cubic quantum number is certain. This can then either be exhibited by one level, which has the given S in the whole d^2 -system, or the cubic number can be exhibited more times. In the $\gamma_{c_3}^2$ group the former case occurs in ${}^3\Gamma_{t_3}$, which can only be the weak field level ${}^3F({}^3\Gamma_{c_2})$ while the latter case occurs in ${}^1\Gamma_{t_3}$, which surely is a ${}^1\Gamma_{c_3}$ state, but which cannot be identified with certainty with any atomic term, since 1D and 1G both have ${}^1\Gamma_{c_3}$ -levels.

In the best determined class, which contains ${}^3\Gamma_{t_3}({}^3F)$, ${}^1\Gamma_{t_2}({}^1G)$, and ${}^3\Gamma_{t_4}({}^3F)$, the energy (given in Table 5) in strong crystal-fields is verified in ref. 5. The partially determined class is represented e. g. by the two ${}^3\Gamma_{t_2}$ -levels:

$$\left. \begin{aligned} {}^3\Gamma_{t_2}({}^3F): & \mu_1 \left[-\frac{4}{35} B_2 - \frac{3}{14} B_4 \right] + \mu_3 \left[\frac{4}{35} B_2 - \frac{2}{7} B_4 \right] \\ {}^3\Gamma_{t_2}({}^3P): & \mu_1 \left[\frac{2}{5} B_2 \right] + \mu_3 \left[-\frac{2}{5} B_2 \right]. \end{aligned} \right\} \quad (23)$$

The former is equal to the energy of $\frac{4}{5} \gamma_{t_5}^2 + \frac{1}{5} \gamma_{t_3} \gamma_{t_4}$, and the latter to $\frac{1}{5} \gamma_{t_5}^2 + \frac{4}{5} \gamma_{t_3} \gamma_{t_5}$. Thus the intermixing coefficients given

in Table 4 seem to apply to the problem of distributing strong tetragonal fields with the intermediate step of strong cubic on the weak tetragonal fields. If it is allowable to use the "centre of gravity"-theorem on the ${}^3T_{c4}$ by beginning tetragonality, it should further be valid that $E(\text{tetr})$ in ${}^3T_{15}$ in the levels should equal $-\frac{1}{2}E(\text{tetr})$ in the corresponding ${}^3T_{12}$. Thus

$$\left. \begin{aligned} {}^3T_{15}({}^3F, c4): \mu_1 \left[\frac{2}{35} B_2 - \frac{11}{28} B_4 \right] + \mu_3 \left[-\frac{2}{35} B_2 - \frac{3}{28} B_4 \right] \\ {}^3T_{15}({}^3P, c4): \mu_1 \left[-\frac{1}{5} B_2 \right] + \mu_3 \left[\frac{1}{5} B_2 \right]. \end{aligned} \right\} \quad (24)$$

The latter result in eq. 24 is again confirmed⁵ while the former result is complicated by the fact that two ${}^3T_{15}$ occur in 3F , and their mutual interaction thus is also reckoned. But the diagonal sum-rule can be applied to all the ${}^3T_{15}$. Their total energy is to be

$$\left. \begin{aligned} \sum {}^3T_{15} &= \gamma_{t3} \gamma_{t5} + \gamma_{t1} \gamma_{t5} + \gamma_{t4} \gamma_{t5} \\ &= \mu_1 \left[-\frac{1}{7} B_2 - \frac{1}{7} B_4 \right] + \mu_3 \left[\frac{1}{7} B_2 - \frac{4}{21} B_4 \right] \end{aligned} \right\} \quad (25)$$

and when the energy of ${}^3T_{15}({}^3P)$ is subtracted,

$$2 {}^3T_{15}({}^3F) = \mu_1 \left[+\frac{2}{35} B_2 - \frac{1}{7} B_4 \right] + \mu_3 \left[-\frac{2}{35} B_2 - \frac{4}{21} B_4 \right] \quad (26)$$

also found by the direct calculation.⁵

Thus it seems possible by application of the best determined levels and by extended use of the theorem concerning the centres of gravity to determine all or nearly all the energies of tetragonal levels. The restriction (also imposed on the method used in ref. 7) is that only average values of several levels with the same $2S+1T_{ln}$ can be estimated.

Special interest is connected with the ground-state of diamagnetic nickel (II) complexes. Due to Pauli's holeequivalence theorem, it is the level among the 1D -levels (see Fig. 3) which has the highest energy in strong tetragonal fields in d^2 -systems. Previously⁵ it has been discussed, if ${}^1T_{12}({}^1G, {}^1T_{c4})$ was the ground-state in the rather strong tetragonal field occurring in the square-planar

complexes of stilbenediamine, cyanide, etc. Rather, the state ${}^1G_{11}({}^1D, {}^1G_{c3})$ transferred to the strong tetragonal field state γ_{13}^2 is lowest, due to second-order effects in the crystal-field strength, while ${}^1G_{12}$ was mentioned as having the lowest energy among the singlet states at more moderate crystal-field strengths.

In cubic complexes, ${}^1G_{c3}({}^1D)$ will at even quite small field strengths have the linear energy expression ($\mu_1 = \mu_2 = \mu_3$)

$$E = \frac{4}{7}({}^1D) + \frac{3}{7}({}^1G) + \mu_1 B_4, \quad (27)$$

while the cubic ground-state ${}^3G_{c2}({}^3F)$ has always

$$E = ({}^3F) + \mu_1 B_4 \quad (28)$$

(see Table 4). The energy differences between the two states are thus nearly constant*, being the differences between terms in the free ion:

$$E({}^1G_{c3}) - E({}^3G_{c2}) = \frac{4}{7}({}^1D) + \frac{3}{7}({}^1G) - ({}^3F). \quad (29)$$

Exceptionally these energies are not known** from atomic spectroscopy,¹² but can with a probable error $\sim 1000 \text{ cm}^{-1}$ be predicted from the theory of CONDON and SHORTLEY¹³ to be $({}^1D) = 13000 \text{ cm}^{-1}$ and $({}^1G) = 22000 \text{ cm}^{-1}$, when $({}^3F) = 0 \text{ cm}^{-1}$. Thus, the energy difference of eq. 29 will be $\sim 17000 \text{ cm}^{-1}$. In $Ni(H_2O)_6^{++}$ measured on the Cary spectrophotometer a very weak band has been found as a shoulder at 18500 cm^{-1} with a half-width 500 cm^{-1} . It may be identified as a ${}^3G_2(F) \rightarrow {}^1G_5(D)$ transition which is predicted $\sim 23000 \text{ cm}^{-1}$, or the similar ${}^1G_3(D)$ predicted $\sim 17000 \text{ cm}^{-1}$.

In tetragonal complexes the energy of ${}^3F({}^3G_{c2})$ has no tetragonal contributions (eq. 10) while $\gamma_{c3}^2({}^1G_{c3})$ will split up, $\gamma_{13}^2({}^1G_{11})$ being the lowest state. If it is assumed (in analogy with the arguments given for the second class of states in Table 5) that the state in eq. 27 will take over also all the strong field

* Nothing is known about the cause of diamagnetism in bis (triarsine) nickel (II) ion¹⁴ which is the only nickel (II) complex supposed to be cubic and diamagnetic.

** Recently, SHENSTONE³⁰ has found 1D at 14032 cm^{-1} and 1G at 23109 cm^{-1} . (Added in proof).

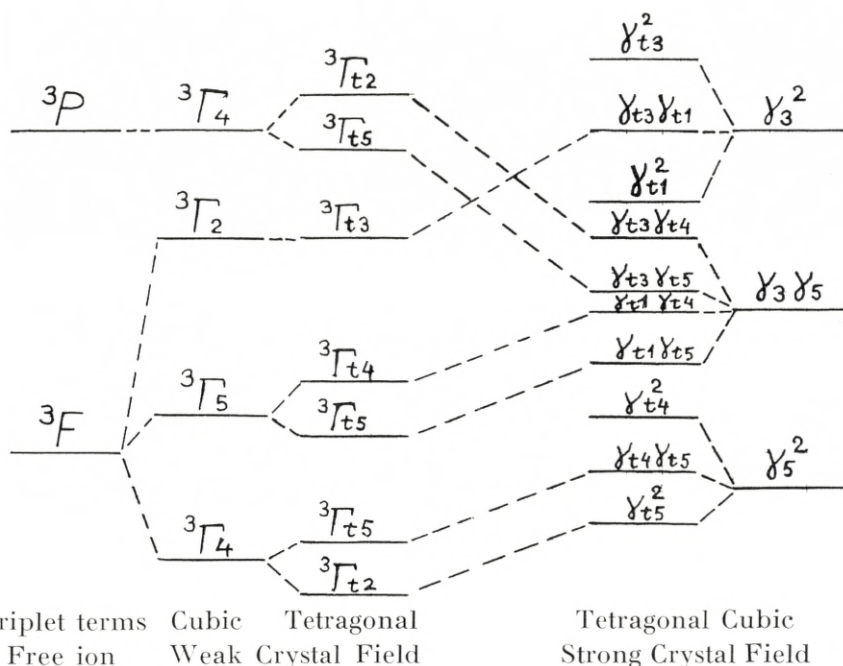


Fig. 2. Triplet states of d^2 in weak and strong crystal fields of cubic and tetragonal symmetry.

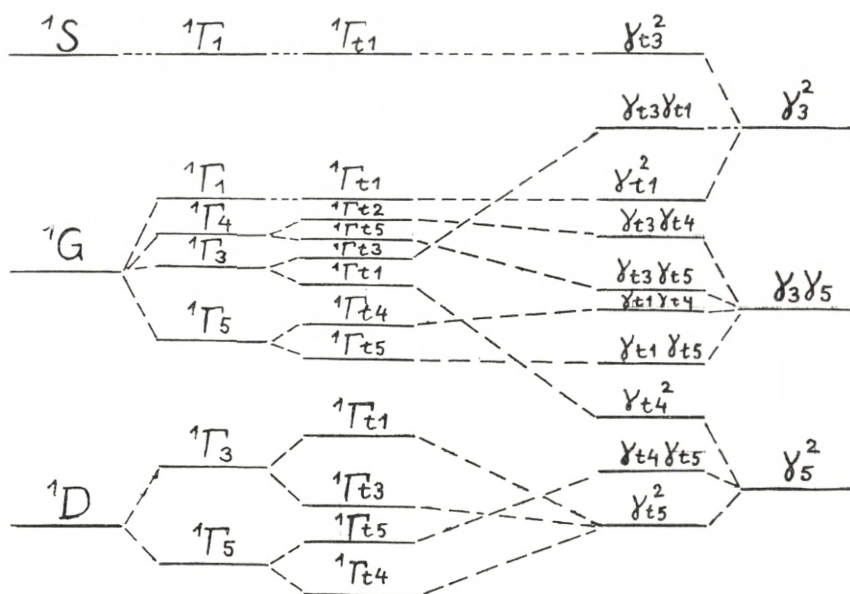
tetragonal splitting by being a strong cubic field state, its energy will be ($\mu_1 = \mu_2 > \mu_3$)

$$E = \frac{4}{7}({}^1D) + \frac{3}{7}({}^1G) + \mu_1 \left[\frac{4}{7}B_2 + \frac{19}{21}B_4 \right] + \mu_3 \left[-\frac{4}{7}B_2 + \frac{2}{21}B_4 \right]. \quad (27)$$

The energy of ${}^1\Gamma_{12}$ (${}^1G, {}^1\Gamma_{c4}$) is then exactly

$$E = ({}^1G) + \mu_1 \left[\frac{4}{7}B_2 + \frac{1}{14}B_4 \right] + \mu_3 \left[-\frac{4}{7}B_2 + \frac{2}{21}B_4 \right]. \quad (28)$$

Since the difference between the energy in eq. 27 and 28 is composed of the positive parts $\frac{4}{7}\{({}^1G) - ({}^1D)\} \sim 5000 \text{ cm}^{-1}$ and $\mu_1 \left[-\frac{5}{6}B_4 \right]$ (this is positive due to the hole-formalism⁴ in d^8 -systems) of the order of magnitude $\frac{1}{2}(E_1 - E_2)$ in the corre-
 2*



Singlet terms Cubic Tetragonal Tetragonal Cubic
Free ion Weak Crystal Field Strong Crystal Field

Fig. 3. Singlet states of d^2 in weak and strong crystal fields of cubic and tetragonal symmetry.

sponding cubic complexes, no nickel (II) complex has the ground-state of eq. 28.

The condition for a nickel (II) complex to be diamagnetic is thus the tetragonal part of eq. 27 being more negative than the energy difference in the free ion of the intermixed states, viz:

$$(\mu_1 - \mu_3) \left[\frac{4}{7} B_2 + \frac{5}{21} B_4 \right] < \langle {}^3F \rangle - \frac{4}{7} \langle {}^1D \rangle - \frac{3}{7} \langle {}^1G \rangle \sim -17000 \text{ cm}^{-1}. \quad (29)$$

If $\mu_3 = 0$, this condition is fulfilled even at $\mu_1 \left[-\frac{5}{3} B_4 \right] = (E_1 - E_2) = 19000 \text{ cm}^{-1}$ when B_2 is put⁵ $= 2.2 B_4$. In reality two opposite tendencies remove a given nickel (II) complex from this simplified model: μ_3 usually is not vanishing, since the diamagnetic complexes have solvate molecules, anions, etc., on the z -axis, while on the other hand μ_1 may very well be larger than in the corresponding cubic complexes ($\mu_1 = \mu_3$) where steric interferences prevent the ligands to be so close to the nickel ion. While

the yellow diamagnetic complexes with their principal band maximum $\sim 22000 \text{ cm}^{-1}$ (with $\text{Ni}(\text{CN})_4^{--}$ on the front with 32000 cm^{-1}) have quite large energy differences between their states, the red ones $\sim 20000 \text{ cm}^{-1}$ are presumably only diamagnetic with some difficulties. E. g. the red nickel (II) inner salt with bis (acetylaceton) ethylenediimine is probably strained by the tendency of the Schiff base-ligand to be planar. The complex, known to be nearest the limit of paramagnetism, is the salmon pink $[\text{Ni en}_2][\text{Ag Br J}]_2$ of NYHOLM¹⁴ (we have also prepared the similar salts with the anions $[\text{Ag Br}_2]^-$ and $[\text{Ag J}_2]^-$ by precipitation with saturated solutions of the silver halide complexes in concentrated solutions of the sodium halides), while the tetra (C, C, C', C') methylsubstituted ethylenediamine¹⁵ forms stable yellow nickel (II) complexes in solution. The absorption spectra of several nickel (II) complexes with these and other amines are now being studied in this laboratory. Fig. 2 and 3 show how the various levels in a d^2 -system are split up by crystal fields of different symmetries. Fig. 2 gives the triplet levels and Fig. 3 the singlet levels.

Three and Four d -Electrons.

As pointed out by SANTEN and WIERINGEN¹⁶ the maximum values of S in d^n -systems give especially regular crystal-field splittings. These are inverted in some cases, viz. for D -states in octahedral complexes:

$$\left. \begin{array}{ll} \text{Regular } (T_5 \text{ lowest}) & \text{Inverted } (T_3 \text{ lowest}) \\ {}^2D (d) & {}^5D (d^4) \\ {}^5D (d^6) & {}^2D (d^9) \end{array} \right\} (30)$$

and for F -states in octahedral complexes:

$$\left. \begin{array}{ll} \text{Regular } (T_4 \text{ lowest}) & \text{Inverted } (T_2 \text{ lowest}) \\ {}^3F (d^2) & {}^4F (d^3) \\ {}^4F (d^7) & {}^3F (d^8) \end{array} \right\} (31)$$

A closer investigation shows that these inversion rules also apply to the tetragonal splitting. Thus the numerical results^{4,5} for

P -, D -, and F -states of highest multiplicity can easily be adapted to these cases.

Since there will hardly be any possibilities of comparing the theory with experimental data for states of lower S in the magnetically normal complexes, the lengthy calculations along the lines given above will not be performed here. It may be noted that the strong tetragonal field states of $\gamma_{t5}^a \gamma_{t4}^b \gamma_{t1}^c \gamma_{t3}^d$ can be found by direct multiplication from Table 2, when the result of γ_{t5}^2 and the hole-formalism $\gamma_{t5}^3 = \gamma_{t5}$ is remembered. But a point of great chemical interest is the behaviour of the lower states of magnetically anomalous complexes. According to SANTEN and WIERINGEN¹⁶ only d^4 -, d^5 -, d^6 -, and d^7 -systems should give magnetically anomalous complexes of cubic symmetry since they are the only ones which have holes in the γ_5 -shell in the magnetically normal state, to which γ_3 -electrons can be transferred under pairing and decrease in S . This is in very good agreement with experience. The best known diamagnetic complexes of the first transition group are the octahedral cobalt (III) complexes. Their ground-state, ${}^1T_{c1}(\gamma_5^6)$ is only once degenerate and is thus undisturbed by tetragonal and rhombic effects. Second-order effects can only occur⁷ from $\gamma_5^4 \gamma_3^2$ states, which are so excited that the effects of nondiagonal elements K of eq. 13 are negligible, except at very small $(E_1 - E_2)$, where they repulse γ_5^6 from its high free-ion energy E (intermixed) down along the line in the Orgel diagram¹¹

$$E = E(\text{intermixed}) - \frac{12}{5}(E_1 - E_2). \quad (32)$$

The value of E (intermixed) must mostly be composite of 1G and 1I . The energies of singlet terms in the free cobalt (III) ion will probably never be found by atomic spectroscopy, Racah's theory¹⁷ for the d^n -terms give the expression in Condon-Shortley parameters:¹³

$$\left. \begin{aligned} E({}^1G) &= 6F_0 - 5F_2 - \frac{13}{2}F_4 \\ &\pm \sqrt{708(F_2 - 5F_4)^2 - 420(F_2 - 5F_4)F_4 + 11025F_4^2} \\ E({}^1I) &= 6F_0 - 15F_2 - 9F_4 \\ E({}^5D) &= 6F_0 - 21F_2 - 189F_4. \end{aligned} \right\} \quad (33)$$

With the reasonable¹³ values of $F_2 = 2000 \text{ cm}^{-1}$ and $F_4 = 200 \text{ cm}^{-1}$ the order of magnitude of the energy difference between the lowest singlet state and 5D is found to be 48000 cm^{-1} . Since the lowest cubic state with $S = 2$, viz. 5T_5 (5D), has the slope $-\frac{2}{5}(E_1 - E_2)$ in the Orgel diagram, it is seen from eq. 32 that $(E_1 - E_2)$ must be at least 24000 cm^{-1} in order to get diamagnetism in cobalt (III). This is already the case in $\text{Co}(\text{H}_2\text{O})_6^{+++}$ as found in alums by ASMUSSEN.¹⁸

While the first band in chromium (III) complexes gives an almost exact measure of $(E_1 - E_2)$ because⁷ the transition 3T_2 (${}^3F, \gamma_5^3$) \rightarrow 3T_5 (${}^3F, \gamma_5^2 \gamma_3$) has no intermixing with different values in strong and weak cubic fields, it is not possible to make a similar statement on cobalt (III) complexes. It is only possible to identify the four states of $\gamma_5^5 \gamma_3$ in strong crystal-fields,^{7, 11} the two strong bands being due to $S = 0$, 1G_4 and 1G_5 , while the weak band discovered in the red⁶ must be due to either 3T_4 or 3T_5 with $S = 1$. The constant energy difference in the two strong bands $\sim 8000 \text{ cm}^{-1}$ is in our opinion due to intermixing of free ion-terms in the diagonal elements in eq. 13, and it would then be accidental if it was equal to $12 F_2 - 60 F_4$ as maintained by ORGEL.¹¹

The two excited states have the tetragonal splittings ${}^1G_{c_4} \rightarrow {}^1G_{t_2} + {}^1G_{t_5}$ and ${}^1G_{c_5} \rightarrow {}^1G_{t_4} + {}^1G'_{t_5}$. If it is assumed that these states have no interaction with other states, their E (tet) (see eq. 10) will be: B_2 and $B_4 > 0$)

$$\left. \begin{aligned} {}^1G_{t_5} &= \gamma_{t_5}^3 \gamma_{t_4}^2 \gamma_{t_1}: (\mu_1 - \mu_3) \left[-\frac{1}{7} B_2 - \frac{25}{126} B_4 \right] \\ {}^1G_{t_2} &= \gamma_{t_5}^4 \gamma_{t_4} \gamma_{t_3}: (\mu_1 - \mu_3) \left[\frac{5}{18} B_4 \right] \\ {}^1G'_{t_5} &= \gamma_{t_5}^3 \gamma_{t_4}^2 \gamma_{t_3}: (\mu_1 - \mu_3) \left[\frac{3}{7} B_2 + \frac{5}{126} B_4 \right] \\ {}^1G_{t_4} &= \gamma_{t_5}^4 \gamma_{t_4} \gamma_{t_1}: (\mu_1 - \mu_3) \left[-\frac{4}{7} B_2 + \frac{5}{126} B_4 \right]. \end{aligned} \right\} \quad (34)$$

The assumption of no interaction between the states will probably not be valid in the case of ${}^1G_{t_5}$ and ${}^1G'_{t_5}$. ORGEL¹¹ is of course

right in maintaining that Γ_{c5} has no first-order tetragonal splitting in contrast to Γ_{c4} . But this situation may be reversed in strong crystal fields. Of the energies in eq. 34 it may be concluded that ${}^1\Gamma_{t2}$ has so small a value of E (tetr) (without B_2 contributions) that if the theorem of centre of gravity can be applied to this and the other level of ${}^1\Gamma_{c4}$, it has a very small tetragonal splitting as compared with the ${}^1\Gamma_{t4}$ plus a mixture of ${}^1\Gamma_{t5}$ and ${}^1\Gamma'_{t5}$, leading to ${}^1\Gamma_{c5}$.

It is empirically well known¹⁹ that the first of the two strong cobalt (III) bands generally show much larger tetragonal splittings than the other. As seen above, it can be interpreted by use of eq. 34 as being the transition to ${}^1\Gamma_{c5}$ contrary to ${}^1\Gamma_{c4}$. In pronounced tetragonal fields, as found in trans-[Co en₂Cl₂]⁺, the lowest excited state is then ${}^1\Gamma_{t4}(\gamma_{t5}^4 \gamma_{t4} \gamma_{t1})$. At a tetragonality so strong that γ_{t4} and γ_{t1} has the same energy (as found e. g. in copper (II) complexes) this state should be competing with ${}^1\Gamma_{c1}(\gamma_{t5}^4 \gamma_{t4}^2)$ as ground-state.

The question of tetragonal splittings in chromium (III) complexes seems quite complicated. Not only does the first strong band show this splitting,¹¹ but as will be shown in another publication by one of us, the second band is strongly split in the bluish grey hydroxo form of the chromium (III) ethylenediaminetetraacetate.²⁰ C. E. SCHÄFFER of this laboratory has discovered that the dinuclear "basic rhodo" complex,²¹ which is formed transiently by air-oxidation of chromium (II) in ammonia water, shows on the Cary spectrophotometer four very narrow bands in the near ultraviolet. The first band ${}^3\Gamma_{c2} \rightarrow {}^3\Gamma_{c5}$ should show little first-order tetragonal splitting, since one of the levels in ${}^3\Gamma_{c5}$ is ${}^3\Gamma_{t4}(\gamma_{t5}^2 \gamma_{t3})$, which has the B_2 -contribution = 0.

Some of the strong bands in magnetically normal complexes predicted by the crystal field theory are not very easily detected. The most prominent examples are:

$$\left. \begin{aligned} d^2: {}^3\Gamma_4({}^3F) &\rightarrow {}^3\Gamma_2({}^3F) \\ d^3: {}^3\Gamma_2({}^3F) &\rightarrow {}^3\Gamma_4({}^3P) \\ d^7: {}^3\Gamma_4({}^3F) &\rightarrow {}^3\Gamma_2({}^3F). \end{aligned} \right\} (35)$$

In d^2 and d^7 the excited states are only once degenerate on a $(2L + 1)$ basis and might be suspected to give weaker bands

than the other, three-fold degenerate states with maximum S . In vanadium (III), the band seems nevertheless observed at 38000 cm^{-1} in the reflection spectrum of $K_2[VF_5H_2O]$ as measured on the Beckman DU. From the other bands in this complex a wave-number 35000 cm^{-1} is predicted. In cobalt (II) the band is now identified with the quite weak band⁶ at 16000 cm^{-1} in $Co(H_2O)_6^{++}$ and the somewhat stronger bands in $Co(NH_3)_6^{++}$ at 18200 cm^{-1} and in $Coen_3^{++}$ at 18500 cm^{-1} as described in the ninth paper of this series.²² Since the band in purely cubic complexes corresponds to the energy $\frac{9}{5}(E_1 - E_2)$, this quantity is now assumed to be 9000 cm^{-1} in the aquo ion, which must be slightly rhombic, as seen above.

d^3 is represented in vanadium (II) and chromium (III). In solutions of vanadium in 6 M HCl , reduced by zinc, a third band can be observed at 26500 cm^{-1} besides the two at 12200 and 18000 cm^{-1} . Since it does not have the place of the second band of vanadium (III), it is most probably one of the bands given in eqs. 35. Since $(E_1 - E_2)$ is as small as 12000 cm^{-1} , the bands are distributed nearly as in $Nien_3^{++}$: the two Γ_4 have nearly their minimum distance⁷ $= 2K$ in eq. 13. In chromium (III), low band at 38000 cm^{-1} observed of TSUCHIDA²³ in $Cr(H_2O)_6^{+++}$ may represent the third strong band with the corresponding $(E_1 - E_2) = 17500\text{ cm}^{-1}$. The red solutions of chromium (III) chloride in absolute ethanol saturated with lithium chloride (probably containing $CrCl_3 \cdot alc_3$) show also the third band clearly. Here the two first bands are shifted much toward the red, 12000 and 19000 cm^{-1} , respectively, while a similar band is observed at 26000 cm^{-1} . Further out in the ultraviolet, the electron transfer spectrum due to the easy remove of electrons from chloride ions are observed.

Five d -Electrons.

These systems⁷ have no first-order crystal-field splittings in complexes of cubic symmetry. Their second-order interactions can be treated by methods given above in the second section. The absorption spectra of magnetically normal manganese (II) and iron (III) consist of very weak bands⁷ due to the transitions

from the ground-state 6S to splittings of quartet states. Besides this, iron (III) compounds have very intense electron transfer spectra as seen in $Fe(OH)^{++}$, $Fe(SCN)_3$, $FeS_2O_3^+$, etc.

Among the quartet states, 4T_1 and 4T_2 are only represented once, and they have both $N = 2$ in eq. 12, as also 6T_1 (6S). 4T_3 is represented twice with $N = 2$ (4D and 4G). They continue also without interaction in strong crystal-fields. Probably the two 4G -levels 4T_3 and 4T_1 are represented in bands⁶ at 24900 and 25150 cm^{-1} . These narrow bands were also found by GIELESSEN²⁴ and in solid manganese (II) salts they split into 12 components. Due to the Kramer degeneracy, more than 6 were not expected, even due to (L, S) coupling effects. But many of the narrow bands found by GIELESSEN are probably coupled with vibrations. Of great importance for the observed spectra are the states 4T_4 , which occur in 4P , 4F , and 4G . They have the energies in the free manganese (II) ion¹² 29200, 43600, and 26800 cm^{-1} respectively. The two terms 4G and 4P are liable to interact strongly due to the small distance of the terms. If in the strong crystal field the lowest level has the energy in cubic complexes

$$Mn(II) {}^4T_4(\gamma_5^4 \gamma_3): 28000 \text{ cm}^{-1} - (E_1 - E_2). \quad (36)$$

$(E_1 - E_2)$ is then = 9200 cm^{-1} in $Mn(H_2O)_6^{++}$, which seems very probable, and similar calculations for $Fe(H_2O)_6^{+++}$ give $(E_1 - E_2) = 22000 \text{ cm}^{-1}$. The middle 4T_4 in $Mn(H_2O)_6^{++}$ should be placed $\sim 30000 \text{ cm}^{-1}$ and is probably the band⁶ at 29700 cm^{-1} . 4T_5 is finally the explanation of the bands at 23000 cm^{-1} in manganese (II) and at 18500 cm^{-1} in iron (III).⁶ The three interacting levels are here due to 4D , 4F , and 4G .

Geometrical Configuration and Absorption Spectrum.

Due to the fact that only three parameters μ_1 , μ_2 , and μ_3 determine the spectrum of a given complex with constant⁴ R , Z and electron configuration, the symmetry of the crystal fields is often surprising high. Table 6 gives the symmetry of complexes with at most three different ligands A , B , C in the octahedral complexes $MA_a B_b C_c$ ($a \geq b \geq c$) with six equal distances.

TABLE 6. Symmetry of octahedral complexes with at most three different ligands A , B and C .

MA_6B c	(1, 2, 6) MA_3B_3 r	(B 1,6 C 2) MA_3B_2C r
MA_5B t	cis (1, 2) MA_4BC r	(B 1,2 C 3,4) $MA_2B_2C_2$ r
cis (1, 2) MA_4B_2 t	trans (1, 6) MA_4BC t	(B 1,2 C 3,5) $MA_2B_2C_2$ t
trans (1, 6) MA_4B_2 t	(B 1,2 C 3) MA_3B_2C t	(B 1,6 C 2,3) $MA_2B_2C_2$ t
(1, 2, 3) MA_3B_3 c	(B 1,2 C 4) MA_3B_2C r	(B 1,6 C 2,4) $MA_2B_2C_2$ r

Among the tetragonal complexes, the tetragonality can be measured by $(\mu_1 - \mu_3)$ as seen from eq. 21 and as also found directly from ref. 4. It is seen that this quantity is (-2) times as small in cis MA_4B_2 as in trans MA_4B_2 , since

$$\left. \begin{array}{ll}
 \text{cis-}MA_4B_2 & \text{trans-}MA_4B_2 \\
 \mu_1 = \mu_2 = \mu_A + \mu_B & \mu_1 = \mu_2 = 2 \mu_A \\
 \mu_3 = 2 \mu_A & \mu_3 = 2 \mu_B \\
 \mu_1 - \mu_3 = \mu_B - \mu_A & \mu_1 - \mu_3 = 2 \mu_A - 2 \mu_B
 \end{array} \right\} (37)$$

This is the explanation of the tetragonal splitting being much more distinct¹⁹ in trans-complexes, while it only gives broadening of the bands in the cis-complexes. Here the splitting is (-1) time the splitting of mono-substituted complexes MA_5B , which have $\mu_1 - \mu_3 = \mu_A - \mu_B$, i. e. the splitting is inverted.

In applying these rules to observed spectra it is necessary to consider several facts. First, chelate ligands are treated as composed of the individual coordinating links. Especially symmetrical chelates such as ethylenediamine or oxalate have AA function. Secondly, when the pure MA_6 and MB_6 complexes have nearly the same spectra, the mixed complexes MA_nB_{6-n} will show very small changes (formally, because $\mu_B - \mu_A \sim 0$). These cases can be found from the spectrochemical series first developed by FAJANS²⁵ and later extended by TSUCHIDA²³:

$$\left. \begin{array}{l}
 J^- < Br^- < Cl^- \lesssim OH^- < RCOO^- < NO_3^- < F^- \lesssim H_2O \\
 < SCN^- \ll NH_3 < en \lesssim NO_2^- < o\text{-phen} \lesssim dip \ll CN^-
 \end{array} \right\} (38)$$

The anions find quite fixed positions between the neutral molecules in this series. Thirdly, the effects of making a purely cubic complex MA_6 less symmetrical by substitution to MA_5B , MA_4B_2 . . .

are different, according to the ground-state being only once degenerate in cubic symmetry (as in chromium (III), nickel (II), diamagnetic cobalt (III) complexes, etc.) or it is several times degenerate (as in titanium (III), cobalt (II), copper (II), etc.). In the former cases the tetragonal splitting of a band does not move its centre of gravity determined by the cubic contribution $\mu_1 + \mu_2 + \mu_3$, while the latter cases have a predominant hypsochromic influence of unsymmetrical substitution, because the ground-state is decreased in energy also by tetragonal fields. Generally spoken, the latter type of complex with several times degenerate ground-state in cubic symmetry can show phenomena such as the "pentammine effect" in copper (II) complexes.⁴ They have a tendency towards showing characteristic coordination numbers 2 and 4 in the sense of J. BJERRUM²⁶, while the non-degenerate cubic ground-states give nearly constant consecutive equilibrium constants, corrected for statistical effects and steric interaction between the ligands.

The non-degenerate, purely cubic type is very promising for calculation of spectra of poly-nuclear species, so abundant in chromium (III) and cobalt (III) chemistry. C. E. SCHÄFFER will elsewhere publish absorption spectra of these compounds. E. g. the brown cation²⁷ $[Co \{ (OH)_2 Co (NH_3)_4 \}_3]^{+6}$ has exactly the spectrum predicted of a mixture of the mono-nuclear links, one part of the hypothetical $[Co (OH)_6]^{-3}$ (determined from eq. 38) and three parts of $cis [Co (NH_3)_4 (OH)_2]^+$, with the strong electron transfer spectrum from $OH^- + Co^{+3} \rightarrow OH + Co^{+2}$ superposed in the near ultraviolet.

***d*-Electrons in Crystal Fields of Trigonal Symmetry.**

The trigonal symmetry D_3 is characterized by the three 3-dimensional vectors ($E, 2 C_3, 3 C_2$)²⁸:

$$\left. \begin{aligned} C(\Gamma_{A1}) &= (1, 1, 1) \\ C(\Gamma_{A2}) &= (1, 1, -1) \\ C(\Gamma_{A3}) &= (2, -1, 0). \end{aligned} \right\} \quad (39)$$

For different values of L , the possible quantum numbers are:

$$\left. \begin{aligned}
 C(S) &= (1, 1, 1) = C(\Gamma_{A1}) \\
 C(P) &= (3, 0, -1) = C(\Gamma_{A2}) + C(\Gamma_{A3}) \\
 C(D) &= (5, -1, 1) = C(\Gamma_{A1}) + 2C(\Gamma_{A3}) \\
 C(F) &= (7, 1, -1) = C(\Gamma_{A1}) + 2C(\Gamma_{A2}) + 2C(\Gamma_{A3}) \\
 C(G) &= (9, 0, 1) = 2C(\Gamma_{A1}) + C(\Gamma_{A2}) + 3C(\Gamma_{A3}) \\
 C(H) &= (11, -1, -1) = C(\Gamma_{A1}) + 2C(\Gamma_{A2}) + 4C(\Gamma_{A3}) \\
 C(I) &= (13, 1, 1) = 3C(\Gamma_{A1}) + 2C(\Gamma_{A2}) + 4C(\Gamma_{A3}),
 \end{aligned} \right\} (40)$$

The multiplication table is:

	Γ_{A1}	Γ_{A2}	Γ_{A3}	
Γ_{A1}	Γ_{A1}	Γ_{A2}	Γ_{A3}	} (41)
Γ_{A2}	Γ_{A2}	Γ_{A1}	Γ_{A3}	
Γ_{A3}	Γ_{A3}	Γ_{A3}	$\Gamma_{A1} + \Gamma_{A2} + \Gamma_{A3}$	

The crystal field of a trigonal bipyramid has this symmetry. If one of the three equal dipoles in the planar triangle is denoted by μ_1 , and one of the two equal dipoles in the perpendicular axis through the centre of the triangle by μ_2 , the energy of the three possible states of one d -electron is:

$$\left. \begin{aligned}
 E(\gamma'_{A3}) &= \mu_1 \left[\frac{3}{7} B_2 + \frac{3}{56} B_4 \right] + \mu_2 \left[-\frac{4}{7} B_2 + \frac{2}{21} B_4 \right] \\
 E(\gamma_{A3}) &= \mu_1 \left[-\frac{3}{14} B_2 - \frac{3}{14} B_4 \right] + \mu_2 \left[+\frac{2}{7} B_2 - \frac{8}{21} B_4 \right] \\
 E(\gamma_{A1}) &= \mu_1 \left[-\frac{3}{7} B_2 + \frac{9}{28} B_4 \right] + \mu_2 \left[+\frac{4}{7} B_2 + \frac{4}{7} B_4 \right].
 \end{aligned} \right\} (42)$$

It is seen that the relative position of these energy levels are highly dependent on the ratio B_2/B_4 and μ_1/μ_2 . For the limiting case $\mu_1 = 0$, the three energies are equal to the similar limits in the tetragonal case for γ_{t3} ($= \gamma_{t4}$), γ_{t5} , and γ_{t1} , respectively.

For the special case $\mu_1 = \frac{4}{3} \mu_2$, the B_2 contributions vanish:

$$\left. \begin{aligned} E(\gamma'_{A3}) &= \mu_2 \left[\frac{1}{6} B_4 \right] \\ E(\gamma_{A3}) &= \mu_2 \left[-\frac{2}{3} B_4 \right] \\ E(\gamma_{A1}) &= \mu_2 [B_4]. \end{aligned} \right\} (43)$$

Just as in the cubic symmetry, the sum of dipole moments in the plane is twice as large as the sum of dipole moments along the perpendicular axis in this particular case. While the other types of crystal field symmetry, treated in this paper, are represented in octahedral complexes, the trigonal symmetry corresponds to only five-coordinated complexes. These are of special interest as a probable intermediate configuration occurring in exchange reactions by dissociation of octahedral complexes involving S_{N1} mechanisms.²⁹

Summary.

The group-theoretical derivation of the possible states in crystal fields of cubic, tetragonal, and rhombic symmetry is presented as operations with simple five-dimensional vectors. The problem of interaction between two states alone by going from weak to strong crystal fields is solved. The behaviour of one d -electron in the fields of different symmetry is discussed. The earlier calculations on d^2 -systems are used for comparison with the strong and weak tetragonal fields. The ground-state of diamagnetic nickel (II) complexes is found. In d^3 - and d^4 -systems, the splitting of states with maximum S is inverted, as compared with the corresponding d^2 - and d^1 -states. The magnetically anomalous complexes of these configurations are discussed, and peculiarities in the tetragonal splitting pointed out. Cubic states of d^5 with $S = \frac{3}{2}$ are in some cases strongly interacting. Finally the relative magnitude of the tetragonal splitting in complexes with different distribution of ligands on the six octahedral places is found. Distinction is made between complexes with only once degenerate ground-state in cubic symmetry (which show more regular evolution of spectra and equilibrium constants with

increasing number of a new ligand) as compared with complexes where this is not the case. These latter, which according to VAN VLECK cannot at all be stable in purely cubic symmetry, show higher wave-numbers of the mixed complexes as compared with the limiting complexes MA_6 and MB_6 .

Acknowledgments.

We are very much indebted to Professor J. BJERRUM for his great interest in the work and for many valuable discussions. Further we want to thank Mr. C. E. SCHÄFFER for his readiness to supply us with the spectra used on p. 24. Dr. L. E. ORGEL is thanked for his kindness in sending us the manuscripts to papers, submitted to the Journal of Chemical Physics. We are also much obliged to the Ole Rømer Foundation for financial support.

*Chemistry Department A,
Technical University of Denmark, Copenhagen.*

References.

1. BETHE, H. Ann. d. Physik [5] **3** (1929) 133.
2. ILSE, F. E. and HARTMANN, H. Z. physik. Ch. **197** (1951) 239.
3. ILSE, F. E. and HARTMANN, H. Z. Naturforschg. **6 a** (1951) 751.
4. BALLHAUSEN, C. J. Dan. Mat. Fys. Medd. **29** (1954) no. 4.
5. BALLHAUSEN, C. J. Dan. Mat. Fys. Medd. **29** (1955) no. 8.
6. JØRGENSEN, C. KLIXBÜLL, Acta Chem. Scand. **8** (1954) 1502.
7. JØRGENSEN, C. KLIXBÜLL, Acta Chem. Scand. **9** (1955) 116.
8. HELLWEGE, K. H. Ann. d. Physik [6] **4** (1949) 150.
9. SUEDA, H. J. Chem. Soc. Japan **56** (1936) 406, 592.
10. VAN VLECK, J. H. J. Chem. Phys. **7** (1939) 61.
11. ORGEL, L. E. J. Chem. Soc. **1952** 4756.
12. MOORE, C. E. Atomic Energy Levels. Nat. Bur. Stand. Circular No. 467 1952.

13. CONDON, E. U. and SHORTLEY, G. H. Theory of Atomic Spectra 1953.
14. NYHOLM, R. S. Chem. Rev. **53** (1953) 263.
15. BASOLO, F. J. Am. Chem. Soc. **72** (1950) 4393.
16. SANTEN, J. H. v. and WIERINGEN, J. S. v. Rec. trav. chim. **71** (1952) 420.
17. RACAH, G. Phys. Rev. **62** (1942) 438.
18. ASMUSSEN, R. W. Magnetokemiske Undersøgelser . . . Thesis. Copenhagen 1944.
19. LINHARD, M. and WEIGEL, M. Z. anorg. Ch. 264 (1951) 321, *ibid.* **271** (1952) 101.
20. BRINTZINGER, H. THIELE, H. and MÜLLER, U. Z. anorg. Chem. **251** (1943) 285.
21. JENSEN, K. A. Z. anorg. Chr. **232** (1937) 257.
22. BALHAUSEN, C. J. and JØRGENSEN, C. KLIXBÜLL. Acta Chem. Scand. **9** (1955).
23. TSUCHIDA, R. J. Chem. Soc. Japan **13** (1938) 388, 426, 471.
24. GIELESSEN, J. Ann. d. Physik [5] **22** (1935) 537.
25. FAJANS, K. Naturwiss. **11** (1923) 165.
26. BJERRUM, J. Metal Ammine Formation . . . Copenhagen 1941.
27. JØRGENSEN, S. M. Z. anorg. Ch. **16** (1898) 184 and WERNER, A. Ber. **40** (1907) 2118.
28. EYRING, H. WALTER, J. and KIMBALL, G. E. Quantum Chemistry 1944.
29. BROWN, D., INGOLD, C. K. and NYHOLM, R. S. J. Chem. Soc. (1953) 2674.
30. SHENSTONE, A. G. J. Opt. Soc. Amer. **44** (1954) 749.

Det Kongelige Danske Videnskabernes Selskab

Matematisk-fysiske Meddelelser, bind **29**, nr. 15

Dan. Mat. Fys. Medd. **29**, no. 15 (1955)

CONSTRUCTION OF A SPECTROMETER
FOR NEUTRINO RECOILS:
INVESTIGATION OF THE DECAY OF A^{37}

BY

O. KOFOED-HANSEN AND A. NIELSEN



København 1955

i kommission hos Ejnar Munksgaard

CONTENTS

	Page
Introduction.....	3
Chapter 1. Theory of the Instrument.....	5
1.1 Principle of the instrument.....	5
1.2 Particles initially at rest.....	8
1.3 Particles with finite initial velocity.....	11
1.4 An example in which $V < T_R$	15
1.5 Motion of the electrons.....	17
1.6 Pressure effects.....	18
Chapter 2. Construction of the Instrument.....	21
2.1 The magnet.....	21
2.2 The collector system.....	24
2.3 The electrical system.....	27
2.4 The potential V_h	30
2.5 The vacuum system.....	31
2.6 Tilting of the instrument.....	34
2.7 Temperature constancy.....	36
2.8 Statistics.....	38
2.9 Dielectric polarization.....	38
Chapter 3. Results with A^{37}	39
3.1 The decay of A^{37}	39
3.2 The currents as functions of medium H values.....	40
3.3 The neutrino momentum.....	43
3.4 The average charge.....	45
3.5 The secondary electrons.....	48
3.6 Measurements in pure magnetic fields.....	50
Conclusions.....	51
Appendix A.....	52
Appendix B.....	57
Appendix C.....	58
References.....	60

A neutrino recoil spectrometer has been constructed. The motion of the recoils has been studied in crossed electric and magnetic fields. The particles have been detected by the charge they give off to the collector system.

First, the theory of the instrument is described; subsequently, details of its construction are given and, finally, results obtained in an investigation of A^{37} are presented. These results are:

The neutrino momentum 812 ± 8 keV
pct. recoils of charge 1 26 ± 3
pct. recoils of charge 2 13 ± 4
pct. recoils of charge 3 38 ± 4
pct. recoils of charge 4 18 ± 2
pct. recoils of charge 5 4 ± 1
pct. recoils of charge 6 1 ± 1

The average charge of the charged recoils $2.64 \pm .08$.

Momentum of the most energetic Auger electrons 162 ± 4 Gauss cm.

pct. of decays leading to such electrons 65 ± 5 .

Average momentum of all electrons 69 ± 1 Gauss cm.

Introduction.

Neutrino recoil particles have in general energies of the order of a few electron volts. The most reliable investigations of such recoils can therefore be carried out with radioactive noble gases. In such experiments, no disturbing effects from source backing or molecular break-up appear.

Ordinarily, it is tried to measure neutrino recoils in instruments which are similar to conventional spectrometers. A radioactive noble gas, however, inevitably spreads out over the whole volume of the chamber. This introduces complications in the evaluation of the resolution curves for the instrument.

In the present article, an instrument is described which has very few similarities to conventional spectrometers. The purpose of this change is to obtain an instrument of sufficient simplicity so that it is feasible to carry through a complete mathematical

analysis of the factors determining intensity and motion of the particles.

We shall study the orbits of the recoils in homogeneous electric and magnetic fields produced inside the volume of a plane parallel condenser. Further, the motion of the particles will be investigated by measuring the charges they give off when they hit the plates of the condenser. The mathematical problem arising is then simply the question of whether a given particle produced in a given position, with a given charge to mass ratio and velocity, will hit a certain one of the condenser plates, or whether it will spiral out between the plates. We then choose such values of the fields which permit the separation of the effects from the different particles. The measuring procedure involves studying small variations in the currents when the fields are changed in such a manner that these changes can be interpreted with respect to the kinematic parameters describing the particles.

With the present choice of the geometry of the instrument, it will be our task to measure currents from particles starting everywhere inside the condenser and with all directions of initial velocity. This obviously leads to many integrations, a fact which makes it evident that we are dealing with very poor geometry. At first sight, it might appear as if the worst possible geometry had been chosen; this suspicion can only be disproved by our results which have provided a body of information that so far had not been obtained by means of more conventional types of spectrometers.

In the following, we shall first enter into the theory of the instrument by solving the mathematical program formulated above. Then, the construction of the instrument is described and an analysis of some necessary measurements is given, which have been carried out in order to determine the behaviour of the instrument. Finally, the results obtained in an investigation of the recoils from K -capture of A^{37} are presented.

Chapter 1. Theory of the Instrument.

1.1 Principle of the Instrument.

In principle, the chamber of the instrument consists of an evacuated space between two condenser plates (Fig. 1). An electric voltage V is applied across the condenser. A magnetic

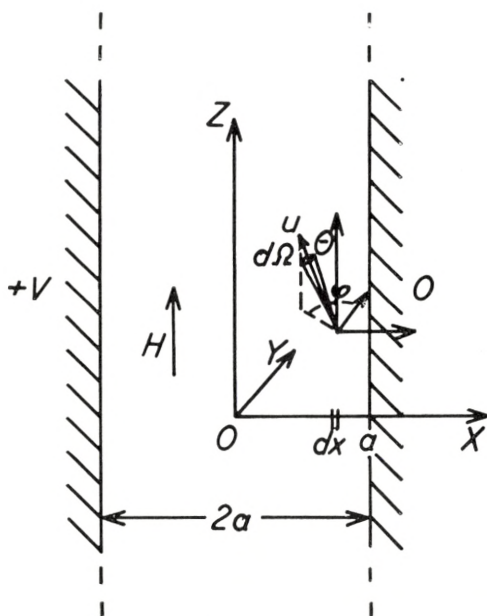


Fig. 1. Principle of the instrument.

field H is introduced parallel to the plane of the condenser plates and a radioactive noble gas is introduced into the space between the plates. When the gas decays, charged particles are created uniformly throughout the space between the plates and with no preferred direction of emission relative to the orientation of the electric and magnetic fields. By β -decay charged recoils appear. Furthermore, secondary effects, such as Auger transitions and influence of nuclear charge changes, give rise to secondary electrons. Thereby high charge values on the recoil atoms may be obtained. In the following, we therefore consider an initially

homogeneously distributed creation of recoil particles with the ionic charge spectrum n_{z_γ} and momentum distribution $P(Mu)$ together with electrons of momentum distribution $P(p)$. The number of recoils created per second inside the interval between x and $x + dx$ (cf. Fig. 1), and with direction of emission inside the solid angle $d\Omega = (1/4 \pi) \sin \theta d\theta d\varphi$ with charge z_γ and momentum between Mu and $Mu + dMu$, is consequently assumed to be given by

$$N n_{z_\gamma} P(Mu) dMu (dx/2a) (1/4 \pi) \sin \theta d\theta d\varphi, \quad (1)$$

where N is the total number of disintegrations per second, and $2a$ is the distance between the condenser plates (cf. Fig. 1). Similarly, the number of electrons created per second between x and $x + dx$, and with momentum between p and $p + dp$, and with the direction of emission inside the solid angle interval $d\Omega$, is given by

$$N \langle z_\gamma \rangle P(p) dp (dx/2a) (1/4 \pi) \sin \theta d\theta d\varphi, \quad (2)$$

where $\langle z_\gamma \rangle$ is the average charge of the recoils. Since we start with neutral atoms, charge conservation tells us that in all $N \langle z_\gamma \rangle$ electrons have to be accounted for. This number of electrons of course includes the decay electrons when we are dealing with a β^- -decay. In the case of β^- -decay including e emission to a bound state, K -capture, and isomeric transitions, only neutral or positively charged recoils appear. We shall restrict our considerations to such cases, although the theory of the instrument, with slight extensions, can also be applied to β^+ -decay.

When charged particles move in crossed electric and magnetic fields, the orbits are determined essentially by the velocity and the charge to mass ratio. Thereby the different contributions to n_z , $P(Mu)$, and $P(p)$ can be found by studying the motion of the particles at different values of the field strengths $F = V/2a$ and H . As mentioned in the Introduction, the variations of the orbits are studied by following the variation of the numbers of particles hitting the plates of the condenser. This number can be examined in essentially two different ways. The number of particles has previously been measured by the tracer method¹⁾ and only electric fields have been applied. In the present investigation,

the particles are detected by the charge they give off to the plates. In cases where the tracer method can be used, both neutral and charged recoils are detected and, furthermore, no contribution from the electrons has to be considered. Such cases appear when the radioactive noble gas has a radioactive daughter substance. When currents are measured, the electrons have also to be taken into account. The large difference between the charge to mass ratio for recoils and that for electrons is the most important factor used in distinguishing between the contribution from each of these types of particles. This difference causes great changes in the orbits of the light and heavy particles. The motion of the electrons is essentially determined by the magnetic fields, and the introduction of small electric fields causes only very small corrections. Conversely, for the recoils the electric fields are of greatest importance.

When currents are measured, neutral particles do not contribute. Thus, in the following, we have to interpret the number N as the number of decays leading to charged particles and our discussions refer to the charged decay products only. In formulas (1) and (2), we have therefore also assumed the following normalization condition

$$\sum_{z\gamma=1}^{\infty} n_{z\gamma} = 1. \quad (3)$$

For completeness, it should be mentioned that the momentum spectra are also assumed to be normalized in the following way:

$$\int_0^{\infty} P(p) dp = 1, \quad (4)$$

$$\int_0^{\infty} P(Mu) dMu = 1. \quad (5)$$

In order to illustrate the procedure of calculating the currents as functions of V and H , we begin with the very simple example which occurs when $Mu = 0$. Such calculations are very illustrative of the procedure adopted in the following, and the results constitute an important limiting case for our later calculations which take into account the momentum of the particles.

1.2 Particles Initially at Rest.

In order to facilitate the understanding of the instrument, we separate the two problems, charge distribution and momentum distribution and, in this section, discuss particles initially at rest. The equations of motion (cf. eq. 33, ref. 2) in the non-relativistic limit are

$$M\dot{x} = z_\gamma eF + (z_\gamma e/c) H\dot{y}, \quad (6)$$

$$M\dot{y} = - (z_\gamma e/c) H\dot{x}, \quad (7)$$

$$M\dot{z} = 0. \quad (8)$$

With the conditions $\dot{x}(t=0) = 0$, we get the well-known cycloidal orbits of the motion

$$x - x_0 = (Mc^2F/z_\gamma eH^2) [1 - \cos(z_\gamma eH/Mc)t], \quad (9)$$

$$y - y_0 = (Mc^2F/z_\gamma eH^2) \sin(z_\gamma eH/Mc)t - (F/H)ct, \quad (10)$$

$$z - z_0 = 0. \quad (11)$$

The motion is a plane motion. It should also be noted that, in (9)–(11), the kinematic parameters and the fields enter through the combinations

$$aB_{z_\gamma} = (Mc^2F/z_\gamma eH^2), \quad (12)$$

$$D = cF/H \quad (13)$$

only.

Due to the periodicity of the orbits as regards the motion in the x -direction, we can obtain an experimental approach to an infinitely extended condenser system by introducing a central collector plate (cf. Figs. 8 and 9 of ref. 2) and the necessary guard rings or protection plates. The necessary sizes of the guard rings are discussed in ref. 2 for the cases of pure magnetic and electric fields. The guard ring discussion in crossed electric and magnetic fields proceeds essentially along the same lines and no further details will be given here. We may only mention that the instrument actually was constructed in such a way as to make it most suitable for our purposes.

We can then proceed as if the condenser were infinitely extended in the y - and x -directions. In order to discuss the number of particles hitting the plates, it is therefore necessary to examine the magnitudes x^{\max} and x^{\min} only. Since, in this special case of the initial velocity $u = 0$, we have

$$x^{\min} = x_0, \quad (14)$$

we are even satisfied when we know the amplitude of the motion in the x -direction, i. e.,

$$x^{\max} - x^{\min} = (2 Mc^2 F / z_\gamma e H^2) = 2 a B_{z_\gamma}. \quad (15)$$

From this information we find immediately the relative number of particles hitting the positive plate

$$h(B) = 0. \quad (16)$$

The number of particles moving out towards infinity is given by

$$g(B) = \left\{ \begin{array}{l} 1 - \frac{x^{\max} - x^{\min}}{2 a} \\ 0 \end{array} \right. = \left\{ \begin{array}{l} 1 - B \text{ for } B < 1 \\ 0 \text{ for } B > 1 \end{array} \right\} \quad (17)$$

and the number of particles hitting the negative plate is given by

$$f(B) = \left\{ \begin{array}{l} \frac{x^{\max} - x^{\min}}{2 a} \\ 1 \end{array} \right. = \left\{ \begin{array}{l} B \text{ for } B < 1 \\ 1 \text{ for } B > 1. \end{array} \right\} \quad (18)$$

It is obvious that the functions h , g , and f fulfill the condition

$$h(B) + g(B) + f(B) = 1. \quad (19)$$

The currents obtained for a certain charge distribution n_{z_γ} are correspondingly given by

$$\left. \begin{array}{l} i_+ \\ i_{\text{out}} \\ i_- \end{array} \right\} = eN \sum_{z_\gamma} z_\gamma n_{z_\gamma} \left\{ \begin{array}{l} h(B) \\ g(B) \\ f(B) \end{array} \right\} \quad (20)$$

and, according to (19), the currents fulfill

$$i_{\text{out}} = eN \langle z_\gamma \rangle - i_+ - i_- \quad (21)$$

In order to get an idea of the accuracy which can be obtained in a determination of n_{z_γ} from measured currents, imagine that i_- has been measured for F equal to integral multiples of (eH^2a/Mc^2) . Furthermore, let us denote the corresponding i_- values by i_1, i_2, i_3 , etc. From (20) it is then seen that the results must be interpreted as

$$\left. \begin{aligned} n_1 + n_2 + n_3 + n_4 + \dots &= i_1/N \\ n_1 + 2n_2 + 2n_3 + 2n_4 + \dots &= i_2/N \\ n_1 + 2n_2 + 3n_3 + 3n_4 + \dots &= i_3/N \\ n_1 + 2n_2 + 3n_3 + 4n_4 + \dots &= i_4/N \end{aligned} \right\} \quad (22)$$

with the solutions

$$\left. \begin{aligned} Nn_1 &= 2i_1 - i_2 \\ Nn_{z_\gamma} &= 2i_{z_\gamma} - i_{z_\gamma-1} - i_{z_\gamma+1}, \end{aligned} \right\} \quad (23)$$

which indicates that a considerable accuracy can be obtained. When, initially, the particles have a distribution in velocity, the set of equations analogous to (22) is more complicated and the accuracy with which n_{z_γ} can be obtained is reduced.

Although we have omitted the initial velocity u in this discussion, all the essential features of the method with respect to a study of the charge distribution of the recoils are given in this section. Especially when $D \gg u$, all the details of i_+ , i_- , and i_{out} are given by (20) to the second order in u/D .

Also the method which we apply for the calculation of h , g , and f as functions of B_{z_γ} and u is essentially similar to those outlined here. The important magnitudes are x^{max} and x^{min} , and we have to separate the number of particles into those hitting the positive plate, those hitting the negative plate, and those spiralling out.

1.3 Particles with Finite Initial Velocity.

For the discussion of an infinitely extended condenser we first show that the motion is periodic in the x -direction. This has been done in ref. 2. Also x^{\max} and x^{\min} have been found in ref. 2. For a discussion of the motion of the heavy particles we take the non-relativistic approximation eq. (40) of ref. 2

$$x^{\max} - x^{\min} - x_0 = aB(1 + A'_y \pm [1 + 2A'_y + A'^2]^{1/2}) = \begin{Bmatrix} \omega a \\ -Wa \end{Bmatrix} \quad (24)$$

where we have introduced

$$A' = [u_x^2 + u_y^2]^{1/2}/D, \quad (25)$$

$$A'_x = u_x/D, \quad (26)$$

$$A'_y = u_y/D. \quad (27)$$

We shall also write

$$A = [u_x^2 + u_y^2 + u_z^2]^{1/2}/D, \quad (28)$$

where

$$\vec{u} = (u_x, u_y, u_z) = (-u \sin \theta \sin \varphi, u \sin \theta \cos \varphi, u \cos \theta). \quad (29)$$

The initial situation is illustrated in Fig. 1. We now introduce the relative numbers f , g , and h as in the preceding section. In order to calculate these numbers we introduce the dimensionless quantities W and ω defined in (24). It is seen that, after averaging over all directions in u , we find that the numbers f , g , and h are functions of A and B only, and that no other combination of the kinematic parameters and the fields appear in our formulas.

In Appendix A, which contains the results of some of the numerical calculations which have to be performed, a picture of the A — B plane is also given. In the present paper, we restrict ourselves to certain regions in this plane where the calculations are especially simple. The procedure will be to compare the quantities W and ω and the relative amplitude of the motion

$$L = W + \omega \quad (30)$$

to 2.

Region I in the A — B plane. The simplest case for our calculations is obtained when

$$\text{and } \left. \begin{array}{l} L \geq 2 \\ W \leq 2 \end{array} \right\} \text{ i. e. } \left\{ \begin{array}{l} B \geq 1/(1-A); A < 1; B < 3 + \sqrt{8} \\ B \leq 4/A^2; A < 1; B > 3 + \sqrt{8}, \end{array} \right\} \quad (31)$$

independent of θ and φ . This case has been treated in detail in ref. 2, together with the simple cases in which we have a pure magnetic field and in which we have a pure electric field. This calculation can also be obtained as a special case of the following more general considerations.

Region II in the A — B plane. Another relatively simple calculation occurs when

$$L < 2, \text{ i. e. } B < 1/(1+A), \quad (32)$$

independent of θ and φ . Both these cases are simple because we can freely integrate over the angles. There is, however, no reason for setting up special derivations for these regions; rather, we prefer to cover the entire region where

$$W \leq 2,$$

i. e.

$$\left. \begin{array}{l} B < 1/(A-1) \text{ for } A \geq 2, \\ B < 4/A^2 \text{ for } 0 < A < 2. \end{array} \right\} \quad (33)$$

Physically, this means that the electric potential V is so large that particles starting out towards the positive plate from the immediate vicinity of the negative plate can never reach, or else can just touch, the positive plate. In the interval $0 < A < 2$ in (33), the condition is, as seen, $B < 4/A^2$ which leads to

$$V \geq T_R, \quad (34)$$

where T_R is the kinetic energy $\frac{1}{2}Mu^2$ of the recoils. Under the restriction (33), we find that ω and W always roughly behave as indicated in Fig. 2 in the special case of $A' = B = 1$.

We have to divide our considerations into two parts according to the magnitude of φ . In each case, we can first estimate the

number of particles hitting the plate towards which it starts to move. Those which miss this plate have then to be separated into those that hit the other plate and those that spiral out, as shown in Fig. 2.

In order to integrate our expressions, we have of course to find the value of φ giving $L = 2$; if no such value exists, the

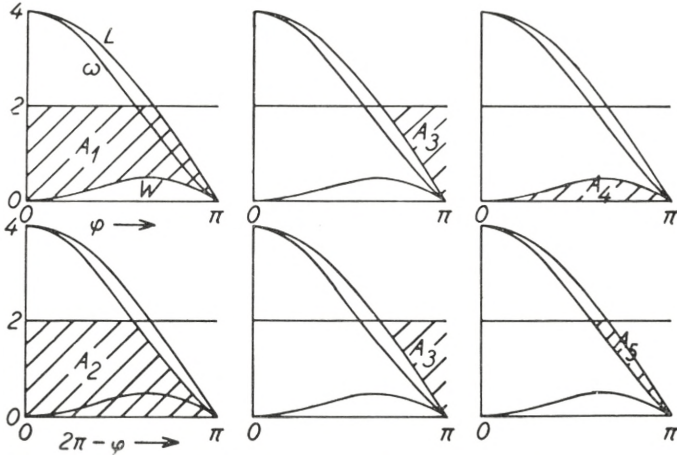


Fig. 2. The curves $W(\varphi)$, $\omega(\varphi)$, and $L(\varphi)$ are drawn for a fixed value of $A' = 1$ and $B = 1$. The number of particles is divided into two parts according to whether they start out towards the negative plate, i.e., $0 \leq \varphi \leq \pi$, or whether they start out towards the positive plate $\pi \leq \varphi \leq 2\pi$. In this way, it is easily seen that the contribution to f is given by $\frac{1}{2}(A_1 + A_2)$, the contribution to g is given by A_3 , and the contribution to h is given by $\frac{1}{2}(A_4 + A_5)$, where the A_i 's are the hatched areas shown in the figures.

limits of integration should be chosen as 0 or π . Thus, the limit of integration is

$$\varphi' = \left\{ \begin{array}{l} 0 \text{ for } B < 1/(1 + A') \\ \text{Arccos} \left[\frac{1}{2A'} \left(\frac{1}{B^2} - 1 - A'^2 \right) \right] \text{ for } 1/(1 + A') < B < 1/(1 - A') \\ \pi \text{ for } B > 1/(1 - A'). \end{array} \right\} \quad (35)$$

Similarly, we have to find the value of φ giving $\omega = 2$. Corresponding to (35), we find

$$\varphi'' = \left\{ \begin{array}{l} 0 \text{ for } B < 1/(1 + A') \\ \text{Arccos } [2/BA' - [(4/BA'^2) + 1]^{1/2}] \text{ for } 1/(1 + A') < B < 1/(1 - A') \\ \pi \text{ for } B > 1/(1 - A'). \end{array} \right\} \quad (36)$$

When no such angles do exist the proper angles to be inserted in the following integrals are given. This occurs in the two simple cases of regions I and II in the A - B plane.

The expressions for the sums of areas in Fig. 2 then lead to

$$\begin{aligned} g(A, B) &= \int_0^{\pi/2} \frac{1}{2\pi} A_3 \sin \theta d\theta \\ &= \int_0^{\pi/2} \int_{\varphi'}^{\pi} (2 - L) \frac{d\varphi}{2\pi} \sin \theta d\theta \\ &= \int_0^{\pi/2} \left\{ \frac{\pi - \varphi'}{\pi} - \frac{2B}{\pi} \left[E\left(k, \frac{\pi}{2}\right) - E\left(k, \frac{\varphi'}{2}\right) \right] (1 + A') \right\} \sin \theta d\theta \end{aligned} \quad (37)$$

and

$$\begin{aligned} h(A, B) &= \int_0^{\pi/2} (1/4 \pi) (A_4 + A_5) \sin \theta d\theta \\ &= \int_0^{\pi/2} \left\{ \int_0^{\pi} W d\varphi / 4\pi + \int_{\varphi'}^{\pi} (2 - \omega) \frac{d\varphi}{4\pi} - \int_{\varphi'}^{\pi} (2 - L) d\varphi / 4\pi \right\} \sin \theta d\theta \\ &= (B/4 \pi) \int_0^{\pi/2} \left\{ (1 + A') [4 E(k, \pi/2) - 4 E(k, \varphi'/2) + 2 E(k, \varphi''/2)] \right. \\ &\quad \left. - 2\pi + \varphi'' + (2/B) (\varphi' - \varphi'') + A' \sin \varphi' \right\} \sin \theta d\theta \end{aligned} \quad (38)$$

and

$$f(A, B) = 1 - g(A, B) - h(A, B), \quad (39)$$

where

$$E(k, \varphi) = \int_0^{\varphi} [1 - k^2 \sin^2 t]^{1/2} dt, \quad (40)$$

$$k^2 = 4 A' / (1 + A')^2. \quad (41)$$

When the particles have initially a distribution in velocity, the functions f , g , and h have to be integrated over this distribution. Such an integration is essentially an integration over A . When

there is a distribution in z_γ one has to sum over this distribution. Such a summation is a sum over different B values. Thus, the final expressions for the currents are given by

$$\left. \begin{array}{l} i_- \\ i_+ \\ i_{\text{out}} \end{array} \right\} = \sum_{z_\gamma} n_{z_\gamma} z_\gamma \int P(u) \left\{ \begin{array}{l} f(A, B) \\ h(A, B) \\ g(A, B) \end{array} \right\} du \cdot Ne \quad \left. \right\} \quad (42)$$

which, under the proper conditions, leads to the approximations (50) and (51) of ref. 2 (cf. also eq. (44) of ref. 2 and the series expansion of the function $S(A)$ in Appendix A).

If experimentally one is mainly interested in the velocity spectrum, one obtains the best results by measuring along $B = \text{const.}$ curves in the A — B plane. When the highest accuracy is desired in the charge distribution, it is convenient to measure along $\langle A \rangle = \text{const.}$ curves in the A — B plane. In the present experiments, we have confined ourselves to an approximation to the latter procedure by measuring along curves for constant V , i. e., along curves of the type

$$B = \text{const}/\langle A \rangle^2. \quad (43)$$

Therefore most information is available about the charge distribution and only $\langle u \rangle$ is obtained. So far nothing is known about the u distribution, which in the present experiments was considered to be a sharp line (cf. section 3.1).

1.4 An Example in which $V < T_R$.

If no magnetic field is applied, the expression for i_+ as a function of V can be found from eqs. (1) and (3) of ref. 2. We find

$$i_+ = \sum_{z_\gamma} n_{z_\gamma} z_\gamma \left\{ \begin{array}{ll} T_R/(6 z_\gamma eV) & \text{for } eV \geq T_R/z_\gamma \\ \frac{1}{2} \left(1 - \frac{2}{3} [z_\gamma eV/T_R]^{1/2} \right) & \text{for } eV < T_R/z_\gamma. \end{array} \right\} \quad (44)$$

In Fig. 3, this expression is plotted as a function of T_R/eV for singly charged atoms (curve A).

If a small magnetic field is applied, we obtain in the region

$eV \geq T_R/z\gamma$, the approximation (44) of ref. 2, corresponding to the series expansion of $S(A)$ given in Appendix A. Furthermore, we know the asymptotic behaviour of i_+ for $V \rightarrow 0$ which is given by the series expansion (17) of ref. 2. This expression we multiply by $1/2$ in order to change to the variable H'_1 which we use here.

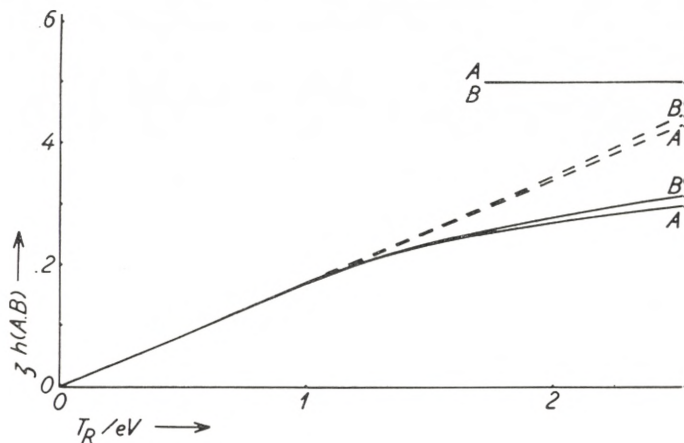


Fig. 3. Theoretical expectations for i_+ as a function of T_R/eV in a pure electric field (curve A). If a small magnetic field is applied, small changes in the curve appear. The general appearance is, however, the same. The curve B corresponding to $9.6 eV$ recoils with charge $z = 1$ and mass 37 amu. has been drawn by joining the known behaviour of the curve for $T_R/eV < 1$ to the known asymptotic behaviour for $V \rightarrow 0$. It should be noted that an upper limit to the deviation from curve A lies around $(1/20) A^2$ (cf. eq. (88) of Appendix A). Particles of the same energy and mass, but of higher charge, will follow the dotted curve.

We shall be interested in the behaviour of $9.6 eV$ singly charged particles of mass ~ 37 amu. moving in a magnetic field $2aH$ of 475 Gauss cm. In this case, the corrected curve for $eV > T_R$ is shown in Fig. 3 curve B, together with the asymptotic behaviour for $V \rightarrow 0$. Instead of carrying out long calculations inside the region IV of Fig. 27, Appendix A, we are content with the approximate curve B in Fig. 3, which is drawn loosely to fit the known behaviour in both ends. Such a procedure is of course rather uncertain. We are interested in the deviation from the dotted continuation of the straight line valid for $eV \geq T_R$ and we need this deviation only to an accuracy of ~ 10 pct. Thus, the present rough approximation is justified.

1.5. Motion of the Electrons.

The motion of the electrons is described in ref. 2. We are especially interested in the approximative expression (49) of ref. 2. In our case, we are dealing with $N \langle z_\gamma \rangle$ electrons. Thus, we get

$$i_{\pm e} = -Ne \langle z_\gamma \rangle [\pi \langle p_e c \rangle / (8aHe) \pm F \langle W_e \rangle / (2aH^2e) + \dots]. \quad (45)^1$$

For the current i_{out} we get, to the same approximation, i. e., to second order terms in F/H ,

$$i_{\text{out } e} = -Ne \langle z_\gamma \rangle [1 - \pi \langle p_e c \rangle / (4aHe) - \dots]. \quad (46)$$

The expressions (45) and (46) are valid only when $eHa > cp_e^{\text{max}}$.

Let us consider n electrons of definite momentum p and, as usually, created uniformly throughout our space between the infinitely extended condenser plates. In a pure magnetic field, we get the total expression covering all H values by combining (13) and (16) of ref. 2 or using (50) of the present paper

$$i_e = \left\{ \begin{array}{ll} en\pi \langle cp \rangle / (8aHe) & \text{for } Hea \geq cp \\ (ne/4) \{ [1 - (Hea/cp)^2]^{1/2} \\ + (cp/Hea) \text{Arcsin}(Hea/cp) \} & \text{for } Hea < cp. \end{array} \right\} \quad (47)$$

This expression is illustrated as a function of pc/Hea in Fig. 4, curve A.

In the following, we are dealing with electrons of kinetic energy $T_e = 2300 \text{ eV}$ moving in an electric potential $V = 30 \text{ eV}$. In order to calculate the exact curve in this case, we would have to apply formulae like those given in (37)—(39) with very high A values and even calculated in the region V of the A — B plane. For $Hae > pc$, we can apply (45) and, for $H \rightarrow 0$, we know the asymptotic behaviour from the expression (3) of ref. 2 or (44) of this paper. Curve B in Fig. 4 is drawn in this way by fitting to the known behaviour in both ends. This procedure is of course uncertain. If a larger number of electrons with smaller energy contributed to i_e , the curve would continue along the dotted

¹ In equation (49) of ref. 2, a factor $1/2$ is missing in the first term. Also the five last lines, including eq. (20) on page 13 of ref. 2, are wrong and should be omitted.

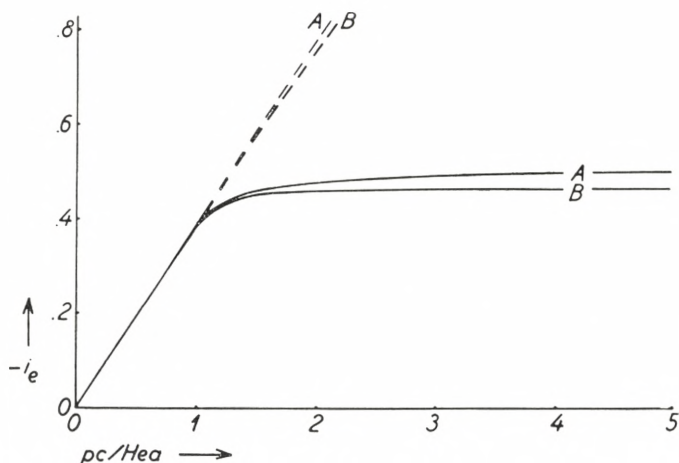


Fig. 4. i_e as a function of pc/Hea for electrons moving in a pure magnetic field (curve A). If a small electric field is applied, changes like those leading to curve B are assumed to appear.

line B which is obtained from (45). The actual curve deviates from this line; we shall use this deviation to an accuracy of 8 pct. only. Therefore it is felt to be safe to apply curve B without carrying through long and laborious calculations.

1.6. Pressure Effects.

When the positive particles collide with residual gas molecules, their charge and momentum are changed, and the current measurements are thereby distorted. We shall not attempt to give a detailed calculation of the complex phenomena occurring in such cases. We only note that pressure effects must be eliminated by carrying out measurements at various pressures and extrapolating to zero pressure.

Order of magnitude estimates of pressure effects are to be found in ref. 2, p. 18 ff. The considerations given there apply to singly charged particles. In the present investigation we are concerned with one more effect connected with pressures, which we will consider now. This effect occurs when a highly charged particle captures an electron, afterwards the fields act on it with reduced strength. A particle which otherwise would

have moved out towards infinity may thereby hit the collector plate. This effect is even increased by the possibility that the particle undergoes several such capture processes.

The pressure is expected to have influence when many particles spiral out. When H and V have such values that no particles can spiral out, the path of the recoils is very short and the pressure effect is a minimum. When particles spiral out, longer orbits occur and particles from the guard ring regions may have to pass the collector region, thereby creating additional possibilities for such effects. This means that the guard ring regions should not be made too large. On the other hand, application of crossed electric and magnetic fields means that all particles obtain an average velocity in the y -direction given by

$$\langle v_y \rangle = Fc/H. \quad (48)$$

This velocity is larger than the recoil velocity by a factor $1/A$. Therefore the particles are very swiftly removed towards the walls of the chamber, and pressure effects are suppressed.

The worst case obviously occurs when $F = 0$. Then even standing orbits appear. Such particles are of course bound to collide. A good idea of the difficulties arising in this case may be provided by the following naive picture. Suppose that the main effect is charge changes and that the averaging mechanism of the instrument completely averages out the momentum changes. Suppose that this includes the gas molecules delivering the charge in question in such a way that the mathematics is defined as follows. Particles hitting a plate before a complete revolution in the motion in the $x - y$ -plane are not affected by pressure. Particles which spiral up or down between the plates may capture an electron, but continue with the same momentum. The particle from which the electron is captured receives so little velocity from the capture process that it is sent out towards infinity with no possibility of hitting the collector.

Furthermore, we assume that the condenser is 2×1 cm long and that we are collecting in an infinitesimally thin region of the condenser only. Finally we also assume that the charge changes by one unit at a time. Then we get the following contributions to the currents to the plates:

$$i_1 = \sum_{z_\gamma=1} n_{z_\gamma} z_\gamma j(pc/Heaz_\gamma), \quad (49)$$

where $j(pc/Heaz_\gamma)$ is given by

$$j_{z_\gamma}(pc/Heaz_\gamma) = 1/2 - \int_0^{\theta'_{z_\gamma}} [(a - \varrho_{z_\gamma})/2a] \sin \theta d\theta, \quad (50)$$

where

$$\varrho_{z_\gamma} = pc \sin \theta / (Hez_\gamma) \quad (51)$$

$$\theta'_{z_\gamma} = \left\{ \begin{array}{ll} \text{Arcsin} [Hez_\gamma/pc] & \text{for } Hez_\gamma \leq cp \\ \pi/2 & \text{for } Hez_\gamma \geq cp \end{array} \right\} \quad (52)$$

(cf. eqs. (13) and (16) of ref. 2). Eq. (49) gives the contribution from those particles which hit the collector before fulfilling one complete revolution. When the integrations in (50) are carried out we obtain (47) of the preceding section.

The contribution to the current from the particles changing charge from z_γ to $z_\gamma - 1$ is then given by

$$i_z = \sum_{z_\gamma=2} (z_\gamma - 1) n_{z_\gamma} k \left(\frac{pc}{Heaz_\gamma}, \alpha_{z_\gamma} \right), \quad (53)$$

where

$$\left. \begin{aligned} k \left(\frac{pc}{Heaz_\gamma}, \alpha_{z_\gamma} \right) &= \int_0^{\theta'_{z_\gamma}} \frac{a - \varrho_{z_\gamma}}{2a} (1 - e^{-\alpha_{z_\gamma}/\cos \theta}) \sin \theta d\theta \\ &- \int_0^{\theta'_{z_\gamma-1}} \frac{a - \varrho_{(z_\gamma-1)}}{2a} (1 - e^{-\alpha_{z_\gamma}/\cos \theta}) \sin \theta d\theta \end{aligned} \right\} \quad (54)$$

and $\alpha_{z_\gamma} = 1/\lambda_{z_\gamma}$, where λ_{z_γ} is the mean free path for a z_γ fold charged ion.

Further contributions from additional charge changes are determined by calculations similar to those involved in the description of a successive radioactive decay. All integrals involved will contain expressions of the following kind only:

$$\int_0^{\theta_{z_\gamma}} \sin^2 \theta (1 - e^{-\alpha/\cos \theta}) d\theta, \quad (55)$$

$$\int_0^{\theta_{z\gamma}} \sin \theta (1 - e^{-a/\cos \theta}) d\theta. \quad (56)$$

The integral (56) can be expressed in terms of known functions (exponential integrals). The functions have been tabulated as functions of $\theta_{z\gamma}$ and a^1 , however, in the present rough treatment the deviations from (50) can be neglected. Thus, the resultant current is still of the form (49), but more complicated expressions are entering (instead of the factors $n_{z\gamma}$).

It is therefore to be expected, at least at not too high pressures, that the main characteristics of (49) appear, although the interpretation of the magnitude of the different charge components is more doubtful. Then only the possibility of determining the momentum of the recoils from the shape of (49) remains. (Cf. Fig. 7 of ref. 2).

One of the above conditions seems not to be fulfilled experimentally, namely, the condition that the molecules from which the charges are taken spiral out; however, it is likely that a diffusion of these ions occurs, giving rise to a constant positive current. This current is not affected by the magnetic field when $Hea > pc$.

The only safe procedure is certainly to carry out experiments at various pressures and to extrapolate to zero pressure.

Chapter 2. Construction of the Instrument.

2.1. The Magnet.

The instrument is shown in Fig. 5. Its main parts are: the magnet with its stabilized generator (A, N). The main vacuum chamber containing the collector system (not visible in Fig. 5), the electrical equipment for measuring small currents and for generating the potential V (B, C, F, J, R), the vacuum system

¹ The authors are indebted to civ.ing. K. O. NIELSEN and fil. lic. G. EHRLING for tabulating the functions (55) and (56) on the electronic computer BESK in Stockholm, Sweden.

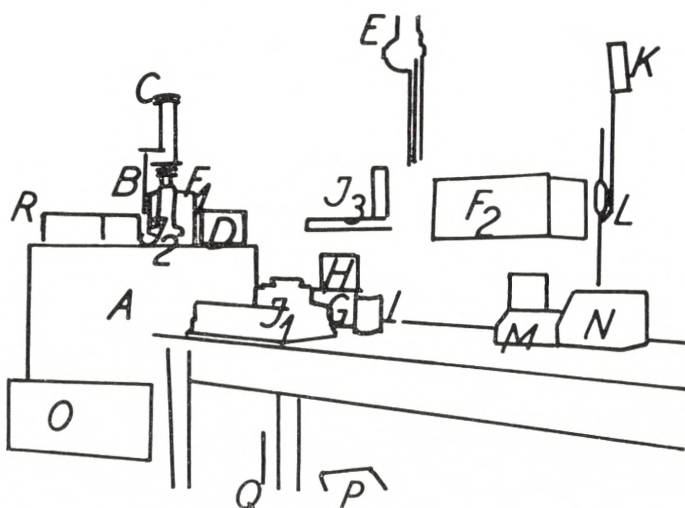
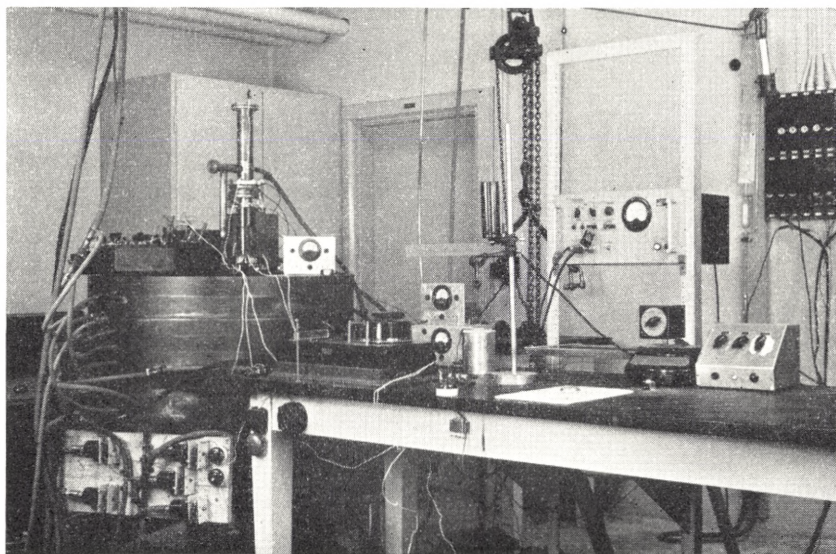


Fig. 5. General view of the instrument. A. Magnet. B. Vacuum tube with wire connection from the central part of the collector plate to the condenser C2 and to the vibrating reed electrometer. C. Vacuum container for the condenser C2. D. Pirani gauge for Ca furnace 2. E. Crane. F_1 . Vibrating reed electrometer with preamplifier. F_2 . Main amplifier and power supply for vibrating reed electrometer. G. Penning gauge. H. Forevacuum Pirani. I. Ice container for thermoelement. J_1 . Compensation instrument P_2 . J_2 . Galvanometer belonging to J_1 . J_3 . Galvanometer scale and lamp belonging to J_1 . K. Liquid air trap. L. McLeod gauge. M. Galvanometer for thermoelement reading. N. Current adjuster for magnetic field. O. Water relays with alarm bell. P. Diffusion pump. Q. Mechanical pump. R. Resistances and voltmeter giving P_2 and P_4 .

and devices for keeping the pressure down without actual pumping (not visible in Fig. 5).

The magnet was constructed by T. B. Thriges factories, Odense, Denmark. The other parts of the equipment were built at this institute.

The magnet is shown in Fig. 6. The iron surrounds a cylindrical gap, which contains the coils with their water cooling and

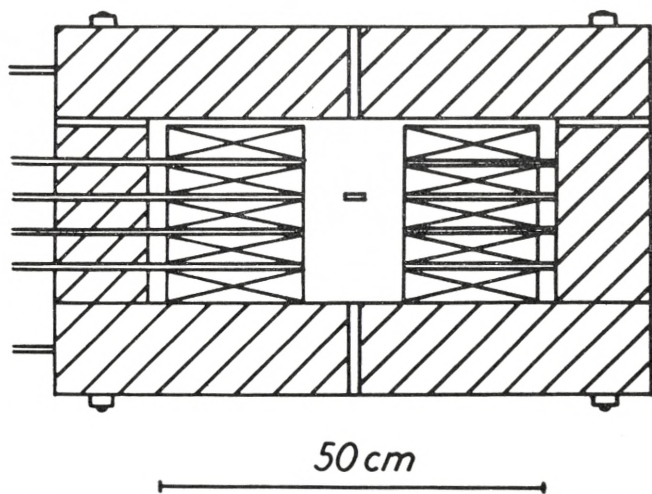


Fig. 6. General diagram of the magnet with coils, water cooling etc.

insulation system. A small cylindrical air gap, 13 cm in diameter and 24 cm long, is left. This air gap constitutes the essential space into which the main vacuum system is introduced. The coils are made of 20 times 1 mm^2 flat copper wires insulated with plastic materials. 10 such flat coils are placed above each other, and between every second coil a water cooled plate is introduced. The magnet is very compact, which involves some difficulties when the main instrument is to be inserted. The main advantage of this construction is the relative cheapness of the magnet. Vacuum and electric and mechanical connections are made through narrow channels in the lid and bottom of the magnet and in one of the cooling plates.

The magnet is fed from a DC generator, which is stabilized in the standard manner applied in this institute³⁾. The homogeneity of the field is measured by moving small test coils up

and down and in the radial direction inside the air gap. The largest inhomogeneities appear around the narrow channels leading into the air gap through the bottom and lid of the magnet. These inhomogeneities do not extend far enough to be of any significance for the main instrument, which, due to the thickness of the vacuum chamber, first begins at about 2 cm from these channels. Apart from these inhomogeneities, slight inhomogeneities of up to 1 pct. appear, making the field slightly weaker in the central plane of the equipment. This is not very satisfactory and it will be seen later that these field inhomogeneities in fact are responsible for the most important source of systematic errors in the measurements.

The linearity of the magnetic field with the input current was investigated by means of a magnetic weight introduced in the air gap and with the possibility of balancing through the air gap between the uppermost coil and the iron lid. The investigation has shown that the field varies linearly with the current to within .1 pct. throughout the whole region applied here (up to 13000 Gauss). The remnant was found to be negligible.

The absolute calibration of the field was taken from a calculation on the magnetic and electric circuits. In fact, this calibration is not necessary, since it can be provided by means of the results (61a) and (77). An error in the calibration would affect these two results in opposite directions.

In the following, the magnetic field was always taken from the measurements of the current in the magnet and calibrated in the above mentioned manner.

The water cooling of the magnet was not adequate for keeping the temperature constant in the air gap. This is another important source of possible systematic errors in the measurements, although it has been largely reduced by inserting an additional water cooled shield between the coils and the vacuum chamber.

2.2. The Collector System.

The collector system is shown in Fig. 7. The whole system is placed in the magnetic field generated in the magnet Fig. 6. A water cooled brass shield *C* is introduced between the coils

and the main instrument. This meant an essential improvement of the instrument. However, even with this extra cooling, the temperature varies when the field operates for a long time. If, say, 70 amps are sent through the coils, the temperature increases by about 35°C during 30 minutes when no water is sent through the channels of the shield, and by about 3°C when the

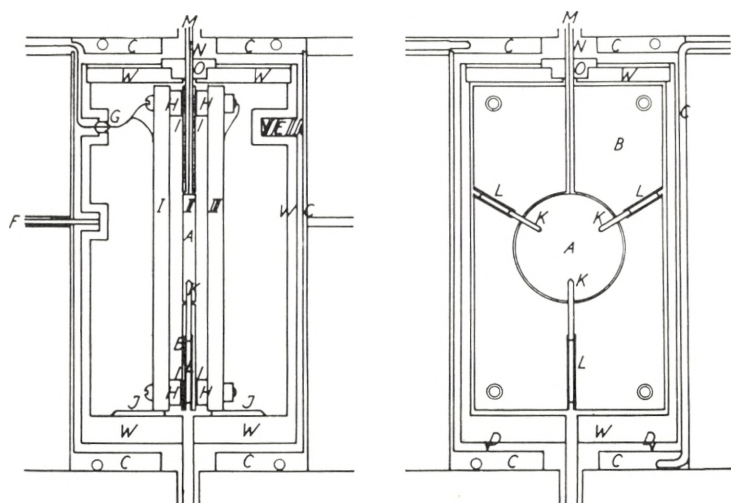


Fig. 7. The vacuum chamber and collector system. I and III. The outer electrodes. II. The inner electrode. A. The collector. B. The guard ring. C. Water cooled shield. V. Vacuum chamber. D. Pivots. E. Phosphor bronze spring. F. Micrometer screw. G. Glass insulator. H. Brass stopper. I. Polystyrene foil. J. Perspex insulator. K. Textolite insulators. L. Brass screws. M. Connection to vibrating reed. N. Guard ring tube. O. Perspex insulator.

shield is cooled. The temperature is measured in the space between the shield and the vacuum chamber W.

The collector system is contained in the vacuum chamber W. W rests on the two pivots D and is kept in position by the phosphor bronze spring E and the micrometer screw F. When the system is put together, vacuum established and A^{37} introduced, the entire system can be tilted so that the collector plates can be adjusted parallel to the lines of force of the magnetic field (cf. section 2.6).

The collector system consists of a double condenser. Duplicity is only introduced for convenience. The two outer condenser plates I and II are short circuited, and the central condenser plate II is supported by .700 cm brass stoppers H and .004 cm

polystyrene foils I, which provide the insulation between I and III and the guard ring part *B* of II. The plates I and III rest on perspex insulators *J*. The whole system is screwed together so that no displacement occurs when the instrument is tilted.

The central part *A* of plate II is the essential collector. It is carefully insulated from *B*. Insulation is provided by the three textolite insulators *K*, which are pressed into position so that *A* and *B* are perfectly plane. The insulators are pressed in position by the brass screws *L*. *A* is connected to the vibrating reed electrometer by means of the thin wire *M*, which is brought out through a thin hole drilled in *B* and completely filled with insulating material, so that A^{37} cannot penetrate into this space and cause false currents. Finally, the insulator is vacuum sealed to the wire and to the thin brass tube *N*, which provides the electric guard ring for the collector connection. *N* is silver soldered to *B* and brought out through the insulator *O*, thus giving the possibility for electric contact to *B*. All electric connections inside the evacuated parts are soldered. This is a very important precaution in order to avoid false potentials due to accidental disconnections when vacuum is established. The inside of the vacuum chamber and of I, II and III is covered with a thin layer of gold in order to minimize effects from surface potentials. Care was taken to make the insulators (as seen from the inside of the system) as small as possible. Such insulators may be charged by the currents and thereby distort the electric field. The dimensions of the instrument are chosen so as to fulfill the conditions (21), (22), and (23) of ref. 2 in order that the central part *A* of the collector represents part of an infinitely extended condenser in all experiments discussed here. At the same time, sufficient homogeneity of the electric field is obtained.

The outer part *B* of the central plate acts as a guard ring and is kept at the same potential as the collector *A*. Nevertheless, contact potentials may cause small currents over the many insulators between *A* and *B*. A special investigation was carried out with the aim of finding insulators which are both rigid enough mechanically and sufficiently well insulated even when they are strongly irradiated with X-rays. This investigation is described in Appendix C. Textolite was found to fulfill these conditions.

2.3. The Electrical System.

The wire *M* of Fig. 7 is connected to a vibrating reed electrometer in the manner shown in Fig. 8. The connection is carried out in a metal vacuum container. Metal was chosen

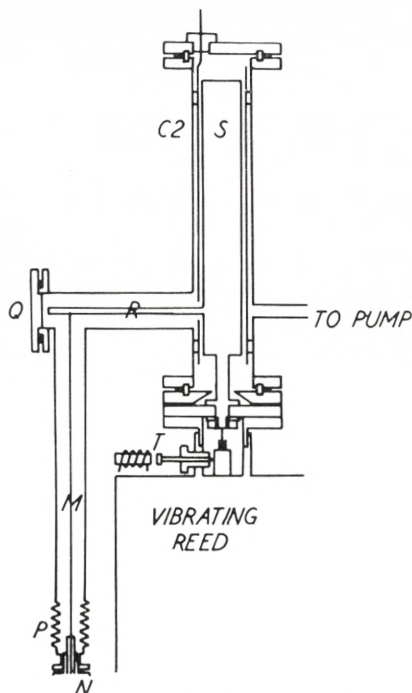


Fig. 8. Connection to vibrating reed, condenser *C2* and magnetic switch. *M*. Wire from the collector *A* of Fig. 7. *P*. Metal bellows. *Q*. Flange. *R*. Rod fixed to the central plate of *C2*. *S*. Central electrode of *C2*. *T*. Magnetic switch.

because the collector system has to be shielded from disturbing electric potentials. The vacuum is necessary in order to ensure that this system should not act as an ionization chamber for cosmic rays or radioactive impurities. The vibrating reed is used as a zero indicator only, and the charge arriving at *M* from the collector is neutralized by charging the additional condenser *C2* from a compensation instrument.

Again all electric contacts inside vacuum are soldered, and current is drawn through all connections in order to ensure contact. The membrane *P* provides the flexibility needed in order

that the main vacuum chamber can be tilted without disturbing the secondary vacuum in the system shown in Fig. 8. The flange Q is only introduced in order to enable us to put the instrument together and to solder M to the fixed rod R which leads to the inner electrode 5 of $C2$. The additional condenser $C2$ rests with its inner electrode in the socket of the vibrating reed electrometer. The magnetically operated switch T makes it possible to set the system free and ready for measurement.

Fig. 9 shows the circuit diagram with the same notation as

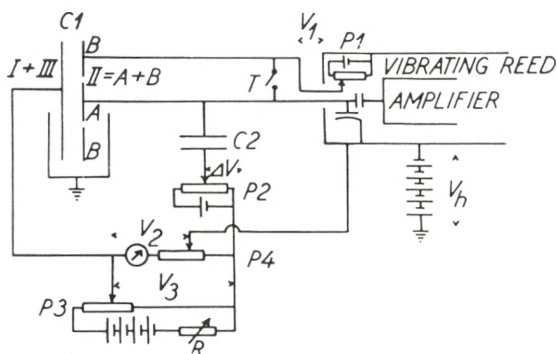


Fig. 9. The circuit diagram.

used previously. The outer condenser plates are connected to a battery of dry cells. The potentiometer $P1$ generates the potential V_1 on A and B .

V_1 is chosen such that it equals the contact potential between the reed and anvil in the vibrating reed electrometer. Thereby the reed indicates zero potential. When the short circuit T is removed the inner system is free and completely insulated from all other conductors in the instrument. $P2$ gives the compensation potential 0—1 volt on $C2$ which is used to keep the reed showing zero when ions are collected on the collector. The time t it takes to charge $C2$ to, say, 1 volt is a measure of the currents i_+ or i_- given in Chapter 1. $P3$ gives the possibility of generating a variable potential V_3 between certain parts of the instrument. V_3 can be adjusted for long time drift by means of the variable resistance R . $P4$ divides V_3 so that a certain portion of V_3 is connected to $C2$ and the remainder, V_2 , is the essential part of the potential V between the outer and inner plates of the collector system. $P4$

is adjusted so that a variation of V_3 causes no indication on the reed. The principle of this procedure is illustrated in Fig. 10. When V' is changed, say, from 0 to W volts, a voltage change in the vibrating reed is measured. This voltage change ΔV is given by

$$\Delta V \cong -W \frac{\Delta}{R_1 + R_2} \frac{C_2}{\Sigma C_i} \quad (57)$$

ΣC_i is the sum of various capacitances between the insulated system and all other parts of the instrument.

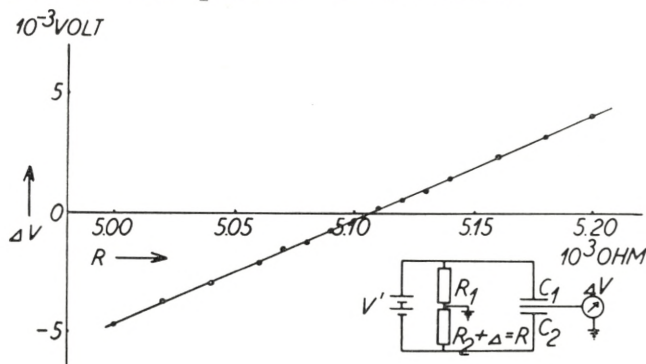


Fig. 10. Indication on vibrating reed for a 3 volt variation of V_3 as a function of the resistance R . Basic circuit diagram is shown.

In Fig. 10 are also given the measured results for ΔV as a function of $R = R_1 + \Delta$ when V' is varied from 0 to 3 volts, which is far more than any drift during a single experiment. It is seen how complete compensation can be obtained by putting $R = 5107$ ohms. Now measurements can be carried out at a potential $V = V_1 - V_2$ across C_1 .

The condenser C_2 is about 60 cm. Therefore, a current of 10^{-14} amp will cause a charging to 0.1 volt in approximately 300 sec. Such an interval of time can be measured by means of a stopwatch with an accuracy of 0.2 sec. Thus it is possible to measure currents of this order with an accuracy of 0.1%. The zero current of the entire instrument, when radioactive Ca is placed in the Ca furnace 2 described in 2.5, is $< 5 \cdot 10^{-18}$ amp and the instrument noise is $< 10^{-4}$ volts which, together with the uncertainty in the time measurement, still permits a 0.1 accuracy.

2.4. The Potential V_h .

When electrons move in our crossed electric and magnetic fields we can, as mentioned in 1.5, practically neglect the influence of the electric field. An electron will thus essentially move in helical orbits. If the electron is created at a point with positive potential, it will not be able to spiral out towards the

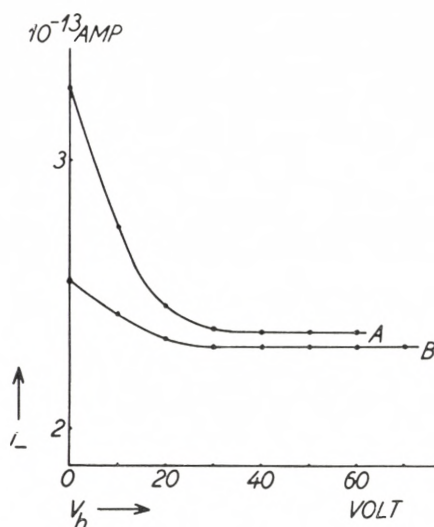


Fig. 11. The figure shows i_- as a function of V_h for $V = 34$ volts and $H = 1450$ Gauss. Curve A corresponds to a pressure of $2 \cdot 10^{-4}$ mm Hg, curve B corresponds to $3.6 \cdot 10^{-5}$ mm Hg.

lid and bottom of the chamber, unless the lid and bottom are placed at a positive potential of approximately the same value as, or a higher value than, that at the point where the electron is created. The effect is similar to that which is utilized in the Penning manometer.

This situation occurs especially when the collector is at zero potential and the plates I and III are at positive potentials. In this case, the electrons will travel up and down in the instrument until they change momentum by collisions with molecules of the residual gas. Thereby the electrons may ionize the molecules giving a new charge which is collected and which falsifies the current measurement.

The effect can easily be removed by applying the potential V_h as shown in Fig. 9. In Fig. 11 the effect of V_h is illustrated. A^{37} has been enclosed in the vacuum system in the manner described in the following, a magnetic field and an electric field of $V = 34$ volts are applied. The current observed is then described as a function of V_h . It is seen that too high positive currents are obtained until $V_h > 34$ volts, i. e., until no electrons are created at higher potential than the potential at the bottom and lid of the vacuum chamber. The curves in Fig. 11 refer to two different values of the pressure, and it is seen that the effect is more pronounced for higher pressures. This is of course a support for the whole picture of the effect.

As a consequence of the present results, V_h was always kept slightly above V in the following experiments. The procedure is not quite satisfactory and, in future instruments of this type, it will be necessary to deal with the fields at the limits of the collector system in a more satisfactory way. Either one field should be applied so as to remove the heavy particles and, as here, the lid and bottom of the instrument kept at a potential V_h , or else a more continuous termination of the electric field should be provided.

2.5. The Vacuum System.

The auxiliary vacuum system is illustrated in Fig. 12. The tube leading from the bottom of the main chamber in Fig. 7 is through a joint U connected to the quartz tube Y containing commercial Ca . The Ca is heated continuously by a stove which is not shown in the figure. In this way, Ca acts as a getter, and the pressure can be kept down in the main instrument for rather long periods of time. A stopcock V leads to a closed system consisting of a stainless steel tube X , which contains 5 g of Ca irradiated for four weeks in the Harwell pile. This Ca contains some millicuries of A^{37} . The closed system also contains a Pirani gauge W . Another stopcock \mathcal{E} leads to the Penning gauge. \mathcal{O} leads to the vacuum pumps, consisting of two oil diffusion pumps and a mechanical pump. \mathcal{A} leads directly to a liquid air trap and further to a McLeod manometer. The liquid air trap prevents Hg vapour from spreading out in the instrument.

When X is heated, A^{37} is liberated and, thus, A^{37} can be introduced into the system. During heating, the pressure rises to very high values inside the closed system defined by V . However, as heating goes on, the pressure again is reduced and, when heating is interrupted, the pressure is further diminished.

When the main system has been pumped down for some time, and the Ca furnace Y has been heated continuously, it is

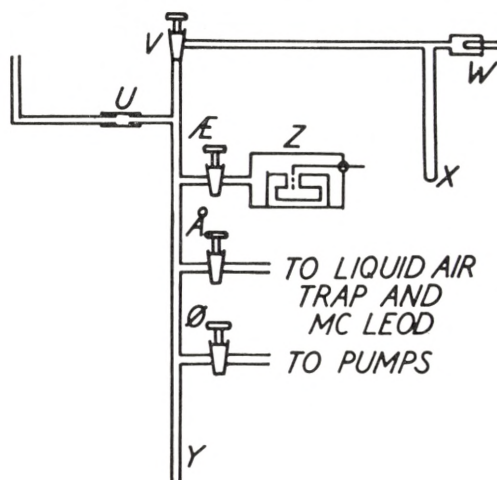


Fig. 12. The auxiliary vacuum chamber. U . Joint. V . Stopcock. W . Pirani gauge belonging to calcium furnace 2. X . Calcium furnace 2. Y . Calcium furnace 1. Z . Penning manometer. E . Stopcock. \emptyset . Stopcock. A . Stopcock.

possible to keep the pressure down at 10^{-6} mm Hg, as read on the Penning gauge, for many days with the stopcock \emptyset to the pump closed. Part of this is due, however, to the fact that the Penning acts as a pump. Gas molecules are ionized and bombarded into the pole pieces of the Penning magnet. This pumping action also diminishes the pressure of Argon, which is not taken by the Ca furnace. This is rather unfortunate since it means that also A^{37} is eaten by the Penning. Such an effect is clearly prohibitive for the entire experiment. That this is so was verified by a direct test using A^{37} as a tracer for A . The current i_- in the instrument was again measured for given values of V and H and followed through half an hour. The current was constant to within the above mentioned uncertainty. Then, as illustrated in Fig. 13, at the time $t = 0$, the stopcock E was opened and the

Penning was permitted to operate. It is seen that the current i_- decreases within an hour to a fraction of the value it had before the Penning was allowed to eat A. The accuracy in the points after $t = 0$ is not too high because shorter time intervals than 300 sec were used for the measurements. Also, the operation conditions are more unstable in this case. The first very sharp

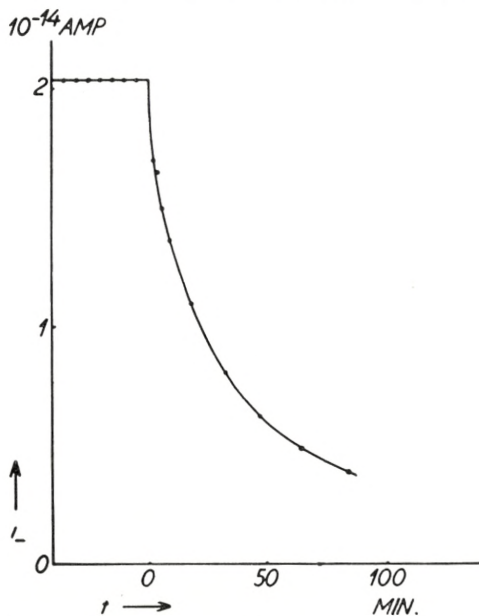


Fig. 13. The Penning manometer eats A. The figure shows the current i_- as a function of time t . At $t = 0$ the Penning is permitted to eat A.

drop is due to the fact that the Penning volume did not contain A^{37} before $t = 0$. It is of course impossible in this way to explain the continued decrease.

It was therefore necessary to use the McLeod only for the measurements of the pressure during the investigations. We could not obtain the very low pressures indicated above, but we had to work with the pressures which the Ca furnace alone could keep. It turned out that, with the present vacuum system, we had a practically constant increase of roughly $3-4 \cdot 10^{-5}$ mm Hg per day when the Penning was not operating. This is presumably due to A leaking into the instrument. The pressure curve as a function of time is shown in Fig. 14. At $t = 0$, a portion of A^{37}

was introduced, and the pressure was rather high for the first few minutes. This is due to gas given off by the irradiated *Ca* when the furnace *X* is heated as mentioned above. After heating, the pressure in the closed system *X* did not go entirely down to zero. Part of this gas was, however, neutralized by the *Ca* furnace *Y*, and within half an hour the pressure decreased to

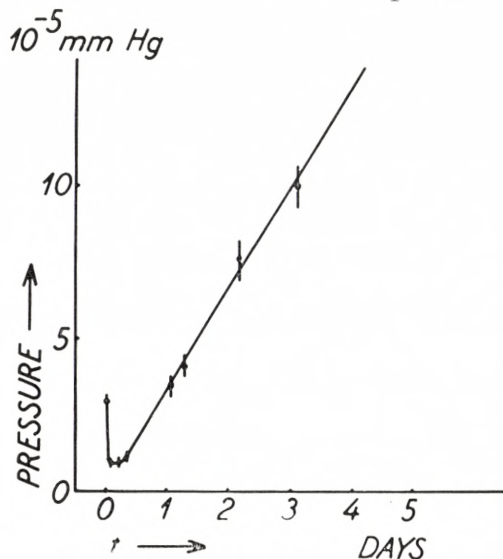


Fig. 14. Pressure in the instrument as a function of time after a portion of radioactive Argon has been introduced at $t = 0$.

a value slightly below 10^{-5} mm Hg, where it stayed for some hours. Thereafter, the pressure increased in the manner described above.

Two millicuries of A^{37} lead to a pressure of about 10^{-6} mm Hg in our approximately 2 liter vacuum system.

2.6. Tilting of the Instrument.

When the plane of the condenser is not parallel to the magnetic field, secondary electrons from the lid and bottom of the instrument spiral up and hit the collector. Thereby the currents to the collector are reduced. One can therefore directly use the current i_- as a function of the micrometer reading (Fig. 15) in order to get the best possible alignment of the instrument. In

the case illustrated in Fig. 15, the instrument has been inserted in the magnet in such a way that the tilting could not be carried further to the right because no more space was available in the two narrow channels of the pole pieces. In other investigations, the curve has been followed further to the right. The curve is thereby shown to be symmetric. If the field were homogeneous and the plates exactly plane, an effect proportional to the numer-

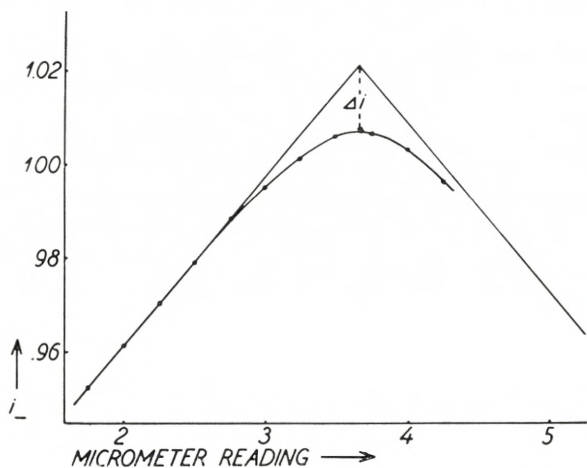


Fig. 15. Tilting of the instrument. The figure shows i_- as a function of the micrometer reading for $V = 60$ volts, $V_h = 70$ volts, $H = 4280$ Gauss, and at a pressure of 10^{-5} mm Hg. The currents are measured in the units used in the following, where i_- for $V = 30$ volts, $H = 2500$ Gauss has been put = 1. The current Δi is the deviation from the asymptotic behaviour. 1 unit micrometer reading corresponds to $\alpha = 25'$.

ical value of the tilting angle α would be expected, i. e., the deviation from the asymptotic behaviour of the curve is a direct measure of the influence of the inhomogeneities in the field and of the lack of planeness of the plates.

In our case, the field inhomogeneities are, as mentioned, so that the field is slightly weaker in the center of the air gap than at the position where the bottom and the lid of the vacuum chamber are placed. The effect is equivalent to the plates being curved away at the ends from the actual space utilized in the instrument. Thus, no shadow effect will occur when the chamber is tilted, and a simple argument shows that the asymptotes in Fig. 15 will intersect in the true point representing α_0 and that

current which would have been obtained if no field inhomogeneities existed. The current Δi thus represents the correction which must be applied on i in order to get the true i value when i is measured in the most favourable position of the instrument. Curves like that given in Fig. 15 were obtained for various values of H and V , but no variation could be found with certainty in Δi ; hence, we have chosen to correct all our later measurements with the mean value observed, $\Delta i = .015$ in the standard units mentioned in the text to Fig. 15. This value is of course somewhat uncertain and must be taken with all due reservation. However, due to its apparent constancy, we need not be much worried when discussing small variations in H and V ; furthermore, we have obtained an independent check on Δi in the arguments given in section 3.4.

2.7. Temperature Constancy.

Obviously, it is important to keep the temperature constant during the investigations, simply because the concentration of A^{37} is strongly affected if different parts of the equipment have differently varying temperatures.

This effect is illustrated in Fig. 16. The instrument was left for some days without cooling water so that room temperature was reached. When measurements were started (in the following referred to as the time $t = 0$), $V = 30$ volts and $H = 2500$ Gauss was applied and cooling water turned on; the curve shown in Fig. 16 was obtained, giving our standard reference current as a function of time measured in units 10^{-16} amp. The variation in temperature in the space between the water cooled shield and the vacuum chamber is also given in Fig. 16.

During the first few minutes after $t = 0$, the outer parts of the vacuum chamber are cooled down, whereas the collector system and the space between them stays at room temperature. Thereby the concentration of A^{37} between the plates is reduced, and the A^{37} concentrates in the outer parts of the vacuum chamber, where it is augmented until somewhat later, when the collector becomes cold and the relative concentration is restored. The final concentration is then slightly larger than the concentration at

$t = 0$ because the vacuum chamber now has a lower temperature relative to the *Ca* furnace, McLeod etc.

The uncertainties indicated in the current measurements in Fig. 16 are $2 \cdot 10^{-17}$ amp, representing 0.1 pct of i_- .

In the experiments described in the following chapter, the measurements have been performed by referring to the present

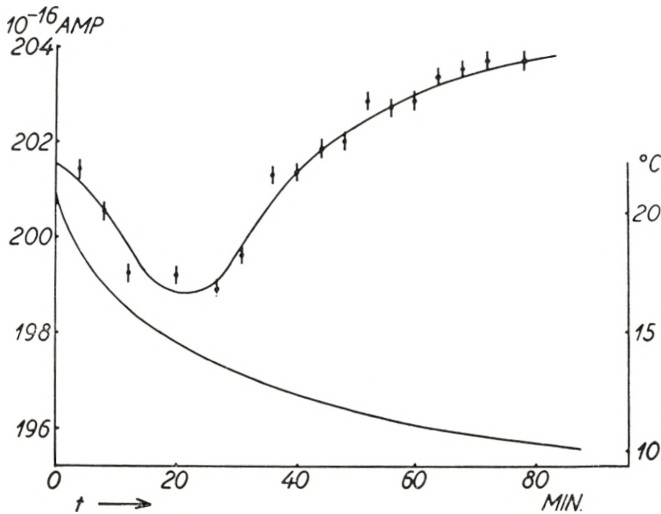


Fig. 16. The figure shows i_- as a function of time measured under our standard reference conditions $V = 30$ volts and $H = 2500$ Gauss. Also the temperature of the instrument is shown as measured in the space between the cooling shield *C* and the main chamber *W* (see Fig. 7).

values of V and H , putting the current obtained here = 1. The data have been taken by measuring the current for this value of V, H , for a new value of V, H , and then again for the present value of V, H and the result has been expressed as the ratio of the second measurement to the average of the first and last measurement. Occasionally, other reference values of V, H have been chosen, but then the new and the old reference points have been checked relative to each other before and after the set of measurements in question. Also each measurement has been repeated, and the results given later represent the average of the repeated measurements.

In this way, it is possible to eliminate the major effect of temperature changes and, simultaneously, the effects from the

decay of A^{37} leading to a decrease in concentration are eliminated.

It should be noted that the temperature changes observed in the present experiment are considerably larger than those encountered when the instrument is already cooled down. (Cf. section 2.2).

2.8. Statistics.

The currents observed vary from 0 to approximately $2 \cdot 10^{-13}$ amp. The latter current corresponds roughly to $1.2 \cdot 10^6$ electronic charges per sec., or to approximately $4 \cdot 10^5$ individual events per sec., if we put the average charge of the recoils to around 3 elementary charges (cf. section 3.4). In order to get a 0.1 pct accuracy in the current measurements, it is necessary to measure for about 200 sec. Thus, the total number of events amounts to about 10^8 , giving statistical fluctuations of about 10^4 . For the small currents, the absolute magnitude of the statistical fluctuations is of course smaller.

This is more than satisfactory for the present investigation but, on the other hand, it shows that an improvement of more than a factor 5 in the accuracy cannot be gained, unless much more time is devoted to each measurement, regardless of any other possible improvement in measuring technique.

2.9. Dielectric Polarization.

When the voltage is suddenly changed, the residual components of the dielectric polarization causes small errors in the currents. The effect can be measured when no radioactivity is present by following the charging up of the collector system due to binding of charges in the two condenser systems $C1$ and $C2$. The effect is similar to that illustrated in Appendix C, but much smaller. The effect takes place in what little can be seen of the insulators inside the entire system and probably also in oxide layers on the surfaces of the condensers.

The essential effect is found to last less than 10 minutes. Consequently, all measurements involving changes in V were carried out after waiting approximately 10 minutes before

starting. Fortunately, this effect does not coincide with the demand of varying the magnetic field and thereby changing the temperature of the instrument, because all curves for varying V are obtained at fixed values of H .

The existence of a heating effect accompanying H changes, and of a dielectric effect accompanying V changes, is the reason why the measurements were carried out at constant H or at constant V , as shown in the following, instead of measuring at constant B and at constant A , as mentioned in section 1.3.

In future constructions of instruments of the present type such effects should of course be avoided.

Chapter 3. Results with A^{37} .

3.1. The Decay of A^{37} .

A^{37} is reported to decay into Cl^{37} by 92 percent K -capture and 8 pct L -capture and with a half life of 34^{d4} . Primarily, electrically neutral recoil atoms are formed. However, successive Auger effects and the charge change of the nucleus from $Z = 18$ to $Z = 17$ cause a considerable ionization within a very short time ($\sim 10^{-10}$ sec) after the decay. The $Cl^{37}(p, n)A^{37}$ threshold gives that 817 ± 4 keV is available for the K -capture. Of this, approximately 3 keV is spent in excitation of the electronic core of Cl^{37} .

The recoil velocity distribution is primarily a sharp line originating from the practically monoenergetic neutrino emission, but is smeared out by ~ 6 per cent due to the recoil from the Auger effect and by a similar amount due to the Brownian motion at s. t. p.

This spread will only cause a ~ 2 keV difference between $c\langle p^2 \rangle^{1/2}$ and $\langle pc \rangle$, the magnitudes with which we are mainly concerned here. We shall therefore neglect the spread in all our expressions and apply the sharp line formulas only. In these formulas we will insert $\langle u \rangle$ everywhere instead of u . Actually, as mentioned in 1.4, the velocity distribution could in principle be found by the present method, especially if measurements were made at suitable A and B values. Due to the effects

mentioned in the preceding sections, it is best, however, that we confine ourselves to the charge distribution and to a measurement of $\langle u \rangle$.

3.2. The Currents as Functions of Medium H Values.

When a potential $V > T_R$ is applied across the condenser, the contribution to i_- or i_+ from the recoils is a constant for

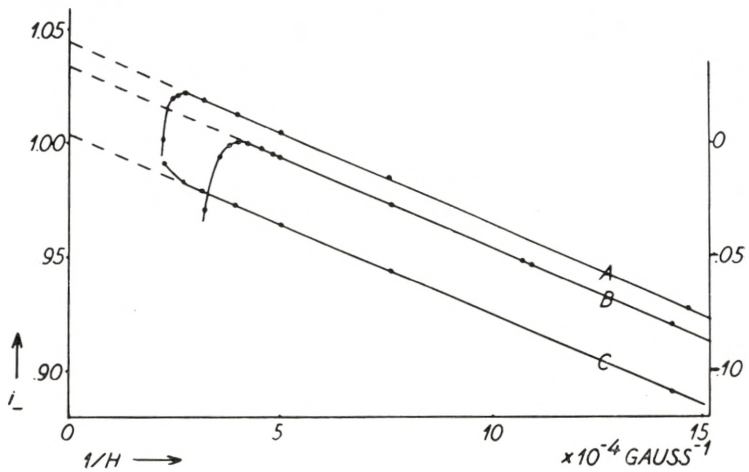


Fig. 17. Curve A: i_- as a function of $1/H$ for $V = 60$ volts, extrapolated to zero pressure, but without correction for Δi . Curve B: i_+ as a function of $1/H$ for $V = 30$ volts, extrapolated to zero pressure, but without correction for Δi . For curves A and B the ordinate is to the left. Curve C: i_- as a function of $1/H$ for $V = 60$ volts and at a pressure of 10^{-5} mm Hg, and without correction for Δi .

For this curve the ordinate is to the right.

low H values (cf. eqs. (50) and (51) of ref. 2). The electrons, however, are collected according to (45) if H is not too small, i. e., to the first approximation we obtain for medium magnetic field currents of the form

$$i_{\pm} = A - B/H. \quad (58)$$

When i is plotted as a function of $1/H$ we should therefore observe a straight line. The results obtained are shown in Fig. 17 for $V = 60, 30,$ and -60 volts. For the first two curves, a set of experiments has been performed at various pressures ranging

from $0.9 \cdot 10^{-5}$ mm Hg and upwards, and an extrapolation to zero pressure has been made. This extrapolation procedure is illustrated in Fig. 18. The magnitude of the correction which must be applied to measurements obtained at 10^{-4} mm Hg is shown in Fig. 19 for $V = 30$ volt and as a function of H . The correction varies linearly with the pressure for sufficiently low pressure values; it is seen that, for measurements performed at

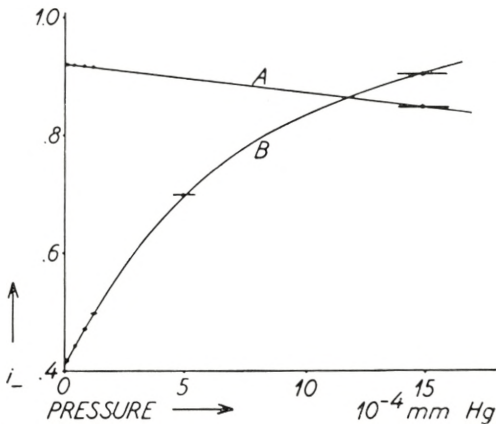


Fig. 18. Two pressure correction curves showing the maximum corrections needed in the present experiment. Both curves are obtained with $V = 30$ volts. Curve A corresponds to $H = 700$ Gauss. Curve B corresponds to $H = 6530$ Gauss. The points represent observed currents without corrections.

10^{-5} mm Hg, the corrections amount to 0.7 pct at most. Fig. 19 is an illustration of the effects discussed in 1.6. At $V = 2500$ Gauss, the positive particles begin to miss the negative plate and spiral out. Thereby the current is reduced and bends away from the straight line, as shown in Fig. 17. At the same time, a change in the behaviour of the pressure correction is observed, and this change clearly shows that pressure effects become more serious when the particles start spiralling.

Curve C in Fig. 17 is obtained at a pressure of 10^{-5} mm Hg. At this pressure, the pressure correction barely affects the straight line part of the curve. This curve bends upwards at approximately the same point where the curve A bends downwards, illustrating that particles missing the negative plate may sometimes hit the positive plate. The points where the deviation from

the straight line shape of the curves begins varies with V according to (42) of ref. 2.

$$\frac{2 Mc^2 V}{ez_\gamma (2 aH)^2} \left(1 - \frac{Hu}{F c} \right) = B_{z_\gamma} (1 - A) = 1, \quad (59)$$

where we have to put $z_\gamma = 6$ in order to obtain agreement with the energy value for the neutrino energy, as mentioned in section 3.1. This will be further illustrated in the following.

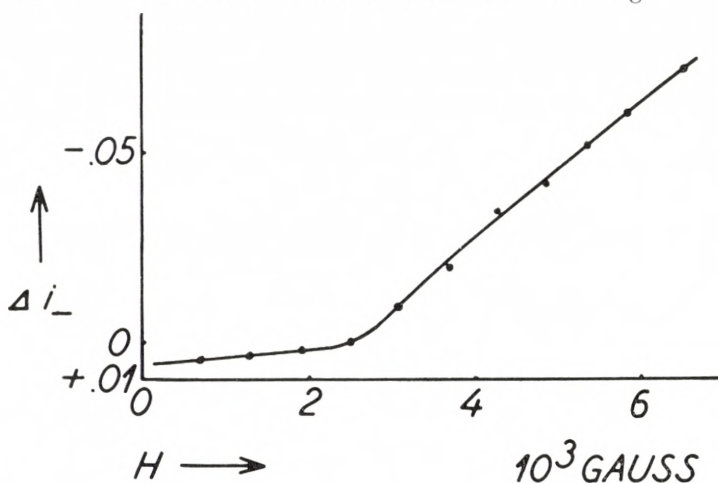


Fig. 19. The pressure correction to be applied to measurements carried out at $V = 30$ volts and a pressure of 10^{-4} mm Hg. The correction is given as a function of H .

From the curves in Fig. 17 it is apparent that the contribution from the electrons at higher values of H can be calculated as the difference between the end point value at $1/H = 0$ for the straight line extrapolated to this point and its value at the H considered.

Furthermore, the slope of the curve can be used to give the average momentum of all the electrons. The result is

$$Ne \langle z_\gamma \rangle \langle p_e \rangle \approx 1.071 \times (67 \pm 1) \text{ Gauss cm}, \quad (60)$$

where we have written the result as a product of two numbers, thereby anticipating later results. Also, we have not used an equality sign in (60) because small corrections have to be taken into account (cf. section 3.5).

3.3. The Neutrino Momentum.

When H reaches a value corresponding to (59) for appropriate values of u and z_j , some recoil particles contributing to i_- begin to miss the collector and either spiral out or add to the current i_+ . As mentioned in the preceding section, this is the reason for the

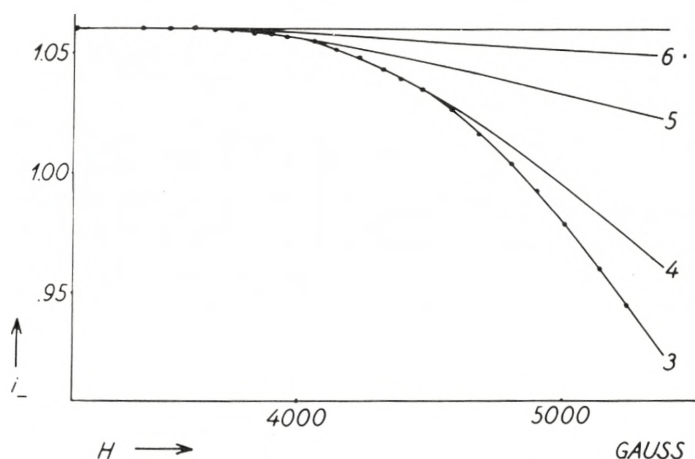


Fig. 20. Recoil contribution to i_- for $V = 60$ volts and as a function of H . The full drawn curves represent calculated contributions corresponding to the data in (61).

sharp drop in i_- and the slight increase in i_+ mentioned in connection with Fig. 17. In order further to investigate this effect we have measured i_- for $V = 60$ volts at higher values of H . The i_- values obtained have been corrected for the contribution from the electrons in the way mentioned in the preceding section. Also a contribution of .015 current units has been added in order to correct for the field inhomogeneity (cf. section 2.6). The results obtained in this way are illustrated in Fig. 20.

First, the data between $H = 3400$ Gauss and $H = 4500$ Gauss have been used to determine the momentum of the recoils. From our approximate knowledge of $Muc = 800$ keV from older recoil measurements⁵⁾ (cf. also section 3.6), or directly from the sequence of apparent humps in the curve in Fig. 20, it is possible to conclude that below $H = 4500$ Gauss only 4 or higher fold charged ions can miss the collector. Using the data in Appendix A,

we can thus calculate the contributions to the currents from 4, 5, 6, etc. charged ions with an assumed Muc value. Such calculations were carried out for a sequence of Muc values, and a least square fit was made of n_6, n_5, n_4 to each set of curves belonging to a definite Muc value. The sum of the squares of the deviations was calculated and the experimental data were found to agree with

$$\left. \begin{aligned} \langle Muc \rangle &= 812 \quad \pm 8 \quad \text{keV} \\ Nn_6 &= .004 \pm .004 \\ Nn_5 &= .015 \pm .005 \\ Nn_4 &= .075 \pm .008. \end{aligned} \right\} \quad (61 \text{ a})$$

Proceeding with the set of curves for $Muc = 812$ keV, one finds from the data for $H > 4500$ Gauss

$$Nn_3 = .155 \pm .015 \quad (61 \text{ b})$$

$$N(1.973 n_2 + 0.973 n_1) = .203 \pm .020. \quad (62)$$

The result for the Muc determination is rather insensitive to the pressure correction. This is quite natural because it merely depends on whether or not particles can spiral out. In other words, it depends on a comparison of H at the point where, say, 4 fold charged particles just begin to miss the collector with the value of H calculated from

$$\frac{Mc^2F}{4H^2a} = 1. \quad (63)$$

The deviation between these two H values is a direct measure of Muc .

Due to the large uncertainties in n_4 and n_5 it becomes very difficult to estimate n_2 by going to still larger values of H . We shall therefore proceed in a different manner in order to determine n_1 and n_2 , namely, by finding N and $N\langle z_\gamma \rangle$.

3.4. The Average Charge.

When i_+ and i_- are measured as functions of V inside the interval where no recoils spiral out, results as those shown in Fig. 21 are obtained.

When $V > T_R/z\gamma$, the curve should follow the expression (50)

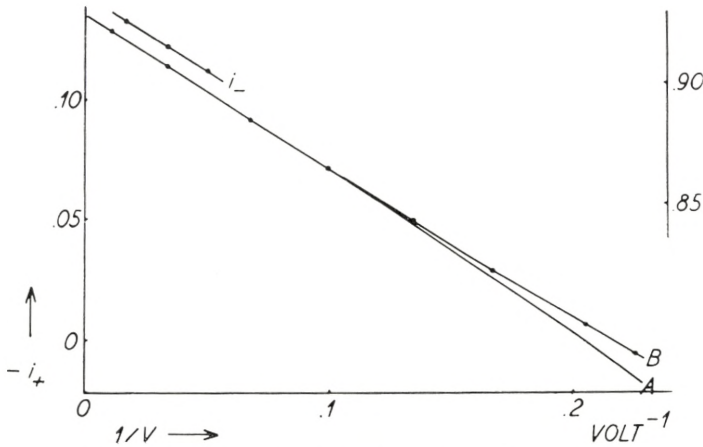


Fig. 21. i_- (scale to the right) and i_+ (scale to the left) as functions of $1/V$. The results represent directly measured currents at 10^{-5} mm Hg without correction for field inhomogeneities. Curve A is the expected curve if no singly charged recoils existed. $H = 675$ Gauss.

of ref. 2 (cf. also eqs. (85) and (88) of Appendix A). To the first approximation, we should thus expect

$$i_+ = -C + D/V. \tag{64}$$

Plotted as a function of $1/V$, a straight line results, as observed in Fig. 21. According to our considerations, $-C$ equals the contribution from the electrons at the magnetic field considered, i. e., at 675 Gauss. This contribution of course includes the current Δi due to field inhomogeneities. From Fig. 21 we obtain

$$-C = .136 \pm .001. \tag{65}$$

From Fig. 17 one obtains, by adding $i = -.014$,

$$-C = .135 \pm .001, \tag{66}$$

which shows that all currents present have been accounted for. This supports the interpretation of the tilting curve given in section 2.6.

The slope of the curve gives $Ne \langle T_R \rangle$. Since Muc is known, N can therefore be found. The result is

$$Ne = .405 \pm .008, \quad (67)$$

where the main uncertainty comes from the uncertainty in Muc . The data given in Fig. 21 and Fig. 17 also give $Ne \langle z \rangle$ which is found to be

$$Ne \langle z_\gamma \rangle = 1.071 \pm .001, \quad (68)$$

i. e., we obtain

$$\langle z_\gamma \rangle = 2.64 \pm .05. \quad (69)$$

We have now all the data required in order to obtain n_1 and n_2 . The results are

$$\left. \begin{aligned} Nn_1 &= .105 \pm .010 \\ Nn_2 &= .051 \pm .015, \end{aligned} \right\} \quad (70)$$

in good agreement with (62).

It is natural to ask whether or not the surprisingly large number of singly charged ions is due to residual gas atoms being ionized by either the electrons or by collisions with the recoil atoms. This question can be answered definitely by following the curve in Fig. 21 down to low V values. According to the theory of the instrument, the curve should then proceed as shown by curve A if no singly charged atoms of energy greater than 4 eV existed, whereas the actual fit is obtained, according to section 1.4, with

$$Nn_1 = .100 \pm .010 \quad (71)$$

and independent of the above energy determination

$$T_R = 10 \pm 1 \text{ eV.} \quad (72)$$

It is thus definitely shown that the singly charged ions have the correct energy corresponding to the neutrino emission. Also the pressure extrapolation clearly excludes the above mentioned possibility, as illustrated in Fig. 22. Note that $\langle z_\gamma \rangle$ is determined from

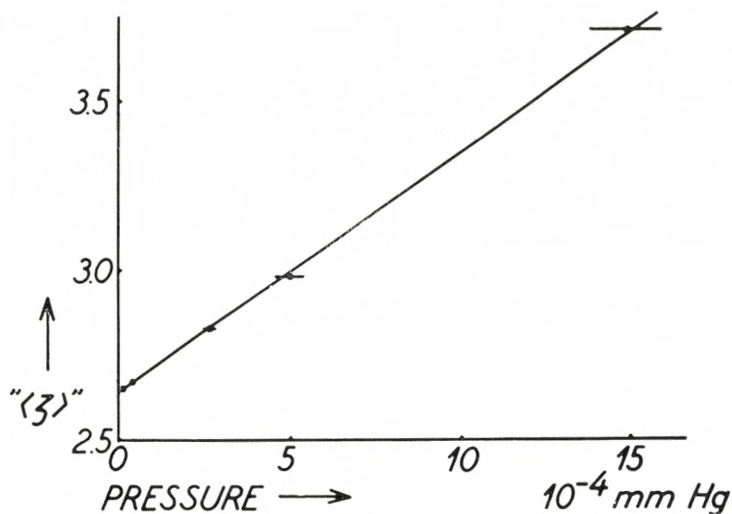


Fig. 22. The calculated $\langle z_{\gamma} \rangle$ value as a function of pressure obtained by calculating from curves not corrected for pressure effects.

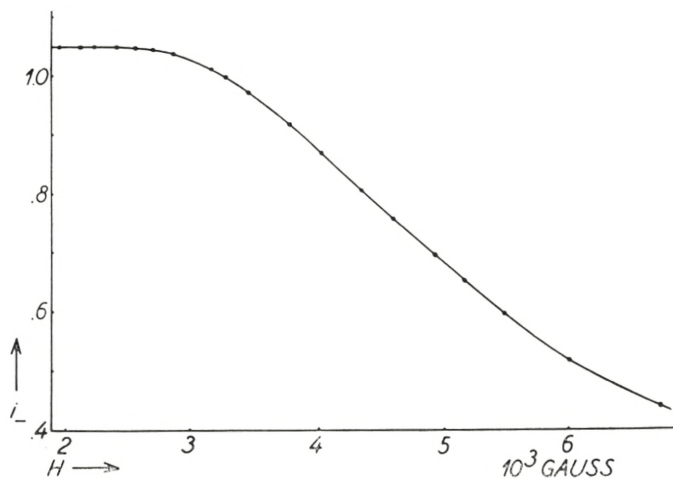


Fig. 23. The recoil contribution to i_{-} as a function of H for $V = 30$ volts.

(50) and (51) of ref. 2 by inserting $\langle T_R \rangle = 9.6$ eV, implying that we are dealing with high energy ions. This figure gives the results for $\langle z_\gamma \rangle$ which are calculated in this way by interpreting curves like Fig. 17 and Fig. 21, obtained at various pressures.

The average charge does not vary drastically with pressure and the pressure effect consists mainly of a current to the negative plate of ionized gas molecules of low initial velocity.

Finally, the picture so obtained is checked in Fig. 23, which shows an $i_-(H)$ curve for $V = 30$ volts extending into the region where also doubly and singly charged ions can miss the collector. The full-drawn curve represents (61) and (70).

The errors given in the different magnitudes derived in the present section are of course not independent of each other. Presumably the statistics of the data would permit narrowing the limits of errors. However, it is not felt that the sources of systematic errors, especially the effects of the field inhomogeneities, justify a long and involved mathematical treatment of the material (cf. also Appendix B).

3.5. The Secondary Electrons.

Since $Ne \langle z_\gamma \rangle$ is now determined, we can immediately get the average momentum of the electrons from (60). The result is 67 Gauss cm when interpreted directly. However, the small terms in (45) have to be taken into account and thereby we obtain

$$\langle pe \rangle = 69 \pm 1 \text{ Gauss cm.} \quad (73)$$

This value may seem surprisingly low when compared with the generally assumed knowledge about Auger probabilities, Auger energies, and also with the results for the A^{37} decay mentioned in section 3.1. From such considerations it seems natural to have ~ 85 pct of the decays accompanied by 166 Gauss cm Auger electrons from the first Auger effect following K -capture. The average momentum for the remainder of the electrons would accordingly be 16 Gauss cm, corresponding to about 23 eV, which is unreasonably small.

The solution to this anomaly is found by following the curves in Fig. 17 to higher values of $1/H$. For $V = 30$ volts the result is shown in Fig. 24.

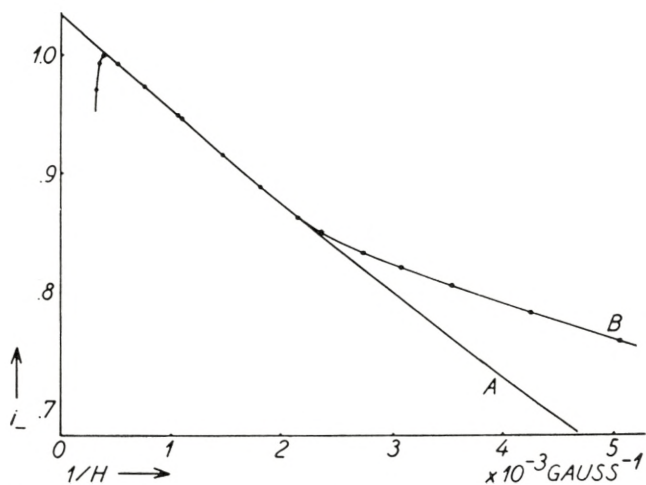


Fig. 24. The same as Fig. 17, but extended to higher l/H values. Curve A is the expected continuation if no electrons of momentum larger than 80 Gauss cm existed. Curve B shows the measurements.

If no electrons of momentum larger than 80 Gauss existed, the points would have to follow the slightly curved line A. The curvature originates from the second term in (45). An analysis of the result according to the picture given in section 1.5 gives the following results:

$$P_{\text{Auger}_I} = 162 \pm 4 \text{ Gauss cm}, \quad (74)$$

corresponding to

$$T_{\text{Auger}_I} = 2320 \pm 120 \text{ eV} \quad (75)$$

and that the intensity of these Auger transitions is

$$N_{\text{Auger}_{I,X}} = 65 \pm 5 \text{ pct.} \quad (76)$$

Correspondingly, the average momentum of the remaining electrons is 32 Gauss cm, corresponding to an energy of 90 eV, which is much more reasonable than the above value, since at least some $L-M$ Auger electrons of energy about 200 eV have to appear¹.

¹ A more detailed analysis of the ionization phenomenon accompanying A^{37} K -capture will be given by A. WINTHER.

3.6. Measurements in Pure Magnetic Fields.

When pure magnetic fields are applied, an especially large pressure correction is expected (cf. section 1.6).

The experimental results obtained in this case are illustrated

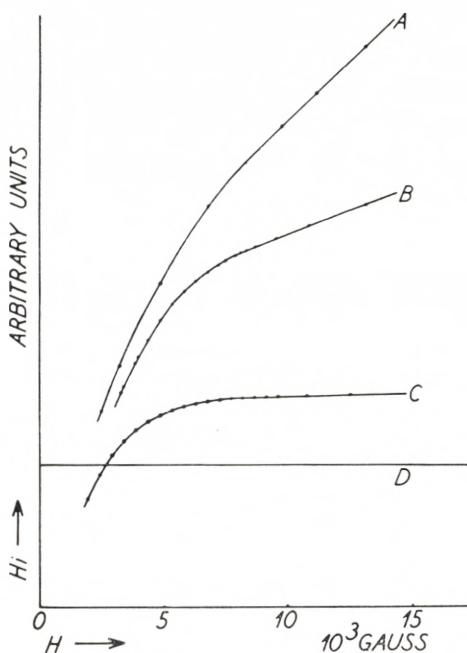


Fig. 25. The figure shows $i(H)$ for $V = 0$. Curve A corresponds to $2 \cdot 10^{-3}$ mm Hg, curve B to $7 \cdot 10^{-4}$ mm Hg, curve C to 10^{-4} mm Hg, and curve D represents the asymptotic behaviour expected from the results in the preceding sections. The currents are given in arbitrary units.

in Fig. 25. Curves are given at various pressures. As expected, the pressure effect is considerably more drastic in these experiments than in the crossed field experiments.

Nevertheless, the points in the 10^{-4} mm Hg curve, where the deviation from the horizontal line occurs, give a good measure of the momentum of the recoils. The determination of M_{uc} gives

$$M_{uc} = 806 \pm 8 \text{ keV}, \quad (77)$$

in agreement with the results measured in crossed fields.

This investigation was actually carried out before the experiments described so far had been performed. The result (77) therefore provided a tool for entering into the analysis of the curve in Fig. 20.

The present curves are of course more uncertain than the curves obtained previously, especially because so high magnetic fields had to be applied that the temperature effect becomes more serious.

Conclusions.

The present investigation gives information about the neutrino recoil momentum in the K -capture of A^{37} . The result is

$$\langle Muc \rangle = 812 \pm 8 \text{ keV}, \quad (78)$$

in agreement with the expectations from the $Cl(p, n) A^{37}$ threshold of $816 \pm 4 \text{ keV}$.

The result (78) has been checked by measuring in pure magnetic fields, "pure" electric fields (72), and crossed electric and magnetic fields.

The charge spectrum is found to be

$$\begin{aligned} n_1 &= 26 \pm 3 \text{ pct.} \\ n_2 &= 13 \pm 4 \text{ pct.} \\ n_3 &= 38 \pm 4 \text{ pct.} \\ n_4 &= 18 \pm 2 \text{ pct.} \\ n_5 &= 4 \pm 1 \text{ pct.} \\ n_6 &= 1 \pm 1 \text{ pct.} \end{aligned}$$

It is ensured that we are dealing with particles of mass $\approx 37 \text{ amu}$. This is due to the fact that really ze/M is measured. We have, furthermore, verified that the charge distribution belongs to particles having the energy corresponding to the neutrino emission.

The average charge of the charged particles is found to be

$$\langle z_7 \rangle = 2.64 \pm .08,$$

which is lower than the values reported previously⁶⁾.

Furthermore, the electrons emitted under the charging of the recoils have been investigated, and it is found that Auger electrons are emitted with an energy of

$$T_{\text{Auger}_l} = 2320 \pm 120 \text{ eV}$$

and the relative intensity per disintegration of these electrons is found to be

$$N_{\text{Auger}_l}/N = 65 \pm 5 \text{ pct.} \quad (82)$$

The average momentum of all the electrons is found to be

$$\langle p \rangle = 69 \pm 1 \text{ Gauss cm.}$$

The total information obtained shows a certain degree of internal consistency, and all currents observed have been accounted for.

The results disagree with previous measurements of $\langle z_\gamma \rangle$ and with previous ideas about the ratio of L to K capture and Auger transition probabilities. These two discrepancies are explained if a rather large fraction of all transitions occurs so that an $A^{37} K$ electron is absorbed but where the resultant Cl^{37} atom, due to the radial correlation between the electrons, appears to have a hole in the L shell only⁷⁾.

The main source of errors is due to the lack of inhomogeneity of the magnetic field, and a considerably improved instrument could be constructed with the experience gained in our investigations. Many interesting problems could then be attacked and high precision in the important investigations of angular correlation in β -decay could be obtained.

Appendix A.

The functions f , g , and h are defined by means of eqs. (37—39) inside the regions I, II, and III of the A , B plane in Fig. 26. Inside the regions IV and V only a few approximate investigations of the functions have been performed.

The functions have been calculated numerically in regions I,

II and III in the following way. First, tables of the limiting angles (35) and (36) have been computed for suitable values of A' and B . Then, the integrands in (37) and (38) have been calculated, apart from the factor $\sin \theta$, as functions of A' and B . The results of these calculations have, for fixed values of $B = 0$,

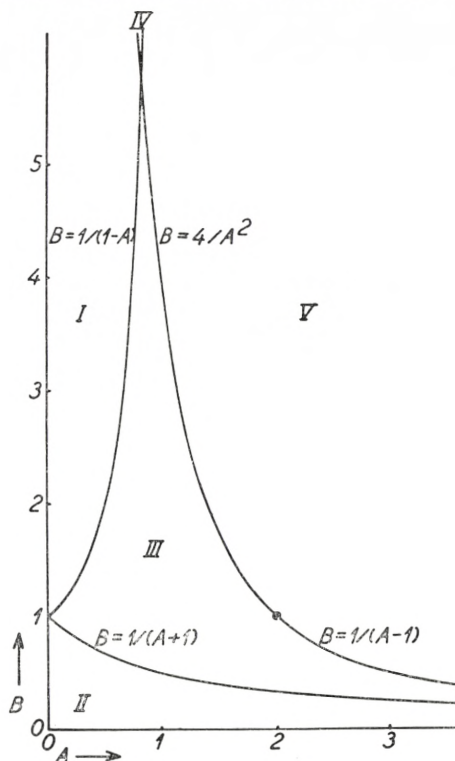


Fig. 26. The regions in the A, B plane.

0.1, 0.2, 3.5, been expressed as curves with A' as abscissa. Then, A values = 0, 0.1, 0.2, . . . have been chosen and tables of $A \sin \theta$ have been constructed for $\theta = 0^\circ, 5^\circ, 10^\circ, \dots, 90^\circ$. The integrands have then been found for these values of A' and multiplied with $\sin \theta$; they have been summed according to Simpson's rule. The functions h and g have thus been obtained with sufficient accuracy for the present investigations, but the accuracy is hardly sufficient when an improved instrument is constructed. The work involved in improved numerical calculations is, however, so great that electronic computers have to be applied.

TABLE 1. $f(A, B) \cdot 1000$.

A	0.0	0.1	0.2	0.3	0.4	0.5	0.6	0.7	0.8	0.9	1.0	1.1	1.2
B													
0.0	000	000	000	000	000	000	000	000	000	000	000	000	000
0.1	100	100	100	101	101	102	103	104	106	107	109	111	114
0.2	200	200	201	202	203	204	206	208	211	214	218	222	227
0.3	300	300	301	302	304	306	309	313	317	321	327	333	340
0.4	400	400	401	403	405	408	412	417	422	428	436	444	454
0.5	500	500	502	504	507	511	515	521	528	536	545	549	
0.6	600	601	602	605	608	613	618	625	629	631	631	627	
0.7	700	701	702	705	710	711	710	708	704	698	691	682	
0.8	800	801	803	805	801	790	778	767	755	743	731	719	
0.9	900	901	893	879	861	842	825	808	791	776	761	747	
1.0	1000	974	951	927	903	881	859	840	820	801	783		
1.1	1000	999	981	961	935	911	887	862	842	820	800		
1.2	1000	1000	996	980	957	931	907	882	858	835	812		
1.3	1000	1000	998	991	970	946	922	897	871	845	820		
1.4	1000	999	998	994	981	959	934	908	881	854			
1.5	1000	999	998	994	986	968	943	917	889	861			
1.6	1000	999	997	994	989	973	950	925	896	867			
1.7	1000	999	997	994	989	976	956	930	901	871			
1.8	1000	999	997	993	988	978	959	933	904	874			
1.9	1000	999	997	993	987	979	962	936	907	876			
2.0	1000	999	997	993	987	979	964	938	909	877			
2.1	1000	999	997	992	986	978	965	939	911	878			
2.2	1000	999	996	992	985	977	965	941	911	878			
2.3	1000	999	996	991	985	976	964	941	911	878			
2.4	1000	999	996	991	984	975	963	941	912	877			
2.5	1000	999	996	991	983	974	961	942	912	877			
2.6	1000	999	996	990	983	973	960	941	913				
2.7	1000	999	996	990	983	973	960	941	913				
2.8	1000	999	995	990	981	971	957	940					
2.9	1000	999	995	989	981	969	956	938					
3.0	1000	999	995	989	980	968	954	936					
3.1	1000	999	995	988	979	967	953	935					
3.2	1000	999	995	988	978	966	951	933					
3.3	1000	999	995	988	978	965	950	931					
3.4	1000	999	994	987	977	964	948	929					
3.5	1000	998	994	987	976	963	946	927					

TABLE 2. $h(A, B) \cdot 1000$.

A	0.0	0.1	0.2	0.3	0.4	0.5	0.6	0.7	0.8	0.9	1.0	1.1	1.2
B													
0.0	000	000	000	000	000	000	000	000	000	000	000	000	000
0.1	0	0	0	1	1	2	3	4	6	7	9	11	14
0.2	0	0	1	2	3	4	6	8	11	14	18	22	27
0.3	0	0	1	2	4	6	9	13	17	21	27	33	40
0.4	0	0	1	3	5	8	12	17	22	28	36	44	54
0.5	0	0	2	4	7	11	15	21	28	36	45	55	66
0.6	0	1	2	5	8	13	18	25	33	41	51	61	
0.7	0	1	2	5	9	15	21	27	35	45	55	66	
0.8	0	1	3	6	10	15	22	28	38	48	60	71	
0.9	0	1	3	6	10	16	22	29	39	51	63	76	
1.0	0	1	3	6	10	16	23	30	40	53	66		
1.1	0	1	2	6	10	16	23	31	42	55	70		
1.2	0	1	2	6	10	16	23	32	43	57	73		
1.3	0	1	2	5	10	17	24	33	45	60	77		
1.4	0	1	2	6	10	17	25	34	47	62	80		
1.5	0	1	3	6	10	18	26	35	48	65	83		
1.6	0	1	3	6	11	18	26	36	50	67	87		
1.7	0	1	3	6	11	19	27	38	52	70			
1.8	0	1	3	7	12	19	28	40	55	72			
1.9	0	1	3	7	13	20	29	42	57	75			
2.0	0	1	3	8	13	21	31	44	60	79			
2.1	0	1	4	8	14	22	32	46	62	81			
2.2	0	1	4	8	15	23	34	48	64	85			
2.3	0	1	4	9	16	24	35	49	68	88			
2.4	0	1	4	9	16	25	37	51	69	92			
2.5	0	1	4	9	17	26	38	53	72	96			
2.6	0	1	4	10	18	27	40	55	73	98			
2.7	0	1	5	10	18	29	41	56	76	104			
2.8	0	1	5	11	19	30	43	59	78				
2.9	0	1	5	11	20	31	44	61					
3.0	0	1	5	11	20	32	46	63					
3.1	0	1	5	12	21	33	47	65					
3.2	0	1	5	12	22	34	49	67					
3.3	0	1	6	12	22	35	51	69					
3.4	0	1	6	13	23	36	52	71					
3.5	0	2	6	13	24	37	54	73					

As long as the deviation from the $A = 0$ case treated in section 1.2 is small, we are, nevertheless, justified in applying the present procedure. Finally, the function f is obtained from formula (39).

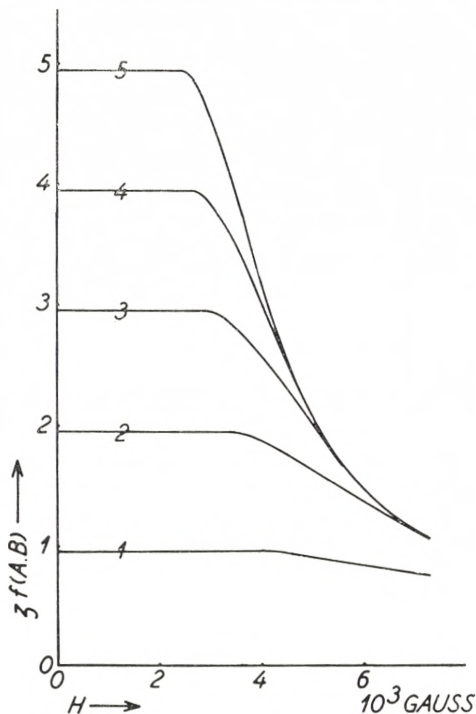


Fig. 27. The current i_- resulting from particles of different charges, $Muc = 812$ keV, $H = 37$ amu, and $V = 30$ volts and $a = .352$ cm as a function of H .

Inside areas I and II the functions are especially simple. Inside area I we have

$$j_I(A, B) = 0 \quad (84)$$

and

$$h_I(A, B) = B \int_0^{\pi/2} \frac{1}{2\pi} \sin \theta (1 + A') E(k, \pi/2) / \theta = B S(A). \quad (85)$$

Inside area II one finds

$$j_{II}(A, B) = 1 - B - 4 B S(A) \quad (86)$$

and

$$h_{II}(A, B) = 2 B S(A). \quad (87)$$

The function $S(A)$ is, for small values of A , given by

$$S(A) \cong \frac{A^2}{24} + \frac{A^4}{480} + \frac{A^6}{2240} + \frac{5A^8}{32256}. \quad (88)$$

The results for the functions f and h are illustrated in Tables 1—2.

By means of the functions f , g , and h one can find the currents belonging to a given charge distribution, say, for a given value of V and as functions of H . This is illustrated in Fig. 27.

Appendix B.

The data obtained in the present investigation are not well suited for a least square fit. The number of decimals needed in handling the mathematics sufficiently precisely is tremendous. This is perhaps best illustrated by a simple example. Suppose that measurements were performed, leading to a set of equations of the type (22). Say, for simplicity,

$$\left. \begin{aligned} n_1 + n_2 + n_3 &= 100.1 \\ n_1 + 2n_2 + 2n_3 &= 175.0 \\ n_1 + 2n_2 + 3n_3 &= 199.9 \end{aligned} \right\} \quad (89)$$

corresponding to $n_1 = 25$, $n_2 = 50$, and $n_3 = 25$ and an accuracy of .1. Now use the method of least squares. Thereby, one finds

$$\left. \begin{aligned} n_1 + 1.667n_2 + 2.000n_3 &= 158.33 \\ n_1 + 1.800n_2 + 2.200n_3 &= 169.98 \\ n_1 + 1.833n_2 + 2.333n_3 &= 174.96 \end{aligned} \right\} \quad (90)$$

which are nearly linearly dependent and need an even larger number of digits than given in order to yield as accurate results as (89).

Appendix C.

The selection of insulator material was made by testing the properties of different insulators by means of the vibrating reed electrometer. We shall describe the results with textolite only because this material was actually used in the instrument. A test

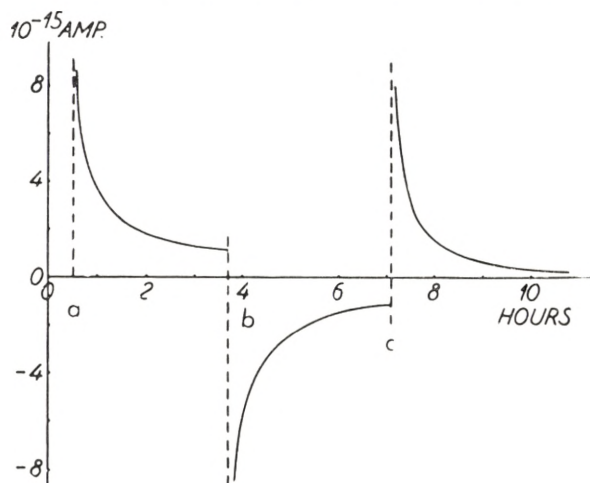


Fig. 28. Currents through textolite insulator as a function of time when a voltage of 120 volts is applied across the insulator. At $t = a$ the voltage is switched on, at $t = b$ the voltage is reversed in sign, and at $t = c$ the voltage is switched off.

body was inserted between two condenser plates, one of which was connected to the electrometer. An extra condenser plate provided the tool for connecting a dry cell across the test body in such a manner that possible drift in the dry cell voltage was eliminated according to the scheme given in Fig. 10 of section 2.3. The test chamber was evacuated in order to eliminate cosmic ray ionization.

When the voltage is switched on, currents occur due to the residual components of the dielectric polarization. This is of course important for the recoil spectrometer also. It means that all insulators which can be seen by the insulated system connected to the vibrating reed have to be left undisturbed as regards electric potential changes for sufficiently long time before measurements can start. The effect is illustrated in Fig. 28.

In our case, the insulators are subjected to heavy irradiations. It is quite reasonable to represent the three insulators K in Fig. 7 of section 2.2 by one textolite resistance of $1/\sigma$ ohms, where σ is the specific conductivity in $\text{ohm}^{-1} \text{cm}^{-1}$. This insulator is placed in a radiation field, but it is fairly well protected by the condenser plate II. Thus we get an overestimate by considering 1 cm^3 textolite placed in the full radiation field. Since we are attempting an approach to an infinitely extended system, the radiation intensity will be given by⁸⁾

$$I = 3.7 \times 10^7 n \times \frac{T}{30} \cdot 4.8 \cdot 10^{-10} \text{ 3600 rep/hour}, \quad (91)$$

where n is the concentration of radioactivity in millicuries per cm^3 and T is the transition energy minus the neutrino energy in eV.

Thus, the conductivity at time t , measured in hours after the gas inlet, will be given by⁹⁾

$$\left. \begin{aligned} \sigma_1 &= gI^h \tanh^\alpha (bgI^h t) \\ &\cong gI^{1/2} \tanh^\alpha (I^{1/2} t/25) \rightarrow gI^{1/2}, \end{aligned} \right\} \quad (92)$$

where g , h , α , b are constants characteristic of the material. The approximation made is sufficient for our purpose because we are especially interested in g and the ultimate value of σ_1 , after a long irradiation. The above mentioned test body was subjected to an irradiation of 250 röntgens per hour for 20 hours so that the ultimate value of σ_1 was obtained. The measurements of σ carried out after termination of the irradiation follow a curve of the form⁹⁾

$$\sigma = \frac{1}{1/\sigma_1 + kt}, \quad (95)$$

where t is measured from the termination of the irradiation, and k is another constant characteristic of the material. From the experimental result, σ_1 is found to be $10^{-16.7}$ and, consequently, one obtains $g = 10^{-17.9}$.

For A^{37} we have $T \approx 3000$ eV, and we are using $u = 10^{-3}$ millicurie per cm^3 . Thus we get $I = 6.4$ röntgen per hour, which leads to $\sigma_1 = 10^{-17.5}$, which is quite satisfactory.

Aknowledgements.

The authors wish to express their sincere gratitude to professor NIELS BOHR for his interest in our experiments and for the facilities placed at our disposal. We also wish to thank Civ. ing. H. TUXEN MEYER for designing the magnet.

*Institute for Theoretical Physics,
University of Copenhagen,
Denmark.*

References.

- 1) J. C. JACOBSEN and O. KOFOED-HANSEN, Phys. Rev. **73**, 675 (1948),
O. KOFOED-HANSEN and P. KRISTENSEN, Dan. Mat. Fys. Medd. **26**,
no. 6 (1951).
- 2) O. KOFOED-HANSEN, Dan. Mat. Fys. Medd. **26**, no. 8 (1951).
- 3) J. R. JENSEN and K. O. NIELSEN, Ingeniøren, Nr. 23 (1952).
- 4) For references, see J. M. HOLLANDER, I. PERLMAN, and G. T. SEABORG, Rev. Mod. Phys. **25**, 469 (1953).
- 5) G. W. RODEBACK and J. S. ALLEN, Phys. Rev. **83**, 215 (1951).
- 6) M. S. PERLMAN and J. A. MISKEL, Phys. Rev. **91**, 899 (1953).
S. WEXLER, Phys. Rev. **93**, 182 (1954).
- 7) P. BENOIST-GUEUTAL, thesis, Paris (1953).
- 8) L. H. GRAY, Proc. Roy. Soc. A **122**, 648 (1928).
O. KOFOED-HANSEN, Arkiv för Fysik **2**, 216 (1950).
- 9) D. K. KELL, S. KAGANOFF, C. H. MAYHEW, and H. G. NORDLIN,
NYO-4518 (1953).

Det Kongelige Danske Videnskabernes Selskab

Matematisk-fysiske Meddelelser, bind **29**, nr. 16

Dan. Mat. Fys. Medd. **29**, no. 16 (1955)

BINDING STATES
OF INDIVIDUAL NUCLEONS IN
STRONGLY DEFORMED NUCLEI

BY

SVEN GÖSTA NILSSON



København 1955

i kommission hos Ejnar Munksgaard

CONTENTS

	Page
I. Introduction	3
II. Calculation of the Binding States in a Deformed Potential	7
a. Choice of field	7
b. Choice of representation	11
c. Details of calculations	14
d. Arrangements of tables and main diagram	18
e. Discussion of the main level diagram	20
III. Examples of Applications of Tables and Diagrams	23
a. Calculation of total energy and equilibrium deformation	23
b. Determination of ground state spin and decoupling factor	25
c. Determination of magnetic moments	27
d. Determination of electromagnetic transition probabilities	29
e. Determination of ft-values for beta transitions	36
IV. Acknowledgements	38
V. Appendix A. Use of an Alternative Representation	39
VI. Appendix B. Asymptotic Solutions in the Limit of Very Strong Deformations	44
VII. Appendix C. The Total Energy as Function of the Deformation Parameter	46
VIII. Tables	48

I. Introduction.

The nuclear shell model has had considerable success in recent years in accounting for various regularities in nuclear properties. In this model one considers the nucleons as moving independently in an averaged potential. For a particular nucleon this potential represents its interaction with all other nucleons in the nucleus. In particular, it has been possible by choosing an appropriate field, containing rather strong spin-orbit coupling, to obtain a succession of single particle states which reproduce the experimentally observed discontinuities associated with the so-called magic numbers.*

In the usual formulation of the shell model the potential is assumed to be isotropic, but it has been found that nuclei with proton and neutron numbers very different from those corresponding to closed shells have large deformations, as evidenced, e. g., by large quadrupole moments. The deformation of the nuclear field may have a great influence on the motion of the individual nucleons, and it is the aim of this paper to consider the binding states of nucleons in such a deformed potential.

The introduction of a non-spherical binding field implies that the nuclear shape and orientation must be considered dynamical variables. These variables are associated with the collective types of nuclear motion which accompany variations in the binding field. The interplay between these collective modes of motion and the individual-particle motion forms the basis of the unified nuclear model.**

* M. G. MAYER, *Phys. Rev.* **75**, 1969 (1949).

O. HAXEL, J. H. D. JENSEN, and H. E. SUESS, *Zs. f. Physik* **128**, 295 (1950).

** A. BOHR, *Dan. Mat. Fys. Medd.* **26**, no. 14 (1952).

A. BOHR and B. MOTTELSON, *Dan. Mat. Fys. Medd.* **27**, no. 16 (1953).

A. BOHR, E. MUNKSGÅRD, Copenhagen (1954).

In the following, these papers are referred to as AB, BM, and AB 1954, respectively.

Cf. also D. HILL and J. A. WHEELER, *Phys. Rev.* **89**, 1102 (1953).

The nuclear properties resulting from this interplay are found to depend essentially on the magnitude of deformation, which again depends on the nucleonic configuration. In the regions of major closed shells the equilibrium shape of the nucleus is spherical, and the individual-particle spectrum may be obtained by considering particle motion in a spherical field, as in the shell model. It is expected, however, that in these regions the nuclei have also additional modes of excitation of the collective vibrational type. The dependence of the particle motion on the nuclear shape implies for these nuclei a small interweaving of collective and particle motion, which may be described by a perturbation treatment. The further addition of particles leads to a larger nuclear deformation. The coupling between collective modes and individual-particle modes of motion may in such cases lead to a very complicated structure of nuclear states.

Still further from the closed shells, however, the situation again simplifies. The nucleus then acquires a large deformation with a resulting stability of orientation. It is then possible to separate approximately between intrinsic nucleonic motion relative to the deformed but fixed nuclear field, and the collective rotational and vibrational motion, which leaves unaffected the intrinsic structure.*

The separation of the different modes of motion is best evidenced empirically by the occurrence of rotational spectra, which are found to obey the simple theoretical expressions with remarkable accuracy.**

The separation of the nuclear motion into collective and intrinsic modes corresponds to the assumption of a wave function of the product type as solution to the nuclear wave equation

$$\Psi = \chi \cdot \varphi_{\text{vib}} \cdot \mathcal{D}_{\text{rot}}.$$

Here χ represents the intrinsic motion of the nucleons, which can be expressed in terms of the independent motion of the

* In AB, BM and AB 1954 this approximate solution of the equations of motion appropriate to strongly deformed nuclei is denoted "the strong coupling scheme".

** Cf., e. g., AB 1954 and A. BOHR and B. MOTTELSON, Chapter 17 of "Beta and Gamma Ray Spectroscopy", ed. by K. SIEGBAHN, North Holland Publishing Co. (1954).

individual particles in the deformed field, which is considered as stationary. The second factor, φ_{vib} , describes the vibrations of the nucleus around its equilibrium shape, while $\mathfrak{D}_{\text{rot}}$ represents the collective rotational motion of the system as a whole.

Most nuclei are expected to prefer shapes of cylindrical symmetry, and this is confirmed by the observed rotational spectra.* Therefore we here restrict ourselves to the consideration of particle states in fields of the spheroidal type.

In this case of axial symmetry, the intrinsic motion is characterized by the quantum numbers Ω_p , the component of angular momentum of each nucleon along the nuclear axis. The total Ω is given by $\Sigma\Omega_p$. Apart from accidental degeneracies, states are doubly degenerate (corresponding to $\pm\Omega_p$), and the total χ , in the following denoted χ_Ω , is therefore simply the antisymmetrized product of individual-particle wave functions χ_{Ω_p} . The presence of direct particle forces produces to first order a shift in the binding energies without, however, affecting the wave functions. The nucleonic coupling scheme will be essentially modified only if the particle forces are comparable with the coupling of individual particles to the nuclear axis.

The rotational motion is characterized by the quantum numbers I , M , and K , i. e. the total angular momentum, its projection on the space fixed axis (later denoted by z''), and its projection on the intrinsic nuclear axis (z'), respectively. (See Fig. 1.)

We shall not here be concerned with the corresponding vibrational quantum numbers, since we always assume that we are in the vibrational ground state.

Beside the rotational symmetry around the nuclear axis we also assume that the nucleus has reflection symmetry through a plane perpendicular to this axis. The wave function has then to be symmetrized (to possess a definite parity). The appropriately symmetrized wave function may be written in the form**

$$|\Omega, IMK\rangle = \sqrt{\frac{2I+1}{16\pi^2}} \varphi_{\text{vib}} \left\{ \chi_\Omega \mathfrak{D}_{MK}^I(\theta_i) + (-)^{I-\Sigma j_r} \chi_{-\Omega} \mathfrak{D}_{M-K}^I(\theta_i) \right\}. \quad (1)$$

* There may be special configurations for which the cylindrically symmetric shape is not stable. The rotational spectra are then of a more complex character than in the symmetric case. Cf. B. SEGALL, Phys. Rev. **95**, 605 A (1954) and M. JEAN and L. WILETS (to be published).

** BM (II.15).

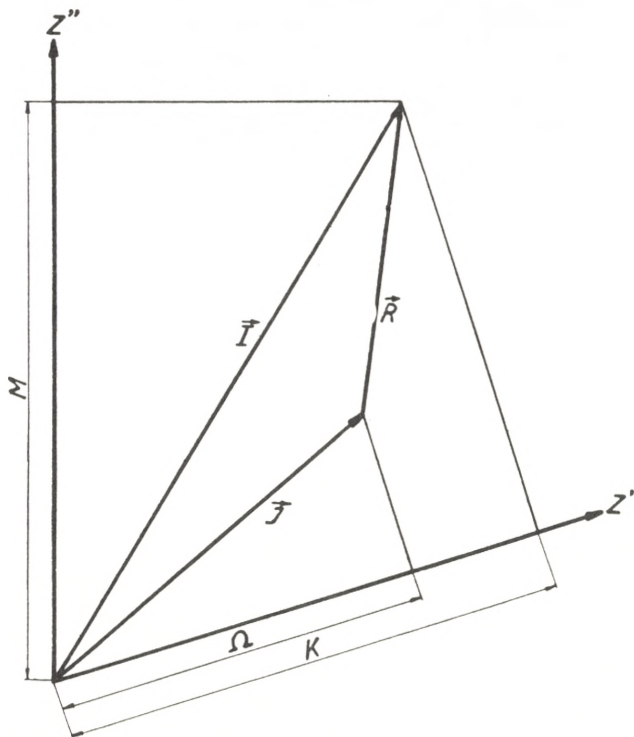


Fig. 1. Angular momentum diagram.

In the unified model the total angular momentum \vec{I} is composed of two parts, one part \vec{R} generated by the collective motion of the nucleus, the other part \vec{J} representing the intrinsic motion of the nucleons.

In the coupling scheme appropriate for large deformations the nucleons move independently with respect to the deformed nuclear field. This motion is characterized by the constants of the motion Ω_p , the component of angular momentum of each nucleon along the nuclear axis. In such a structure the magnitude of the total \vec{J} is not a constant of the motion, though its component on the nuclear symmetry axis is a good quantum number and is denoted Ω , where $\Omega = \sum_p \Omega_p$.

Finally the rotational state of the system is described in terms of the quantum numbers I , the total angular momentum, its z'' -component M , and its z' -component K .

In the ground state, \vec{R} is perpendicular to z' ($\Omega = K$), i. e. the collective rotation takes place around an axis perpendicular to the nuclear symmetry axis.

The phase $(-)^{I-\Sigma j_p}$ is thought of as a matrix when j_p (the angular momentum of the p^{th} particle relative to the potential) is not a constant of the motion. The normalization factor comes from the particular normalization of the rotational wave functions $\mathfrak{D}_{MK}^I(\theta_i)$, where θ_i refers to the Eulerian angles. The normalization

is such that the wave functions represent unitary transformations from the coordinate system (x'', y'', z'') to the nuclear coordinate system (x', y', z') .

The present paper consists of two main parts. In the first part a model is formulated for the interaction of the nucleons with the deformed nuclear field by introducing a single-particle Hamiltonian of a simple type, essentially containing a modified ellipsoidal oscillator potential and a spin-orbit term. A convenient representation, using the eigenvectors of an isotropic three-dimensional harmonic oscillator as a basic set, is then introduced. The calculated single-particle eigenvalues and eigenfunctions, obtained by means of an electronic digital computer, are arranged in tables and diagrams.

In the second part of the paper the applications of the single-particle states which have been calculated are discussed. First, we deal with the possibility of obtaining the total internal energy of the nucleus, the equilibrium deformation, and levels of particle excitation. Finally, expressions for the decoupling factor in rotational spectra, the magnetic moment, and the electromagnetic transition probabilities are given in terms of the particular wave-function representation chosen.

An analysis of empirical data (e. g. level spins, parities, magnetic moments, excitation spectra, and transition probabilities) compared with the results of the model is to be undertaken at a later date.* Already at this point, however, the general results of the calculations are published because of their wide range of application to different problems of nuclear physics.

II. Calculation of the Binding States in a Deformed Potential.

a. *Choice of field.*

To represent the interaction of one nucleon with the nuclear field we assume a single-particle Hamiltonian of the following

* Note added in proof: For preliminary results of such an analysis cf. B. MOTTELSON and S. G. NILSSON, *Zs. f. Physik* **141**, 217 (1955), and B. MOTTELSON and S. G. NILSSON, *Phys. Rev.* (in press).

form^{*}, ^{**}. (For the sake of completeness we should really add a suffix p to all the quantities in this section, referring to the fact that they are single-particle quantities. However, we simplify the notation by dropping this index from the beginning.)

$$H = H_0 + C \bar{l} \cdot \bar{s} + D \bar{l}^2, \quad (2)$$

where

$$H_0 = -\frac{\hbar^2}{2M} \Delta' + \frac{M}{2} (\omega_x^2 x'^2 + \omega_y^2 y'^2 + \omega_z^2 z'^2), \quad (2a)$$

where x' , y' , z' are the coordinates of a particle in a coordinate system fixed in the nucleus.

This means that an oscillator potential is first adopted for the sake of simplicity. To this is added the usual spin-orbit term. The \bar{l}^2 -term then gives a correction to the oscillator potential especially at large distances (important for high l -values). This serves to depress the high angular momentum states. One might also say it has some of the features of the interpolation, between the square well and the oscillator potential, which is usually employed in the shell model. In the case of spherical symmetry, we must require that (2) and (2a) give the known sequence of single-particle levels considered in the shell model. This puts a strong limitation on the choice of C and D (see further the discussion on p. 15). In Fig. 2 one can compare the level scheme (with our parameter choice) for the spherical case, with the level spectrum proposed by KLINKENBERG^{***}, which represents a compilation of empirical data interpreted on the basis of the shell model.

It is expected that many features of nuclear states obtained

* The author is indebted to Dr. A. BOHR, Dr. B. MOTTELSON, and Prof. I. WALTER for suggestions regarding the choice of a simple potential.

** Several authors have considered the motion of nucleons in deformed fields. E. FEENBERG and K. C. HAMMACK, Phys. Rev. **81**, 285 (1951), and S. GALLONE and C. SALVETTI, Il Nuovo Cimento (9) **8**, 970 (1951), consider an ellipsoidal square well, and D. PFIRSCH, Zs. f. Physik **132**, 409 (1952), treats the anisotropic harmonic oscillator, all using perturbation theory. S. GRANGER and R. D. SPENCE, Phys. Rev. **83**, 460 (1951), report that they have an exact solution for an infinitely deep spheroidal well, without any $\bar{l} \cdot \bar{s}$ -term in the Hamiltonian, however. Finally, PFIRSCH, in the publication mentioned, and S. GALLONE and C. SALVETTI, Il Nuovo Cimento (9) **10**, 145 (1953), have studied the exact solutions of an anisotropic harmonic oscillator without spin-orbit force.

*** P. F. A. KLINKENBERG, Rev. Mod. Phys. **24**, 63 (1952).

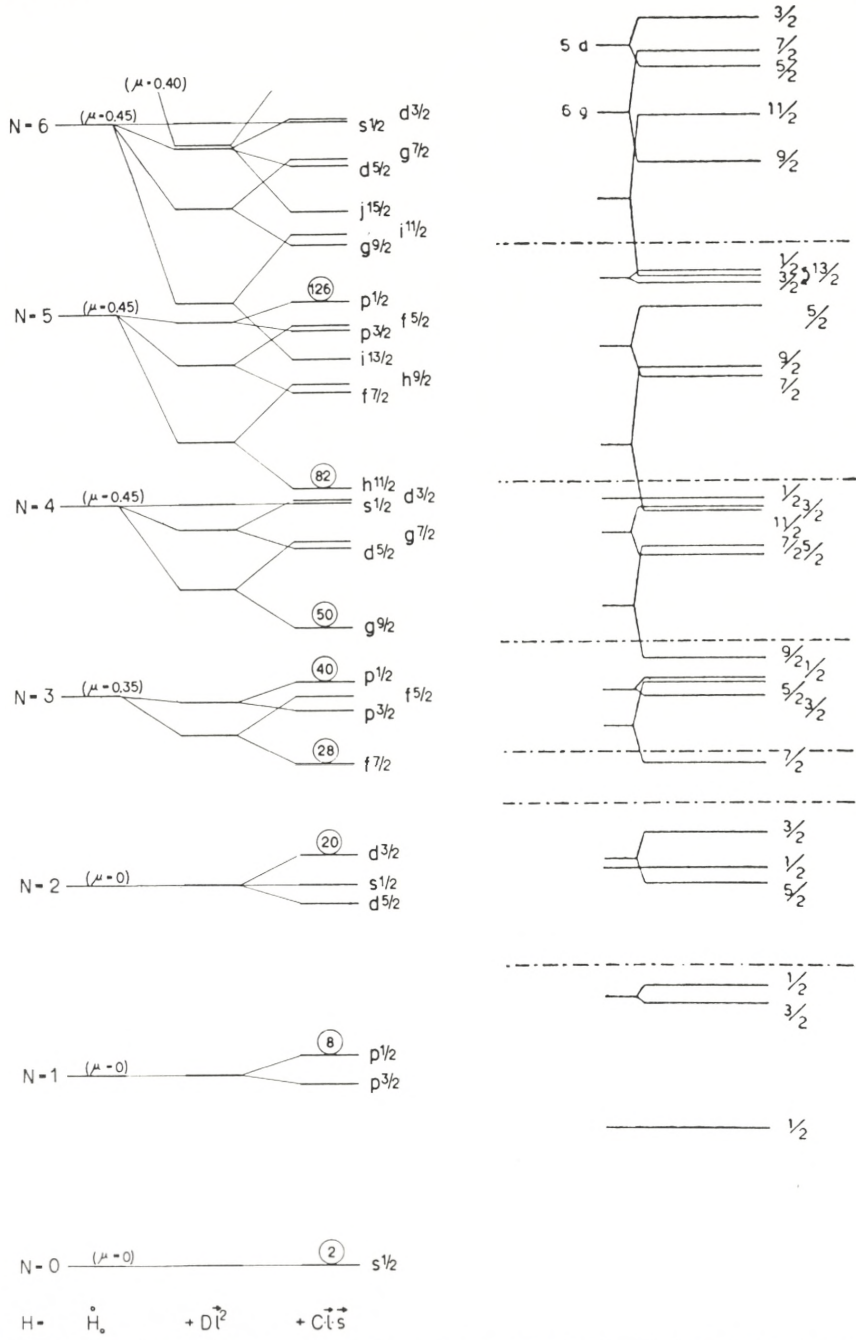


Fig. 2. Level order for the spherical case compared with the shell model level order.

Energy levels of the potential assumed in formula (2) for the spherical case ($\delta = 0$) are plotted to the left. The right part of the figure shows the level scheme proposed by P. KLINCKENBERG, which he has obtained from empirical data interpreted according to the shell model. The level scheme of Dr. KLINCKENBERG is reproduced by his kind permission from Reviews of Modern Physics.

from (2) are more general than the particular field employed, since the structure is especially determined by the angular properties, while the radial matrix elements alone reflect the detailed properties of the nuclear field.

We confine ourselves to the case of cylindrical symmetry and further introduce one single parameter of deformation δ

$$\omega_x^2 = \omega_0^2 \left(1 + \frac{2}{3} \delta\right) = \omega_y^2 \quad (3a)$$

$$\omega_z^2 = \omega_0^2 \left(1 - \frac{4}{3} \delta\right). \quad (3b)$$

Neglecting the $\vec{l} \cdot \vec{s}$ - and \vec{l}^2 -terms the problem is separable in x' , y' , z' . In this case a change, e. g., of ω_x only changes the scale of the wave function along the x' -axis. As the scale is proportional to $\frac{1}{\sqrt{\omega_x}}$, the condition of constant volume of the nucleus leads to

$$\omega_x \omega_y \omega_z = \text{const.}$$

Keeping this condition in the general case together with (3a) and (3b), ω_0 has to depend on δ in the following way

$$\omega_0(\delta) = \dot{\omega}_0 \left(1 - \frac{4}{3} \delta^2 - \frac{16}{27} \delta^3\right)^{-1/6}. \quad (4)$$

$\dot{\omega}_0$ is the value of $\omega_0(\delta)$ for $\delta = 0$. It turns out that δ is related to the quantity β , used in the papers by A. BOHR and B. MOTTELSON, to first-order as*

$$\delta \simeq \frac{3}{2} \sqrt{\frac{5}{4\pi}} \beta \simeq 0.95 \beta. \quad (5)$$

We introduce new coordinates

$$x = \sqrt{\frac{M\omega_0}{\hbar}} x' \quad \text{etc.}, \quad (6)$$

and split H_0 into a spherically symmetric term \dot{H}_0 and a term H_δ representing the coupling of the particle to the axis of the deformation

* Cf. (16) and BM (V. 7).

$$H_0 = \hat{H}_0 + H_\delta, \tag{7}$$

where

$$\hat{H}_0 = \hbar \omega_0 \frac{1}{2} [-\Lambda + r^2] \tag{7a}$$

$$H_\delta = -\delta \hbar \omega_0 \frac{4}{3} \sqrt{\frac{\pi}{5}} r^2 Y_{20}. \quad * \tag{7b}$$

b. *Choice of representation.*

A representation is chosen with \hat{H}_0 diagonal, together with \bar{l}^2 , l_z , and s_z , which all commute with \hat{H}_0 . The corresponding quantum numbers are denoted l , Λ and Σ .

None of the above operators commute with the total Hamiltonian. A commuting operator, however, is $j_z = l_z + s_z$. We denote the corresponding quantum number by Ω . For the states corresponding to a given Ω , the vectors $|N\Lambda\Sigma\rangle$ with $\Lambda + \Sigma = \Omega$ are used as basic vectors. The quantum number N represents the total number of oscillator quanta. One has

$$\hat{H}_0 |N\Lambda\Sigma\rangle = \left(N + \frac{3}{2}\right) \hbar \omega_0 |N\Lambda\Sigma\rangle.$$

In configuration space representation the basic vector looks like

$$\langle \bar{r} | N\Lambda\Sigma \rangle \sim r^l e^{-\frac{1}{2}r^2} F\left(-n, l + \frac{3}{2}, r^2\right) Y_{l\Lambda} f_{s\Sigma}, \tag{8}$$

where the relation

$$2n + l = N \tag{8a}$$

defines n . Further $F\left(-n, l + \frac{3}{2}, r^2\right)$ is the confluent hypergeometric function.

In this representation the different parts of the total Hamil-

* We assume here and throughout this paper that the phases of the spherical harmonics are chosen in accordance with E. U. CONDON and G. H. SHORTLEY, *The Theory of Atomic Spectra*, Camb. Univ. Press, London (1935).

tonian have very simple matrix elements; in particular are \vec{l}^2 and \hat{H}_0 diagonal in this representation.

The matrix elements $\langle l' A' \Sigma' | \vec{l} \cdot \vec{s} | l A \Sigma \rangle$ have the following selection rules

$$l = l', \quad A = \begin{cases} A' \\ A' \pm 1 \end{cases}, \quad \Sigma = \begin{cases} \Sigma' \pm 1 \\ \Sigma' \end{cases}, \quad A + \Sigma = A' + \Sigma'.$$

We write down, for completeness, the non-vanishing elements

$$\langle l A \pm 1 \mp | \vec{l} \cdot \vec{s} | l A \pm \rangle = \frac{1}{2} \sqrt{(l \mp A)(l \pm A + 1)} \quad (9a)$$

$$\langle l A \pm | \vec{l} \cdot \vec{s} | l A \pm \rangle = \pm \frac{1}{2} A, \quad (9b)$$

denoting $\Sigma = +\frac{1}{2}$ and $\Sigma = -\frac{1}{2}$ simply by + and -, respectively, in the vectors.

The only part of the Hamiltonian not immediately given is H_δ , which is proportional to $r^2 Y_{20}$. It is easy to show that

$$\langle l' A' | Y_{20} | l A \rangle = \sqrt{\frac{5}{4\pi}} \sqrt{\frac{2l+1}{2l'+1}} \langle l 2 A 0 | l 2 l' A' \rangle \langle l 2 0 0 | l 2 l' 0 \rangle \quad (10)$$

in the Condon-Shortley notation for Clebsch-Gordon coefficients.

Matrix elements of r^2 are calculated most easily with the help of recursion formulae for confluent hypergeometric functions. The general matrix element for r^2 is given later in (41), but the simplified expressions for $\lambda = 2$ are given here:

$$\langle Nl | r^2 | Nl \rangle = N + \frac{3}{2} \quad (11a)$$

$$\langle Nl-2 | r^2 | Nl \rangle = 2 \sqrt{(n+1) \left(n + l + \frac{1}{2} \right)} \quad (11b)$$

$$\langle N-2l | r^2 | Nl \rangle = \sqrt{n \left(n + l + \frac{1}{2} \right)} \quad (11c)$$

$$\langle N-2 \ l-2 \mid r^2 \mid Nl \rangle = \sqrt{\left(n+l+\frac{1}{2}\right)\left(n+l-\frac{1}{2}\right)} \quad (11\text{ d})$$

$$\langle N-2 \ l+2 \mid r^2 \mid Nl \rangle = \sqrt{n(n-1)}. \quad (11\text{ e})$$

The selection rules for $r^2 Y_{20}$ are

$$A = A', \quad \Sigma = \Sigma', \quad l = \begin{cases} l' \\ l' \pm 2 \end{cases}, \quad N = \begin{cases} N' \\ N' \pm 2 \end{cases}.$$

The selection rules for $r^2 Y_{20}$ imply that there is a coupling between states with different N (the difference in N being an even number). The approximation is made, however, that this coupling is neglected. Levels belonging to, e. g., the N -shell and the $(N+2)$ -shell are on the average separated by an energy of $2 \hbar\omega_0$, which, for most values of the parameters, is much larger than the corresponding non-diagonal coupling energies.

In fact, it can be shown by changing the representation slightly, that these couplings between shells of different N can be accounted for by a small change in the interpretation of the parameters δ , ω_0 etc., and a small modification of the $\bar{l}\cdot\bar{s}$ - and \bar{l}^2 -terms (cf. Appendix A).

Non-vanishing matrix elements of H are thus considered only between base vectors $\mid NlA\Sigma \rangle$ belonging to the same N and Ω .

A note should be made at this point that there are a few cases when levels of the same spin and parity (but belonging to N -shells with N different by two) cross each other within the range of the parameter η considered. Fig. 5 shows two such crossings between levels of the $N = 4$ and the $N = 6$ shells. One crossing occurs between the $\Omega = 1/2$ levels # 51 and # 60 and the other between the $\Omega = 3/2$ levels # 42 and # 57. (Concerning the labelling of the levels, see p. 19.) These crossings are removed when account is taken of the neglected coupling terms between the N - and the $(N+2)$ -shells.* The coupling terms between the crossing levels are calculated in Table II.

* The corresponding energy levels of the Hamiltonian H_t , considered in Appendix A, actually cross in the exact treatment for a deformation different from zero. With that form of the Hamiltonian (H_t) there is, however, associated an additional degeneracy compared to the case considered here.

c. Details of calculations.

From (2) and (7) we have

$$H = \hat{H}_0 + H_\delta + C\bar{l}\cdot\bar{s} + D\bar{l}^2.$$

As \hat{H}_0 is diagonal in the representation chosen, and its matrix elements are all equal for a constant N , it is advantageous to bring \hat{H}_0 out of the matrix H and only consider $H - \hat{H}_0$.

We introduce new parameters μ and \varkappa instead of C and D

$$\varkappa = -\frac{1}{2} \frac{C}{\hbar\hat{\omega}_0} \quad (12a)$$

$$\mu = \frac{2D}{C}. \quad (12b)$$

Further we introduce a new \varkappa -dependent deformation parameter

$$\eta = \frac{\delta\omega_0(\delta)}{\varkappa\hat{\omega}_0} = \frac{\delta}{\varkappa} \left[1 - \frac{4}{3}\delta^2 - \frac{16}{27}\delta^3 \right]^{-1/6}. \quad (12c)$$

We can write

$$H_\delta = \delta\hbar\omega_0 U = \varkappa\hbar\hat{\omega}_0 \cdot \eta \cdot U,$$

where

$$U = -\frac{4}{3} \sqrt{\frac{\pi}{5}} r^2 Y_{20} \quad (12d)$$

which does not depend on δ .

It is then convenient to write

$$H - \hat{H}_0 = \varkappa\hbar\hat{\omega}_0 R, \quad (12e)$$

where

$$R = \eta U - 2\bar{l}\cdot\bar{s} - \mu\bar{l}^2 \quad (12f)$$

is an operator that depends only on two parameters, η and μ .

The final calculations now consist of an exact diagonalization of the (dimensionless) matrix R in the representation chosen. R is treated as a function of the deformation parameter η , and it is diagonalized for a sequence of η -values (cf. below). The only other parameter that enters R is μ , which is independent of the deformation. The choice of μ is discussed below.

From the diagonalization of R , or rather its submatrices

belonging to certain N and Ω , we obtain the eigenvalues $r_\alpha^{N\Omega}(\eta)$. (Here α numbers the different eigenvalues of the matrix.) The corresponding energy eigenvalues of the total H are then given as

$$E_\alpha^{N\Omega} = \left(N_\alpha + \frac{3}{2} \right) \hbar \omega_0(\delta) + \kappa \hbar \omega_0 r_\alpha^{N\Omega}. \quad (13)$$

Let us denote the corresponding eigenvector $|N\Omega\alpha\rangle$. Its configuration space representation is denoted by $\chi_{\Omega\alpha}$ in the Introduction.

The values of κ and μ are chosen, as mentioned earlier, in such a way that for $\delta = 0$ the sequence of levels of the shell model are reproduced. Of course we are free to let both κ and μ vary from shell to shell, i. e. vary with N .

The parameter μ determines the sequence of levels within the group of states belonging to a particular N by depressing (for $\mu > 0$) the levels corresponding to higher l -values. The total energy spread of levels belonging to the same N -shell is determined primarily by the parameter κ . In the numerical calculations we have assigned values of μ for each N -shell so as to reproduce (for $\delta = 0$) the assumed sequence of shell model levels as well as possible.

In the numerical calculations μ is chosen in the following manner

$N = 0, 1, 2$	$\mu = 0$
$N = 3$	$\mu = 0.35$ (0, 0.50)
$N = 4$	$\mu = 0.45$ (0.55)
$N = 5, 6$	$\mu = 0.45$
$N = 7$	$\mu = 0.40$.

In general, this choice of μ means that in the lower N -shells we use a pure oscillator and for higher N -values we approach more to a square well (cf. Fig. 2).

In order to examine the sensitivity of our results to the particular choice of μ , we have performed calculations for the shell with $N = 3$ employing a sequence of different μ -values. The resulting level spectra are plotted as functions of the deformation parameter η in Figs. 3a, b, c. It is seen that, even for rather different choices of the level spectrum in the spherical potential ($\eta = 0$), the results become quite similar for large η .

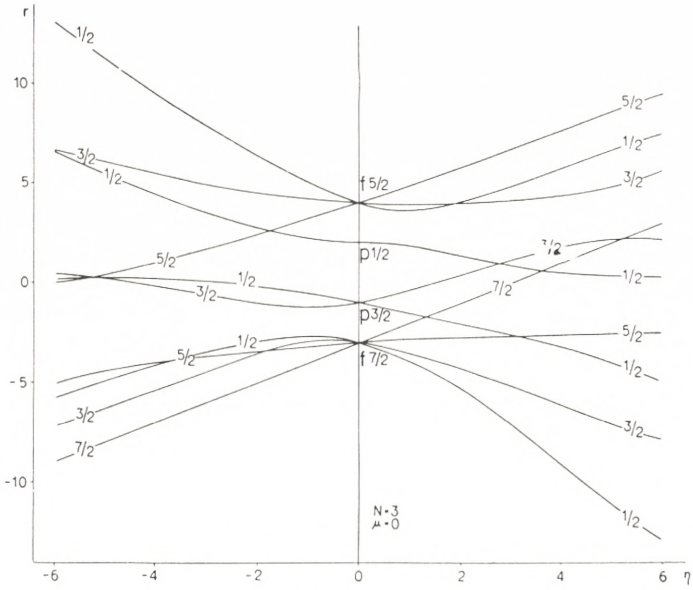


Fig. 3 a.

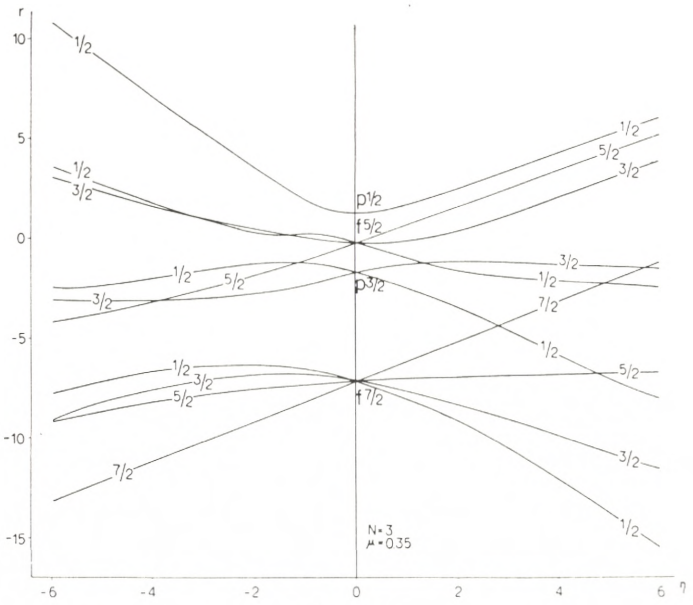


Fig. 3 b.

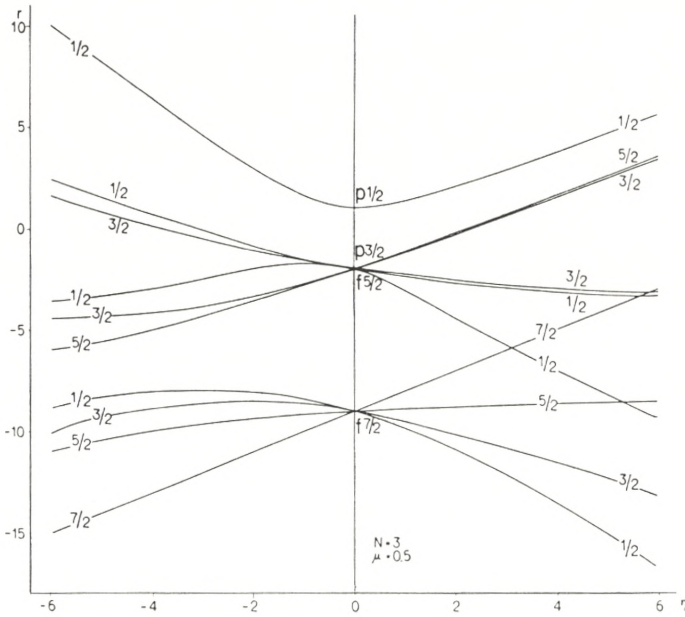


Fig. 3 c.

Fig. 3 a, b, c. The influence of the choice of \bar{l}^2 -admixture in the potential on the energy eigenvalues.

Eigenvalues $r(\eta)$ corresponding to $N = 3$ are depicted as functions of the deformation parameter η , with three different choices of μ , the parameter of \bar{l}^2 -admixture in the assumed potential. The connection between the eigenvalues $r(\eta)$ and the level energy E is given by (13). One may notice that for large η -values (large deformations) the level order within the $N = 3$ groups of levels is rather independent of μ .

Finally, as regards the choice of \varkappa , one sees from (13) that the level spread within each N -shell is directly proportional to \varkappa . As the N -shells overlap for a larger number of nucleons, \varkappa has to be chosen within certain limits to reproduce for $\delta = 0$ the level order of the shell model. The arbitrariness in the choice of \varkappa is important particularly for $N \leq 3$.

In the final plot (Fig. 5) the value of \varkappa is taken to be 0.05 for all levels. It is, however, easy to modify the plotting and use the result of the calculation for another \varkappa -value. This will mean two things: a) the same value of η now corresponds to another deformation δ according to (12c), b) the second term in (13) is changed.

A reasonable value for $\hat{\omega}_0$ may be obtained by taking

the mean value of r'^2 for all the nucleons to be equal to $\frac{3}{5} \cdot (1.2 \cdot 10^{-13} A^{\frac{1}{3}})^2 \text{ cm}^2$, which gives $\hbar \omega_0 \simeq 41 A^{-\frac{1}{3}} \text{ MeV}$.*

Thus for $A \simeq 100$ one has $\hbar \omega_0 \simeq 8.8 \text{ MeV}$. This choice of $\hbar \omega_0$ and the choice of κ made in the plot ($\kappa = 0,05$) give, e. g., a spin-orbit splitting between $g_{9/2}$ and $g_{7/2}$ of 4.0 MeV.

In the calculation, submatrices of R were diagonalized up to and including $N = 6$. The largest, which corresponds to $N = 6$, $\Omega = \frac{1}{2}$, is then a 7×7 matrix. The calculation is repeated for

six values of η ($\eta = -6, -4, -2, 2, 4, 6$). Matrices of order 3×3 and higher were treated with the help of the digital computing machine BESK in Stockholm. A method due to JACOBI was used in the machine calculations for matrix diagonalization.

Finally, the case $\delta = 0$ (or $\eta = 0$) corresponds to spherical symmetry and is already worked out. One obtains the behaviour of the levels in the vicinity of $\delta = 0$ by introducing an $|Nlj\Omega\rangle$ -representation. Here the Hamiltonian is diagonal except for H_δ , which can be treated as a perturbation for small δ .

d. Arrangements of tables and main diagram.

Table I gives the eigenvalues $r(\eta)$ and the corresponding eigenfunctions as a sequence of coefficients $A_{l\Omega-1/2}$ and $A_{l\Omega+1/2}$, defined by

$$|N\Omega\alpha\rangle = \sum_l \{A_{l\Omega-1/2} |Nl(\Omega-1/2)+\rangle + A_{l\Omega+1/2} |Nl(\Omega+1/2)-\rangle\}, \quad (14)$$

where the normalization of A_{lA} is discussed below. (If we write (14) with coefficients a_{lA} , we assume a normalization $\sum_{lA} a_{lA}^2 = 1$.)

The basic vectors $|Nl(\Omega-1/2)+\rangle$ and $|Nl(\Omega+1/2)-\rangle$ are given above each separate table.

Consider, as an example, $N = 5, \Omega = \frac{5}{2}$. Above the table are written the base vectors $|552+\rangle, |532+\rangle, |553-\rangle$, and

* An estimate for the harmonic oscillator potential in accordance with the Thomas-Fermi statistical model agrees with what one obtains by using the wave functions of the individual nucleons.

$|533-\rangle$. The eigenvalues r_1, r_2, \dots, r_4 are listed for each value of η . Below each of them there are four numbers, which are the coefficients A_{52}, A_{32}, \dots with a normalization such that the first listed coefficient equals 1. Take, e. g., $\eta = -4$. The largest eigenvalue is -2.676 . To this corresponds the eigenfunction $1.000 |552+\rangle + 1.355 |532+\rangle - 1.030 |553-\rangle - 1.074 |533-\rangle$.

The numbers to the left in Tables I are referring to the curves in Fig. 5. In some instances these numbers are missing. This means that the level in question lies outside the range of the energy scale used in the diagram. Curves coming into the drawing from above left are labelled by letters.

Fig. 5 shows the energy eigenvalues E_α given by (13) as functions of the deformation parameters η or δ , to which latter η is related by (12c). The scales for η and δ are shown at the bottom of the drawing. The calculated points corresponding to $\eta = -6, -4, -2, 0, 2, 4, 6$ are fitted by curves with the further requirement of a given slope at $\eta = 0$ (determined from perturbation calculations, cf. above). The curves are labelled by the Ω -number and the parity sign. The energy scale is $\hbar\omega_0(\delta)$; this δ -dependent unit is chosen rather than the constant unit $\hbar\omega_0^\circ$ to simplify the drawing. What is plotted is $\frac{E_\alpha}{\hbar\omega_0} = \left(N_\alpha + \frac{3}{2}\right) + \frac{\omega_0^\circ}{\omega_0(\delta)} \cdot r_\alpha$. Notice, further, that the true energy scale is different for nuclei with different A , as $\hbar\omega_0$ may be assumed to vary with A as $A^{-1/3}$ (cf. p. 18).

The bottom level, corresponding to $\Omega = \frac{1}{2}+$, which is a pure $|000+\rangle$ -state, is left out in Fig. 5 in order to save space.

Of the $N = 7$ states only the $\Omega = \frac{15}{2}$ state has been calculated, and thus one must expect additional levels in the diagram for energies above, say, $6.6 \hbar\omega_0$.

Added in proof: In the analysis of the empirical level spectra (B. MOTTELSON and S. G. NILSSON, Phys. Rev., in press) it has been found that an improved fit for the protons in the $N = 4$ shell is obtained by increasing slightly the value of μ . The calculations have therefore been performed also for $\mu = 0.55$. The results are given in Table 1b. (The eigenvectors are normalized

such that $\sum_{lA} a_{lA}^2 = 1$.) The corresponding energy level diagram is shown in the above reference. In this diagram z is chosen = 0.0613, compared to 0.05 in Fig. 5.

e. *Discussion of the main level diagram.*

Many of the features of the level diagram in Fig. 5 can be understood from simple considerations.

Thus, in the neighbourhood of spherical shape, the states can be labelled by the l and j quantum numbers. The degeneracies corresponding to $\delta = 0$ are removed by the surface coupling term in such a manner that for a positive δ the energies increase with increasing Ω . For negative δ the level order is the opposite.

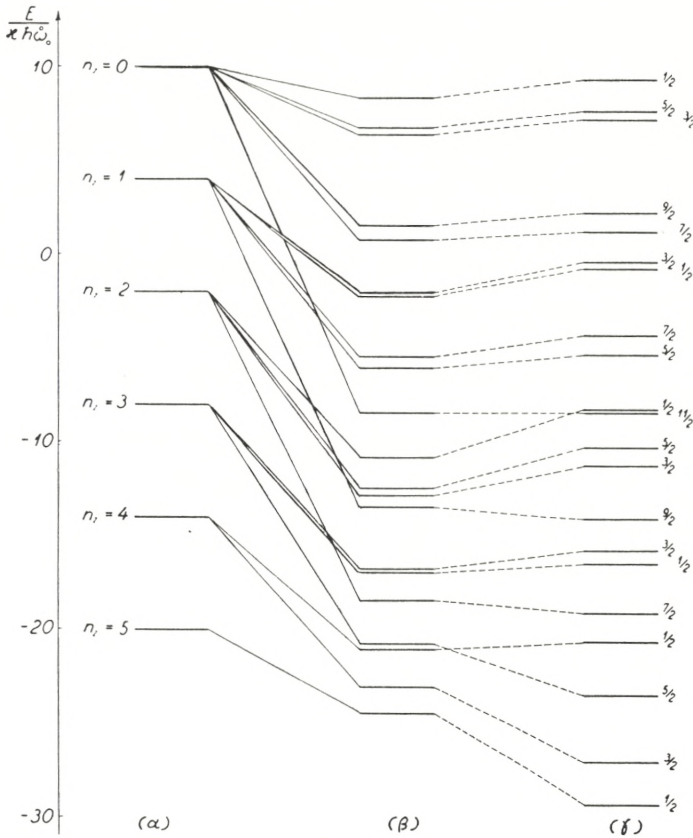
With increasing deformation, the states of different j and l (but the same Ω and parity) are coupled together, and for intermediate deformations the situation may be rather complex, as seen from the peculiar variations with δ of some of the energy levels.

For sufficiently large deformations, the situation again simplifies since for this case one may consider as a zeroth approximation the levels of a pure (anisotropic) harmonic oscillator potential and treat the $\bar{l}\cdot\bar{s}$ - and \bar{l}^2 -terms as a perturbation. In this limit the states may be labelled by the quantum numbers N , n_z (number of oscillator quanta along the z' -axis), A and Σ .

The quantum numbers appropriate at large deformations can easily be assigned to the energy levels in Fig. 5 by noting the following rules. For the levels in the shell N the lowest state of $\Omega = 1/2$, assuming positive deformation, has $n_z = N$, the next has $n_z = N - 1$ etc., so that the highest $\Omega = 1/2$ level has $n_z = 0$. Similarly for $\Omega = 3/2$ the lowest level has $n_z = N - 1$, the next $n_z = N - 2$ etc. After the n_z -values have been assigned, the A -values can be simply obtained by noting that A is even or odd according to whether $(N - n_z)$ is even or odd. Since Ω is known, this determines A and Σ uniquely.

As an example, it is in this way found that in the $N = 5$ shell the levels corresponding to $n_z = 0$ for large positive deformations are the ones labelled 28, 48, 40, 70, 61, and A. It is also seen that all these levels tend to become parallel and to increase steeply with the deformation, corresponding to the fact that for

these levels the oscillations are in the plane of the small nuclear axes. At the same time it is apparent that the $\bar{l} \cdot \bar{s}$ - and \bar{l}^2 -terms in the Hamiltonian, which are responsible for the spin-orbit



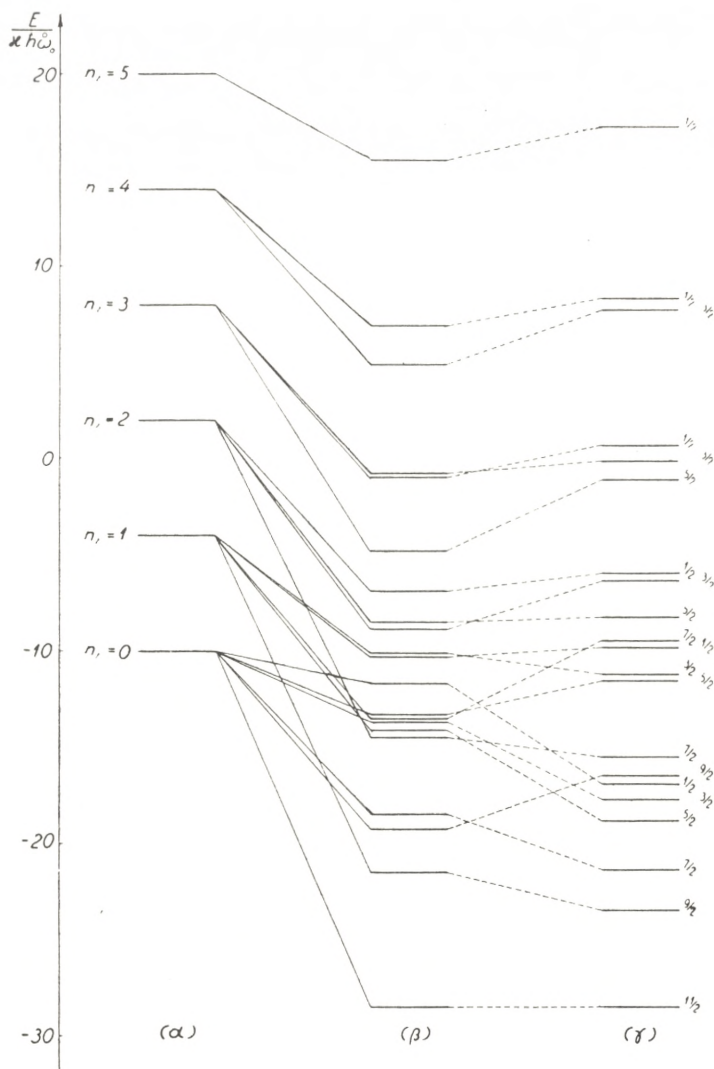


Fig. 4 b.

are the pure oscillator levels (α), while the levels (β) include the diagonal values of the $\bar{l} \cdot \bar{s}$ - and \bar{l}^2 -terms, which are calculated in Appendix B. The comparison with the numerically calculated levels (γ) shows that such a first order perturbation calculation, for the very large deformations in question, reproduces the main trends of the level order, even though there are still a number of significant differences between the level spectra (β) and (γ). This is especially the case for negative deformations (cf. Fig. 4b).

III. Examples of Applications of Tables and Diagrams.

We consider below a number of the nuclear properties which may be treated by means of the calculation given above. It should be remembered that the essential condition, underlying all of the work in the present paper, is that the nuclear deformation is essentially larger than the fluctuations. This condition is found to be satisfied only for configurations far removed from the closed shells.

a. Calculation of total energy and equilibrium deformation.

The total energy of the nucleus is not the sum of the energies for each individual particle because, in that case, two-particle interactions would be counted twice, three-particle interactions three times, etc.

The expression to be used thus depends on which kind of interaction is postulated. Assuming only two-body forces, the Hamiltonian for the i :th particle is

$$H_i = T_i + V_i = T_i + \sum_{j(j \neq i)} V_{ij}.$$

The Hamiltonian for the total nucleus, however, should be

$$\mathfrak{H} = \sum_i T_i + \frac{1}{2} \sum_{\substack{i,j \\ (i \neq j)}} V_{ij} = \frac{1}{2} \sum_i H_i + \frac{1}{2} \sum_i T_i. \quad (15)$$

The total wave function of all the nucleons, describing their motion relative to the deformed potential, is the product of the wave functions for each occupied particle state, appropriately antisymmetrized. To find the total energy $\mathfrak{E}(\delta)$ we then have to find the expectation value of \mathfrak{H} with respect to the calculated single-particle wave functions.

The equilibrium deformation δ_{eq} is now given by $\left(\frac{\partial \mathfrak{E}(\delta)}{\partial \delta} \right)_{\delta_{\text{eq}}} = 0$, which gives the minimum total energy $\mathfrak{E}_{\text{min}}$. The energy values are calculated with good accuracy for seven points on all the levels. As the levels cross, different combinations of levels will give the lowest total energy within different ranges of δ (or η).

For each single combination of levels the energy minimum is to be found, e. g., from an interpolation formula utilizing several or possibly all of the calculated points corresponding to this particular level combination. The lowest minimum gives the ground state. Other minima, corresponding to other level combinations, give particle levels of the excitation spectrum.

In this connection it should be emphasized that the total nuclear excitation spectrum will have three distinct modes. On each particle level, characterized by Ω , there will be superimposed a vibrational band, and furthermore on each level (including the vibrational levels) a rotational band. The level distance for heavy nuclei is for the particle spectrum of order 100 KeV (see Fig. 5), for the vibrational spectrum of the order of a few MeV. Finally, the rotational energies depend on the nuclear deformation, but for heavy nuclei and large deformations they are much smaller than the vibrational energies.

To calculate the equilibrium deformation in the prescribed way it turns out to be essential to take the couplings between different N -shells into account. This can be done, as pointed out on p. 13, by reinterpreting the machine calculations as performed in a slightly different representation, accompanied by a small change in the definition of the parameters (cf. Appendix A).

This coupling causes a slight repression of all the energy levels without affecting the level order. It thus amounts to a change in the whole energy scale (cf. (A4), (4), and (13)). Furthermore the scale factor is dependent on deformation.

The effect is important in decreasing the effective restoring force of the nucleus against deformation. The energy minimum is thus shifted towards larger deformations. An approximate expression for the total energy \mathcal{E} , taking these effects into account, is given in Appendix C.

It should be emphasized that the determination of δ_{eq} involves a number of simplifying approximations. Apart from the assumption regarding the shape of the nuclear potential and the two-body character of the interactions, we have neglected the effect of residual interactions between the nucleons not included in the average potential (as, e. g., the pairing energy terms).

However, in the application of the model an independent estimate of δ is obtained from the empirically determined

quadrupole moment. Assuming a charge distribution in accordance with the Thomas-Fermi statistical model applied to the oscillator potential, one obtains to second order in δ

$$Q_0 \simeq 0.8 \cdot Z \cdot R_Z^2 \cdot \delta \cdot \left(1 + \frac{2}{3} \delta\right), \quad (16)$$

where R_Z is to be taken equal to the radius of charge of the nucleus or $R_Z \simeq 1.2 \cdot 10^{-13} \cdot A^{1/3}$ cm. In obtaining this result the convention has been employed to put the mean value of r'^2 for all the protons (cf. p. 18) equal to $3/5 R_Z^2$.

The relation between the measured quadrupole moment, denoted by Q_s , and Q_0 is given by*

$$Q_s = \frac{3 K^2 - I(I+1)}{(I+1)(2I+3)} Q_0. \quad (17)$$

As regards the particle levels of the excitation spectrum, one cannot expect to obtain the exact level order and even less the correct energy differences between the levels. The diagram should tell, however, which level spins and parities are likely to appear in the lowest states of the spectrum.

b. Determination of ground state spin and decoupling factor.

The component of angular momentum along the axis of deformation Ω_p is a constant of the motion for each particle. Ω_p is given for each of the energy states drawn in Fig. 5. In the strong coupling limit the total Ω equals $\sum_p \Omega_p$. Each energy state is degenerate corresponding to $\pm \Omega$. If we have two groups a and b of equivalent particles — neutrons and protons — the particles of each group fill pairwise in the levels independently of the other group. If the number of particles in the group a is even, $\Omega_a = 0$, if odd, then Ω_a equals the Ω_p of the last unpaired particle.

If one of the groups is even, the case is simple enough for the ground state, Ω equals Ω_b , if b is the odd group. If both a and b are odd, the states with $\Omega = |\Omega_a \pm \Omega_b|$ are degenerate

* BM (V. 6).

in first order. The diagonal contribution of n - p -forces and the rotational energy decide which Ω corresponds to the ground state.

It turns out that always the ground state spin of the nucleus $I_0 = \Omega = K$, except when $\Omega = \frac{1}{2}$, in which case the ground state spin I_0 is given from Table III once the decoupling factor a is determined.* (See below.)

The decoupling factor a appears in the expression for the rotational energy for odd- A nuclei with $\Omega = \frac{1}{2}$ **

$$E_{\text{rot}} = \frac{\hbar^2}{2\mathfrak{I}} \left[I(I+1) + a (-)^{I+1/2} \left(I + \frac{1}{2} \right) \right] \quad (18)$$

and is thus experimentally measurable. In the j - Ω -representation, with quantum numbers l, s, j, Ω , where χ_Ω is written $\sum_j c_j \langle \bar{r} | Nlj\Omega \rangle$,

$$a = \sum_j (-)^{j-1/2} \left(j + \frac{1}{2} \right) |c_j|^2,$$

and it can be transformed to the l - A -representation with quantum numbers l, s, A, Σ , where $\chi_\Omega = \sum_{lA} a_{lA} \langle \bar{r} | Nl(s)A\Sigma \rangle$, by means of the relations

$$c_j = \sum_{A\Sigma} \langle l \frac{1}{2} A\Sigma | l \frac{1}{2} j \Omega \rangle a_{lA}.$$

In the l - A -representation then

$$a = (-)^l \sum_l (a_{l0}^2 + 2\sqrt{l(l+1)} a_{l0} a_{l1}), \quad (19)$$

where $(-)^l$ is the parity of the state in question, and where the coefficients a_{lA} are, as before, the representatives of the particle wave function χ_Ω in the $|NlA\Sigma\rangle$ -representation. The

* Cf. BM p. 30. Table III is based on BM (II.24). I_0 is determined as the half integer spin I which gives the minimum rotational energy W_{rot} .

** See A. BOHR and B. MOTTELSON "Collective Nuclear Motion and the Unified Model", Chapter 17 of "Beta and Gamma Ray Spectroscopy" edited by K. STEGBAHN, North Holland Publishing Co. (1954).

values of a_{lA} for the calculated eigenstates are the same as the coefficients listed in Tables I, apart from a different normalization (cf. p. 18).

c. Determination of magnetic moments.

We next consider the magnetic moment for an odd- A nucleus in which all the particles except the last one fill the different orbits in pairs. The generalization to configurations in which several particles move in unpaired orbits is straightforward.

By definition, the magnetic moment expressed in units of the nuclear magneton is

$$\mu = \frac{\langle \bar{\mu}^{\text{op}} \cdot \bar{I} \rangle}{I+1},$$

where

$$\bar{\mu}^{\text{op}} = g_s \bar{s} + g_l \bar{l} + g_R \bar{R},$$

and \bar{R} is the angular momentum of the surface.

Using $\bar{j} = \bar{l} + \bar{s}$ and $\bar{j} + \bar{R} = \bar{I}$ we can write μ as

$$\mu = \frac{1}{I+1} [(g_s - g_l) \langle \bar{s} \cdot \bar{I} \rangle + (g_l - g_R) \langle \bar{j} \cdot \bar{I} \rangle + g_R \langle \bar{I}^2 \rangle]. \quad (20)$$

Here $\langle \bar{j} \cdot \bar{I} \rangle$ is given in the j - Ω -representation of BM.* It can be written

$$\langle \bar{j} \cdot \bar{I} \rangle = \Omega K + \frac{1}{2} \left(I + \frac{1}{2} \right) a (-)^{I-1/2} \delta_{\Omega, 1/2} \delta_{K, 1/2}, \quad (21)$$

where the l - A -representation of a is given directly from (19).

For $\langle \bar{s} \cdot \bar{I} \rangle$ it is more convenient to use the l - A -representation from the beginning. The part of the wave function (1) which is written $(-)^{I-j} \chi_{-\Omega}$ has the meaning $\sum_j (-)^{I-j} c_j \chi_{-\Omega}^j$. In the l - A -representation then

$$\sum_j (-)^{I-j} c_j \chi_{-\Omega}^j = (-)^{I-1/2+l} \sum_{lA\Sigma} a_{lA} \langle \bar{r} | Nl - A - \Sigma \rangle. \quad (22)$$

One obtains

* BM II.18.

$$\langle \bar{s} \cdot \bar{I} \rangle = \frac{K}{2} \sum_l (a_{l+}^2 - a_{l-}^2) + \frac{1}{2} \left(I + \frac{1}{2} \right) (-)^{I+1/2+l} \sum_l a_{l_0}^2 \delta_{\Omega, 1/2} \delta_{K, 1/2}. \quad (23)$$

For the case $\Omega = K = I = \frac{1}{2}$, (23) simplifies to

$$\langle \bar{s} \cdot \bar{I} \rangle = \frac{1}{2} \sum_l a_{l_0}^2 [1 + (-)^l] - \frac{1}{4} \quad (23a)$$

(where we have utilized $\sum_l (a_{l_0}^2 + a_{l_1}^2) = 1$). Specializing further to a state of odd parity,

$$\langle \bar{s} \cdot \bar{I} \rangle = -\frac{1}{4}. \quad (23b)$$

Turning now to μ , we first consider the case $\Omega \neq \frac{1}{2}$. From (20), (21), and (23) one obtains

$$\mu = \frac{1}{I+1} \left\{ (g_s - g_l) \frac{1}{2} K \sum_l (a_{l_{\Omega-1/2}}^2 - a_{l_{\Omega+1/2}}^2) + (g_l - g_R) \Omega K + g_R I(I+1) \right\}, \quad (24)$$

which for $I = \Omega = K$ (still $\neq \frac{1}{2}$) simplifies to

$$\mu = \frac{I}{I+1} \left\{ (g_s - g_l) \frac{1}{2} \sum_l (a_{l_{\Omega-1/2}}^2 - a_{l_{\Omega+1/2}}^2) + g_l I + g_R \right\}. \quad (24a)$$

It may be pointed out that (24) can be rewritten in the formally simple form

$$\mu = \frac{\Omega K}{I+1} (g_\Omega - g_R) + g_R I, \quad (24b)$$

where

$$g_\Omega = \frac{1}{\Omega} \{ g_s \langle s_z \rangle + g_l \langle l_z \rangle \}. \quad (24c)$$

For the case $\Omega = K = \frac{1}{2}$ (when some extra terms enter due to the symmetrization of the wave function) equation (24) is somewhat modified

$$= \frac{1}{I+1} \left\{ (g_s - g_l) \left[\frac{1}{4} \sum_l (a_{l0}^2 - a_{l1}^2) + (-)^{I-1/2+l} \frac{1}{2} \left(I + \frac{1}{2} \right) \sum_l a_{l0}^2 \right] + (g_l - g_R) \left[\frac{1}{4} + (-)^{I-1/2} \frac{1}{2} \left(I + \frac{1}{2} \right) a \right] + g_R I (I + 1) \right\}, \quad (25)$$

where a is given by (19). For free nucleons one has $g_s = \begin{pmatrix} 5,585 \\ -3,826 \end{pmatrix}$ and $g_l = \begin{pmatrix} 1 \\ 0 \end{pmatrix}$ for protons and neutrons, respectively. Under the assumption that the rotational motion can be described in terms of an irrotational flow of uniformly charged nuclear matter, $g_R \simeq \frac{Z}{A}$.

For the case $I = \Omega = K = \frac{1}{2}$ and odd parity, when $\langle \bar{s} \cdot \bar{I} \rangle$ according to (23b) is independent of the internal wave function, (25) simplifies to

$$\mu = \frac{1}{3} \left\{ (g_l - g_R) a - \frac{1}{2} g_s + g_l + g_R \right\}, \quad (26)$$

which means that, for this particular case, there exists between the quantities a and μ a relation that involves only the gyro-magnetic ratios g_s , g_l , and g_R , but not the nucleonic wave functions.

c. Determination of electromagnetic transition probabilities.

The electric and magnetic multipole operators in the space fixed system (x'' , y'' , z'') are given by*

$$\mathfrak{M}_e''(\lambda, \mu) = \sum_p \left[e_p + (-)^{\lambda} \frac{Ze}{A^{\lambda}} \right] \cdot r_p^{\lambda} Y_{\lambda\mu}(\vartheta_p'', \varphi_p'') + \frac{3}{4\pi} ZeR_0^{\lambda} a_{\lambda\mu}^{\dagger} \quad (27a)$$

$$\left. \begin{aligned} \mathfrak{M}_m''(\lambda, \mu) &= \frac{e\hbar}{2Mc} \sum_p \left(g_s \bar{s} + \frac{2}{\lambda+1} g_l \bar{l} \right)_p \cdot \bar{\nabla}_p [r_p^{\lambda} Y_{\lambda\mu}(\vartheta_p'', \varphi_p'')] \\ &+ \frac{e\hbar}{Mc} \frac{1}{\lambda+1} g_R \int \bar{\mathfrak{R}}(\bar{r}) \cdot \bar{\nabla} [r^{\lambda} Y_{\lambda\mu}(\vartheta, \varphi)] d\tau. \end{aligned} \right\} \quad (27b)$$

The first terms in the expressions represent the transition moments of the most loosely bound particles which can be

* BM (VII. 5, 6).

individually excited (thus the sum over p is to be taken only over the transforming nucleons), while the last terms represent the multipole moments generated by the collective motion of the nucleus. The recoil effect of the nuclear core (important for dipole transitions) is included in the particle part of (27a).

The term $a_{\lambda\mu}^\dagger$ in (27a) is the Hermitian conjugate of the coordinate describing the deformation of the nuclear surface in the coordinate system fixed in space.* R_0 is the nuclear radius. As regards the collective part of the magnetic multipole operator, $\mathfrak{M}(\vec{r})$ is the collective angular momentum density, and one has $\int \mathfrak{M}(\vec{r}) d\tau = \vec{R}$. This part is in general difficult to handle, except in the case $\lambda = 1$. In that case, it can be incorporated into the first term simply by changing g_s to $g_s - g_R$ and g_l to $g_l - g_R$.

For the strongly deformed nuclei one can distinguish between particle transitions which are associated with a change in the intrinsic wave function χ_Ω , and collective transitions which leave the internal particle structure unaffected. Of the collective transitions those that have been most studied are the rotational ones which leave φ_{vib} unaffected and only change the rotational state \mathfrak{D} of the system.

The intrinsic structure χ_Ω affects the transition probabilities for particle transitions and for rotational transitions of M1 type. We shall in the following limit ourselves to those cases. We can then simply leave the last term of (27a) out of consideration since it is effective only in collective transitions (and we shall not consider rotational E2 transitions)**.

It is useful to introduce the reduced transition probability

$$B(\lambda, I \rightarrow I') = \sum_{\mu M'} \left| \langle \Omega', I' K' M' | \mathfrak{M}'(\lambda, \mu) | \Omega, I K M \rangle \right|^2. \quad (28)$$

The probability for a γ -transition with a frequency ω , where $\hbar\omega$ is the energy difference between the initial and final state, is then***

* AB (1).

** Cf., however, G. ALAGA, K. ALDER, A. BOHR, and B. MOTTELSON (Dan. Mat. Fys. Medd. **29**, no. 9, 1955). In this paper, the authors take into account a small decoupling of the rotational from the intrinsic motion, leaving Ω only approximately a constant of the motion. This effect may render the collective term of (27a) important for certain particle transitions, particularly of E2 type.

*** BM (VII.1), cf. also J. M. BLATT and V. F. WEISSKOPF, Theoretical Nuclear Physics, J. Wiley and Sons, New York (1952), chapter XII.

$$T(\lambda) = \frac{8\pi(\lambda+1)}{\lambda[(2\lambda+1)!!]^2} \frac{1}{\hbar} \left(\frac{\omega}{c}\right)^{2\lambda+1} B(\lambda). \tag{29}$$

$B(E\lambda)$ also enters the expression for the $E\lambda$ Coulomb excitation cross sections*.

As pointed out, the coordinates x'' etc. in (27 a, b) refer to a coordinate system fixed in space. It is convenient to transform the multipole operators to the coordinate system fixed in the nucleus

$$\mathfrak{M}''(\lambda, \mu) = \sum_{\nu} \mathfrak{D}_{\mu\nu}^{\lambda}(\theta_i) \mathfrak{M}'(\lambda, \nu), \tag{30}$$

where \mathfrak{M}' is of the same functional form as \mathfrak{M}'' but depends on the new coordinates x' . The functions \mathfrak{D} , depending on the Eulerian angles θ_i , are the same as those used in (1).

In the matrix elements in (28) the integration over the Eulerian angles can now be performed and the summation over μ and M' can be carried out.** One then obtains

$$B(\lambda, I \rightarrow I') = \left| \langle I\lambda K K' - K | I\lambda I' K' \rangle \int \chi_{\Omega}^{\dagger} \mathfrak{M}(\lambda, K' - K) \chi_{\Omega} d\tau \right. \\ \left. - \langle I\lambda K -K' -K | I\lambda I' -K' \rangle \int [(-)^{I-I'} \chi'_{-\Omega}]^{\dagger} \mathfrak{M}(\lambda, -K' -K) \chi_{\Omega} d\tau \right|^2. \tag{31}$$

The second term contributes only for the empirically rather unusual case $\lambda \geq K + K'$. In evaluating $B(\lambda)$, we have used

$$\int \mathfrak{D}_{M'K'}^{I'\dagger} \mathfrak{D}_{\mu\nu}^{\lambda} \mathfrak{D}_{MK}^I d\Omega^3 = \frac{8\pi^2}{2I'+1} \langle I\lambda M \mu | I\lambda I' M' \rangle \langle I\lambda K \nu | I\lambda I' K' \rangle, \tag{32}$$

where $d\Omega^3$ signifies integration over all three Eulerian angles. We shall later need the closely related formula

$$Y_{I'A'}^{\dagger} Y_{\lambda\nu} Y_{IA} d\Omega^2 = \sqrt{\frac{(2I+1)(2\lambda+1)}{4\pi(2I'+1)}} \langle I\lambda A \nu | I\lambda I' A' \rangle \langle I\lambda 0 0 | I\lambda I' 0 \rangle \tag{33}$$

Equation (10) is a special case of (33).

It is of advantage to make the transformation to dimensionless

* BM (Ap VI.17, 18).

** Cf. G. ALAGA et al., loc. cit.

variables (6). This gives a factor $\left(\frac{\hbar}{M\omega_0}\right)^{\lambda/2}$ for the electric multipole operator and a factor $\left(\frac{\hbar}{M\omega_0}\right)^{\lambda-1}$ for the magnetic multipole operator when r' is replaced by r .

The operator $\vec{l} \cdot (\vec{\nabla} r^\lambda Y_{\lambda\nu})$ can be rewritten*

$$\vec{l} \cdot (\vec{\nabla} r^\lambda Y_{\lambda\nu}) = \left. \begin{aligned} & \sqrt{\frac{2\lambda+1}{2\lambda-1}} \left[\sqrt{\lambda^2 - \nu^2} \cdot l_z r^{\lambda-1} Y_{\lambda-1\nu} + \frac{1}{2} \sqrt{(\lambda-\nu)(\lambda-\nu-1)} \right. \\ & \cdot L_- r^{\lambda-1} Y_{\lambda-1\nu+1} - \frac{1}{2} \sqrt{(\lambda+\nu)(\lambda+\nu-1)} L_+ r^{\lambda-1} Y_{\lambda-1\nu-1} \left. \right] \end{aligned} \right\} \quad (34)$$

where

$$l_+ = l_x + il_y, \quad l_- = l_x - il_y. \quad (34a)$$

The same formula holds for $\vec{s} \cdot (\vec{\nabla} r^\lambda Y_{\lambda\nu})$ with s_- exchanged for l_- etc.

For particle transitions due to electric multipoles, we can write

$$\left. \begin{aligned} B(E\lambda, I \rightarrow I') &= e^2 \left(1 + (-)^{\lambda} \frac{Z}{A^\lambda} \right)^2 \left(\frac{\hbar}{M\omega_0} \right)^{\lambda} \frac{2\lambda+1}{4\pi} \\ & \cdot \left| \langle I\lambda K K' - K | I\lambda I' K' \rangle + b_{E\lambda} (-)^{I+K'} \langle I\lambda K - K' - K | I\lambda I' - K' \rangle \right|^2 \cdot G_{E\lambda}^2 \end{aligned} \right\} \quad (35)$$

where

$$\left. \begin{aligned} b_{E\lambda} &= \frac{(-)^{K'+1/2+\nu}}{G_{E\lambda}} \left\{ \sum_{I'} \langle N'I' | r^\lambda | NI \rangle \sqrt{\frac{2I+1}{2I'+1}} \langle I\lambda 0 0 | I\lambda I' 0 \rangle \right. \\ & \cdot \left. \sum_{A'\Lambda\Sigma'\Sigma} \delta_{\Sigma'\Sigma} a'_{I'A'} a_{IA} \langle I\lambda A - K' - K | I\lambda I' - A' \rangle \right\} \end{aligned} \right\} \quad (35a)$$

$$\left. \begin{aligned} G_{E\lambda} &= \sum_{I'} \langle N'I' | r^\lambda | NI \rangle \sqrt{\frac{2I+1}{2I'+1}} \langle I\lambda 0 0 | I\lambda I' 0 \rangle \\ & \cdot \sum_{A'\Lambda\Sigma'\Sigma} \delta_{\Sigma'\Sigma} a'_{I'A'} a_{IA} \langle I\lambda A K' - K | I\lambda I' A' \rangle \end{aligned} \right\} \quad (35b)$$

* Cf. H. BETHE, Quantenmechanik der Ein- und Zwei-Elektronenprobleme, p. 559, Handbuch der Physik, XXIV/1, Berlin (1933). Note, however, our different choice of phases which agrees with that of E. U. CONDON and G. H. SHORTLEY, The Theory of Atomic Spectra. Cf. also M. E. ROSE and R. K. OSBORN, Phys. Rev., **93**, 1322 (1954).

For transitions due to magnetic multipoles we shall for $\lambda > 1$ omit the last term in (27b), which is expected to have a relatively minor influence. One then obtains

$$(M\lambda, I \rightarrow I') = \left(\frac{e\hbar}{2Mc} \right)^2 \left(\frac{\hbar}{M\omega_0} \right)^{\lambda-1} \cdot \frac{1}{4} \cdot \frac{2\lambda+1}{4\pi} |\langle I\lambda K K'-K | I\lambda I'K' \rangle + b_{M\lambda} (-)^{I+K'} \langle I\lambda K -K'-K | I\lambda I' -K' \rangle|^2 G_{M\lambda}^2, \quad (36)$$

where

$$G_{M\lambda} = \frac{(-)^{K'+1/2+I'}}{G_{M\lambda}} \sum_{I''} \langle N'I'' | r^{\lambda-1} | NI \rangle \langle I\lambda -100 | I\lambda -1 I' 0 \rangle \sqrt{\frac{2I+1}{2I'+1}} \left\{ \sum_{A'\Sigma'} a'_{I'A'} a_{IA} \cdot \left[g_s \left[A(q) \delta_{-\Sigma', \Sigma} (-)^{\Sigma-\frac{1}{2}} \langle I\lambda -1 Aq | I\lambda -1 I' -A' \rangle + B(q) \delta_{\Sigma', \frac{1}{2}} \delta_{\Sigma, \frac{1}{2}} \langle I\lambda -1 Aq+1 | I\lambda -1 I' -A' \rangle - C(q) \delta_{\Sigma', -\frac{1}{2}} \delta_{\Sigma, -\frac{1}{2}} \langle I\lambda -1 Aq-1 | I\lambda -1 I' -A' \rangle \right] + \frac{2}{\lambda+1} g_l \delta_{-\Sigma', \Sigma} \left[A(q) \cdot (-2A') \langle I\lambda -1 Aq | I\lambda -1 I' -A' \rangle + B(q) \sqrt{(I'+A')(I'-A'+1)} \langle I\lambda -1 Aq+1 | I\lambda -1 I' -A'+1 \rangle - C(q) \sqrt{(I'-A')(I'+A'+1)} \langle I\lambda -1 Aq-1 | I\lambda -1 I' -A'-1 \rangle \right] \right\} \quad (36a)$$

$$G_{M\lambda} = \sum_{I''} \langle N'I'' | r^{\lambda-1} | NI \rangle \langle I\lambda -100 | I\lambda -1 I' 0 \rangle \sqrt{\frac{2I+1}{2I'+1}} \sum_{A'\Sigma'} a'_{I'A'} a_{IA} \cdot \left\{ g_s \left[A(k) \delta_{\Sigma', \Sigma} (-)^{\Sigma-\frac{1}{2}} \langle I\lambda -1 Ak | I\lambda -1 I' A' \rangle + B(k) \delta_{\Sigma', -\frac{1}{2}} \delta_{\Sigma, \frac{1}{2}} \langle I\lambda -1 Ak+1 | I\lambda -1 I' A' \rangle - C(k) \delta_{\Sigma', \frac{1}{2}} \delta_{\Sigma, -\frac{1}{2}} \langle I\lambda -1 Ak-1 | I\lambda -1 I' A' \rangle \right] + \frac{2}{\lambda+1} g_l \delta_{\Sigma', \Sigma} \left[A(k) \cdot 2A' \langle I\lambda -1 Ak | I\lambda -1 I' A' \rangle + B(k) \sqrt{(I'-A')(I'+A'+1)} \langle I\lambda -1 Ak+1 | I\lambda -1 I' A'+1 \rangle - C(k) \sqrt{(I'+A')(I'-A'+1)} \langle I\lambda -1 Ak-1 | I\lambda -1 I' A'-1 \rangle \right] \right\} \quad (36b)$$

and where in turn

$$A(v) = \sqrt{\lambda^2 - v^2} \quad (36c)$$

$$B(v) = \sqrt{(\lambda - v)(\lambda - v - 1)} \quad (36d)$$

$$C(v) = \sqrt{(\lambda + v)(\lambda + v - 1)} \quad (36e)$$

$$k = K' - K \quad (36f)$$

$$q = -K' - K. \quad (36g)$$

For $\lambda = 1$, as pointed out above, we can easily handle the last term of (27b) and incorporate it in the first term. All the expressions derived for $\lambda > 1$ are then valid if g_s is replaced by $(g_s - g_R)$ and g_l by $(g_l - g_R)$ everywhere.

For M1 transitions within one rotational band, equations (36) simplify greatly, and one obtains

$$G_{M1} = (g_\Omega - g_R) \cdot 2\Omega. \quad (37a)$$

Further, b_{M1} is different from zero only if $\Omega = K = \frac{1}{2}$. (For this latter case we denote b_{M1} by $b_0\sqrt{2}$ and G_{M1} by G_0 .) One has

$$b_0 = -\frac{(-)^l}{g_\Omega - g_R} \left\{ (g_s - g_R) \sum_l a_{l0}^2 + 2(g_l - g_R) \sum_l \sqrt{l(l+1)} a_{l0} a_{l1} \right\}. \quad (37b)$$

The reduced transition probability for a transition of this kind from a level $I' + 1$ to a level I' (both belonging to the same rotational band) has then the simple form

$$B_0(M1) = \frac{3}{64\pi} \left(\frac{e\hbar}{2Mc} \right)^2 \frac{2I' + 1}{I' + 1} G_0^2 \cdot |1 + b_0 (-)^{I'-1/2}|^2. \quad (37c)$$

For a rotational band with $\Omega = \frac{1}{2}$, we have given expressions for the four measurable quantities a , μ , G_0 , and b_0 in (19), (25), (37a), and (37b), respectively. As the dependence of the internal wave function on all these quantities is contained in the expressions $\sum_l a_{l0}^2$ and $\sum_l \sqrt{l(l+1)} a_{l0} a_{l1}$, it is apparent that between a , μ , G_0 , and b_0 there must exist relations that are independent of the nucleonic structure.

We have already found such a relation between a and μ for $I = \Omega = K = \frac{1}{2}$ and odd parity, in which case formula (26) holds.

One can further for this case derive the second relation

$$2 b_0 G_0 = G_0 - 2 (g_l - g_R) a + g_s - 2 g_l + g_R. \quad (38)$$

For the case $I = \Omega = K = \frac{1}{2}$ and even parity the two corresponding relations are

$$G_0 = 3 \mu - a (g_l - g_R) - \frac{1}{2} g_s + g_l - 2 g_R \quad (39)$$

and

$$b_0 = -\frac{1}{2 G_0} \left[3 \mu + a (g_l - g_R) + \frac{1}{2} g_s - g_l - g_R \right]. \quad (40)$$

For the case $I \neq \Omega = K = \frac{1}{2}$, one can also establish relations of the same kind as (39) and (40).

The radial matrix element $\langle N'l' | r^\lambda | Nl \rangle$ is given by the formula*

$$\left. \begin{aligned} \langle N'l' | r^\lambda | Nl \rangle &= \left[\frac{\Gamma(n+1) \Gamma(n'+1)}{\Gamma(n+t-v+1) \cdot \Gamma(n'+t-v'+1)} \right]^{1/2} v'! v! \\ &\sum_{\sigma} \frac{\Gamma(t+\sigma+1)}{\sigma!(n-\sigma)!(n'-\sigma)!(\sigma+v-n)!(\sigma+v'-n)!} \end{aligned} \right\} \quad (41)$$

where

$$n = \frac{1}{2}(N-l) \quad (41 a)$$

$$n' = \frac{1}{2}(N'-l') \quad (41 b)$$

$$v = \frac{1}{2}(l' - l + \lambda) \quad (41 c)$$

$$v' = \frac{1}{2}(l - l' + \lambda) \quad (41 d)$$

* See, e. g., P. MORSE and H. FESHBACH, *Methods of Theoretical Physics*, McGraw-Hill (1953), p. 785. The extra phase factor appearing in this reference is due to the fact that $|Nl\rangle_{MF} \sim (-)^n |Nl\rangle_{\text{here}}$. Formulae (11 a-e) are given from (41) for $\lambda = 2$.

$$t = \frac{1}{2}(l + l' + \lambda + 1), \quad (41 e)$$

and where the condition on the summation variable σ is

$$\begin{array}{ccc} n & & n - \nu \\ & \geq \sigma \geq & \\ n' & & n' - \nu'. \end{array} \quad (42)$$

This means that σ has to be smaller than or equal to the smallest of n and n' etc. If this condition cannot be fulfilled by any σ , the integral vanishes. An equivalent necessary condition (expressed in N, l , and λ) for the matrix element of r^λ to be different from zero can be formulated as

$$l + \lambda \geq l' \geq l - \lambda \quad (42 a)$$

$$N + \lambda \geq N' \geq N - \lambda. \quad (42 b)$$

e. Determination of ft-values for beta transitions.

As it is the purpose of this paragraph merely to illustrate the application of the strong coupling wave functions in the field of beta transitions, we limit ourselves to considering only allowed transitions and a select group of forbidden transitions, namely those which imply a parity change of $(-)^{\Delta I + 1}$ (with $I \neq 0$). This latter group is of a pure Gamow-Teller type.

The treatment of β -transitions is similar to that of γ -transitions and it is useful to introduce the concept of reduced transition probability* defined in analogy to (28)

$$D_{GT}^F(n) = \sum_{\mu M'} \left| \langle \Omega', I'M'K' | \mathfrak{D}_{GT}^F(n, \mu) | \Omega, IMK \rangle \right|^2. \quad (43)$$

Here $\mathfrak{D}_{GT}^F(n, \mu)$ is the Fermi respectively the Gamow-Teller transition operator, and n is the degree of forbiddenness, $n = \Delta I - 1$.

The comparative half lives or the ft-values can now be defined in terms of these reduced transition probabilities.

* See BM, chapter VIII.

For allowed transitions we can write

$$f_0 t = B_g [(1-x) D_F(0) + x D_{GT}(0)]^{-1}, \quad (44)$$

where t is the half life, f_0 the integrated Fermi function for allowed transitions, $g(1-x)^{1/2}$ and $gx^{1/2}$ are the Fermi and Gamow-Teller coupling constants, and the constant B_g is given as

$$B_g = \frac{2 \pi^3 \hbar^7 \ln 2}{g^2 m_e^5 e^4}. \quad (45)$$

For forbidden transitions of the particular type considered here (parity change = $(-)^{\Delta I + 1}$ etc.) one has

$$f_n t = B_g [x D_{GT}(n)]^{-1}, \quad (46)$$

where f_n is the integrated Fermi function corresponding to the order of forbiddenness n [for definition and normalization see BM (VIII.6)].

It turns out that $D_{GT}(n)$ has a structure very similar to the reduced transition probability for a γ -transition of the magnetic multipole type with $\lambda = n + 1$. The corresponding operator is defined as

$$\mathfrak{D}_{GT}(n, \mu) = S(n) \sum_p \bar{s}_p \cdot \bar{\nabla}_p [r_p^{n+1} Y_{n+1\mu}(\vartheta_p, \varphi_p)] \tau_{\pm}^{\nu}, \quad (47)$$

where

$$S(n) = \left[\frac{4 \pi 2^{n+3}}{(2n+3)!} \right]^{1/2} \frac{[(n+1)!]^2}{n+1} \left(\frac{mc}{\hbar} \right)^n. \quad (47a)$$

In general the sum over p is to be taken over all particles involved in the transition. We restrict ourselves, however, to transitions between odd- A nuclei with only one unpaired particle which then undergoes the β -transition. τ_+ and τ_- are the isotopic spin creation and annihilation operators, transforming a proton into a neutron, and vice versa.

By formally putting $g_s = 1$ and $g_l = g_R = 0$ in (27b) we obtain exactly the above expression apart from a multiplicative numerical factor and the isotopic spin operator. Making this formal change we can then use formula (36) of the preceding paragraph for calculating $D_{GT}(n)$. Thus,

$$\begin{aligned}
 D_{GT}(n) &= S(n)^2 \left(\frac{\hbar}{M\omega_0} \right)^n \frac{1}{4} \frac{2n+3}{4\pi} \\
 &\cdot \left| \langle I n + 1 K K' - K \mid I n + 1 I' K' \rangle \right. \\
 &+ \beta_{n+1} (-)^{I+K'} \left. \langle I n + 1 K - K' - K \mid I n + 1 I' - K' \rangle \right|^2 \gamma_{n+1}^2
 \end{aligned} \quad (48a)$$

where

$$\gamma_{n+1} = G_{Mn+1}(g_s = 1, g_l = g_R = 0) \quad (48b)$$

$$\beta_{n+1} = b_{Mn+1}(g_s = 1, g_l = g_R = 0). \quad (48c)$$

For the case of mirror transitions, this simplifies to

$$D_{GT}(0) = \left| \langle I 1 K 0 \mid I 1 I K \rangle + \beta_1 (-)^{I+K} \langle I 1 K - 1 \mid I 1 I - K \rangle \right|^2 \gamma_1^2, \quad (48d)$$

where

$$\gamma_1 = \sum_l (a_{l\Omega-1/2}^2 - a_{l\Omega+1/2}^2) = 2 \langle s_z \rangle \quad (48e)$$

$$\beta_1 = \frac{(-)^{I+1}}{\gamma_1} \sqrt{2} \sum_l a_{l0}^2 \delta_{\Omega, 1/2} \delta_{K, 1/2}. \quad (48f)$$

Finally, in this same case, the Fermi part $D_F(0)$ is simply

$$D_F(0) = \sum_{M'} \left| \langle \Omega, IM'K \mid \tau_{\pm}^I \mid \Omega, IMK \rangle \right|^2 = 1. \quad (49)$$

Collecting the terms, we can write for mirror transitions in odd- A nuclei

$$f_0 t = B_g \left\{ (1-x) \cdot 1 + x \frac{K^2}{I(I+1)} \left[1 + \beta_1 (-)^{I+1/2} \sqrt{2} \left(I + \frac{1}{2} \right) \right]^2 \gamma_1^2 \right\}^{-1}, \quad (50)$$

where B_g is given by (45).

IV. Acknowledgements.

This problem was suggested by Drs. A. BOHR and B. MOTTELSON. I want to thank them cordially for all help and suggestions they have generously given me during the course of the work, and the time they have set apart for discussions. This work was done partly in Copenhagen and partly in Lund, and I wish to

thank, in Copenhagen Professors N. BOHR and C. MØLLER for their kind hospitality, in Lund particularly Professor T. GUSTAFSON and Dr. G. KÄLLÉN for their help and interest. In addition, thanks are due fil. lic. G. EHRLING and civ.ing. O. CARLQVIST, members of the mathematical staff at the Electronic Computer BESK in Stockholm. The financial support of the Swedish Atomic Energy Commission is gratefully acknowledged.

*CERN (European Organization for Nuclear Research)
Theoretical Study Division at the Institute for
Theoretical Physics, University of Copenhagen,
and
The Institute of Theoretical Physics,
University of Lund.*

V. Appendix A.

Use of an Alternative Representation.

In the diagonalization of the Hamiltonian (2), cross terms with different total quantum number N have been neglected. It is possible, however, to obtain an improved solution by making a small change of representation and in this manner to exhibit in a simple way the effect of the neglected non-diagonal terms in N .

Starting from (2) and (2 a)

$$H = H_0 + C\vec{l} \cdot \vec{s} + D\vec{l}^2 \quad (\text{A } 1)$$

$$H_0 = -\frac{\hbar^2}{2M} \Delta' + \frac{M}{2} (\omega_x^2 x'^2 + \omega_y^2 y'^2 + \omega_z^2 z'^2), \quad (\text{A } 1 \text{ a})$$

we make a slight parameter change and define ε and $\omega_0(\varepsilon)$, differently from δ and $\omega_0(\delta)$, as

$$\omega_x = \omega_y = \omega_0(\varepsilon) \left(1 + \frac{1}{3} \varepsilon \right) \quad (\text{A } 2 \text{ a})$$

$$\omega_z = \omega_0(\varepsilon) \left(1 - \frac{2}{3} \varepsilon \right). \quad (\text{A } 2 \text{ b})$$

The following relations hold between the old and the new parameters

$$\varepsilon = \delta + \frac{1}{6} \delta^2 + O(\delta^3) \quad (\text{A } 3)$$

$$\omega_0(\varepsilon) = \omega_0(\delta(\varepsilon)) \left[1 - \frac{1}{9} \varepsilon^2 + O(\varepsilon^3) \right] = \overset{\circ}{\omega}_0 \left[1 + \frac{1}{9} \varepsilon^2 + O(\varepsilon^3) \right]. \quad (\text{A } 4)$$

We further perform a coordinate transformation

$$\xi = x' \sqrt{\frac{M \omega_x}{\hbar}} \quad (\text{A } 5 \text{ a})$$

$$\eta = y' \sqrt{\frac{M \omega_y}{\hbar}} \quad (\text{A } 5 \text{ b})$$

$$\zeta = z' \sqrt{\frac{M \omega_z}{\hbar}} \quad (\text{A } 5 \text{ c})$$

H_0 is then separable in ξ , η , ζ

$$H_0 = H_\xi + H_\eta + H_\zeta, \quad (\text{A } 6)$$

where

$$H_\xi = \frac{1}{2} \hbar \omega_x \left(-\frac{\partial^2}{\partial \xi^2} + \xi^2 \right) \text{ etc.} \quad (\text{A } 6 \text{ a})$$

For later use a note should be made at this point that a representation that obviously makes H_0 diagonal is $|n_\xi\rangle |n_\eta\rangle |n_\zeta\rangle$, where $|n_\xi\rangle$ is defined by

$$H_\xi |n_\xi\rangle = \left(n_\xi + \frac{1}{2} \right) \hbar \omega_x |n_\xi\rangle. \quad (\text{A } 7)$$

We proceed, however, to split H_0 in a manner analogous to (7)

$$H_0 = \overset{\circ}{H}_0 + H_\varepsilon, \quad (\text{A } 8)$$

where

$$\overset{\circ}{H}_0 = \hbar \omega_0(\varepsilon) \frac{1}{2} [-\Delta_\xi + \varrho^2] \quad (\text{A } 8 \text{ a})$$

$$H_\varepsilon = \frac{1}{6} \varepsilon \hbar \omega_0(\varepsilon) \left[\left(-\frac{\partial^2}{\partial \xi^2} + \xi^2 \right) + \left(-\frac{\partial^2}{\partial \eta^2} + \eta^2 \right) - 2 \left(-\frac{\partial^2}{\partial \zeta^2} + \zeta^2 \right) \right], \quad (\text{A } 8 \text{ b})$$

and

$$\varrho^2 = \xi^2 + \eta^2 + \zeta^2.$$

In conformity with the new coordinates ξ, η, ζ introduced it is useful also to introduce an operator \bar{l}_l defined analogously to \bar{l} as

$$(l_l)_z = -i \left(\eta \frac{\partial}{\partial \zeta} - \zeta \frac{\partial}{\partial \eta} \right) \text{ etc.} \quad (\text{A } 9)$$

(We denote the component by $(l_l)_x$ instead of $(l_l)_\xi$ to emphasize that the directions of the new coordinates coincide with the old ones.)

We now introduce a representation which makes \hat{H}_0 diagonal together with $(l_l)_z$ and \bar{l}_l^2, s_z and \bar{s}^2 . The eigenvalues of $(l_l)_z$ and \bar{l}_l^2 are denoted as A_l and $l_l(l_l + 1)$.

Thus,

$$\begin{aligned} \hat{H}_0 |N_l l_l A_l \Sigma\rangle &= \hbar \omega_0 \frac{1}{2} (-\Delta_\xi + \varrho^2) |N_l l_l A_l \Sigma\rangle \\ &= \left(N_l + \frac{3}{2} \right) \hbar \omega_0 |N_l l_l A_l \Sigma\rangle. \end{aligned} \quad \left. \vphantom{\hat{H}_0} \right\} (\text{A } 10)$$

We rewrite (A 1) in the form

$$H = H_l + H_{\text{pert}}, \quad (\text{A } 11)$$

where

$$H_l = \hat{H}_0 + H_\varepsilon + C \bar{l}_l \cdot \bar{s} + D \bar{l}_l^2 \quad (\text{A } 11 \text{ a})$$

and

$$H_{\text{pert}} = C (\bar{l} - \bar{l}_l) \cdot \bar{s} + D (\bar{l}^2 - \bar{l}_l^2). \quad (\text{A } 11 \text{ b})$$

By using the identity

$$\frac{\partial^2}{\partial \xi^2} + \frac{\partial^2}{\partial \eta^2} - 2 \frac{\partial^2}{\partial \zeta^2} = \frac{1}{8} [A, [A, \xi^2 + \eta^2 - 2 \zeta^2]]$$

and exploiting (A 10), one can show that

$$\begin{aligned} &\langle N'_l l'_l A'_l \Sigma' | H_\varepsilon | N_l l_l A_l \Sigma \rangle \\ &= \delta_{N'_l N_l} \langle N'_l l'_l A'_l \Sigma' | \frac{1}{3} \varepsilon \hbar \omega_0 (\xi^2 + \eta^2 - 2 \zeta^2) | N_l l_l A_l \Sigma \rangle. \end{aligned} \quad \left. \vphantom{\langle N'_l l'_l A'_l \Sigma' | H_\varepsilon | N_l l_l A_l \Sigma \rangle} \right\} (\text{A } 12)$$

The fact that H_ε has vanishing matrix elements between states of different N_l can also be seen from (A 8b), (A 6a), and (A 7), remembering that the $|N_l l_t A_t\rangle$ -vector is a particular sum of $|n_\xi\rangle |n_\eta\rangle |n_\zeta\rangle$ product vectors with $n_\xi + n_\eta + n_\zeta = N_l$.

It follows now that H_l has the same matrix elements in the $|N_l l_t A_t \Sigma\rangle$ -representation as H has in the $|N l A \Sigma\rangle$ -representation apart from, first, the change of parameters (ε and $\omega_0(\varepsilon)$ in the former representation and δ and $\omega_0(\delta)$ in the latter one) and, secondly, the fact that the matrix elements of H_l between states with N_l differing by two vanish identically in the $|N_l l_t A_t \Sigma\rangle$ -representation.

The next step is to investigate the effect of the H_{pert} -term. The three \bar{l} -components l_+ ($= l_x + i l_y$), l_- ($= l_x - i l_y$), and l_z may be transformed as follows

$$l_+ = a (l_t)_+ - b f_+ \quad (\text{A 13a})$$

$$l_- = a (l_t)_- - b f_- \quad (\text{A 13b})$$

$$l_z = (l_t)_z, \quad (\text{A 13c})$$

where

$$a = \frac{1}{2} \left[\sqrt{\frac{1 + \frac{1}{3}\varepsilon}{1 - \frac{2}{3}\varepsilon}} + \sqrt{\frac{1 - \frac{2}{3}\varepsilon}{1 + \frac{1}{3}\varepsilon}} \right] = 1 + \frac{1}{8}\varepsilon^2 + O(\varepsilon^3) \quad (\text{A 13d})$$

$$b = \frac{1}{2} \left[\sqrt{\frac{1 + \frac{1}{3}\varepsilon}{1 - \frac{2}{3}\varepsilon}} - \sqrt{\frac{1 - \frac{2}{3}\varepsilon}{1 + \frac{1}{3}\varepsilon}} \right] = \frac{1}{2}\varepsilon + \frac{1}{12}\varepsilon^2 + O(\varepsilon^3), \quad (\text{A 13e})$$

and where the operators f_+ and f_- can be conveniently written in the form

$$f_+ = \frac{1}{2} [A, -\zeta (\xi + i\eta)] = \sqrt{\frac{2\pi}{15}} [A, \varrho^2 U_{21}] \quad (\text{A 14a})$$

$$f_- = \frac{1}{2} [A, +\zeta (\xi - i\eta)] = \sqrt{\frac{2\pi}{15}} [A, \varrho^2 U_{2-1}]. \quad (\text{A 14b})$$

Here U_{21} is the normalized spherical harmonic of order 2,1, expressed in the angles of the coordinate system ξ, η, ζ .

From (A 10) and (14 a, b) one finds

$$\langle N_l | f_{\pm} | N_l \rangle = \sqrt{\frac{8\pi}{15}} (N'_l - N_l) \langle N'_l | \varrho^2 U_{2\pm 1} | N_l \rangle. \quad (\text{A } 15)$$

Next, using (13 a, b) and expanding in powers of ε , one can show that

$$H_{\text{pert}} = \varepsilon H_1 + \varepsilon^2 H_2 + \dots, \quad (\text{A } 16)$$

where

$$H_1 = -\frac{1}{4} C \{ f_{+s_-} + f_{-s_+} \} - \frac{1}{2} D \{ (l)_- f_+ + f_- (l)_+ \} \quad (\text{A } 16 \text{ a})$$

and

$$\left. \begin{aligned} H_2 = \frac{1}{16} C \left\{ (l)_{+s_-} + (l)_{-s_+} - \frac{3}{2} (f_{+s_-} + f_{-s_+}) \right\} \\ + \frac{1}{4} D \left\{ (l)_- (l)_+ + f_- f_+ - \frac{1}{3} [(l)_- f_+ + f_- (l)_+] \right\}. \end{aligned} \right\} \quad (\text{A } 16 \text{ b})$$

Now it follows from (A 15) that the matrix elements of εH_1 between states of the same N_l vanish. On the other hand, εH_1 causes a coupling in the $|N_l l_t A_t \Sigma\rangle$ -representation between states differing by two in their N_l -value of formally a very similar kind [cf. (A 15) and (7 b)] to the coupling caused by H_δ in the $|N l A \Sigma\rangle$ -representation between the N and $N + 2$ shells. An estimate of the εH_1 coupling terms shows, however, that their order of magnitude is only 1/10 of the H_δ coupling terms, or something similar to the ratio of the matrix elements of the $\bar{l} \cdot \bar{s}$ - and \bar{l}^2 -terms to the matrix elements of H_0 .

The second order terms in (A 16) amount only to the order of a per cent of the total $\bar{l} \cdot \bar{s}$ - and \bar{l}^2 -terms and are therefore negligible.

By interpreting the representatives A_{lA} , listed in Table I, as being representatives $A_{l_t A_t}$ of eigenfunctions in the $|N_l l_t A_t \Sigma\rangle$ -representation, one should thus obtain an improved approximation.

The uncorrected more simple eigenfunctions are, however, used in the main part of this paper since they are sufficiently accurate for most of the applications. Thus, the matrix elements

for operators as μ and a and those involved in M1 transitions, which all contain exclusively \bar{l} and \bar{s} , are affected only to the order ϵ^2 by the change in the wave functions. Moreover, the correction term of this order involves a small coefficient [cf. (A 13d)] and is therefore of little significance. The situation is somewhat different for operators like the quadrupole moment and E2 transition operators, and in an estimate of matrix elements of these quantities it may sometimes be important to use the improved representation.

Finally, it may be added that, apart from the smallness of H_{pert} , it is even questionable which Hamiltonian H or H_t best describes the nuclear conditions.

The $\bar{l} \cdot \bar{s}$ -term for the nuclear case is modelled after the spin-orbit coupling term for an electron moving in an electrostatic field. This term is of the form $\bar{s} \cdot (\bar{v} \times \text{grad } V)$ which only for an isotropic potential reduces to $\bar{l} \cdot \bar{s}$. For a deformed oscillator potential, the difference between such a coupling term and the $\bar{l} \cdot \bar{s}$ -term is of the same order of magnitude as the difference between $\bar{l} \cdot \bar{s}$ and $\bar{l}_t \cdot \bar{s}$.

Similarly for the \bar{l}^2 -term, which is thought of as a correction at larger distances for the too fast rising of the oscillator walls, there is no reason to assume a spherically symmetric correction when the oscillator potential itself becomes elliptically deformed.

Thus, it appears that the effect of H_{pert} lies entirely within the range of ambiguity in the definition of the $\bar{l} \cdot \bar{s}$ - and \bar{l}^2 -terms for the deformed nucleus.

Appendix B.

Asymptotic Solutions in the Limit of Very Strong Deformations.

The notation and parameters used in this section are identical with those employed in Appendix A.

We first consider the Hamiltonian H_0 (A 1 a) containing only kinetic energy and oscillator field terms. It follows from (A 6, A 7) that the energy eigenvalues corresponding to H_0 are of the form

$$E_0 = \left(n_\xi + \frac{1}{2} \right) \hbar \omega_z + (n_\xi + n_\eta + 1) \hbar \omega_x,$$

which can be rewritten in terms of the deformation parameter ε [cf. (A2 a, b)]

$$E_0 = \hbar \omega_0(\varepsilon) \left[\left(N + \frac{3}{2} \right) + \varepsilon \frac{n_\perp - 2 n_\xi}{3} \right], \quad (\text{B1})$$

where $n_\perp = n_\xi + n_\eta$. The energy eigenvalues in units of $\hbar \omega_0(\varepsilon)$, plotted as functions of ε , are then straight lines. The corresponding eigenfunctions are $|n_\xi\rangle |n_\eta\rangle |n_\zeta\rangle$.

Such a level characterized by n_ζ and n_\perp is degenerate to the order $n_\perp + 1$ (number of combinations of n_ξ and n_η that fulfil $n_\xi + n_\eta = n_\perp$). To this degeneracy is then added the spin degeneracy.

We further introduce linear combinations $|n_\perp A\rangle$ of base vectors $|n_\xi\rangle |n_\eta\rangle$ (with $n_\xi + n_\eta = n_\perp$) such that

$$[(l)_z - A] |n_\perp A\rangle = 0.$$

The vectors $|n_\xi\rangle |n_\perp A\rangle | \Sigma \rangle$ form a complete set, and H_0 is further diagonal in such a representation. Here $A = \pm 1, \pm 3, \dots, \pm n_\perp$ if n_\perp is odd, and $= 0, \pm 2, \dots, \pm n_\perp$ if n_\perp is even.

We now consider elements of $\bar{l}_i \cdot \bar{s}$ and \bar{l}_i^2 in this representation. As before, we can have coupling terms only between states of the same Ω and $N (= n_\zeta + n_\perp)$. Apart from diagonal elements, non-vanishing matrix elements of $\bar{l}_i \cdot \bar{s}$ occur only between states differing by one unit in A and n_\perp . As regards \bar{l}_i^2 , this operator is diagonal in A and has non-vanishing elements only between states with n_\perp equal or different by two.

The diagonal elements of $\bar{l}_i \cdot \bar{s}$ are given immediately as

$$\langle n_\zeta n_\perp A \Sigma | \bar{l}_i \cdot \bar{s} | n_\zeta n_\perp A \Sigma \rangle = A \Sigma. \quad (\text{B2})$$

Employing operator relations of the type used in Appendix A, one can show

$$\langle n_\zeta n_\perp A \Sigma | \bar{l}_i^2 | n_\zeta n_\perp A \Sigma \rangle = A^2 + 2 n_\perp n_\zeta + 2 n_\zeta + n_\perp. \quad (\text{B3})$$

Figs. 4a and 4b give a comparison of the energy levels of the $N = 5$ shell by perturbation treatment and exact calculation, for

the largest deformations calculated in the numerical treatment. The level group (α) corresponds to the harmonic oscillator levels (B1) while (β) employs the diagonal terms of (B2) and (B3). Finally (γ) shows the exact levels.

These asymptotic solutions corresponding to the $|n_\xi n_\perp A\Sigma\rangle$ -states may be of interest in providing new approximate selection rules for particle transitions in this region of deformation, connected with the occurrence of the new constants of the motion n_\perp and Σ .

Appendix C.

The Total Energy as Function of the Deformation Parameter.

We shall here evaluate the expectation value of the total energy Hamiltonian \mathfrak{H} , defined by (15), employing the notation and results of Appendix A, i. e. taking into account the effect on the wave functions of the coupling between shells characterized by different N -values. We write

$$\mathfrak{H} = \frac{1}{2} \sum_i H_i + \frac{1}{2} \sum_i T_i = \frac{3}{4} \sum_i H_i - \frac{1}{4} \sum_i (V_i - T_i).$$

The eigenvalues of H_i are just the calculated single-particle energy eigenvalues E_i . Separating out l -dependent terms of the difference $V_i - T_i$ we can write

$$V_i - T_i = W_i + U_i, \quad (\text{C1})$$

where in the notation of Appendix A (dropping the index i)

$$W = \hbar \omega_x \left[\frac{\partial^2}{\partial \xi^2} + \xi^2 + \frac{\partial^2}{\partial \eta^2} + \eta^2 \right] + \hbar \omega_z \left[\frac{\partial^2}{\partial \zeta^2} + \zeta^2 \right] \quad (\text{C1 a})$$

$$U = C \bar{l} \cdot \bar{s} + D \bar{l}^2 \simeq C \bar{l}_t \cdot \bar{s} + D \bar{l}_t^2. \quad (\text{C1 b})$$

Noting that the single-particle wave functions can be written as linear combinations of $|n_\xi\rangle |n_\eta\rangle |n_\zeta\rangle$, with the requirement $n_\xi + n_\eta + n_\zeta = N_t$, it follows immediately from the virial theorem for one-dimensional harmonic oscillators that

$$\langle W_i \rangle = 0. \quad (\text{C2})$$

Figs. 4a and 4b further demonstrate that U_i is approximately diagonal at the largest deformations with respect to the wave functions which are appropriate at these deformations. The approximate expectation values of U_i can be calculated from (B2) and (B3). To the extent this approximation is valid, U_i is independent of the deformation.

Using the equivalent of formula (13) (employing ε instead of δ) and formula (A4), one finally obtains *, **

$$\mathcal{G}(\varepsilon) = \frac{3}{4} \hbar \omega_0 \left\{ \sum_i \left(N_i + \frac{3}{2} \right) \left(1 + \frac{1}{9} \varepsilon^2 \right) + \sum_i \kappa r_i(\varepsilon) \right\} + \frac{1}{4} \sum_i \langle U_i \rangle. \quad (\text{C3})$$

The equilibrium deformation ε_{eq} is then obtained by solving

$$\frac{\partial \mathcal{G}(\varepsilon)}{\partial \varepsilon} = 0.$$

The relation between the deformation parameters ε and δ , employed here and in the main text, respectively, is given by (A3).

* A correction to (C3) is obtained by considering the diagonal terms of the neglected Coulomb interaction between the protons. This effect will tend to increase the equilibrium deformation. For, e. g., a homogeneously charged ellipsoid of an average radius R_0 one has to second order in ε

$$E_{cl} = \frac{3}{5} \frac{Z^2 e^2}{R_0} \left(1 - \frac{4}{45} \varepsilon^2 \right).$$

(Cf., e. g., N. BOHR and J. A. WHEELER, Phys. Rev. 56, 426 (1939).)

The ε^2 -dependent term is negligible for the lighter nuclei, and even for nuclei around $A = 200$ it does not amount to more than 10 per cent of the "surface tension" term (second order term) in (C3).

** Note added in proof: It is possible to estimate the effect of the residual interactions by employing the two-nucleon model used by A. BOHR and B. MOTTELSON (Dan. Mat. Fys. Medd., in press). These interactions tend always to reduce the deformation from that calculated for completely independent particle motion as above. The effect becomes less important for increasing deformation. For $\varepsilon = 0.3$ and a strength of interaction $v = 0.3$, as defined in the above reference, the equilibrium deformation is reduced by 10 per cent. (Private communication from B. MOTTELSON.)

Tables.

TABLE I. Eigenvalues and Eigenfunctions for the Deformed Field.

$$N = 0 \quad \Omega = \frac{1}{2}$$

eigenvalue: $r = 0$, eigenvector: $|000 + \rangle$.

$$N = 1 \quad \Omega = \frac{3}{2}$$

eigenvalue: $r = \frac{1}{3}\eta - 1$, eigenvector: $|111 + \rangle$.

	$\eta = -6$	-4	-2	2	4	6
2	-3.000	-2.333	-1.667	-0.333	0.333	1.000

$$N = 1 \quad \Omega = \frac{1}{2}$$

base vectors: $|110 + \rangle, |111 - \rangle$.

	$\eta = -6$	-4	-2	2	4	6
4	4.372	3.228	2.333	2.228	2.706	3.275
	1.000	1.000	1.000	1.000	1.000	1.000
	-0.263	-0.397	-0.707	-2.518	-3.798	-5.144
3	-1.372	-0.895	-0.667	-1.895	-3.039	-4.275
	1.000	1.000	1.000	1.000	1.000	1.000
	3.798	2.518	1.414	0.397	0.263	0.194

$$N = 2 \quad \Omega = \frac{5}{2}$$

eigenvalue: $r = \frac{2}{3}\eta - 2$, eigenvector: $|222 + \rangle$.

	$\eta = -6$	-4	-2	2	4	6
5	-6.000	-4.667	-3.333	-0.667	0.667	2.000

$$N = 2 \quad \Omega = \frac{3}{2}$$

base vectors: $|221 + \rangle, |222 - \rangle$.

	$\eta = -6$	-4	-2	2	4	6
8	2.000	1.895	2.228	4.035	5.198	6.424
	1.000	1.000	1.000	1.000	1.000	1.000
	-0.500	-0.781	-1.281	-2.851	-3.766	-4.712
7	-3.000	-2.228	-1.895	-2.368	-2.865	-3.424
	1.000	1.000	1.000	1.000	1.000	1.000
	2.000	1.281	0.781	0.351	0.266	0.212

$$N = 2 \quad \Omega = \frac{1}{2}$$

base vectors: $|220 + \rangle, |200 + \rangle, |221 - \rangle$.

	$\eta = -6$	-4	-2	2	4	6
11	8.719	6.379	4.368	2.630	3.298	4.394
	1.000	1.000	1.000	1.000	1.000	1.000
	0.649	0.591	0.432	-0.717	-1.143	-1.287
	-0.428	-0.605	-0.907	-1.066	-0.675	-0.454
9	2.568	1.693	0.667	0.120	-0.237	-0.853
	1.000	1.000	1.000	1.000	1.000	1.000
	2.203	2.227	2.828	-15.696	15.901	6.635
	5.672	3.827	2.449	11.489	-25.472	-16.609
6	-4.287	-3.072	-2.035	-3.751	-6.069	-8.542
	1.000	1.000	1.000	1.000	1.000	1.000
	-1.319	-1.227	-0.927	0.503	0.622	0.662
	0.336	0.453	0.662	0.600	0.428	0.325

$$N = 3 \quad \Omega = \frac{7}{2}$$

eigenvalue: $r = \eta - 7.2$, eigenvector: $|333 + \rangle$.

	$\eta = -6$	-4	-2	2	4	6
10	-13.200	-11.200	-9.200	-5.200	-3.200	-1.200

$$N = 3 \quad \Omega = \frac{5}{2}$$

base vectors: $|332 + \rangle, |333 - \rangle.$

	$\eta = -6$	-4	-2	2	4	6
15	-4.200	-3.200	-1.828	1.572	3.424	5.321
	1.000	1.000	1.000	1.000	1.000	1.000
	-0.817	-1.225	-1.785	-3.173	-3.929	-4.703
12	-9.200	-8.200	-7.572	-6.972	-6.824	-6.721
	1.000	1.000	1.000	1.000	1.000	1.000
	1.225	0.817	0.560	0.315	0.255	0.213

$$N = 3 \quad \Omega = \frac{3}{2}$$

base vectors: $|331 + \rangle, |311 + \rangle, |332 - \rangle.$

	$\eta = -6$	-4	-2	2	4	6
19	3.058	1.614	0.483	0.381	2.091	3.967
	1.000	1.000	1.000	1.000	1.000	1.000
	0.574	0.560	0.473	-1.816	-2.300	-2.322
	-0.601	-0.829	-1.178	-1.225	-0.737	-0.513
16	-3.054	-3.124	-2.765	-1.129	-1.319	-1.491
	1.000	1.000	1.000	1.000	1.000	1.000
	2.137	3.280	11.837	2.543	1.585	1.416
	3.703	3.421	5.599	-2.953	-3.590	-4.460
13	-9.104	-7.590	-6.819	-8.352	-9.872	-11.576
	1.000	1.000	1.000	1.000	1.000	1.000
	-1.262	-0.917	-0.408	0.204	0.303	0.356
	0.458	0.587	0.685	0.514	0.412	0.337

$$N = 3 \quad \Omega = \frac{1}{2}$$

base vectors: $|330 + \rangle, |310 + \rangle, |331 - \rangle, |311 - \rangle.$

	$\eta = -6$	-4	-2	2	4	6
26	10.824	7.100	3.594	2.512	4.265	6.126
	1.000	1.000	1.000	1.000	1.000	1.000
	1.460	1.518	1.650	-1.495	-1.161	-1.049
	-0.474	-0.620	-0.854	-1.554	-2.053	-2.587
	-0.307	-0.449	-0.823	4.547	5.248	6.244
20	3.620	1.779	0.257	-1.636	-2.151	-2.373
	1.000	1.000	1.000	1.000	1.000	1.000
	-4.476	-3.201	-1.730	-0.645	-0.926	-0.950
	-8.469	-4.424	-1.803	-0.837	-0.468	-0.300
	-4.959	-2.482	-0.379	-0.718	-0.578	-0.444
17	-2.465	-2.012	-1.275	-3.480	-5.829	-8.066
	1.000	1.000	1.000	1.000	1.000	1.000
	-0.539	-0.379	0.328	7.020	5.302	5.955
	-0.030	-0.136	-0.197	-4.641	-6.453	-10.375
	0.740	1.134	2.076	0.503	-1.542	-3.458
14	-7.779	-6.666	-6.376	-9.196	-12.086	-15.487
	1.000	1.000	1.000	1.000	1.000	1.000
	-0.582	-0.484	-0.303	0.359	0.637	0.809
	1.432	1.088	0.918	0.777	0.632	0.500
	-1.718	-0.912	-0.347	0.164	0.198	0.183

$$N = 4 \quad \Omega = \frac{9}{2}$$

eigenvalue: $r = \frac{4}{3}\eta - 13$, eigenvector: $|444 + \rangle.$

	$\eta = -6$	-4	-2	2	4	6
18	-21.000	-18.333	-15.667	-10.333	-7.667	-5.000

$$N = 4 \quad \Omega = \frac{7}{2}$$

base vectors: $|443 + \rangle, |444 - \rangle.$

	$\eta = -6$	-4	-2	2	4	6
25	-10.628	-8.632	-6.392	-1.518	1.018	3.589
	1.000	1.000	1.000	1.000	1.000	1.000
	-1.192	-1.662	-2.219	-3.470	-4.131	-4.804
21	-16.372	-15.035	-13.942	-12.148	-11.351	-10.589
	1.000	1.000	1.000	1.000	1.000	1.000
	0.839	0.602	0.451	0.288	0.242	0.208

$$N = 4 \quad \Omega = \frac{5}{2}$$

base vectors: $|442 + \rangle$, $|422 + \rangle$, $|443 - \rangle$.

	$\eta = -6$	-4	-2	2	4	6
31	-3.373	-3.871	-4.087	-2.217	0.277	2.838
	1.000	1.000	1.000	1.000	1.000	1.000
	0.552	0.558	0.517	-3.610	-3.561	-3.352
	-0.809	-1.081	-1.451	-1.201	-0.757	-0.547
27	-9.282	-8.360	-6.780	-3.855	-3.470	-3.008
	1.000	1.000	1.000	1.000	1.000	1.000
	2.465	5.272	90.857	1.119	0.946	0.914
	2.918	3.646	33.064	-2.532	-3.127	-3.773
22	-15.045	-13.469	-12.833	-13.628	-14.506	-15.530
	1.000	1.000	1.000	1.000	1.000	1.000
	-1.034	-0.611	-0.232	0.127	0.200	0.245
	0.531	0.610	0.607	0.451	0.380	0.325

$$N = 4 \quad \Omega = \frac{3}{2}$$

base vectors: $|441 + \rangle$, $|421 + \rangle$, $|442 - \rangle$, $|422 - \rangle$.

	$\eta = -6$	-4	-2	2	4	6
42	4.911	2.230	0.171	2.276	4.651	7.148
	1.000	1.000	1.000	1.000	1.000	1.000
	1.244	1.404	2.026	-3.127	-2.112	-1.784
	-0.629	-0.809	-1.071	-1.816	-2.246	-2.689
	-0.431	-0.713	-1.871	9.992	9.053	9.513
33	-2.239	-3.332	-3.800	-4.457	-4.200	-3.765
	1.000	1.000	1.000	1.000	1.000	1.000
	-148.417	-7.290	-0.671	-1.560	-1.677	-1.597
	-208.425	-7.611	-1.393	-0.961	-0.566	-0.379
	-121.847	-4.315	0.605	-0.763	-0.642	-0.512
29	-7.119	-5.521	-4.335	-5.846	-7.524	-9.133
	1.000	1.000	1.000	1.000	1.000	1.000
	-0.545	-0.233	3.603	2.001	1.780	1.835
	-0.297	-0.510	0.727	-2.294	-3.008	-3.917
	1.181	1.524	4.020	0.109	-0.441	-0.868
23	-12.952	-12.111	-12.104	-14.706	-16.994	-19.649
	1.000	1.000	1.000	1.000	1.000	1.000
	-0.623	-0.462	-0.245	0.215	0.373	0.482
	0.969	0.829	0.763	0.627	0.537	0.456
	-0.891	-0.450	-0.167	0.081	0.110	0.114

$$N = 4 \quad \Omega = \frac{1}{2}$$

base vectors: $|440 + \rangle, |420 + \rangle, |400 + \rangle, |441 - \rangle, |421 - \rangle$.

	$\eta = -6$	-4	-2	2	4	6
51	13.736	8.749	4.034	2.039	4.403	6.898
	1.000	1.000	1.000	1.000	1.000	1.000
	2.266	2.555	3.410	-4.291	-3.337	-2.987
	1.561	1.843	2.667	6.641	4.782	4.099
	-0.511	-0.639	-0.835	-0.814	-0.613	-0.488
	-0.698	-1.052	-2.135	2.532	1.293	0.870
43	5.508	2.566	0.188	-1.353	-1.477	-1.202
	1.000	1.000	1.000	1.000	1.000	1.000
	-1.275	-0.938	-0.205	-1.173	-0.441	-0.215
	-2.191	-2.308	-3.435	-2.734	-1.886	-1.691
	-3.821	-2.644	-1.728	-1.567	-2.106	-2.709
	-4.813	-3.764	-3.474	4.285	4.063	4.563
34	-1.437	-2.333	-3.037	-6.163	-8.057	-9.716
	1.000	1.000	1.000	1.000	1.000	1.000
	0.085	0.172	0.136	-0.504	-0.644	-0.589
	-0.559	-0.465	-0.142	-0.258	-0.504	-0.573
	-0.290	-0.472	-0.841	-0.816	-0.438	-0.261
	0.670	0.840	0.838	-0.834	-0.777	-0.615
30	-6.733	-5.465	-4.165	-7.293	-11.045	-14.793
	1.000	1.000	1.000	1.000	1.000	1.000
	6.922	-17.873	-9.735	3.961	3.743	5.130
	-9.733	20.639	7.376	1.714	2.139	3.283
	10.840	-17.270	-5.376	-2.728	-4.024	-7.444
	-5.800	4.197	-3.760	0.947	-0.933	-3.180
24	-12.474	-11.584	-11.753	-15.296	-18.558	-22.587
	1.000	1.000	1.000	1.000	1.000	1.000
	-0.868	-0.554	-0.263	0.267	0.531	0.758
	0.659	0.302	0.071	0.055	0.181	0.318
	0.791	0.892	0.914	0.853	0.770	0.658
	-0.491	-0.408	-0.221	0.187	0.295	0.325

$$N = 5 \quad \Omega = \frac{11}{2}$$

eigenvalue: $\frac{5}{3}\eta - 18.5$, eigenvector: $|555 + \rangle$.

	$\eta = -6$	-4	-2	2	4	6
28	-28.500	-25.177	-21.833	-15.177	-11.833	-8.500

$$N = 5 \quad \Omega = \frac{9}{2}$$

base vectors: $|554 + \rangle, |555 - \rangle.$

	$\eta = -6$	-4	-2	2	4	6
40	-16.500	-13.636	-10.616	-4.322	-1.105	2.139
	1.000	1.000	1.000	1.000	1.000	1.000
	-1.581	-2.065	-2.599	-3.745	-4.341	-4.946
32	-23.500	-21.698	-20.050	-17.011	-15.562	-14.139
	1.000	1.000	1.000	1.000	1.000	1.000
	0.632	0.484	0.385	0.267	0.230	0.202

$$N = 5 \quad \Omega = \frac{7}{2}$$

base vectors: $|553 + \rangle, |533 + \rangle, |554 - \rangle.$

	$\eta = -6$	-4	-2	2	4	6
48	-9.480	-9.049	-8.384	-5.218	-2.054	1.176
	1.000	1.000	1.000	1.000	1.000	1.000
	0.497	0.490	0.433	-4.295	-4.425	-4.149
	-1.056	-1.361	-1.732	-1.439	-0.888	-0.636
41	-15.523	-13.722	-11.256	-6.609	-5.512	-4.366
	1.000	1.000	1.000	1.000	1.000	1.000
	2.442	5.528	37.895	1.145	0.870	0.814
	2.098	2.726	10.044	-2.723	-3.210	-3.741
35	-21.397	-19.628	-18.760	-18.573	-18.834	-19.210
	1.000	1.000	1.000	1.000	1.000	1.000
	-0.871	-0.461	-0.168	0.096	0.155	0.194
	0.537	0.569	0.535	0.408	0.354	0.309

$$N = 5 \quad \Omega = \frac{5}{2}$$

base vectors: $|552 + \rangle$, $|532 + \rangle$, $|553 - \rangle$, $|533 - \rangle$.

	$\eta = -6$	- 4	- 2	2	4	6
61	- 1.116	- 2.676	- 3.119	1.371	4.423	7.580
	1.000	1.000	1.000	1.000	1.000	1.000
	1.129	1.355	2.466	- 4.479	- 2.914	- 2.403
	- 0.816	- 1.030	- 1.306	- 1.992	- 2.368	- 2.753
	- 0.587	- 1.074	- 3.540	15.268	12.525	12.386
50	- 8.258	- 8.569	- 7.442	- 7.416	- 6.489	- 5.388
	1.000	1.000	1.000	1.000	1.000	1.000
	9.749	- 4.844	- 0.035	- 1.917	- 2.198	- 2.094
	10.595	- 4.599	- 1.386	- 1.184	- 0.692	- 0.463
	5.725	- 0.772	0.769	- 0.782	- 0.722	- 0.590
44	- 11.586	- 9.284	- 8.749	- 8.607	- 9.501	- 10.393
	1.000	1.000	1.000	1.000	1.000	1.000
	- 0.454	0.350	21.498	1.944	1.461	1.413
	- 0.506	- 0.455	7.169	- 2.428	- 2.893	- 3.491
	1.534	1.809	12.613	0.188	- 0.287	- 0.582
36	- 18.840	- 17.937	- 17.823	- 19.815	- 21.567	- 23.599
	1.000	1.000	1.000	1.000	1.000	1.000
	- 0.618	- 0.425	- 0.206	0.162	0.279	0.362
	0.785	0.714	0.667	0.546	0.479	0.419
	- 0.575	- 0.291	- 0.107	0.053	0.076	0.083

$$N = 5 \quad \Omega = \frac{3}{2}$$

base vectors: $|551 + \rangle, |531 + \rangle, |511 + \rangle, |552 - \rangle, |532 - \rangle.$

	$\eta = -6$	-4	-2	2	4	6
70	7.808	3.907	0.568	0.918	3.947	7.097
	1.000	1.000	1.000	1.000	1.000	1.000
	1.890	2.226	3.338	-5.411	-4.112	-3.623
	0.976	1.232	2.039	12.795	8.865	7.343
	-0.667	-0.827	-1.048	-0.987	-0.740	-0.586
	-0.870	-1.390	-3.159	4.393	2.149	1.407
62	-0.191	-2.274	-3.276	-1.865	-1.323	-0.438
	1.000	1.000	1.000	1.000	1.000	1.000
	-4.359	-2.719	-1.115	-2.461	-1.306	-0.946
	-4.856	-4.512	-8.014	-3.718	-2.318	-1.948
	-7.139	-3.871	-2.218	-1.717	-2.134	-2.583
	-8.290	-5.329	-5.299	7.183	5.864	5.942
52	-6.357	-6.436	-6.565	-9.164	-10.375	-11.357
	1.000	1.000	1.000	1.000	1.000	1.000
	-0.048	0.071	0.052	-0.823	-1.124	-1.077
	-0.500	-0.339	-0.046	-0.235	-0.483	-0.566
	-0.467	-0.708	-1.099	-1.036	-0.578	-0.351
	0.841	0.953	0.707	-0.790	-0.822	-0.678
46	-11.233	-9.299	-7.877	-10.230	-12.980	-15.877
	1.000	1.000	1.000	1.000	1.000	1.000
	2.985	13.310	141.387	3.477	2.431	2.483
	-5.559	-17.369	-85.487	0.887	0.858	0.997
	4.330	11.111	59.345	-2.665	-3.114	-4.047
	-1.922	0.032	74.877	0.874	-0.423	-1.205
37	-17.727	-16.931	-17.216	-20.692	-23.635	-27.126
	1.000	1.000	1.000	1.000	1.000	1.000
	-0.754	-0.475	-0.229	0.214	0.399	0.546
	0.546	0.211	0.043	0.027	0.081	0.138
	0.780	0.810	0.794	0.701	0.631	0.555
	-0.474	-0.337	-0.161	0.116	0.180	0.205

$$N = 5 \quad \Omega = \frac{1}{2}$$

base vectors: $|550 + \rangle, |530 + \rangle, |510 + \rangle, |551 - \rangle, |531 - \rangle, |511 - \rangle.$

	$\eta = -6$	-4	-2	2	4	6
A	17.207	10.952	5.017	3.162	6.118	9.237
	1.000	1.000	1.000	1.000	1.000	1.000
	2.944	3.426	4.884	-4.742	-3.082	-2.542
	3.717	4.688	8.018	6.313	3.072	2.252
	-0.558	-0.681	-0.857	-1.391	-1.720	-2.061
	-1.148	-1.723	-3.469	8.472	7.414	7.644
	-0.632	-1.081	-3.043	-23.071	-16.614	-15.753
71	8.305	4.175	0.577	-2.149	-1.654	-0.781
	1.000	1.000	1.000	1.000	1.000	1.000
	-0.069	0.327	1.517	-3.818	-2.730	-2.359
	-2.803	-3.133	-4.467	3.716	2.449	1.981
	-2.853	-2.132	-1.506	-0.822	-0.606	-0.469
	-5.438	-4.780	-4.972	2.074	0.780	0.420
	-2.826	-2.665	-2.914	2.656	1.431	0.993
63	0.663	-1.195	-1.835	-4.868	-6.961	-8.308
	1.000	1.000	1.000	1.000	1.000	1.000
	0.743	1.011	2.203	-1.007	0.082	0.438
	-0.683	-0.652	-0.455	-4.445	-2.549	-2.161
	-0.402	-0.559	-0.768	-1.545	-2.077	-2.735
	0.384	0.310	-0.524	4.172	3.179	3.313
	0.681	1.157	3.480	0.659	1.207	1.649
53	-5.968	-6.278	-6.309	-10.324	-13.537	-16.571
	1.000	1.000	1.000	1.000	1.000	1.000
	-5.341	-2.350	-0.424	-0.092	-0.353	-0.303
	3.586	1.279	0.121	-0.085	-0.464	-0.622
	-7.107	-2.545	-1.091	-0.946	-0.499	-0.262
	0.251	-0.040	0.401	-0.678	-0.887	-0.735
	3.619	0.691	-0.184	-0.153	-0.305	-0.299
47	-9.867	-7.850	-7.135	-11.269	-15.732	-20.742
	1.000	1.000	1.000	1.000	1.000	1.000
	-0.482	0.068	4.020	15.520	5.093	6.911
	0.138	-0.175	-1.629	7.570	4.087	6.789
	-0.073	-0.161	0.987	-7.545	-4.822	-8.888
	0.846	1.192	3.905	8.387	-0.393	-3.757
	-1.326	-1.419	-2.239	2.459	0.195	-0.742
38	-16.940	-16.403	-16.915	-21.152	-24.834	-29.436
	1.000	1.000	1.000	1.000	1.000	1.000
	-0.654	-0.458	-0.234	0.237	0.479	0.712
	0.260	0.140	0.041	0.046	0.183	0.379
	0.994	0.944	0.928	0.888	0.843	0.765
	-0.724	-0.440	-0.211	0.192	0.343	0.428
	0.502	0.188	0.039	0.024	0.071	0.110

$$N = 6 \quad \Omega = \frac{13}{2}$$

eigenvalue: $2\eta - 24.9$, eigenvector: $|666 + \rangle$.

	$\eta = -6$	-4	-2	2	4	6
39	-36.900	-32.900	-28.900	-20.900	-16.900	-12.900

$$N = 6 \quad \Omega = \frac{11}{2}$$

base vectors: $|665 + \rangle$, $|666 - \rangle$.

	$\eta = -6$	-4	-2	2	4	6
56	-23.128	-19.476	-15.721	-8.035	-4.139	-0.221
	1.000	1.000	1.000	1.000	1.000	1.000
	-1.955	-2.432	-2.938	-4.002	-4.550	-5.103
45	-31.672	-29.324	-27.079	-22.766	-20.661	-18.579
	1.000	1.000	1.000	1.000	1.000	1.000
	0.512	0.411	0.340	0.250	0.220	0.196

$$N = 6 \quad \Omega = \frac{9}{2}$$

base vectors: $|664 + \rangle$, $|644 + \rangle$, $|665 - \rangle$.

	$\eta = -6$	-4	-2	2	4	6
66	-16.305	-15.010	-13.535	-9.123	-5.290	-1.392
	1.000	1.000	1.000	1.000	1.000	1.000
	0.454	0.437	0.371	-4.776	-5.265	-4.938
	-1.305	-1.623	-1.983	-1.689	-1.017	-0.721
59	-22.640	-19.912	-16.602	-10.291	-8.490	-6.661
	1.000	1.000	1.000	1.000	1.000	1.000
	2.719	6.371	33.063	1.240	0.833	0.755
	1.712	2.332	6.685	-2.915	-3.325	-3.785
49	-28.854	-26.878	-25.663	-24.386	-24.020	-23.747
	1.000	1.000	1.000	1.000	1.000	1.000
	-0.698	-0.348	-0.127	0.077	0.126	0.159
	0.524	0.522	0.480	0.376	0.332	0.296

$$N = 6 \quad \Omega = \frac{7}{2}$$

base vectors: $|663 + \rangle, |643 + \rangle, |664 - \rangle, |644 - \rangle.$

	$\eta = -6$	-4	-2	2	4	6
	-7.780	-8.110	-6.895	-0.473	3.260	7.085
	1.000	1.000	1.000	1.000	1.000	1.000
	1.099	1.453	3.248	-5.916	-3.740	-3.025
	-1.007	-1.240	-1.517	-2.154	-2.493	-2.838
	-0.810	-1.672	-6.277	21.577	16.514	15.604
67	-15.209	-13.845	-12.205	-11.281	-9.688	-7.920
	1.000	1.000	1.000	1.000	1.000	1.000
	9.127	-0.484	0.120	-2.138	-2.684	-2.570
	8.182	-1.454	-1.565	-1.409	-0.815	-0.543
	3.443	1.255	0.600	-0.773	-0.791	-0.661
64	-16.823	-14.934	-14.132	-12.307	-12.452	-12.639
	1.000	1.000	1.000	1.000	1.000	1.000
	-0.203	4.223	25.832	2.081	1.317	1.216
	-0.627	1.807	7.150	-2.594	-2.914	-3.375
	1.739	2.926	11.799	0.265	-0.202	-0.442
54	-25.988	-24.910	-24.569	-25.738	-26.920	-28.326
	1.000	1.000	1.000	1.000	1.000	1.000
	-0.574	-0.372	-0.171	0.129	0.222	0.290
	0.684	0.639	0.598	0.493	0.440	0.392
	-0.395	-0.200	-0.073	0.038	0.056	0.063

$$N = 6 \quad \Omega = \frac{5}{2}$$

base vectors: $|662 + \rangle, |642 + \rangle, |622 + \rangle, |663 - \rangle, |643 - \rangle.$

	$\eta = -6$	-4	-2	2	4	6
	1.230	-1.526	-3.467	-1.132	2.568	6.381
	1.000	1.000	1.000	1.000	1.000	1.000
	1.758	2.180	3.683	-6.606	-4.943	-4.302
	0.796	1.074	1.971	20.348	13.926	11.254
	-0.826	-1.008	-1.239	-1.151	-0.856	-0.676
	-1.104	-1.867	-4.645	6.763	3.192	2.042
	-6.774	-7.855	-7.295	-3.487	-2.228	-0.688
	1.000	1.000	1.000	1.000	1.000	1.000
	-16.275	-5.331	-2.222	-3.633	-2.035	-1.525
	-16.446	-9.117	-18.549	-4.837	-2.748	-2.197
	-19.525	-5.516	-2.787	-1.860	-2.210	-2.583
	-22.252	-7.957	-8.672	10.540	7.928	7.548
	-12.017	-11.415	-11.176	-13.048	-13.595	-13.901
	1.000	1.000	1.000	1.000	1.000	1.000
72	-0.078	0.047	0.058	-1.004	-1.509	-1.477
	-0.408	-0.204	-0.035	-0.196	-0.452	-0.546
	-0.658	-0.940	-1.296	-1.240	-0.706	-0.434
	0.980	0.980	0.592	-0.750	-0.867	-0.739
	-16.668	-14.185	-12.795	-14.039	-15.961	-18.090
	1.000	1.000	1.000	1.000	1.000	1.000
65	2.503	7.250	26.193	3.590	2.013	1.874
	-4.837	-8.414	-10.944	0.644	0.519	0.560
	2.984	4.856	8.652	-2.776	-2.920	-3.460
	-0.829	1.543	14.032	0.949	-0.244	-0.775
	-24.271	-23.519	-23.767	-26.794	-29.285	-32.203
	1.000	1.000	1.000	1.000	1.000	1.000
55	-0.658	-0.414	-0.197	0.173	0.316	0.427
	0.393	0.138	0.027	0.015	0.046	0.078
	0.739	0.736	0.708	0.615	0.558	0.500
	-0.413	-0.266	-0.119	0.080	0.126	0.148

$$N = 6 \quad \Omega = \frac{3}{2}$$

base vectors: $|661 + \rangle, |641 + \rangle, |621 + \rangle, |662 - \rangle, |642 - \rangle, |622 - \rangle.$

	$\eta = -6$	-4	-2	2	4	6
	10.761	5.658	1.285	3.270	6.868	10.631
	1.000	1.000	1.000	1.000	1.000	1.000
	2.571	3.121	4.948	-6.377	-4.023	-3.253
	2.483	3.385	7.184	14.197	6.316	4.398
	-0.698	-0.842	-1.033	-1.533	-1.819	-2.115
	-1.376	-2.161	-4.760	12.321	9.797	9.519
	-0.698	-1.344	-5.119	-49.751	-29.946	-25.832
	2.006	-1.194	-3.531	-4.003	-2.832	-1.320
	1.000	1.000	1.000	1.000	1.000	1.000
	-1.497	-0.651	1.655	-4.837	-3.465	-2.970
	-5.024	-5.355	-5.770	6.958	4.680	3.719
	-4.106	-2.721	-1.564	-0.987	-0.724	-0.560
	-7.338	-5.968	-5.286	3.693	1.462	0.817
	-3.381	-2.952	-1.072	3.571	2.008	1.393
	-4.789	-5.332	-4.347	-6.198	-7.446	-8.179
	1.000	1.000	1.000	1.000	1.000	1.000
	0.607	1.054	3.209	-2.192	-0.817	-0.376
	-0.714	-0.674	1.207	-5.616	-3.098	-2.487
	-0.553	-0.728	-0.825	-1.679	-2.075	-2.532
	0.396	0.124	-1.140	6.616	4.690	4.435
	0.899	1.749	6.218	0.389	1.150	1.504
73	-11.500	-10.961	-10.573	-14.358	-16.884	-19.214
	1.000	1.000	1.000	1.000	1.000	1.000
	-10.085	-0.974	-0.132	-0.345	-0.737	-0.738
	8.500	0.511	0.012	-0.138	-0.485	-0.652
	-12.091	-1.431	-1.153	-1.114	-0.646	-0.360
	1.047	0.682	0.508	-0.659	-0.893	-0.779
	4.543	-0.432	-0.155	-0.104	-0.223	-0.237
68	-13.717	-11.779	-11.794	-15.386	-18.894	-22.914
	1.000	1.000	1.000	1.000	1.000	1.000
	-0.279	1.453	11.255	8.624	3.440	3.212
	-0.030	-1.143	-4.328	2.757	1.747	1.977
	-0.185	0.605	3.513	-4.475	-3.609	-4.429
	1.012	1.625	8.045	3.864	-0.089	-1.321
	-1.508	-1.752	-3.188	0.796	0.130	-0.153
57	-22.962	-22.593	-23.240	-27.524	-31.011	-35.204
	1.000	1.000	1.000	1.000	1.000	1.000
	-0.628	-0.424	-0.211	0.205	0.395	0.562
	0.273	0.131	0.033	0.029	0.103	0.196
	0.865	0.840	0.819	0.751	0.699	0.636
	-0.546	-0.340	-0.160	0.132	0.225	0.278
	0.302	0.108	0.021	0.012	0.033	0.051

$$N = 6 \quad \Omega = \frac{1}{2}$$

base vectors: $|660 + \rangle, |640 + \rangle, |620 + \rangle, |600 + \rangle, |661 - \rangle,$
 $|641 - \rangle, |621 - \rangle.$

	$\eta = -6$	-4	-2	2	4	6
	20.703	13.179	6.009	3.047	6.636	10.396
	1.000	1.000	1.000	1.000	1.000	1.000
	3.642	4.348	6.495	-7.352	-5.077	-4.300
	6.358	8.496	16.462	23.764	12.993	9.905
	4.037	5.649	12.004	-34.171	-17.158	-12.525
	-0.598	-0.714	-0.874	-0.862	-0.697	-0.581
	-1.658	-2.483	-4.971	5.484	2.800	1.888
	-1.709	-3.009	-8.870	-12.174	-4.392	-2.551
	11.182	5.874	1.264	-1.158	-0.286	1.113
	1.000	1.000	1.000	1.000	1.000	1.000
	0.910	1.476	3.282	-4.449	-2.472	-1.857
	-2.356	-2.508	-2.531	2.535	0.142	-0.273
	-2.769	-3.742	-8.776	9.588	4.365	3.219
	-2.380	-1.866	-1.416	-1.365	-1.696	-2.056
	-6.154	-5.848	-6.970	7.890	6.323	6.331
	-5.976	-6.372	-10.012	-15.544	-9.244	-8.186
	2.886	-0.154	-2.437	-6.473	-7.838	-8.605
	1.000	1.000	1.000	1.000	1.000	1.000
	1.430	1.862	3.257	-3.672	-2.368	-1.936
	-0.190	0.017	0.545	1.983	1.119	0.736
	-0.864	-0.983	-0.980	1.343	1.251	1.124
	-0.482	-0.629	-0.855	-0.853	-0.613	-0.462
	-0.015	-0.345	-1.901	2.129	0.521	0.147
	1.068	1.660	3.333	3.422	1.818	1.208
	-4.471	-5.273	-4.443	-8.425	-12.460	-15.518
	1.000	1.000	1.000	1.000	1.000	1.000
	-2.275	-1.386	0.225	-1.078	0.351	0.879
	-1.051	-2.133	-7.489	-6.249	-2.765	-2.021
	3.089	3.545	7.386	-3.250	-1.945	-1.712
	-3.756	-2.417	-1.749	-1.581	-2.058	-2.746
	-2.325	-2.538	-5.201	4.927	2.906	2.621
	2.694	1.631	-0.539	-0.011	1.419	2.034
	-10.435	-10.131	-10.266	-15.117	-19.353	-23.659
	1.000	1.000	1.000	1.000	1.000	1.000
	-0.163	-0.148	-0.235	0.113	-0.113	-0.121
	-0.235	-0.036	0.060	0.009	-0.256	-0.482
	0.296	0.032	-0.026	0.003	-0.116	-0.268
	-0.322	-0.685	-1.033	-1.021	-0.626	-0.299
	0.853	0.885	0.418	-0.493	-0.892	-0.816
	-0.653	-0.493	-0.115	-0.125	-0.416	-0.495

Continued next page

Continuation of

$$N = 6 \quad \Omega = \frac{1}{2}$$

base vectors: $|660 + \rangle, |640 + \rangle, |620 + \rangle, |600 + \rangle, |661 - \rangle,$
 $|641 - \rangle, |621 - \rangle.$

	$\eta = -6$	-4	-2	2	4	6
69	-13.673	-11.555	-11.349	-16.175	-20.943	-26.907
	1.000	1.000	1.000	1.000	1.000	1.000
	9.085	10.291	6.560	-14.612	12.536	10.379
	-13.400	-9.981	-2.819	-6.223	10.248	11.336
	12.883	7.570	1.088	-1.686	4.288	5.538
	11.185	7.818	1.830	4.984	-10.418	-12.297
	-3.429	3.850	5.694	-10.813	2.228	-4.031
	-0.061	-3.798	-2.214	-3.733	2.374	-0.462
60	-22.392	-22.141	-22.979	-27.899	-31.957	-37.020
	1.000	1.000	1.000	1.000	1.000	1.000
	-0.658	-0.432	-0.216	0.217	0.436	0.657
	0.356	0.149	0.036	0.037	0.151	0.337
	-0.209	-0.059	-0.007	0.006	0.041	0.120
	0.934	0.943	0.937	0.910	0.883	0.836
	-0.582	-0.397	-0.197	0.187	0.354	0.480
	0.251	0.121	0.031	0.027	0.093	0.170

TABLE Ia. Eigenvalues for the Spherical Case ($\delta = 0$).

Level designation in the spherical case		r	Label on level in Fig. 5
$N = 0$	$s_{1/2}$	0.000	
$N = 1$	$p_{3/2}$	- 1.000	2, 3
	$p_{1/2}$	2.000	4
$N = 2$	$s_{1/2}$	0.000	9
	$d_{5/2}$	- 2.000	5, 6, 7
	$d_{3/2}$	3.000	8, 11
$N = 3$	$p_{3/2}$	- 1.700	16, 17
	$p_{1/2}$	1.300	26
	$f_{7/2}$	- 7.200	10, 12, 13, 14
	$f_{5/2}$	- 0.200	15, 19, 20
$N = 4$	$s_{1/2}$	0.000	43
	$d_{5/2}$	- 4.700	27, 29, 30
	$d_{3/2}$	0.300	42, 51
	$g_{9/2}$	- 13.000	18, 21, 22, 23, 24
	$g_{7/2}$	- 4.000	25, 31, 33, 34
$N = 5$	$p_{3/2}$	- 1.900	70, 71
	$p_{1/2}$	1.100	A
	$f_{7/2}$	- 8.400	41, 44, 46, 47
	$f_{5/2}$	- 1.400	61, 62, 63
	$h_{11/2}$	- 18.500	28, 32, 35, 36, 37, 38
	$h_{9/2}$	- 7.500	40, 48, 50, 52, 53
$N = 6$	$s_{1/2}$	0.000	
	$d_{5/2}$	- 4.700	B
	$d_{3/2}$	0.300	
	$g_{9/2}$	- 13.000	59, 64, 65, 58, 69
	$g_{7/2}$	- 4.000	
	$i_{13/2}$	- 24.900	39, 45, 49, 54, 55, 57, 60
	$i_{11/2}$	- 11.900	56, 66, 67, 72, 73, 74
$N = 7$	$j_{15/2}$	- 29.400	58

TABLE Ib. Eigenvalues and Eigenfunctions of the Shell $N = 4$ with the Parameter $\mu = 0.55$ (added in proof).

$$\Omega = \frac{9}{2}$$

eigenvalue: $r = \frac{4}{3} \eta - 15$, eigenvector: $|444 + \rangle$.

	$\eta = -6$	-4	-2	2	4	6
18	-23.000	-20.333	-17.667	-12.333	-9.667	-7.000

$$\Omega = \frac{7}{2}$$

base vectors: $|443 + \rangle, |444 - \rangle$.

	$\eta = -6$	-4	-2	2	4	6
25	-12.628	-10.632	-8.392	-3.519	-0.982	1.589
	-0.643	-0.516	-0.411	-0.277	-0.235	-0.204
	0.766	0.857	0.912	0.961	0.972	0.979
21	-18.372	-17.035	-15.942	-14.148	-13.351	-12.589
	0.766	0.857	0.912	0.961	0.972	0.979
	0.643	0.516	0.411	0.277	0.235	0.204

$$\Omega = \frac{5}{2}$$

base vectors: $|442 + \rangle, |422 + \rangle, |443 - \rangle$.

	$\eta = -6$	-4	-2	2	4	6
31	-5.119	-5.644	-5.891	-2.948	-0.447	2.111
	0.705	-0.625	-0.521	-0.179	-0.228	-0.257
	0.458	-0.455	-0.485	0.972	0.964	0.959
	-0.541	0.634	0.702	0.152	0.137	0.119
27	-10.702	-9.435	-7.619	-5.741	-5.390	-4.948
	0.139	0.016	-0.138	-0.383	-0.316	-0.266
	0.659	0.805	0.860	-0.211	-0.207	-0.188
	0.739	0.593	0.492	0.899	0.926	0.946
22	-16.479	-15.221	-14.790	-15.611	-16.463	-17.463
	-0.695	0.780	0.842	0.906	0.921	0.929
	0.596	-0.381	-0.159	0.102	0.167	0.211
	-0.401	0.496	0.515	0.410	0.352	0.302

$$\Omega = \frac{3}{2}$$

base vectors: $|441 + \rangle$, $|421 + \rangle$, $|442 - \rangle$, $|422 - \rangle$.

	$\eta = -6$	-4	-2	2	4	6
42	3.732	1.135	-0.667	1.631	3.969	6.444
	0.531	0.443	0.252	0.078	0.091	0.089
	0.746	0.745	0.684	-0.292	-0.218	-0.175
	-0.316	-0.338	-0.259	-0.145	-0.210	-0.246
	-0.249	-0.368	-0.634	0.942	0.949	0.949
33	-3.575	-4.513	-4.994	-5.389	-5.138	-4.732
	-0.031	-0.063	0.154	-0.311	-0.409	-0.464
	0.490	0.579	0.660	0.870	0.851	0.841
	0.712	0.604	0.112	0.198	0.180	0.148
	0.501	0.544	0.727	0.326	0.275	0.237
29	-8.286	-6.688	-5.564	-7.513	-9.237	-10.881
	0.595	0.544	-0.553	-0.448	-0.344	-0.269
	-0.300	-0.165	0.266	-0.364	-0.386	-0.355
	-0.259	-0.421	0.752	0.815	0.846	0.876
	0.699	0.707	-0.240	0.050	0.132	0.187
23	-14.471	-13.868	-14.041	-16.661	-18.861	-21.431
	-0.602	0.710	0.779	0.834	0.840	0.840
	0.336	-0.286	-0.163	0.157	0.280	0.369
	-0.571	0.587	0.596	0.525	0.456	0.388
	0.446	-0.264	-0.109	0.060	0.084	0.090

$$\Omega = \frac{1}{2}$$

base vectors: $|440 + \rangle$, $|420 + \rangle$, $|400 + \rangle$, $|441 - \rangle$, $|421 - \rangle$.

	$\eta = -6$	-4	-2	2	4	6
51	13.130	8.188	3.551	1.811	4.142	6.614
	0.298	0.248	0.159	0.091	0.140	0.170
	0.745	0.725	0.670	-0.478	-0.531	-0.556
	0.537	0.559	0.596	0.833	0.810	0.796
	-0.144	-0.149	-0.125	-0.068	-0.079	-0.077
	-0.218	-0.282	-0.393	0.253	0.189	0.151
43	4.517	1.723	-0.319	-1.955	-2.266	-2.091
	-0.142	-0.166	-0.146	0.150	0.176	0.163
	0.152	0.116	-0.064	-0.271	-0.123	-0.062
	0.318	0.425	0.635	-0.437	-0.343	-0.279
	0.531	0.443	0.256	-0.235	-0.373	-0.445
	0.757	0.763	0.711	0.811	0.835	0.833
34	-2.734	-3.610	-4.315	-7.297	-9.189	-10.887
	0.721	-0.651	0.438	-0.412	-0.578	-0.653
	0.132	-0.242	0.539	0.669	0.539	0.477
	-0.458	0.423	-0.394	0.289	0.370	0.414
	-0.219	0.286	-0.207	0.192	0.204	0.158
	0.454	-0.507	0.565	0.511	0.444	0.387
30	-7.698	-6.293	-5.173	-8.602	-12.320	-16.125
	-0.050	0.194	-0.492	-0.498	-0.305	-0.187
	0.450	-0.552	0.479	-0.470	-0.549	-0.493
	-0.553	0.553	-0.292	-0.172	-0.281	-0.289
	0.628	-0.574	0.664	0.707	0.702	0.741
	-0.308	0.151	-0.036	0.047	0.181	0.299
24	-13.815	-13.275	-13.676	-17.224	-20.301	-24.111
	0.608	0.671	0.720	0.743	0.723	0.695
	-0.450	-0.314	-0.162	0.169	0.332	0.466
	0.308	0.149	0.037	0.031	0.103	0.183
	0.505	0.608	0.660	0.635	0.565	0.471
	-0.280	-0.243	-0.137	0.121	0.192	0.211

TABLE II. Matrix Elements of the Coupling Energy between some Particular States with N Differing by Two. (The energy unit is $\varkappa \hbar \omega_0$.)

	$\eta = 2$	$\eta = 4$	$\eta = 6$
$\frac{1}{\varkappa \hbar \omega_0} \cdot \langle N = 4 \ \Omega = \frac{3}{2}, \#42 H_\delta N = 6 \ \Omega = \frac{3}{2}, \#57 \rangle$	0.006	0.015	0.017
$\frac{1}{\varkappa \hbar \omega_0} \cdot \langle N = 4 \ \Omega = \frac{1}{2}, \#51 H_\delta N = 6 \ \Omega = \frac{1}{2}, \#60 \rangle$	0.007	0.013	0.018

TABLE III. Connection between Ground State Spin I_0 and Decoupling Factor a .

Range of a	I_0
— 14 < a < — 10	11/2
— 10 < a < — 6	7/2
— 6 < a < — 1	3/2
— 1 < a < 4	1/2
4 < a < 8	5/2
8 < a < 12	9/2
12 < a < 16	13/2

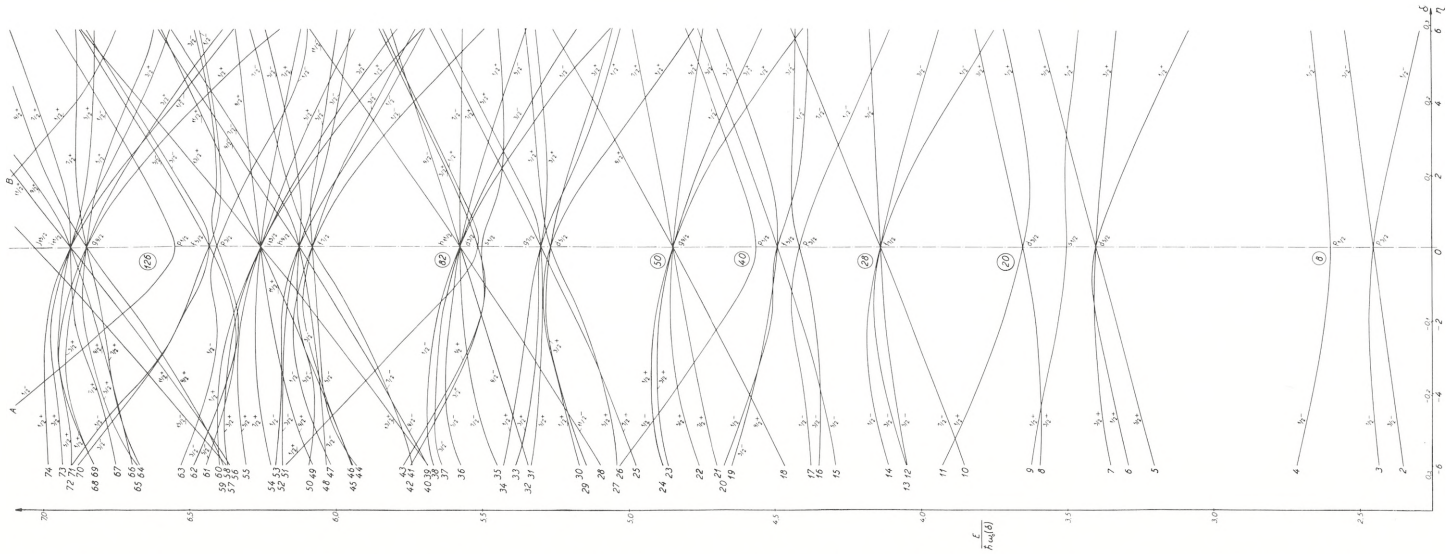


Fig. 5. Energy levels of the model as functions of the deformation. There is a scale for both of the deformation variables γ and δ . To first order δ equals the deformation parameter β used in the papers of A. BOHR and B. MOTTELSON. The energy is plotted in the A- and δ -dependent energy unit $\propto \hbar\omega_0(\delta)$, where $\hbar\omega_0$ varies with A as $A^{-1/3}$. Further, for $A \approx 100$ one expects $\hbar\omega_0 \approx 8.8$ MeV. The constant α is chosen equal to 0.05 in the diagram. The levels are labelled by the Ω -number and the parity. The numbers to the left of the curves refer to Table 1.

Det Kongelige Danske Videnskabernes Selskab

Matematisk-fysiske Meddelelser, bind **29**, nr. 17

Dan. Mat. Fys. Medd. **29**, no. 17 (1955)

FOURTH ORDER VACUUM POLARIZATION

BY

G. KÄLLÉN AND A. SABRY



København 1955

i kommission hos Ejnar Munksgaard

CONTENTS

	Page
I. Introduction.....	3
II. General outline of the method.....	4
III. Discussion of the part $\Pi_a^{(3)}(p^2)$	9
IV. The real part of the vacuum polarization kernel.....	14
Appendix.....	17

The real and imaginary parts of the kernel for the fourth order vacuum polarization are calculated for all values of the four-dimensional energy momentum vector. If an expansion in powers of the square of this quantity is used, the first coefficient agrees with a result previously obtained by BARANGER *et. al.*

I. Introduction.

In a previous paper, one of us¹ has developed a formulation of renormalized quantum electrodynamics that is slightly different from the standard techniques used by most authors. This modification was introduced because of its convenience in discussions of general principles. It has been applied, for example, to a discussion, avoiding perturbation theory, of the magnitude of the renormalization constants.² In the present paper, we wish to show that the new method can also be used with advantage in practical calculations in which perturbation theory is applied, and, as an illustration, the fourth order vacuum polarization has been chosen. BARANGER, DYSON and SALPETER³ have computed those terms in this effect which are important in the Lamb shift. They present, however, only the result and very few intermediary steps of the calculation. On the other hand, we attempt to give a fairly detailed account of our calculations, and compute not only the terms of immediate experimental interest, but also the complete vacuum polarization kernel as a function of the four-dimensional momentum. As will be seen later, our calculation is simplified to a certain extent by the fact that we can use the result of an earlier calculation of the lowest-order radiative corrections to the current operator⁴ and thereby avoid some

¹ G. KÄLLÉN, *Helv. Phys. Acta* **25**, 417 (1952), in the following quoted as I.

² G. KÄLLÉN, *Dan. Mat. Fys. Medd.* **27**, no. 12 (1953).

³ M. BARANGER, F. J. DYSON, and E. E. SALPETER, *Phys. Rev.* **88**, 680 (1952).

⁴ J. SCHWINGER, *Phys. Rev.* **76**, 790 (1949).

integrations. Since the main work involved in the calculation of a high-order effect is connected with the integrations over the so-called "Feynman auxiliary variables", a simplification at this point is not without interest. A further advantage of our method is that the questions of regularization¹ and of the so-called "overlapping divergences"² are completely avoided. Finally, due to the application of the known expression for the current operator, we need not carry out any explicit mass renormalization in our calculations.

II. General Outline of the Method.

We start from the following formulae given in I:

$$\langle 0 | j_{\mu}^{\text{ind}}(x) | 0 \rangle = \frac{1}{(2\pi)^4} \int dp e^{ipx} (-\bar{\Pi}(p^2) + \bar{\Pi}(0) - i\pi \varepsilon(p) \Pi(p^2)) j_{\mu}^{\text{ext}}(p), \quad (1)$$

$$\bar{\Pi}(p^2) - \bar{\Pi}(0) = -p^2 \int_0^{\infty} \frac{da \Pi(-a)}{a(a+p^2)}, \quad (2)$$

$$\Pi(p^2) = \frac{V}{-3p^2} \sum_{p^{(\varepsilon)}=p} \langle 0 | j_{\mu} | z \rangle \langle z | j_{\mu} | 0 \rangle. \quad (3)$$

The notation is the same as in I and will be used here without further explanation. If the matrix elements of the current operator are expanded in powers of e ,

$$j_{\mu} = e j_{\mu}^{(0)} + e^2 j_{\mu}^{(1)} + e^3 j_{\mu}^{(2)} + \dots, \quad (4)$$

the first non-vanishing contribution to the function $\Pi(p^2)$ will be

$$\Pi^{(0)}(p^2) = \frac{Ve^2}{-3p^2} \sum_{p^{(\varepsilon)}=p} \langle 0 | j_{\mu}^{(0)} | z \rangle \langle z | j_{\mu}^{(0)} | 0 \rangle. \quad (5)$$

¹ W. PAULI and F. VILLARS, *Rev. Mod. Phys.* **21**, 434 (1949). The regularization of the fourth order vacuum polarization has been discussed by E. KARLSON, *Arkiv f. Fysik* **7**, 221 (1954).

² A. SALAM, *Phys. Rev.* **82**, 217 (1951). For the special problem of fourth order vacuum polarization, the overlapping divergences have been discussed by R. JOST and J. M. LUTTINGER, *Helv. Phys. Acta* **23**, 201 (1949).

This expression can be computed easily and gives

$$\Pi^{(0)}(p^2) = \frac{e^2}{12\pi^2} \left(1 - \frac{2m^2}{p^2}\right) \sqrt{1 + \frac{4m^2}{p^2}} \theta(-p^2 - 4m^2), \quad (6)$$

$$\theta(x) = \frac{1}{2} \left[1 + \frac{x}{|x|} \right], \quad (6a)$$

$$\left. \begin{aligned} & \bar{\Pi}^{(0)}(p^2) - \bar{\Pi}^{(0)}(0) = \\ & - \frac{e^2}{12\pi^2} \left[\frac{4m^2}{p^2} - \frac{5}{3} + \left(1 - \frac{2m^2}{p^2}\right) \sqrt{1 + \frac{4m^2}{p^2}} \log \frac{1 + \sqrt{1 + \frac{4m^2}{p^2}}}{1 - \sqrt{1 + \frac{4m^2}{p^2}}} \right]. \end{aligned} \right\} \quad (7)$$

The subsequent term in the expansion of the function $\Pi(p^2)$ is of order e^4 , and contains the following terms:

$$\Pi^{(1)}(p^2) = \Pi_a^{(1)}(p^2) + \Pi_b^{(1)}(p^2), \quad (8)$$

$$\Pi_a^{(1)}(p^2) = \frac{Ve^4}{-3p^2} \sum_{p^{(2)}=p} \langle 0 | j_\mu^{(1)} | z \rangle \langle z | j_\mu^{(1)} | 0 \rangle, \quad (9)$$

$$\Pi_b^{(1)}(p^2) = \frac{Ve^4}{-3p^2} \sum_{p^{(2)}=p} \langle 0 | j_\mu^{(2)} | z \rangle \langle z | j_\mu^{(0)} | 0 \rangle + \text{complex conjugate.} \quad (10)$$

The expansion of the current operator has been computed earlier.¹ From these results it can be seen that the term (9) gets contributions from states with one in-coming pair and one in-coming photon.² These matrix elements are

$$\left. \begin{aligned} \langle 0 | j_\mu^{(1)} | q, q', k \rangle &= \frac{e^2}{V^{3/2} \sqrt{2\omega}} \bar{u}^{(-)}(-q') \left[\gamma_\mu \frac{i\gamma(q+k) - m}{2qk - \mu^2} \gamma e \right. \\ & \left. - \gamma e \frac{i\gamma(q'+k) + m}{2q'k - \mu^2} \gamma_\mu \right] u^{(+)}(q). \end{aligned} \right\} \quad (11)$$

The notation in the last expression is self-explanatory, except possibly for the quantities $u^{(\pm)}(q)$. These are the normalized

¹ Cf., e. g., G. KÄLLÉN, Arkiv f. Fysik 2, 371 (1950).

² For the definition of particle numbers for these physical states, cf., e. g., G. KÄLLÉN, Physica 19, 850 (1953).

plane-wave solutions of the free-particle Dirac equation. The index (+) refers to solutions with positive energy and the index (−) to solutions with negative energy. The vector e is the polarization vector of the photon; V is the volume of periodicity and μ a small photon mass introduced to handle infrared divergences. In the computation of the function $\Pi_a^{(1)}(p^2)$, we must “square” the expression (11) and sum over all states where $k + q + q' = p$. Using well-known properties of the functions u , and taking the limit $V \rightarrow \infty$, we can write this sum as an integral

$$\begin{aligned}
 & e^4 V \sum_{q+q'+k=p} \langle 0 | j_\mu^{(1)} | q, q', k \rangle \langle k, q', q | j_\mu^{(1)} | 0 \rangle = \\
 & - \frac{e^4}{(2\pi)^6} \int dk dq dq' \delta(p - q - q' - k) \delta(q^2 + m^2) \theta(q) \delta(q'^2 + m^2) \theta(q') \\
 & \times \delta(k^2 + \mu^2) \theta(k) Sp \left[(i\gamma q' + m) \left(\gamma_\mu \frac{i\gamma(q+k) - m}{2qk - \mu^2} \gamma_\lambda \right. \right. \\
 & \left. \left. - \gamma_\lambda \frac{i\gamma(q'+k) + m}{2q'k - \mu^2} \gamma_\mu \right) (i\gamma q - m) \left(\gamma_\mu \frac{i\gamma(q'+k) + m}{2q'k - \mu^2} \gamma_\lambda \right. \right. \\
 & \left. \left. - \gamma_\lambda \frac{i\gamma(q+k) - m}{2qk - \mu^2} \gamma_\mu \right) \right].
 \end{aligned} \tag{12}$$

The evaluation of this integral, which is the main task in our computation, is given in a later paragraph.

The first approximation to the current, $j_\mu^{(0)}$, has matrix elements which connect the vacuum only to states with one incoming pair. Hence, the expression (10) will reduce to a sum over states with one in-coming pair

$$\Pi_b^{(1)}(p^2) = \frac{Ve^4}{-3p^2} \sum_{q+q'=p} \langle 0 | j_\mu^{(2)} | q, q' \rangle \langle q', q | j_\mu^{(0)} | 0 \rangle + \text{complex conjugate}. \tag{1}$$

As has been mentioned in the introduction, the matrix elements $\langle 0 | j_\mu^{(2)} | q, q' \rangle$ have been computed by SCHWINGER.¹ We write his result as

$$\begin{aligned}
 e^2 \langle 0 | j_\mu^{(2)} | q, q' \rangle = & \left[-\bar{\Pi}^{(0)}(p^2) + \bar{\Pi}^{(0)}(0) + \bar{R}(p^2) - \bar{R}(0) + \bar{S}(0) - i\pi(\Pi^{(0)}(p^2) \right. \\
 & \left. - R(p^2)) \right] \langle 0 | j_\mu^{(0)} | q, q' \rangle - \frac{1}{2m} (q_\mu - q'_\mu) [\bar{S}(p^2) + i\pi S(p^2)] \langle 0 | \bar{\psi}^{(0)} \psi^{(0)} | q, q' \rangle,
 \end{aligned} \tag{1}$$

¹ Footnote 4, p. 3.

$$R(p^2) = \frac{e^2}{8\pi^2} \left\{ \frac{1 + \frac{2m^2}{p^2}}{1 + \frac{4m^2}{p^2}} \log \left(-\frac{p^2 + 4m^2}{\mu^2} \right) - \frac{3}{2} \sqrt{1 + \frac{4m^2}{p^2}} \theta(-p^2 - 4m^2), \right. \quad (15)$$

$$\begin{aligned} \bar{R}(p^2) - \bar{R}(0) = & \frac{e^2}{4\pi^2} \left[\frac{1 + \frac{2m^2}{p^2}}{\sqrt{1 + \frac{4m^2}{p^2}}} \left[-\Phi \left(\frac{1 - \sqrt{1 + \frac{4m^2}{p^2}}}{1 + \sqrt{1 + \frac{4m^2}{p^2}}} \right) + \frac{\pi^2}{4} \theta(-p^2) \right. \right. \\ & \left. \left. - \frac{1}{4} \log^2 \left[\frac{1 + \sqrt{1 + \frac{4m^2}{p^2}}}{1 - \sqrt{1 + \frac{4m^2}{p^2}}} \right] + \log \left[\frac{1 + \sqrt{1 + \frac{4m^2}{p^2}}}{1 - \sqrt{1 + \frac{4m^2}{p^2}}} \right] \cdot \log \frac{2\sqrt{1 + \frac{4m^2}{p^2}}}{1 + \sqrt{1 + \frac{4m^2}{p^2}}} \right] \right. \\ & \left. + \frac{3}{4} \left[\sqrt{1 + \frac{4m^2}{p^2}} \log \frac{1 + \sqrt{1 + \frac{4m^2}{p^2}}}{\left| 1 - \sqrt{1 + \frac{4m^2}{p^2}} \right|} - 2 \right] \right. \\ & \left. + \log \frac{m}{\mu} \left[1 - \frac{1 + \frac{2m^2}{p^2}}{\sqrt{1 + \frac{4m^2}{p^2}}} \log \frac{1 + \sqrt{1 + \frac{4m^2}{p^2}}}{\left| 1 - \sqrt{1 + \frac{4m^2}{p^2}} \right|} \right] \right\}, \quad (16) \end{aligned}$$

$$S(p^2) = -\frac{e^2}{4\pi^2} \frac{m^2 \theta(-p^2 - 4m^2)}{p^2 \sqrt{1 + \frac{4m^2}{p^2}}}, \quad (17)$$

$$\bar{S}(p^2) = \frac{e^2}{8\pi^2} \frac{2\frac{m^2}{p^2} \log \frac{1 + \sqrt{1 + \frac{4m^2}{p^2}}}{\left| 1 - \sqrt{1 + \frac{4m^2}{p^2}} \right|}}{\sqrt{1 + \frac{4m^2}{p^2}}}. \quad (18)$$

The connection between the functions $R(p^2)$ and $\bar{R}(p^2)$, and between $S(p^2)$ and $\bar{S}(p^2)$, is the same as the connection between $\Pi(p^2)$ and $\bar{\Pi}(p^2)$, which is given in Eq. (2). This is a consequence of the "causal" structure of the theory which says that the value of the current in one point x can depend only on the

previous history of the system inside the retarded light-cone belonging to x . If Eq. (14) is written in x -space, we get a relation of the form

$$\left. \begin{aligned} \langle 0 | j_{\mu}^{(2)}(x) | q, q' \rangle &= \int dx' F(x-x') \langle 0 | j_{\mu}^{(0)}(x') | q, q' \rangle \\ + \int G(x-x') \langle 0 | \frac{\partial \bar{\psi}^{(0)}(x')}{\partial x'_{\mu}} \psi^{(0)}(x') - \bar{\psi}^{(0)}(x') \frac{\partial \psi^{(0)}(x')}{\partial x'_{\mu}} | q, q' \rangle. \end{aligned} \right\} \quad (14a)$$

Causality requires $F(x)$ and $G(x)$ to vanish if $x_0 < 0$ and this gives, in a well-known way, the relations involving the Hilbert transformations. This offers a new possibility of computing the matrix element under discussion by first computing the "imaginary parts" $R(p^2)$ and $S(p^2)$, which can be obtained by integrating over finite domains in momentum space and, subsequently, computing the "real parts" with the aid of Hilbert transformations. Actually, a calculation of this kind has been performed. However, it has not been found to be much simpler than the standard methods for this problem. On the other hand, arranging the computation in this way is certainly not a more complicated procedure. We will not insist on this point here, but accept the results (14) — (18) as they stand. Consequently, the computation of the function $\Pi_b^{(1)}(p^2)$ will be reduced to simple algebraic manipulations of these expressions. The function $\Phi(x)$ in (16) is defined by the integral

$$\Phi(x) = \int_1^x \frac{dt}{t} \log |1+t|. \quad (19)$$

Hereby it is supposed that the argument x is real, *i. e.* that $1 + \frac{4m^2}{p^2} > 0$. This will be sufficient at this stage. The integral $\Phi(x)$ has many interesting properties which will be of some use in our calculation and that are discussed in the Appendix.

We now write the function $\Pi_b^{(1)}(p^2)$ as

$$\left. \begin{aligned} \Pi_b^{(1)}(p^2) &= 2 \Pi^{(0)}(p^2) [-\bar{\Pi}^{(0)}(p^2) + \bar{\Pi}^{(0)}(0) + \bar{R}(p^2) \\ &\quad - \bar{R}(0) + \bar{S}(0)] + 2 \bar{S}(p^2) X(p^2), \end{aligned} \right\} \quad (20)$$

where

$$X(p^2) = \left. \begin{aligned} & \frac{4e^2}{3 p^2} \frac{1}{(2\pi)^3} \int dq dq' \delta(p-q-q') \\ & \times \delta(q^2+m^2) \theta(q) \delta(q'^2+m^2) \theta(q') (qq'+m^2). \end{aligned} \right\} \quad (21)$$

The last expression is easily computed

$$X(p^2) = \frac{e^2}{24 \pi^2} \left(1 + \frac{4 m^2}{p^2}\right)^{3/2} \theta(-p^2 - 4 m^2). \quad (22)$$

Collecting all these results, we have

$$\left. \begin{aligned} I_b^{(1)}(p^2) = & \frac{e^4}{48 \pi^4} \left[\frac{\delta}{3} (3 - \delta^2) \left(-\frac{17}{3} + \delta^2 \right) + \frac{\delta^2}{2} \left(7 - 3 \delta^2 + \frac{1}{3} \delta^4 \right) \log \frac{1+\delta}{1-\delta} \right. \\ & - \log \frac{m}{\mu} \delta (3 - \delta^2) \left(1 - \frac{1+\delta^2}{2\delta} \log \frac{1+\delta}{1-\delta} \right) - \frac{1}{2} (3 - \delta^2) (1 + \delta^2) \left(\Phi \left(-\frac{1-\delta}{1+\delta} \right) \right. \\ & \left. \left. - \frac{\pi^2}{4} + \frac{1}{4} \log^2 \frac{1+\delta}{1-\delta} - \log \frac{1+\delta}{1-\delta} \cdot \log \frac{1+\delta}{2\delta} \right) \right] \theta(1-\delta), \end{aligned} \right\} \quad (23)$$

where

$$\delta = \sqrt{1 + \frac{4 m^2}{p^2}} > 0. \quad (24)$$

III. Discussion of the Part $\Pi_a^{(1)}(p^2)$.

The remaining part of the function $\Pi(p^2)$, the integral (12), can be treated in the following way. We first compute the trace of the γ -matrices. This is a straightforward calculation and the necessary work can be considerably reduced by performing first the summations over the indices μ and λ . This can be done with the aid of the well-known formulae

$$\gamma_\lambda \gamma_{v_1} \gamma_{v_2} \cdots \gamma_{v_{2n+1}} \gamma_\lambda = -2 \gamma_{v_{2n+1}} \cdots \gamma_{v_2} \gamma_{v_1} \quad (25)$$

$$\gamma_\lambda \gamma_{v_1} \gamma_{v_2} \gamma_\lambda = 4 \delta_{v_1 v_2}. \quad (26)$$

The complete trace can then be written

$$Sp [\dots] = \frac{S^{(1)}(q, q')}{(2qk - \mu^2)^2} + \frac{S^{(1)}(q', q)}{(2q'k - \mu^2)^2} + \frac{S^{(2)}(q, q') + S^{(2)}(q', q)}{(2qk - \mu^2)(2q'k - \mu^2)}, \quad (27)$$

$$S^{(1)}(q, q') = -32 [kq \cdot kq' + 2m^2 qk + m^2 q'k + m^2 (qq' - 2m^2)], \quad (28)$$

$$S^{(2)}(q, q') = -16 [2(qq')^2 - 4m^2 \cdot qq' + 2(kq + kq')qq' - m^2(kq + kq')]. \quad (29)$$

Terms containing μ^2 have been dropped in (28) and (29), as they will obviously vanish in the limit $\mu \rightarrow 0$.

Our next task is to compute an integral of the form

$$J = \int dk dq dq' \delta(p - k - q - q') \delta(q^2 + m^2) \delta(q'^2 + m^2) \delta(k^2 + \mu^2) \left. \begin{array}{l} \\ \times \theta(q) \theta(q') \theta(k) F(qk, q'k, qq'). \end{array} \right\} \quad (30)$$

This can conveniently be done in two steps. We first consider

$$I(p'^2, kp') = \int dq \delta(q^2 + m^2) \theta(q) \delta((p' - q)^2 + m^2) \theta(p' - q) \left. \begin{array}{l} \\ \times F(qk, p'k - qk, p'q - q^2). \end{array} \right\} \quad (31)$$

This is a *finite* integral and we compute it in the special coordinate system where the space-like components of the vector p' vanish. We then obtain

$$I(-p_0'^2, -k_0 p_0') = \pi \int_{x_1}^{x_2} \frac{dx}{2p_0' |\bar{k}|} F\left(x, -k_0 p_0' - x, m^2 - \frac{1}{2} p_0'^2\right) \theta(p_0'^2 - 4m^2), \quad (32)$$

$$x_{1,2} = -\frac{1}{2} k_0 p_0' \mp |\bar{k}| \sqrt{\frac{1}{4} p_0'^2 - m^2}. \quad (32a)$$

We now write this result in an invariant way, as

$$I(p'^2, kp') = \frac{\pi}{2\sqrt{(kp')^2 + \mu^2 p'^2}} \int_{x_1}^{x_2} dx F\left(x, kp' - x, m^2 + \frac{1}{2} p'^2\right) \theta(-p'^2 - 4m^2), \quad (33)$$

$$x_{1,2} = \frac{1}{2}kp' \mp \frac{1}{2}\sqrt{(kp')^2 + \mu^2 p'^2} \cdot \sqrt{1 + \frac{4m^2}{p'^2}}, \quad (33a)$$

and treat the next integration similarly. The result is

$$J = \int dk \delta(k^2 + \mu^2) \theta(k) I((p-k)^2, kp + \mu^2) = \left. \begin{aligned} & -\frac{\pi^2}{2p^2} \int_{\mu\sqrt{-p^2}}^{-\frac{1}{2}(p^2+4m^2)} dy \int_{-\xi}^{+\xi} dz F\left(\frac{z-y+\mu^2}{2}, \frac{-z-y+\mu^2}{2}, y+m^2 + \frac{p^2-\mu^2}{2}\right), \\ & \xi = \sqrt{1 + \frac{4m^2}{p^2-\mu^2+2y}} \cdot \sqrt{y^2 + \mu^2 p^2}. \end{aligned} \right\} \quad (34)$$

Applying this technique to the integral (12), we get

$$H_a^{(1)}(p^2) = \frac{e^2}{12\pi^4 p^4} (A + B) \theta(-p^2 - 4m^2), \quad (35)$$

$$A = \int_{\mu\sqrt{-p^2}}^{-\frac{1}{2}(p^2+4m^2)} dy \int_{-\xi}^{+\xi} dz \left[-\frac{1}{2} + \frac{m^2-y}{z-y} + \frac{y}{y^2-z^2} (p^2-m^2) \right], \quad (36)$$

$$B = \int_{\mu\sqrt{-p^2}}^{-\frac{1}{2}(p^2+4m^2)} dy \int_{-\xi}^{+\xi} dz (p^2-2m^2) \left[\frac{m^2}{(z-y)^2} + \frac{1}{2} \frac{p^2+2m^2}{y^2-z^2} \right]. \quad (37)$$

To obtain these expressions, we have introduced the quantities y and z into (27), which becomes

$$Sp [\dots] = -32 \left\{ \begin{aligned} & -\frac{1}{2} + \frac{m^2-y}{z-y} + \frac{m^2(p^2-2m^2)}{(z-y)^2} \\ & + \frac{1}{y^2-z^2} \left(y(p^2-m^2) + \frac{1}{2}(p^4-4m^4) \right) \end{aligned} \right\} \quad (38)$$

The quantity A will stay finite in the limit $\mu \rightarrow 0$ and can be expressed in elementary functions. After some straightforward calculations we get the result

$$A = \frac{3}{64} p^4 \left[2\delta (5 - 3\delta^2) - (5 + 6\delta^2 - 3\delta^4) \log \frac{1 + \delta}{1 - \delta} \right]. \quad (39)$$

The quantity B is a little more tricky to handle and the limit $\mu \rightarrow 0$ cannot be performed in all terms. We write (37) as

$$B = \frac{1}{8} p^4 (3 - \delta^2) [-(1 - \delta^2) B^{(1)} + (1 + \delta^2) B^{(2)}], \quad (40)$$

where

$$B^{(1)} = 2 I(1), \quad (41)$$

$$B^{(2)} = \int_{-1}^{+1} I(z) dz, \quad (42)$$

$$I(z) = \int_{\mu \sqrt{1-p^2}}^{-\frac{p^2}{2} \xi} \frac{\delta dy}{y^2 - \xi^2 z^2} = \int_{\varepsilon}^{\delta^2} dy \frac{\sqrt{y^2 - \varepsilon^2} \sqrt{1 - \frac{1 - \delta^2}{1 - y}}}{y^2 - z^2 (y^2 - \varepsilon^2)} \left[1 - \frac{1 - \delta^2}{1 - y} \right], \quad (43)$$

$$\varepsilon = \frac{2\mu}{\sqrt{1-p^2}}. \quad (43a)$$

The term containing the logarithmic dependence on μ in $I(z)$ can be split off in the following way:

$$I(z) = \int_{\varepsilon}^{\delta^2} \frac{\sqrt{y^2 - \varepsilon^2} \cdot \delta dy}{y^2 - \delta^2 z^2 (y^2 - \varepsilon^2)} + \int_0^{\delta^2} \frac{dy}{y} \left[\frac{\sqrt{1 - \frac{1 - \delta^2}{1 - y}}}{1 - z^2 \left(1 - \frac{1 - \delta^2}{1 - y} \right)} - \frac{\delta}{1 - \delta^2 z^2} \right]. \quad (44)$$

In the first integral, we make the transformation $1 - \frac{\varepsilon^2}{y^2} = t^2$ and rewrite it as

$$\left. \begin{aligned} & \int_{\varepsilon^2}^{\delta^2} \frac{dy}{y} \frac{\delta \cdot \sqrt{1 - \varepsilon^2/y^2}}{1 - z^2 \delta^2 (1 - \varepsilon^2/y^2)} = \frac{\delta}{1 - z^2 \delta^2} \int_0^{\sqrt{1 - \varepsilon^2/\delta^2}} \frac{dt}{1 - t} \\ & + \delta \int_0^1 \frac{dt}{1 - t} \left[\frac{2t^2}{(1+t)(1 - z^2 \delta^2 t^2)} - \frac{1}{1 - z^2 \delta^2} \right]. \end{aligned} \right\} \quad (45)$$

The remaining integrations can now be performed without difficulty, and $I(z)$ is found to be

$$I(z) = \frac{1}{1-z^2} \left(z \log \frac{1+\delta z}{1-\delta z} - \log \frac{1+\delta}{1-\delta} \right) - \left(\frac{1}{2z} + \frac{3\delta^2 z}{2(1-\delta^2 z^2)} \right) \log \frac{1+\delta z}{1-\delta z} + \frac{\delta}{1-\delta^2 z^2} \log_{\varepsilon} \frac{8\delta^2}{(1-\delta^2)}. \quad (46)$$

The last integration in (42) introduces again the function $\Phi(x)$. With the aid of the formulae given in the Appendix we can write the result as

$$I^{(2)} = -3\Phi\left(-\frac{1-\delta}{1+\delta}\right) - 2\Phi\left(\frac{1-\delta}{1+\delta}\right) - \frac{3}{4}\pi^2 + \log \frac{1+\delta}{1-\delta} \left[\log \frac{m}{\mu} + \frac{1}{4} \log \frac{1+\delta}{1-\delta} + \log \frac{(1+\delta)^2}{4\delta} \right]. \quad (47)$$

The remaining part of the calculation is purely algebraic in nature. Collecting previous results, we get

$$I_a^{(1)}(p^2) = \frac{e^4}{48\pi^4} \left[\frac{\delta}{8}(39-17\delta^2) + \frac{1}{16}(33-10\delta^2+\delta^4) \log \frac{1+\delta}{1-\delta} - \frac{\delta}{2}(3-\delta^2) \log \frac{64\delta^4}{(1-\delta^2)^3} - \delta(3-\delta^2) \left[1 - \frac{1+\delta^2}{2\delta} \log \frac{1+\delta}{1-\delta} \right] \cdot \log \frac{m}{\mu} - \frac{(3-\delta^2)(1+\delta^2)}{2} \left(3\Phi\left(-\frac{1-\delta}{1+\delta}\right) + 2\Phi\left(\frac{1-\delta}{1+\delta}\right) + \frac{3}{4}\pi^2 - \frac{1}{4} \log^2 \frac{1+\delta}{1-\delta} - \log \frac{1+\delta}{1-\delta} \log \frac{(1+\delta)^2}{4\delta} \right) \right] \theta(1-\delta). \quad (48)$$

Adding (48) and (23), we find that the terms depending on μ cancel. In this way we obtain

$$I^{(1)}(p^2) = \frac{\alpha^2}{3\pi^2} \left\{ \delta \left[-\frac{19}{24} + \frac{55}{72}\delta^2 - \frac{\delta^4}{3} - \frac{3-\delta^2}{2} \log \frac{64\delta^4}{(1-\delta^2)^3} \right] + \log \frac{1+\delta}{1-\delta} \left[\frac{33}{16} + \frac{23}{8}\delta^2 - \frac{23}{16}\delta^4 + \frac{1}{6}\delta^6 + \left(\frac{3}{2} + \delta^2 - \frac{\delta^4}{2} \right) \log \frac{(1+\delta)^3}{8\delta^2} \right] + \left(\frac{3}{2} + \delta^2 - \frac{1}{2}\delta^4 \right) \left[4\Phi\left(-\frac{1-\delta}{1+\delta}\right) + 2\Phi\left(\frac{1-\delta}{1+\delta}\right) + \frac{\pi^2}{2} \right] \right\} \theta(1-\delta), \quad (49)$$

$$\alpha = \frac{e^2}{4\pi}. \quad (49a)$$

This is our expression for the imaginary part of the kernel (1). According to (2), the real part is obtained after a Hilbert transformation of this expression. This will be discussed in the next paragraph.

IV. The Real Part of the Vacuum Polarization Kernel.

So far, all our results are given as functions of the quantity δ defined in (24). It is therefore convenient to introduce a new variable of integration instead of a in (2). If we put

$$1 - \frac{4m^2}{a} = z^2, \quad (50)$$

we get

$$\bar{H}^{(1)}(p^2) - \bar{H}^{(1)}(0) = 2 \int_0^1 \frac{z dz}{z^2 - \delta^2} H^{(1)}(\delta = z). \quad (51)$$

Not all the integrations in (51) can be carried out explicitly, with the result expressed by elementary functions or by the function $\Phi(x)$. The new integrals which appear can be written in the standard form

$$F(x, y) = \int_0^1 \frac{dt}{t} \log |1 + xt| \cdot \log |1 + yt|. \quad (52)$$

All the necessary integrals over the function $\Phi(x)$ can be expressed in terms of this $F(x, y)$

$$P \int_0^a \frac{dz}{z+b} \Phi(z) = \Phi(a) \log \left| 1 + \frac{a}{b} \right| - F\left(a, \frac{a}{b}\right). \quad (53)$$

In our final result, one of the variables in $F(x, y)$ has only a very small number (three) of different values. We therefore introduce the following three integrals, each of which depends on only one variable:

$$F(x) = \int_{-1}^{+1} \frac{dt}{t} \log(1+t) \log \left| 1 - \frac{t^2}{x} \right|, \tag{54}$$

$$G(x) = \int_{-1}^{+1} \frac{dt}{1+t} \log \frac{1-t}{2} \cdot \log \left| 1 - \frac{t^2}{x} \right|, \tag{55}$$

$$H(x) = \int_{-1}^{+1} \frac{dt}{1+t} \log |t| \log \left| 1 - \frac{t^2}{x} \right|. \tag{56}$$

The remaining integrations are then straightforward, and not too time consuming. The result can be written as

$$\left. \begin{aligned} \overline{\Pi}^{(1)}(p^2) - \overline{\Pi}^{(1)}(0) = & \frac{\alpha^2}{3\pi^2} \left\{ -\frac{13}{108} + \frac{11}{72} \delta^2 - \frac{1}{3} \delta^4 + \delta \left(\frac{19}{24} - \frac{55}{72} \delta^2 \right. \right. \\ & \left. \left. + \frac{1}{3} \delta^4 \right) \log \frac{1+\delta}{|1-\delta|} - \left(\frac{33}{32} + \frac{23}{16} \delta^2 - \frac{23}{32} \delta^4 + \frac{\delta^6}{12} \right) \left(\log^2 \frac{1+\delta}{|1-\delta|} - \pi^2 \theta(1-\delta) \right) \right. \\ & \left. + \delta(3-\delta^2) \left[\Phi \left(\frac{1-\delta}{1+\delta} \right) + 2 \Phi \left(-\frac{1-\delta}{1+\delta} \right) + \frac{\pi^2}{4} - \frac{3}{4} \pi^2 \theta(1-\delta) \right. \right. \\ & \left. \left. - \frac{3}{4} \log^2 \frac{1+\delta}{|1-\delta|} + \frac{1}{2} \log \frac{1+\delta}{|1-\delta|} \log \frac{64 \delta^4}{|1-\delta^2|^3} \right] \right. \\ & \left. + (3 + 2\delta^2 - \delta^4) \left[F(\delta^2) + \frac{3}{2} G(\delta^2) - H(\delta^2) \right] \right\}. \tag{57} \end{aligned}$$

If this expression is expanded in powers of δ^{-1} , the first non-vanishing term will be of order δ^{-2} . The same conclusion can also be obtained from a study of Eq. (51). If this expression is expanded in powers of δ^{-1} , we get immediately

$$\overline{\Pi}^{(1)}(p^2) - \overline{\Pi}^{(1)}(0) = -\frac{2}{\delta^2} \int_{-1}^{+1} z dz \Pi^{(1)}(\delta = z) + \dots \tag{58}$$

The numerical coefficient of the first power of δ^{-2} has been computed from Eq. (57) and with the aid of the integration indicated in Eq. (58). The agreement of the results serves as a check on the calculations. In either way we obtain

$$\bar{\Pi}^{(1)}(p^2) - \bar{\Pi}^{(1)}(0) = -\frac{1}{\delta^2} \cdot \frac{\alpha^2}{\pi^2} \cdot \frac{82}{81} + \dots = -\frac{p^2 \alpha^2}{m^2 \pi^2} \frac{41}{162} + \dots \quad (59)$$

This also agrees with the result obtained by BARANGER, DYSON, and SALPETER.¹

In Eq. (57) it is supposed that δ is real, that is, p^2 is either positive or less than $-4 m^2$. For $0 < -p^2 < 4 m^2$, δ will be purely imaginary. In this case we have to substitute arctangent functions for logarithms, according to the following rules:

$$\delta \log \frac{1 + \delta}{|1 - \delta|} \rightarrow 2 \eta \operatorname{arctang} \frac{1}{\eta}, \quad (\eta = i \delta > 0), \quad (60 \text{ a})$$

$$\log^2 \frac{1 + \delta}{|1 - \delta|} - \pi^2 \theta(1 - \delta) \rightarrow -4 \operatorname{arctang}^2 \frac{1}{\eta}, \quad (60 \text{ b})$$

$$\left. \begin{aligned} & \delta \left[\Phi \left(\frac{1 - \delta}{1 + \delta} \right) + 2 \Phi \left(-\frac{1 - \delta}{1 + \delta} \right) + \frac{\pi^2}{4} - \frac{3}{4} \pi^2 \theta(1 - \delta) - \frac{3}{4} \log^2 \frac{1 + \delta}{|1 - \delta|} \right. \\ & \left. + \frac{1}{2} \log \frac{1 + \delta}{|1 - \delta|} \log \frac{64 \delta^4}{|1 - \delta^2|^3} \right] \rightarrow \eta \left[\psi \left(2 \operatorname{arctang} \frac{1}{\eta} \right) - 2 \psi(2 \operatorname{arctang} \eta) \right. \\ & \left. + \operatorname{arctg} \frac{1}{\eta} \log \frac{64 \eta^4}{(1 + \eta^2)^3} \right], \end{aligned} \right\} \quad (60 \text{ c})$$

$$\psi(x) = \sum_1^{\infty} \frac{\sin(nx)}{n^2}. \quad (60 \text{ d})$$

At the point $p^2 = -4 m^2$, or $\delta = 0$, the expression (57) has a logarithmic singularity. If, during the calculation, the photon mass μ had been kept different from zero in *all* places, our result would have shown a finite peak at this point. For practical applications, the weak logarithmic infinity will not be very harmful, as one is in general interested in convolution integrals involving the function $\bar{\Pi}(p^2) - \bar{\Pi}(0)$. In such expressions, the result (57) will be sufficient. For large values of $|p^2/m^2|$, our function behaves as $\log^2 |p^2/m^2|$. Fig. 1 gives a qualitative idea of the behaviour of the fourth approximation of the vacuum polarization kernel as a function of $-p^2/m^2$. A figure of the corresponding behaviour of the functions $\bar{\Pi}^{(0)}(p^2)$ and $\bar{\Pi}^{(0)}(p^2) - \bar{\Pi}^{(0)}(0)$ would be rather

¹ Footnote 3, page 3.

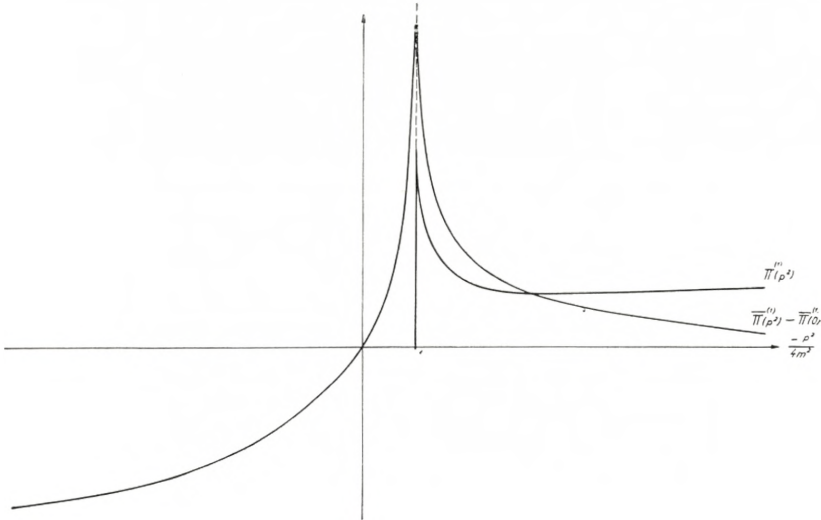


Fig. 1. Qualitative behaviour of the e^4 approximation of the real and of the imaginary parts of the vacuum polarization kernel.

similar to Fig. 1. The only qualitative difference would be that the function $\overline{\Pi}^{(0)}(p^2)$ vanishes at the point $-p^2 = 4m^2$ and that the function $\overline{\Pi}^{(0)}(p^2) - \overline{\Pi}^{(0)}(0)$ has a finite peak at this point.

Appendix.

In the following are given some formulae involving the function $\Phi(x)$, defined in Eq. (19). Although practically all these expressions can be found in the literature,¹ we add this summary for the reader's convenience.

If x is real, our function is defined by

$$\Phi(x) = \int_1^x \frac{dz}{z} \log |1+z|. \tag{A. 1}$$

If we consider

$$\Phi\left(\frac{1}{x}\right) = \int_1^{1/x} \frac{dz}{z} \log |1+z|, \tag{A. 2}$$

¹ Cf., e.g., K. MITCHELL, Phil. Mag. **40**, 351 (1949) and W. GRÖBNER, N. HOFREITER, Integraltafeln, Wien and Innsbruck, 1950.

and make the variable transformation $t = z^{-1}$, we get the fundamental relation

$$\left. \begin{aligned} \Phi\left(\frac{1}{x}\right) &= -\int_1^x \frac{dt}{t} \log \left| \frac{1+t}{t} \right| - 2\theta(-x) \int_{-1}^{+1} \frac{dz}{z} \log |1+z| \\ &= -\Phi(x) + \frac{1}{2} \log^2 |x| - \frac{\pi^2}{2} \theta(-x) \end{aligned} \right\} \quad (\text{A. 3})$$

or

$$\Phi(x) + \Phi\left(\frac{1}{x}\right) = \frac{1}{2} \log^2 |x| - \frac{\pi^2}{2} \theta(-x). \quad (\text{A. 4})$$

An integration by parts in the definition (A. 1) will give another useful formula

$$\left. \begin{aligned} \Phi(x) &= \int_1^x \log |z| \log |1+z| - \int_1^x \frac{dz}{1+z} \log |z| \\ &= \log |x| \cdot \log |1+x| - \int_2^{1+x} \frac{dz}{z} \log |1-z|, \end{aligned} \right\} \quad (\text{A. 5})$$

or

$$\Phi(x) + \Phi(-1-x) = -\frac{\pi^2}{3} + \log |x| \cdot \log |1+x|. \quad (\text{A. 6})$$

Besides (A. 4) and (A. 6), we also mention the formula

$$\left. \begin{aligned} \Phi(x) + \Phi(-x) &= \int_1^x \frac{dz}{z} \log |1-z^2| + \int_{-1}^{+1} \frac{dz}{z} \log |1-z| \\ &= \frac{1}{2} \Phi(-x^2) - \frac{\pi^2}{8}. \end{aligned} \right\} \quad (\text{A. 7})$$

Another relation which has been of some use in the calculations can be obtained in the following way:

$$\Phi(x) - \Phi(-x) = \int_1^x \frac{dz}{z} \log \left| \frac{1+z}{1-z} \right| + \frac{\pi^2}{4}. \quad (\text{A. 8})$$

The transformation $1 + t = \frac{1 - z}{1 + z}$ transfers this integral to

$$\left. \begin{aligned} \Phi(x) - \Phi(-x) &= \frac{\pi^2}{4} - \int_{-1}^{-\frac{2x}{1+x}} dt \left[\frac{1}{t} - \frac{1}{2+t} \right] \log |1+t| \\ -\theta(-1-x) \int_{-\infty}^{+\infty} \frac{2 dt}{t(1+t)} \log |1+t| &= \frac{\pi^2}{4} - \pi^2 \theta(-1-x) \\ &\quad - \Phi\left(\frac{-2x}{1+x}\right) + \Phi\left(\frac{-2}{1+x}\right). \end{aligned} \right\} \text{(A. 9)}$$

Using (A. 6), we can write (A. 9) as

$$\left. \begin{aligned} \Phi(x) - \Phi(-x) &= \frac{\pi^2}{4} - \pi^2 \theta(-1-x) + \Phi\left(-\frac{1-x}{1+x}\right) \\ &\quad - \Phi\left(\frac{1-x}{1+x}\right) + \log|x| \cdot \log\left|\frac{1+x}{1-x}\right|. \end{aligned} \right\} \text{(A. 10)}$$

For complex values of x we can still define the function $\Phi(x)$ as the integral (A. 1), making this definition unique with the aid of a cut along the real axis below the point -1 . This function fulfils an equation similar to (A. 4),

$$\Phi(x) + \Phi\left(\frac{1}{x}\right) = \frac{1}{2} \log^2 x, \tag{A. 11}$$

where the definition of the logarithm is made unique by the prescription just mentioned. From (A. 11), we conclude that

$$\operatorname{Re} \Phi(e^{i\vartheta}) = -\frac{1}{4} \vartheta^2. \tag{A. 12}$$

For $|x| \leq 1$, we have the power series expansion

$$\Phi(x) = -\frac{\pi^2}{12} + \sum_1^{\infty} \frac{(-1)^{n+1} \cdot x^n}{n^2}. \tag{A. 13}$$

From (A. 13), it follows that

$$\operatorname{Im} \Phi(-e^{i\vartheta}) = - \sum_1^{\infty} \frac{\sin(n\vartheta)}{n^2} = -\psi(\vartheta). \quad (\text{A. 14})$$

Numerical values of $\Phi(x)$ for real x can be obtained from the paper by MITCHELL. The function $\psi(\vartheta)$ in (A. 14) has been tabulated by CLAUSEN¹.

¹ T. CLAUSEN, Jour. f. Math. (Crelle) 8, 298 (1832).

*CERN (European Organization for Nuclear Research),
Theoretical Study Division, Copenhagen, Denmark
and
Institute for Theoretical Physics, University of Copenhagen.*

Det Kongelige Danske Videnskabernes Selskab

Matematisk-fysiske Meddelelser, bind **29**, nr. 18

Dan. Mat. Fys. Medd. **29**, no. 18 (1955)

MATRIX ELEMENTS
BETWEEN STATES IN THE
COULOMB FIELD

BY

KURT ALDER AND AAGE WINTHER



København 1955

i kommission hos Ejnar Munksgaard

CONTENTS

	Pages
I. Introduction	3
II. Non-relativistic matrix elements	4
III. Recursion formulae	8
IV. Specializations	10
a) Discrete-discrete transitions	10
b) Discrete-continuous transitions	11
c) Continuous-continuous transitions	12
V. Relativistic matrix elements	12
Appendix: Some properties of the generalized hypergeometric function of two variables, F_2	16
References	18

It is shown that the matrix elements between radial eigensolutions in a Coulomb field of functions of the type $r^p \exp(-qr)$ can be expressed explicitly by means of hypergeometric functions of two variables. The calculation is made separately for the non-relativistic and relativistic case. Recursion formulae connecting the matrix elements are discussed and specializations to discrete-discrete, discrete-continuous, and continuous-continuous transitions are given.

I. Introduction.

In quantum mechanical perturbation treatments one often has to evaluate matrix elements between the eigenstates of the Coulomb field. In point of fact, this problem arose as one of the first in wave mechanics in connection with the calculation of the intensity of the hydrogen lines¹.

Other cases where one encounters Coulomb matrix elements are, e. g., the theory of bremsstrahlung, photoeffect, internal conversion, Auger effect, and Coulomb excitation, when one includes the Coulomb interaction in the unperturbed Hamiltonian.

In all these cases the integration over angles can be readily performed, giving the selection rules for the angular momenta. The remaining radial integral is generally of the type

$$\int_0^\infty R_i e^{-qr} r^p R_j^* r^2 dr,$$

where R is the radial eigenfunction in the Coulomb field belonging to either the discrete or the continuous spectrum. For $p = \pm 1$, GORDON² has given general formulae for discrete-discrete, discrete-continuous, and continuous-continuous tran-

sitions. For a positive integer, p , the matrix elements may be obtained by means of recursion formulae. For $p = -2$ and $q = 0$, one may use the equation of motion in the Coulomb field and reduce it to the case $p = 1$. For negative integers, $p < -2$, the matrix elements are more difficult and have until now been calculated only in some special cases of discrete-continuous transitions.

It will be shown here that a quite general explicit expression for Coulomb matrix elements of the above mentioned types can be given.

Section II of this paper is concerned with the derivation of this explicit expression for non-relativistic matrix elements. In the next section, methods will be given by which it is possible to derive recursion formulae connecting different matrix elements of the aforementioned type. Section IV deals with the specializations of the general formulae for the cases of discrete-discrete, discrete-continuous, and continuous-continuous transitions. These expressions embrace the earlier calculations of Gordon and others, corresponding to special choices of the parameters. In the last section, we shall give the exact expression also for the matrix elements with relativistic Coulomb wave functions.

The application of the method introduced here to the theory of Coulomb excitation will be given in a following paper³.

II. Non-Relativistic Matrix Elements.

The non-relativistic eigenfunctions of a particle of charge $Z_1 e$ in a Coulomb potential $\frac{Z_2 e}{r}$ are in spherical coordinates r, θ, φ

$$\Psi_{l, m}(\lambda, r) = N_{\lambda, l} Y_{l, m}(\theta, \varphi) R_l(r/\lambda). \quad (1)$$

$N_{\lambda, l}$ is the normalization factor to be specified later; $Y_{l, m}(\theta, \varphi)$ are the normalized spherical harmonics. The radial wave function $R_l(r/\lambda)$ is a solution of the differential equation

$$\frac{d^2 R_l}{dr^2} + \frac{2}{r} \frac{dR_l}{dr} - \left(\lambda^{-2} + \frac{2}{ar} + \frac{l(l+1)}{r^2} \right) R_l = 0. \quad (2)$$

l and m are the angular momentum quantum numbers. λ^{-2} is connected with the energy E and the mass m of the particle through

$$\lambda^{-2} = -\frac{2m}{\hbar^2} E. \tag{3}$$

The K orbit radius a is given by

$$a = \hbar^2/Z_1 Z_2 m e^2, \tag{4}$$

where Z_1 and Z_2 have the signs of the charges.

The general solution of the radial equation (2) can be expressed by the confluent hypergeometric function ${}_1F_1$ or by the Whittaker function M through*

$$\left. \begin{aligned} R_l(r/\lambda) &= (2r/\lambda)^l e^{-r/\lambda} {}_1F_1(l+1+\lambda/a, 2l+2, 2r/\lambda) \\ &= (2r/\lambda)^{-1} M_{-\lambda/a, l+1/2}(2r/\lambda) \\ &= (-1)^l (-2r/\lambda)^{-1} M_{\lambda/a, l+1/2}(-2r/\lambda). \end{aligned} \right\} \tag{5}$$

A discrete spectrum $E < 0$ occurs only when a is negative, and one finds

$$\lambda = -na. \tag{6}$$

n is the principal quantum number which can take on the values $l+1, l+2, \dots$, while the radial quantum number $n' = n-l-1$ takes on the values $0, 1, 2, \dots$. In the confluent hypergeometric function of formula (5) the first parameter is a negative integer, namely $-n'$, and the radial wave function may be expressed by a Laguerre polynomial**

$$R_l(r/\lambda) = \frac{(n-l-1)!(2l+1)!}{(l+n)!} \left(\frac{2r}{n|a|}\right)^l e^{-\frac{r}{n|a|}} L_{n-l-1}^{2l+1}\left(\frac{2r}{n|a|}\right).$$

* For the definition of these functions, see ERDÉLYI et al.: Higher Transcendental Functions, McGraw Hill 1953, vol. I, chap. VI. This reference will hereafter be quoted as HTF.

** HTF, vol. II, chapter X.

The normalization is given by the condition $\int |\psi|^2 d^3r = 1$, i. e.

$$N_{l, \lambda} = \frac{2}{(2l+1)! n^2} \sqrt{\frac{(n+l)!}{(n-l-1)!}} |a|^{-3/2}. \quad (7)$$

For the *continuous spectrum*, $E > 0$, one has

$$\lambda = i\eta a = \frac{i}{k}. \quad (8)$$

The "Sommerfeld number" η is defined as $\eta = \frac{Z_1 Z_2 e^2}{\hbar v}$.

In all scattering phenomena this is a very important number, since it measures the strength of the interaction. For $\eta \ll 1$ the interaction is weak and in the limit the Born approximation applies. For $\eta \gg 1$ one may similarly in the limit use classical concepts^{5, 6}.

The quantities $k = mv/\hbar$ and v are the wave number and the velocity, respectively, at infinity.

The normalization is here

$$N_{l, \lambda} = e^{-\frac{\pi}{2}\eta} \frac{|\Gamma(l+1+i\eta)|}{(2l+1)!} i^l, \quad (9)$$

which makes the so-called Coulomb wave function

$$F_l = N_{l, \lambda} kr R_l(-ikr)$$

real with the following asymptotic behaviour

$$F_l \cong \sin(kr - l\frac{\pi}{2} + \sigma_l - \eta \log 2kr). \quad (10)$$

The Coulomb phase σ_l is defined as

$$\sigma_l = \arg \Gamma(l+1+i\eta).$$

We shall now consider the radial matrix element of the following type

$$J_{l_i, l_f}^{p, q} = \int_0^\infty R_{l_i}(r/\lambda_i) r^p e^{-qr} R_{l_f}^*(r/\lambda_f) r^2 dr. \tag{11}$$

For its evaluation, we use an integral representation of the confluent hypergeometric function*

$$R_l = \left(\frac{2r}{\lambda}\right)^l e^{-r/\lambda} \frac{(2l+1)!}{\Gamma\left(l+1-\frac{\lambda}{a}\right)\Gamma\left(l+1+\frac{\lambda}{a}\right)} \int_0^1 e^{2ru/\lambda} u^{l+\frac{\lambda}{a}} (1-u)^{l-\frac{\lambda}{a}} du. \tag{12}$$

Hereby one obtains, carrying out the integration over r ,

$$\left. \begin{aligned} & J_{l_i, l_f}^{p, q} = \\ & \frac{(2l_i+1)!(2l_f+1)!(2/\lambda_i)^{l_i}(2/\lambda_f^*)^{l_f}(l_i+l_f+p+2)! \left(\frac{1}{\lambda_i} + \frac{1}{\lambda_f^*} + q\right)^{-(l_i+l_f+p+3)}}{\Gamma\left(l_i+1-\frac{\lambda_i}{a}\right)\Gamma\left(l_i+1+\frac{\lambda_i}{a}\right)\Gamma\left(l_f+1-\frac{\lambda_f^*}{a}\right)\Gamma\left(l_f+1+\frac{\lambda_f^*}{a}\right)} \\ & \int_0^1 \int_0^1 du dv u^{l_i+\frac{\lambda_i}{a}} (1-u)^{l_i-\frac{\lambda_i}{a}} v^{l_f+\frac{\lambda_f^*}{a}} (1-v)^{l_f-\frac{\lambda_f^*}{a}} (1-ux-vy)^{-(l_i+l_f+p+3)} \\ & \quad x = \frac{2/\lambda_i}{1/\lambda_i+1/\lambda_f^*+q} \quad y = \frac{2/\lambda_f^*}{1/\lambda_i+1/\lambda_f^*+q}. \end{aligned} \right\} \tag{13}$$

The remaining double integral is just one of the integral representations of the Appell function F_2 .**

$$\left. \begin{aligned} & J_{l_i, l_f}^{p, q} = (l_i+l_f+p+2)! x^{l_i} y^{l_f} \left(\frac{1}{\lambda_i} + \frac{1}{\lambda_f^*} + q\right)^{-(p+3)} \\ & F_2\left(l_i+l_f+p+3, l_i+1+\frac{\lambda_i}{a}, l_f+1+\frac{\lambda_f^*}{a}, 2l_i+2, 2l_f+2, x, y\right). \end{aligned} \right\} \tag{14}$$

By means of the functional equation for the F_2 function (Appendix A5) one may give alternative formulae, e. g.,***

* HTF, vol. I, chapter VI.

** HTF, vol. I, chapter V.

*** In the derivation, one has to put limits to the parameters so that the integral representation (12) has a meaning. Once, however, we have got the closed formula (14) this must be true for any values of the parameters.

The formula (14) is a special case of a general formula for the integral of products of Whittaker functions given by A. ERDÉLYI⁷.

$$\left. \begin{aligned}
 J_{l_i, l_f}^{q, q} &= (-1)^{l_i + p + 3} (l_i + l_f + p + 2)! \left(\frac{1}{\lambda_i} - \frac{1}{\lambda_f^*} - q \right)^{-(p+3)} u^{l_i} v^{l_f} \\
 F_2 \left(l_i + l_f + p + 3, l_i + 1 - \frac{\lambda_i}{a}, l_f + 1 + \frac{\lambda_f^*}{a}, 2l_i + 2, 2l_f + 2, u, v \right) \\
 \text{with} \\
 u &= \frac{2/\lambda_i}{1/\lambda_i - 1/\lambda_f^* - q} \quad v = \frac{-2/\lambda_f^*}{1/\lambda_i - 1/\lambda_f^* - q}
 \end{aligned} \right\} \quad (14 \text{ a})$$

The generalized hypergeometric functions of two variables have been studied by several authors, the standard work on the subject being the monograph by APPELL and KAMPÉ DE FÉRIET⁸. Some of the properties of these functions are given in the Appendix.

The radial matrix element is given by J through

$$M_{l_i, l_f}^{p, q} = N_{l_i, \lambda_i} N_{l_f, \lambda_f}^* J_{l_i, l_f}^{p, q}. \quad (15)$$

III. Recursion Formulae.

One can derive a large number of recursion formulae which connect matrix elements with different values of l_i , l_f , and p . The general form of these recursion formulae can be determined from a theorem[†] which states that any five F_2 functions of the form

$$F_2(\alpha + n_1, \beta + n_2, \beta' + n_3, \gamma + n_4, \gamma' + n_5, x, y)$$

(where n_r are positive or negative integers) are connected by a linear relationship. The coefficients are polynomials in x and y . Since the matrix elements are proportional to an F_2 function, also five matrix elements of the form

$$M_{l_i + n', l_f + n''}^{p + n, q}$$

are linearly connected.

If the F_2 function is reduced to an F_1 function, e. g., in the case $l_i = l_f \pm (p + 1)$, already four matrix elements are con-

[†] APPELL and KAMPÉ de FÉRIET (ref. 8, chapter I) state that this theorem holds already for four F_2 functions, but this does not seem to be true.

nected in this way. In the case where the F_2 function is reduced to an ordinary hypergeometric function, three will suffice. Since the above mentioned theorem holds for three ordinary confluent hypergeometric functions ${}_1F_1$, three radial Coulomb wave functions of the type R_{l+n} are connected by a linear relation. Some of the recursion formulae for the matrix elements can be derived from these recursion formulae. One has, e. g.,*

$$\left. \begin{aligned} \left(\frac{l}{r} + \frac{1}{la} + \frac{d}{dr}\right)rR_l &\equiv {}^+H^l rR_l = 2(2l+1)r/\lambda R_{l-1} \\ \left(\frac{l+1}{r} + \frac{1}{(l+1)a} - \frac{d}{dr}\right)rR_l &\equiv {}^-H^{l+1}rR_l = -\frac{1}{l+1} \cdot \frac{(l+1)^2 - (\lambda/a)^2}{(2l+2)(2l+3)} \frac{r}{\lambda} R_{l+1}. \end{aligned} \right\} (16)$$

Recursion formulae for Coulomb matrix elements can now be obtained by considering the following expression:

$$\int_0^\infty rR_{l_i} r^p e^{-qr} [x_1 {}^+H^{l_i+1} + x_2 {}^+H^{l_i} + x_3 {}^-H^{l_i+1} + x_4 {}^-H^{l_i}] rR_{l_i}^* dr.$$

For the moment we leave the constant coefficients x_1 to x_4 undetermined. By partial integration in the first and fourth term and application of the recursion formulae (16) one obtains, by identifying the result with the direct evaluation

$$\left. \begin{aligned} -x_1 \frac{1}{\lambda_i(l_i+1)} \frac{(l_i+1)^2 - (\lambda_i/a)^2}{(2l_i+2)(2l_i+3)} J_{l_i+1, l_i}^{p, q} + x_2 \frac{2}{\lambda_j^*} (2l_j+1) J_{l_i, l_j-1}^{p, q} \\ -x_3 \frac{1}{\lambda_j^*(l_j+1)} \frac{(l_j+1)^2 - (\lambda_j/a)^2}{(2l_j+2)(2l_j+3)} J_{l_i, l_j+1}^{p, q} + x_4 \frac{2}{\lambda_i} (2l_i+1) J_{l_i-1, l_i}^{p, q} \\ = [x_1(l_i+1+p) + x_2 l_j + x_3(l_j+1) + x_4(l_i-p)] J_{l_i, l_i}^{p-1, q} \\ -\frac{1}{a} \left[x_1 \left(\frac{1}{l_i+1} + qa \right) + x_2 \frac{1}{l_j} + x_3 \frac{1}{l_j+1} + x_4 \left(\frac{1}{l_i} - qa \right) \right] J_{l_i, l_i}^{p, q} \\ + (x_1 + x_2 - x_3 - x_4) \int_0^\infty rR_{l_i} r^p e^{-qr} \frac{d}{dr} (rR_{l_i}^*) dr. \end{aligned} \right\} (17)$$

* These formulae can be derived directly from the properties of the ${}_1F_1$ functions (HTF, vol. I, chapter VI) or by the factorization method⁹.

To get recursion formulae between Coulomb matrix elements we choose the x'_n 's so that the last term vanishes, i. e.,

$$x_1 + x_2 - x_3 - x_4 = 0. \quad (18)$$

In accordance with the parity selection rule one will often employ the further condition

$$x_1 \left(\frac{1}{l_i + 1} + qa \right) + x_2 \frac{1}{l_j} + x_3 \frac{1}{l_j + 1} + x_4 \left(\frac{1}{l_i} - qa \right) = 0. \quad (19)$$

In the resulting recursion relation we still have freedom in the choice of the x_n 's. In particular, one can get a recursion formula with p fixed by the extra condition

$$x_1 (l_i + p + 1) + x_2 l_j + x_3 (l_j + 1) + x_4 (l_i - p) = 0. \quad (20)$$

For $q = 0$, the relations containing $p - 1$ as well as p become singular for $p = -2$, which illustrates the more complicated character of matrix elements of the quadrupole type, as compared with that of dipole matrix elements.

Other recursion formulae may be obtained directly from the properties of the generalized hypergeometric functions. An example will be given in connection with the theory of Coulomb excitation (II).

IV. Specializations.

In this section, we give a few examples of the reduction of the general formula (14) for the case $q = 0$, which is of special interest.

a) *Discrete-discrete transitions.*

In this case, the second and third parameters in the F_2 function become negative integers, namely $l_i + 1 - n_i = -n'_i$ and $l_j + 1 - n_j = -n'_j$. The F_2 function is then reduced to a polynomial in x and y .¹⁰

$$M_{l_i, l_f}^p = (l_i + l_f + p + 2)! \alpha^p \left(\frac{1}{n_i} + \frac{1}{n_f} \right)^{-p-3} \frac{4 x^{l_i} y^{l_f}}{n_i^2 n_f^2 (2 l_i + 1)! (2 l_f + 1)!} \sqrt{\frac{(n_i + l_i)! (n_f + l_f)!}{(n_i - l_i - 1)! (n_f - l_f - 1)!} \sum_{r=0}^{n_i - l_i - 1} \sum_{s=0}^{n_f - l_f - 1} \frac{(l_i + l_f + p + 3)_{r+s} (l_i + 1 - n_i)_r (l_f + 1 - n_f)_s}{(2 l_i + 2)_r (2 l_f + 2)_s r! s!} x^r y^s} \quad (21)$$

with

$$x = \frac{2 n_f}{n_i + n_f} \quad y = \frac{2 n_i}{n_i + n_f}.$$

This formula contains, e. g., the matrix elements needed for the calculation of the intensity of hydrogen lines.

b) *Discrete-continuous transitions.*

Here, the parameter $\beta = l_i + 1 - n_i = -n'_i$ will become a negative integer. The F_2 function can, in this case, be reduced to a finite sum of ordinary hypergeometric functions (A 3).

$$M_{l_i, l_f}^p = (l_i + l_f + p + 2)! \alpha^{p + 3/2} \left(\frac{1}{n_i} + \frac{i}{\eta_f} \right)^{-p-3} \frac{2 x^{l_i} y^{l_f}}{n_i^2 (2 l_i + 1)!} \sqrt{\frac{(n_i + l_i)!}{(n_i - l_i - 1)!}} \times \frac{|\Gamma(l_f + 1 + i \eta_f)|}{(2 l_f + 1)!} i^{-l_f} e^{-\frac{\pi}{2} \eta_f} \times \sum_{r=0}^{n_i - l_i - 1} \frac{(l_i + l_f + p + 3)_r (l_i + 1 - n_i)_r}{(2 l_i + 2)_r r!} x^r {}_2F_1(l_i + l_f + p + 3 + r, l_f + 1 + i \eta_f, 2 l_f + 2, y) \quad (22)$$

with

$$x = \frac{2 i \eta_f}{n_i - i \eta_f} \quad y = \frac{2 n'_i}{n_i - i \eta_f}.$$

This formula applies, e. g., for the matrix elements occurring in the theory of electron emission by radioactive α -disintegration¹¹.

c) *Continuous-continuous transitions.*

In the general case, the F_2 function cannot easily be reduced to more elementary functions. The matrix element is

$$\left. \begin{aligned}
 M_{l_i l_f}^p &= (l_i + l_f + p + 2)! a^{p+3} \left(\frac{1}{\eta_i} - \frac{1}{\eta_f} \right)^{-p-3} \frac{x^{l_i} y^{l_f} i^{l_i - l_f + p + 3}}{(2l_i + 1)! (2l_f + 1)!} \\
 & \left| \Gamma(l_i + 1 + i\eta_i) \right| \cdot \left| \Gamma(l_f + 1 + i\eta_f) \right| e^{-\frac{\pi}{2}(\eta_i + \eta_f)} \\
 & F_2(l_i + l_f + p + 3, l_i + 1 - i\eta_i, l_f + 1 + i\eta_f, 2l_i + 2, 2l_f + 2, x, y), \\
 \text{where } x &= \frac{2\eta_f}{\eta_f - \eta_i} \quad \text{and } y = \frac{-2\eta_i}{\eta_f - \eta_i}.
 \end{aligned} \right\} \quad (23)$$

Since $x + y > 1$, it is essential for the application of this formula to investigate the analytic continuation of the F_2 function beyond the domain of convergence of the series expansion (A1). This problem will be treated in detail in (II) in connection with the theory of Coulomb excitation. In the case $p = -1$ and $l_i = l_f$, the F_2 function is reduced directly to the usual hypergeometric function (A6) and one obtains an expression which is identical with the formula of GORDON (loc. cit.).

V. Relativistic Matrix Elements.

The relativistic eigensolution for an electron in a Coulomb field $-Ze/r$ is, in the notation of ROSE and OSBORN¹²,

$$\psi_{\kappa, m} = \begin{pmatrix} -if_{\kappa} \chi_{-\kappa}^m \\ g_{\kappa} \chi_{\kappa}^m \end{pmatrix}, \quad (24)$$

where

$$\chi_{\kappa}^m = \sum_{\tau} \langle l_{\kappa}, m - \tau; \frac{1}{2}, \tau | j, m \rangle \chi_{\nu/2, \tau} Y_{l_{\kappa}, m - \tau}$$

with

$$\begin{aligned}
 l_{\kappa} &= |\kappa| + \frac{1}{2} (\text{sign } \kappa - 1) \\
 j &= |\kappa| - \frac{1}{2}
 \end{aligned}$$

and

$$\chi_{1/2, 1/2} = \begin{pmatrix} 1 \\ 0 \end{pmatrix} \quad \chi_{1/2, -1/2} = \begin{pmatrix} 0 \\ 1 \end{pmatrix}.$$

The radial wave functions are solutions of the differential equations

$$\frac{d}{dr} \begin{pmatrix} f \\ g \end{pmatrix} = \begin{pmatrix} \frac{\kappa-1}{r}, & -\frac{1}{\hbar c} \left(W - mc^2 - \frac{Ze^2}{r} \right) \\ \frac{1}{\hbar c} \left(W + mc^2 + \frac{Ze^2}{r} \right), & -\frac{\kappa+1}{r} \end{pmatrix} \begin{pmatrix} f \\ g \end{pmatrix}, \quad (25)$$

where W is the total energy (including the rest energy). The solution may be written in the following form:

$$\begin{pmatrix} f \\ g \end{pmatrix} = N_{\lambda, \kappa} \begin{pmatrix} F \\ G \end{pmatrix}, \quad (26)$$

where $N_{\lambda, \kappa}$ is a normalization factor and

$$\begin{pmatrix} F \\ G \end{pmatrix} = \sqrt{\frac{mc^2}{W} \mp 1} \left(\frac{\lambda}{r} \right)^{3/2} \left[(N - \kappa) M_{\gamma + n' + 1/2, \gamma} \left(\frac{2r}{\lambda} \right) \pm n' M_{\gamma + n' - 1/2, \gamma} \left(\frac{2r}{\lambda} \right) \right].$$

We have used the following abbreviations:

$$\left. \begin{aligned} \lambda &= \lambda_0 \frac{mc^2}{\sqrt{m^2c^4 - W^2}} & \lambda_0 &= \frac{\hbar}{mc}, \\ N &= \frac{\hbar c}{a \sqrt{m^2c^4 - W^2}} & a &= \frac{\hbar^2}{Zme^2}, \\ \gamma &= \sqrt{\kappa^2 - Z^2\alpha^2} & \alpha &= \frac{e^2}{\hbar c}, \\ n' &= \frac{\alpha ZW}{\sqrt{m^2c^4 - W^2}} - \gamma. \end{aligned} \right\} \quad (27)$$

For the *discrete spectrum* $W < mc^2$, n' is the radial quantum number taking on the values $0, 1, \dots$. The quantum number N is then

$$N = \sqrt{n'^2 + \kappa^2} + 2n'\gamma \quad (28)$$

and the parameter λ becomes

$$\lambda = Na. \quad (19)$$

The normalization is determined by the condition

$$\int \bar{\psi} \psi d^3r = 1,$$

giving

$$N_{\gamma, \varkappa} = - \frac{\sqrt{\Gamma(2\gamma + n' + 1)}}{\Gamma(2\gamma + 1)\sqrt{(n')!}} \frac{(Na)^{-3/2}}{\sqrt{4N(N-\varkappa)} \sqrt{1 + \frac{\alpha^2 Z^2}{(n' + \gamma)^2}}}. \quad (30)$$

For the *continuous spectrum* $W > mc^2$ the parameters have the following values:

$$\left. \begin{aligned} \lambda &= \frac{i}{k}, & k &= p/\hbar, \\ N &= \frac{i}{ka}, \\ n' &= i\eta - \gamma, & \eta &= \frac{Ze^2}{\hbar v} = Z\alpha \frac{W}{pc}, \end{aligned} \right\} \quad (31)$$

where p is the momentum at infinity. The normalization is

$$N_{\lambda, \varkappa} = ke^{i(\frac{\pi}{2}\gamma - \delta)} \frac{e^{\frac{\pi}{2}\eta} |\Gamma(\gamma + i\eta)|}{\Gamma(2\gamma + 1)} (2i)^{-3/2}, \quad (32)$$

which makes the wave function real with the following asymptotic behaviour:

$$\left(\begin{array}{l} f \\ g \end{array} \right) \sim \sqrt{1 \mp \frac{W}{mc^2}} \begin{pmatrix} -\sin \\ \cos \end{pmatrix} \left[kr + \eta \log 2kr - \sigma_l + \delta - \frac{\pi}{2}\gamma \right]. \quad (33)$$

The phases σ_l and δ are defined by

$$\left. \begin{aligned} \sigma_l &= \arg \Gamma(\gamma + i\eta), \\ \delta &= \frac{1}{2} \arg \frac{-\varkappa + \frac{i}{ka}}{\gamma + i\eta}. \end{aligned} \right\} \quad (34)$$

Since the relativistic wave functions are expressed by confluent hypergeometric functions, the matrix elements of $r^p e^{-qr}$ may be calculated in the same way as the non-relativistic matrix elements (formula 14). Here, we shall give the result only:

$$\left. \begin{aligned}
 & \int_0^\infty \begin{pmatrix} f_i \\ g_i \end{pmatrix} r^p e^{-qr} (f_j, g_j) r^2 dr = \\
 & N_{\kappa_i, \lambda_i} N_{\kappa_f, \lambda_f} 2 \lambda_i \lambda_f \lambda_i^{-\gamma_i} \lambda_f^{-\gamma_f} \left(q + \frac{1}{\lambda_i} + \frac{1}{\lambda_f} \right)^{-\gamma_i - \gamma_f - p - 1} \Gamma(\gamma_i + \gamma_f + p + 1) \\
 & \sqrt{\frac{(mc^2 + \varepsilon_1 W_i)(mc^2 + \varepsilon_2 W_f)}{W_i W_f}} \\
 & \left. \begin{aligned}
 & \left\{ \varepsilon_3 (N_i - \kappa_i)(N_f - \kappa_f) F_2(\gamma_i + \gamma_f + p + 1, -n_i, -n_f, 2\gamma_i + 1, 2\gamma_f + 1, x, y) \right. \\
 & \varepsilon_4 n_i n_f \quad F_2(\gamma_i + \gamma_f + p + 1, -n_i + 1, -n_f + 1, 2\gamma_i + 1, 2\gamma_f + 1, x, y) \\
 & \varepsilon_5 (N_i - \kappa_i) n_f \quad F_2(\gamma_i + \gamma_f + p + 1, -n_i - n_f + 1, 2\gamma_i + 1, 2\gamma_f + 1, x, y) \\
 & \left. \varepsilon_6 (N_f - \kappa_f) n_i \quad F_2(\gamma_i + \gamma_f + p + 1, -n_i + 1, -n_f, 2\gamma_i + 1, 2\gamma_f + 1, x, y) \right\}
 \end{aligned} \right\} (35)
 \end{aligned}$$

The signs ε_n are given by

$$\left. \begin{aligned}
 \varepsilon_1 &= \begin{pmatrix} - & - \\ + & + \end{pmatrix} & \varepsilon_2 &= \begin{pmatrix} - & + \\ - & + \end{pmatrix} & \varepsilon_3 &= \begin{pmatrix} + & + \\ + & + \end{pmatrix} \\
 \varepsilon_4 &= \begin{pmatrix} + & - \\ - & + \end{pmatrix} & \varepsilon_5 &= \begin{pmatrix} + & - \\ + & - \end{pmatrix} & \varepsilon_6 &= \begin{pmatrix} + & + \\ - & - \end{pmatrix}
 \end{aligned} \right\} (36)$$

Further,

$$x = \frac{2/\lambda_i}{1/\lambda_i + 1/\lambda_f + q} \quad y = \frac{2/\lambda_f}{1/\lambda_i + 1/\lambda_f + q}. \quad (37)$$

With this formula one can, e. g., write down directly the internal conversion matrix elements.

Acknowledgements.

The authors are indebted to Mr. JENS LINDHARD for many enlightening discussions and wish also to thank Professor NIELS BOHR and Drs. AAGE BOHR and BEN MOTTELSON for their interest in this work.

Appendix:

Some properties of the generalized hypergeometric function of two variables, F_2 .

The F_2 function is defined by a series expansion

$$F_2(\alpha, \beta, \beta', \gamma, \gamma' x, y) = \sum_{m, n=0}^{\infty} \frac{\alpha_{m+n} \beta_m \beta'_n}{\gamma_m \gamma'_n m! n!} x^m y^n, \quad (\text{A1})$$

where

$$\alpha_m = \frac{\Gamma(a+m)}{\Gamma(a)} = a(a+1) \cdots (a+m-1).$$

This double series has the following domain of absolute convergence

$$|x| + |y| \leq 1. \quad (\text{A2})$$

By summation over n , one gets an alternative series expansion

$$F_2(\alpha, \beta, \beta', \gamma, \gamma' x, y) = \sum_{m=0}^{\infty} \frac{\alpha_m \beta_m}{\gamma_m m!} x^m {}_2F_1(\alpha + m, \beta', \gamma', y). \quad (\text{A3})$$

The analytic continuation of the function F_2 beyond the domain A2 may be given by the integral representation

$$F_2(\alpha, \beta, \beta', \gamma, \gamma', x, y) = \frac{\Gamma(\gamma) \Gamma(\gamma')}{\Gamma(\beta) \Gamma(\beta') \Gamma(\gamma - \beta) \Gamma(\gamma' - \beta')} \left. \int_0^1 \int_0^1 du dv u^{\beta-1} v^{\beta'-1} (1-u)^{\gamma-\beta-1} (1-v)^{\gamma'-\beta'-1} (1-ux-vy)^{-\alpha} \right\} (\text{A4})$$

The integral representation has a meaning only when the following inequalities are fulfilled,

$$Re\beta > 0 \quad Re\beta' > 0 \quad Re(\gamma - \beta) > 0 \quad Re(\gamma' - \beta') > 0.$$

There exist three transformations corresponding to the Euler transformations of the ordinary hypergeometric functions,

$$\left. \begin{aligned} F_2(\alpha, \beta, \beta', \gamma, \gamma' x, y) &= (1-x)^{-\alpha} F_2\left(\alpha, \gamma - \beta, \beta', \gamma, \gamma' \frac{x}{x-1}, \frac{y}{1-x}\right) \\ &= (1-y)^{-\alpha} F_2\left(\alpha, \beta, \gamma' - \beta', \gamma, \gamma' \frac{x}{1-y}, \frac{y}{y-1}\right) \\ &= (1-x-y)^{-\alpha} F_2\left(\alpha, \gamma - \beta, \gamma' - \beta', \gamma, \gamma' \frac{x}{x+y-1}, \frac{y}{x+y-1}\right). \end{aligned} \right\} \quad (A5)$$

The F_2 function reduces, for special choices of the parameters, to a simpler function.

If the first index α is a negative integer, the series A1 breaks off and the F_2 function is thus a polynomial. The same is true when both parameters β and β' are negative integers. If only one of them is a negative integer, the series A3 reduces to a finite sum of ordinary hypergeometric functions. There exist also other special reduction formulae of which we use only

$$\left. \begin{aligned} F_2(\alpha, \beta, \beta', \alpha, \alpha, x, y) &= (1-x)^{-\beta} (1-y)^{-\beta'} \\ &\times {}_2F_1\left(\beta, \beta', \alpha, \frac{xy}{(1-x)(1-y)}\right). \end{aligned} \right\} \quad (A6)$$

*CERN (European Organization for Nuclear Research)
Theoretical Study Division, Copenhagen,
and
Institute for Theoretical Physics,
University of Copenhagen.*

References.

1. E. SCHRÖDINGER, Ann. d. Phys. **80**, 437 (1926).
2. W. GORDON, Ann. d. Phys. **2**, 1031 (1929).
3. K. ALDER and A. WINTHER, Dan. Mat. Fys. Medd. **29**, no. 19 (1955).
4. A. ERDÉLYI ET. AL., Higher Transcendental Functions, McGraw Hill (1953).
5. A. SOMMERFELD, Atombau und Spektrallinien II. Vieweg, Braunschweig (1939), pp. 534, 562.
6. N. BOHR, Dan. Mat. Fys. Medd. **18**, no. 8 (1948).
7. A. ERDÉLYI, Math. Z. **40**, 693 (1936).
8. P. APPELL et J. KAMPÉ DE FÉRIET, Fonctions Hypergéométriques etc. Paris, Gauthiers-Villars (1926).
9. L. INFELD and T. E. HULL, Rev. Mod. Phys. **23**, 21 (1950).
10. K. MAYR, Math. Z. **39**, 597 (1935).
11. J. S. LEVINGER, Phys. Rev. **90**, 11 (1953).
12. M. E. ROSE and R. K. OSBORN, Phys. Rev. **93**, 1315 (1954).



Det Kongelige Danske Videnskabernes Selskab

Matematisk-fysiske Meddelelser, bind **29**, nr. 19

Dan. Mat. Fys. Medd. **29**, no. 19 (1955)

ON THE EXACT
EVALUATION OF THE COULOMB
EXCITATION

BY

KURT ALDER AND AAGE WINTHER



København 1955

i kommission hos Ejnar Munksgaard

DET KONGELIGE DANSKE VIDENSKABERNES SELSKAB udgiver følgende publikationsrækker:

L'Académie Royale des Sciences et des Lettres de Danemark publie les séries suivantes:

	Bibliografisk forkortelse <i>Abréviation bibliographique</i>
Oversigt over selskabets virksomhed (8°) <i>(Annuaire)</i>	Dan. Vid. Selsk. Overs.
Historisk-filologiske Meddelelser (8°)	Dan. Hist. Filol. Medd.
Historisk-filologiske Skrifter (4°) <i>(Histoire et Philologie)</i>	Dan. Hist. Filol. Skr.
Arkæologisk-kunsthistoriske Meddelelser (8°)	Dan. Arkæol. Kunsthist. Medd.
Arkæologisk-kunsthistoriske Skrifter (4°) <i>(Archéologie et Histoire de l'Art)</i>	Dan. Arkæol. Kunsthist. Skr.
Filosofiske Meddelelser (8°) <i>(Philosophie)</i>	Dan. Filos. Medd.
Matematisk-fysiske Meddelelser (8°) <i>(Mathématiques et Physique)</i>	Dan. Mat. Fys. Medd.
Biologiske Meddelelser (8°)	Dan. Biol. Medd.
Biologiske Skrifter (4°) <i>(Biologie)</i>	Dan. Biol. Skr.

Selskabets sekretariat og postadresse: Dantes plads 5, København V.

L'adresse postale du secrétariat de l'Académie est:

*Det Kongelige Danske Videnskabernes Selskab,
Dantes plads 5, København V, Danmark.*

Selskabets kommissionær: EJNAR MUNKSGAARD's forlag, Nørregade 6, København K.

Les publications sont en vente chez le commissionnaire:

EJNAR MUNKSGAARD, éditeur, Nørregade 6, København K, Danmark.

Det Kongelige Danske Videnskabernes Selskab

Matematisk-fysiske Meddelelser, bind **29**, nr. 19

Dan. Mat. Fys. Medd. **29**, no. 19 (1955)

ON THE EXACT
EVALUATION OF THE COULOMB
EXCITATION

BY

KURT ALDER AND AAGE WINTHER



København 1955

i kommission hos Ejnar Munksgaard

CONTENTS

	Pages
I. Introduction	3
II. Reduction of the Coulomb Cross Section to Radial Matrix Elements ...	3
III. Evaluation of the Radial Matrix Elements	5
IV. Recursion Formulae	7
V. Limiting Cases	10
VI. Conclusions	13
VII. Numerical Results	14
Appendix: Some Properties of Generalized Hypergeometric Functions of Two Variables	18
References	20

It is shown that the calculation of the total cross section for Coulomb excitation can be reduced to the calculation of radial matrix elements between eigenstates in the Coulomb potential. With the method developed in the preceding paper, one is able to give closed expressions, convenient series expansions, and recursion formulae for these matrix elements. The case of vanishing energy loss and the semi-classical limit are also discussed.

I. Introduction.

The exact evaluation of the Coulomb excitation cross section has hitherto only been performed in the dipole case^{1,2}. The radial matrix elements for the higher multipoles are more complicated and have previously been treated only in the WBK approximation³. With the method developed in the preceding paper⁴, one is able, however, to give closed expressions and suitable series developments of these matrix elements.

The closed expression given there contains a generalized hypergeometric function of two variables. It is one of the main points of this paper to give the analytical continuation of this function into the domain where it is of physical interest and from which the numerical evaluation can be performed. Once this is derived it will be easy to discuss the different limiting cases. We shall deal here especially with the limit of no energy loss and the classical limit. Furthermore, we shall give a number of recursion formulae which will considerably facilitate a numerical evaluation.

II. Reduction of the Coulomb Cross Section to Radial Matrix Elements.

The electromagnetic excitation of nuclear levels by means of impinging charged particles is a phenomenon analogous to the nuclear photoeffect, since specific nuclear properties enter only through matrix elements identical with those encountered in radia-

tion theory. If one neglects the penetration of the projectile into the nucleus, one finds easily in the non-relativistic limit the following differential cross section for excitations by means of the electric field:

$$\frac{d\sigma}{d\Omega} = \frac{4m_i^2 Z_1^2 e^2 v_f}{\hbar^4 v_i} \sum_{\lambda, \mu} \frac{B(E\lambda)}{(2\lambda + 1)^3} |\langle \vec{k}_i | r^{-\lambda-1} Y_{\lambda\mu}(\vartheta, \varphi) | \vec{k}_j \rangle|^2. \quad (1)$$

m_i , Z_1 , and v are the mass, the charge, and the velocity of the projectile, respectively. The indices i and f refer to the initial and final states. $B(E\lambda)$ is the square of the nuclear 2^λ pole electric transition matrix element in the notation of BOHR and MOTTELSON⁵. The states $|\vec{k}\rangle$ are eigenstates in the Coulomb field of the nucleus which, at distances far from the nucleus, behave as "plane waves" (distorted by the Coulomb field) with definite wave numbers k . These states may be decomposed in partial waves⁶:

$$|\vec{k}\rangle = \sum_{l=0}^{\infty} 4\pi (-1)^m i^l e^{i\sigma_l} Y_{l-m}(\vec{k}) Y_{lm}(\vartheta, \varphi) k r F_l(kr), \quad (2)$$

where $\sigma_l = \arg \Gamma(l+1+i\eta)$ is the Coulomb phase and $F_l(kr)$ the regular solution of the wave equation behaving as

$$\sin\left(kr - \frac{1}{2}l\pi - \eta \ln 2kr + \sigma_l\right) \text{ for } kr \gg 1.$$

Introducing this into (1) one may integrate over the angles, utilizing the formula*

$$\int Y_{l_1 m_1} Y_{l_2 m_2} Y_{l_3 m_3} d\Omega = \sqrt{\frac{(2l_1+1)(2l_2+1)(2l_3+1)}{4\pi}} \begin{pmatrix} l_1 & l_2 & l_3 \\ 0 & 0 & 0 \end{pmatrix} \begin{pmatrix} l_1 & l_2 & l_3 \\ m_1 & m_2 & m_3 \end{pmatrix}. \quad (3)$$

By integrating over the direction of k one obtains the total cross section

$$\sigma_{el} = \left. \begin{aligned} & \frac{64\pi^2 Z_1^2 e^2 m_i^2 v_f}{\hbar^4 v_i} \sum_{\lambda} \frac{B(E\lambda)}{(2\lambda + 1)^2} \\ & \times \sum_{l_i l_f} (2l_i + 1)(2l_f + 1) \begin{pmatrix} l_i & l_f & \lambda \\ 0 & 0 & 0 \end{pmatrix}^2 |M_{l_i l_f}^{-\lambda-1}|^2 \end{aligned} \right\} \quad (4)$$

* Here we use the Wigner notation for the vector addition coefficients. The relation between those and the Clebsch-Gordon coefficients of Condon and Shortley (E. U. CONDON and G. H. SHORTLEY, Theory of Atomic Spectra, Oxford 1936) is

$$\begin{pmatrix} l_1 & l_2 & l_3 \\ m_1 & m_2 & m_3 \end{pmatrix} = \frac{(-1)^{l_1-l_2-m_3}}{\sqrt{2l_3+1}} \langle l_1 m_1 l_2 m_2 | (l_1 l_2) l_3 - m_3 \rangle.$$

with

$$M_{l_i l_f}^{-\lambda-1} = \frac{1}{k_i k_f} \int_0^\infty F_{l_i}(k_i r) r^{-\lambda-1} F_{l_f}^*(k_f r) dr. \quad (5)$$

The selection rules for the angular momenta l_i and l_f are directly seen from equation (3):

$$|l_i - l_f| \leq \lambda \leq l_i + l_f \quad \text{and} \quad l_i + l_f + \lambda \quad \text{even.}$$

The evaluation of the total cross section is thus reduced to the evaluation of the radial integrals $M^{-\lambda-1}$. The differential cross section and the angular distribution of subsequent γ quanta can also be expressed by these radial matrix elements. In a forthcoming review article⁷, formulae will be given for these cross sections together with a more complete discussion of electromagnetic excitations.

III. Evaluation of the Radial Matrix Elements.

According to the formula (22) of I, the radial matrix element is given by

$$M_{l_i l_f}^{-\lambda-1} = \left. \begin{aligned} & \frac{|\Gamma(l_i + 1 + i\eta_i)| |\Gamma(l_f + 1 + i\eta_f)|}{(2l_i + 1)! (2l_f + 1)!} \\ & (l_i + l_f - \lambda + 1)! i^{l_i + l_f - \lambda + 2} x^{l_i} y^{l_f} e^{-\frac{\pi}{2}(\eta_i + \eta_f)} (k_i - k_f)^{\lambda - 2} \\ & F_2(l_i + l_f - \lambda + 2, l_i + 1 - i\eta_i, l_f + 1 + i\eta_f, 2l_i + 2, 2l_f + 2, x, -y), \end{aligned} \right\} (6)$$

where

$$x = \frac{2\eta_f}{\xi} \quad \text{and} \quad y = \frac{2\eta_i}{\xi};$$

further

$$\xi = \eta_f - \eta_i \quad \text{and} \quad \eta = \frac{Z_1 Z_2 e^2}{\hbar v}.$$

Since the series expansion of the F_2 function only converges for x and y in the neighbourhood of zero, one has for the numerical evaluation to find the analytic continuation of this function in the neighbourhood of infinity.

The analytic continuation is in fact given by the Barnes integral representation⁸, and suitable asymptotic expansions may easily be derived from this. However, we shall here use only the

analytic continuation for the special case $l_i = l_f \pm \lambda$ and derive the other matrix elements by means of recursion formulae.

In these matrix elements, where the change of l is maximum (maximal matrix elements), the F_2 function reduces to an F_1 according to formula A5. This may again be expressed by an F_3 function (A5) for which an analytic continuation in terms of F_2 functions is known (A4). One thus obtains immediately, e.g.,

$$\left. \begin{aligned}
 & F_2(2l+2, l+\lambda+1-i\eta_i, l+1+i\eta_f, 2l+2\lambda+2, 2l+2, x, -y) = \\
 & (-1)^{l+1-i\eta_f} (2l+2\lambda+1)! \left[(-x)^{-2l-2} \frac{|F(\lambda+i\xi)|^2}{\Gamma(2\lambda) |\Gamma(l+\lambda+1+i\eta_i)|^2} \right. \\
 & F_2\left(-2\lambda+1, l+1-i\eta_f, l+1+i\eta_f, -\lambda+1-i\xi, -\lambda+1+i\xi, \frac{1}{x}, \frac{1}{x}\right) \\
 & + 2 \operatorname{Re} \left\{ (-x)^{-2l-\lambda-2-i\xi} \frac{\Gamma(-\lambda-i\xi)}{\Gamma(l+1-i\eta_f) \Gamma(l+\lambda+1+i\eta_i)} \right. \\
 & \left. \left. \times F_2\left(-\lambda+1+i\xi, l+\lambda+1-i\eta_i, l+1+i\eta_f, \lambda+1+i\xi, -\lambda+1+i\xi, \frac{1}{x}, \frac{1}{x}\right) \right\} \right] \quad (7)
 \end{aligned} \right\}$$

With this formula one gets for the radial matrix element*

$$\left. \begin{aligned}
 & M_{l+\lambda, l}^{-\lambda-1} = e^{\frac{\pi}{2}\xi} \left| \frac{\Gamma(l+1+i\eta_f)}{\Gamma(l+1+i\eta_i)} \right| \left(\frac{\eta_i}{\eta_f} \right)^l (2k_i)^{\lambda-2} \times \left\{ \frac{|F(\lambda+i\xi)|^2}{(2\lambda-1)!} \right. \\
 & F_2\left(-2\lambda+1, l+1-i\eta_f, l+1+i\eta_f, -\lambda+1-i\xi, -\lambda+1+i\xi, \frac{\xi}{2\eta_f}, \frac{\xi}{2\eta_f}\right) \\
 & + 2 \operatorname{Re} \left[\left(e^{i\pi} \frac{\xi}{2\eta_f} \right)^{\lambda+i\xi} \frac{\Gamma(l+\lambda+1-i\eta_i) \Gamma(-\lambda-i\xi)}{\Gamma(l+1-i\eta_f)} \right. \\
 & \left. \left. \times F_2\left(-\lambda+1+i\xi, l+\lambda+1-i\eta_i, l+1+i\eta_f, \lambda+1+i\xi, \right. \right. \right. \\
 & \left. \left. \left. -\lambda+1+i\xi, \frac{\xi}{2\eta_f}, \frac{\xi}{2\eta_f} \right) \right] \right\} \quad (8)
 \end{aligned} \right\}$$

* Dr. L. C. BIEDENHARN has kindly communicated to us an independent derivation of expressions equivalent to formulae (8) and (9) which were obtained directly without explicit use of the properties of the hypergeometric functions.

Similarly, for the other maximal matrix element, one obtains

$$\begin{aligned}
 M_{l,l+\lambda}^{-\lambda-1} &= e^{-\frac{\pi}{2}\xi} \left\{ \frac{\Gamma(l+1+i\eta_i)}{\Gamma(l+\lambda+1+i\eta_f)} \left| \left(\frac{\eta_f}{\eta_i} \right)^l (2k_f)^{\lambda-2} \times \left[\frac{\Gamma(\lambda+i\xi)^2}{(2\lambda-1)!} \right. \right. \right. \\
 &F_2 \left(-2\lambda+1, l+1+i\eta_i, l+1-i\eta_i, -\lambda+1-i\xi, -\lambda+1+i\xi, \frac{-\xi}{2\eta_i}, \frac{-\xi}{2\eta_i} \right) \\
 &+ 2 \operatorname{Re} \left[\left(\frac{\xi}{2\eta_i} \right)^{\lambda+i\xi} \frac{\Gamma(l+\lambda+1+i\eta_f) \Gamma(-\lambda-i\xi)}{\Gamma(l+1+i\eta_i)} \right. \\
 &\times F_2 \left(-\lambda+1+i\xi, l+\lambda+1+i\eta_f, l+1-i\eta_i, \lambda+1+i\xi, \right. \\
 &\quad \left. \left. \left. -\lambda+1+i\xi, \frac{-\xi}{2\eta_i}, \frac{-\xi}{2\eta_i} \right) \right] \right\} \quad (9) \\
 &= e^{-\pi\xi} M_{l+\lambda,l}^{-\lambda-1}(\eta_i \rightleftharpoons -\eta_f).
 \end{aligned}$$

In the first F_2 function of these formulae, the first parameter, $-2\lambda+1$, is a negative integer. Thus the functions are reduced to polynomials which for the lowest multipole orders are given explicitly by

$$\begin{aligned}
 &F_2 \left(-2\lambda+1, l+1-i\eta_f, l+1+i\eta_f, -\lambda+1-i\xi, -\lambda+1+i\xi, \frac{\xi}{2\eta_f}, \frac{\xi}{2\eta_f} \right) \\
 &= \begin{cases} 0 & \text{for } \lambda = 1 \\ \frac{1}{2(1+\xi^2)} \cdot \frac{\eta_i(\eta_i+\eta_f)}{\eta_f^2} & \text{for } \lambda = 2 \\ \frac{1}{2(1+\xi^2)(4+\xi^2)} \cdot \frac{\eta_i(\eta_i+\eta_f)}{\eta_f^4} [5l(\eta_i+\eta_f)\xi + 4(3\eta_f^2 - 2\eta_i^2)] & \text{for } \lambda = 3. \end{cases} \quad (10)
 \end{aligned}$$

The formulae (8) and (9) are well suited for a numerical evaluation, since the series expansion of F_2 converges for nearly all interesting values of the parameters. However, for $l \gg \eta$ the convergence is rather slow.

IV. Recursion Formulae.

The non-maximal radial matrix elements can be derived from the maximal ones through recursion formulae. We shall first derive a recursion relation of this type, which we shall use for quadrupole matrix elements.

Recursion relations connecting different multipoles can be used, e. g., for the calculation of the octupole matrix elements from the quadrupole ones.

For the numerical evaluation of the maximal matrix elements, it may also be advantageous to use recursion formulae connecting successive maximal matrix elements.

From the general formula I (17) one gets a recursion formula of the first type by demanding the condition

$$x_1(l_i - \lambda) + x_2 l_f + x_3(l_f + 1) + x_4(l_i + \lambda + 1) = 0 \quad (11)$$

besides the two conditions I (18, 19). In the quadrupole case, this leads to two recursion formulae, where one has to set $l_i = l_f - 1$ and $l_i = l_f + 1$, respectively.

$$y_1 M_{l+1, l+1}^{-3} + y_2 M_{l l}^{-3} + y_3 M_{l l+2}^{-3} + y_4 M_{l-1 l+1}^{-3} = 0, \quad (12)$$

$$y'_1 M_{l+2 l}^{-3} + y'_2 M_{l+1 l-1}^{-3} + y'_3 M_{l+1 l+1}^{-3} + y'_4 M_{l l}^{-3} = 0, \quad (13)$$

where

$$\left. \begin{aligned} y_1 &= k_i(l+2)(2l+3)|l+1+i\eta_i| & y'_1 &= -3k_i(l+1)(2l+1)|l+2+i\eta_i| \\ y_2 &= -k_f l(2l+1)|l+1+i\eta_f| & y'_2 &= 3k_f(l+1)(2l+3)|l+i\eta_f| \\ y_3 &= 3k_f(l+1)(2l+1)|l+2+i\eta_f| & y'_3 &= -k_f(l+2)(2l+3)|l+1+i\eta_f| \\ y_4 &= -3k_i(l+1)(2l+3)|l+i\eta_i| & y'_4 &= k_i l(2l+1)|l+1+i\eta_i|. \end{aligned} \right\} (14)$$

By elimination of the matrix element $M_{l+1, l+1}^{-3}$ from (12) and (13) one obtains a recursion formula of the desired type

$$z M_{l l}^{-3} = z_1 M_{l l+2}^{-3} + z_2 M_{l-1 l+1}^{-3} + z_3 M_{l+2 l}^{-3} + z_4 M_{l+1 l-1}^{-3} \quad (15)$$

with

$$\left. \begin{aligned} z &= \frac{l(l+1)}{3}(\eta_f^2 - \eta_i^2) \\ z_1 &= -\eta_i^2 |l+1+i\eta_f| |l+2+i\eta_i| & z_3 &= \eta_f^2 |l+1+i\eta_i| |l+2+i\eta_i| \\ z_2 &= \eta_i \eta_f \frac{2l+3}{2l+1} |l+i\eta_i| |l+1+i\eta_f| & z_4 &= -\eta_i \eta_f \frac{2l+3}{2l+1} |l+i\eta_f| |l+1+i\eta_i|. \end{aligned} \right\} (15)$$

By means of (15) the non-maximal quadrupole matrix elements are determined from the maximal ones already calculated in (8) and (9).

The recursion relation connecting matrix elements of different multipoles may also be derived from I (17). One relation involving octupole matrix elements is, e. g., obtained with the subsidiary condition $x_1 = 0$. This leads to

$$y'' M_{l+1}^{-4} = y_1'' M_{l+1}^{-3} + y_2'' M_{l+2}^{-3} + y_3'' M_{l+1}^{-3}, \tag{17}$$

where

$$y'' = \left. \begin{aligned} y_1'' &= 2 k_f |l + 1 + i\eta_f| \\ y_2'' &= k_f (2l + 1) |l + 2 + i\eta_f| \\ y_3'' &= -k_i (2l + 3) |l + i\eta_i|. \end{aligned} \right\} \tag{18}$$

In order to obtain recursion relations which involve only maximal matrix elements, we shall use the general properties of the F_1 functions which occur in these matrix elements. The property which we shall utilize is the following:

$$F_1(\alpha + n_1, \beta + n_2, \beta' + n_3, \gamma + n_4, x, y) = \left[A(x, y) + B(x, y) \frac{\partial}{\partial x} + C(x, y) \frac{\partial}{\partial y} \right] F_1(\alpha, \beta, \beta', \gamma, x, y), \tag{19}$$

where n_r are arbitrary positive or negative integers and $A, B,$ and C rational functions in x and y .

A method of deriving recursion formulae is then to eliminate $\frac{\partial}{\partial x} F_1$ and $\frac{\partial}{\partial y} F_1$ between three such equations. The F_1 function which occurs in the maximal matrix elements is, for $l_i = l_f + \lambda,$

$$F_1(l + \lambda + 1 - i\eta_i, l + 1 + i\eta_f, l + 1 - i\eta_f, 2l + 2\lambda + 2, x, y) = F_1(l) \left. \begin{aligned} & \text{with } x = \frac{2\eta_i}{\eta_f + \eta_i} \quad y = \frac{2\eta_f}{\eta_f - \eta_i}. \end{aligned} \right\} \tag{20}$$

One easily obtains

$$F_1(l + 1) = \left. \begin{aligned} & \frac{(2l + 2\lambda + 2)(2l + 2\lambda + 3)}{|l + \lambda + 1 + i\eta_i|^2 |l + 1 + i\eta_f|^2} \frac{1}{(x - y)} \\ & \left\{ (l + 1 - i\eta_f)(x - 1) \frac{\partial}{\partial x} - (l + 1 + i\eta_f)(y - 1) \frac{\partial}{\partial y} \right\} F_1(l). \end{aligned} \right\} \tag{21}$$

Similar expressions for $F_1(l-1)$ and $F_1(l+2)$ can be derived. The elimination of the derivatives gives the desired recursion formula

$$w_1 M_{l+\lambda-3, l-3}^{-\lambda-1} + w_2 M_{l+\lambda-2, l-2}^{-\lambda-1} + w_3 M_{l+\lambda-1, l-1}^{-\lambda-1} + w_4 M_{l+\lambda, l}^{-\lambda-1} = 0 \quad (22)$$

with

$$\left. \begin{aligned} w_1 &= 2 \eta_i \eta_f |l-2 + i\eta_f| |l-1 + i\eta_f| |l+\lambda-2 + i\eta_i| \\ w_2 &= - |l-1 + i\eta_f| [l^2(2\eta_i^2 + 4\eta_f^2) + l[4(\lambda-2)(\eta_i^2 + \eta_f^2) + \eta_i^2 - \eta_f^2] \\ &\quad + (\lambda-2)[(2\lambda-3)\eta_i^2 - 3\eta_f^2] + 6\eta_i^2\eta_f^2] \\ w_3 &= \frac{\eta_f}{\eta_i} |l+\lambda-1 + i\eta_i| [l^2(4\eta_i^2 + 2\eta_f^2) + l[4(\lambda-2)\eta_i^2 + \eta_i^2 - \eta_f^2] \\ &\quad - 2(\lambda-2)\eta_i^2 + 6\eta_i^2\eta_f^2] \\ w_4 &= -2\eta_f^2 |l+\lambda-1 + i\eta_i| |l+\lambda + i\eta_i| |l+i\eta_f|. \end{aligned} \right\} (23)$$

V. Limiting Cases.

We shall here study two limiting cases of the general formulae for the Coulomb matrix elements. The one is the case of vanishing energy loss, i. e. $\eta_f - \eta_i = \xi = 0$, where one easily can obtain a simple expression for an arbitrary Sommerfeld number. The second case is the classical limit where $\eta_i, \eta_f \gg 1$, while $\eta_f - \eta_i$ is finite. This must lead to expressions identical with the usual classical integrals^{10, 11}.

a) $\xi = 0$.

For the maximal matrix elements, the second term of equations (8) and (9) is zero* while the first F_2 function is equal to one. One gets thus immediately the result

$$M_{l, l+\lambda}^{-\lambda-1} = M_{l+\lambda, l}^{-\lambda-1} = (2k)^{\lambda-2} \frac{[(\lambda-1)!]^2}{(2\lambda-1)!} \left| \frac{\Gamma(l+1+i\eta)}{\Gamma(l+\lambda+1+i\eta)} \right|. \quad (24)$$

The other matrix elements can be obtained by means of the recursion formulae. For the quadrupole case one may use equation (15)**. However, this becomes singular for $\xi = 0$, and the limiting process $\xi \rightarrow 0$ has to be performed with some care.

* This is not true for $\lambda = 1$, the result (24) is, however, right also in this case.

** The formula (25) has been found also by L. C. BIEDENHARN and C. M. GLASS¹² who have given a numerical evaluation of the total cross section and one of the coefficients for the angular distribution of the subsequent γ 's for the case $\xi = 0$.

$$\left. \begin{aligned}
 M_{l,l}^{-3} &= -\frac{\eta^2}{2(2l+1)l(l+1)} \lim_{\xi \rightarrow 0} \frac{1}{\xi} \left[\left| \frac{\Gamma(l+1+i\eta_f)}{\Gamma(l+1+i\eta_i)} \right| \frac{\eta_i}{\eta_f^2} e^{\frac{\pi}{2}\xi} \right. \\
 &- \left. \left| \frac{\Gamma(l+1+i\eta_i)}{\Gamma(l+1+i\eta_f)} \right| \frac{\eta_f}{\eta_i^2} \left(\frac{\eta_f}{\eta_i} \right)^{2l-2} e^{-\frac{\pi}{2}\xi} \right] \\
 &= \frac{1}{2l(l+1)(2l+1)} \{ 2l+1 - \pi\eta + i\eta [\psi(l+1-i\eta) - \psi(l+1+i\eta)] \}.
 \end{aligned} \right\} (25)$$

We have here used the expansion $\Gamma(x + \delta) \cong \Gamma(x) [1 + \delta\psi(x)]$, where $\psi(x)$ is the logarithmic derivative of the Γ -function.

For the octupole case one may use equation (17), and one gets directly

$$\left. \begin{aligned}
 M_{l,l+1}^{-4} &= \frac{k}{3l(l+1)(l+2)(2l+1)(2l+3) |l+1+i\eta|} \{ 3 |l+1+i\eta|^2 \\
 &[2l+1 - \pi\eta + i\eta (\psi(l+1-i\eta) - \psi(l+1+i\eta))] - l(l+1)(2l+1) \}.
 \end{aligned} \right\} (26)$$

The limiting case $\eta = 0$, i. e., the case where a plane wave Born approximation applies, is immediately obtained from (24) and (25).

For $\eta \gg 1$ one obtains the classical limit for $\xi = 0$. The deflection angle θ is there determined through $\text{tg } \theta/2 = \eta/l$ (see below) and one gets, e. g., for the quadrupole case

$$\left. \begin{aligned}
 M_{l,l+2}^{-3} &= M_{l+2,l}^{-3} = \frac{1}{\eta^2} \frac{1}{6} \sin^2 \theta/2 \\
 M_{l,l}^{-3} &= \frac{1}{\eta^2} \cdot \frac{1}{2} \text{tg}^2 \theta/2 \left[1 - \frac{\pi - \theta}{2} \text{tg } \theta/2 \right].
 \end{aligned} \right\} (27)$$

These matrix elements are just $4/\eta^2$ times the classical integrals for $\xi = 0$ given by Ter-Martirosyan (loc. cit.). The connection between the matrix elements and the classical integrals is obtained by the WBK approximation.

b) *The classical limit.*

In the classical limit $\eta \gg 1$, the main contribution to the matrix element $\langle \vec{k}_i | r^{-\lambda-1} Y_{\lambda\mu} | \vec{k}_f \rangle$ of equation (1) will arise from a narrow region of l values around¹³

$$l = \frac{mv}{\hbar} p = \eta \cotg \theta/2, \quad (28)$$

where p is the classical impact parameter and θ the angle between k_i and k_f .

For $\eta \gg 1$ and ξ finite, the F_2 functions of (8) and (9) approach the confluent hypergeometric functions of two variables Ψ_2 according to equation (A3). One obtains thus, in view of equation (28),

$$\left. \begin{aligned} M_{l+l}^{-\lambda-1} &= \frac{k^{\lambda-2}}{4 \eta^\lambda} I_{\lambda, -\lambda}(\theta) = \frac{k^{\lambda-2}}{4 \eta^\lambda} 2^\lambda \sin^\lambda \theta/2 e^{-\xi (\cot \theta/2 + \theta/2 - \pi/2)} \\ &\times \left\{ \frac{|\Gamma(\lambda + i\xi)|^2}{(2\lambda - 1)!} \Psi_2(-2\lambda + 1, -\lambda + 1 - i\xi, -\lambda + 1 + i\xi, z, z^*) \right. \\ &\left. + 2 \operatorname{Re} [e^{-\pi\xi} \Gamma(-\lambda - i\xi) z^{\lambda+i\xi} \Psi_2(-\lambda + 1 + i\xi, \lambda + 1 + i\xi, -\lambda + 1 + i\xi, z, z^*)] \right\} \end{aligned} \right\} (29)$$

with

$$z = \frac{\xi}{2} (\cot \theta/2 - i) = e^{-i\theta/2} \frac{\xi}{2 \sin \theta/2}.$$

The classical integrals $I_{\lambda\mu}(\theta)$ are defined in ref. 10. Similarly, one obtains

$$\left. \begin{aligned} M_{l+l}^{-\lambda-1} &= \frac{k^{\lambda-2}}{4 \eta^\lambda} I_{\lambda\lambda}(\theta) \\ &= \frac{k^{\lambda-2}}{4 \eta^\lambda} 2^\lambda \sin^\lambda \theta/2 e^{\xi (\cot \theta/2 + \theta/2 - \pi/2)} \\ &\times \left\{ \frac{|\Gamma(\lambda + i\xi)|^2}{(2\lambda - 1)!} \Psi_2(-2\lambda + 1, -\lambda + 1 - i\xi, -\lambda + 1 + i\xi, -z^*, -z) \right. \\ &\left. + 2 \operatorname{Re} [\Gamma(-\lambda - i\xi) (z^*)^{\lambda+i\xi} (-1)^\lambda \Psi_2(-\lambda + 1 + i\xi, \lambda + 1 + i\xi, -\lambda + 1 + i\xi, -z^*, -z)] \right\} \\ &= (-1)^\lambda e^{-\pi\xi} \frac{k^{\lambda-2}}{4 \eta^\lambda} I_{\lambda-\lambda}(-\theta). \end{aligned} \right\} (30)$$

The non-maximal matrix elements may be obtained by means of the recursion formulae.

The series expansion (A3) of the Ψ_2 function converges for all values of the variables, and the formulae (29) and (30) are thus directly suited for a numerical evaluation.

Since the limiting formula (A3) also holds for any value of η in the limit $l \gg 1$, the formulae (29) and (30) constitute the limits of the general formula (6) for large values of l_i and l_j .

VI. Conclusions.

By means of the results obtained in this paper it is possible to calculate the exact matrix elements needed for the computation of the total and differential cross sections in Coulomb excitation. The main difficulty encountered in a numerical evaluation is the rather large number of angular momenta which contribute to the process. The main contribution will in fact arise from l values of the order $l = \eta$, but also much higher l values must be taken into account. A direct application of the formulae for the matrix elements is made difficult by the fact that the F_2 functions converge rather slowly for $l > \eta$. However, this difficulty is overcome by the use of recursion formulae, whereby one may compute all matrix elements from the maximal matrix element, corresponding to $l = 0, 1$, and 2. Furthermore, in the limit $l \gg 1$, the matrix elements approach always the classical integrals $k^{\lambda-2}/4 \eta^\lambda I_{\lambda\mu}(\theta, \xi)$, with $\text{tg } \theta/2 = \eta/l$. Extensive tables of these integrals have recently been compiled*.

VII. Numerical Results.**

A numerical evaluation along the above mentioned lines has been carried out on the high speed electronic computer BESK in Stockholm. The first three maximal matrix elements were calculated with an accuracy of 10^{-11} . A comparison between the directly evaluated matrix elements and those obtained by the recursion formulae proved that this accuracy was sufficient for the application of successive recursion from these three first matrix elements.

* This tabulation, which was made by the authors, is not published, but parts of it are available on request.

** This chapter has been added to the original manuscript on May 10th 1955. We are greatly indebted to Prof. G. BREIT for drawing our attention to an error of sign in the numerical calculation of ref. 11.

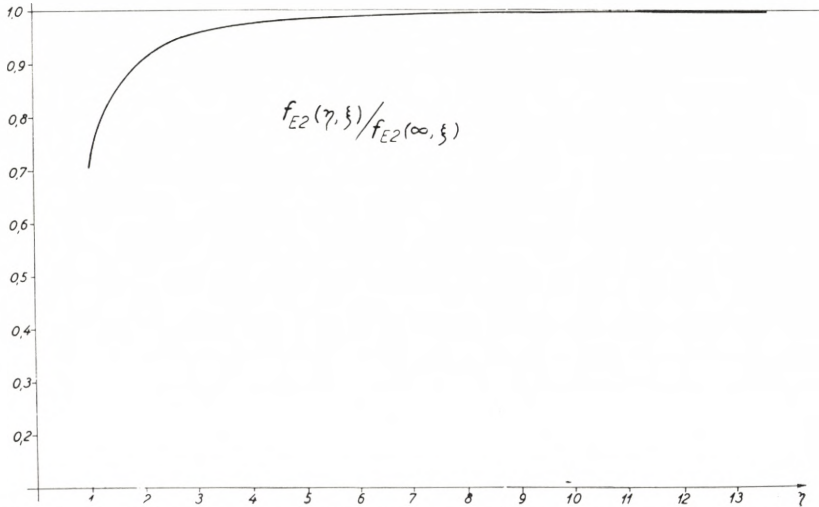


Fig. 1. The ratio of the exact to the classical total cross section function $f_{E2}(\eta, \xi) / f_{E2}(\infty, \xi)$ for electric quadrupole excitation as a function of η . The curves for different values of $\xi \leq 2$ coincide within the accuracy of drawing for $\eta > 1$.

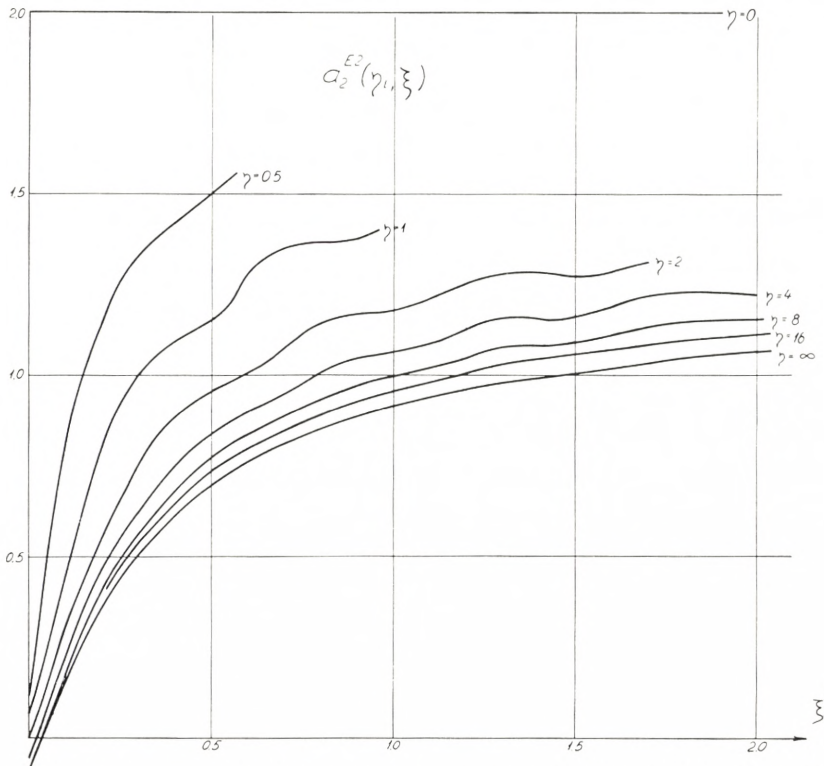


Fig. 2. The angular distribution coefficient a_2 as a function of ξ for different values of η .

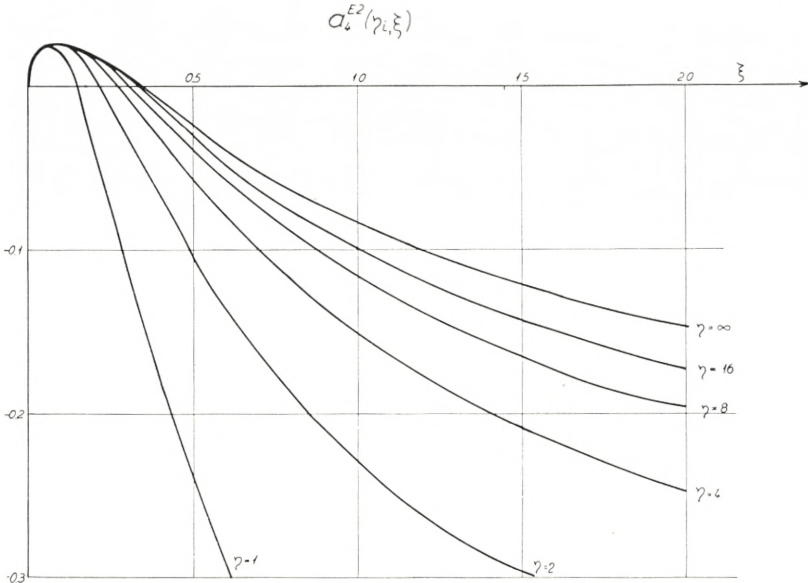


Fig. 3. The angular distribution coefficient a_4 as a function of ξ for different values of η_i .

An extract of the results is shown in Figs. 1—3.

The total cross section function $f_{E2}(\eta, \xi)$ is connected with the total cross section for electric quadrupole excitation through

$$\sigma_{E2} = \frac{m_1^2 v_f^2}{Z_2^2 e^2 \hbar^2} B(E2) f_{E2}(\eta_i, \xi).$$

With this definition one expects from the WKB approximation that the quantum mechanical corrections on f are small. Thus

$$f_{E2}(\eta_i, \xi) = \frac{64 \pi^2}{25} \eta_i \eta_f b_0$$

$$b_0 = \sum_l \left\{ \frac{3l(l-1)}{2(2l-1)} (M_{l-2,l}^{-3})^2 + \frac{l(l+1)(2l+1)}{(2l-1)(2l+3)} (M_{ll}^{-3})^2 + \frac{3(l+1)(l+2)}{2(2l+3)} (M_{l+2,l}^{-3})^2 \right\}.$$

The classical limit of this function is

$$f_{E2}(\infty, \xi) = \int_0^\pi \sin \theta \, d\theta \frac{8 \pi^3}{125} \sum_\mu |Y_{2\mu}(\frac{\pi}{2}, 0)|^2 |I_{2\mu}(\theta, \xi)|^2 \sin^{-4} \theta / 2.$$

This function was tabulated earlier (ref. 11) and is reproduced in Table 1. The results for the total cross section function is plotted in Fig. 1 as the ratio $f_{E2}(\eta, \xi) / f_{E2}(\infty, \xi)$. Within the accuracy of drawing the curves for different values of $\xi \leq 2$ coincide for $\eta > 1$.

The angular distribution coefficients are given by

$$a_2 = b_2/b_0 \quad \text{and} \quad a_4 = b_4/b_0$$

with

$$\begin{aligned} b_2 = & \sum_l \left\{ \frac{3 l(l-1)(l-2)}{(2l-1)^2} (M_{l-2,l}^{-3})^2 - \frac{l(l+1)(2l+1)(2l-3)(2l+5)}{(2l-1)^2(2l+3)^2} (M_{l,l}^{-3})^2 \right. \\ & + \frac{3(l+1)(l+2)(l+3)}{(2l+3)^2} (M_{l+2,l}^{-3})^2 \\ & - 6 \frac{(l-1)l(l+1)}{(2l-1)^2} M_{l-2,l}^{-3} M_{l,l}^{-3} \cos(\sigma_l - \sigma_{l-2}) \\ & \left. - 6 \frac{l(l+1)(l+2)}{(2+3)^2} M_{l+2,l}^{-3} M_{l,l}^{-3} \cos(\sigma_l - \sigma_{l+2}) \right\}, \\ b_4 = & - \sum_l \left\{ \frac{9 l(l-1)(l-2)(l-3)}{16 (2l-1)^2(2l+1)} (M_{l-2,l}^{-3})^2 + \frac{9(l-1)l(l+1)(l+2)(2l+1)}{4 (2l-1)^2(2l+3)^2} (M_{l,l}^{-3})^2 \right. \\ & + \frac{9(l+1)(l+2)(l+3)(l+4)}{16 (2l+1)(2l+3)^2} (M_{l+2,l}^{-3})^2 \\ & - \frac{15(l-2)(l-1)l(l+1)}{4 (2l-1)^2(2l+3)} M_{l-2,l}^{-3} M_{l,l}^{-3} \cos(\sigma_l - \sigma_{l-2}) \\ & - \frac{15 l(l+1)(l+2)(l+3)}{4 (2l-1)(2l+3)^2} M_{l+2,l}^{-3} M_{l,l}^{-3} \cos(\sigma_l - \sigma_{l+2}) \\ & \left. + \frac{105(l-1)l(l+1)(l+2)}{8 (2l-1)(2l+1)(2l+3)} M_{l+2,l}^{-3} M_{l-2,l}^{-3} \cos(\sigma_{l+2} - \sigma_{l-2}) \right\}. \end{aligned}$$

The results for a_2 and a_4 are plotted in Figs. 2 and 3. The classical curves ($\eta = \infty$) calculated earlier¹¹ contain an error of sign. The curves for $\eta_i = 0$ are discontinuous having the values

$$a_2(\eta_i = 0, \xi) = \begin{cases} \frac{1}{2} & \text{for } \xi = 0 \\ 2 & \text{for } \xi \pm 0 \end{cases}$$

$$a_4(\eta_i = 0, \xi) = \begin{cases} \frac{1}{16} & \text{for } \xi = 0 \\ -\frac{3}{2} & \text{for } \xi \pm 0 \end{cases}$$

Table 1.

ξ	$f_{E2}(\infty, \xi) \cdot 10^{+P}$	P
0.0	0.8954	0
0.1	0.8638	0
0.2	0.7289	0
0.3	0.5608	0
0.4	0.4046	0
0.5	0.2781	0
0.6	0.1844	0
0.7	0.1189	0
0.8	0.7511	1
0.9	0.4663	1
1.0	0.2855	1
1.2	0.1035	1
1.4	0.3628	2
1.6	0.1238	2
1.8	0.4143	3
2.0	0.1363	3

The classical total cross section function for electric quadrupole excitation for $\xi \leq 2$.

Acknowledgement.

The authors wish to thank Professor NIELS BOHR and Drs. AAGE BOHR and BEN MOTTELSON for their continued interest in this work.

Appendix:
Some Properties of Generalized Hypergeometric Functions
of Two Variables.

Besides the function F_2 defined in I, we shall here use the following Appell functions:

$$\left. \begin{aligned} F_1(\alpha, \beta, \beta', \gamma, x, y) &= \sum_{m, n=0}^{\infty} \frac{\alpha_{m+n} \beta_m \beta'_n}{\gamma_{m+n} m! n!} x^m y^n \\ F_3(\alpha, \alpha', \beta, \beta', \gamma, x, y) &= \sum_{m, n}^{\infty} \frac{\alpha_m \alpha'_n \beta_m \beta'_n}{\gamma_{m+n} m! n!} x^m y^n, \end{aligned} \right\} \quad (\text{A } 1)$$

where

$$a_n = \frac{\Gamma(a+n)}{\Gamma(a)} = a(a+1) \dots (a+n-1).$$

These double series have the following domain of absolute convergence:

$$|x| < 1 \quad |y| < 1. \quad (\text{A } 2)$$

From these hypergeometric functions one can obtain related functions by a limiting process, (the so-called confluence), e. g.,

$$\lim_{\substack{\varepsilon_1 \rightarrow 0 \\ \varepsilon_2 \rightarrow 0}} F_2\left(\alpha, \frac{1}{\varepsilon_1}, \frac{1}{\varepsilon_2}, \gamma, \gamma', \varepsilon_1 x, \varepsilon_2 y\right) = \Psi_2(\alpha, \gamma, \gamma', x, y), \quad (\text{A } 3)$$

where

$$\Psi_2(\alpha, \gamma, \gamma', xy) = \sum_{m, n=0}^{\infty} \frac{\alpha_{m+n}}{\gamma_m \gamma'_n m! n!} x^m y^n$$

is a series expansion which converges for all values of x and y . There exist a large number of functional relations connecting

different hypergeometric functions. Some of these represent an analytic continuation, such as

$$\left. \begin{aligned}
 &F_3(\alpha, \alpha', \beta, \beta', \gamma, x, y) = f(\alpha, \alpha', \beta, \beta') (-x)^{-\alpha} (-y)^{-\alpha'} \\
 &F_2\left(\alpha + \alpha' + 1 - \gamma, \alpha, \alpha', \alpha + 1 - \beta, \alpha' + 1 - \beta', \frac{1}{x}, \frac{1}{y}\right) \\
 &+ f(\alpha, \beta', \beta, \alpha') (-x)^{-\alpha} (-y)^{-\beta'} \\
 &F_2\left(\alpha + \beta' + 1 - \gamma, \alpha, \beta', \alpha + 1 - \beta, \beta' + 1 - \alpha', \frac{1}{x}, \frac{1}{y}\right) \\
 &+ f(\beta, \alpha', \alpha, \beta') (-x)^{-\beta} (-y)^{-\alpha'} \\
 &F_2\left(\beta + \alpha' + 1 - \gamma, \beta, \alpha', \beta + 1 - \alpha, \alpha' + 1 - \beta', \frac{1}{x}, \frac{1}{y}\right) \\
 &+ f(\beta, \beta', \alpha, \alpha') (-x)^{-\beta} (-y)^{-\beta'} \\
 &F_2\left(\beta + \beta' + 1 - \gamma, \beta, \beta', \beta + 1 - \alpha, \beta' + 1 - \alpha', \frac{1}{x}, \frac{1}{y}\right),
 \end{aligned} \right\} \quad (A4)$$

where

$$f(\lambda, \mu, \varrho, \sigma) = \frac{\Gamma(\gamma) \Gamma(\varrho - \lambda) \Gamma(\sigma - \mu)}{\Gamma(\varrho) \Gamma(\sigma) \Gamma(\gamma - \lambda - \mu)}.$$

Others represent the reductions which occur for special choices of the parameters. We shall here use the following reduction formulae:

$$\left. \begin{aligned}
 &F_2(\alpha, \beta, \beta', \gamma, \alpha, x, y) = (1 - y)^{-\beta'} F_1\left(\beta, \alpha - \beta', \beta', \gamma, x, \frac{x}{1 - y}\right) \\
 &F_2(\alpha, \beta, \beta', \alpha, \gamma', x, y) = (1 - x)^{-\beta} F_1\left(\beta', \beta, \alpha - \beta, \gamma', \frac{y}{1 - x}, y\right) \\
 &F_3(\alpha, \alpha', \beta, \gamma - \beta, \gamma, x, y) = (1 - y)^{-\alpha'} F_1\left(\beta, \alpha, \alpha', \gamma, x, \frac{y}{y - 1}\right).
 \end{aligned} \right\} \quad (A5)$$

CERN (European Organization for Nuclear Research)
 Theoretical Study Division, Copenhagen

and

Institute for Theoretical Physics, University of Copenhagen.

References.

1. R. HUBY and H. C. NEWNS: Proc. Phys. Soc. **64**A, 619 (1951).
2. C. T. MULLIN and E. GUTH: Phys. Rev. **82**, 141 (1951).
3. K. ALDER and A. WINTHER: Phys. Rev. **96**, 237 (1954).
4. K. ALDER and A. WINTHER: Dan. Mat. Fys. Medd. **28**, no. 18 (1955).
Quoted as I.
5. A. BOHR and B. MOTTELSON: Dan. Mat. Fys. Medd. **27**, no. 16 (1953).
6. N. F. MOTT and H. MASSEY: Theory of Atomic Collisions, Oxford 1949.
7. K. ALDER, A. BOHR, T. HUUS, B. MOTTELSON and A. WINTHER: Rev. Mod. Phys. in preparation.
8. ERDÉLYI ET AL: Higher Transcendental Functions, Mc Graw-Hill 1953.
9. P. APPELL et J. KAMPÉ DE FÉRIET: Fonctions Hypergéométriques etc. Paris, Gauthier-Villars 1926.
10. K. A. TER-MARTIROSYAN: Journ. Exp. Theor. Phys. U. S. S. R. **22**, 284 (1952).
11. K. ALDER and A. WINTHER: Phys. Rev. **91**, 1578 (1953).
12. L. C. BIEDENHARN and C. M. CLASS: Phys. Rev. in press.
13. N. BOHR: Dan. Mat. Fys. Medd. **18**, no. 8 (1948).

Det Kongelige Danske Videnskabernes Selskab

Matematisk-fysiske Meddelelser

Dan. Mat. Fys. Medd.

Bind 28 (kr. 73.00)

	kr. ø.
1. HUUS, TORBEN, and ZUPANČIČ, ČRTOMIR: Excitation of Nuclear Rotational States by the Electric Field of Impinging Particles. 1953	2.00
2. WEBER, SOPHUS: Über den Zusammenhang zwischen der laminaren Strömung der reinen Gase durch Rohre und dem Selbstdiffusionskoeffizienten. 1954	20.00
3. ALAGA, G., KOFOED-HANSEN, O., and WINTHER, A.: On the Pseudoscalar Interaction in β -Decay. 1953	2.00
4. CHOUDHURY, D C.: Intermediate Coupling Calculations in the Unified Nuclear Model. 1954	2.00
5. LÜDERS, GERHART: On the Equivalence of Invariance under Time Reversal and under Particle-Antiparticle Conjugation for Relativistic Field Theories. 1954	2.00
6. BELINFANTE, F. J., and MØLLER, C.: On the Relation between the Time-Dependent and Stationary Treatments of Collision Processes. 1954	7.00
7. BOHR, NIELS, and LINDHARD, JENS: Electron Capture and Loss by Heavy Ions Penetrating through Matter. 1954	4.00
8. LINDHARD, J.: On the Properties of a Gas of Charged Particles. 1954	6.00
9. KOFOED-HANSEN, O.: Theoretical Angular Correlations in Allowed Beta Transitions. 1954	3.00
10. RASMUSEN, HANS Q., and HESSELBERG, O. K.: An Appropriate Method for Integration of the Motion of Periodic Comets. 1954	5.00
11. D'ESPAGNAT, B.: Meson Production in Meson-Nucleon Collisions. 1954	6.00
12. KRISTENSEN, P.: Configuration Space Representation for Non-Linear Fields. 1954	8.00
13. TORNEHAVE, HANS: On Almost Periodic Movements. 1954	6.00

Bind 29 (kr. 85.50)

1. FØLNER, ERLING: On the Dual Spaces of the Besicovitch Almost Periodic Spaces. 1954	5.00
2. EBEL, MARVIN E.: Causal Behaviour of Field Theories with Non-Localizable Interactions. 1954	5.00
3. WILETS, LAWRENCE: Excitation of Nuclear Rotational States in μ -Mesonic Atoms. 1954	3.00
4. BALLHAUSEN, C. J.: Studies of Absorption Spectra. II. Theory of Copper (II)-Spectra. 1954	3.00

	kr. ø.
5. NAUR, PETER: The Energy Production in Convective Cores in Stars. 1954.....	3.00
6. NIELSEN, O. B., and KOFOED-HANSEN, O.: A Six Gap β -Ray Spectrometer. 1955.....	2.00
7. JØRGENSEN, CHR. KLIXBÜLL: Studies of Absorption Spectra. VI. Actinide Ions with two 5 f -Electrons. 1955.....	<u>2.00</u>
8. BALLHAUSEN, C. J.: Studies of Absorption Spectra. V. The Spectra of Nickel (II) Complexes. 1955.....	3.00
9. ALAGA, G., ALDER, K., BOHR, A., and MOTTELSON, B. R.: Intensity Rules for Beta and Gamma Transitions to Nuclear Rotational States. 1955.....	3.00
10. BOHR, A., FRÖMAN, P. O., and MOTTELSON, B. R.: On the Fine Structure in Alpha Decay. 1955.....	2.00
11. JØRGENSEN, CHR. KLIXBÜLL: Studies of Absorption Spectra. VII. Systems with three and more f -Electrons. 1955.....	3.50
12. HAAG, R.: On Quantum Field Theories. 1955.....	6.00
13. HERMANSEN, ALFRED: A Theory of Interference Filters. 1955..	<u>15.00</u>
14. BALLHAUSEN, C. J., and JØRGENSEN, CHR. KLIXBÜLL: Studies of Absorption Spectra. X. d -Electrons in Crystal Fields of Different Symmetries. 1955.....	<u>5.00</u>
15. KOFOED-HANSEN, O., and NIELSEN, A.: Construction of a Spectrometer for Neutrino Recoils: Investigation of the Decay of A^{87} . 1955.....	8.00
16. NILSSON, SVEN GÖSTA: Binding States of Individual Nucleons in Strongly Deformed Nuclei. 1955.....	8.00
17. KÄLLÉN, G., and SABRY, A.: Fourth Order Vacuum Polarization. 1955.....	4.00
18. ALDER, KURT, and WINTHER, AAGE: Matrix Elements between States in the Coulomb Field. 1955.....	2.00
19. ALDER, KURT, and WINTHER, AAGE: On the Exact Evaluation of the Coulomb Excitation. 1955.....	3.00